Universität Potsdam

W.-R. Hamann | A. Feldmeier | L. Oskinova (eds.)

Clumping in Hot-Star Winds

Proceedings of an International Workshop held in Potsdam, Germany, 18. - 22. June 2007

Universitätsverlag Potsdam

Clumping in Hot-Star Winds

Wolf-Rainer Hamann, Achim Feldmeier, Lidia Oskinova (eds.)

Clumping in Hot-Star Winds

Proceedings of an International Workshop
held in Potsdam, Germany, 18. - 22. June 2007

Universitätsverlag Potsdam 2008

Bibliografische Information der Deutschen Nationalbibliothek
Die Deutsche Nationalbibliothek verzeichnet diese Publikation in der Deutschen Nationalbibliografie; detaillierte bibliografische Daten sind im Internet über http://dnb.d-nb.de abrufbar.

Universitätsverlag Potsdam 2008
http://info.ub.uni-potsdam.de/verlag.htm

Universitätsverlag Potsdam, Am Neuen Palais 10, 14469 Potsdam
Tel.: +49 (0)331 977 4623 / Fax: 4625
E-Mail: ubpub@uni-potsdam.de

Elektronisch veröffentlicht auf dem Publikationsserver der Universität Potsdam
URL http://pub.ub.uni-potsdam.de/volltexte/2008/1398/
URN urn:nbn:de:kobv:517-opus-13981
[http://nbn-resolving.de/urn:nbn:de:kobv:517-opus-13981]

Zugleich gedruckt erschienen im Universitätsverlag Potsdam:
ISBN 978-3-940793-33-1

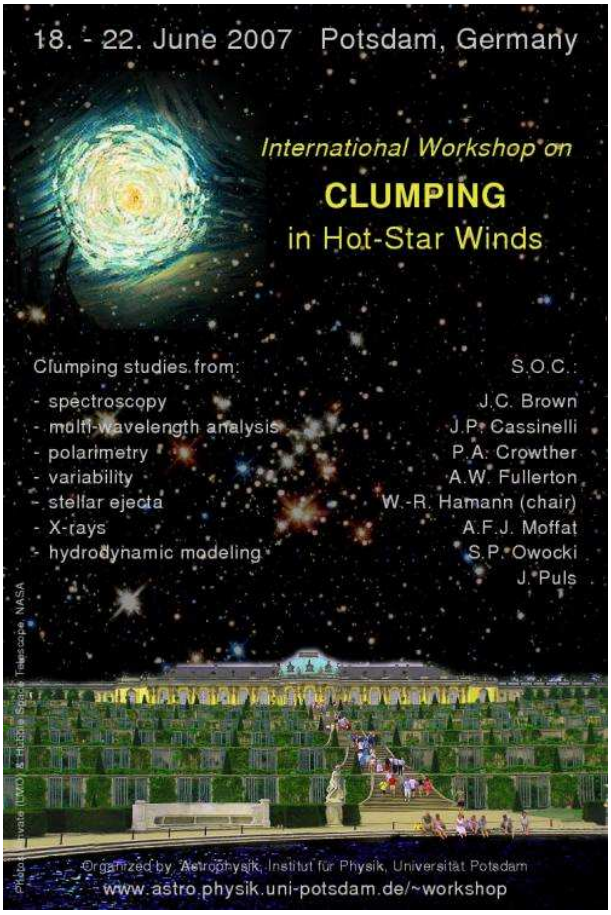

Workshop Poster

Abstract

Stellar winds play an important role for the evolution of massive stars and their cosmic environment. Multiple lines of evidence, coming from spectroscopy, polarimetry, variability, stellar ejecta, and hydrodynamic modeling, suggest that stellar winds are non-stationary and inhomogeneous. This is referred to as 'wind clumping'.

The urgent need to understand this phenomenon is boosted by its far-reaching implications. Most importantly, all techniques to derive empirical mass-loss rates are more or less corrupted by wind clumping. Consequently, mass-loss rates are extremely uncertain. Within their range of uncertainty, completely different scenarios for the evolution of massive stars are obtained. Settling these questions for Galactic OB, LBV and Wolf-Rayet stars is prerequisite to understanding stellar clusters and galaxies, or predicting the properties of first-generation stars.

In order to develop a consistent picture and understanding of clumped stellar winds, an international workshop on 'Clumping in Hot Star Winds' was held in Potsdam, Germany, from 18. - 22. June 2007. About 60 participants, comprising almost all leading experts in the field, gathered for one week of extensive exchange and discussion. The Scientific Organizing Committee (SOC) included John Brown (Glasgow), Joseph Cassinelli (Madison), Paul Crowther (Sheffield), Alex Fullerton (Baltimore), Wolf-Rainer Hamann (Potsdam, chair), Anthony Moffat (Montreal), Stan Owocki (Newark), and Joachim Puls (Munich). These proceedings contain the invited and contributed talks presented at the workshop, and document the extensive discussions.

Acknowledgements. The editors thank Helge Todt for developing the LaTeX scheme and template of these proceedings. We thank Ghazal Khan and Christina Winter for their help in transcribing the discussions.

Clumping in Hot Star Winds
W.-R. Hamann, A. Feldmeier & L.M. Oskinova, eds.
Potsdam: Univ.-Verl., 2008
URN: http://nbn-resolving.de/urn:nbn:de:kobv:517-opus-13981

Contributions

Stellar evolution

Chair: A. Pollock

Clumping in Hot Star Winds
W.-R. Hamann, A. Feldmeier & L.M. Oskinova, eds.
Potsdam: Univ.-Verl., 2008
URN: http://nbn-resolving.de/urn:nbn:de:kobv:517-opus-13981

The impact of reduced mass loss rates on the evolution of massive stars

Raphael Hirschi
University of Keele, United Kingdom

Mass loss is a very important aspect of the life of massive stars. After briefly reviewing its importance, we discuss the impact of the recently proposed downward revision of mass loss rates due to clumping (difficulty to form Wolf-Rayet stars and production of critically rotating stars). Although a small reduction might be allowed, large reduction factors around ten are disfavoured.

We then discuss the possibility of significant mass loss at very low metallicity due to stars reaching break-up velocities and especially due to the metal enrichment of the surface of the star via rotational and convective mixing. This significant mass loss may help the first very massive stars avoid the fate of pair-creation supernova, the chemical signature of which is not observed in extremely metal poor stars. The chemical composition of the very low metallicity winds is very similar to that of the most metal poor star known to date, HE1327-2326 and offer an interesting explanation for the origin of the metals in this star.

We also discuss the importance of mass loss in the context of long and soft gamma-ray bursts and pair-creation supernovae. Finally, we would like to stress that mass loss in cooler parts of the HR-diagram (luminous blue variable and yellow and red supergiant stages) are much more uncertain than in the hot part. More work needs to be done in these areas to better constrain the evolution of the most massive stars.

1 Introduction

Mass loss has a crucial impact on the evolution of massive stars. It affects evolutionary tracks, lifetimes and surface abundances. It also determines the population of massive stars (number of stars in each Wolf-Rayet subtype for example). It influences the type of supernova at the death of the star (SNII, Ib, Ic, or a pair-creation supernova) and the final remnant (neutron star or black hole). Mass loss releases matter and energy back into the interstellar medium in amounts comparable to supernovae (for stars above 30 $M_{\odot}$). Finally, it affects the hardness of the ionizing radiation coming from massive stars. It is therefore very important to understand mass loss in order to understand and model the evolution of massive stars.

2 Impact of reduced mass loss rates at solar metallicity

The concept of clumping is not new (see contribution from Moffat in this volume, or a general review from Kudritzki & Puls 2000). However, new observations suggest clumping factors leading to downward revision of mass loss rates between three to ten or even more for massive stars (Bouret et al. 2005, Fullerton et al. 2006). Here we discuss the implications of a reduction factor around ten. A 120 $M_{\odot}$ star, using current mass loss prescriptions at solar metallicity (Vink et al. 2000, 2001, Kudritzki & Puls 2000), loses on average $2 \cdot 10^{-5}\, M_{\odot}$ per year. The lifetime of a 120 $M_{\odot}$ star is about 2.5 million years. This implies that, on the main sequence, a 120 $M_{\odot}$ star loses approximately 50 $M_{\odot}$. If mass loss rates are reduced by a factor 10, such a star would only lose 5 $M_{\odot}$. The question is then, how to produce a WR star with such low mass loss rates? The first possibility is that mass loss is high in other evolutionary stages, like the luminous blue variable (continuum-driven winds in LBVs, Smith & Owocki 2006) and the red supergiant (RSG) stages. Mass loss rates are harder to determine in these two stages and therefore uncertainties are still large. Nevertheless clumping may also affect mass loss determination in other stages. Another possibility would be that all massive stars are in close binary systems (Kobulnicky et al. 2006). However, if this were true, then it would be hard to produce the many RSG stars observed. Furthermore, the fraction of Wolf-Rayet stars in close binary systems in the Magellanic Clouds is found to be only 30-40% (Foellmi et al. 2003, 2003). This means that single stars must still be able to lose enough mass to become WRs on their own. The last possibility discussed here is that rotation (possibly coupled to magnetic fields) induces such a strong mixing that WRs are produced by mixing rather than mass loss

(Maeder 1987, Yoon & Langer 2005). This scenario works only for fast rotators, which represent only a small fraction at $Z_{\odot}$ and therefore this cannot produce all the WR stars observed.

Another important impact of strongly reduced mass loss rates is that it implies that the angular momentum loss is much weaker. This would lead to many critically rotating stars near the end of the main sequence, similar to Be stars. This in turn would lead to an increase in mass loss rates, which could possibly compensate for a modest reduction factor. Additional models are necessary to give a quantitative answer. More interestingly, mass loss would become strongly anisotropic (Maeder & Desjacques 2001) and possibly produce disks when the Ω-limit is reached as is observed around Be type stars (See e.g. the review by Porter & Rivinius 2003). The lack of observations of critically rotating very massive stars is an argument against mass loss being extremely low on the main sequence and high only later on during the LBV and RSG stages. Note that rotation is able to compensate for a reduction factor 2 for mass loss since comparable number of WR stars are produced with enhanced mass loss rates (Meynet et al. 1994) and with normal mass loss rates + rotation (Meynet & Maeder 2005).

3 Metallicity dependence

The metallicity (Z) dependence of mass loss rates is usually included using the formula: $\dot{M}(Z) = \dot{M}(Z_{\odot})(Z/Z_{\odot})^{\alpha}$. The exponent α varies between 0.5-0.6 (Kudritzki & Puls 2000, Kudritzki 2002) and 0.7-0.86 (Vink and collaborators 2001, 2005) for O-type and WR stars (See Mokiem et al. 2007 for a recent comparison between mass loss prescriptions and observed mass loss rates). Until very recently, most models use at best the total metal content present at the surface of the star to determine the mass loss rate. However, the surface chemical composition becomes very different from the solar mixture, due either to mass loss in the WR stage or by internal mixing (convection and rotation) after the main sequence. It is therefore important to know the contribution from each chemical species to opacity and mass loss. Recent studies (Vink et al. 2000, 2005) show that iron is the dominant element concerning radiation line-driven mass loss for O-type and WR stars. In the case of WR stars, there is however a plateau at low metallicity due to the contributions from light elements like carbon, nitrogen and oxygen (CNO). In the RSG stage, rates generally used are still those of Nieuwenhuijzen & de Jager (1990). Observations indicate that there is a very weak dependence of dust-driven mass loss on metallicity and that CNO elements and especially nucleation seed components like silicon and titanium are dominant (Van Loon 2000, 2006, Ferrarotti & Gail 2006). See van Loon et al. (2005) for recent mass loss rate prescriptions in the RSG stage. In particular, the ratio of carbon to oxygen is important to determine which kind of molecules and dusts form. If the ratio of carbon to oxygen is larger than one, then carbon-rich dust would form, and more likely drive a wind since they are more opaque than oxygen-rich dust at low metallicity (Höfner & Andersen 2007).

In between the hot and cool parts of the HR-diagram, mass loss is not well understood. Observations of the LBV stage indicate that several solar masses per year may be lost and there is no indication of a metallicity dependence. Chromospheric activity could also play a role in stars having surface temperature similar to the Sun. Thermally driven winds and pulsations are still other ways to lose mass. Even though there are still large uncertainties in the dependence of the mass loss rates on metallicity in the cooler part of the HR-diagram, it is very useful to use models and observations at various metallicities. Indeed, clumping appears to be metallicity independent and therefore comparisons between models and observations should yield the same conclusions at different metallicities. Furthermore, using models at lower metallicity already give a very good estimate of what the impact of clumping may be on the evolution of the star. The mass loss rate is a factor 1.6-2.2 (depending on alpha) and 2.2-4.0 lower at the metallicity of the large and small Magellanic Clouds (LMC and SMC) respectively. Comparing models calculated at the SMC metallicity with observations at solar metallicity shows the impact of a reduction factor around three.

Several groups recently computed massive star models and compared them to observed populations around solar metallicities. Here we present a few of them. Meynet & Maeder (2005) compare the ratio or WR to O-type stars using α=0.5 for O-type star and no metallicity dependence for WR stars. They find that rotating models better reproduce the WR/O ratio and also the ratio of type Ib+Ic to type II supernova as a function of metallicity compared to non-rotating models, which underestimate these ratios. Reducing the mass loss rates by even a factor two would not fit the observations as well as with the current mass loss prescriptions. Eldridge & Vink (2006) use mass loss rates dependent on metallicity in the WR stage and find a better agreement with observations for the WC/WN ratio compared to metallicity independent mass loss rates in the WR stage. Again, reducing the mass loss rates by a factor 2 or more would not fit the data better than with the current mass loss prescriptions. However Vanbeveren et al. (2007) includes binary stars in the comparison and find a good fit with a mass loss rate reduced by a factor two.

Including all the arguments discussed above, from the current stellar evolution point of view the observations of the populations of massive stars would not be better reproduced with mass loss rate pre-

scriptions reduced by a factor greater than two.

4 First stellar generations

As we saw in the previous sections, mass loss plays a crucial in the evolution of solar metallicity stars. In this section, we discuss the importance of mass loss on the evolution of the first stellar generations. The first massive stars died a long time ago and will probably never be detected directly (see however Scannapieco et al. 2005). There are nevertheless indirect observational constraints on the first stars coming from observations of the most metal poor halo stars (Beers & Christlieb 2005). The first stars are very important because they took part in the re-ionisation of the universe at the end of the dark ages (roughly 400 million years after the Big Bang). They are therefore tightly linked to the formation of the first structures in the universe and can provide valuable information about the early evolution of the universe. The first stellar generations are different from solar metallicity ($Z_\odot$) stars due to their low metal content or absence of it. First, very low-Z stars are more compact due to lower opacity. Second, *metal free* stars burn hydrogen in a core, which is denser and hotter. This implies that the transition between core hydrogen and helium burning is much shorter and smoother. Furthermore, hydrogen burns via the pp-chain in shell burning. *These differences make the metal free (first) stars different from the second or later generation stars!* (Ekström & Meynet 2007). Third, mass loss is metallicity dependent (at least for radiation-driven winds) and therefore mass loss is expected to become very small at very low metallicity. Finally, the initial mass function of the first stellar generations is expected to be top heavy below a certain threshold (Bromm & Loeb 2003).

Mass loss is expected to be very small. What could change this expectation? An additional mechanism or the chemical enrichment of the envelope of the star are two possible ways to increase mass loss at very low Z. Models of metal free stars including the effect of rotation (Ekström et al. 2005) show that stars may lose up to 10 % of their initial mass due to the star rotating at its critical limit (also called break-up limit). The mass loss due to the star reaching the critical limit is non-negligible but at the same time not important enough to change drastically the fate of the first generation stars.

The situation is very different at very low but non-zero metallicity (Meynet et al. 2006 and Hirschi 2007). The total mass of an $85\,M_\odot$ model at $Z = 10^{-8}$ is shown in Fig. 1 with the top solid line. This model, like metal free models, loses around 5% of its initial mass when its surface reaches break-up velocities in the second part of the main sequence. At the end of core H-burning, the core contracts and the envelope expands, thus decreasing the surface velocity and its ratio to the critical velocity. The mass loss rate becomes very low again until the star crosses the HR diagram and reaches the RSG stage. At this point the convective envelope dredges up CNO elements to the surface increasing its overall metallicity. The total metallicity, Z, is used in this model (including CNO elements) for the metallicity dependence of the mass loss.

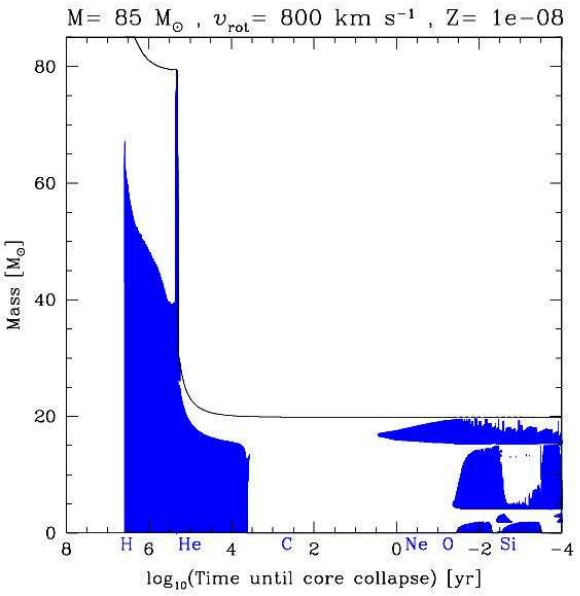

Figure 1: Structure evolution diagram of the 85 $M_\odot$ model at $Z = 10^{-8}$. Coloured areas corresponds to convective zones along the lagrangian mass coordinate as a function of time left until the core collapse. The top solid line shows the total mass of the star. The burning stage abbreviations are given below the time axis.

Therefore depending on how much CNO is brought up to the surface, the mass loss becomes very large again. The CNO brought to the surface comes from primary C and O produced in He-burning. Rotational and convective mixing brings these elements into the H-burning shell. A large fraction of the C and O is then transformed into primary nitrogen via the CNO cycle. Additional convective and rotational mixing is necessary to bring the primary CNO to the surface of the star. The whole process is complex and depends on mixing. Multi-dimensional models would be very helpful to constrain mixing between the hydrogen and carbon rich layers, which releases a large amount of energy and strongly affects the structure of the star.

The strongest mass loss occurs in these models in the cooler part of the HR diagram. Dust-driven winds appear to be metallicity independent as long as C-rich dust can form. For this to occur, the sur-

face effective temperature needs to be low enough ($\log(T_{\rm eff}) < 3.6$) and carbon needs to be more abundant than oxygen. Note that nucleation seeds (probably involving titanium) are still necessary to form C-rich dust. It is not clear whether extremely low-Z stars will reach such low effective temperatures. This depends on the opacity and the opacity tables used in these calculations did not account for the non-standard mixture of metals (high CNO and low iron abundance, see Marigo 2002 for possible effects). It is interesting to note that the wind of the 85 $M_\odot$ model is richer in carbon than oxygen, thus allowing C-rich dust to form if nucleation seeds are present. There may also be other important types of wind, like chromospheric activity-driven, pulsation-driven, thermally-driven or continuum-driven winds.

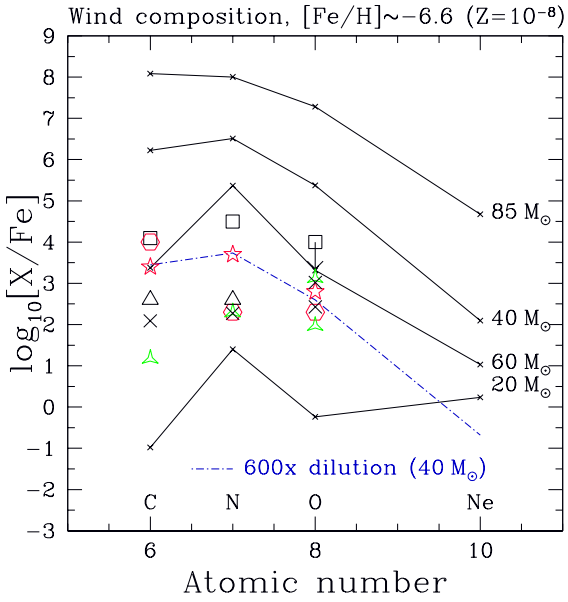

Figure 2: Composition in [X/Fe] of the stellar wind for the $Z = 10^{-8}$ models (solid lines). For HE1327-2326 (*red stars*), the best fit for the CNO elements is obtained by diluting the composition of the wind of the 40 $M_\odot$ model by a factor 600 (see Hirschi 2007 for more details).

Significant mass loss in very low-Z massive stars offers an interesting explanation for the strong enrichment in CNO elements of the most metal poor stars observed in the halo of the galaxy (see Meynet et al. 2006 and Hirschi 2007). The most metal poor stars known to date, HE1327-2326 (Frebel et al. 2006) is characterised by very high N, C and O abundances, high Na, Mg and Al abundances, a weak s–process enrichment and depleted lithium. The star is not evolved so has not had time to bring self–produced CNO elements to its surface and is most likely a subgiant. By using one or a few SNe and using a very large mass cut, Limongi et al. (2003) and Iwamoto et al. (2005) are able to reproduce the abundance of most elements. However they are not able to reproduce the nitrogen surface abundance of HE1327-2326 without rotational mixing. A lot of the features of this star are similar to the properties of the stellar winds of very metal poor rotating stars. HE1327-2326 could therefore have formed from gas, which was mainly enriched by stellar winds of rotating very low metallicity stars. In this scenario, a first generation of stars (PopIII) pollutes the interstellar medium to very low metallicities ([Fe/H]∼-6). Then a PopII.5 star (Hirschi 2005) like the 40 $M_\odot$ model calculated here pollutes (mainly through its wind) the interstellar medium out of which HE1327-2326 forms. This would mean that HE1327-2326 is a third generation star. In this scenario, the CNO abundances are well reproduced, in particular that of nitrogen, which according to the new values for a subgiant from Frebel et al. (2006) is 0.9 dex higher in [X/Fe] than oxygen. This is shown in Fig. 2 where the abundances of HE1327-2326 are represented by the red stars and the best fit is obtained by diluting the composition of the wind of the 40 $M_\odot$ model by a factor 600. When the SN contribution is added, the [X/Fe] ratio is usually lower for nitrogen than for oxygen. Although the existence of a lower limit for the minimum metallicity Z for low mass stars to form is still under debate, it is interesting to note that the very high CNO yields of the 40 $M_\odot$ stars brings the total metallicity Z above the limit for low mass star formation obtained in Bromm & Loeb (2003).

5 Gamma-ray bursts and pair-creation supernovae

Long and soft gamma-ray bursts (GRBs) have now been firmly connected to the death of type Ic supernovae (see Woosley & Bloom 2006 for a recent review). In one of the most promising models, the collapsar model (Woosley 1993), GRB progenitors must form a black hole, lose their hydrogen rich envelope (become a WR) and retain enough angular momentum in their core during the pre-supernova stages. The strong mass loss discussed in the previous section make it possible for single massive stars in the first stellar generations to become WR stars and even to retain enough angular momentum to produce a GRB (Hirschi 2007). A wider grid of models at metallicities around solar shows that the rate of fast rotating WO stars is compatible with the rate of GRBs with an upper limit around the LMC metallicity, in agreement with observations (Hirschi et al. 2005). More recent models including the effects of magnetic fields (Yoon & Langer 2005) show that another mechanism is possible to produce GRBs at

low Z. This mechanism is the quasi-chemical evolution of very fast rotating massive stars. In this scenario, WR stars are produced by mixing and not mass loss. This last scenario however does not predict GRB at metallicities equal or higher than the SMC. This upper limit is too low compared to recent observations (Fruchter et al. 2006). Taking into account the anisotropy in the wind of these fast rotating stars (Meynet & Maeder 2007) may help reduce the discrepancy between models and observations. Note that the downward revision of solar metallicity (Asplund et al. 2005) may help resolve the problem.

Apart from GRBs, pair-creation supernovae (PCSNe) are very energetic explosions, which could be observed up to very high redshifts (Scannapieco et al. 2005). PCSNe are expected to follow the death of stars in the mass range between 100 and 250 $M_{\odot}$, assuming that they do not lose a significant fraction of their mass during the pre-supernova stages. Amongst the very first stars formed in the Universe, one expects to have PCSN due to the lack of mass loss and to the low opacity unable to stop the accretion on the star during its formation. However, the EMP stars observed in the halo of the galaxy do not show the peculiar chemical signature of PCSN (strong odd-even effect, see Heger & Woosley 2002). This means that either too few or even no PCSN existed. One possible explanation to avoid the production of very low-Z or metal free PCSNe is the strong mass loss in the cool part of the HR diagram due to the surface enrichment in CNO elements induced by rotational and convective mixing (see previous section) or the star reaching the $\Omega\Gamma$-limit (Ekström & Meynet 2007).

I wish to thank G. Meynet and S. Ekström for their help for this review.

References

Asplund, M., Grevesse, N., & Sauval, A. J. 2005, in ASP Conf. Ser. 336: Cosmic Abundances as Records of Stellar Evolution and Nucleosynthesis, 25

Beers, T. C. & Christlieb, N. 2005, ARA&A, 43, 531

Bouret, J.-C., Lanz, T., & Hillier, D. J. 2005, A&A, 438, 301

Bromm, V. & Loeb, A. 2003, Nature, 425, 812

Ekström, S., Meynet, G., & Maeder, A. 2007, ArXiv e-prints:0709.0202, First Stars III conference proceedings

Ekström, S., Meynet, G., & Maeder, A. 2006, in ASP Conf. Series, Vol. 353, Stellar Evolution at Low Metallicity: Mass Loss, Explosions, Cosmology, ed. H. J. G. L. M. Lamers, N. Langer, T. Nugis, & K. Annuk, 141

Eldridge, J. J. & Vink, J. S. 2006, A&A, 452, 295

Ferrarotti, A. S. & Gail, H.-P. 2006, A&A, 447, 553

Foellmi, C., Moffat, A. F. J., & Guerrero, M. A. 2003a, MNRAS, 338, 360

Foellmi, C., Moffat, A. F. J., & Guerrero, M. A. 2003b, MNRAS, 338, 1025

Frebel, A., Christlieb, N., Norris, J. E., Aoki, W., & Asplund, M. 2006, ApJ, 638, L17

Fruchter, A. S., Levan, A. J., Strolger, L., et al. 2006, Nature, 441, 463

Fullerton, A. W., Massa, D. L., & Prinja, R. K. 2006, ApJ, 637, 1025

Heger, A. & Woosley, S. E. 2002, ApJ, 567, 532

Hirschi, R., Meynet, G., & Maeder, A. 2005, A&A, 443, 581

Hirschi, R. 2005, in IAU Symposium 228, ed. V. Hill, P. François, & F. Primas, 331–332

Hirschi, R. 2007, A&A, 461, 571

Höfner, S. & Andersen, A. C. 2007, A&A, 465, L39

Iwamoto, N., Umeda, H., Tominaga, N., Nomoto, K., & Maeda, K. 2005, Science, 309, 451

Kobulnicky, H. A., Fryer, C. L., & Kiminki, D. C. 2006, astro-ph/0605069, ApJ accepted

Kudritzki, R. P. 2002, ApJ, 577, 389

Kudritzki, R.-P. & Puls, J. 2000, ARA&A, 38, 613

Limongi, M., Chieffi, A., & Bonifacio, P. 2003, ApJ, 594, L123

Maeder, A. 1987, A&A, 178, 159

Maeder, A. & Desjacques, V. 2001, A&A, 372, L9

Marigo, P. 2002, A&A, 387, 507

Meynet, G., Ekström, S., & Maeder, A. 2006, A&A, 447, 623

Meynet, G. & Maeder, A. 2007, A&A, 464, L11

Meynet, G. & Maeder, A. 2005, A&A, 429, 581

Meynet, G., Maeder, A., Schaller, G., Schaerer, D., & Charbonnel, C. 1994, A&AS, 103, 97

Mokiem, M. R., de Koter, A., Vink, J. S., et al. 2007, ArXiv e-prints, 708

Nieuwenhuijzen, H. & de Jager, C. 1990, A&A, 231, 134

Porter, J. M. & Rivinius, T. 2003, PASP, 115, 1153

Scannapieco, E., Madau, P., Woosley, S., Heger, A., & Ferrara, A. 2005, ApJ, 633, 1031

Smith, N. & Owocki, S. P. 2006, ApJ, 645, L45

van Loon, J. T. 2006, in ASP Conf. Ser. 353: Stellar Evolution at Low Metallicity: Mass Loss, Explosions, Cosmology, ed. H. J. G. L. M. Lamers, N. Langer, T. Nugis, & K. Annuk, 211

van Loon, J. Th., Cioni, M.-R. L., Zijlstra, A. A. & Loup, C., A&A, 438, 273

van Loon, J. T. 2000, A&A, 354,125

Vanbeveren, D., Van Bever, J., & Belkus, H. 2007, ApJ, 662, L107

Vink, J. S. & de Koter, A. 2005, A&A, 442, 587

Vink, J. S., de Koter, A., & Lamers, H. J. G. L. M. 2000, A&A, 362, 295

Vink, J. S., de Koter, A., & Lamers, H. J. G. L. M. 2001, A&A, 369, 574

Woosley, S. E. 1993, ApJ, 405, 273

Woosley, S. E. & Bloom, J. S. 2006, ARA&A, 44, 507

Yoon, S.-C. & Langer, N. 2005, A&A, 443, 643

Townsend: Just a couple of comments: I am skeptical that 1D models for rotating stars can give correct values for the mass loss when a star reaches critical rotation. I am likewise skeptical of the ability of the bi-stability mechanism to lead to a thin equatorial disk. Photons are lazy, and will tend to avoid driving the disk.

Vink: Just a comment regarding Richard's "lazy photons" and the bi-stability effect. One should realize that the mass loss rate is set close to the photosphere. Bi-stability may well increase the mass flux from the equator, in e.g. B(e) supergiants. But one would still need to understand the dynamics in the outer disk wind.

Puls: The increase of $\dot{M}$ because of the bi-stability effect is due to the larger number of lines in Fe III compared to Fe IV before the bi-stability jump. Predictions from Vink say that the increase in $\dot{M}$ over compensates for the decrease in v_∞. Recent observations and analyses by Markova and myself suggest that $\dot{M}$ increases only by a factor of two, so that the product $\dot{M}v_\infty$ remains conserved over the jump. One "philosophical" comment: even for zero metallicty, the mass loss rate is not zero because of driving by H/He lines (even at hotter $T_{\rm eff}$).

Smith: When you are comparing the observed WR/O ratio to model predictions, whether or not the luminous WN stars are included is important, because there may actually be core H burning stars and should probably be counted with O stars rather than with WR stars. That would lower the observed WR/O ratio, more in line with even lower mass loss rates.

Hirschi: The WN stars are included in the WR group in both models and observations, so for the comparison of the WR/O ratio, this is not biased.

Hamann: I wonder what really happens when a star reaches critical rotation. Matter is then at Keplerian velocity, but still bound to the system. How it can be accelerated to escape?

Hirschi: An decretion disk would form and viscosity could transport angular momentum and a fraction of the matter outside. The rest of the matter could fall back on the star. Work on decretion disks is done by A. T. Okazaki and collaborators.

Spectroscopy and mass loss diagnostic: observations

Chairs: A. Pollock, D. Cohen

Clumping in Hot Star Winds
W.-R. Hamann, A. Feldmeier & L.M. Oskinova, eds.
Potsdam: Univ.-Verl., 2008
URN: http://nbn-resolving.de/urn:nbn:de:kobv:517-opus-13981

Observational overview of clumping in hot stellar winds

Anthony F.J. Moffat
Université de Montréal, Canada

In the old days (pre ∼1990) hot stellar winds were assumed to be smooth, which made life fairly easy and bothered no one. Then after suspicious behaviour had been revealed, e.g. stochastic temporal variability in broadband polarimetry of single hot stars, it took the emerging CCD technology developed in the preceding decades (∼1970-80's) to reveal that these winds were far from smooth. It was mainly high-S/N, time-dependent spectroscopy of strong optical recombination emission lines in WR, and also a few OB and other stars with strong hot winds, that indicated all hot stellar winds likely to be pervaded by thousands of multiscale (compressible supersonic turbulent?) structures, whose driver is probably some kind of radiative instability. Quantitative estimates of clumping-independent mass-loss rates came from various fronts, mainly dependent directly on density (e.g. electron-scattering wings of emission lines, UV spectroscopy of weak resonance lines, and binary-star properties including orbital-period changes, electron-scattering, and X-ray fluxes from colliding winds) rather than the more common, easier-to-obtain but clumping-dependent density-squared diagnostics (e.g. free-free emission in the IR/radio and recombination lines, of which the favourite has always been Hα). Many big questions still remain, such as: What do the clumps really look like? Do clumping properties change as one recedes from the mother star? Is clumping universal? Does the relative clumping correction depend on $\dot{M}$ itself?

1 Preamble

Between 1978 and 1995 when it was active, the International UV Explorer satellite (IUE) made great strides in the area of hot-star winds, leading to the discovery, mostly in strong resonant lines, of large-scale wind structures. These were referred to as discrete absorption components (DACs), seen mainly in the absorbing column between the observer and the projected disk of the star. Their variation with time (more or less periodically) is commonly believed to be due to large-scale corotating interactive regions (CIR), as seen in the Solar wind. In hot-star winds, CIRs are probably produced by some kind of rotating inhomogeneity at the surface of the star: non-radial pulsations or local magnetic loops come to mind, which then perturb the rotating wind (e.g. Cranmer & Owocki 1996). It is possible that all hot-star winds contain CIRs, but this remains to be proven (e.g. difficult in WR stars?).

But what we now normally refer to as clumping in hot-star winds is something that appears to be much more widespread and pervasive in all hot-star winds than DACs/CIRs. While many different phenomena pointed towards the presence of some kind of granulation in the winds, it took high-S/N, moderately-high time-resolved spectroscopy as the final clue to say that virtually all parts of all hot-star winds are stochastically inhomogeneous on various (mainly small) scales. This was first revealed in time-resolved optical spectra of WR stars, where their strong, broad emission lines probe the whole wind simultaneously, not just the column along the line-of-sight. It was also in the optical where mostly recombination lines are seen and where it is relatively easy to obtain very high S/N with CCD detectors, unlike the photon-counting systems used in the UV from space.

2 Indirect evidence for clumping

One of the first indications that hot-star winds are not smooth arose from a study of the light-curve eclipses of the Rosetta Stone among WR + O binaries, V444 Cygni by Cherepashchuk et al. (1984). While the primary eclipse (WR in front) shape changes little in passing from optical to near-IR wavelengths, the secondary minimum (O star blocking the WR star) becomes significantly deeper and wider in the IR. This can only occur if most of the IR emission comes from density-squared dependent free-free emission processes in the bright WR wind which must be clumpy, compared to linear density-dependent electron scattering in the optical. If the WR wind were smooth, this would not make a difference. However, one sees a big difference, although the actual nature of the clumpy wind-structure could

not be deduced from these data alone. Nevertheless, the clumping must be something that pervades most of the wind where IR-dominated f-f emission originates.

Another phenomenon that had been noticed for some time is electron-scattering wings seen to the red of strong WR emission lines. This is also a contributing factor making WR-star emission-line radial velocities (RVs) more positive than systemic. A clear recent case is WR111, a bright, single Galactic WC5 star, with high-quality available optical and UV spectra, for which Hillier & Miller (1999) deduce a wind filling-factor of f = 0.1 (1 = non-clumped). Assuming the observed lines to be optically thin, this leads to the need for revision of the mass-loss rate down by a factor $1/f^{0.5} \approx 3$. However, this phenomenon yields no obvious constraint on the nature of the clumps (e.g. shells could produce the same effect as stochastic clumps).

In the X-ray domain several clues have arisen, athough the lack so far of detected stochastic variability in X-ray flux from any single hot star (e.g. Berghöfer & Schmitt 1995) might be considered as evidence for absence of clumping. However in fact, the apparently general lack of stochastic X-ray variability is likely to be quite compatible with small-scale multi-clumping, given the limited sizes of X-ray telescopes combined with the relatively low X-ray fluxes, that make detection of the expected <1% variability difficult. On the other hand, massive X-ray binaries (MXRB) containing OB stars sometimes exhibit slow X-ray flickering on timescales of 10's of minutes. A good example of this is the out-of-eclipse X-ray lightcurve of 2U1700-37 = HD153919, O6Iaf + NS, P = 3.41d (Haberl et al. 1989). The apparently random flickering could very well be due to rarer large clumps being accreted onto the NS or its accretion disk, although this has never been analyzed in this vein. Perhaps the X-ray flaring of eta Car could also de due to similar circumstances (Corcoran & Moffat, in prep.). More recently, X-ray spectroscopy has revealed that OB-star winds must have reduced mass-loss rates (although not necessarily porous) in order to account for the line shapes (Owocki & Cohen 2006).

As for photometric and polarimetric variability, the former is less obvious to relate to inhomogeneous winds, since other factors can be at play, such as pulsations, rotation modulation, etc. However, in (linear, where electron scattering is key) polarization, localized inhomogeneities can more easily account for the observed variability, even if it does occur at a very small level. The best examples are for WR stars, which have been extensively and systematically monitored in linear polarization (e.g. Drissen et al. 1987; St-Louis et al. 1987), although some single hot stars of other types have also revealed stochastic variability (e.g. P Cyg: Taylor et al. 1991). At two extremes are the WR stars WR111, WC5, which did not vary during 6 weeks in linear polarization significantly more than the instrumental noise, ∼0.01%, and WR40, WN8, which showed stochastic variations in Stokes' Q and U up to ∼1%. The latter is as large as the strictly periodic variability seen in the strongest-modulated, short-period WR + O binaries, where the free electrons that do the polarizing are mostly associated with the WR wind as a whole, rather than in large clumps. However, it is known that WN8 stars are also the most highly intrinsically *photometric* variables (up to ∼10%) among all WR stars, possibly due in large part to stellar pulsations affecting the winds (Lefèvre et al. 2005).

From the coherent polarimetric variability of WR + O systems, one can also derive mass-loss rates, independent of wind clumping (St-Louis et al. 1988). Along with mass-loss rates based on electron-scattering wings, these were among the first observations to suggest that previous density-squared based $\dot{M}$'s were overestimated by factors of 2-5. The best example of this is V444 Cyg, where $\dot{M}(WR)/(10^{-5} M_{\odot}/yr)$ is 2 or more from thermal radio and IR lines, and 0.7 from polarimetry (from two independent ways: orbital modulation and eclipses) and dynamical period change. I.e. we see the same factor ∼3 here as for the electron-scattering wings in WR111.

However, all of these observations can only be related indirectly to clumping. We now look at more direct lines of evidence.

3 Direct evidence for clumping

Ideally, one would like to actually have enough spatial resolution to image wind clumps directly. To resolve clumps of typical size ≈1 $R_{\odot}$ at a distance of close O stars (∼ 1000 pc) would require microarcsec resolution. However, as clumps expand with the wind flow, they will be much larger if they survive into the outer wind. It is tempting to associate the stochastic structures seen in some WR ring nebulae as due to wind clumps. The best example of this is M1-67 around WR124 (WN8h) (Grosdidier et al. 1998), where the "young" WR wind is just starting to ram into the slow wind of the previous LBV (or possibly RSG) stage. However, one can probably not distinguish between new clumps from the interaction and those left from the expanding wind, although the numerous as-yet unexplained small (∼1") expanding Hα-emitting knots are quite intriguing in the context of wind clumping.

Perhaps the chances are better in resolved thermal radio images of hot-star winds. The best example of this is probably WR147, a WN8 star (accompanied by a 0.6" separated OB companion and a NT wind-wind interaction region between the 2 stars) whose thermal wind has been resolved by the Merlin array (Williams et al. 1997). In this image, one does see

knots of several degrees across (as seen from the central star), as expected if the largest clumps survived out this far, i.e. ∼4000 stellar radii. This is only slightly larger than in the simulations of Runacres & Owocki (2002).

Possibly the most convincing evidence for clumpy structures in hot-star winds comes from time-resolved spectroscopic monitoring of WR emission lines (Schumann & Seggewiss 1975 - although in a binary, where the interpretation could be ambiguous; Moffat et al. 1988; McCandliss et al. 1988; Robert 1992). These now well-known spectral series show clear stochastic subpeaks of various sizes moving in a direction from line centre to line edge, interpreted as wind clumps whose projected velocities we see as they propagate with the outflow. Although the stars are not resolved, one reaches effectively a poor-man's resolution with the aid of Doppler expansion of the wind, which cannot unambiguously locate the structures other than in a ring of constant angle from the central star. Nevertheless, **this was the first time that it became clear that small-scale wind-structures are essentially universal at least in the strong winds of WR stars.**

4 Clump characteristics

Early analysis of the 9 WR stars for which adequate series of spectral time-series were available used gaussian fits and wavelet analysis of the spectral subpeaks, assuming each to be associated with a clump. General salient properties of the substructures can be summarized as follows (Moffat & Robert 1992, 1994; Moffat et al. 1994):

- ∼10 subpeaks are seen at any given time, on average
- relative line variability is typically a few percent
- the width of the subpeak features is FWHM ∼2-5 Å (100 - 300 km/s)
- they are seen at all times and last typically ∼10 hours
- within the errors, they always move away from line centre
- they are much narrower near line centre
- lines of lower ionization potential tend to be more variable
- the level of variability tends to follow the same wavelength-dependent profile as the emission-line itself, but P Cyg absorption edges tend to be more variable

Assuming most lines to be optically thin, the second-last point above implies that the instabilities tend to grow as they move from the inner to the outer wind, as expected in hydrodynamic simulations at the time of Owocki (1994). The last point suggests that *the wind is the clumps*, i.e. all clumps follow on average the same expansion law and formation profile in the wind.

Using wavelets allowed one to probe down to smaller substructures propagating across the line profiles. It was found that in general, real repeating substructures tend to follow a simple power law relation between substructure flux and substructure width in velocity space: $f \propto \sigma_v^{2.0\pm0.4}$. Non-repeating substructures both in the line and in the neighbouring continuum followed a flatter-slope power law, as expected if due to noise associated with a constant detection limit in substructure height $h = f/\sigma_v$. Furthermore, a less-reliable but feasible relation was found for the substructure lifetimes: $\tau \propto f^{0.8\pm0.2}$.

One of the main signatures of turbulence is the presence of scaling laws among the various structures in a turbulent medium. This is quite evident in the ISM for GMC strucures, which reveal strong evidence for supersonic, compressible turbulence, driven ultimately by fluctuations in the local gravitational field (Henriksen 1991). In that case, one expects typical clump lifetimes of $\tau \sim l/\sigma_v \sim 1/\sqrt{G\rho}$, i.e. the free-fall time in virial equilibrium. Also, for constant gas pressure, $P \sim \rho\sigma_v^2 \sim$ const. ¿From these, it follows that $\rho \propto 1/l$ (i.e. opacity $\rho l =$ const) and $\sigma_v \propto l^{1/2}$. Unfortunately, ρ and l are not directly observable, but one can also use τ and $f \propto \rho^2 l^3$ for an ideal gas, from which follow that $f \propto l \propto \sigma^2$ and $\tau \propto l^{1/2} \propto f^{1/2}$. These are quite close to what is observed in WR winds, as noted in the previous paragraph!

Furthermore, one can also look at the numbers of substructures of different flux level or mass, such that $\mathrm{N}(f)df = N(\mathrm{m})\mathrm{dm}$. From the wavelet analysis of the observed emission-line fluctuations of the WR stars, one finds that $\mathrm{N}(f) \propto f^{\alpha}$, with typical α = -1.9 ±0.2. Then with a clump mass m $\propto \rho l^3 \propto l^2 \propto f^2$ one finds $N(\mathrm{m}) \propto \mathrm{m}^{\gamma}$, where $\gamma = (\alpha - 1)2 = -1.5 \pm 0.1$, like in GMCs on average (Stutzki 1994)!

The similarity of these scaling laws for the clumps to what one sees in GMCs leads one to believe that the clumpy structure of hot-star winds is also a result of full-scale anisotropic turbulence, with scaling laws like those seen in the fractalized ISM. The only real difference is that in the winds, the driver is radiative instabilities, while in the ISM it is small-scale fluctuating gravity. As R.N. Henriksen always used to remind me (see also Henriksen 1994), **"In astrophysical turbulent media, it often doesn't matter what the physics is - the result is always about the same!"**. Indeed, the presence of scaling laws in a medium is a good signature of turbulence, with lots

of structure and subscale elements, both nested and not nested in superscale elements (Henriksen 1991).

Later, Sébastien Lépine (1998) in his PhD thesis re-analyzed the same repeated spectra for the 9 WR stars using Mexican-hat wavelets that Carmelle Robert analyzed using gaussians in her thesis (Robert 1992). From this new work (Lépine & Moffat 1999, with even more intense data for the single WC8 star WR135: Lépine et al. 2000), it became clear that the individual subpeaks seen moving across spectral emission lines are not due to individual clumps. This may not matter regarding the above results based on the opposite assumption, given the nested nature of turbulence! Nevertheless, the newer work represents a fresh, more rigorous look at the problem.

In particular, Lépine & Moffat (1999) found from their mean wavelet power-spectral analysis that the dominant scale occurs at mean line-of-sight velocities of ∼100 km/s for all 9 analyzed WR stars, except WR134 with ∼350 km/s, due to a velocity component from rotating CIRs in that case. In their analysis, Lépine & Moffat made line-profile variation (LPV) simulations assuming a β-expansion law for the wind occupied by a large number of discrete wind-emission elements (DWEEs), whose fluxes obeyed a power-law distribution within the line-emitting region (LER). In all cases, at least 10^4 DWEEs were needed to simulate the observed LPVs in each WR star, assuming that there are no other components besides DWEEs in the wind. Interestingly, the number of simulated spectral subpeaks was ∼10 on average, but varying with the actual line width, as the actual data show. By varying the anisotropy of the simulated emitting DWEEs in the ratio of radial to lateral emission and velocity dispersion, they found that the simulations which best matched the observations were with isotropic emission but larger radial than transverse velocity dispersion by a factor 4. This latter value is actually probably much higher, as a result of projection effects, as shown by Dessart & Owocki (2002). This means that the velocity dispersion occurs mostly in the radial direction, where in fact the bulk of the radiative force (and instabilities associated with it) occur.

Lépine & Moffat (1999) also devised what they called a "degradation function", used to correlate the ensemble of varying patterns in successive spectra in a statistical way. From this, they deduced that the (assumed constant) wind acceleration for any given line in any given WR star lies in the range 4-25 m/s^2, with the largest value for WR134, with its unusually broad CIRs. With these adopted acceleration values for each star, they then found from when the pattern correlation completely broke down, that the DWEE lifetimes are the same order as the propagation time through the LERs, i.e. typically 6-10 hours. Unfortunately, they could not constrain the wind accleration β parameter by itself; they could only constrain the product β R$_*$ to lie in the range 20-80 R$_\odot$. These values have been reduced by the patch-method simulations of Dessart & Owocki (2005) by a factor 2-3. Nevertheless, they still remain large enough to say that the β values where most WR lines are formed are >>1, i.e. much softer winds than in O stars. An exception to this is found in the Of-like WN3ha star WR3 (see Chené et al., these proceedings).

5 Not only classical WR-star winds are clumped!

Although the easiest, most obvious results have emerged for "classical" WR stars because of their intense, broad emission lines, it is now clear that virtually all hot-star winds likely show similar effects. One obvious general target to investigate was the WC-type central stars of planetary nebulae. Not many of these (they are faint!) have been observed sufficiently yet, but those that have, tend to show almost identical effects as do the clumps in population I WR stars, except that the timescales are much shorter in the CSPN [WC] stars, because their radii are smaller. The best current example is the [WC8] star NGC 40 (Grosdidier et al. 2001).

Among pop I O stars, only Of stars have strong enough winds to allow probing fine structures on their optical emission lines, where it is still easiest to obtain the highest S/N time-resolved spectra. This was demonstrated for the first time by Eversberg et al. (1998) for the bright (both apparently and intrinsically!) O4I(n)f star ζ Puppis. Although its optical emission lines (the strongest being at HeII 4686 and Hα) are an order of magnitude weaker than those of typical WR stars, with spectra of S/N > 1000 Eversberg et al. showed that its wind behaves almost identically with respect to LPV as any WR star. In fact, the relative stochastic LPV due to clumping is the same, i.e. several %, implying (for optically thin lines) that the overdensities in typical clumps in ζ Pup's wind are similar to those in the winds of WR stars. Another satisfying result of the Eversberg et al. study is that ζ Pup shows a normal wind-acceleration value (β ∼1) from the clump trajectories, as expected for OB stars.

In the meantime, Lépine & Moffat (in prep.) have observed ζ Pup again, along with another Of star (HD 93129A in the Tr14 cluster of the Carina Nebula), as well as the 2 WN6ha (Of-like) WR stars in the same Carina Nebula, WR24 and WR25. Again, the same general trend prevails as in the first monitoring of ζ Pup by Eversberg et al., suggesting that indeed clumping appears to be universal.

Other types of hot-star winds in which clumps have been seen recently include novae (Lépine et al. 1999) and supernovae (Matheson et al. 2000).

6 Importance of hot-star wind-clumping

The most important results relating to clumping (in the small-scale sense) in hot-star winds can probably be summarized as follows:

- The presence of clumping and its characteristics is universal in all hot-star winds.
- The root cause is likely connected to turbulence driven by radiative instabilities in the radial direction of the wind flow.
- Hot-star winds provide a unique astrophysical laboratory to study (anisotropic) supersonic compressible turbulence in action on tractable time scales.
- True mass-loss rates are a factor 2-5 (3 on average) lower than those based on Hα and thermal radio fluxes assuming smooth flows.
- Lower mass-loss rates have a significant impact on stellar evolution, e.g. decreasing the initial masses based on observed masses and increasing the importance of luminous blue variables (LBVs)to allow O stars to evolve into WR stars, since the winds of O stars can no longer be considered strong enough to do it by themselves.
- One should be able to empirically trace and tie down the wind expansion velocity-law using clumps in lines of various ionization/excitation potential.
- Clumps will soften collisions both between winds in hot-star binaries (where observed X-ray fluxes are low by orders of magnitude cf. those expected based on flow rates) and by interaction with the ISM.
- In binaries, the presence of clump overdensities will better allow one to understand how dust forms in the winds of some WC + O binaries, and possible even in some single WC stars; clumps also widen secondary eclipses and can cause X-ray flickering in MXRBs.
- Hot-star wind clumps could conceivably contribute to the clumpiness of the ISM.

7 Future needs

In order to advance our understanding of hot-star wind clumping, the most pressing needs in my view are:

- One needs ultimately to spatially resolve the clumps, starting where it may be easiest, i.e. for nearby objects in the radio, where large arrays are beginning to provide sufficient resolution combined with sensitivity.
- One also needs to carry out full (M?)H-D in 3D, given that turbulence is basically a 3D phenomenon.

References

Berghöfer, T.W. & Schmitt, J.H.M.M. 1995, AdSpR, 16, 163

Cherepashchuk, A.M., Khaliullin, K.F., Eaton, J.A. 1984, ApJ, 281, 774

Cranmer, S.R. & Owocki, S.P. 1996, ApJ, 462, 469

Drissen, L., et al. 1987, ApJ, 322, 888

Dessart, L. & Owocki, S.P. 2002, A&A, 393, 991

Dessart, L. & Owocki, S.P. 2005, A&A, 432, 281

Eversberg, T., Lépine, S. & Moffat, A.F.J. 1998, ApJ, 494, 799

Grosdidier, Y., et al. 1998, ApJ, 506, L127

Grosdidier, Y., Acker, A., Moffat, A.F.J. 2001, A&A, 370, 513

Haberl, F., White, N.E., Kallman, T.R. 1989, ApJ, 343, 409

Henriksen, R.N. 1991, ApJ, 377, 500

Henriksen, R.N. 1994, Ap&SS, 221, 137

Hillier, D.J. & Miller, D.L. 1999, ApJ, 519, 354

Lefèvre, L., et al. 2005, 634, L109

Lépine, S. 1998, PhD Thesis, Université de Montréal

Lépine, S. & Moffat, A.F.J. 1999, ApJ, 514, 909

Lépine, S., et al. 1999, ApJ, 522, L121

Lépine, S., et al. 2000, ApJ, 120, 3201

Matheson, T., et al. 2000, AJ, 120, 1499

McCandliss, S.R. 1988, PhD Thesis, Colorado Univ., Boulder

Moffat, A.F.J., et al. 1988, ApJ, 334, 1038

Moffat, A.F.J. & Robert, C. 1992, ASPC, 22, 203

Moffat, A.F.J. & Robert, C. 1994, ApJ, 421, 313

Moffat, A.F.J. 1994, Rev. Mod. Astronomy, 7, 51

Moffat, A.F.J., et al. 1994, ApSpSc, 216, 55

Owocki, S.P. 1994, ApSpSc, 221, 3

Owocki, S.P. & Cohen, D. 2006, ApJ, 648, 565

Robert, C. 1992, PhD Thesis, Université de Montréal

Runacres, M.C. & Owocki, S.P. 2002, A&A, 381, 1015

Schumann, J.D. & Seggewiss, W. 1975, IAUS, 67, 299

St-Louis, N., et al. 1987, ApJ, 322, 870

St-Louis, N., et al. 1988, ApJ, 330, 286

Stutzki, J. 1994, Rev. Mod. Astron., 6, 209

Taylor, M., et al. 1991, AJ, 102, 1197

Williams, P.M., et al. 1997, MNRAS, 289, 10

Feldmeier: How can you derive 10^4 clouds from only 100 spectral features seen? I guess you make the difference between model and observations ever smaller by increasing the cloud number. But what prevents you from going to infinity with the number of clouds in order to make this error go to zero?

Moffat: Actually one sees typically ~ 10 (not 100) spectral sub-peaks at any given time in WR spectral lines. Some $> 10^4$ DWEES are deduced in the context ot the simple Lépine et al. (1999) model to give the best match to what we actually see varying in the spectra. In reality, probably the number of large clumps, which dominate, will be considerably below 10^4.

Prinja: I think an important constraint will ultimately come from an understanding of how small-scale structure (clumping) coexists with large-scale spatial structure (such as diagnosed via DACs). Whilst the two forms of structure are known to co-exist in OB stars, do you think the extensive clumping in WR stars may obliterate extended coherent structures in WR stars?

Moffat: No, the two are sometimes seen together, depending mainly on the quality of the data. In the case of WR stars, WR 134 in the Galaxy is a good example.

Cassinelli: You showed a slide in which there were large scatter on the polarization Q, U plane. This would mean there is a relatively small number of clumps and each is fairly massive. Have you tried to estimate clump masses from this?

Moffat: The time-sampling I showed ($\sim$ a day) is inadequate to say that one has a small number of clumps. In any case, spectra show typically only ~ 10 bumps, although one suspects $> 10^4$ substructures that overlap and combine to give a small number of apparent features.

Vink: Regarding Joe's comment: large polarization variations must be due to a few large clumps. But I will show tomorrow that there are two regimes, and recent polarization monitoring of LBVs favours the scenario of many small clumps.

Hillier: There does appear to be evidence that the volume filling factor you determine depends on v_∞. In particular, in LBVs (AG Car, P Cygni) the measured volume filling factors are clearly larger than the canonical value of 0.1 (e.g. 0.2 to 0.4) and thus different from many O and WR stars (which have higher terminal velocities). These values are determined from the strength of the electron-scattering wings, which are readily seen and measured. Such a scaling might be consistent with that expected from radiation driven instabilities.

Owocki: You emphasized a similarity between wind turbulence with that in the ISM. But I think that a key difference is that ISM turbulence is likely to be (statistically) isotropic, whereas your (and collaborators) observations show quite clearly that wind turbulence has a stronger velocity dispersion in the radial than lateral directions. The hydrodynamic simulations by Luc Dessart and myself are able to match the observed profile variations, including the variation of turbulent speed across the profile, without any fine tuning, except to choose a lateral scale size of about 3 degrees.

Clumping in Hot Star Winds
W.-R. Hamann, A. Feldmeier & L.M. Oskinova, eds.
Potsdam: Univ.-Verl., 2008
URN: http://nbn-resolving.de/urn:nbn:de:kobv:517-opus-13981

Revised mass-loss rates for O stars from the P v resonance line

A. W. Fullerton[1], D. L. Massa[2] & R. K. Prinja[3]
[1] *Space Telescope Science Institute, USA*
[2] *SGT, Inc., NASA Goddard Space Flight Center, USA*
[3] *University College London, England*

The P v $\lambda\lambda$1118, 1128 resonance doublet is an extraordinarily useful diagnostic of O-star winds, because it bypasses the traditional problems associated with determining mass-loss rates from UV resonance lines. We discuss critically the assumptions and uncertainties involved with using P v to diagnose mass-loss rates, and conclude that the large discrepancies between mass-loss rates determined from P v and the rates determined from "density squared" emission processes pose a significant challenge to the "standard model" of hot-star winds. The disparate measurements can be reconciled if the winds of O-type stars are strongly clumped on small spatial scales, which in turn implies that mass-loss rates based on Hα or radio emission are too large by up to an order of magnitude.

1 Diagnostics of mass loss

Wind profiles of the resonance lines of ionized metals are the most sensitive indicators of the outflows from hot, massive stars because they are caused by the scattering of photons by individual particles. However, resonance lines cannot generally be used for quantitative measurements of the mass flux, because the strength of the absorption trough of a P Cygni profile only determines $\dot{M}q$, where $\dot{M}$ is the mass-loss rate and q is the ion fraction of the species. Consequently, resonance lines provide direct determinations of $\dot{M}$ only when they are due to the dominant ion of an element (i.e., $q \approx 1$).

Unfortunately, estimating q for any given resonance line is problematical. Of course, ion fractions can be predicted via detailed modelling, e.g., with `CMFGEN` or `FASTWIND`, but the overall reliability of these predictions depends on other, poorly constrained factors and assumptions, e.g., concerning X-rays, line blanketing/blocking, etc.. Ion fractions cannot be determined empirically, since access to resonance lines from consecutive stages of ionization is not generally available in the far-UV and UV regions. Finally, even in cases where a particular ion of an abundant element is expected to be dominant (e.g., C^{3+} in mid- to late-O stars), the resonance line is almost always saturated, so that even in these favorable cases only lower limits to the amount of material in the wind can be estimated. As a result, mass-loss determinations have relied on recombination lines (particularly Hα) or free-free radio emission. In contrast to scattering, these processes require the interaction of two particles; i.e., they are "density squared" ("ρ^2") processes.

However, the P v $\lambda\lambda$1118, 1128 resonance doublet accessible to *FUSE* side-steps the traditional problems associated with metallic resonance lines, essentially because the cosmic abundance of P is so low that the doublet is not saturated even when P^{4+} is the dominant ion. Consider, e.g., that in the Sun the abundance of P is $\sim$0.09% of the abundance of C! As illustrated in the *FUSE* atlases of Galactic and Magellanic OB spectra (Pellerin et al. 2002; Walborn et al. 2002), the doublet is very weak for the earliest O spectral types, exhibits a broad maximum, and then weakens substantially between O9.5 and B0. This behavior is consistent with the ion fraction of P^{4+} achieving a maximum for mid O-type stars. Model atmosphere calculations suggest that P^{4+} is the dominant ion of P in the outer winds of stars with temperature classes between $\sim$O7.5 and O9.7.

2 The P v problem

If $q(P^{4+})\approx1$ for some range of O temperature classes, then measurements of the strength of its P Cygni profile should provide an independent estimate of $\dot{M}$, which can be compared with precise values determined from radio or Hα measurements. Fullerton et al. (2006) performed this comparison for a carefully selected sample of 40 Galactic O stars, all of which have well-determined values of $\dot{M}$ from "ρ^2" diagnostics. Fits to the wind profiles provide reliable estimates of the radial optical depth of a wind, while requiring a minimal number of assumptions beyond those of the "standard model". For a given velocity law (which can be constrained by fitting wind profiles of saturated resonance lines), the optical depths

are directly related to mass-loss rates via:

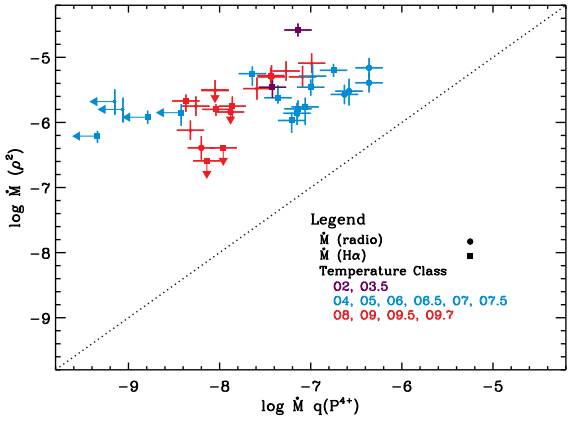

Figure 1: Comparison of $\dot{M}(\rho^2)$ with $\dot{M}q(\mathrm{P}^{4+})$. From Fullerton et al. (2006).

$$\tau_{rad} \propto \dot{M}\, q(\mathrm{P}^{4+})\, A_P \qquad (1)$$

where A_P is the assumed abundance of P relative to H by number.

Figure 1 shows that $\dot{M}q(\mathrm{P}^{4+})$ is typically less than $\dot{M}(\rho^2)$ by a factor of ∼10 for mid-range O stars, and by substantially larger factors for earlier and later spectral types. Contrary to expectations, the two mass-loss indicators *never* agree with each other, even though both are determined precisely.

Of course, we did not expect agreement for all stars in our sample. Since the empirical behavior of the P V doublet suggests that the $q(\mathrm{P}^{4+})$ is largest for mid-range O-stars, we thought that the diagnostics would be within a factor of ∼2 for these objects, and that discrepancies for the earliest and latest spectral types would be due to the fact that $q(\mathrm{P}^{4+})$ is small. However, for these mid-range stars, the median discrepancy $\dot{M}(\rho^2)/\dot{M}q(\mathrm{P}^{4+}) = 20$. If "standard" model atmospheres correctly predict the range of spectral types where (P^{4+}) is the dominant ion, the median discrepancy is a factor of ∼130. This discrepancy is the "P V problem".

3 Re-examining assumptions

Since the implications of this discrepancy are significant, a critical assessment of the assumptions associated with the measurements of the P V resonance line is in order. Eq. (1) shows that there are three assumptions that affect the interpretation of τ_{rad}: (a) a value of A_P is assumed; (b) it is assumed that $q(\mathrm{P}^{4+}) \approx 1$ for some range of O temperature classes; (c) the structure of the wind is described by the "standard model", which assumes that the wind is spherically symmetric, homogeneous, and stationary with a monotonically increasing velocity law.

3.1 The Galactic abundance of P

Fullerton et al. (2006) assumed a solar abundance for P. A smaller abundance would shift points in Fig. 1 to the right and reduce the discrepancy. However, there is no evidence to support a reduction of the magnitude required. On the contrary, analysis of P II lines in the diffuse interstellar medium (e.g., Lebouteiller et al. 2005, and references therein) confirm that the abundance of P is solar along several lines of sight. Since this is the raw material from which O stars form, and since the abundance of P is not altered by nuclear processes over the evolutionary lifetime of a star, there is no reason to suspect that the abundance of P is systematically subsolar. Further support is supplied by the persistence of the "P V problem" for O stars in the Large Magellanic Cloud (Massa et al. 2003); i.e., in an environment with a globally reduced metallicity.

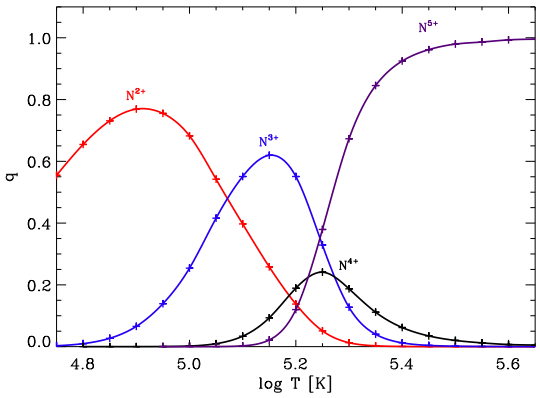

Figure 2: The collisional ionization equilibrium for nitrogen (Sutherland & Dopita 1993).

3.2 Is the maximum value of q(P^{4+})∼1?

By asserting that $\dot{M} \approx \dot{M}q(\mathrm{P}^{4+})$ for *some* range of temperature classes, we are explicitly assuming that the ion fraction of $\mathrm{P}(^{4+})$ peaks near unity. Although Fig. 4 of Fullerton et al. (2006) suggests that the ion fraction goes through a maximum for mid-range O stars, the value of the peak is not known a priori. This is a serious concern, since species with one valence electron like $\mathrm{P}(^{4+})$ typically exhibit maximum ion fractions that are substantially less than 1 in calculations of collisional equilibria. Fig. 2 illustrates this "fragility" in the case of N^{4+} (which is the analog of P^{4+} in the preceding row of the periodic table), by indicating a peak value of $q(\mathrm{N}^{4+}) \sim$ 0.2. The

obvious counter-argument is that the ionization balance in hot-star winds is dominated by photoionization, not collisions; and more relevant models (computed, e.g., with `FASTWIND` or `CMFGEN`) show that $q(\mathrm{P}^{4+})$ does indeed approach unity over much of the wind for stars of the appropriate temperatures; see, e.g., Puls et al. (2006).

The basic problem is that we simply do not know a priori how $q(\mathrm{P}^{4+})$ varies in the winds of O-type stars. Model atmosphere calculations provide valuable guidance, although a variety of issues connected with the ionization equilibrium of stellar winds must be resolved. Despite these uncertainties, there is at present no reason to suspect that the mean ion fraction of P^{4+} is always less than $\sim$0.1 for O stars, as would be required to explain the discrepancy.

3.3 Resolution: Relaxing the assumptions of the standard model

The only remaining assumptions associated with the P V analysis define the "standard model", which forms the basis of the determination of $\dot{M}$ by any of the usual techniques: sphericity, homogeneity, stationarity, and monotonicity. To resolve the "P V problem", at least one of these assumptions must be relaxed. However, relaxing any of them is tantamount to acknowledging that the density structure is inhomogeneous. Thus, the discrepancy between $\dot{M}(\rho^2)$ and $\dot{M}q(\mathrm{P}^{4+})$ signals that the winds of O stars are inhomogeneous, or "clumped".

The spatial scale associated with the clumps is not known: a variety of scales may be involved, since the winds of many O-type stars are structured on large scales (as indicated, e.g., by the presence of discrete absorption components). Optically thin clumps (which have spatial scales that are smaller than the mean free path of a photon) are easily incorporated in stellar atmosphere models, and permit progress to be made despite uncertainties concerning the mechanism(s) responsible for generating structure in the wind (though the line-driven instability is certainly implicated). In the optically thin limit, the discrepancy between $\dot{M}(\rho^2)$ and $\dot{M}q(\mathrm{P}^{4+})$ is resolved by recognizing that ρ^2 diagnostics are inherently biased: in the presence of clumps, they *systematically over-estimate* mass-loss rates if they are modelled with the assumptions of the "standard model". Thus, a fundamental consequence of clumping in hot-star winds is that the values of $\dot{M}(\rho^2)$ *must be reduced*. The only question is: by how much? If the entire discrepancy is assigned to this effect alone, then the mass-loss rates derived from ρ^2 diagnotics are too large by an order of magnitude and the clumped material must occupy a tiny fraction of the volume of the wind.

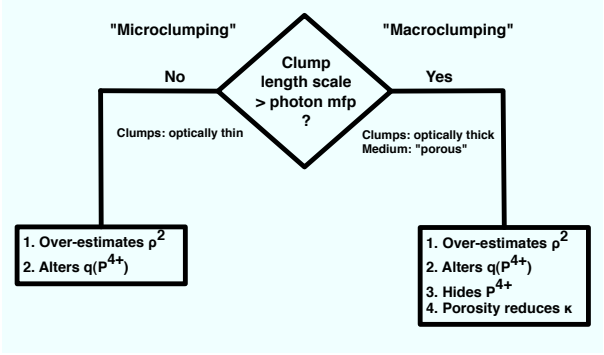

Figure 3: A schematic representation of the effects of clumping.

However, other competing factors might come into play, since density enhancements also change the ionization structure of the wind, particularly $q(\mathrm{P}^{4+})$. Furthermore, as noted by Oskinova et al. (2007), clumps may be optically thin for one diagnostic but not another; i.e., the effects of clumping are not the same for all mass-loss diagnostics. Radiative transfer through a medium in which optically thick clumps are embedded (i.e, a "porous" medium) is quite different from the case of a medium comprised of optically thin clumps. As discussed by Hamann, Townsend, Feldmeier, Oskinova, & Owocki at this workshop, porosity leads to a variety of ways of reinterpreting the observed optical depth of a resonance line. Fig. 3 provides a simplified scheme to characterize these consequences. At present it is not clear whether one of these effects dominates, or whether several of them are required to resolve the mass-loss discrepancy. Regardless, the fundamental conclusion remains: *O-star winds are clumpy.*

References

Fullerton, A. W., Massa, D. L., & Prinja, R. K. 2006, ApJ, 637, 1025

Lebouteiller, V., Kuassivi, & Ferlet, R. 2005, A&A, 443, 509

Massa, D., Fullerton, A. W., Sonneborn, G., & Hutchings, J. B. 2003, ApJ, 586, 996

Oskinova, L. M., Hamann, W.-R., & Feldmeier, A. 2007, A&A, 476, 1331

Pellerin, A., et al. 2002, ApJS, 143, 159

Puls, J., Markova, N., & Scuderi, S. 2006, preprint arXiv:astro-ph/0607290v1

Sutherland, R. S., & Dopita, M. A. 1993, ApJS, 88, 253

Walborn, N. R., et al. 2002, ApJS, 141, 443

Cohen: Does the P IV resonance line provide any useful information about either abundances or the ionization balance in the wind?

Fullerton: For Galactic O stars, extinction usually prevents any meaningful observations of the far-ultraviolet spectrum below ∼1000 Å. The situation is much more favourable for stars in the Magellanic Clouds. Even there, the P IV λ951 resonance line is badly blended with the interstellar Lyman δ line of H at 949.7 Å and the red component of the S VI doublet. So, it is not immediately obvious how it could be used to constrain the behavior of phosphorous in a wind. Despite the blending, we know P IV is present with some strength because in the two cases where we have long time series observations we can see it vary. It is an unusual situation: the variations about the mean, blended profile are present with large amplitude (larger than in P V), though we cannot even see, let alone measure, the mean profile.

Ignace: By "variable", do you mean the P IV resonance line is different across spectral types?

Fullerton: No; in this case "variable" refers to changes in the profile of the P IV resonance line of a single object. Of course, we would also expect the mean profile to change with spectral type. It is really too bad that we cannot make better use of it.

Cassinelli: You assume that P V is a dominant ion stage even inside a clump. However, as I will discuss later, the clumps have a bow shock surrounding them that produces X-rays. This intense X-ray radiation should greatly increase the ionization state in the clump via the Auger mechanism (say to P VII or P VIII), so P V would not provide a true measure of the optical depth through the wind; i.e. your ion fractions q(P V) are too large, and the mass loss rate is not necessarily reduced.

Fullerton: I think this is an interesting way of changing the ion fraction of P V within a clump. I guess that the change in the global ion fraction will depend on the competing process of recombination, which will be a function of the density and dimensions of the clump. But the upshot could very well be an overall reduction in q(P V) from dominant values, which will reduce the mass loss discrepancy, particularly if clumps represent the bulk of the wind. Of course, the basic conclusion of the analysis – that the discrepant P V-Hα mass loss rates indicate the presence of significant clumping – would remain, but with more modest decreases in the mass loss rates.

Prinja: We should note that an ionization "issue" also extends beyond the O stars and P V to B supergiants and the fact that Si IV never appears to be the dominant ion of silicon in line synthesis analysis, while models (CMFGEN, etc.) predict that it should be.

Fullerton: I think that the ionization balance in hot-star winds needs to be revisited, with particular emphasis on the effect of localized density enhancements.

Clumping in Hot Star Winds
W.-R. Hamann, A. Feldmeier & L.M. Oskinova, eds.
Potsdam: Univ.-Verl., 2008
URN: http://nbn-resolving.de/urn:nbn:de:kobv:517-opus-13981

Independent signs of lower mass-loss rates for O-type stars

Nathan Smith
University of California, Berkeley, USA

I discuss observational evidence – independent of the direct spectral diagnostics of stellar winds themselves – suggesting that mass-loss rates for O stars need to be revised downward by roughly a factor of three or more, in line with recent observed mass-loss rates for clumped winds. These independent constraints include the large observed mass-loss rates in LBV eruptions, the large masses of evolved massive stars like LBVs and WNH stars, WR stars in lower metallicity environments, observed rotation rates of massive stars at different metallicity, supernovae that seem to defy expectations of high mass-loss rates in stellar evolution, and other clues. I pay particular attention to the role of feedback that would result from higher mass-loss rates, driving the star to the Eddington limit too soon, and therefore making higher rates appear highly implausible. Some of these arguments by themselves may have more than one interpretation, but together they paint a consistent picture that steady line-driven winds of O-type stars have lower mass-loss rates and are significantly clumped.

1 Introduction

Before giving a list of observational reasons to favor clumped-wind mass-loss rates, I'll just clarify a few terms. When I mention "standard" or "unclumped" mass-loss rates, I am referring to the mass-loss rates derived primarily from Hα or radio continuum observations with the assumption of homogeneous winds (de Jager et al. 1988; Nieuwenhuijzen & de Jager 1990). When I refer to "lower" or "clumped" mass-loss rates, I am referring to these same mass-loss rates reduced by adopting a clumping factor. I do not refer to theoretical mass-loss predictions, such as those by Vink et al. (2001), which appear to be in line with the moderately-clumped rates.

2 Mass Budget: LBV Eruptions

In the evolution of very massive stars with initial masses above $\sim$60 $M_\odot$, the standard mass-loss rates would have an O star shed most of its initial mass by the end of the main sequence, followed by a WNH or LBV line-driven wind that removes the remaining H envelope to yield a $\lesssim$20 $M_\odot$ WR star. This scenario does not allow room for giant eruptions of LBVs, which can remove something like 10 $M_\odot$ in a few years, and which seem to happen multiple times (see Smith & Owocki 2006). I have discussed these events and their role in stellar evolution ad nauseam, but the main point here is that line-driven winds on the main sequence need to be lower by a factor of a few in order leave enough mass on the star at the end of core-H burning so that they can supply enough ejecta for these outbursts.

3 Mass Budget: High Masses of LBVs and WNH Stars

By the same token, O-star mass-loss rates need to be lower than the standard rates in order to agree with measured masses of stars at the end of core-H burning. An example that I sometimes mention is η Carinae, because it is well studied. We think the primary star in the η Car system has a present-day mass of order 100 $M_\odot$ (it could be higher) if it is not violating the classical Eddington limit, and we think it has reached the end or passed the end of core-H burning because of the observed nitrogen enrichment in its ejecta. It has lost at least 20 $M_\odot$, perhaps 30 $M_\odot$, in violent LBV eruptions in just the past few thousand years (Smith et al. 2003), in addition to its steady wind. That means the star made it to the end of the main sequence with a mass of 120–130 $M_\odot$ still bound to the star. If we believe that the upper limit to the initial mass of stars is about 150 $M_\odot$ (e.g., Figer 2005), then η Car could have lost only about 20-30 $M_\odot$ as an O star and WNH star combined during its first 3 Myr. This could only be the case if O star mass-loss rates are reduced by at least a factor of 3, probably more.

Similar arguments apply to the Pistol star and the luminous WNH stars (see Smith & Conti 2008), with estimated present-day masses as high as 80–120 $M_\odot$ measured in binaries. These stars are at or very near the end of core-H burning, having suffered mass loss from steady line-driven winds as O stars for roughly

3 Myr as well. With the standard mass-loss rates, they could not exist with their present-day masses.

4 Feedback and High Mass-Loss

Another problem is that the higher "standard" mass-loss rates lead to an unphysical predicament – they make the star go berzerk too early. I am referring to a feedback loop introduced by high mass-loss rates (see Smith & Conti 2008). Namely, as mass loss reduces a star's mass and its luminosity simultaneously climbs due to core evolution, the star will creep closer to the Eddington limit. However, as the Eddington factor climbs, CAK theory (Castor et al. 1975) tells us that the mass-loss rate will climb even faster. Eventually the star will exceed the classical Eddington limit; when this happens depends essentially on the initial mass-loss rate.

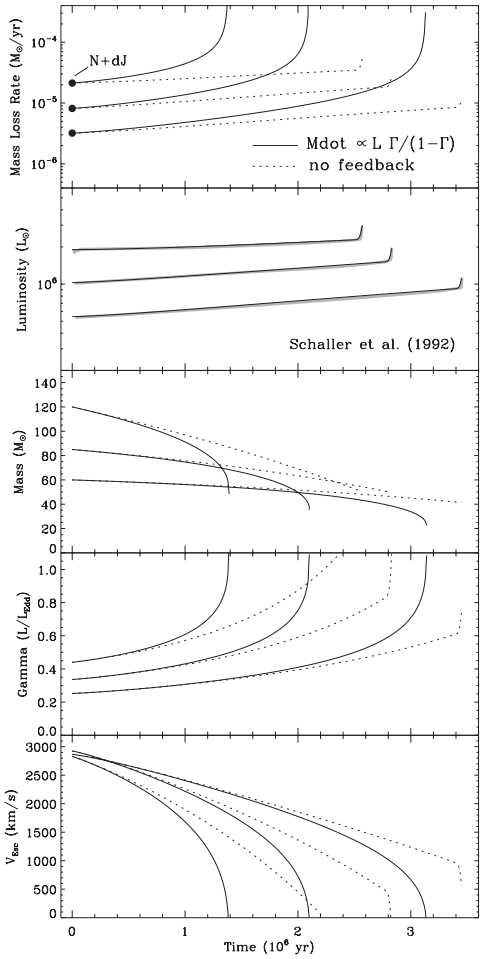

Figure 1: Mass-loss rate evolution adopting standard (NdJ) initial mass-loss rates with feedback (solid) and without (dashed). See Smith & Conti (2008).

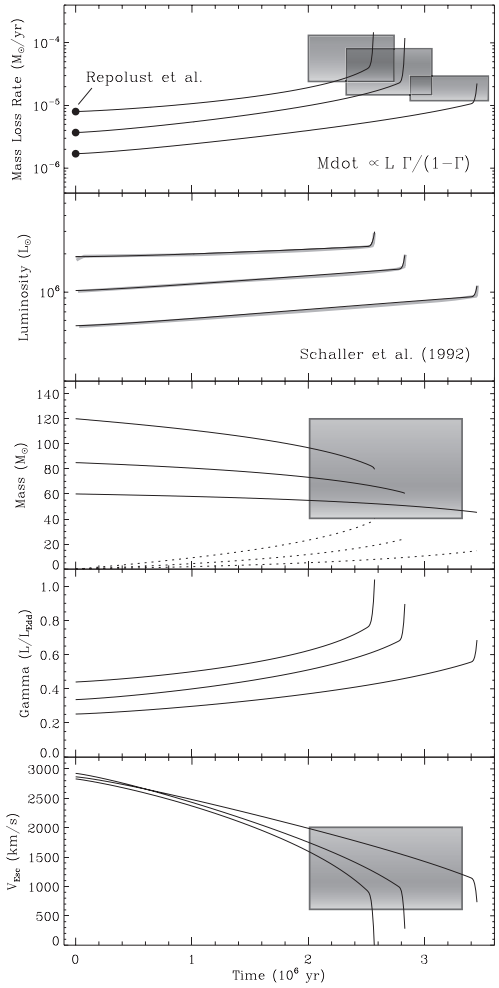

Figure 2: Mass-loss rate evolution adopting moderately-clumped initial mass-loss rates from Repolust et al. (2006) with feedback. Shaded boxes indicate observed range of properties for WNH stars; see Smith & Conti (2008).

Figure 1 shows the mass-loss rate evolution predicted on the main-sequence, taking the standard mass-loss rates as the intial rates. For higher masses and luminosities, the mass-loss rate skyrockets and the star exceeds the classical Eddington limit after only about 1 Myr. This is too early, since almost no massive stars in very young clusters are surrounded by LBV-type shells (η Car is the only one, and its age is thought to be $\sim$3 Myr). Furthermore, the predicted *change* in mass-loss rate with feedback disagrees with the observed trend (dashed in Fig. 1).

By contrast, Figure 2 shows a more sensible mass-loss evolution, starting with initial mass-loss rates for O stars that are reduced by a factor of about 3 (rates from Repolust et al. 2006). These rates, in-

cluding the expected effects of feedback, yield stellar properties near the end of core-H burning that agree with observations of WNH stars. This topic is discussed in more detail by Smith & Conti (2008).

5 Type IIn Supernovae

There exists a population of supernovae that argues against strong mass loss in steady line-driven winds as the dominant mode of mass-loss in massive stars. These are the Type IIn supernovae, named for the "narrow" lines of H in their spectra. There are two reasons they contradict high mass-loss rates.

The first reason is because Type IIn supernovae are thought to mark the deaths of very massive stars – in some cases the *most* massive stars like η Car. Their deaths prove that in some cases, at roughly Solar metallicity, massive stars face death with their H envelopes intact. Second, the Type IIn supernovae show evidence for huge blasts of eruptive mass loss shortly before they exploded. These supernova precursor events are suspiciously similar to giant LBV eruptions (Smith & Owocki 2006), shedding a few to 10s of $M_{\odot}$ of H-rich material in the decade before core collapse. Thus, Type IIn supernovae argue against the conventional wisdom that all massive stars should shed their H envelopes via line-driven winds to form WR stars. See Smith et al. (2007) and Gal-Yam et al. (2007) for more details.

6 GRBs and WR Stars at Low-Z

A prediction of the relatively high "standard" mass-loss rates is that winds will dominate mass loss for massive stars, steadily removing the outer layers of a star through line-driven winds until a He-rich WR star appears. Because these winds are metallicity dependent, it becomes more difficult to make WR stars at low metallicity. This runs counter to the observations that long-duration GRBs (associated with Type Ic supernovae that result from the deaths of WR stars) are found only in low metallicity galaxies, and that WR stars are seen in abundance in some low-Z galaxies, like IC 10 and I Zw 18. The existence of WR stars at low Z is sometimes explained by close binary mass transfer, but this cannot explain all of them. Moffatt et al. (these proceedings) have shown that the binary fractions among WR stars in the SMC, LMC, and Milky Way are not significantly different (i.e., there are single WR stars or WR stars in very wide binaries in the SMC). This suggests that some mechanism other than binary interaction (i.e. continuum-driven LBV eruptions; Smith & Owocki 2006) must be responsible for the envelope removal that leads to WR stars in all three environments, not line-driven winds. One alternative way to explain the existence of WR stars at low Z is that rapid rotation and efficient mixing leads to homogeneous evolution (e.g., Hirschi, these proceedings), but the high initial rotation rates required will only apply to a small fraction of stars.

7 Z-Independent O-Star Rotation

Mass-loss via steady line-driven winds throughout core-H burning as O stars should lead to significant loss of angular momentum if the "standard" mass-loss rates apply. Thus, there should be a clear trend in rotation rate and metallicity among O stars. Penny et al. (2004) have searched for this effect, but find no convincing difference in the rotation period distribution of O stars in the Galaxy, LMC, and SMC. This, in turn, would argue strongly that the mass and angular momentum loss is in fact much lower than given by the standard rates, arguing that winds are indeed clumped. The mass-loss reduction needs to be enough that line-driven winds no longer dominate the mass lost during a star's lifetime.

8 Summary: Factor of 3

For most of the observational clues that mass-loss rates are lower, a reduction by a factor of three seems to suffice. It could be more, but *at least* a factor of three seems to be needed. These clues are important because they are independent of the mass-loss rates and clumping factors derived from the analysis of O-star winds.

References

Castor, J.I., Abbott, D.C., & Klein, R. 1975, ApJ, 195, 157

de Jager, C., et al. 1988, A&AS, 72, 259

Figer, D.F. 2005, Nature, 434, 192

Gal-Yam, A., et al. 2007, ApJ, 656, 372

Nieuwenhuijzen, H., & de Jager, C. 1990, A&A, 231, 134

Penny, L., et al. 2004, ApJ, 617, 1316

Repolust, T. et al. 2006, 415, 349

Smith, N., & Conti, P.S. 2008, ApJ, submitted

Smith, N., & Owocki, S.P. 2006, ApJ, 645, L45

Smith, N., et al. 2003, AJ, 125, 1458

Smith, N., et al. 2007, ApJ, 666, 1116

Vink et al. 2001, A&A, 369, 574

Oskinova: Kinetic energy input into the ISM is higher when the bulk of mass is lost via stellar winds compared with LBV outflows. Can observations of diffuse X-ray emission from (super-)bubbles in massive star clusters discriminate between these two (LBV vs. stellar wind mass loss)?

Smith: Well, to begin with, I would disagree that kinetic energy input to the ISM is dominated by stellar winds. Instead, giant H II regions and superbubbles are inflated by radiation pressure and supernova. By comparison to these effects, the ram pressure of stellar winds is not terribly relevant. Therefore, reducing Hα and radio mass loss rates by factors of two or three or even ten and replacing them with LBV mass loss would not matter.

Zinnecker: Can you explain again how to produce WR stars in low-metallicity dwarf galaxies such as IZw18? And why some of these WR stars would be rapidly rotating (to become progenitors of GRBs)?

Smith: If O star winds are too weak because of the metallicity dependence (and because of clumping), then it seems likely that continuum driven LBV eruptions might be able to shed the remaining mass. Observationally, it seems that LBV mass loss is inherently bipolar, but I really do not know if that is enough of an effect for the star to retain enough angular momentum to make a GRB. However, it is likely that LBV mass loss will shed less angular momentum than the same amount of mass shed in a steady spherical wind.

Massa: Do the numbers of LBVs versus WRs and O stars in the Galaxy agree with your expectations? Can you make up for the reduction in WR production?

Smith: The relative number ratio of LBVs, WRs, and O stars really just tells us the relative lifetimes in each phase, and the variety of LBVs just means that their lifetimes are short, like a few 10^4 years. However, that is not really the crux of the problem, because we know that LBV mass loss is dominated by giant eruptions when the star can shed $\sim 10\,M_\odot$ in a couple years. We know that these eruptions can, in principle, happen repeatedly. So, in principle, yes they can make up the deficit of mass loss left by reduced O star rates. The question that we do not know the answer to with confidence is how much mass is lost each time and how many total eruptions there are as a function of luminosity.

Clumping in Hot Star Winds
W.-R. Hamann, A. Feldmeier & L.M. Oskinova, eds.
Potsdam: Univ.-Verl., 2008
URN: http://nbn-resolving.de/urn:nbn:de:kobv:517-opus-13981

Clumping in O-type Supergiants

J.-C. Bouret[1], T. Lanz[2] , D.J. Hillier[3] & C. Foellmi[4]
[1]*Laboratoire d'Astrophysique de Marseille, France*
[2]*University of Maryland, USA*
[3]*University of Pittsburgh, USA*
[4]*Laboratoire d'Astrophysique de Grenoble, France*

We have analyzed the spectra of seven Galactic O4 supergiants, with the NLTE wind code CMFGEN. For all stars, we have found that clumped wind models match well lines from different species spanning a wavelength range from FUV to optical, and remain consistent with Hα data. We have achieved an excellent match of the P V $\lambda\lambda$1118, 1128 resonance doublet and N IV λ1718, as well as He II λ4686 suggesting that our physical description of clumping is adequate. We find very small volume filling factors and that clumping starts deep in the wind, near the sonic point. The most crucial consequence of our analysis is that the mass loss rates of O stars need to be revised downward significantly, by a factor of 3 and more compared to those obtained from smooth-wind models.

1 Introduction

Massive O-type stars stars are characterized by dense, highly-supersonic mass outflows. These stellar winds have a significant effect on the stars' evolution, as O stars will loose a sizable fraction of their total mass during their lifetime. Mass-loss rates are therefore a crucial parameter of stellar evolution models. Aside from their effect on the ultimate evolution of the stars, the deposition of mechanical energy and momentum have a greatly impact on the circumstellar environment and play a prominent role in the chemical and dynamical evolution of galaxies. Establishing reliable mass-loss rates of O stars is therefore a crucial undertaking which impacts a broad segment of Astrophysics.

The winds of O-type stars are radiatively driven. This process is unstable and, theoretically, should lead to the formation of structures (clumps, shocks) and the emission of X-rays. Observationally, there is growing evidence that O stars have highly structured winds: *i)* Discrete Absorption Components are observed in O-star wind line profiles, and might indicate the propagation of disturbances throughout the wind *ii)* Spectral properties of X-ray line profiles observed with Chandra and XMM-Newton are best explained by considering highly fragmented (or porous) winds, starting close to the photosphere *iii)* NLTE analyses with state-of-the-art atmosphere models require the use of inhomogeneous (clumped) winds to simultaneously fit UV and optical wind line profiles, as well as IR and radio fluxes (e.g. Bouret et al. 2005; Puls et al. 2006). Fullerton et al. (2006) also had to consider highly clumped winds to reconcile $\dot{M}q(P^{+4})$ with mass-loss rates measurent from radio and Hα emission. A consequence of the introduction of clumping is that the inferred mass-loss rates had to be revised downward by a factor 3 or more, compared to those obtained from smooth-wind models, with strong consequences on the predicted evolution of O-type stars.

While these results show that we cannot trust the mass-loss rates derived from homogeneous models, we cannot conclude that the revised values from the clumped wind models can be adopted just yet because of the crude physical description of clumping in current models. It is thus essential to investigate if a consistent picture can be drawn from the different diagnoses of wind clumping, P V $\lambda\lambda$1118-1128, O V λ1371, N IV λ1718, He II λ4686 and Hα, ensuring that these are not spuriously affected by abundance or ionization effects.

We have selected 7 galactic early-type O supergiants (spectral types O4 If+ to O6.5 Iaf) to derive their properties and address these issues. These stars, namely HD 14947, HD 15570, HD 16691, HD 190429A, HD 66811 (ζ Puppis), HD 163758 and HD 210839 (λ Cephei) are considered as "bona fide" as possible objects representative of early-O supergiants, whose strong winds are expected to exhibit most conspicuous signatures of clumping.

2 Observational material

We have extracted IUE short wavelength, large aperture, high resolution spectra from the IUE Newly Extracted Spectra (INES) archive. The SWP spectra cover the spectral range, $\lambda\lambda$1150-2000 Å, at a resolving power $R = 10,000$. The spectra of all stars show a large number of narrow lines of interstellar

(IS) origin. This becomes an issue for HD 15570, for which it dominates the whole UV spectrum.

All stars but ζ Puppis have been observed with the FUSE $30'' \times 30''$ LWRS aperture. The nominal spectral resolution is 20,000 and the wavelength range goes from 905 Å to 1187 Å. The processed FUSE spectra have been retrieved from MAST. For ζ Puppis, we used the COPERNICUS spectra available from MAST.

Northern stars were observed with the ELODIE spectrograph at Observatoire de Haute-Provence, while southern stars were observed with the ESO/FEROS spectrograph at La Silla Observatory. The spectral resolution is R=42,000 and 45,000 (for ELODIE and FEROS, respectively). The wavelength coverage is 3895-6815 Å for ELODIE, 3700-9000 Åfor FEROS. The exposure time were chosen to ensure a signal-to-noise ratio of at least 100 at 5200 Å. Each order was normalized by a polynomial fit to the continuum; the successive orders were then merged to reconstruct the full spectrum for each star.

3 Spectral Modeling

The spectral analysis has been performed using model atmospheres calculated with the unified model code CMFGEN (Hillier & Miller 1998). We use a hydrostatic density structure computed with TLUSTY (Lanz & Hubeny 2003) in the deep layers, and the wind part is described with a standard β-velocity law.The photosphere and the wind are connected below the sonic point at $v(r) \approx 15$ km s^{-1} .

To investigate spectral signatures of clumping in the winds of our sample stars, and its consequences on the derived wind parameters, we have thus constructed clumped wind models with CMFGEN. A simple, parametric treatment of wind clumping is implemented in CMFGEN, which is expressed by a volume filling factor, f, and which assumes a void interclump medium and the clumps to be small compared to the photons mean free path. The filling factor is such that $\bar{\rho} = f\rho$, where $\bar{\rho}$ is the homogeneous (unclumped) wind density. The filling factor decreases exponentially with increasing radius (or, equivalently, with increasing velocity) $f = f_\infty + (1 - f_\infty)\exp(-v/v_{\rm cl})$, where $v_{\rm cl}$ is the velocity at which clumping starts. By default, we have adopted $v_{\rm cl} = 30$ km s^{-1}, that is, clumps start forming just above the sonic point (cf. Bouret et al. 2005) some specific cases, we had to tune $v_{\rm cl}$ to improve the fit to some observed lines, but we kept in within a few tenths of stellar radii above the photosphere (i.e. $v_{\rm cl} \leq 150$ km s^{-1}).

4 Results

Clumping related quantities ($\dot{M}$, $v_{\rm cl}$ and f_∞) have been derived from P V $\lambda\lambda$1118-1128, O V λ1371, N IV λ1718, in the FUV/UV domain. We found that Si IV $\lambda\lambda$1394, 1403 are also sensitive to clumping, especially for the cooler stars of the sample, where Si IV is the dominant ions of Silicium. In the optical, clumping sensitive lines are primarily He II λ4686 and Hα, although all the lines (including photospheric lines) we looked at presented some sensitivity to the adopted filling factor (and scaled $\dot{M}$). For photospheric lines, this is essentially caused by a lower wind contribution (emission) in clumped models, thus producing deeper absorption, compared to smooth-wind models.

We find that only clumped wind models consistently improve the match to lines from FUV to the optical wavelength range. The dramatic improvement of the fits to the lines listed hereabove is presented in Fig. (1) and Fig. (2). The winds of our sample stars are highly clumped, as expressed by very small volume filling factors: $0.01 \leq f_\infty \leq 0.08$. In most cases clumping must starts deep in the wind, just above the sonic point $v_{\rm cl} \approx 30$ km s^{-1}.

For ζ Pup and λ Cep (both being rapid rotators), we had to use $v_{\rm cl} \approx 130$ km s^{-1} to reduce emissivity in the lower wind and improve the fit to the central absorption seen on the Hα profile (Fig. 1).

Lower mass-loss rates are derived from the clumped models, here by a factor of 3 to 10, with respect to those derived form smooth-wind models, which is expected to significantly alter the predicted evolution of O-type stars.

We emphasize that for all but one star, we succeeded in matching the observed profiles of P V $\lambda\lambda$1118-1128 with the reduced solar abundances for Phosphorus from Asplund et al. (2005). This suggests that the very low mass-loss rates we derive do not result from any uncertainty about the exact abundance of this element, and further confirm that the ionization structure of Phosphorus in our models is correct. For HD 190429A, the best fit to the P V FUV resonance doublet is then obtained for $\rm P/P_\odot = 0.7$, further confirming the apparent depletion in phosphorus of this star (see Bouret et al. 2005).

References

Asplund, M., Grevesse, N., Sauval, A. J. 2005, ASPC, 336, 25

Bouret, J.-C., Lanz T., Hillier, D.J. 2005, A&A, 438, 301

Fullerton, A. W., Massa, D. L., Prinja, R. K. 2006, ApJ, 637, 1025

Hillier, D. J. & Miller, D. L. 1998, ApJ, 496, 407

Lanz, T. & Hubeny, I. 2003, ApJS, 164, 417

Puls, J., Markova, N., Scuderi, S., et al. 2006, A&A, 454, 625

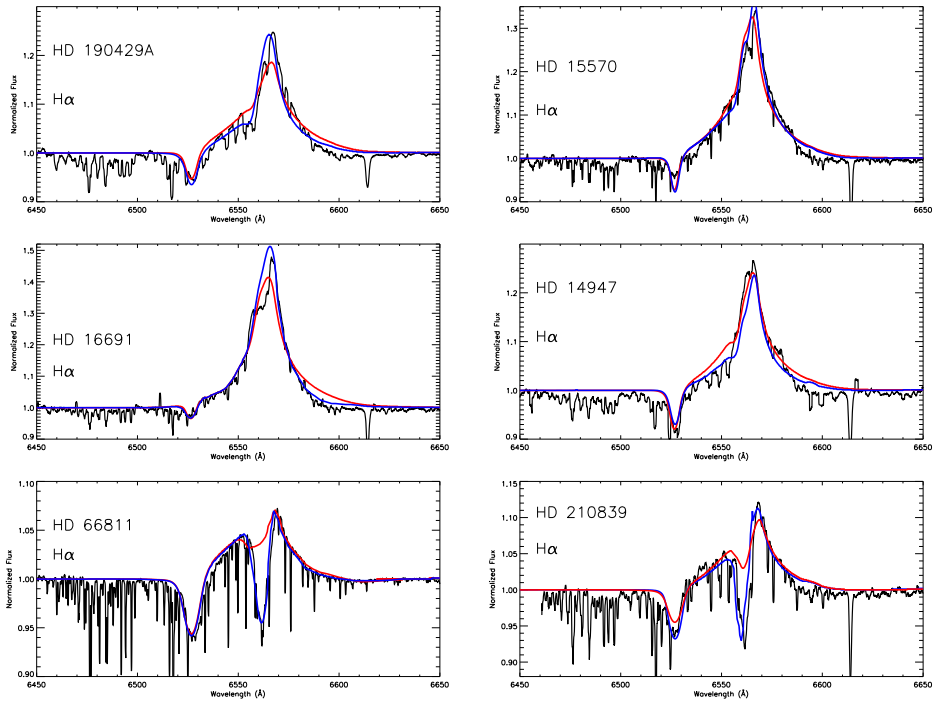

Figure 1: Best fit to observed Hα line profiles (black line) of 6 stars of our sample, obtained with smooth (red line) and clumped (blue line) models

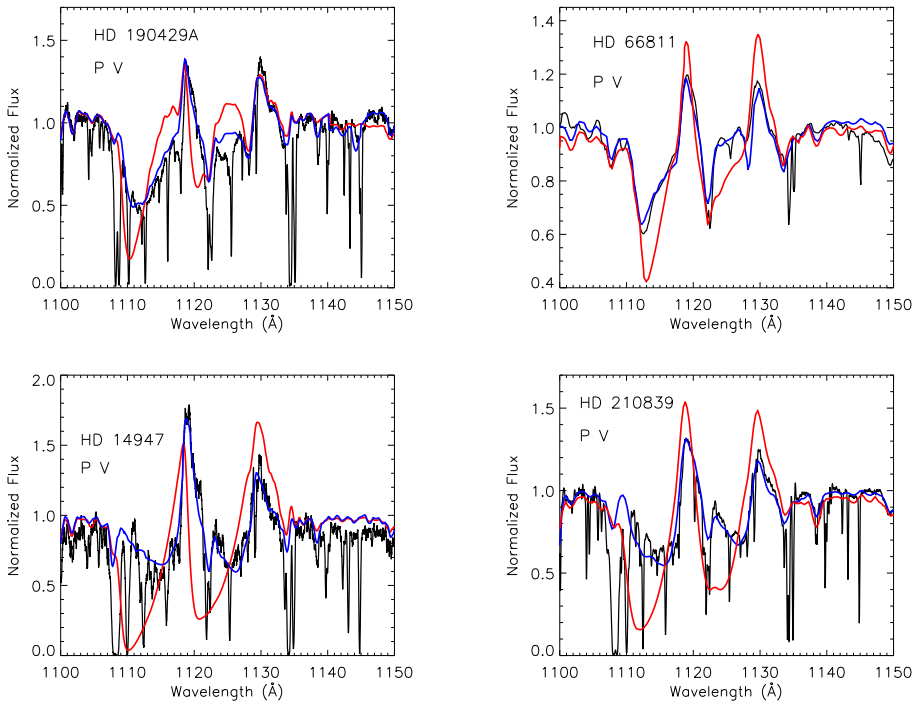

Figure 2: Best fit to observed P V λλ1118, 1128 line profiles (black line) of the four O4 If+ stars of our sample, obtained with smooth (red line) and clumped (blue line) models

Cohen: Please keep an open mind about X-ray profiles: whether they really imply that large scale clumping exists or whether the data simply imply $\dot{M}$ reductions. Can you comment on the relatively high smooth $\dot{M}$ for ζ Pup?

Bouret: Thanks for your comment. Concerning your question, I do not think you can say the smooth $\dot{M}$ is high; it is in any case compatible with values published elsewhere (for instance Puls et al. 2006). $\dot{M}$ depends strongly on the distance adopted for ζ Pup. In the present case, the lower value $d \approx 460$ pc is used.

Moffat: Just because the models seem to fit the observed spectum fairly well does not necessarily mean that the model is correct. It is a necessary condition but not sufficient. So, my question is, how confident are you that your description of clumping and its consequence is correct?

Bouret: True! Nevertheless I would like to stress for instance that our clumped models match the two P V resonance lines very well, providing strong evidence that the wind ionization is correct and that there is no particular issue such as covering factors with our treatment of clumps.

Puls: Just let me mention that He II 4686 in ζ Pup and λ Cep is strongly variable on (rather) short time scales. So it might be not so problematic that you cannot fit one specific observation.

Bouret: Very good point indeed. It is one of the issues of this work that we try to derive parameters from data obtained in some cases about 25 years apart. And short-term variability does not help either.

Najarro: What is the effect of such strong clumping on the cores of the Balmer lines and He I lines? Do they not get too deep?

Bouret: As I said in my talk, we first derive the stellar parameters (including $\dot{M}$) from the UV and FUV spectra and when we look at the optical spectrum, we find that Balmer lines and some He lines are too weak in the model. This is caused indeed by wind filling, and a very efficient way to reduce that is to introduce clumping. Lines then get deeper, in better agreement with the observations most of the time, although in some cases they might get too deep indeed.

Clumping in Hot Star Winds
W.-R. Hamann, A. Feldmeier & L.M. Oskinova, eds.
Potsdam: Univ.-Verl., 2008
URN: http://nbn-resolving.de/urn:nbn:de:kobv:517-opus-13981

Clumping in O-star winds

J.Puls[1], N. Markova[2], F. Najarro[3] & M.M. Hanson[4]
[1] *Universitätssternwarte München, Germany*
[2] *Institute of Astronomy, Bulgarian National Astronomical Observatory, Smolyan, Bulgaria*
[3] *Instituto de Estructura de la Materia, CSIC, Madrid, Spain*
[4] *Department of Physics, The University of Cincinnati, Cincinnati, OH 45221, USA*

We review various diagnostics of clumping in O-star winds, with special emphasis on its radial stratification. Implications and problems are discussed, and promising NIR methods are presented.

1 A word of warning

Instead of a conventional introduction, let us begin with a word of warning: *Almost all evidence for clumping in OB-stars is only indirect* (except for the detection of "outward moving inhomogeneities" in He II λ4686 from ζ Pup, Eversberg et al. 1998), and relies strongly on our belief in results from theoretical modeling: (i) time-dependent hydrodynamic simulations predict a highly structured wind due to the line-driven instability; (ii) spectroscopic NLTE analyses based on homogeneous models produce lines in different wavelength bands which do not fit the observations simultaneously; (iii) predictions from wind models do not agree with "observed" mass-loss rates. Moreover, there are several phenomena which strongly suggest that the "standard model" of a stationary, homogeneous wind needs to be revised: The denser, but also line-driven Wolf Rayet star winds display moving substructures on top of emission lines and reveal inconsistencies between the strengths of recombination lines and their electron scattering wings. Other clues are provided by the presence of X-Ray emission in single stars ($\rightarrow$ shocks) and "black throughs" in saturated P Cygni lines ($\rightarrow$ non-monotonic velocity fields).

2 Indications of significant clumping in OB-star winds

Various diagnostics have been used to derive constraints on the clumping properties of OB stars in different wavelength bands. Typical examples from the recent few years are cited in the following (but see also the references given therein).

- From radio/submm observations, Blomme et al. (2002: ε Ori; 2003: ζ Pup) found a submm-*excess*, suggesting the intermediate wind to be clumped.
- Assuming optically thin clumps and a void interclump medium, NLTE model atmosphere analyses of UV and optical spectra of O-star winds allowed to derive clumping factors, $f_{\rm cl} = \langle\rho^2\rangle/\langle\rho\rangle^2$, of order 10...50, with clumping starting already close to the wind base (Crowther et al. 2002, Hillier et al. 2003, Bouret et al. 2003, 2005, and this volume).
- From the mismatch of predicted and derived wind-momentum rates of O-type supergiants, Markova et al. (2004) and Repolust et al. (2004) suggested this disagreement to be the consequence of wind-clumping: Any ρ^2 dependent diagnostics such as Hα over-predicts the mass-loss rate by a factor of $\sqrt{f}_{\rm cl}$, when the analysis is performed using a smooth model, but the wind consists of optically thin clumps. Both analyses implied clumping factors of the order of 5 to 7.
- The greatest challenge for the standard model resulted from the analysis of the unsaturated FUV resonance doublet of P V for a large sample of O-stars (see Fullerton et al. 2006 and this volume): mass-loss rates derived from these lines were found to be a factor of 10 (or more) lower than those obtained from Hα and radio emission. Interpreted in terms of wind clumping, this would correspond to $f_{\rm cl} \geq 100$!

3 A combined Hα/IR/mm/radio analysis

Recently, Puls et al. (2006) were able to derive constraints on the radial stratification of the clumping factor, by simultaneously modeling Hα and the IR/mm/radio emission from a sample of 19 O-stars with well-known parameters. This is possible since Hα and the IR form in the lower/intermediate wind (1-5 $R_\star$) whereas the mm/radio emission forms in the outer regions (10-50 $R_\star$).

Notably, the derived stratification does not or only marginally agree with the theoretical predictions, the latter suggesting the maximum of the clumping factor to be reached in the intermediate wind (10-20 $R_\star$, see Fig. 1). In contrast, our analysis in-

dicates that in *denser* winds considerable clumping is present already close to the star (in agreement with other investigations, see above), which then remains rather constant over a large volume before decreasing in the outer wind. On average, the ratio of clumping factors in the inner and outer wind is of the order 3 to 6. For the best constrained object, ζ Pup, we found that the maximum of $f_{\rm cl}$ is reached already in the innermost wind region.

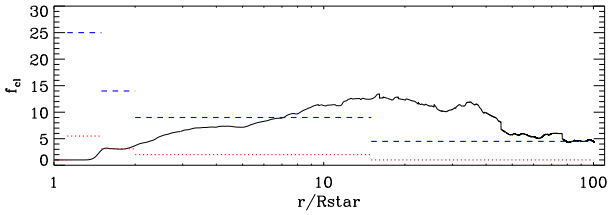

Figure 1: Theoretical predictions for the clumping factor (solid, from Runacres & Owocki 2002), compared to "observed" results from ζ Pup. The red (dotted) solution corresponds to an unclumped outer wind (from Puls et al. 2006), whereas the blue (dashed) solution (with an assumed $f_{\rm cl}$= 4.5 in the radio-emitting region) gives the same fit quality, when the mass-loss rate is reduced by a factor of $1/\sqrt{4.5}$. See text.

For *weaker* winds, on the other hand, the clumping factor is the same in the inner ($r < 2R_\star$) and outermost regions. (Due to missing diagnostics, the intermediate wind remains unconstrained.) This finding points to a physical difference in the clumping properties of weaker and stronger winds, and may be related to the excitation mechanism of the structure formation. In terms of "conventional" mass-loss rates, we find $\dot{M}$(radio) $\approx$ $\dot{M}$(Hα) for weak winds with Hα in absorption, whereas for all stars with Hα in emission we obtain $\dot{M}$(radio) $\approx 0.4 \ldots 0.5$ $\dot{M}$(Hα).

A major shortcoming of our investigation is that only *relative* clumping factors could be derived, normalized to the values in the outermost, radio-emitting region, since *all* considered diagnostics depend on ρ^2. This dilemma is illustrated by the two different solutions for the run of $f_{\rm cl}$ in the wind of ζ Pup (Fig. 1), which cannot be discriminated by our analysis. In other words, $\dot{M}$(REAL) $\leq$ $\dot{M}$(radio), since until now the clumping in the radio emitting region is still unknown. Only if $f_{\rm cl}$(radio) were unity, we would have $\dot{M}$(REAL) = $\dot{M}$(radio). Thus, the issue of absolute values for $\dot{M}$ still remains unresolved, though - at least for the analyzed sample - the observed wind-momentum luminosity relation (WLR) would agree quite nicely with the predicted one (Vink et al. 2000) if one assumes the outer wind to be unclumped!

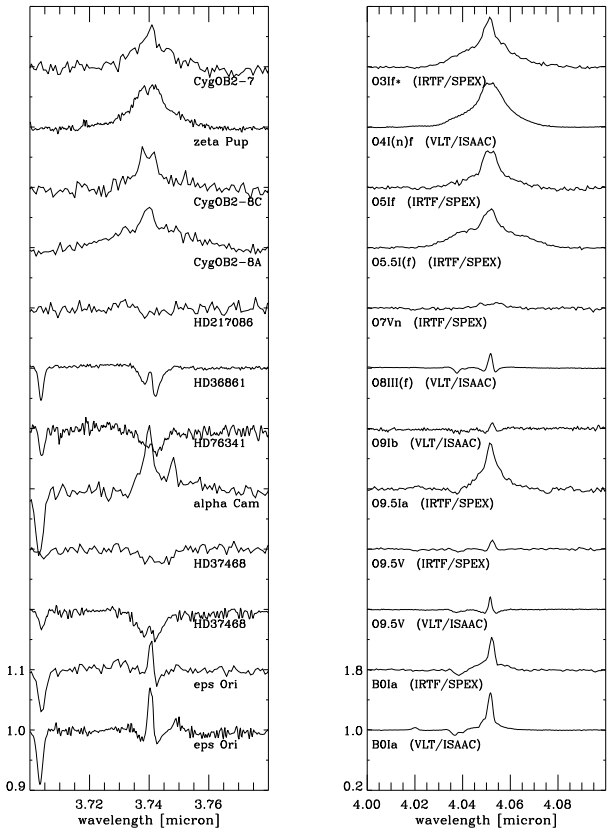

Figure 2: He I 3.70 + Pfγ (left) and Brα(right) for a sample of OB stars with thin and thick winds, as observed by ISAAC@VLT and SPeX@IRTF (observations by Puls, Hanson & Najarro).

4 Implications - problems

In the latter case then, most results obtained from the F(UV) would become questionable and would need to be re-interpreted. A possible way out of the apparent dilemma has been suggested by Oskinova et al. (see Hamann, this volume), who argue that *porosity* effects are able to diminish the effective (line-)opacities and thus would lead to lower clumping factors/higher mass-loss rates than implied by the F(UV) analyses assuming optically thin clumps exclusively.

If, on the other hand, those values were correct, we would have to conclude that the outer wind is significantly clumped, and that the suggested match of observed and predicted WLR is purely coincidental. This, of course, would imply severe problems for radiation driven wind theory (see Krtička and de Koter, this volume), and, most importantly, for

the stellar evolution in the upper HRD (Hirschi and Smith, this volume).

Before final conclusions are possible, a number of open problems have to be solved. Since any instability needs some time to grow and to become nonlinear, our present treatment of clumping is most likely inadequate in those regions where the instability is not fully grown. In these (lowermost) wind regions, the assumption of a void inter-clump matter is certainly questionable. For diagnostics exploiting optically thick lines, the present treatment of the velocity field is certainly wrong (see Owocki, this volume). And finally, as has been suggested recently by Lucy (2007), the influence of photospheric microturbulence on the wind-properties needs to be investigated in more detail.

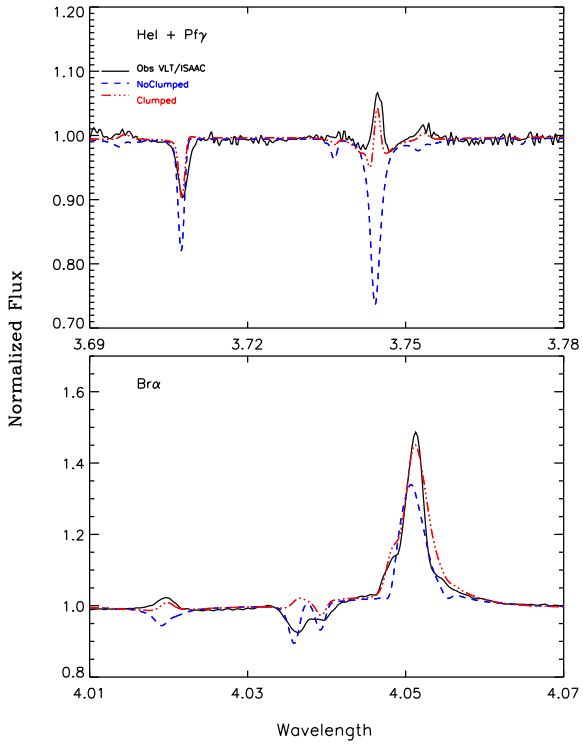

Figure 3: L'-Band diagnostics for ε Ori, by means of unclumped (blue, dashed) and clumped (red, dashed-dotted) models. The need for clumping is clearly visible. The derived $\dot{M}$ is a factor of ≈ 3 lower than implied by unclumped models. From Najarro et al., in prep for A&A.

5 Future perspectives: NIR spectroscopy

Independent clues on the degree of clumping and its stratification are imprinted into IR lines, due to their extreme sensitivity on mass-loss/clumping effects. For objects with large $\dot{M}$, Brα samples the intermediate wind, enabling us to derive constraints on the (local) clumping factor, and in combination with other indicators (UV, Hα, Brγ, Pfγ), to derive "true" mass-loss rates. For objects with weak winds, on the other hand, this line provides not just upper limits (as Hα) but *reliable* constraints on $\dot{M}$. Our models predict a narrow emission peak, superimposed on rather shallow Stark-wings, where the peak height reacts strongly on $\dot{M}$ (increasing with decreasing $\dot{M}$), enabling a measurement of even the weakest wind strengths and, again in combination with other diagnostics, insight into their clumping properties.

During a recent project, we obtained high S/N (> 150) L'-band spectra of ten OB stars covering Brα, Pfγ and He I 3.70 (Fig. 2). A comparison of these spectra with our model predictions (Fig. 3) clearly demonstrates the potential of NIR line diagnostics (see also Najarro, this volume).

Financial support by the NF "Scientific Research" to the Bulgarian MES, grant No 1407/2004 (Markova), and by the Spanish MEC through project AYA2004-08271-CO2 (Najarro) is gratefully acknowledged.

References

Blomme, R., Prinja, R.K., Runacres, M.C., et al. 2002, A&A, 382, 921

Blomme, R., Van den Steene, G.C., Prinja, R.K., et al. 2003, A&A, 408, 715

Bouret, J.-C., Lanz, T., Hillier, D.J., et al. 2003, ApJ, 595, 1182

Bouret, J.-C., Lanz, T., Hillier, D.J. 2005, A&A, 438, 301

Crowther, P.A., Hillier, D.J., Evans, C.J., et al. 2002, ApJ, 579, 774

Eversberg, T., Lepine, S., Moffat, A.F.J. 1998, ApJ, 494, 799

Fullerton, A.W., Massa, D.L., Prinja, R.K. 2006, ApJ, 637, 1025

Hillier, D.J., Lanz, T., Heap, S.R., et al. 2003, ApJ, 588, 1039

Lucy, L.B. 2007, A&A, 468, 649

Markova, N., Puls, J., Repolust, T., et al. 2004, A&A, 413, 693

Puls, J., Markova, N., Scuderi, S., et al. 2006, A&A, 454, 625

Repolust, T., Puls, J., Herrero, A. 2004, A&A, 415, 349

Runacres, M.C., & Owocki, S.P. 2002, A&A, 381, 1015

Vink, J., de Koter, A., Lamers, H.J.G.L.M. 2000, A&A, 362, 295

Feldmeier: You find a clumping factor > 1 close to the photosphere for dense winds and $= 1$ for thin winds. Has this something to do with the effect you found in the paper with Stan Owocki from 1998, on the influence of velocity curvature on the source function?

Puls: First, these are only "relative" clumping factors, i.e. normalized to the unknown clumping in the radio domain. So, weak winds have the same clumping in the lower and outer wind, whereas stronger winds have larger clumping factors. I have no idea on the origin of this difference, but it might be related to the effect discussed (source function gradient).

Hillier: I think there is a real problem with the analysis of O stars with weak winds. First, there is a lack of diagnostics. Second, there are problems with the computation of the ionization structure using standard assumptions (as calculated for example with CMFGEN). Third, the X-rays play (appear to play) a much larger role in the wind. The fraction of the wind emitting X-rays is large, and there are issues of whether the shocks can cool.

Puls: I completely agree. Therefore, we (Paco Najarro and myself) have suggested to use L-band H/He diagnostics for these winds, which are the diagnostics less contaminated by the aforementioned effects. In my talk, however, I was *not* referring to these stars, but to more normal stars with lower luminosity, which follow the WLR, but have H in absorption, i.e. are thinner than the supergiant winds at the same $T_{\rm eff}$.

Ignace: So, whether thick or thin winds, non of your empirical results for $f(r)$ agree with the trends of the Runacres and Owocki simulations?

Puls: Either the outer and inner wind are similarly clumped (which might be unified with hydrodynamic simulations allowing for an earlier onset of clumping), or the clumping is strongest in the lowermost wind, and then decreasing. At least the latter finding is completely inconsistent with hydrodynamic simulations.

Owocki: I just want to point out that the Runacres and Owocki instability model you cite was a conservative model for instability-generated clumping, with *no* photospheric perturbation to seed the wind instability. With base perturbations, one can get clumping starting much closer to the stellar surface, perhaps as high as $f_{\rm cl} = 5$, but not the $f_{\rm cl} = 25$ that you suggest in the more extreme cases.

Runacres: In your paper there is a star (HD 15570) for which the derived clumping factor appears to continue to rise out to larger distances than for the star you showed here, and agrees better with theoretical predictions. Could you comment on what makes this star different?

Puls: Indeed, this is true, but HD 15570 is more or less the only object in our sample which behaves like this. Since this star is not a typical one regarding other parameters, I have no idea about the origin of this difference.

Clumping in Hot Star Winds
W.-R. Hamann, A. Feldmeier & L.M. Oskinova, eds.
Potsdam: Univ.-Verl., 2008
URN: http://nbn-resolving.de/urn:nbn:de:kobv:517-opus-13981

Do clumping corrections increase with decreasing mass-loss rates?

N. St-Louis & A.F.J. Moffat
Université de Montréal (Qc), Canada

We report on new mass-loss rate estimates for O stars in six massive binaries using the amplitude of orbital-phase dependent, linear-polarimetric variability caused by electron scattering off free electrons in the winds. Our estimated mass-loss rates for luminous O stars are independent of clumping. They suggest similar clumping corrections as for WR stars and do not support the recently proposed reduction in mass-loss rates of O stars by one or two orders of magnitude.

1 Introduction

There are many ways to estimates mass-loss rates of massive stars. For some time, it was thought that rates obtained from fitting recombination lines such as H_α (e.g. Markova et al. 2004) or based on radio/IR free-free emission fluxes (Wright & Barlow 1975) were the most accurate. However, when winds were discovered to be clumpy, it was realised that these two methods actually overestimate mass-loss rates, as they depend on the square of the wind density.

Therefore, other methods were sought to alleviate this problem. Fullerton et al. (2006) fitted line profiles to the PV resonance doublet of 40 Galactic O stars. The advantage of using these lines is that P^{+4} is a trace ion in the wind of massive O stars, which insures that the line is not saturated. However, the estimated values of the mass-loss rates were found to be surprisingly low; reduction factors have a median value of ∼20 for O4 to O7 stars and ∼130 for O7 to O9.7 stars. To check if mass-loss rates of O stars need to be so drastically reduced, other methods need to be used.

Alternative methods to get reliable clumping-independent mass-loss rates involve binary systems. Of course, the method that is the most direct is the orbital period lengthening due to symmetric mass-loss as used, for example, by Khaliullin (1974). However, this requires extremely long timescales as the period changes are very small. Another method, suggested by Lamontagne et al. (1996), is the modelling of atmospheric eclipses. The companion star's light shines through the wind and the depth of the light-curve variation depends on the density in the wind and therefore on the mass-loss rate.

Finally, St-Louis et al. (1988) devised a method based on linear polarisation variability as a function of orbital phase for massive WR+O binaries. This method has the advantage that the detailed fit of the polarisation modulation provides an estimate of the orbital inclination (Brown et al. 1978) while the amplitude of the change gives the mass-loss rates. The basic principle is that in a WR+O binary, the light from the O star acts as a probe of the WR wind via electron scattering. O-star photons scatter off the abundant free electrons in the WR wind, which polarises the light received by the observer. The level of polarisation of the observed light depends on the angle between the O-star light source and the scatterers in the WR wind (i.e. the orbital phase for circular orbits) and the total number of scatterings and therefore on the number of free electrons. This latter value is in turn related to the mass-loss rate of the WR star via some simple assumptions. St-Louis et al. (1988) have shown that:

$$\dot{M} = \frac{2.33 \times 10^{-7} A_p \; a(R_\odot) v_\infty (\mathrm{km\ s^{-1}})}{(1+\cos^2 i) f_c I} M_\odot / yr,$$

where A_p is the semi-amplitude of the polarisation ellipse in the Q-U plane, a is the semi-major axis of the orbit, v_∞ is the terminal velocity of the WR wind, i is the orbital inclination, f_c is the fraction of the total flux coming from the companion and I is the numerical value of an integral over solid angles and depends on the β value of the velocity law and the radius beyond which single electron scattering dominates.

Here we have adapted this formalism to O+O binaries. We have searched for published linear polarisation curves in the literature and came up with a sample of 6 massive O binaries, whose names are listed in Table 1. Also given are their orbital period, spectral type, flux fraction for the less luminous of the two stars, the orbital inclination, the semi-major axis of the orbit and the terminal velocity of the dominant wind. All references are given as footnotes. The last parameter that must be specified is the number of free electron per nucleon, α. Here we have assumed in all cases that hydrogen is

Table 1: Data and mass-loss rate estimates for our sample of massive O stars

Star	HD 149404	HD 152248	HD 47129 Plasket's Star	HD 57060 29 CMa	Sk-67^{o}105 (LMC)	LSS 3074
Orbital Period (d)	9.81	5.81	14.40	4.39	3.30	2.185
Spectral Type	O8.5I +O6.5III	O7.5III(f) +O7III(f)	O7.5I +O6I	O7.5Iab +O9.7Ib	O4f +O6V	O4f +O6-7
f_c	0.5[2]	0.5[4]	0.5[6]	0.24[10]	0.31	0.4
i(^{o})	30[2]	72[4]	71[7]	74[10]	71.5	50
a($R_\odot$)	62[2]	54[4]	119[8]	37[11]	42	20.6
$v_\infty(km/s)$	2300[1]	2200[5]	2400[9]	1425[5]	2500	2500
A_p	0.002[3]	0.0006[3]	0.0002[7]	0.0015[12]	0.0145	0.0125
I	12	12	12	12	12	12
α	1	1	1	1	1	1
$\dot{M}(M_\odot)$	$\mathbf{3.1\times10^{-6}}$	$\mathbf{2.3\times10^{-6}}$	$\mathbf{1.8\times10^{-6}}$	$\mathbf{11\times10^{-6}}$	$\mathbf{21\times10^{-6}}$	$\mathbf{3.1\times10^{-6}}$

[1]Penny (1996) [2]Penny et al. (1999a) [3]Luna (1988) [4]Penny et al. (1999b) [5]Howarth et al. (1997) [6]Bagnuolo et al. (1992) [7]Rudy & Herman (1978) [8]Stickland (1987) [9]Prinja et al. (1990) [10]Bagnuolo et al. (1994) [11]Based on the masses of Bagnuolo et al. (1994) [12]Lupie & Nordsieck (1987)

the dominant ion and that it is fully ionised, leading to a value of $\alpha = 1$. The value of the integral I is taken from St-Louis et al. (1988). We have adoted a value of $\beta = 0.8$. In all cases, the value of a/R_* was found to be around 2, leading to a value of $I = 12$.

In the case of WR+O binaries, the wind of the O star is assumed to be negligible with respect to that of the WR star and therefore only the electron scattering of O star photons by WR-wind free electrons is taken into account. In the case of O+O binaries, the two winds can have comparable strengths and therefore both must be taken into account. Most of the binary sytems in our sample are very well studied, which gave us a good idea of the relative strengths of the two winds. In several cases, we have assumed equal-strength winds. In such a situation, the polarisation variability is the result of scattering off photons in the two winds and consequently, the published polarisation amplitude must be divided by two. For a given mass-loss rate of one of the O stars, the polarisation amplitude is therefore doubled (in relative terms) compared to the case of a WR+O binary. This partly compensates for the fact that the mass-loss rates of O stars are generally much smaller than those of WR stars and therefore the absolute values of the linear-polarisation amplitudes are smaller. In Figure 1 we show an example of Q and U curves. The data are for the O8.5I+O6.5III binary HD 149404 and are reproduced from Luna (1988). The characteristic double-wave curve is clearly seen. The literature values of the polarisation amplitudes, A_p, for the 6 binaries in our sample are given in Table 1.

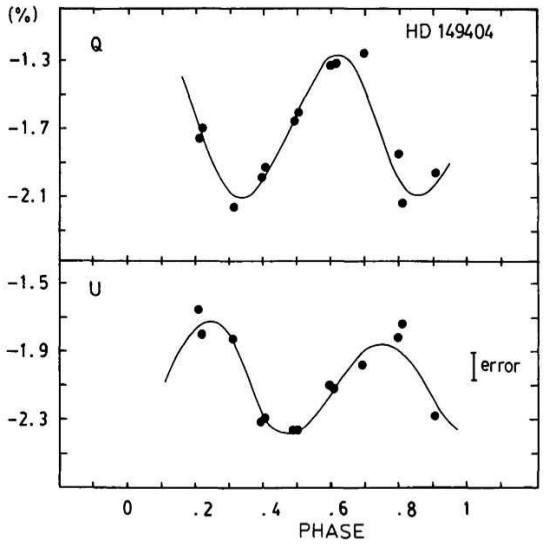

Figure 1: Q and U as a function of orbital phase for the O8.5I+O6.5III binary HD 149404. Reproduced from Luna (1988).

The values of the mass-loss rates that we obtain from the equation of St-Louis et al. (1988) given above are listed in the last line of Table 1. For the first three stars, we have assumed equal winds and therefore the value given is for each component. For the last three stars, the value of the mass-loss rate is for the primary, as the secondary is assumed to

have a negligible wind in comparison to that of the primary. The mass-loss rate values are certainly not two orders of magnitude smaller than average values from free-free emission fluxes or recombination-line fits. Unfortunately, in most cases it is impossible to obtain mass-loss rate estimates by fitting H_α line profiles since, although observed extensively, they are greatly affected by wind-wind collision effects.

Only one of the stars in our sample, HD 149404, has a measured radio thermal flux. The initial mass-loss estimate from Lamers & Leitherer (1993) has been corrected for the revised temperature scale for O dwarfs (Martins et al. 2005) by Fullerton et al. (2006). The resulting value of the mass-loss rate is $\dot{M}$=6.17 $\times 10^{-6}$ $M_\odot$/yr. However, to our knowledge, this estimate does not take into account that the radio flux actually comes from both O stars taken together; therefore it should be divided by two. Our estimated mass-loss rate for each star in this binary is 3.1 $\times 10^{-6}$ $M_\odot$/yr, which is amazingly similar to the radio value (after dividing by two).

We can also compare our estimated mass-loss rate for HD 149404 with the predictions of Vink et al. (2000). Using their theoretical mass-loss recipe for O-type stars in the temperature range 30000–50000 K and stellar parameters for HD 149404 from Penny et al. (1999a) ($T = 36000\ K, log(L_*) = 5.74, M_* = 17\ M_\odot, R_* = 20\ R_\odot$ and $v_\infty = 2300\ km\ s^{-1}$), we calculate $\dot{M} = 6.5 \times 10^{-6} M_\odot/yr$. The temperature used here is appropriate for an O6.5III star, according to the temperature scale of Martins et al. (2005). If instead we adopt $T = 31000\ K$, which is the value given by Martins et al. (2005) for an O8.5I star, we obtain a slightly lower value for the mass-loss rate, $\dot{M} = 4.4 \times 10^{-6} M_\odot/yr$. These value are quite similar to the polarisation and radio values (3.1 $\times 10^{-6}$ $M_\odot$/yr) considering the number of stellar parameters, each with their own error, that enter into these estimates. Furthermore, these theoretical predictions do not include the effects of clumping and therefore are most likely too high.

On the other hand, from fits to the FUSE-band PV resonance doublet, Fullerton et al. (2006) obtain a value of 5.37 $\times 10^{-8}$ $M_\odot$/yr for this star, when they assume that P^{+4} is the dominant P ion in the wind, a value two orders of magnitude below the two above-mentioned estimates. No other star in our sample is also part of the sample of Fullerton et al. (2006).

Therefore the polarisation mass-loss rate estimates do not support a reduction in the mass-loss rates of O stars by two orders of magnitude, at least for the most luminous O stars such as those we have in our sample.

References

Bagnuolo, W. G. Jr.,Gies, D.R., & Wiggs, M.S. 1992, ApJ, 385, 708

Bagnuolo, W.G., Gies, D.R., Hahula, M.E., Wiemker, R., & Wiggs, M.S. 1994, ApJ, 423, 446

Brown, J.C., McLean, I.S., & Emslie, A.G. 1978, A&A, 68, 415

Fullerton, A.W., Massa, D.L., & Prinja, R.K. 2006, ApJ, 637, 1025

Howarth, I.D., Siebert, K.W., Husain, A.J., & Prinja, R.K. 1997, MNRAS, 284, 265

Khaliullin, K. F. 1974, Astronomicheskii Zhurnal, 51, 395

Lamers, H.J.G.L.M., & Leitherer, C. 1993, ApJ, 412, 771

Lamontagne, R., Moffat, A.F.J., Drissen, L., Robert, C., & Matthews, J.M. 1996, AJ, 112, 2227

Luna, H.G. 1988, A&A Sup. Series, 74, 427

Lupie, O. L., & Nordsieck, K. H. 1987, AJ, 93, 214

Markova, N., Puls, J., Repolust, T., & Markov, H. 2004, A&A, 413, 693

Martins, F., Schaerer, D., & Hillier, D.J. 2005, A&A, 436, 1049

Martins, F., Schaerer, D., & Hillier, D.J. 2005, A&A, 436, 1049

Penny, L.R. 1996, ApJ, 463, 737

Penny, L.R., Gies, D.G., & Bagnuolo Jr, W. G. 1999a, In *Proc. IAU Symp. 193*, 86

Penny, L.R., Gies, D.R., & Baguolo, W.G. Jr. 1999b, ApJ, 518, 450

Prinja, R. K., Barlow, M. J., & Howarth, I. D. 1990, ApJ, 361, 607

Rudy, R.J., & Herman, L.C. 1978, PASP, 90 163

St-Louis, N., Moffat, A.F.J., Drissen, L., Bastien, P., & Bastien, P. 1988, ApJ, 330, 286

Stickland, D. J. 1987, The Observatory, 107, 68

Vink, J.S., de Koter, A., & Lamers, H.J.G.L.M. 2000, A&A, 362, 295

Wright, A. E., & Barlow, M. J. 1975, MNRAS, 170, 41

Hillier: These O stars have significantly weaker winds than other O stars. As a consequence, the optical depth of the wind to electron scattering is low. I was therefore wondering what fraction of the polarization signal comes from scattering off the photosphere.

St-Louis: I have not taken that into account in these estimates. Certainly the mass loss rates will have to be reduced because of this effect, but I do not know what the level of the corrections will be; I would have to work them out.

Cassinelli: The photospheres are optically thick. Therefore, radiation that enters is multiply scattered and so scattering from the photosphere will probably be very small.

Moffat: If clumps are optically thick, then this could also hide electrons. So, does the fact that you observe such relatively large mass loss rates from polarization imply that clumps are not optically thick?

Hillier: The clumps are optically thick to lines but not to electron scattering.

Clumping in Hot Star Winds
W.-R. Hamann, A. Feldmeier & L.M. Oskinova, eds.
Potsdam: Univ.-Verl., 2008
URN: http://nbn-resolving.de/urn:nbn:de:kobv:517-opus-13981

Tracking the Clumping in OB Stars from UV to radio

F. Najarro[1], J. Puls[2], A. Herrero[3], M.M. Hanson[4], J. Martín-Pintado[1] & D.J. Hillier[5]
[1] *DAMIR, Instituto de Estructura de la Materia, CSIC, Serrano 121, 28006-Madrid, Spain*
[2] *Universitäts-Sternwarte München, Scheinerstr. 1, D-81679 München, Germany*
[3] *Instituto de Astrofísica de Canarias, E-38200 La Laguna, Tenerife, Spain*
[4] *Department of Physics, The University of Cincinnati, Cincinnati, OH 45221, USA*
[5] *Dep. of Physics and Astronomy, Univ. of Pittsburgh, 3941 O'Hara Street, Pittsburgh, PA 15260, USA*

We review different line and continua diagnostics from the UV to radio, which can be utilized to simultaneously constrain the clumping structure throughout the stellar wind of massive OB stars.

1 Introduction

Theoretically, the intrinsic instability of radiation driven winds predicts the formation of shocks and inhomogeneities (clumps) which have been continuously studied during the last twenty years (Owocki et al. (1988), Feldmeier et al. (1997), Runacres & Owocki (2002)). Observationally, clearest evidence of clumping has been provided by Eversberg et al. (1998), by means of moving structures in the He IIλ4686 wind line profile of ζPuppis. Finally, from the modelling point of view, clumping has been invoked in stellar winds to explain inconsistencies arising between ρ (density) and ρ^2 diagnostics. For a given mass-loss, clumping causes an enhancement of ρ^2 processes while leaving unaltered those which depend linearly on ρ. Further, if mass-loss rate and clumping are scaled without changing the $\dot{M}/f^{0.5}$ ratio, the ρ-dependent diagnostics vary while the recombination lines profiles ($\propto \rho^2$) remain basically unaltered. Thus, models including clumping where developed by Abbott et al. (1981) and Puls et al. (1993) to study its effects on the IR and radio continua of OB stars as well on the resonance lines, while Hillier (1991) investigated in detail the effects on the electron scattering wings of emission lines of WR-stars. Since then, clumping has increasingly gained relevance in the hot-stars business deserving its own workshop (see this proceedings).

In this paper, we make use of observations from the UV to radio of OB stars and identify key diagnostics lines to obtain the clumping structure throughtout the stellar wind. We also give a couple of guidelines to constrain the degree of clumping in stellar winds for different stellar types.

2 Models and Observations

We have used CMFGEN, the iterative, non-LTE line blanketing method which solves the radiative transfer equation in the co-moving frame and in spherical geometry for the expanding atmospheres of early-type stars. We refer to Hillier & Miller (1998) and Hillier & Miller (1999) for a detailed discussion of the code. To test our models we have used a compilation of observations from the UV to radio of the O3If$^+$ star CyOB2#7. Below we concentrate on the clumping structure utilized in our models.

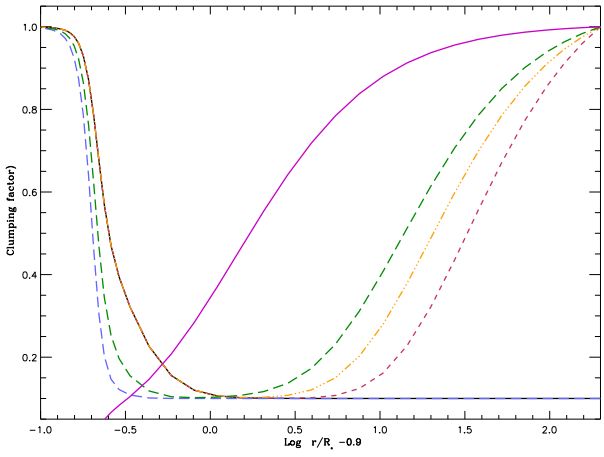

Figure 1: Radial structure of clumping factor for different values of CL_2 and CL_3 according to Eq. 1. The wind velocity structure (in units of V_∞) is also displayed to illustrate the onset of the clumping variations.

To investigate the clumping we introduce the following clumping law (see Fig. 1:

$$f = CL_1 + (1 - CL_1)e^{\frac{-V}{CL_2}} + (CL_4 - CL_1)e^{\frac{(V-V_\infty)}{CL_3}} \quad (1)$$

where CL_1 and CL_4 are volume filling factors and CL_2 and CL_3 are velocity terms defining locations

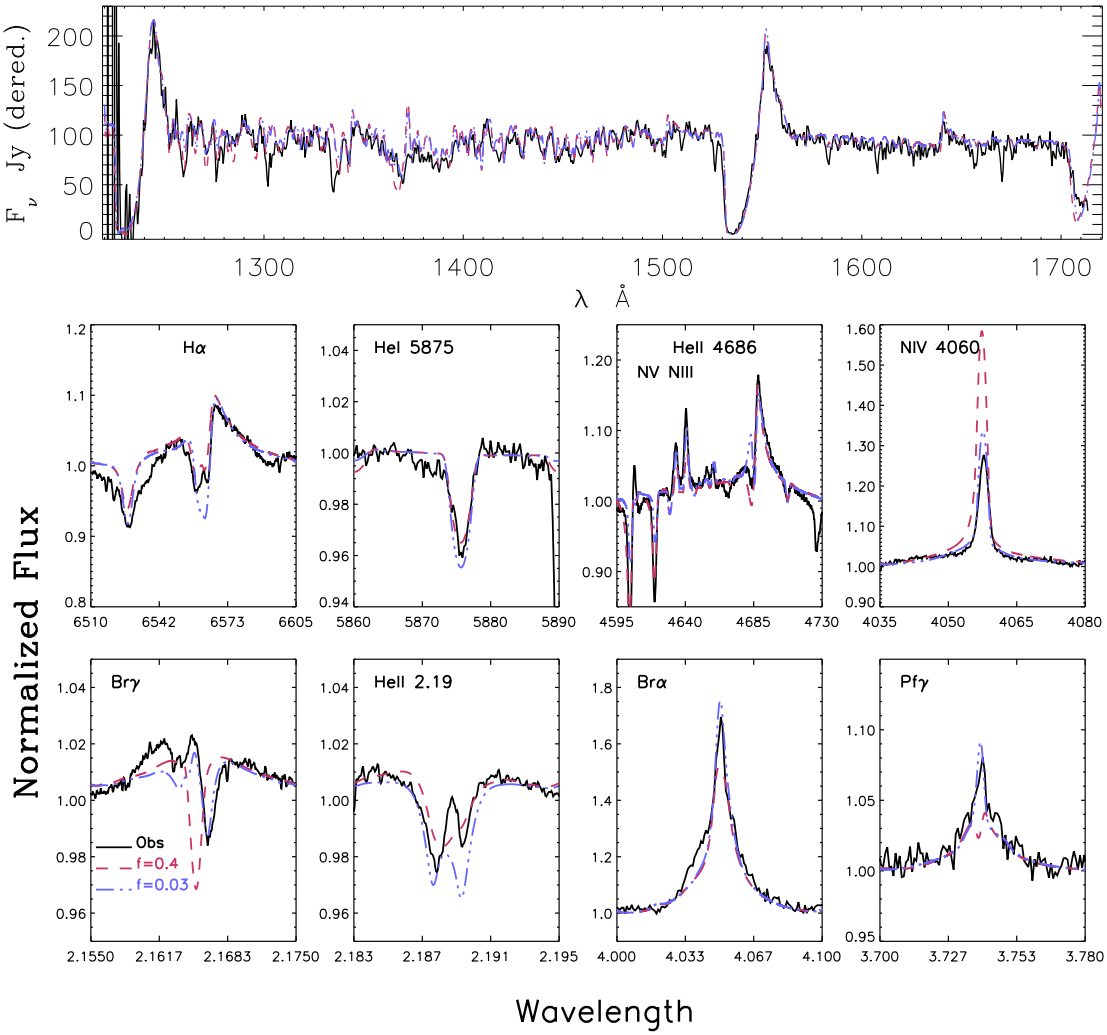

Figure 2: Model best fits to UV, optical and infrared profiles of CygOB2 #7, for two values of the main clumping value $f = \mathrm{CL}_1$.

in the stellar wind where the clumping structure changes. CL_1 sets the maximum degree of clumping reached in the stellar wind (provided $\mathrm{CL}_4 > \mathrm{CL}_1$) while CL_2 determines the velocity of the onset of clumping. CL_3 and CL_4 control the clumping structure in the outer wind. This is illustrated in Fig. 1 which displays the behavior of clumping in the stellar wind for different values of CL2 and CL3. Overploted is also the velocity field in units of V_∞. From Eq.1 we note that as the wind velocity approaches V_∞, so that $(\mathrm{V}-V_\infty) \leq \mathrm{CL}_3$, clumping starts to migrate from CL_1 towards CL_4. If CL_4 is set to unity, the wind will be unclumped in the outermost region. Such behavior was already suggested by Nugis et al. (1998) and was utilized by Figer et al. (2002) and Najarro et al. (2004) for the analysis of the WNL stars in the Arches Cluster. Recently, Puls et al. (2006) also have found similar behavior from Hα and radio studies of OB stars with dense winds. Furthermore, our clumping parametrization seems to follow well the results from hydrodynamical calculations by Runacres & Owocki (2002). From Eq. 1 we note that if CL_3, and therefore CL_4, is not considered ($\mathrm{CL}_3 \rightarrow 0$), we recover the law proposed by Hillier & Miller (1999). To avoid entering free parameters heaven we set $\mathrm{CL}_4 = 1$ in all of our investigations, aiming to get an appropriate amount of leverage on the amount of non-constant clumping in the outer wind regions.

The general impact of clumping on line profiles that was described in the introduction of this paper will occur provided the ionization equilibrium is on the "safe" side. We consider the "safe" re-

gion to be where the population of the next ionization stage clearly dominates over the one the line belongs to (i.e., H II ≫ H I for the hydrogen lines). Noting, however, that ionization depends linearly on density whereas recombination is proportional to ρ^2, a "changing" ionization situation may occur, where two adjacent ionization stages have similar populations. In such a case clumping, which enhances recombination, will cause a net reduction of the mean ionization. This will result in weaker lines.

Finally, in the infrared, via bound-free and free-free processes ($\propto \rho^2$), not only the lines but also the continuum will depend on clumping, resulting in high sensitivity of the continuum-rectified line profiles to CL_1 and CL_2.

One may, therefore, distinguish between lines formed on the "safe" region and those arising from the "changing" region. Figure 2 shows that the N IV λ4058 and N V λ4600 lines in CygOB2 #7 are clearly formed on a "changing" region, as confirmed in our models, while the rest of optical lines are less affected by the large change on clumping and seem to follow the "safe" region behavior. On the other hand, Fig. 2 shows that, contrary to the optical, most of the infrared lines react strongly to changes on clumping. This is because, as discussed above, both line and continua are affected by clumping. Interestingly, our best current models for CygOB2 #7 (Najarro et al. in prep.), which favor a large clumping starting relatively close to the photosphere, provide *consistent* simultaneous fits to the UV, optical and IR observations of this object (see Fig. 2).

We note that while the optical and IR spectra of CygOB2 #7 provide strong constraints on CL_1 and CL_2, the UV spectra and submillimeter and radio observations constitute crucial diagnostics to determine CL_1 and CL_3. Indeed, our UV and submillimeter data (see Fig.3) support the presence of constant clumping, at least, up to mid-outer wind regions where the millimeter continua of CygOB2 #7 are formed. However, recent radio observations by Puls et al. (2006), which continua form at much larger radii, show that clumping may start to vanish at the outermost regions of the stellar wind. The expected emission of our models with constant clumping severely overestimate the upper limits provided by the observations by Puls et al. (2006) of CygOB2 #7. This demonstrates the need of multi-wavelength observations to constrain the run of the clumping structure.

Finally, we tentatively provide some diagnostic optical lines that, depending on the stellar type of the object, could be used to constrain the absolute degree of wind clumping. These are intimately related to the "changing" region situation presented in this paper. No strong UV lines are included as they may strongly be affected by X-rays. For early O supergiants, the N IV λ4058 and N V λ4600 lines. For late O supergiants the He II, N III and C III lines turn into important clumping diagnostic lines. Valuable clumping information may be obtained from cool LBVs for which the He I and Fe II] lines will arise from "changing" regions.

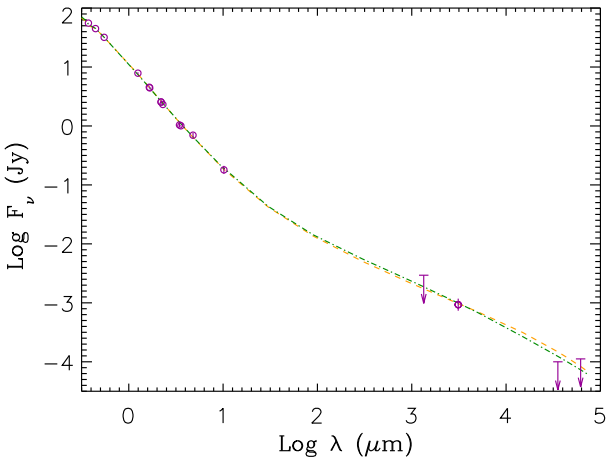

Figure 3: Potential of the submillimeter and radio observations to track the behavior of clumping in the outer wind (see text).

References

Abbott, D. C., Bieging, J. H., & Churchwell, E. 1981, ApJ, 250, 645

Eversberg, T., Lepine, S., & Moffat, A. F. J. 1998, ApJ, 494, 799

Feldmeier, A., Puls, J., Pauldrach, A.W.A. 1997, A&A 322, 878

Figer, D. F., et al. 2002, ApJ, 581, 258

Hillier, D. J. 1991, A&A, 247, 455

Hillier, D. J. & Miller, D. L. 1998, ApJ, 496, 407

Hillier, D. J. & Miller, D. L. 1999, ApJ, 519, 354

Najarro, F., Figer, D. F., Hillier, D. J., & Kudritzki, R. P. 2004, ApJl, 611, L105

Nugis, T., Crowther, P. A., & Willis, A. J. 1998, A&A, 333, 956

Owocki, S. P., Castor, J. I., & Rybicki, G. B. 1988, ApJ, 335, 914

Puls, J., Pauldrach, A. W. A., Kudritzki, R.-P., Owocki, S. P., & Najarro, F. 1993, Reviews in Modern Astronomy, 6, 271

Puls, J., Markova, N., Scuderi, S., Stanghellini, C., Taranova, O. G., Burnley, A. W., & Howarth, I. D. 2006, A&A, 454, 625

Runacres, M. C.,& Owocki, S. P. 2002, A&A, 381, 1015

Smith: If you are using IR/sub-mm/radio fluxes to derive the clumping at various radii, do you not need to worry about variability, if the observations are not obtained simultaneously? Rather, do you have a sense yet for how much variability there is in the sub-mm/radio?

Najarro: Of course variability plays an important role. The problem is that, appart from optical spectra which do show variability, we just have single measurements.

Hamann: You have shown an excess of emission at about 10 μm in the spectrum of Cyg OB2 no. 11. Can this be due to warm circumstellar dust? While hot stars usually do not show such dust emission in the mid-IR, we found unexpectedly warm dust around two WN stars in the dense environment of the Galaxy.

Najarro: The excess was consistent with bound-free and free-free emission. Unfortunately we are missing the wavelength gap $10\,\mu\mathrm{m} - 30\,\mu\mathrm{m}$, where we could see traces of warm circumstellar dust.

Clumping in Hot Star Winds
W.-R. Hamann, A. Feldmeier & L.M. Oskinova, eds.
Potsdam: Univ.-Verl., 2008
URN: http://nbn-resolving.de/urn:nbn:de:kobv:517-opus-13981

Constraints on wind clumping from the empirical mass-loss vs. metallicity relation for early-type stars

A. de Koter[1], J.S. Vink[2] & L. Muijres[1]
[1]*Astronomical Institute 'Anton Pannekoek', University of Amsterdam, The Netherlands*
[2]*Armagh Observatory, Northern Ireland, UK*

We present the latest results on the observational dependence of the mass-loss rate in stellar winds of O and early-B stars on the metal content of their atmospheres, and compare these with predictions. Absolute empirical rates for the mass loss of stars brighter than $10^{5.2} L_{\odot}$, based on Hα and ultraviolet (UV) wind lines, are found to be about a factor of two higher than predictions. If this difference is attributed to inhomogeneities in the wind this would imply that luminous O and early-B stars have clumping factors in their Hα and UV line forming regime of about a factor of 3–5. The investigated stars cover a metallicity range Z from 0.2 to 1 $Z_{\odot}$. We find a hint towards smaller clumping factors for lower Z. The derived clumping factors, however, presuppose that clumping does not impact the predictions of the mass-loss rate. We discuss this assumption and explain how we intend to investigate its validity in more detail.

1 Introduction

In the context of the *VLT-FLAMES Survey of Massive Stars* (Evans et al. 2005, 2006) we studied the stellar and wind properties of close to 100 O- and early B-type stars in several young clusters in the Magellanic Clouds. The data was complemented by a set of Galactic stars (Mokiem et al. 2005). One of the goals of this VLT Large Program is to establish the empirical relation between mass loss and metal content. Theoretical predictions of this relation assume a power-law dependence, i.e. $\dot{M} \propto Z^m$ where $m \sim 0.7$ (Vink et al. 2001, Krtička 2006). So far, a robust empirical value of m was lacking. The reasons for this are both observational and theoretical in nature. The total number of stars that need to be observed and analyzed in order to obtain a meaningful value of m is large, at least 20–30 per galaxy (amounting to 60–90 stars for the Galaxy and Magellanic Clouds). The quantitavive spectral modeling that is required is complex, as non-LTE effects, line blocking/blanketing and an accelerating outflow need to be accounted for. Fortunately, the last decade has shown great progress in both instrumentation developments on large telescopes as well as in the development of (more) realistic stellar atmosphere models.

The most recent step forward in the modeling technique has been the development of an automated fitting method, opening up a means to analyse large samples in a homogeneous way (Mokiem et al. 2005). This valuable asset in the quest for the $\dot{M}(Z)$-relation is briefly discussed in Section 2. The empirical $\dot{M}(Z)$-relation is presented in Section 3 with special emphasis on constraints on the small scale clumping properties implied by the results. In Section 4 we discuss effects of clumping on the predictions of mass-loss rates. We end with conclusions.

2 Spectral analysis

To facilitate a homogeneous analysis we apply an automated spectral fitting method capable of global optimization in a multi-dimensional parameter space of arbitrary size (see Mokiem et al. 2005 for details). The method consists of two main components, the non-LTE stellar atmosphere code FASTWIND by Puls et al. (2005) and the genetic algorithm based optimization routine PIKAIA from Charbonneau (1995). Genetic algorithms represent a class of heuristic optimization techniques, which are inspired by the notion of biological evolution by means of natural selection. Like genes are the coded parameters in case of real life evolution, in our case these can be expressed by the fundamental parameters of the star. So far, the fitted parameters are the effective temperature, surface gravity, luminosity $L_{\star}$, helium abundance, turbulent velocity, mass-loss rate, rate of acceleration and terminal velocity v_{∞} of the outflow, and projected rotational velocity.

The fitness criterion is defined such that individual spectral lines can be assigned weighing factors. Though in principle any line can be modeled we concentrated on optical lines, making Hα the most important mass-loss diagnostic. The modeling technique is sufficiently powerful to exclude – if necessary – the Hα line core, which may suffer from nebular contamination, from the fitting process though clearly this will be reflected in the associated error

bars. The error bars are derived from the fitness properties around the global fit optimum, and will show a degenerate result if the lines lack sensitivity to a certain parameter (for instance mass loss) or when a combination of parameters yields a similar fit quality.

3 The empirical dM/dt(Z) relation

With the lion's share of the data analyzed using the automated fitting method, Mokiem et al. (2007b), based on results presented in Mokiem et al. (2005, 2006, 2007a), determined the empirical relation between mass loss and surface metallicity. The outcome is shown in Fig. 1 in terms of the so-called modified wind momentum – luminosity (WLR) relation,

$$\begin{aligned} \log D_{\rm mom} &\equiv \log(\dot{M} v_\infty \sqrt{R_\star}) \\ &\simeq x \log(L_\star/L_\odot) + \log D_\circ \end{aligned} \quad (1)$$

where $R_\star$ is the stellar radius. The metallicity dependence of $D_{\rm mom}$ is contained in the relative offset of the curves for the individual galaxies. The solid lines represent the empirical result for Galactic ($Z = Z_\odot$), LMC ($0.5\,Z_\odot$) and SMC ($0.2\,Z_\odot$) stars; one sigma confidence intervals are shown as grey areas. One finds

$$\dot{M} \propto Z^{0.83\pm0.16}. \quad (2)$$

Also shown in Fig. 1 are the theoretical predictions of $D_{\rm mom}(L_\star)$ by Vink et al. (2001) using dashed lines. Note that the empirical curves lie above the predictions (for each galaxy). The reason may be the neglect of small scale clumping in the spectral analysis. As the (wind) emission in Hα is the result of recombination, the line strength scales with the square of the density. This implies that $\dot{M}$(clumped wind) $\times \sqrt{f} = \dot{M}$(smooth wind), where f is the clumping factor. Hence, clumping would decrease the empirical curves allowing for a match with predictions.

Therefore, Fig. 1 allows for the following statements regarding clumping: *i)* As the slopes of the non-clumping corrected empirical and theoretical WLRs are very similar over a wide range in wind strengths, clumping is not a strong function of the wind density. *ii)* Taken at face value, the offset at $L_\star = 10^{5.75} L_\odot$ corresponds to a clumping factor $f \sim 5$ for Galactic stars, and $f \sim 3$ for SMC stars. The LMC value is intermediate between these two. We note that the uncertainties on these estimates are such that it is premature to firmly conclude that clumping is a function of metal content. This issue requires a more detailed investigation.

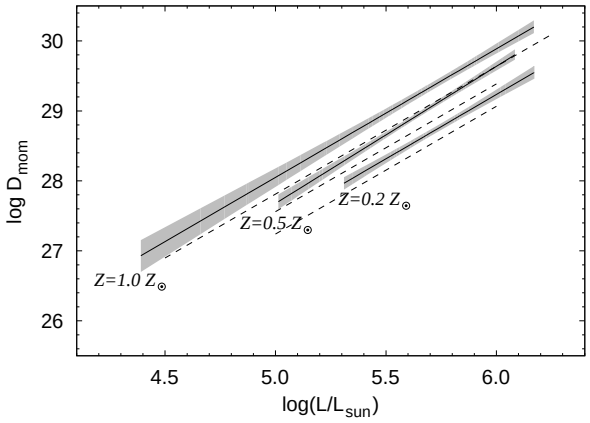

Figure 1: Confrontation between the empirical (solid lines; grey areas denote error bars) and theoretical (dashed lines) modified wind momentum – luminosity relation for Galactic (top), LMC (middle), and SMC (bottom) stars. The empirical results imply a systematically larger $D_{\rm mom}$, which may be due to clumping. From Mokiem et al. (2007b).

4 The effect of small scale clumping on mass-loss predictions

The predictions of $D_{\rm mom}(L_\star)$ assume a smooth wind, therefore the above statements are only valid if clumping does not affect the theoretical mass-loss rates. Is this presumption correct?

One-dimensional time-dependent simulations of the line-driving process shows that extensive but highly unstable wind structure arises quite naturally (e.g. Owocki & Puls 1999). Typically (given assumptions on the line source function) this structure is dominated by reverse shocks that separate high-speed, low-density rarefactions from slower, high-density compressions. In the absence of explicit perturbations, it is essentially found that the mean flow dynamics relax to a steady state (smooth wind) solution. This would imply that, in the context of these models, clumping does not affect the mass loss properties.

Recent determinations of the empirical clumping stratification in O star winds (Puls, these proceedings; Najarro et al., these proceedings) reveal a $f(r)$ that is not compatible with that implied by the line-driven instability mechanism: where observations show that clumping is strong near the photosphere relative to regions further out in the wind, the opposite behavior is predicted. It is currently unknown

whether the *ad hoc* inclusion of strong perturbations at the base of the wind would significantly alter the predicted (mean) mass-loss rate. What's more, the line-driven instability computations so far do not account for the feedback of ionization/excitation changes as a result of structure formation. Such a feedback may be expected to have an effect on the predicted mass loss (see below). The above arguments therefore warrant caution regarding the current paradigm of the impact of wind structure on $\dot{M}$, i.e. that there would be no significant effect.

4.1 Predictions of mass loss in clumped winds

We have taken first steps towards a consistent implementation of structure inhomogeneities in our Monte Carlo method to predict the mass-loss rates of early-type stars (documented in de Koter et al. 1997 and Vink et al. 2000). The problem involves many issues, including: *a)* the feedback of clumping on the ionization and excitation of the gas; *b)* the spatial dimension of the 'clumps' relative to that of the region in which a spectral line can absorb. The latter may be estimated from the (direction dependent) Sobolev length. Two limiting cases can be identified: the size of the clumps is large or small relative to the Sobolev length. *c)* The velocity dispersion of material inside individual clumps, as well as the velocity dispersion of the clump ensemble. *d)* The radial behavior of the clumping and of the velocity dispersions mentioned above. *e)* The potential occurrence of 'porosity', which may occur in a medium in which the clumps are optically thick for continuum radiation.

If we adopt a constant clumping factor throughout the photosphere and wind, we find that if we single out effect *a* the predicted mass-loss is *increased*. This is consistent with results obtained by Krtička (these proceedings). To match the discrepancy in mass loss between theory and observations only a mild value of f – a few – is required though we point out that this assumes a clumping factor that is constant throughout the photosphere and wind. If clumping is negligible in the photosphere, larger values of f may be required. Still, these pilot calculations imply that *if* an inhomogeneous wind is only affected by feedback effects on the state of the gas, a match of the empirical and theoretical WLR seems to require only very mild clumping (recall that clumping also *decreases* the empirical $\dot{M}$).

A more consistent approach of clumping, accounting for more of the above listed effects, is underway.

5 Conclusions

A confrontation of the empirical and theoretical modified wind momentum – luminosity relation can be used to constrain the clumping properties of the winds of luminous O- and early-B stars. If clumping does not affect the amount of mass-loss that is driven by line radiation pressure, this confrontation implies clumping factors $3-5$. A clumping factor $f \sim 5$ is found for Galactic stars, while for SMC stars $f \sim 3$. This may hint towards smaller clumping factors for lower Z (but see Marchenko 2007), though uncertainties are presently too large to make a firm statement about this.

Predictions of the line-driven instability of stellar winds (see e.g. Owocki & Puls 1999) do not predict that the rate of mass loss suffers from wind inhomogeneities. However, we have pointed out that not all effects of clumping have been accounted for in these simulations. For instance, the feedback of clumping on the ionization and excitation (not accounted for in these simulations) leads to a higher predicted mass loss. Taking this into account, only very mild clumping factors would be required to match the empirical and theoretical WLR.

References

Charbonneau, P. 1995, ApJS, 101, 309

de Koter, A., Heap, S.R., & Hubeny, I. 1997, ApJ, 477, 792

Evans, C.J., et al. 2005, A&A, 437, 467

Evans, C.J., Lennon, D.J., Smartt, S.J., & Trundle, C. 2006, A&A, 456, 623

Krtička, J. 2006, MNRAS, 367, 1282

Marchenko, S.V., Foellmi, C., Moffat, A.F.J., Martins, F., Bouret, J.-C., & Depagne, E. 2007, ApJL, 656, L77

Mokiem, M.R., de Koter, A., Puls, J., Herrero, A., Najarro, F., & Villamariz, M.R. 2005, A&A, 441, 711

Mokiem, M. R., et al. 2006, A&A, 456, 1131

Mokiem, M.R., et al. 2007a, A&A, 465, 1003

Mokiem, M.R., et al. 2007b, A&A, in press, astro-ph/0708.2042

Owocki, S.P., & Puls, J. 1999, ApJ, 510, 355

Puls, J., Urbaneja, M.A., Venero, R., Repolust, T., Springmann, U., Jokuthy, A., & Mokiem, M.R. 2005, A&A, 435, 669

Vink, J.S., de Koter, A., & Lamers, H.J.G.L.M. 2000, A&A, 362, 295

Vink, J.S., de Koter, A., & Lamers, H.J.G.L.M. 2001, A&A, 369, 574

Massa: I am a little surprised that the change in mass loss rates caused by clumping is so large since weak lines are important drivers and they are insensitive to clumping.

de Koter: The mass loss rates that are shown in the calculations are underpredicted because they do not account for the velocity dispersion inside clumps and of the clump ensemble. We are working to implement this.

Puls: As Jirí Krtička will show tomorrow, the reduction of the acceleration has a similar dependence on α (thin vs. thick lines) as the line force itself, i.e. only the optically thin lines are affected.

de Koter: After verifying with Krtička it turns out that for the same set of assumptions (clump size large relative to Sobolev line region; constant clumping factor; feedback on ionization included) we recover the same dependence of mass loss on clump size.

Cassinelli: You showed some models with "enhanced driving" of a sector within a clump. However, would this not imply a sector with a different velocity gradient from the rest of the clump, and if this is the case, it seems that it would drive the clump apart very quickly. I would think that a persisting clump would have no velocity gradient across it and the whole clump is at the same velocity.

de Koter: An enhanced driving only results from the effect that a clumped medium has on the ionization structure.

Feldmeier: Since the clump size is much larger than the photon mean free path, you are in the limit of macroturbulence. So you should seperately solve the complete radiative transfer for each single realisation of the wind structure, and take the average $\langle I_{\rm emerg} \rangle$ from all these realisations. How do you do the radiative transfer?

de Koter: So far the feedback of clumping on the ionization/excitation structure is done in the limit of optically thin clumps.

Owocki: For this kind of simulation, is the rather smooth velocity law inside the clumps not more important than the large variations in the surrounding, optically thin medium?

de Koter: In the calculations that I have shown, the velocity dispersion inside a clump is essentially the velocity gradient of the smooth flow times the size of the clump. The ensemble of clumps is assumed to follow the smooth flow to achieve a meaningful comparison with the velocity pattern implied by, for instance, the line driven instability. This needs to be accounted for in our Monte Carlo method. Such a comparison will also require that we do not account for the feedback of a clumped structure on the ionization structure of the medium (which has an impact on the driving). This is done in our models (so we need to switch this off). The latter effect by itself causes an increase of the predicted mass loss. Obviously, we are also interested in implementing empirical clumping structures, which appear to deviate from those predicted by the line driven instability, to see the effect on the mass loss rate.

Hillier: In your procedure to compute $\dot{M}$ you use the global momentum balance of the wind. This technique will clearly be sensitive to the details of clumping in the wind. An alternative technique is to determine $\dot{M}$ by solving the momentum equation below the critical point. This has the advantage that it will be insensitive to details of the clumping in the wind, although a disadvantage is that it may be sensitive to microturblence.

de Koter: We are in the process of implementing the local momentum balance in our Monte Carlo code. As I explained in my reply to Stan's question, the inclusion of a velocity dispersion is the next step.

Gräfener: What kind of clumping geometry did you assume? I guess that a patchy structure would influence your results considerably and also the spectral diagnostics are affected.

de Koter: We took the usual assumption that the clumps are cubes. Different clump realisations might indeed have an effect on the driving efficiency assuming a prefered direction can be assigned to the clumps. The latter may be expected given the almost radial streaming of photons.

Clumping in Hot Star Winds
W.-R. Hamann, A. Feldmeier & L.M. Oskinova, eds.
Potsdam: Univ.-Verl., 2008
URN: http://nbn-resolving.de/urn:nbn:de:kobv:517-opus-13981

Wind emission of OB supergiants and the influence of clumping

M. Kraus[1], **J. Kubát**[1] **& J. Krtička**[2]
[1] *Astronomický ústav, Akademie věd České republiky, Ondřejov, Czech Republic*
[2] *Ústav teoretické fyziky a astrofyziky PřF MU, Brno, Czech Republic*

The influence of the wind to the total continuum of OB supergiants is discussed. For wind velocity distributions with $\beta > 1.0$, the wind can have strong influence to the total continuum emission, even at optical wavelengths. Comparing the continuum emission of clumped and unclumped winds, especially for stars with high β values, delivers flux differences of up to 30% with maximum in the near-IR. Continuum observations at these wavelengths are therefore an ideal tool to discriminate between clumped and unclumped winds of OB supergiants.

1 Introduction

The spectra of hot stars show often excess emission at IR and radio wavelengths that can be ascribed to free-free and free-bound (ff-fb) emission from their wind zones (see e.g. Panagia & Felli 1975).

Waters & Lamers (1984) have investigated this excess emission for $\lambda \geq 1\,\mu$m and winds with a β-law velocity distribution of varying β, pointing already to the sensitivity of the wind emission to the chosen velocity distribution.

Over the last few years, two major effects have become obvious that both strongly influence the wind continuum emission: (i) the winds of hot stars seem to be clumped, and (ii) many OB supergiants have winds with $1.0 \leq \beta \leq 3.5$ (see Table 1).

We investigate the wind continuum emission of OB supergiants especially at optical wavelengths. First, the influence of high β values is discussed, and later on the effects of clumping are studied.

Table 1: Range of β values found for OB supergiants in the Galaxy (Markova et al. 2004 = Ma; Crowther et al. 2006 = Cr; Kudritzki et al. 1999 = Ku) and the Magellanic Clouds (Evans et al. 2004 = Ev; Trundle & Lennon 2005 = TL; Trundle et al. 2004 = Tr).

Sp. Type	β	Ref.
O4 – O9.7	0.7 – 1.25	Ma
O9.5 – B3	1.2 – 3.0	Cr
B0 – B3	1.0 – 3.0	Ku
O8.5 – B0.5	1.0 - 3.5	Ev
B0.5 – B2.5	1.0 - 3.0	TL
B0.5 – B5	1.0 - 3.0	Tr

2 Continuum of OB supergiants

The calculation of the continuum emission of a typical OB supergiant is performed in three steps: (i) we first calculate the stellar emission of the supergiant with no stellar wind, (ii) then we calculate the emission of the wind with the stellar parameters $(R_*, T_{\rm eff})$ as boundary conditions, (iii) and finally we combine the two continuum sources whereby the stellar emission still has to pass through the absorbing wind. To simulate a typical OB supergiant we adopt the following set of stellar parameters: $T_{\rm eff} = 28\,000\,$K, $R_* = 27.5\,R_\odot$, $\log L_*/L_\odot = 5.62$, and $\log g = 3.1$. With these parameters we compute the stellar continuum emission with the code of Kubát (2003), suitable for the calculation of NLTE spherically-symmetric model atmospheres.

The spherically symmetric wind is assumed to be fully ionized, isothermal, and in LTE. This reduces the problem to a pure 1D treatment of the simplified radiation transfer (e.g. Panagia & Felli 1975). The electron temperature is fixed at 20 000 K, and the density distribution in the wind follows from the equation of mass continuity, relating the density at any point in the wind to the mass loss rate and the wind velocity.

The velocity of hot star winds can be approximated with a β-law

$$v(r) = v_0 + (v_\infty - v_0)\left(1 - \frac{R_*}{r}\right)^\beta \qquad (1)$$

where β describes the steepness of the velocity increase at the base of the wind, and v_0 defines the velocity on the stellar surface. A more detailed description of the calculations will be given elsewhere.

2.1 The influence of the velocity

The range in β found for Galactic and Magellanic Cloud OB supergiants is listed in Table 1. Increasing β means that the wind is accelerated more slowly. Consequently, the density in these regions is enhanced because $n_e(r) \sim \dot{M}/v(r)$. These density peaks close to the stellar surface with respect to the wind density with $\beta = 1.0$ are shown in Fig. 1.

Even though these density peaks are rather narrow in radius, they strongly influence the optical depth and therefore the emission of the ff and especially the fb processes. Now, the wind can become (at least partially) optically thick even at optical wavelengths. This leads to an enhanced wind emission meanwhile the stellar flux suffers from the simultaneously increasing wind absorption.

Our test supergiant is assumed to have a wind with $\dot{M} = 5 \times 10^{-6}\, M_\odot \mathrm{yr}^{-1}$, $v_\infty = 1550\,\mathrm{km\,s}^{-1}$, and we calculate the continuum emission for $\beta = 1, 2,$ and 3. The results are shown in Fig. 2. It is obvious that with increasing β the wind creates a near-IR excess, absorbs more of the stellar emission, and contributes to the total emission even at optical wavelengths.

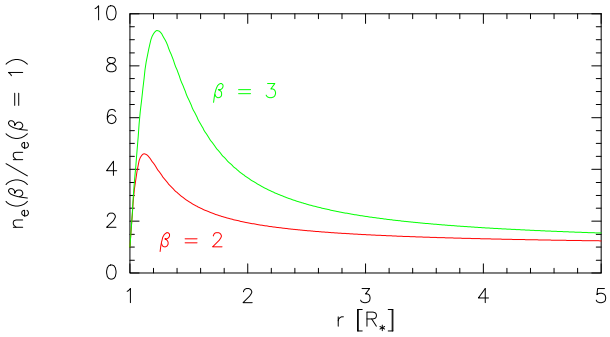

Figure 1: Pronounced density peaks close to the surface (compared to the density for $\beta = 1$) that grow with increasing β.

2.2 The influence of clumping

Hillier et al. (2003) introduced a formalism to account for the presence of wind clumping, and in our calculations we use their filling factor defined by

$$f(r) = f_\infty + (1 - f_\infty) e^{-v(r)/v_{\mathrm{cl}}} \qquad (2)$$

and setting $f_\infty = 0.1, v_{\mathrm{cl}} = 30\,\mathrm{km\,s}^{-1}$, and $v(R_*) = v_{\mathrm{thermal}}$. Since f depends on the velocity distribution, this filling factor is a function of radius as well, constructed such that it quickly reaches its terminal value (top panel of Fig. 3). This way of clumping introduction requests, however, that in order to maintain the same radio flux, the mass loss rate has to be decreased, i.e. $\dot{M}_{\mathrm{cl}} = \sqrt{f_\infty}\, \dot{M}_{\mathrm{smooth}}$, while the absorption coefficient of the ff-fb processes increases, $\langle\kappa\rangle_{\mathrm{cl}} = f(r)^{-1}\, \kappa_{\mathrm{smooth}}$, due to its density squared dependence. Our clumped models automatically account for this mass loss reduction.

At those positions in the wind where $f(r) = f_\infty$ there is no difference between the clumped and the unclumped wind. However, in those regions where $f(r) \neq f_\infty$, which are also the regions where β has its strongest influence, the wind opacity is sensitive to the clumping. But while β enhances the density, clumping (for the same input $\dot{M}_{\mathrm{smooth}}$) reduces the density again. A wind with high β and clumping will therefore have a different opacity in the innermost wind region than a wind with low β and clumping, and the clumped wind will have a different opacity than the smooth wind. This is shown in the lower panel of Fig. 3 where we plotted the opacity ratio of the clumped with respect to the smooth wind for different values of β. The higher β, the stronger the effect. In Fig. 4 we compare the continuum of a clumped with an unclumped wind for $\beta = 3.0$.

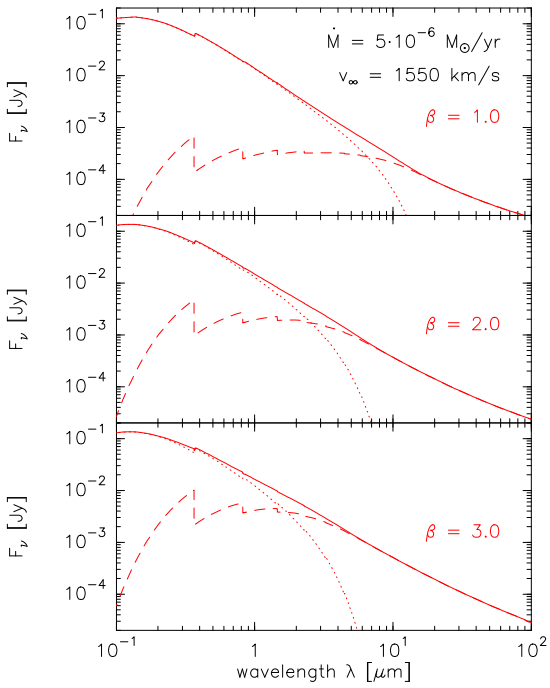

Figure 2: Continuum emission of the test OB supergiant for different values of β. Shown are the stellar emission having passed through the absorbing wind (dotted), the ff-fb emission from the wind (dashed) and the total continuum (solid).

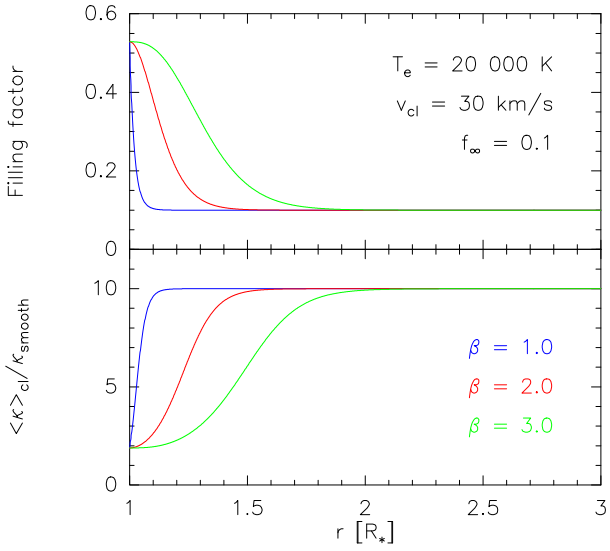

Figure 3: Top: Filling factor for different values of β. Bottom: Opacity ratio between clumped wind model and unclumped wind model.

It is obvious that the clumped model generates less wind emission for $\lambda < 10\,\mu$m. For a better visualization we calculated the flux ratios between unclumped and clumped models (Fig. 5). They show a maximum of up to 30% at near-IR wavelengths. Continuum observations at these wavelengths are therefore an ideal tool to discriminate whether the winds of OB stars with $\beta > 1.0$ are clumped.

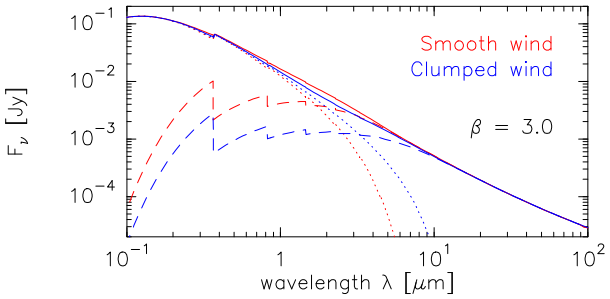

Figure 4: Clumped versus unclumped wind with $\beta = 3.0$. The clumped model produces less wind emission for $\lambda < 10\,\mu$m, resulting in a lower total near-IR flux.

3 Conclusions

For OB supergiants with high β values the ff and especially the fb emission can strongly influence the total continuum, even at optical wavelengths.

Clumping, introduced by the filling factor approach, also influences the wind opacity and therefore the continuum emission. Whether the wind of an OB supergiant is clumped or not can be checked based on continuum observations in the optical and near-IR region. Especially winds with high β are found to have fluxes that differ by about 30% (see Fig. 5). The optical and near-IR continuum are therefore ideal to discriminate between clumped and unclumped winds.

M.K. acknowledges financial support from GA AV grant number KJB 300030701.

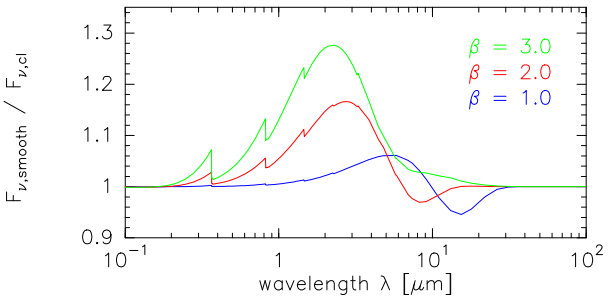

Figure 5: Continuum flux ratio between the unclumped and clumped wind models. The ratio increases with β having a maximum in the near-IR.

References

Crowther, P. A., Lennon, D. J., & Walborn, N. R. 2006, A&A, 446, 279

Evans, C. J., Crowther, P. A., Fullerton, A. W., & Hillier, D. J. 2004, ApJ, 610, 1021

Hillier, D. J., Lanz, T., Heap, S. R., et al. 2003, ApJ, 588, 1039

Kubát, J. 2003, in Modelling of Stellar Atmospheres, ed. N. Piskunov, W. W. Weiss, & D. F. Gray (San Francisco: ASP), IAU Symp., 210, A8

Kudritzki, R. P., Puls, J., Lennon, D. J., et al. 1999, A&A, 350, 970

Markova, N., Puls, J., Repolust, T., & Markov, H. 2004, A&A, 413, 693

Panagia, N., & Felli, M. 1975, A&A, 39, 1

Trundle, C., & Lennon, D. J. 2005, A&A, 434, 677

Trundle, C., Lennon, D. J., Puls, J., & Dufton, P. L. 2004, A&A, 417, 217

Waters, L. B. F. M., & Lamers, H. J. G. L. M. 1984, A&AS, 57, 327

Cohen: Have you considered non-isothermal winds?

Kraus: A non-isothermal wind will not change the spectrum significantly. The free-free emission is hardly temperature dependent, and the free-bound emission, which does depend on temperature, is created in the innermost wind region where the wind temperature is highest. An isothermal wind at high electron temperature is therefore a reasonable assumption for our continuum calculations.

Clumping in Hot Star Winds
W.-R. Hamann, A. Feldmeier & L.M. Oskinova, eds.
Potsdam: Univ.-Verl., 2008
URN: http://nbn-resolving.de/urn:nbn:de:kobv:517-opus-13981

Wind inhomogeneities in low-Z environment: observations

S.V. Marchenko
Western Kentucky University, USA

We discuss the results of time-resolved spectroscopy of three presumably single Population I Wolf-Rayet stars in the Small Magellanic Cloud, where the ambient metallicity is $\sim 1/5 Z_{\odot}$. We were able to detect and follow numerous small-scale wind-embedded inhomogeneities in all observed stars. The general properties of the moving features, such as their velocity dispersions, emissivities and average accelerations, closely match the corresponding characteristics of small-scale inhomogeneities in the winds of Galactic Wolf-Rayet stars.

1 Introduction

The fast, dense winds of Wolf-Rayet (W-R) stars are driven by radiation pressure exerted on multiple lines of mainly heavy elements. Hence, W-R mass-loss rates should be sensitive to the ambient metallicity content, as well as to the locally enhanced chemical composition of the wind. The former sensitivity, though suggested from general principles (Lamers & Cassinelli 1999), has escaped detection until recently (see Crowther 2006, Gräfener & Hamann 2006, and references therein). Numerous spectroscopic observations of Galactic W-R and OB stars (see, e.g., Lépine et al. 2000; Fullerton et al. 2006 and references therein) demonstrated the omnipresence of wind-embedded clumps, usually taking on the form of discrete density enhancements outmoving with an accelerating wind. Though wind-clumping was widely anticipated to operate also in low-Z environments (Hamann & Koesterke 1998; Crowther et al. 2002; Bouret et al. 2003), any *direct* proof was lacking.

2 Our targets and observing strategy

We targeted three presumably single (Foellmi et al., 2003) early-type WN stars in the SMC: SMC-WR 1 (WN3ha), WR 2 (WN5ha) and WR 4 (WN6h), thus forming a representative sample of the small SMC W-R population (12 known Population I W-R stars, most of them early-type WNs: Massey et al. 2003). We tried to avoid the binaries, as, quite frequently, a large-amplitude, phase-related line-profile variability prevents detection of relatively faint details ascribed to the wind-clumping. We monitored the stars in continuous, ∼1h 40 min-long loops for two consecutive nights in August, 2006 (between HJD 2,453,974.538 and ...75.877), alternating among the 3 targets. We used the UVES spectrograph at the ESO-VLT-UT2 8-m telescope, sampling the region $\lambda 3927-6031$Å and obtaining 5-6 spectra/night/star, all with comparable signal-to-noise ratios $S/N \simeq 120-160$, and ~ 0.3Å spectral resolution (for more details see Marchenko et al. 2007). Previously a similar setup has led to robust detections of small-scale inhomogeneities in the winds of Galactic W-R stars.

3 Properties of the Clumps

Applying a widely-accepted procedure (appropriately filtered differences: individual profiles minus night averages - see, e.g., Lépine et al. 2000), we detected, as anticipated, numerous wind-embedded, stochastically appearing and gradually outmoving (notice the typical **V**-shaped structures in Fig. 1) clumps in all 3 targets and all major emission lines, namely, HeII 4686, 4859 and 5412 Å . The line-profile variability of WR1 and WR2 closely resembles the behavior of emission lines in the Galactic W-R stars. However, in WR4 one may notice the synchronized *redward* migration of weak emission features in the first half of Night 1 (Fig. 1), as well as the gradual disappearance of the broad emission feature at $\lambda \sim 4690$ during Night 2, both phenomena reminiscent of a large-scale, relatively long-lasting perturbation in the wind. These are usually linked to a co-rotating interacting. region (e.g., Massa et al. 1995). The existence of a photometric period (Foellmi et al. 2003: P=6.55 d) calls for an even closer analogy with EZ CMa, a Galactic W-R CIR proto-type (St-Louis et al. 1995). However, any direct analogy promptly ends at the inspection of the available data from FUSE (Fig. 2): where one expects to detect a coherent variability across the spectrum (St-Louis et al. 1995), we see none substantially exceeding the instrumental noise. Hence, we conclude that

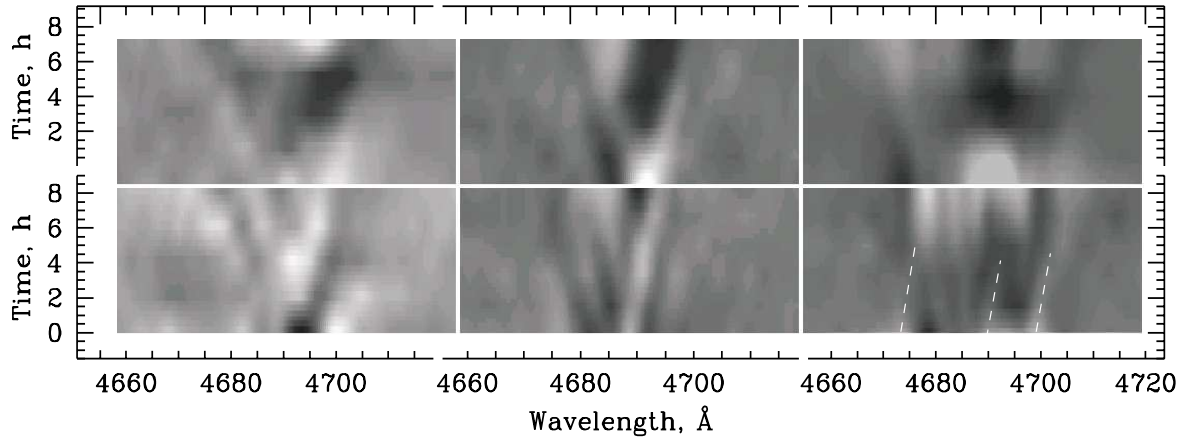

Figure 1: Grayscale plots of time-interpolated and smoothed difference (individual - night-average) spectra of WR1 (left panels), WR2 (central panels) and WR4 (right panels) for Night 1 (lower panels) and Night 2 (upper panels). The intensity ranges are -0.03 (black) to +0.03 (white) in the local continuum units (≡ 1). The dashed lines in the lower-right panel for WR4 mark the features presumably related to CIRs (see text).

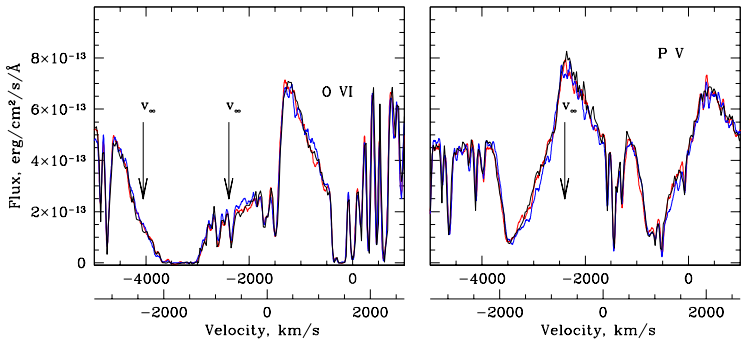

Figure 2: The line-profile variability (or, rather, a lack of variability) in WR4 observed with FUSE. Black lines: data from 14 June, 2001 (Willis et al. 2004); red lines - 06 August, 2006; blue lines - 01 October, 2006. The double X-axis shows velocity scales for the two components of the OVI and P V doublets. Their v_∞ edges are marked by vertical arrows.

practically all the variability patterns seen in Fig. 1 are caused by stochastical appearance of small-scale overdensities in the winds of the SMC W-R stars.

Evaluating the characteristics of wind-clumps, we apply the well-developed suite of techniques, such as time-averaged cross-correlation functions, the degradation functions, etc. (see Lépine et al. 2000) and find that the basic properties of the Galactic wind-clumps are indistinguishable from those in the SMC sample (Fig. 3).

Two unveiled characteristics deserve special attention:

(i) the simultaneous appearance of some clumps in all studied HeII lines allows to address the important question of the optical depth of the detected clumps. The limited amount of spectra, as well as insufficiently high (for this particular purpose) S/N do not provide a single answer. However, we are left with only two potentially viable alternatives: (a) the clumps are optically thick in all transitions *and* the winds have rather low volume filling factors (e.g., Owocki & Cohen 2006), or (b) all clumps are optically thin;

(ii) even more interesting is the the lack of any dependence of clump FWHMs on spectral class or terminal velocity of the W-R winds (Fig. 3, left section). Such 'insensitivity' may signify that the clumps are direct products of supersonic turbulence operating in compressible outflows. Indeed, evaluating the expected velocity dispersions in a shock-bound cold dense layer (Folini & Walder 2006), we find a reasonably close match with the observed FWHMs of

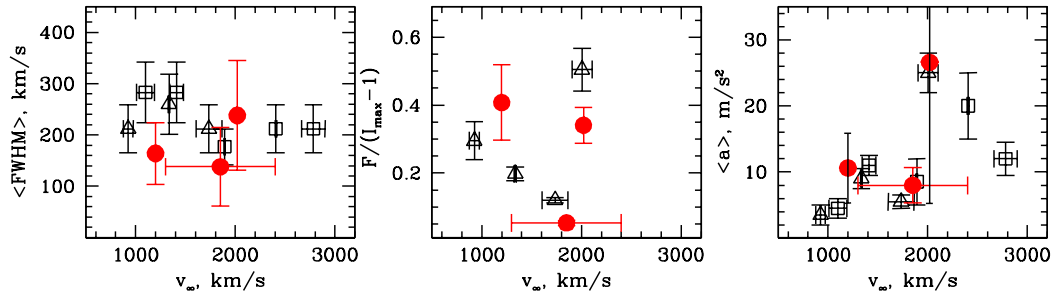

Figure 3: The left panel shows the average FWHMs of the clumps observed in the HeII 5412Å profile in the SMC stars (red circles), as well as Galactic WC (open squares) and WN (open triangles) stars (see Lépine & Moffat 1999). The data are arranged by the corresponding terminal velocities of the WR winds. The middle panel shows the average fluxes (F) of the clumps detected in the HeII 5412Å line and normalized by the maximum intensity of this emission profile ($I_{max} - 1$), in order to be compared with the measurements of Robert (1992). The right panel shows the average accelerations of outmoving clumps.

wind-clumps.

4 Conclusions

The general properties of wind-clumps are the same in the Galactic and SMC stars.

The clumps should be considered as direct products of supersonic turbulence operating in a compressible outflow. The observed FWHMs of the wind-clumps (Fig. 3) point to the filling factor $f \sim 0.1$, in line with the widely accepted value (e..g, Hamann & Koesterke 1998).

Presently, we are not able to choose between the two possibilities: (a) either the clumps are optically thin or (b) the filling factor f is very low.

The author is grateful to his long-term collaborators, C. Foellmi, A.F.J. Moffat, F. Martins, J.-C. Bouret and E. Depagne, for their valuable contributions to this project. The program was partially supported from the NASA grant NNX07AC73G.

References

Bouret, J.-C., et al. 2003, ApJ, 595, 1182

Crowther, P.A. 2006, Stellar Evolution at Low Metallicity: Mass-Loss, Explosions, Cosmology, H. Lamers, N. Langer, & T. Nugis, ASP Conf. Series, 353, 157

Crowther, P.A., Dessart, L., Hillier, D.J., Abbott, J.B., & Fullerton, A.W. 2002, A&A, 392, 653

Foellmi, C., Moffat, A. F. J., & Guerrero, M. A. 2003, MNRAS, 338, 360

Folini, D., & Walder, R. 2006, A&A, 459, 1

Fullerton, A.W., Massa, D.L., & Prinja, R.K. 2006, ApJ, 637, 1025

Gräfener, G., & Hamann, W.-R. 2006, Stellar Evolution at Low Metallicity: Mass-Loss, Explosions, Cosmology, H. Lamers, N. Langer, & T. Nugis, ASP Conf. Series, 353, 171

Hamann, W.-R., & Koesterke, L. 1998, A&A, 335, 1003

Lamers, H.J.G.L.M, & Cassinelli, J.P. 1999, Introduction to Stellar Winds, Cambridge: Cambridge University Press

Lépine, S., & Moffat, A.F.J. 1999, ApJ, 514, 909

Lépine, S., et al. 2000, AJ, 120, 3201

Marchenko, S.V., Foellmi, C., Moffat, A.F.J., et al. 2007, ApJL, 656, L77

Massa, D., et al. 1995, ApJL, 452, L53

Massey, P., Olsen, K. A. G., & Parker, J. W. 2003, PASP, 115, 1265

Owocki, S.P., & Cohen, D.H. 2006, ApJ, 648, 565

Robert, C. 1992, Ph.D. Thesis, Université de Montréal

St-Louis, N., Dalton, M.J., Marchenko, S.V., Moffat, A.F.J., Willis, A.J. 1995, ApJL, 452, L57.

Willis, A.J., et al. 2004, ApJS, 154, 651

Clumping in Hot Star Winds
W.-R. Hamann, A. Feldmeier & L.M. Oskinova, eds.
Potsdam: Univ.-Verl., 2008
URN: http://nbn-resolving.de/urn:nbn:de:kobv:517-opus-13981

Mass-loss rate and clumping in LBV stars: the impact of time-dependent effects

J.H. Groh [1], D.J. Hillier[2] & A. Damineli[3]
[1] *Max-Planck-Institut für Radioastronomie, Germany*
[2] *University of Pittsburgh, USA*
[3] *Universidade de São Paulo, Brazil*

This paper outlines a newly-developed method to include the effects of time variability in the radiative transfer code CMFGEN. It is shown that the flow timescale is often large compared to the variability timescale of LBVs. Thus, time-dependent effects significantly change the velocity law and density structure of the wind, affecting the derivation of the mass-loss rate, volume filling factor, wind terminal velocity, and luminosity. The results of this work are directly applicable to all active LBVs in the Galaxy and in the LMC, such as AG Car, HR Car, S Dor and R 127, and could result in a revision of stellar and wind parameters. The mass-loss rate evolution of AG Car during the last 20 years is presented, highlighting the need for time-dependent models to correctly interpret the evolution of LBVs.

1 Introduction

In order to analyze the complex winds of massive stars major improvements, such as the inclusion of wind clumping and a consistent treatment of line blanketing, have been incorporated into radiative transfer codes during the last decade (e.g. Hillier & Miller 1998; Gräfener et al. 2002; Puls el al. 2005). However, a steady-state outflow is still assumed by the models. While this is probably valid for single Wolf-Rayet and O-type stars, it is invalid for LBV stars.

LBVs are characterized by strong photometric and spectroscopic variability on timescales from days to decades, arising from changes in stellar and wind parameters (Humphreys & Davidson 1994; van Genderen 2001). A careful evaluation of the wind timescales, and how they compare to the variability timescale, is required to quantify the impact of time-dependent effects in the spectroscopic analysis of LBVs.

2 The flow timescale

The flow timescale ($t_{\rm flow}$) is the time required for the material ejected from the surface of the star ($R_\star$) to reach a distance r in the wind. Thus, a lower limit can be estimated as $(r - R_\star)/v$, where v is the wind velocity at r. As the wind of LBVs usually have a beta-type velocity law, a more realistic $t_{\rm flow}$ can be obtained by integrating the inverse of the velocity law.

As LBVs show a wide range of physical parameters, the value of $t_{\rm flow}$ can vary significantly from minimum (i.e. hot) to maximum (i.e. cool) phases. We present in Figure 1 the flow timescale and the line formation region calculated for models assuming the physical parameters found in LBVs at minimum (panels *a* and *b*, respectively) and maximum phases (panels *c* and *d*, respectively).

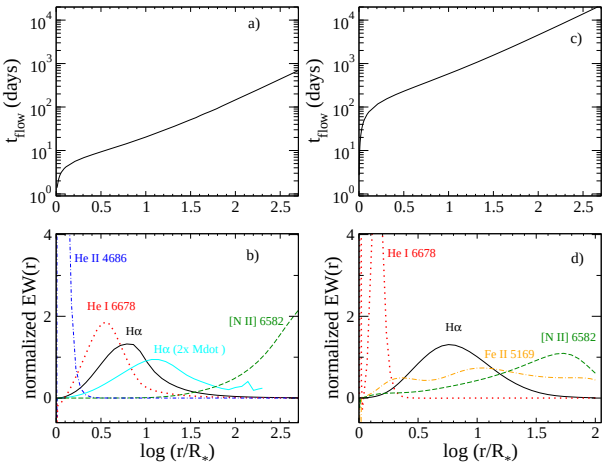

Figure 1: Flow timescale as a function of distance in the wind for minimum phases (panel *a*) and maximum phases (panel *c*). The formation region of the strongest diagnostic lines used to analyze minimum and maximum phases is also shown in panels *b* and *d*, respectively. Notice that the flow timescale can be large for Hα even during minimum.

At minimum phases, $t_{\rm flow}$ is less than a 100 days for distances up to 100 $R_\star$. All the diagnostic lines used in the spectroscopic analysis (e.g. He II 4686, Hα, He I 6678, etc.) are formed in the inner 100 $R_\star$ region, which translates to a small impact of time-dependent effects.

During maximum phases, however, $t_{\rm flow}$ increases dramatically, as the wind terminal velocity is typically 4 times lower than during minimum, and the stellar radius is increased by a factor of 8 (Stahl et al. 2001; Groh et al. 2007). Therefore, it is anticipated that most diagnostic lines will be affected by time-dependent effects. Moreover, physical parameters obtained through steady-state models will be significantly biased. As can be seen in the right panels of Figure 1, time-dependent effects are especially crucial to model Hα, which has an extended line formation region, with $t_{\rm flow} = 300$ – 1000 days.

It is important to point out that, as LBV stars have very dense winds, the recombination timescale is very short (few days) for distances smaller than $\sim$ 500 $R_\star$. Typically, $t_{\rm flow}$ is at least one or two orders of magnitude larger than the recombination timescale, and hereafter we neglect the latter.

3 Including time-dependent effects in CMFGEN

The long flow timescales found for LBVs will change significantly the wind density structure, and the velocity field. We developed a code to obtain a realistic description of $v(r)$ and $\rho(r)$, and use them as an input to the radiative transfer code CMFGEN (Hillier & Miller 1998). The main steps involved in our code are:

1. We consider two epochs: epoch 1 (initial), and epoch 2 (final), which are separated in time by Δt days. We assume that the physical parameters of the star are known for epoch 1, while they will be determined for epoch 2 accounting for time-dependent effects.

2. We obtain rough values for the wind terminal velocity and stellar radius for epoch 2, using a CMFGEN steady-state model. The refined values are determined later through a detailed spectroscopic analysis.

3. We determine the flow timescale for epoch 2:

$$t_{flow}(r) = \int_{R_\star}^{r'} (v_\infty - v_0)^{-1} (1 - R_\star/r)^{-\beta}\, dr' \ .$$

4. Using $t_{\rm flow}$, we calculate how the wind "terminal velocity" and $\dot{M}$ change as a function of r. We assume both vary linearly as a function of time:

$$v_\infty(r) = v_{\infty,i} + \frac{(v_{\infty,f} - v_{\infty,i})[\Delta t - t_{flow}(r)]}{\Delta t} \ ,$$

$$\dot{M}(r) = \dot{M}_i + \frac{(\dot{M}_f - \dot{M}_i)[\Delta t - t_{flow}(r)]}{\Delta t} \ .$$

5. The velocity field is then obtained, assuming a beta-type law at each point and a constant value of $v_0 = 5.0$ km s^{-1}:

$$v(r) = v_0 + [v_\infty(r) - v_0][1 - R_\star(r)/r)^\beta] \ .$$

For $v < v_0$, the beta-type law is smoothly connected to a hydrostatic structure.

6. Finally, the density structure, which includes the effects of clumping through a volume filling factor $f(r)$, is derived using the equation of continuity:

$$\rho(r) = \frac{\dot{M}(r) f(r)^{-1/2}}{4\pi r^2 v(r)} \ .$$

4 Results: AG Carinae

We analyzed the 20-year spectroscopic and photometric evolution of AG Carinae, which has been the most variable LBV in the Galaxy in the last decades (van Genderen 2001). We obtained the stellar parameters using CMFGEN, taking into account the time-dependent effects in the velocity field and density structure as outlined above. Further details about the observational data, technique, and results can be found in Groh et al. 2006, Groh 2007, and Groh et al. 2007.

4.1 Mass-loss rate evolution

To highlight the need for time-dependent models, we shown in Figure 2 (panel *a*) the evolution of the mass-loss rate of AG Car during the last 20 years, comprising two full S-Dor cycles. The J-band lightcurve is also shown as a reference for the maximum and minimum phases.

Striking differences are seen in the results obtained by steady-state models and time-dependent models. The steady-state models predict an increase in the mass-loss rate from minimum to maximum, with a peak of very high mass-loss rate around the lightcurve maximum. This is qualitatively similar to the results obtained by Stahl et al. 2001, besides quantitative differences due to the inclusion of clumping and full line blanketing in our models.

However, when time-dependent effects are taken into account, the mass-loss rate still increases from minimum to maximum, but without a peak of very

high mass-loss rate around maximum. Instead, the mass-loss rate reaches approximately a constant value during the maximum phase. Indeed, the apparent peak in the mass-loss rate during maximum obtained by steady-state models is an artifact caused by the neglecting the time-dependent effects in the density structure. Those effects have a key impact in the formation of Hα and other strong emission lines which are formed by recombination and thus are density-squared dependent. As Hα and other strong hydrogen lines are usually the main diagnostics for the mass-loss rate, *extreme* caution has to be used if they are used to derive the mass-loss rate for active LBVs, such as AG Car, HR Car, R127 and S Dor.

4.2 How clumpy are LBV winds?

Another interesting result obtained from the analysis of the AG Car spectra is the evolution of the volume filling factor f during the S-Dor cycle, which is shown in Figure 2 (panel c). As the physical parameters of the star and the wind are very different from minimum to maximum, AG Car is an ideal laboratory to study how of the wind clumping changes as a function of the stellar temperature (panel b of Fig.2), for instance.

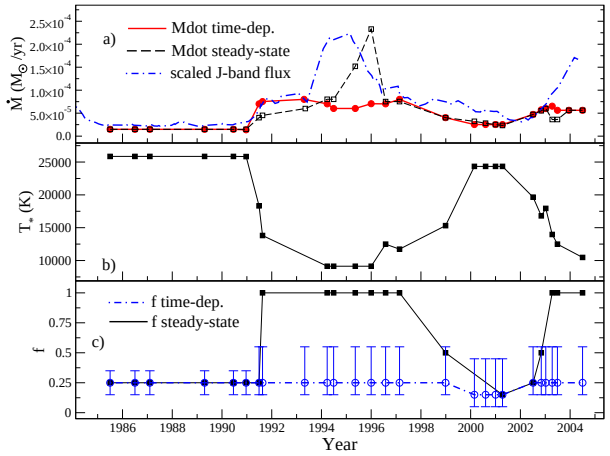

Figure 2: Evolution of the mass-loss rate (panel a), stellar temperature (b) and volume filling factor (c) during the last 20 years for AG Car.

The results obtained using steady state models show that f increases from 0.25 during minimum (high $T_{\rm eff}$) to 1.0 during maximum (low $T_{\rm eff}$). This happens because the electron-scattering wings become very strong during maximum, and they are used to constrain the value of f. However, the change in f occurs in a short timescale of 3 months, which is difficult to be explained.

When time-dependent models are used, the changes in f as a function of time are small or none at all. The changes compared to the steady-state results are due to a modified density structure due to the long flow timescale of the wind (order of a few years). Therefore, because the density structure of the wind is modified compared to the steady-state models, strong electron-scattering wings are present for smaller values of f in time-dependent models.

Moreover, we assume for simplicity that the mass-loss rate and wind terminal velocity change linearly as a function of time. Different variations as a function of time also produce changes in the electron-scattering wings, which can account for the observed line profiles. Clearly, time-dependent models are required to derive the volume filling factor of LBV winds.

5 Summary and Conclusions

The long flow timescales of LBVs have a significant impact in the density structure and velocity law of the wind, which makes steady-state models usually invalid for active LBVs.

Strong hydrogen recombination lines such as Hα, Hβ, Paβ, and Brγ are formed through a large volume of the wind, and are the most affected by time-dependent effects. Therefore, physical parameters obtained using those lines will be biased, especially the mass-loss rate, and the aforementioned emission lines are proportional to the square of the density.

The inclusion of time-dependent effects in the radiative transfer codes is required to obtain reliable stellar and wind parameters for such active LBVs, as shown here for AG Car. Ongoing work by our group might lead to significant revision of stellar and wind parameters of those active LBVs, and might provide key insights on the evolution during the LBV phase.

References

Gräfener, G., Koesterke, L., & Hamann, W.-R. 2002, A&A, 387, 244

Groh, J. H. 2007, PhD Thesis, Universidade de São Paulo (Brazil)

Groh, J. H., Hillier, D. J., & Damineli, A. 2006, ApJL, 638, L33

Groh, J. H., Damineli, A., & Hillier, D. J. 2007, astro-ph/0702612

Hillier, D. J. & Miller, D. L. 1998, ApJ, 496, 407

Humphreys, R. M. & Davidson, K. 1994, PASP, 106, 1025

Puls, J., Urbaneja, M. A., Venero, R., et al. 2005, A&A, 435, 669

Stahl, O., Jankovics, I., Kovács, J., et al. 2001, A&A, 375, 54

van Genderen, A. M. 2001, A&A, 366, 508

Najarro: The radio variability of LBVs is usually explained in terms of changes of ionization rather than to flow of the material, due to the short time scale of the variability. Have you checked the effects of ionization fronts associated with your radial dependent mass loss?

Groh: The recombination time scale is an order of magnitude lower than the flow time scale, therefor I think that, even for the radio emission, the long-term variability will be dominated by changes in the $\dot{M}$ and v_∞. But you are right, the ionization fronts will dominate the radio variability on shorter time scales of days to months.

Smith: If a slightly faster wind is overtaking a slow wind, and the flow time scale is comparable to the variability time scale, you may expect hydrodynamic instabilities to develop in the slower shell that may induce large scale clump formation. Have you considered this?

Groh: No. Right now I only consider changes in the velocity law and density structure as a function of time. The faster wind will only overtake the slow wind during minimum, and for those epochs I use lines formed in the inner wind as diagnostics for the stellar parameters. As the interaction between fast and slow wind will produce a non-monotonic velocity field, I cannot deal with that in the radiative transfer at the moment.

Clumping in Hot Star Winds
W.-R. Hamann, A. Feldmeier & L.M. Oskinova, eds.
Potsdam: Univ.-Verl., 2008
URN: http://nbn-resolving.de/urn:nbn:de:kobv:517-opus-13981

Structure in the fast wind of NGC6543

R.K. Prinja[1], S.E. Hodges[1], D.L. Massa[2], A.W. Fullerton[3] & A.W. Burnley[1]
[1] *University College London, UK*
[2] *SGT, Inc., NASA Goddard Space Flight Center, USA*
[3] *Space Telescope Science Institute, USA*

We exploit time-series *FUSE* spectroscopy to *uniquely* probe spatial structure and clumping in the fast wind of the central star of the H-rich planetary nebula NGC 6543 (HD 164963). Episodic and recurrent optical depth enhancements are discovered in the Pv absorption troughs, with some evidence for a ~ 0.17-day modulation time-scale. The characteristics of these features are essentially identical to the 'discrete absorption components' (DACs) commonly seen in the UV lines of massive OB stars, suggesting the temporal structures seen in NGC 6543 likely have a physical origin that is similar to that operating in massive, luminous stars. The mechanism for forming coherent perturbations in the outflows is therefore apparently operating equally in the radiation-pressure-driven winds of widely differing momenta ($\dot{M}v_\infty R_\star^{0.5}$) and flow times, as represented by OB stars and CSPN.

1 Introduction

The fast winds of CSPN provide a probe of the *current* mass-loss, and represent a valuable setting for the study of radiative and mechanical interactions between stars and their environments. An improved understanding of variability and structure in the fast winds of CSPN is important since (i) spatial structure and clumping can modify how the supersonic outflow interacts with the nebular material, (ii) substantial clumping can impose downward revisions to estimates of the mass-loss rates from the central stars, (iii) the source of the X-rays from the central star vicinity remains uncertain, and one possible origin would be the presence of shock-heated gas arising from instabilities in a variable fast wind (e.g. Guerrero et al. 2001; Akashi, Soker & Behar, 2006).

To date, studies of variability in PN fast winds have primarily relied on (limited) multiple UV spectra obtained with the *IUE* satellite (e.g. Patriarchi & Perinotto, 1997). Generally however the detection of wind line variability with *IUE* (or *HST*) was extremely difficult since the only UV resonance lines accessible are strongly saturated, thus masking all changes except at the extreme violet edges of the line profiles. We have therefore embarked on a new project to directly probe variability in the fast winds of CSPN by exploiting *FUSE* ($\lambda\lambda$905 to 1187 Å) time-series observations. *FUSE* can uniquely deliver the requisite high signal-to-noise data in short integration times, while also potentially providing access to *unsaturated* resonance lines.

We present here a summary of our study of structure and variability in the fast wind of the central star of the planetary nebula NGC 6543 (HD 164963; BD $+66^o$ 1066). The target has a complex nebula (Balick 2004), and exhibits X-ray emission which is consistent with a point source at the central star and diffuse emission from the within the hot central cavity of the nebula (Chu et al. 2001). Key adopted parameters for the central star in NGC 6543 are $R_\star$ = 0.6R$\odot$, $T_{\rm eff}$ = 63000K, mass-loss rate $\sim 1{\times}10^{-7}$ M$\odot$ yr^{-1} (Georgiev et al. 2006), and we estimate $v_\infty \sim 1400$ km s^{-1} (and a wind flushing time of $\sim$ 45 mins for a 'β=1'-type velocity law).

1.1 FUSE dataset

The data for this investigation were secured between 2007 January 13 to 16 (Program F034; P.I. – D.L. Massa). The observations were obtained through the MDRS ($4" \times 20"$) aperture, spanning a total wavelength range of 905 to 1187 Å at a spectral resolution of ~ 15 km s^{-1}, with individual integration times in HIST mode of ~ 10 minutes. The primary time-series discussed below are 59 spectra (processed through CalFUSE version 3.1.8) in the LiF2 channel (segment A; $\lambda\lambda$1086 to 1182 Å) which covers the strategic (unsaturated) P Cygni line of Pv $\lambda\lambda$1117.98, 1128.01.

Unambiguous flux changes are evident in the absorption trough of Pv at ~ 10 to 20% of the continuum level, spanning a range of ~ -500 to -1300 km s^{-1}. The Svi $\lambda\lambda$933.38, 944.52 and Ovi $\lambda\lambda$1031.92, 1037.62 P Cygni lines are saturated, and the weaker lines of excited Niv λ955.34 and Ciii λ1175.67 do not reveal any evidence for variability.

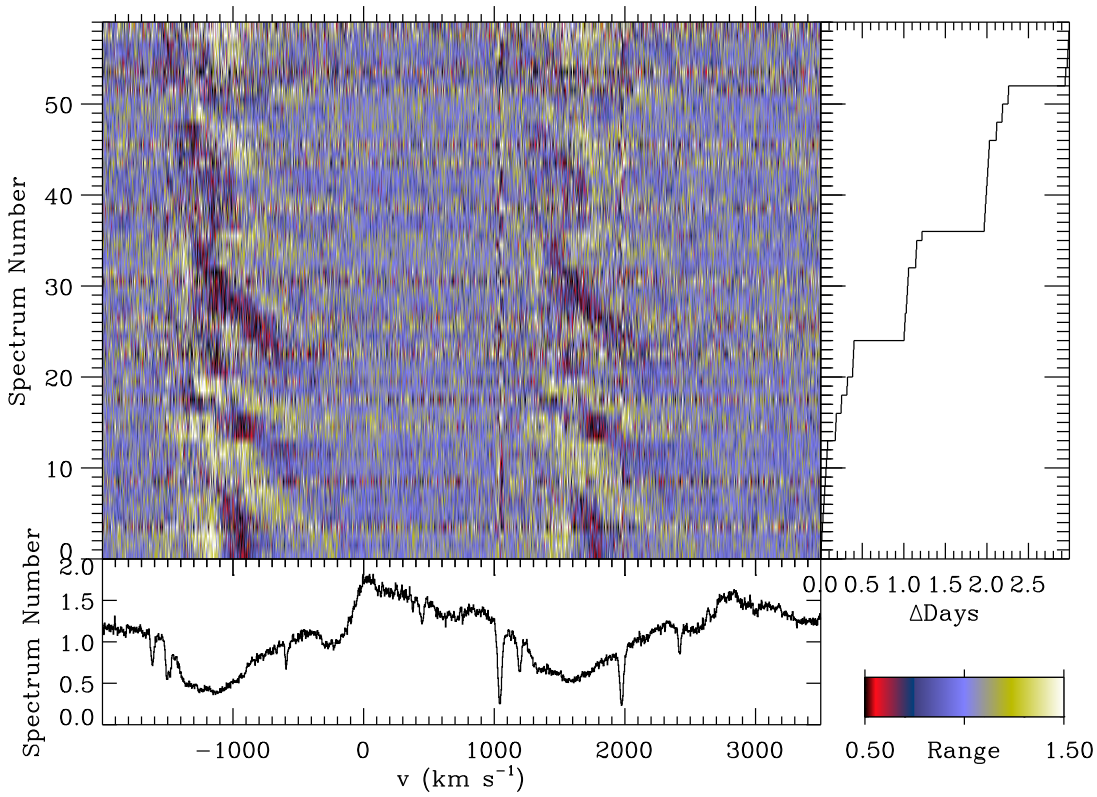

Figure 1: Dynamic spectrum representations of *organised*, hourly variability in Pv $\lambda\lambda$1118,1128. The ordinate is the sequential spectrum number, and the panel on its right is a temporal plot showing the relative time of each exposure.

2 Discrete Absorption Components

Greyscale representations of the variability evident in the Pv doublet are displayed in Figure 1. The images reveal clear evidence for systematic and organised line profiles changes. Specifically, localised (in velocity) absorption enhancements are seen migrating blueward from ~ -400 to ~ -1000 km s^{-1}. We identify at least 4 separate episodes of recurring features. The characteristics in Fig. 1 are essentially identical to the 'discrete absorption components' (DACs) commonly seen in UV resonance lines formed in the radiation-pressure-driven winds of massive OB stars (e.g. Kaper et al. 1996; Prinja, Massa & Fullerton, 2002). We measure (linear) accelerations for the DACs of between 3×10^{-2} km s^{-2} to 8×10^{-2} km s^{-2}. The values for NGC 6543 are up to a factor of 10 faster than typical acceleration rates measured for migrating features in OB star winds. Note, however, that the characteristic radial flow time of the wind (which scales as $\sim R_\star/v_\infty$) in NGC 6543 is only $\sim$ 5 minutes, compared to $\sim$ hours for O stars. The time-scales associated with the DACs in NGC 6543 are therefore significantly greater than the wind flushing time over the line formation region, which suggests that it is very unlikely the wind structures in the PN central star are due to processes entirely intrinsic to the fast wind. The DACs cannot, for example, be due to mass-conserved shells or blobs 'riding' with the outflow from the star. The empirical evidence provided here suggests that the physical mechanism for initiating wind structure in the fast wind of NGC 6543 may be the same as that operating in massive, luminous stars.

A periodogram analysis was carried out to search for evidence of repetitive or cyclic properties in the Pv line profile changes. The basic Fourier method employed uses the iterative CLEAN algorithm (Roberts, Lehár & Dreher 1987) to deconvolve the features of the window function from the discrete Fourier transform. We identify as potentially interesting the main power peak in Pv at $\sim$

5.85 ± 0.5days^{-1}, corresponding to a period of ∼ 0.17 day. The individual spectra normalised to the mean are shown in Fig. 2 phased on the 0.17 day period. The diagnostic PV data do clearly show some coherency on this modulation time-scale. The modulation is represented by the occurrence of two sequential episodes of migrating structures in the wind. (Recall that the total length of the *FUSE* time-series combined here is ∼ 3 days, and therefore spans several 'cycles'.)

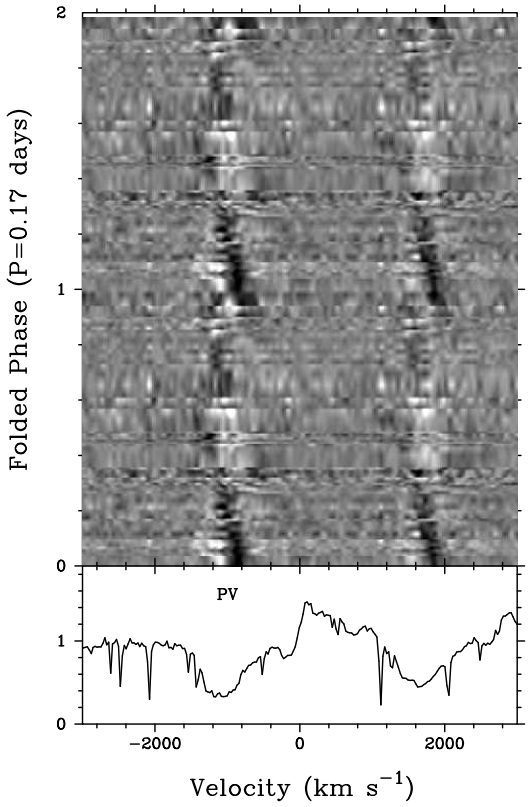

Figure 2: Individual PV spectra are shown phased over two cycles on a period of 0.17 days; a clearly coherent behaviour is evident.

3 Concluding remarks

The suggestion of quasi-periodic wind variability in NGC 6543 may be evidence that the DACs are spectroscopic signatures of spatial structures in the fast wind that are causally connected to stellar surface irregularities, such as pulsation or magnetic fields. (Unfortunately the rotation rate of the central star in NGC 6543 is not well constrained.) For example, according to the scenario for the formation of co-rotating interaction regions (CIRs; e.g. Cranmer & Owocki 1996), the photospheric inhomogeneities cause the wind from different longitudinal sectors on the stellar surface to emerge with different densities and/or velocities. The consequence is to form different adjacent streams, that meet to create spiral-shaped CIRs. Key observational properties of the DACs can be matched with this model, with variable optical depth enhancements arising from the combination of a plateau in the radial velocity as well as a density perturbation.

Our results provide the constraint that the mechanism for forming coherent perturbations in the outflows is apparently operating equally in the radiation-pressure-driven winds of widely differing momenta ($\dot{M}v_\infty R_\star^{0.5}$) and flow times, as represented by OB stars and CSPN. UV (and optical) evidence for spatial structure and clumping in the fast winds of CSPN may ultimately imply downward revisions in the central star mass-loss rates, and alter the dynamics of the hot central cavity excavated by the fast wind, thus modifying its interaction with the surrounding nebula, including contributions to the X-ray emission.

(A more complete version of this paper, including results on spectral signatures of clumping based on CMFGEN models, has been submitted to MNRAS.)

References

Akashi, M., Soker, N., Behar, E. 2006, MNRAS, 368, 1706

Balick, B., 2004, AJ, 127, 2262

Chu, Y.-H., Guerrero, M.A., Gruendl, R.A., Williams, R.M., Kaler, J.B. 2001, ApJ, 553, 55

Cranmer, S.R., Owocki, S.P. 1996, ApJ, 462, 469

Georgiev, L.N., Hillier, D.J., Richer, M.G., Arrieta, A. 2006, IAU Symp. 234, 'Planetary Nebulae in our Galaxy and Beyond', eds. M.J. Barlow & R.H. Mendez., CUP, 119

Guerrero, M.A., Chu, Y.-H., Gruendl, R.A., Williams, R.M., Kaler, J.B. 2001, ApJ, 553, L55

Guerrero, M.A., Chu, Y.-H., Gruendl, R.A., Williams, R.M., Kaler, J.B. 2001, ApJ, 553, L55

Kaper, L. et al. 1996, A&AS, 116, 257

Patriarchi, P., Perinotto, M. 1997, A&AS, 126, 385

Prinja, R.K., Massa, D., Fullerton, A.W. 2002, A&A, 388, 587

Roberts, D.H., Lehár, J., Dreher, J.W. 1987, AJ, 93, 968

Clumping in Hot Star Winds
W.-R. Hamann, A. Feldmeier & L.M. Oskinova, eds.
Potsdam: Univ.-Verl., 2008
URN: http://nbn-resolving.de/urn:nbn:de:kobv:517-opus-13981

Clumping in the winds of O-type CSPNs

M. A. Urbaneja[1], R.-P. Kudritzki[1] & J. Puls[2]
[1] *University of Hawaii Institute for Astronomy, USA*
[2] *Universitäts-Sternwarte München, Germany*

Recent studies of massive O-type stars present clear evidences of inhomogeneous and clumped winds. O-type (H-rich) central stars of planetary nebulae (CSPNs) are in some ways the low mass–low luminosity analogous of those massive stars. In this contribution, we present preliminary results of our on-going multi-wavelength (FUV, UV and optical) study of the winds of Galactic CSPNs. Particular emphasis will be given to the clumping factors derived by means of optical lines (Hα and HeII 4686) and "classic" FUV (and UV) lines.

1 Introduction

H-rich O-type central stars of planetary nebulae (CSPNs) are "downscaled" versions of massive O-type stars, at least with respect to their physical properties as derived from spectroscopic studies (see Kudritzki et al. 2006 and references therein). In the canonical picture of a planetary nebula, the fast wind coming from the central star is extremely important for the structure of the nebula, as well as for the subsequent evolution of the star itself. So far, the analysis of these winds have been based on sophisticated non-LTE models under the consideration of homogeneous winds (Kudritzki el al. 1997; Pauldrach et al. 2004). However, this assumption seems to be unrealistic, as could be suspected from recent studies of the winds of their massive (false) relatives (see A. Fullerton, J.C. Bouret, J. Puls or F. Najarro, this volume). Moreover, independent hints of the presence of inhomogeneous winds have been presented for the Of-type CSPN NGC 6543: first, the detection of X-ray emission coming from the central star (Chu et al. 2001), that could be only explained as the result of the presence of shocks in the stellar wind (in analogy with massive O-stars) and, secondly, the detection of discrete absorption components in FUV/UV profiles (see the contribution of R. Prinja in these proceedings).

Recently, we have re-analyzed the optical spectra of a sample of CSPNs by means of NLTE models atmospheres with inhomogeneous winds (Kudritzki et al. 2006), computed with FASTWIND (Puls et al. 2005). It was possible to estimate wind clumping properties for some of the targets in the sample, using a novel technique based on the relative strength of Hα and HeII 4686 (see below). In order to check the results, and also to extend the analysis to other O-type CSPNs, we started a program aimed at the quantitative analysis of their UV spectra. In the following, we present (some) results of this complementary FUV/UV study on the winds of these objects.

2 Spectroscopy of CSPNs

Due to space constraints, we will not discuss the methodology followed in the analysis. The reader is referred to any of the many works published in recent years on quantitative spectroscopy techniques of massive stars. We will just provide some detail concerning clumping assumptions.

Regarding the model atmosphere codes, we used FASTWIND for the optical analysis, and CMFGEN (Hillier & Miller 1998) for the FUV/UV analysis. Clumping is treated presently in both codes under the *micro-clumping* formalism, i.e. *small-scale* density inhomogeneities in the wind redistribute the matter into clumps of enhanced density, embedded in an almost void (inter-clump) medium. Clumping is then characterized in the models by the *clumping factor* $f_{\rm cl}$, which represents the overdensity in the clumps with respect to the smooth medium $\rho_{\rm cl} = f_{\rm cl}\,\rho$. Under the current assumptions, $f_{\rm cl}$ corresponds to the inverse of the volume filling factor.

2.1 Optical analysis

The analysis of the optical spectra has been presented by Kudritzki et al. (2006). With regard to the distribution of the clumping, we assumed a constant clumping factor $f_{\rm cl}$ for velocities larger than twice the characteristic isothermal speed of sound, and unity for lower velocities. This clumping distribution is basically equivalent to an exponential law rising (almost) at the base of the wind.

Below Teff$\sim$37–36 kK (depending on the gravity) He II becomes the dominant ionization stage, thus the lines' optical depths present a linear dependence with density. On the other hand, neutral hydrogen is a trace ion at these Teffs, hence its lines depend on ρ^2. Therefore, it would be possible to estimate wind clumping factors by comparing the relative strenthgs of H and HeII lines with significant wind contribution. In the optical domain, Hα and

HeII 4686 are the lines of choice. Using this concept, Kudritzki et al. (2006) estimated the clumping factors for three CSPNs, ranging from 1 to 50 (see Tab. 1). This same technique has been recently applied by Hultzsch et al. (2007) to a sample of CSPNs in the Galactic Bulge.

Table 1: Parameters derived from the analysis of the optical spectra.

ID	Teff (kK)	log g (dex)	$f_{\rm cl}$	$\log \dot{M}$ ($M_\odot\,{\rm yr}^{-1}$)
IC 418	36	3.2	50	-7.43
Hen 2-108	34	3.4	1	-7.46
Hen 2-131	32	3.2	8	-6.88

2.2 FUV/UV analysis

It is a well known fact that there are differences regarding the derived parameters when analyzing optical or UV spectra. These differences are most likely linked to subtle differences in the preferred codes used in each spectral windows. Seeking for consistency, we used our FASTWIND models (the atmospheric structure, both pseudo-static photosphere and wind) as an input for CMFGEN. In such way, the density distribution used to synthesize the FUV/UV spectrum is the same that was used for the optical analysis. Nevertheless, some minor corrections have to be applied to the parameters derived from the optical analysis. In particular, and for the domain explored here, the SiIV 1063–74, CIII 1176 and SiIV 1394–1402 Å lines present a high sensitivity to Teff. In general, these lines require a reduction in Teff of ∼1–1.5 kK, within the uncertainties of the analysis.

Concerning clumping, we used the standard implementation in CMFGEN, an exponential law. As previously quoted, this is consistent with the constant clumping form used in the optical analysis, provided that the constant value is reached soon enough (fast rising). Only in a very limited number of tests we have tried a distribution with clumping vanishing ($f_{\rm cl}$ becoming unity) in the outer parts of the wind (F. Najarro, this volume).

We display in Fig. 1 line profiles for two different cases, IC 418, for which we could infer clumping from the optical analysis, and IC 4593, a CSPN too hot to use the Hα–HeII 4686 method. For each star, three different lines are presented: the bluest component of the PV 1118–28 doublet, HeII 1640 and NIV 1719. In the first case, these three lines change strongly when considering inhomogeneous wind models. For the second star, the HeII line does not change at all: at this high Teff, HeIII is the dominant ionization stage, and hence HeII lines behave as Hα with respect to wind clumping.

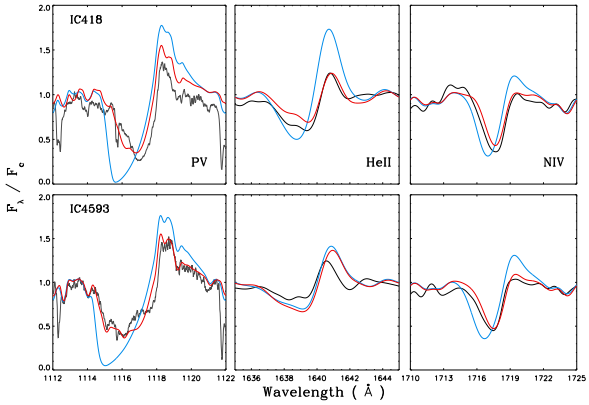

Figure 1: Observed (black) spectral lines compared with theoretical profiles for homogeneous (blue) and clumped (red) winds.

Other lines are also affected by clumping, such as SiVI 933–45 Å. To a lesser degree, and most likely as a consequence of an "indirect" effect (due to the reduced $\dot{M}$), photospheric lines (FeV and OIV) display variations in the sense that the fits are improved when (wind) clumping is considered.

All the CSPNs in our sample for which FUV data (either FUSE, COPERNICUS or TUES) are available present features that can be associated with the OVI 1032–38 Å lines. These *super-ionization* features (as well as NV 1238–42 Å) are related to X-rays, usually explained as produced by shocks in the winds. We have tried to model these features in some (few) cases, to investigate the sensitivity of the primary clumping diagnostics to the presence of X-rays. While we did not manage to produce completely satisfactory fits, these tests have shown that all the clumping indicators are insensitive to the presence of X-rays (note that present implementations of X-rays in model atmosphere codes are very crude).

3 Discussion

While we have results presently for a handful of objects, there are a number of conclusions that can be drawn from this preliminary work. First, it seems to be possible to achieve good fits to FUV/UV spectra with the parameters derived from the optical analysis (see Fig. 2). The ability of reproducing simultaneously ultraviolet and optical ranges increases our confidence on that the physics considered in the models is a fair representation of the true one (i.e. we are not missing any important contribution). Secondly, FUV/UV clumping sensitive lines support $f_{\rm cl}$ values derived using Hα–HeII 4686 for

the coolest objects. There is not an apparent reason why this method should not work also for massive O-stars in the appropriated Teff–log g domain. Thirdly, and most important, CSPNs with very similar fundamental parameters have substantial differences in their clumping properties. To the best of our knowledge, this has not been found (yet) in the case of massive O-stars. Should this be confirmed, it would have tremendous implications for (theoretical) predictions of CSPNs mass-loss rates.

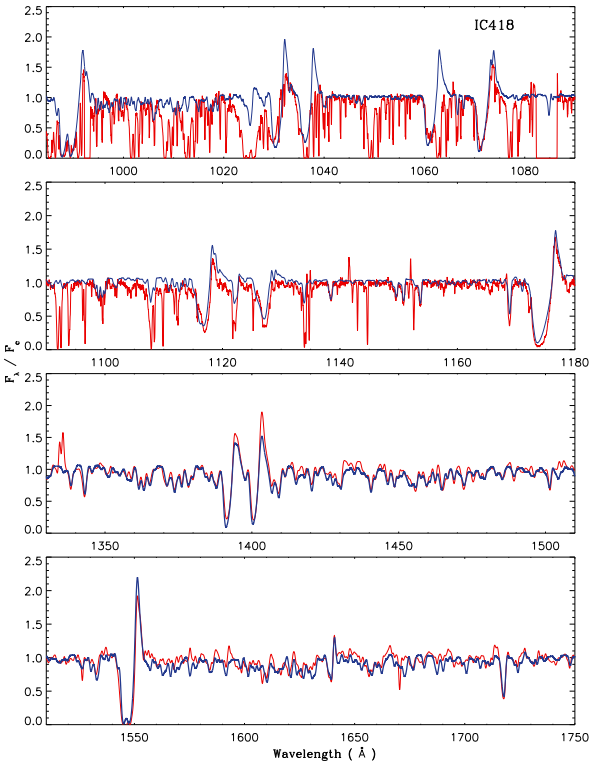

Figure 2: IC 418 FUSE and IUE data (red). A model including clumping ($f_{\rm cl} = 50$) and X-rays ($\log L_{\rm x}/L_{\odot} = -4.27$) is shown in blue. Note the heavy contamination of FUSE ranges by the medium surrounding the star.

There are a number of open issues related to the comparison of the derived properties with the corresponding expected theoretical values, from the point of view of post-AGB evolution as well as from the radiatively driven wind (RDW) theory. First, for some of the objects we still derive uncomfortably high spectroscopic masses. Since these objects are evolving directly to the WD phase, CSPN masses above $\sim$0.8–0.9 $M_{\odot}$ (as derived for IC 418, Tc 1 and NGC 2392) seem unrealistic (WD mass distribution peaks around $\sim$0.6 $M_{\odot}$). Secondly, the ratios of the measured wind terminal velocities to the derived escape velocities are in general higher than the values expected from the RDW theory. Increasing the masses will bring these ratios closer to the expected values, but this would badly affect the comparison with post-AGB evolutionary models, increasing the number of objects with extremely high spectroscopic mass.

At present, it is not clear where the solution to these two problems resides. Is there any important ingredient missing in our model atmospheres? As previously quoted, our ability to reproduce a wide spectral range (FUV/UV/optical) seems to argue against this possibility, although it cannot be completely ruled out. On the other hand, wind hydrodynamics are based on the assumption of smooth winds. Theoretical predictions have to be checked with the inclusion of clumped winds (deKoter and Kriticka, this volume).

References

Chu, Y.-H., Guerrero, M.A., Gruendl, R. A., Williams, R.M. & Kaler, J.B. 2001, ApJ, 553, L69

Hillier, D.J. & Miller, D.L. 1998, ApJ, 496, 407

Hultzsch, P.J.N., Puls, J., Méndez, R.H., Pauldrach, A.W.A., Kudritzki, R.-P., Hoffmann, T.L. & McCarthy, J.K. 2007, A&A, 467, 1253

Kudritzki, R.-P., Méndez, R.H., Puls, J. & McCarthy, J.K. 1997, IAUS, 180, 64

Kudritzki, R.-P., Urbaneja, M.A. & Puls, J. 2006, IAUS, 234, 119

Pauldrach, A.W.A, Hoffmann, T.L. & Méndez, R.H. 2004, A&A, 419, 1111

Puls, J., Urbaneja, M.A., Venero, R., Repolust, T., Springmann, U., Jokuthy, A. & Mokiem, M.R. 2005, A&A, 435, 669

Najarro: In your He II 4686 plot did you try a higher value for the velocity at which clumping starts? The line should really react to that value.

Urbaneja: Not yet, but we will do a detailed analysis as I have shown for IC418, for as many objects in the sample as possible.

Hillier: Just a quick comment regarding the exponential formula for the variations of the volume filling factor with velocity (radius). The formula was based on very little physics. It was simply designed to go from $f = 1$ in the photosphere to $f = \text{const}$ in the wind in a smooth fashion with a minimal number of parameters.

Urbaneja: In fact, we used a constant clumping starting at twice the speed of sound when doing the analysis of the optical spectra with FASTWIND. Both clumping laws (constant and exponential) produce basically the same profiles. We have also explored models with fading clumping law, showing that for FUV, UV and optical it makes (basically) no difference.

Cassinelli: Planetary Nebulae have very odd shapes and some axial symmetry; so I ask if the rotation rate of the stars is known or if you have accounted for rotation.

Urbaneja: The objects in our sample have relatively low projected rotational velocity, around 80 km/s as derived from UV photospheric lines. As for the shapes, their PNs are classified as round (mostly).

Puls: I just want to stress (once more), that here we have the situation that two similar objects have completely different clumping properties. This "fact", to my knowledge, has never been seen in "normal" O stars.

Urbaneja: This is something to be carefully considered. Perhaps there is something missing here. However, if this result is confirmed, it would mean that there is not a unique relationship between the fundamental parameters ($T_{\rm eff}$, luminosity) and the clumping (wind) properties.

Kubat: I do not completely understand why you were not satisfied by stellar masses around the Chandrasekhar limit. Central stars are not white dwarfs and their gravity is about 4 orders of magnitude lower than that of white dwarfs.

Urbaneja: The mass distribution function of white dwarfs presents a narrow peak around $0.6 - 0.7 M_{\odot}$. Our objects are supposed to be evolving very quickly to the white dwarfs phase. Therefore, these objects (H-rich CSPNs) for which we derived masses are close to the Chandrasekhar limit and should get rid of around half of their masses with no wind in no time. That is a bit unresting.

Clumping in Hot Star Winds
W.-R. Hamann, A. Feldmeier & L.M. Oskinova, eds.
Potsdam: Univ.-Verl., 2008
URN: http://nbn-resolving.de/urn:nbn:de:kobv:517-opus-13981

Discussion: Spectroscopy and Mass-Loss Diagnostics

Moderator: Derck Massa

Cassinelli: Planetary nebulae central stars have fast and fairly high mass loss rates. These winds collide with the surrounding slower outflow. So there should be a very large X-ray flux from the PN. However, the X-rays from the interaction are down by a factor of 100 from theoretical predictions. A solution to this is to have the winds collide with a clumpy medium and in the interaction the clumps become dispersed and "mass-load" the wind, thereby making the "wind" slower and reducing the X-ray production ability. So this is one effect of clumps. Another is that such disposal of clumps could increase the density far out in the flow and this could be the cause of the extra radio flux that several speakers mentioned.

Gull: We have heard descriptions today of clumping, and observations of clumping events that occur on a time scale of hours and days. Microclumping, macroclumping, short- and long-lasting clumps. Just what is an appropriate definition of a clump?

Cohen: Porosity, which requires optically thick clumps, implies spatially large clumps, so Alex's "macroclumping".

Ignace: I was impressed by Tony Moffat's example of using $\dot{P}$ in a binary to get a quite secure $\dot{M}$. It seems important to calibrate our different perspectives and approaches to clumping against mass loss values that are robust and independent of micro/macroclumping and porosity. How hard would it be to increase this kind of sample? Are there more such robust methods?

Moffat: V444 Cyg is unique. There is no other system to get a dynamical $\dot{M}$ with such high precision.

Leutenegger: Porosity depends on wavelength: a wind may be porous at one wavelength and "effectively smooth" at another. Furthermore, continuum opacity is only affected by geometrical clumping, while line opacity depends also on the velocity dispersion within the clumps and the velocity distribution of the clumps.

Owocki: I think it is important to distinguish between large-scale structure that might be induced by some sort of surface features and so have a certain coherence like rotational modulation, and the small-scale stochastic clumping from turbulence. This issue of scale is also relevant for distinguishing between porosity and the traditional clumping volume filling factor f (defined as the root of the ratio of the square of the mean density divided by the mean of the density squared). The latter is the factor relevant for correcting the mass loss inferred from, e.g. density-squared diagnostics.
But porosity can effect even single-density diagnostics like bound-free absorption of X-rays.The key, however, is that individual clumps become optically thick, so that some material in the clump can effectively "hide" behind other material at the front of the clump, and so effectively reduce its overall effect in absorption. But for this you require a large "porosity length" h, defined by the ratio of the clump size to the volume filling factor. In fact, among other things, this porosity length can be thought of as the mean free path between optically thick clumps, and so to make a given medium effectively more transparent, it has to be bigger than the characteristic length scale of the medium. For a wind, that would typically be the local radius of the formation of whatever diagnostic you are looking at. Note, however, that it does *not* require that the individual clumps themselves be necessarily large, and for that reason I think a term like "macroclumping" is a bit misleading. But if the clumps are small, then they must also have a very small volume filling factor to make the medium porous.

Gull: Given the different definitions of clumps we hear, can we bound the clumping definition? As an example, in the large clump limit, do clumps seen in PNs or ejecta come from clumping or major ejection events?

Smith: I would like to switch gears a bit and ask about the space in between the clumps. I mean, we talk about these clumping factors as if we have blobs at some density separated by a vacuum. Of course the densest region will tend to dominate the emission because of ρ^2 effects, but if clumping factors are only ~ 4 or 5, then I wonder if the interclump medium may contribute significantly to the total mass loss even if we cannot see it. Are there observational diagnostics of the interclump medium? How much does it matter?

Cohen: From Vela X-1 ASCA (Sako et al 1999), you see spectral signatures from both the clumped and interclump medium.

Owocki: Well, one point here is that a simple picture of a medium with clumps of just a single size

separated by a completely empty medium is surely too simple. More likely the clumped structure contains a range of scales and compression factors, with perhaps also a floor level for the density even between the denser clumps. Such structure can be modeled phenomenologically using for example a "power-law porosity" approach, but ultimately one needs a dynamical model to predict the true nature of such structure.

Hamann: Sure, $\langle\rho^2\rangle/\langle\rho\rangle^2$ is a clear definition of the clumping density contrast. However, for the spectrum formation the actual distribution of density also matters, because high density enhances recombination. In the process of fitting WR spectra, we often encounter stars which show three subsequent ionization stages, e.g. N III, N IV and N V. With our models, it is sometimes impossible to produce all three stages with the observed line strength. I would attribute this to the scatter or stratification of densities in the clumps, which is neglected when assuming a fixed density contrast.

Cohen: Can we use the ISM as an analogy? The thermal pressure keeps clouds and intercloud medium separate. Maybe there is a magnetic field at cloud surfaces. If we could fly into an O star wind, what would the boundaries of clumps look like? Would they be sharp?

Smith: I think the clumps and cometary structures that you see in planetary nebulae like the Helix or the Ring Nebula are very different from the clumps in O star winds. Instead of forming directly out of an instability in the driven wind, they probably form as a result of the strong interaction of two winds, i.e. Rayleigh-Taylor-like instabilities as a hot fast wind overtakes a slow wind.

Gull: The ejecta around η Car show very well-defined clumps, bullets and diffuse structures. However, they all appear to have come from the same nitrogen-enriched source. Indeed the 513 km/s Homunculus contains molecules mixed at the same velocity. What feedback mechanism makes these single shells and otherwise clumps?

Sonneborn: The observed structure in supernova remnants is the result of Rayleigh-Taylor instabilities in the expanding SN ejecta (blast wave) with circumstellar and/or interstellar media. This is primarily a ballistic process, not a radiatively driven one as in O stars.

Smith: With respect to the velocity-dependent radiative driving leading to clumping in O stars, it may (or may not) be worth mentioning that we know from observations (like OH, H_2O and SiO masers) that cool supergiants have winds that are highly clumped, yet in those objects the driving force is not velocity-dependent (radiation pressure on dust). It may be interesting to consider if there is anything to be learned from (or applied to) those winds.

Vink: The central question is whether the mass loss rates are down and by what factor. But before we "vote" on this, we should probably first define what we compare it to: the ρ^2 diagnostics (Hα and radio) or the smooth radiation-driven wind models, as these two values are discrepant by a factor of two (with the theory underpredicting the unclumped ρ^2 data).

Runacres: Even though the radiative acceleration is negligible beyond $30\,R_*$, the wind can remain clumped out to very large distances ($\gtrsim 1000\,R_*$). The main reason is that the clumps have different speeds and therefore collide. The collision produces a dense clump and enhances the clumping factor. This partly counteracts the pressure-expansion of the clumps.

Feldmeier: One should also keep in mind that the extent of clumping may depend on the photospheric seed perturbations for the line-driven instability. Since the line-drag effect of Lucy causes the flow to be marginally stable directly above the photosphere, stochastic perturbations with quite a substantial velocity dispersion of, say, one third of the sound speed are required in the photosphere, in order to produce cloud-cloud collisions in the wind that can account for the observed X-ray emission, and that can counteract the pressure expansion at large radii, as Marc (Runacres) just noted.

Moffat: We should not be loath to make analogies of clumping in winds with the ISM, where we resolve the matter and can describe its nature. In winds you do have the inconvenience of having to deal with spherical geometry, but in Moffat & Robert (1994) we calculated the filling factor for a hypothetical wind with similar scaling laws as in the ISM. We found f values giving $\dot{M}$ corrections of $3-4$ for very reasonable ratios of the largest and smallest scales.

Feldmeier: We must clearly distinguish between micro- and macroturbulence, i.e. whether the photon mean free path is longer or shorter than the length-scale of the clumps.

Spectral modeling

Chair: R. Ignace

Clumping in Hot Star Winds
W.-R. Hamann, A. Feldmeier & L.M. Oskinova, eds.
Potsdam: Univ.-Verl., 2008
URN: http://nbn-resolving.de/urn:nbn:de:kobv:517-opus-13981

Spectrum formation in clumpy stellar winds

W.-R. Hamann, L.M. Oskinova & A. Feldmeier
Universität Potsdam, Germany

Modeling expanding atmospheres is a difficult task because of the extreme non-LTE situation, the need to account for complex model atoms, especially for the iron-group elements with their millions of lines, and because of the supersonic expansion. Adequate codes have been developed e.g. by Hillier (CMFGEN), the Munich group (Puls, Pauldrach), and in Potsdam (PoWR code, Hamann et al.). While early work was based on the assumption of a smooth and homogeneous spherical stellar wind, the need to account for clumping became obvious about ten years ago. A relatively simple first-order clumping correction was readily implemented into the model codes. However, its simplifying assumptions are severe. Most importantly, the clumps are taken to be optically thin at all frequencies ("microclumping"). We discuss the consequences of this approximation and describe an approach to account for optically thick clumps ("macroclumping"). First results demonstrate that macroclumping can generally reduce the strength of spectral features, depending on their optical thickness. The recently reported discrepancy between the Hα diagnostic and the P V resonance lines in O star spectra can be resolved without decreasing the mass-loss rates, when macroclumping is taken into account.

1 Modeling hot-star winds

Adequate stellar atmosphere models are prerequisite to analyze the spectra of early-type stars and to determine their mass-loss rate. The model calculations must account for the supersonic expansion, and for the strong departure from Local Thermodynamical Equilibrium (LTE).

Non-LTE modeling means to solve consistently two sets of equations. For a given source function that depends on the population numbers, $S(n)$, the radiation field J is obtained by solving the transfer equation, symbolically written as a linear mapping $\mathbf{\Lambda}$:

$$\mathbf{J} = \mathbf{\Lambda}\,\mathbf{S}(n)\ . \tag{1}$$

The second set of equations describes the statistical equilibrium between the level populations. These equations are linear in n and must be fulfilled at each spatial point:

$$\vec{n}\cdot\mathbf{P}(\mathbf{J}) = [0,...,0,1] \tag{2}$$

The transition probabilities in the matrix P contain frequency integrals over the radiation field,

$$R_{lu} = \int \frac{4\pi}{h\nu}\ \sigma_{lu}(\nu)\ J_\nu\ \mathrm{d}\nu\ , \tag{3}$$

thus closing the circle of mutual dependence between radiation field and population numbers. The radiation transfer couples in space, and the radiative transition rates couple in frequency; a solution of the full 3-D problem is therefore extremely demanding, especially since complex model atoms and millions of spectral lines must be taken into account for realistic models. For the formal solution of the radiative transfer in multi-dimensional geometries, short-characteristic methods are most promising.

The problem becomes even more complex, when time-dependent hydrodynamic modeling is required. The 3-dimensional density and velocity structure must be obtained from solving the hydrodynamic equations, while the full 3-D radiation transfer provides the radiation pressure.

This situation can only be handled with drastical simplifications. For instance, one may reduce the full non-LTE problem to two atomic levels (cf. the Wind3D code: Lobel, these proceedings). The absorption of X-rays by wind clumps may be treated statistically (see Oskinova et al., these proceedings). For the line formation in turbulent media, analytic solutions have been developed by Gail et al. (1980).

In the following section we will describe the treatment of radiative transfer in the approximation of optically thin clumping, and in Sect. 3 we will present a new approach to line transfer with optically thick clumping.

2 Clumping in 1st approximation: "microclumping"

Clumping in first approximation is taken into account in all up-to-date stellar wind codes like CMFGEN, PoWR, or WMbasic. The assumption is that the clumps are smaller than the mean free path of the photons for all frequencies. Furthermore, it is assumed that inside the clumps the density is uniform, and enhanced by a factor D compared to a

smooth model with same mass-loss rate. The volume filling factor of the clumps is $f_V = D^{-1}$, because the interclump medium is assumed to be void.

Thanks to the latter assumption, the rate equations have to be solved only for the clump medium, where the density is $D\rho$ instead of ρ in the smooth case. In the equation of radiation transfer, we must replace the opacity $\kappa(\rho)$ and emissivity $\eta(\rho)$ by

$$\kappa_D = f_V\ \kappa_C(D\rho) \quad \text{and} \quad \eta_D = f_V\ \eta_C(D\rho), \qquad (4)$$

respectively. The filling factor f_V appears here, because statistically any given ray is for the fraction f_V of its path crossing clumps, and for the rest crossing the interclump void.

For processes which are *linear* in density, f_V and D cancel out in Eqs. 4. For processes scaling with the *square* of density, however, opacities and emissivities are effectively enhanced by the factor D.

Line absorption, for instance, scales linearly with ρ. In contrast, emission lines are typically formed in recombination cascades, and therefore ρ^2-dependent. In addition, strong emission lines show weak, extended line wings that are due to the frequency redistribution of line photons by electron scattering. (Because of their small mass, electrons have a high thermal speed, e.g. $v_{th} = 550\,\mathrm{km/s}$ for $T_e = 10\,\mathrm{kK}$.) The electron scattering opacity scales *linearly* with density.

Indeed, homogeneous wind models notoriously predict too strong electron scattering wings for strong WR emission lines (see Fig. 2). When increasing the clumping factor D, and reducing the mass-loss rate $\dot{M}$ such that $\dot{M}\sqrt{D}$ is preserved, the emission lines approximately keep their strength, but the electron-scattering wings are reduced. This effect can be used to determine the clumping factor D, as pointed out first by Hillier (1991).

For WR stars this method yields typical clumping factors D between 4 and 10 (e.g. Hamann & Koesterke 1998). For a few [WC]-type Central Stars, Todt et al. (these proceedings) find marginal evidence for the same effect. Unfortunately, the method is not applicable for O stars, since their spectra do not show suitable emission line wings. In this case, only the resonance line absorptions remain as a ρ-linear diagnostic, especially the unsaturated P V doublet (cf. Sect. 3.2).

Simplicity is the only justification for assuming a universal density contrast D everywhere in the wind. Puls et al. (2006 and these proceedings) compared ρ^2-diagnostics from different formation radii (Hα, IR and radio free-free continuum) for OB stars and determined the dependence of clumping on the radial coordinate, i.e. $D(r)$. For WN stars, Liermann et al. (these proceedings) compared the radio and line forming region. The agreement with *theoretical predictions* for $D(r)$ from HD modeling is not yet convincing (e.g. Runacres, these proceedings). Vice versa, the clumping stratification $D(r)$ strongly affects the HD models (Gräfener, these proceedings).

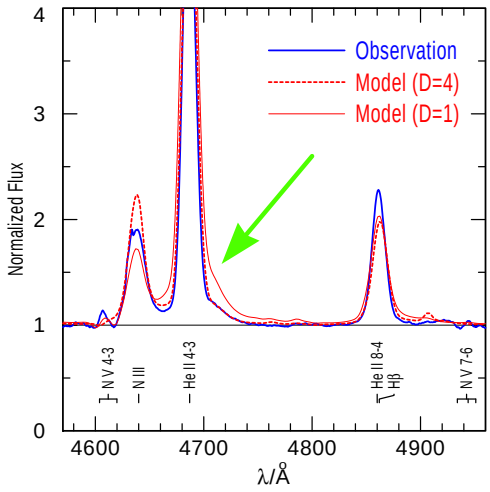

Figure 1: Estimating the microclumping density contrast from electron-scattering line wings, for the WN7 star LMC Brey 24. The observed wing of the He II 4686 line (plotted thick blue) is weaker than calculated with the homogeneous model (D=1, red thin), but perfectly matched by the clumped model with D=4 (red dashed).

3 Macroclumping

3.1 X-rays: continuous absorption

According to the widely accepted scenario, X-rays from hot-star winds are produced in shock-heated gas, while the bulk of the stellar wind is in cool clumps which absorb part of the X-rays before they can emerge. The X-rays are mainly emitted in spectral lines, while the absorption is continuous (K-shell photoionization). This decoupling of emission and absorption greatly facilitates a semi-empirical modeling.

Monte-Carlo calculations have been applied to model the emergent X-ray line profiles with randomly distributed line emitters and absorbing clumps (Oskinova et al. 2004, 2006).

Alternatively, one may introduce a statistical treatment that is based on the assumption that the emitting spots and the absorbing clumps are numerous (Feldmeier et al. 2003, Owocki & Cohen 2006). When there are n_C clumps per unit volume, and each clump is optically thick with a cross section σ_C, the effective opacity becomes

$$\kappa_{eff} = n_C\ \sigma_C \qquad (5)$$

in full analogy to the usual atomic opacity. If the clumps are not opaque, σ_C is their geometrical cross section diminished by the fraction of transmitted radiation.

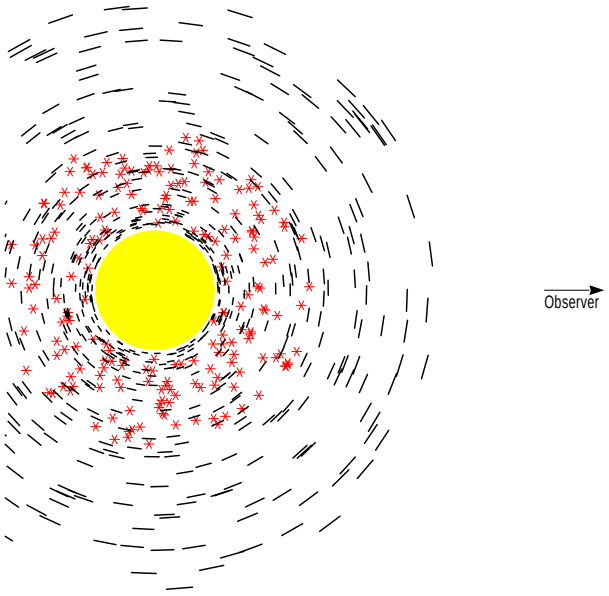

Figure 2: 'Shell fragment' model for the formation of X-ray line profiles (Oskinova et al. 2004). Line emission from randomly located spots (red asterisks) is absorbed by shell fragments of continuous opacity.

The Potsdam group (Feldmeier et al. 2003, Oskinova et al. 2004, 2006) found that the observed X-ray line profiles can be explained best if the "clumps" are assumed to have the shape of "pancakes" or "shell fragments" (see Fig. 2). This idea is also supported by the theoretical consideration that the forces which compress the clumps act mainly in radial direction. If clumps are anisotropic, their *projected* cross section must be inserted for $\sigma_{\rm C}$ in Eq. (5). This leads to a "venetian blind effect", where in the limit of entirely flat fragments the opacity scales proportional to $\mu = \cos\vartheta$ (Fig. 3). With the corresponding effective opacity becoming angle-dependent as $\kappa_{\rm eff} \propto \mu$, the optical depth increment for a ray of any impact parameter growth with the change of radius: $\mathrm{d}\tau \propto |\mathrm{d}r|$, in contrast to the isotropic case where $\mathrm{d}\tau = \kappa\, \mathrm{d}z$.

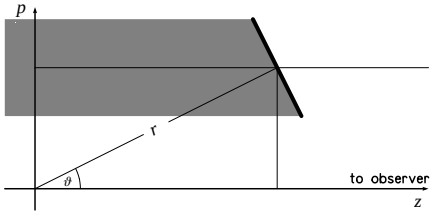

Figure 3: Venetian-blind effect from oriented absorbing slabs. The projected area, and thus the effective opacity, scales with $\cos\vartheta$.

3.2 Line transfer

The microclumping approximation holds when clumps are small compared to the mean free path of photons. Given the large atomic opacity in many spectral lines, this approximation is not generally justified. It has been relaxed in a recent paper (Oskinova et al. 2007) in favor of a statistical approach to macroclumping in the formal integral of the PoWR stellar-wind code.

It is again assumed that the matter density inside the clumps is enhanced by a factor D compared to a smooth model with the same mass-loss rate, while the interclump medium is void (clump volume filling factor $f_{\rm V} = D^{-1}$). For macroclumping, it is now adopted that the clumps have a uniform size with a linear diameter ℓ. Center-to-limb variation of ℓ across a clump is neglected. For this first study, clumps are assumed to be isotropic.

The clumps are statistically distributed with average separation L. Both $\ell(r)$ and $L(r)$ may vary with radial location and are related via the filling factor,

$$f_{\rm V} = \frac{\ell^3}{L^3} \quad \text{or} \quad D = \frac{L^3}{\ell^3}\ . \tag{6}$$

The optical depth across one clump of size ℓ is

$$\tau_{\rm C} = \kappa_{\rm C}\ \ell = \kappa_{\rm D}\ D\ \ell\ , \tag{7}$$

when $\kappa_{\rm C} = \kappa(D\rho)$ denotes the opacity of the clump material, and $\kappa_{\rm D} = f_{\rm V}\ \kappa_{\rm C}$ the mean opacity in the microclumping approximation (cf. Eq. 4). This can be expressed as

$$\tau_{\rm C} = \kappa_{\rm D}\ L^3/\ell^2 = \kappa_{\rm D}\ h \tag{8}$$

with the definition of the *porosity length* $h := L^3/\ell^2$ (Owocki et al. 2004). In terms of the average clump separation L, the clump optical thickness reads

$$\tau_{\rm C} = \kappa_{\rm D}\ D^{2/3}\ L \tag{9}$$

The effective absorption cross section of a single clump, $\sigma_{\rm C}$, is its geometrical cross section times the fraction of absorbed photons, i.e.

$$\sigma_{\rm C} = \ell^2\ \left(1 - e^{-\tau_{\rm C}}\right)\ . \tag{10}$$

As the number density of clumps is $n_{\rm C} = L^{-3}$, the effective opacity of the clumpy medium, $\kappa_{\rm eff} = n_{\rm C}\ \sigma_{\rm C}$, becomes

$$\kappa_{\rm eff} = \frac{\ell^2}{L^3}\ \left(1 - e^{-\tau_{\rm C}}\right) = h^{-1}\ \left(1 - e^{-\tau_{\rm C}}\right)\ . \tag{11}$$

As we have $\tau_{\rm C} = \kappa_{\rm D}\ h$, this is equivalent to

$$\kappa_{\rm eff} = \kappa_{\rm D}\ \frac{1 - e^{-\tau_{\rm C}}}{\tau_{\rm C}}\ . \tag{12}$$

For optically thin clumps ($\tau_{\rm C} \ll 1$) the microclumping approximation $\kappa_{\rm eff} = \kappa_{\rm D}$ is recovered. In

the limit of optically thick clumps ($\tau_{\rm C} \gg 1$) the effective opacity becomes $\kappa_{\rm eff} = h^{-1}$, i.e. the porosity length h has the meaning of the photon's mean free path. In this limit the effective opacity is reduced by a factor of $\tau_{\rm C}$ compared to the microclumping approximation.

In order to evaluate the general opacity reduction factor $(1 - e^{-\tau_{\rm C}})/\tau_{\rm C}$ with the help of Eq. (8), the porosity length $h(r)$ must be specified. Adopting that the clumping contrast D can be constrained otherwise, the remaining free parameter is the average clump separation $L(r)$.

For the radial dependence of $L(r)$ we assume that clumps are conserved entities and move radially with $v(r)$. Then the number density of clumps obeys an equation of continuity, $n_{\rm C} \propto (r^2\ v(r))^{-1}$. As the average separation of clumps is related to $n_{\rm C}$ by $L^3 = n_{\rm C}^{-1}$, the radial dependence of $L(r)$ becomes

$$L(r) = L_0 \left(r^2 \frac{v(r)}{v_\infty} \right)^{1/3} , \qquad (13)$$

where the free parameter L_0 describes the typical clump separation in units of the stellar radius.

The total number of clumps that are found at a given instant of time in the radial range between r_1 and r_2 is

$$N_{\rm C} = \int_{r_1}^{r_2} n_{\rm C}(r)\ 4\pi\ r^2\ {\rm d}r = \frac{4\pi}{L_0^3}\ (t_2 - t_1) , \qquad (14)$$

where $t_2 - t_1$ is the flight time between r_1 and r_2 in units of the dynamical time scale, R_*/v_∞. Considering e.g. the radial range from 1.05 to 10.0, and adopting a β=1 velocity law, the total number of clumps amounts to $N_{\rm C} = 178\ L_0^{-3}$.

Which choice of L_0 is realistic for hot-star winds? The 1-D hydrodynamic simulations by Feldmeier et al. (1997) indicate that one or few radial shells may be launched within one dynamical timescale, which implies that $L_0 \lesssim 1$ (in units of R_*). From *line profile variability* in WR stars, Lépine & Moffatt (1999) conclude that $\gtrsim 10^4$ clumps are generated per hour, which corresponds to $L_0 \approx 0.25$. Our fitting of X-ray line profiles (Oskinova et al. 2006) required $L_0 \lesssim 1$.

Now we consider specifically the case of spectral *line* formation, for which we have to address the issue of Doppler shifts. In our one-component model *the clumps are the wind*. Hence clumps as such move with the wind velocity field $v(r)$. In a supersonically expanding medium, rays of a given (observer's frame) frequency can only interact with clumps near the *surface of constant radial velocity* (CRVS). The line opacity of the other clumps is Doppler-shifted out of the resonance. Hence the porosity effect for lines is very pronounced, as illustrated in Fig. 4. Note that even if the "clumps" would have the shape of shell fragments with large cone angle, the CRVS would look porous.

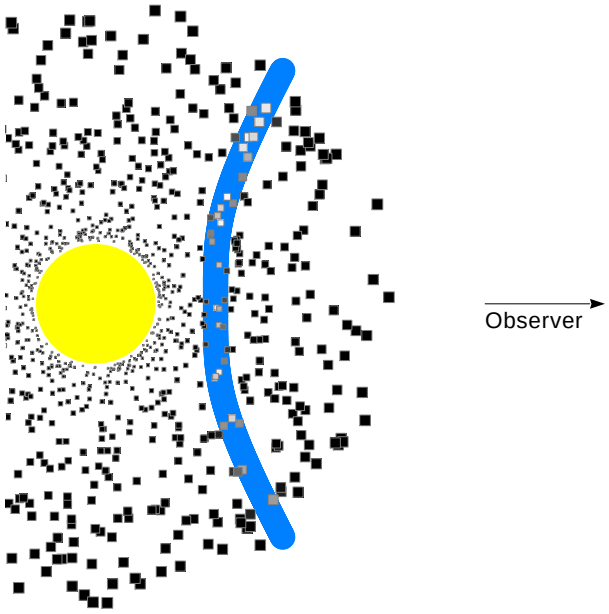

Figure 4: Porosity in the case of line opacity. At a given observer's frame frequency, rays can only interact with those clumps (shaded white or light grey) that are close to the *constant radial velocity surface* (CRVS, blue), while other clumps (black) are out of the line resonance.

Accounting for the finite width of the clump's absorption profile, the CRVS widens to a resonance *zone*. The absorption profile depends on the velocity distribution inside the clump. Broadening can be caused by stochastic motion (thermal, microturbulent), and by velocity gradients, e.g. due to the clump's expansion in radial or lateral direction. For simplicity we adopt that all these effects can be described by a single Gaussian distribution of velocities. Empirically it is known that the narrowest spectral features from stellar winds, like the DACs (discrete absorption components), still have typical widths corresponding to 40 ... 100 km/s. Therefore we evaluate the optical depth across one clump, $\tau_{\rm C}$, as for a *static* medium with a microturbulence velocity $v_{\rm D}$ in the mentioned range. Note that the degree of porosity for line radiation depends on this parameter: for smaller $v_{\rm D}$, the opacity profile of a clump profile peaks to a higher maximum, resulting in a smaller effective opacity of the atmosphere.

The described approach to macroclumping has been implemented in the *Potsdam Wolf-Rayet* (PoWR) code. As the only modification, the opacity has been replaced in the *Formal Integral* by the reduced "effective opacity" (Eq. 12). The non-LTE source function is taken from the microclumping model, i.e. the feedback of macroclumping effects on the population numbers is neglected. Al-

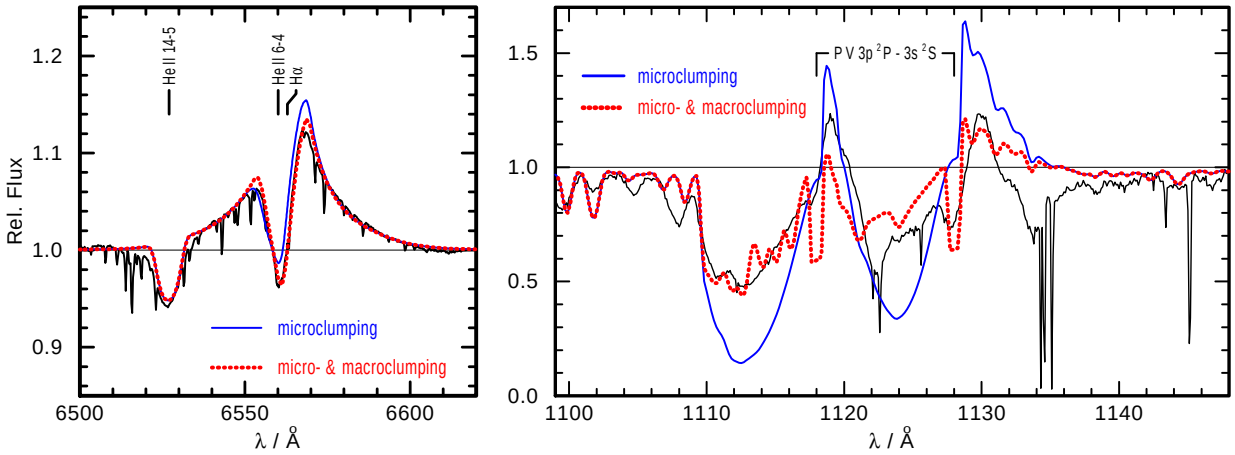

Figure 5: Observed line profiles for ζ Puppis (black), compared with synthetic profiles without macroclumping (blue smooth line) and with macroclumping (red dotted). The Hα profile is not affected by macroclumping (left panel). The P V resonance doublet (right panel), however, is predicted much stronger than the observation if neglecting macroclumping, while the model with macroclumping yields a profile of about the observed strength.

though dictated by the need to keep the problem tractable, one can give some justification for this approximation. Most transition rates are not changed by macroclumping, namely all collisional rates, and those radiative transitions for which clumps are optically thin. For those few frequencies where clumps are opaque (i.e. in strong line cores), the average radiation field neglecting macroclumping provides a rough approximation to evaluate the radiative transition rates in the *outer layers* of the clumps. Moreover, the absorption part of the resonance lines from leading ions (e.g. the debated P V line in O stars!) is especially robust against second-order effects on population numbers.

Oskinova et al. (2007) demonstrated the macroclumping effect by means of a model for ζ Puppis ($\log L/L_\odot = 5.9$, $\log \dot{M} = -5.56$, $T_* = 39\,$kK, $v_\infty = 2250\,$km/s, $v_D = 40\,$km/s). For the clumping parameters, a density contrast of $D = 10$ and an average clump separation parameter $L_0 = 0.2$ was adopted. The latter gives a reasonable total number of $2.2 \cdot 10^4$ clumps between $r = 1.05$ and 10. Clumping assumed to start at the sonic point. As shown in Fig. 5, the effect of macroclumping on Hα is negligible, because this line is not optically thick in the wind. The P V resonance line is predicted much too strong by the model neglecting macroclumping. Its fit would require a ten times smaller $\dot{M}$ (Fullerton et al. 2006). However, with the macroclumping formalism the model yields the P V line in about the observed strength. Thus macroclumping can resolve the discrepancy between $\dot{M}$ from resonance line and ρ^2-diagnostics without decreasing the mass-loss rates.

4 Conclusions

Microclumping leads to *smaller* empirical mass-loss rates from ρ^2-diagnostics (Hα line, WR emission lines, radio free-free emission).

Macroclumping leads to *higher* empirical mass-loss rates if derived from resonance lines, and is also important for modeling X-ray emission line profiles.

References

Castor, J.I., Abbott, D.C., & Klein, R. 1975, ApJ, 195, 157
Feldmeier, A., Puls, J., Pauldrach, A.W.A. 1997, A&A, 322, 878
Feldmeier, A., Oskinova, L. M., & Hamann, W.-R. 2003, A&A, 403, 217
Fullerton, A. W., Massa, D. L., & Prinja, R. K. 2006, ApJ, 637, 1025
Gail, H.P., Hundt, E., Kegel, W.H., et al., 1974, A&A, 32, 65
Hamann, W.-R., & Koesterke, L. 1998, A&A, 335, 1003
Hillier, D. J. 1991, A&A, 247, 455
Lépine, S., & Moffat, A. F. J. 1999, ApJ, 514, 909
Oskinova, L. M., Feldmeier, A., & Hamann, W.-R. 2004, A&A, 422, 675
Oskinova, L. M., Feldmeier, A., & Hamann, W.-R. 2006, MNRAS, 372, 313
Oskinova, L. M., Hamann, W.-R., & Feldmeier, A. 2007, A&A, 476, 1331
Owocki, S. P., & Cohen, D. H. 2006, ApJ, 648, 565
Owocki, S. P., Gayley, K. G., & Shaviv, N. J. 2006, ApJ, 616, 525
Puls, J., Markova, N., Scuderi, S., et al. 2006, A&A, 454, 625

Hillier: It is important to point out that the increase in mass loss arising from including macroclumping is relative to models using microclumping and the volume filling approach. The derived mass loss rates are still less than those derived from fitting Hα using homogeneous models.

Hamann: This is what I wanted to say. The macroclumping is potentially counteracting the microclumping, but will not overcome. At best, I hope that we can keep $\dot{M}$ reductions of factors of 2 to 4 compared to the homogeneous analysis, and can attribute the excessive weakness of the P V resonance line to the porosity effect.

Townsend: In principle, we could make the P V profiles disappear completely with the correct choice of clump parameters. What parameters do you use in your model?

Hamann: Well, not completely disappear, but weaken significantly. The clumping parameters for the ζ Pup model shown are $D = 10$ for the clumping contrast, and $L_0 = 0.2\,R_*$ for the clump separation parameter.

Moffat: Nobody can believe that clumps are all the same size at a given distance from the star, as is commonly assumed. The question is how close to reality your and others' models are. What can we really believe? Have you done any kind of reality tests?

Hillier: You cannot learn running before you can walk!

Hamann: Thank you, John, for your support. We must start with simplified models.

Ignace: Your prescription for $L(r)$ suggests that clumps do not expand with constant solid angle. Is that true?

Hamann: Yes. We assume for simplicity that the density contrast $D(r)$ (= inverse filling factor) remains constant (except for the static layers below $v = 30$ km/s where clumping is switched off), and adopt that the number density of clumps follow the equation of continuity (clump conservation). A further condition (like conservation of solid angle) would over-determine the problem.

Clumping in Hot Star Winds
W.-R. Hamann, A. Feldmeier & L.M. Oskinova, eds.
Potsdam: Univ.-Verl., 2008
URN: http://nbn-resolving.de/urn:nbn:de:kobv:517-opus-13981

Modeling DACs in UV lines of massive hot stars

A. Lobel
Royal Observatory of Belgium

We apply the 3-dimensional radiative transport code WIND3D to 3D hydrodynamic models of Corotating Interaction Regions to fit the detailed variability of Discrete Absorption Components observed in Si IV UV resonance lines of HD 64760 (B0.5 Ib). We discuss important effects of the hydrodynamic input parameters on these large-scale equatorial wind structures that determine the detailed morphology of the DACs computed with 3D transfer. The best fit model reveals that the CIR in HD 64760 is produced by a source at the base of the wind that lags behind the stellar surface rotation. The non-corotating coherent wind structure is an extended density wave produced by a local increase of only 0.6% in the smooth symmetric wind mass-loss rate.

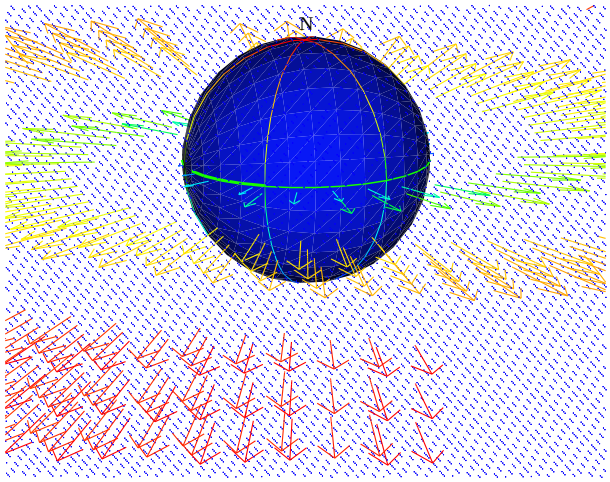

Figure 1: Schematic representation of two CIRs in the plane of the equator used in 3D radiative transfer calculations with WIND3D.

1 Introduction

Discrete Absorption Components (DACs) observed in the broad P Cygni profiles of UV resonance lines are important tracers of the dynamics of line driven winds in massive hot stars. DACs are observed to propagate bluewards through the UV line profiles on time scales comparable to the stellar rotation period (Massa et al. 1995; Prinja 1998). Hydrodynamic models of Corotating Interaction Regions (CIRs) have been proposed by Cranmer & Owocki (1996) to explain the observed DAC properties qualitatively. These large-scale wind structures are spiral-shaped density- and velocity-perturbations winding up in or above the plane of the equator that can extend from the stellar surface to possibly several tens of stellar radii. The CIRs can be produced by intensity irregularities at the stellar surface, such as dark and bright spots, magnetic loops and fields, or non-radial pulsations. The surface intensity variations alter the radiative wind acceleration locally, which creates streams of faster and slower wind material.

We investigate to what extent the CIR wind model can *quantitatively* explain the *detailed* DAC properties observed in B0.5 Ib supergiant HD 64760. Fullerton et al. 1997 pointed out how exceptional IUE data from the MEGA campaign (Massa et al. 1995) have made it a key object for studying the origin and nature of hot-star wind variability. We discuss the development of a new 3D radiative transfer code WIND3D to best fit the DAC morphology (e.g. shape and flux changes) observed in the unsaturated absorption portion of the Si IV λ1395 line. The hydrodynamic CIR models developed for this purpose are discussed in a companion paper (Blomme 2007). Animations are online at `alobel.freeshell.org/conference.html`.

2 3D radiative transfer: Wind3D

WIND3D computes 3D spatial non-LTE radiative transfer in the 2-level atom approximation for optically thick resonance lines formed in scattering dominated extended winds of massive hot stars. Its implementation is based on the finite element method described by Adam (1990). The code accepts arbitrary 3D wind-density and -velocity distributions. The 3D transfer scheme further extends Adam's Cartesian method with three new aspects: (i) We considerably accelerate the (exact) lambda iteration of the source function on 71^3 grid points with appropriate starting values from the Sobolev approximation. (ii) Since the lambda iteration is the bottleneck of the numerical transfer problem we fully parallelize the mean intensity integration over 80^2 spatial an-

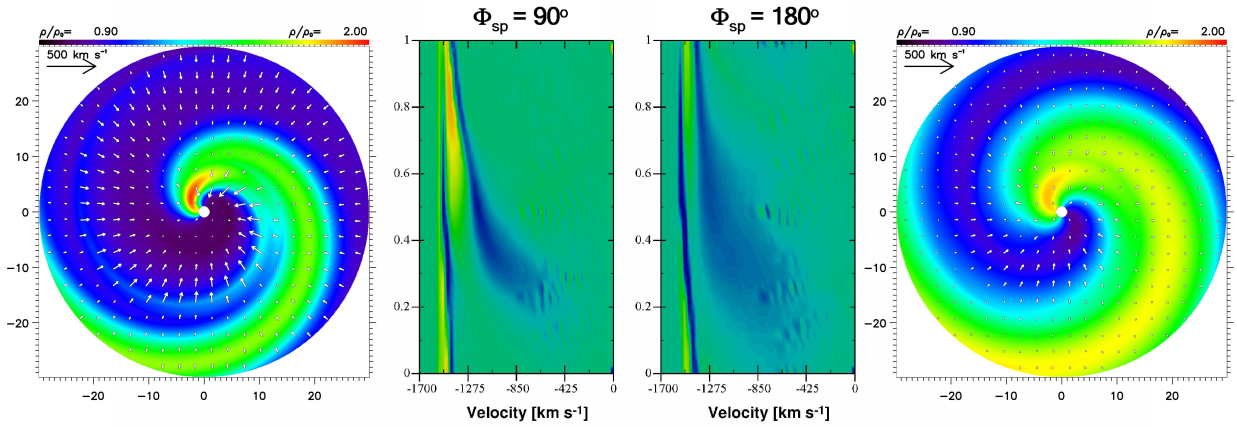

Figure 2: Hydrodynamic CIR models for spot opening angles $\Phi_{\rm sp}$=90° (left-hand panel) & 180° (right-hand panel). The dynamic spectra (middle panels) reveal width changes of the DAC base for an observer viewing the rotating models from the south side of the images in the equatorial plane.

gles. (iii) We introduce a new technique that 3D interpolates the converged (non-Sobolev) source function to a higher resolution (spatial) grid of 700^3 grid points to solve the final 3D transfer equation for very narrow line profile functions. This method resolves the small flux variations in the absorption portions of very broad unsaturated P Cygni profiles.

Parameterized 3D models of CIRs already provide comprehensive comparisons to general properties observed in DACs. We consider a β-velocity law for an isothermal wind with $\beta \simeq 1$. The smooth wind is perturbed with 3D spiraling density enhancements wound around the central star (Fig. 1). The wind velocities inside the CIRs also assume the β-law and are directed radially (velocity vectors drawn in the equatorial plane). The CIR model of Fig. 1 causes the width of DACs computed for an observer in the plane of the equator to decrease because the range of velocities in the CIR projected in the observer's line of sight (inside the cylinder in front of the stellar disk) decreases at larger distances from the star.

For the hydrodynamic CIR models a local radiation force enhancement (or surface 'spot') is introduced at the base of the stellar wind (Blomme 2007). The resulting equatorial density- and velocity-structures are inserted around the star with a thickness of 1 R_* around the equatorial plane. Outside this region, the model density and velocity assume the smooth wind values. In Fig. 2 the spot opening angle $\Phi_{\rm sp}$ is increased from 90° to 180°. The spot co-rotates with the stellar surface $v_{\rm sp} = v_{\rm rot}$, and the spot intensity $A_{\rm sp} = 0.5$. The increase of $\Phi_{\rm sp}$ considerably alters the FWHM evolution of the DAC computed in Si IV λ1395. The DAC base broadens because extra wind material injected by the spot becomes more spread out over the equatorial plane. The maximum of ρ/ρ_0 in the CIR occurs within ~5 R_* above the stellar surface. Inside this region extra wind material is distributed over a larger geometric region above the bright spot, which also considerably broadens the density contrast in the tail of the CIR. When this region rotates in front of the stellar disk (around rotation phase 0.2 in the dynamic spectra) the DAC base broadens because the range of velocities projected in the observer's line of sight (that contribute to the DAC opacity) increases. The wind streams almost radially through the CIR density structure. The wind flow decelerates due the relative increase of wind density in a region behind the CIR density contrast maximum. It causes a trailing velocity plateau (between the star and CIR) which strongly contributes to the DAC absorption at larger distances from the star since the line optical depth in the Sobolev approximation is $\tau \simeq \rho \,/\, |dv/dr|$.

3 Modeling DACs in HD 64760

We determine a recurrence period of 10.3±0.5 d for the two DACs (right-hand panel of Fig. 3) observed in the Si IV lines of HD 64760 in 1995 January 13-29 (Massa et al. 1995) by flux filtering the nearly horizontal rotational modulations (Lobel & Blomme 2007). We can assume that this star is observed equator-on (sin i≃1). The surface rotation velocity of the fast-rotating supergiant is $v_{\rm rot}$=265 km s^{-1} which, for R_*=22 $R_\odot$, yields a rotation period of 4.13 d. The latter period is 2.5 times shorter than the observed DAC recurrence period. It reveals that the spot cannot co-rotate with the stellar surface. We therefore use a single bright spot with the spot parameter $v_{\rm sp}$ set equal to $v_{\rm rot}$ / 2.5 in the hydrodynamic wind models. We compute a large grid of dynamic spectra from a grid of hydrodynamic mod-

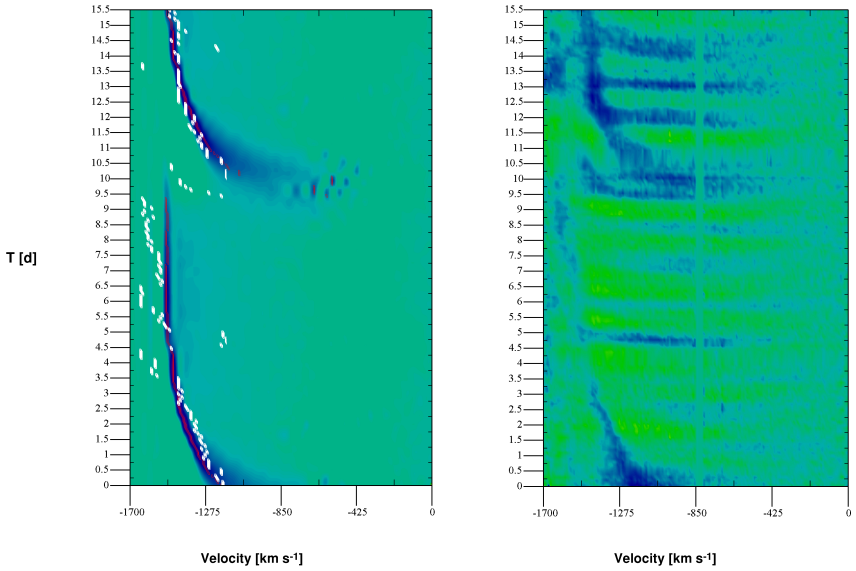

Figure 3: Best fit dynamic spectrum (left-hand panel) of Si IV λ1395 compared to the observed spectrum (right-hand panel) of HD 64760. The computed DAC shape fits the observations in detail.

els for a broad range of spot parameters $\Phi_{\rm sp}$ and $A_{\rm sp}$, using the smooth wind properties of HD 64760. We obtain a best fit from a least-squares fit procedure between the observed and computed DACs for $\Phi_{\rm sp} = 50^\circ \pm 5^\circ$ and $A_{\rm sp} = 0.1 \pm 0.05$ (see the hydrodynamic model in Fig. 1 of Blomme 2007). In the left-hand panel of Fig. 3 the velocity positions of the flux minima in the computed DAC differ by less than $\sim$50 km s^{-1} from the observed velocity positions (white dots) for 0 d $\leq T \leq$ 3.5 d, and 10 d $\leq T$ 15.5 d. The FWHM of the computed DAC decreases from $\sim$100 km s^{-1} at $T = 0\dot{\rm d}$ to $\sim$ 20 km s^{-1} around $T = 3.5\dot{\rm d}$, in agreement with the narrowing of the observed DAC. The DAC width remains almost constant over the following 6.5 d, after which it fades away. The 'tube-like' extension of the DAC base is also observed (right-hand panel). This characteristic DAC morphology can only correctly be computed with hydrodynamic structured wind models.

4 Conclusions

We demonstrate with 3D radiative transfer calculations in hydrodynamic CIR models of HD 64760 that the DACs observed in the Si IV UV resonance lines are due to a region of enhanced mass-loss at the base of the wind that lags 2.5 times behind the surface rotation. Our detailed DAC modeling reveals that this region is not locked to the stellar surface. It indicates that magnetic fields at the equator are an unlikely source for additional wind material yielding an asymmetric structured wind with an extended density wave in the equatorial plane. The integration of the best fit hydrodynamic CIR model for HD 64760 provides a very small increase of only 0.6% in the mass-loss rate of the spherically symmetric smooth wind model. It signals that DACs are generally expected in hot-star winds since they result from rather small variations of the spherically symmetric mass-loss rate. These coherent CIR structures may become perturbed by wind clumping on much smaller length scales. They will however built up again very rapidly as well, provided that the perturbation time-scales are sufficiently short for the large-scale wind structures to completely develop and to produce the slowly blueward drifting recurring DACs in unsaturated UV spectral lines.

This work has been supported by the Belgian Federal Science Policy - Terugkeermandaten.

References

Adam, J. 1990, A&A, 240, 541

Blomme, R., 2007, these proceedings

Cranmer, S.R., & Owocki, S.P. 1996, ApJ, 462, 469

Fullerton, A.W., Massa D.L., Prinja, R.K., Owocki, S.P., & Cranmer, S.R. 1997, A&A, 327, 699

Lobel, A., & Blomme, R. 2007, ApJ, submitted

Massa, D., Fullerton, A.W., Nichols, J.S., et al. 1995, ApJ, 452, L53

Prinja, R.K. 1998, in "Cyclical Variability in Stellar Winds", Eds. L. Kaper & A.W. Fullerton, ESO Astroph. Symp., Springer, Berlin, 92

Massa: First, I am happy to see data we obtained over 15 years ago still being used. Second, do you have any thoughts on how to put all of the different effects into the wind, i.e. DACs, CIRs and clumps?

Lobel: Thank you. These IUE data are a real treasure. My detailed fits to DACs with WIND3D show that the mass source of the "large-scale" wind structures (CIRs) is not locked onto the stellar surface. It reveals something fundamental about this source at the base of the wind (possibly an interference pattern caused by non-radial pulsations). Since I find a density increase in CIRs of only $\sim 20\%$, any other kind of wind perturbation (large or small scale) can break them up, but only small mass loss rate enhancements suffice to build them up again. My best guess for the source of the clumps is a cascading phenomenon down to smaller length scales due to Rayleigh-Taylor instability. The horizontal "modulations" in the lines are hard to fit with hydrodynamic models (as opposed to kinematic models), so my best guess is that their origin is very different from the DACs, possibly some unusual hydrodynamic effect at the photosphere in the plane of the equator.

Fullerton: I like the simulations of DACs in HD 64760 very much. I think this is the first time these features have been modelled, and your success is very encouraging. Could you comment further on the hydrodynamic problems associated with trying to reproduce the modulations? I am puzzled that they do not figure in your CIR simulations, since their "phase bowing" is thought to be a signature of spiral-shaped structures.

Lobel: The main problem with calculations of bow-shaped modulations in HD 64760 is that the ratio $v_\infty / v_{\rm rot}$ makes them to drift too slowly bluewards compared to the IUE observations in Si IV. The spot model is adequate to explain the "slowly" shifting DACs, but for the modulations it fails to match them quantitatively. Kinematic models with sector-like density enhancements do produce the phase bowing on nearly horizontal line structures, but with full hydrodynamic models they always drift too slowly using simple spot models at the surface. Perhaps some kind of highly supersonic expansion at the base of the wind near the photosphere (much faster than what the spot models produce) could provide models that work?

Clumping in Hot Star Winds
W.-R. Hamann, A. Feldmeier & L.M. Oskinova, eds.
Potsdam: Univ.-Verl., 2008
URN: http://nbn-resolving.de/urn:nbn:de:kobv:517-opus-13981

Techniques for simulating radiative transfer through porous media

Rich Townsend
Bartol Research Institute, University of Delaware, Newark, DE 19716, USA

In this contribution, I discuss some basic techniques that can be used to simulate radiative transfer through porous media. As specific examples, I consider scattering transfer through a clumped slab, and X-ray emission line formation in a clumped wind.

1 Introduction

A porous medium is one that is macroclumped: the typical scale of the clumps is larger than the mean free path $\bar{\ell}$ of photons. This represents the opposite end of the 'clumping spectrum' to a microclumped medium, for which the clump scale is smaller than $\bar{\ell}$. The distinction between these two limits is more than academic; although microclumping usually only affects the volume emissivity of a medium (which depends on the local density squared), porosity/macroclumping can result in the medium having an effective opacity $\kappa_{\rm eff}$ that is significantly smaller than the microscopic value κ of the material comprising it.

Recent investigations of porosity (e.g., Oskinova, Feldmeier & Hamann 2004; Owocki & Cohen 2006) have been focused primarily toward evaluating its observable consequences. As such, these studies have relied largely on very simple models for the radiative transfer. In this contribution, I discuss some of the basic techniques and codes that I have devised to move beyond these simplified models, allowing consideration of the full radiative transfer problem for a clumped medium.

The standard approach to radiative transfer is to solve the radiative transfer equation (RTE),

$$\frac{{\rm d}I}{{\rm d}\tau} = I - S, \tag{1}$$

where I is the specific intensity, S the source function, and τ the optical depth coordinate. However, solving the RTE is not the only way to tackle the problem. Instead of the I-based 'field' approach embodied by the RTE, one can adopt a 'particle' approach, following individual photons as they propagate through a medium. This is precisely what Monte-Carlo radiative transfer entails, and in the following section I apply this approach to model scattering transfer through a clumped slab.

2 A clumped scattering slab

To investigate radiative transfer in a clumped scattering medium, I have developed FREYR, a Monte-Carlo code for simulating the propagation of photons through a plane-parallel slab composed of discrete, spherical clumps. The clumps are randomly positioned, but each has the same radius $r_{\rm c}$ and a uniform density $\rho_{\rm c}$. Photons are introduced at the bottom of the slab with a random upward direction. A nominal 'optical distance to travel' τ is assigned to each photon based on the expression

$$\tau = -\log x, \tag{2}$$

where x is a uniform random deviate in the range $0 < x \leq 1$. This optical distance is converted into a physical distance ℓ by inverting the optical depth equation

$$\tau = \int_0^\ell \kappa\rho(\ell')\,{\rm d}\ell'; \tag{3}$$

here, the microscopic opacity κ is assumed to be constant, while the local density ρ varies with position as the photon passes in and out of spheres. After moving a distance ℓ in the appropriate direction, the photon is scattered: a new random direction is chosen (corresponding to isotropic scattering), and a new optical distance is picked using Eq. (2). This procedure is repeated until the photon escapes from the top or the bottom of the slab; periodic boundary conditions are applied at the sides of the slab.

Conceptually, this procedure is quite straightforward; but from an implementation perspective the tricky part comes in inverting the optical depth equation Eq. (3). The key to this task lies in the recognition that along any given ray through the slab, the density is a piecewise-constant function. Changes in ρ arise only at those discrete points where the ray enters or exits a sphere. To locate these points, the parametric equation for the ray traversed by a photon is written as

$$\mathbf{r} = \mathbf{r}_0 + \ell\mathbf{dr}. \tag{4}$$

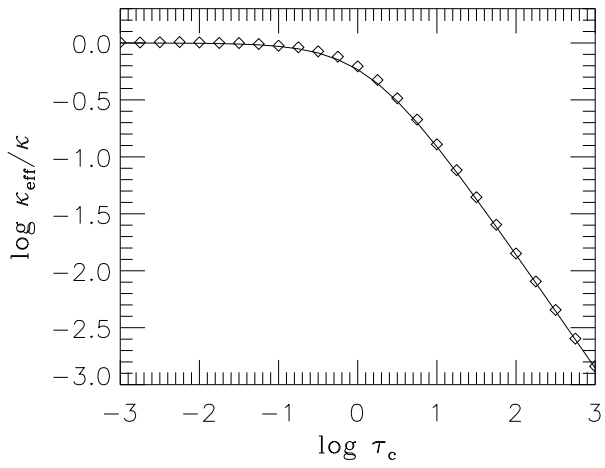

Figure 1: The ratio between the effective opacity $\kappa_{\rm eff}$ and the microscopic opacity κ, plotted (diamonds) as a function of clump optical thickness $\tau_{\rm c}$. The solid line shows the corresponding prediction of the simple bridging law Eq. (14).

Here, $\mathbf{r}_0$ is the starting position vector of the photon, and the unit vector $\mathbf{dr}$ gives the photon's direction. To establish whether this ray intersects a sphere located at $\mathbf{r}_{\rm s}$, FREYR calculates the following quantities:

$$\mathbf{v} = \mathbf{r}_0 - \mathbf{r}_{\rm s} \tag{5}$$

$$B = 2\mathbf{dr}\cdot\mathbf{v} \tag{6}$$

$$C = \mathbf{v}\cdot\mathbf{v} - r_{\rm c}^2 \tag{7}$$

$$D = B^2 - 4C \tag{8}$$

If $D > 0$, then the ray pierces the sphere at the locations

$$\ell_{\rm s} = \frac{-B \pm \sqrt{D}}{2}; \tag{9}$$

these correspond to the points where the density undergoes a jump. Between these points, ρ is constant, and τ varies linearly – so it is straightforward to reconstruct the function $\tau(\ell)$ from Eq. (3), and then to invert this function to find ℓ given τ.

For each leg of a photon's journey, the ray-sphere intersection test (Eqs. 5–9) must be performed against *every* sphere contained in the slab. Potentially, this can be quite time consuming, and so FREYR uses a spatial partitioning approach to reduce the number of tests that must be done. After the distribution of spheres is calculated (i.e., a set $\{\mathbf{r}_{\rm s}\}$ of random centers), the slab is divided up into a 3-dimensional array of voxels. Each voxel stores a index list of those spheres that fall part or all of the way inside it. To find out which spheres a ray intersects, it is then only necessary to test the subset of spheres that are indexed by the voxels that the ray passes through. Efficient algorithms exist (e.g., Amanatides & Woo 1987) for quickly finding these voxels.

Having described the basic principles of FREYR, let me now present some illustrative results. Fig. 1 plots the ratio $\kappa_{\rm eff}/\kappa$ between the effective and microscopic opacities of a clumped slab, as a function of the averaged clump optical thickness

$$\tau_{\rm c} = \frac{4\kappa\rho_{\rm c} r_{\rm c}}{3}. \tag{10}$$

To obtain the $\kappa_{\rm eff}$ datum at each $\tau_{\rm c}$ abscissa, a FREYR simulation is used to determine an empirical value for the slab transmittance

$$T \equiv \frac{N_{\rm esc}}{N_{\rm inj}}; \tag{11}$$

here, $N_{\rm inj}$ is the number of photons injected at the bottom of the slab during the simulation, and $N_{\rm esc}$ is the number that eventually escape through the top. Formally, the transmittance is a function only of the slab optical thickness, so that

$$T = f(\kappa_{\rm eff}\bar{\rho}\Delta z) \tag{12}$$

for some function $f()$. Thus, armed with the empirically-measured value of T, and the known values of the slab mean density $\bar{\rho}$ and vertical extent Δz, the effective opacity follows as

$$\kappa_{\rm eff} = \frac{f^{-1}(T)}{\bar{\rho}\Delta z}. \tag{13}$$

The only difficulty is to determine the inverse of the transmittance function, $f^{-1}()$, but this can be done numerically using Monte-Carlo simulations of a homogeneous, isotropically scattering slab.

Looking at Fig. 1, the onset of porosity is plain to see. Once the clumps become optically thick (i.e., $\tau_{\rm c} > 1$), the effective opacity of the slab begins to fall well below the microscopic value κ. This drop-off is well approximated by

$$\frac{\kappa_{\rm eff}}{\kappa} = \frac{C}{C+\tau_{\rm c}} \tag{14}$$

(shown in the figure by the solid line), where the constant $C \approx 1.4$. This expression is a modified form of the bridging law introduced by Cohen & Owocki (2006). In the limit of small $\tau_{\rm c}$, it correctly reproduces the microclumping case, for which $\kappa_{\rm eff}$ equals the microscopic opacity κ. In the opposite limit of large $\tau_{\rm c}$ (i.e., macroclumping), the effective opacity has a scaling

$$\kappa_{\rm eff} = \frac{\kappa C}{\tau_{\rm c}} = \frac{3C}{4\rho_{\rm c} r_{\rm c}}. \tag{15}$$

Multiplying through by the clump mass $4\pi\rho_{\rm c} r_{\rm c}^3/3$ then gives the effective cross section of the clumps,

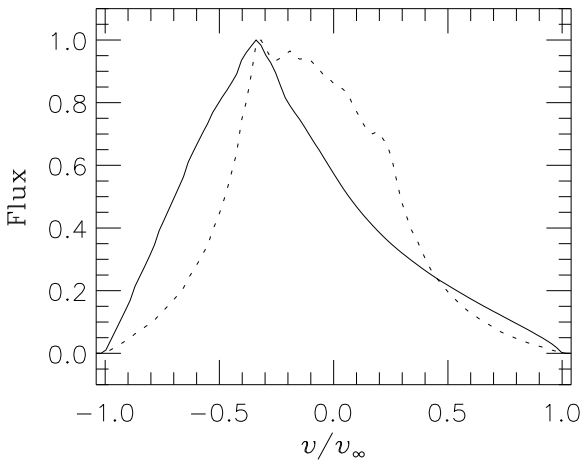

Figure 2: X-ray line profiles for a $\tau_* = 3$ clumped wind. The solid (dotted) profile corresponds to optically thin (optically thick) clumps; both profiles are normalized to have a maximum flux of unity.

$$\sigma_{\rm eff} = C\pi r_{\rm c}^2. \qquad (16)$$

This can be recognized as the geometric cross section $\pi r_{\rm c}^2$, scaled by the constant C. The basis for this result is that the clumps – when they become extremely optically thick – behave like individual scattering centers, with an interaction cross section equal to their geometric cross section. The appearance of the constant C is to correct for the angular scattering profile of each individual clump. If this profile were isotropic, then we would obtain $C = 1$; but in fact the profile is that of a sphere with a Lambert-law surface (see Schoenberg 1929), leading to the 'observed' value $C = 13/9 \approx 1.4$.

3 A clumped absorbing wind

The utility of Monte-Carlo is that it works in cases such as scattering where the source function S is difficult to obtain. If in fact S is already available, then a simple formal solution of the RTE (cf. Eq. 1) is

$$I = \int S\ {\rm e}^{-\tau} {\rm d}\tau. \qquad (17)$$

Calculating the intensity I using this expression is invariably faster than performing an equivalent Monte-Carlo simulation. (This is a specific instance of a general rule: *Monte-Carlo is guaranteed to be the slowest way to solve a radiative transfer problem.* Of course, sometimes – as with scattering – it is the only straightforward way.)

The calculation of X-ray emission line profiles in clumped winds (see, e.g., the contribution by David Cohen) is a specific example of a case where the formal solution Eq. (17) can be used. X-ray line photons are emitted according to some simple parametric function of radius, meaning that the source function is easy to calculate. These photons are then re-absorbed by an opacity associated with a distribution of clumps. As with the Monte-Carlo simulations, the tricky part in modeling this re-absorption involves evaluating the optical depth τ.

Fortunately, for spherical clumps the same set of techniques (cf. Sect. 2) can be applied. If the inter-clump medium is a vacuum, then once again the density along any given ray is a piecewise-continuous function, and the ray-sphere intersection testing (cf. Eqs. 5–9) can be used to reconstruct $\tau(\ell)$. If, more realistically, there is a smooth inter-clump medium following a wind expansion law $\rho = \dot{M}/(4\pi r^2 v)$, then the contribution of this medium to the optical depth along a ray can be added in using numerical quadrature.

Figure 2 shows some example X-ray line profiles calculated using BOREAS, a simple formal solver for a spherical-clump wind. For both profiles, the optical depth τ_* to the star (cf. Owocki & Cohen 2006) is 3; however, the profiles differ in the nature of the clumping. The solid-line profile is for a configuration composed of many optically thin clumps, and it shows the characteristic asymmetric (blue-skewed) shape usually associated with a smooth wind. Conversely, the dotted-line profile is for a configuration composed of fewer, optically thick clumps. With porosity acting to reduce the effective opacity of the wind, a much more symmetric line profile is seen in this latter case.

4 Summary

The spherical clumps considered herein admittedly rather idealized. However, it is precisely for such simple, idealized cases that one can hope to fully understand the precise manner in which porosity modifies the effective opacity of a medium. Both FREYR and BOREAS – and the techniques they implement – will certainly prove useful in developing such an understanding.

References

Amanatides, J., & Woo, A. 1987, in Eurographics '87, p. 3

Oskinova, L.M., Feldmeier, A., & Hamann, W.-R. 2004, A&A, 422, 675

Owocki, S.P., Cohen, D.H. 2006, ApJ, 648, 565

Schoenberg, E. 1929, Handb. Astro., 2, 255

Feldmeier: Your emmission line profile from a highly porous wind is flat-topped and symmetric and not blueshifted, but centered at the rest-frame frequency. In my own models of a porous wind the line is flat-topped and symmetric and blueshifted by $v_\infty/2$. How does this difference occur? Is it because you assume spherical blobs and we assume flat, pancake-like shell fragments?

Townsend: It could be a variety of things: different treatments of emission, different clumps as you suggest (spherical blobs vs. pancakes), or, perhaps, come about due to how the wind at large radii is treated.

Clumping in Hot Star Winds
W.-R. Hamann, A. Feldmeier & L.M. Oskinova, eds.
Potsdam: Univ.-Verl., 2008
URN: http://nbn-resolving.de/urn:nbn:de:kobv:517-opus-13981

Mid-IR observations of WC stars, and the connection to wind clumping

O. Schnurr & P.A. Crowther
University of Sheffield, UK

We present preliminary results of a tailored atmosphere analysis of six Galactic WC stars using UV, optical, and mid-infrared Spitzer IRS data. With these data, we are able to sample regions from 10 to 10^3 stellar radii, thus to determine wind clumping in different parts of the wind. Ultimately, derived wind parameters will be used to accurately measure neon abundances, and to so test predicted nuclear-reaction rates.

1 Introduction

Classical Wolf-Rayet (WR) stars are almost bare, helium-burning cores of evolved, massive ($M_i \gtrsim 25 M_\odot$ with dense and fast, stellar winds. A star enters the WR phase as WN star, displaying CNO-processed material in its envelope (i.e. N and He). As the wind erodes the outer layers of the WN star, helium-burning products emerge in the wind, mainly carbon and, in more advanced stages, oxygen – the star is then classified as WC (or WO) star.

Theory of nuclear-reaction rates predicts that neon (Ne) abundances rise sharply when CNO-produced nitrogen is processed into Ne during helium burning (Maeder 1983). In fact, Ne becomes the fourth most abundant element after He, C, and O, and is exposed in the wind. Thus, the accurate determination of Ne abundances in WC stars becomes a powerful tool to test theoretical models.

In WC stars, Ne recombination lines are present in the ultraviolet (UV) and optical spectrum, which is formed at high densities (10^{11} to 10^{12} cm^{-3}) of the inner part (few stellar radii) of the wind. However, the Ne lines are weak and severely blended with broad lines of other elements, and thus practically unobservable. In the mid-infrared one has access to forbidden fine-structure lines, such as [NeII]λ12.8μm and [NeIII]λ15.5μm. These Ne emission lines are relatively strong and well-isolated, but they form only where the wind density has dropped below the critical density (10^5 to 10^6 cm^{-3}), at a few thousand stellar radii from the star.

From both theory and UV/optical observations it is well known that radiatively-driven winds are clumped, and that mass-loss rates, which are a vital quantity to derive Ne abundances, have to be modified by the related volume-filling factor f, such that $\dot{M}_{\rm clumped} = \dot{M}_{\rm smooth}/\sqrt{f}$. However, from hydrodynamical considerations it is expected that wind clumping decreases with distances from the star, and that the wind becomes smooth in the outer parts again (Runacres & Owocki 2002; see their Fig. 6). If this is true, then one cannot rely on f-values which have been obtained for the *inner* wind (e.g. from UV/optical diagnostics) to derive Ne abundances from emission lines which form in the *outer* wind.

2 Present project

We have embarked on a project to carry out tailored-atmosphere analysis of six Galactic WC stars in order to determine wind properties ranging from the inner (UV/optical) to the outer (mid-IR) parts of the wind. Our sample comprises WR4 (WC5), WR15 (WC7), WR23 (WC6), WR52 (WC4), WR135 (WC8), and WR144 (WC4), for which we have high-quality, flux-calibrated spectroscopy covering 0.4 to 1.1 (ground-based) and 5 to 35 μm (Spitzer IRS) spectroscopy; for some of the stars, IUE short/long HIRES and near-infrared data are also available.

Synthetic spectra are computed using the latest, 1D, line-blanketed CMFGEN model-atmosphere code (Hillier & Miller 1998) which assumes a spherically symmetric and stationary wind, and imposes a standard velocity law with $\beta = 1$. Clumping is treated as "shellular" (Hillier 1991). The following analytical prescription by Najarro (priv.comm.) is used to describe the radial dependence of the volume-filling factor f:

$$f(r) = f_{\rm max} + (1 - f_{\rm max}) \times \times \left[e^{-v(r)/v_1} + e^{-(v(r)-v_\infty)/v_2} \right]$$

A typical example for the run of the volume-filling factor is shown in Fig. 1, where the radius is expressed in terms of Rosseland opacity. The innermost wind (large opacities) starts smooth, but clumping quickly sets in at low wind velocities ($v_1 = 100$ kms^{-1}) to reach a predefined level (here: $f_{\rm max} =$

0.1) at 2 R_*. Two cases are shown, one with a constant clumping throughout the wind (black) and one where the wind increasingly becoming smooth again ($f = 0.6$ at 100 R_*, $v_2 = 100$ km s^{-1}; shown in red).

Most emission lines visible in the spectrum are recombination lines, hence their strength depends on ρ^2; on the other hand, the electron-scattering wing, which is mainly visible on the red flank of emission lines (cf. Hillier 1991), depends only on ρ. Thus, only a particular combination of $\dot{M}$ and f will reproduce correctly the strength and shape of the emission line. As an example, the CIVλ2530 lines in WR23 is shown in Fig. 2. Three models are computed using different volume-filling factors, but holding the effective mass-loss rate $\dot{M}_{\rm smooth}/\sqrt{f}$ constant, so that one can study the influence of clumping alone. The model with a volume-filling factor $f = 0.1$ clearly reproduces the line in an excellent way.

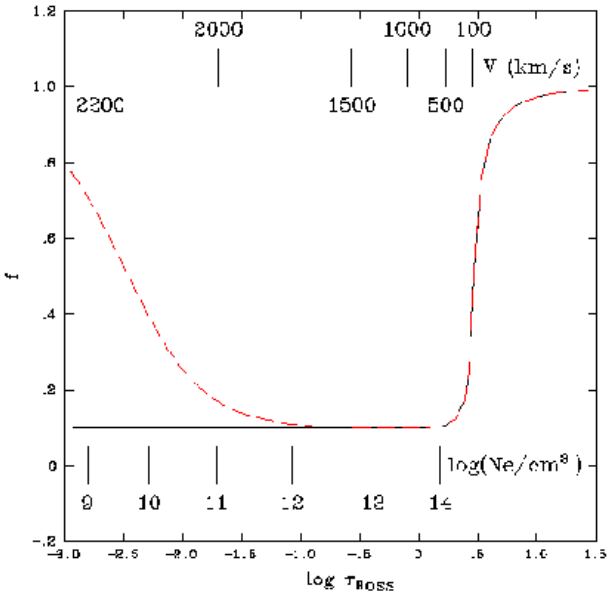

Figure 1: Parametrization of the volume-filling factor (i.e. inverse clumping factor), f, as a function of Rosseland optical depth (as measure of radius). This "clumping law" is used in the models.

Due to their ionized winds, massive stars display continuum free-free (i.e. *bremsstrahlung*) excess emission at longer wavelengths (infrared and beyond) whose strength depends on ρ^2. Radio fluxes therefore can be (and already have been) used to derive mass-loss rates of O and WR stars. However, such measures cannot provide information on wind clumping because radio observations are monochromatic; also the radio emission originates from the outer part of the wind (at thousands of R_*) that has already reached its terminal velocity. The mid-IR spectrum, in contrast, is formed only at few hundreds of R_*, where the wind is still accelerating, and because WR stars have such high mass-loss rates, their free-free excees is readily observable in the mid-IR.

In Fig. 3, we show the Spitzer data for WR23. The model with constant clumping ($f = 0.1$) throughout the wind is able to reproduce the continuum slope, whereas the model with decreasing clumping ($f = 0.6$ at 100 R_*) does not generate enough free-free emission. Note that both models reproduce the UV/optical emission spectrum equally well, as the inner-wind clumping factors are identical. Given that models have to successfully reproduce both the emission-line spectrum and the SED over a very large spectral range, resulting wind parameters and, by consequence, Ne abundances, are very reliable.

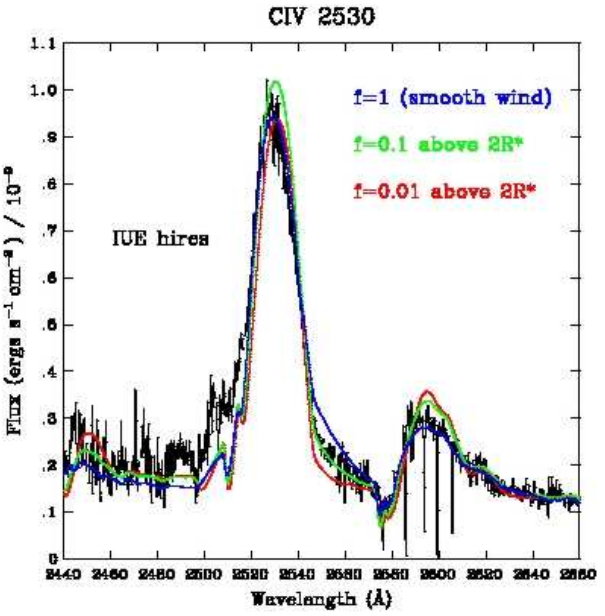

Figure 2: CIVλ2530 lines in WR23. Overplotted are model spectra with three different volue-filling factors: $f = 1$ (i.e. unclumped wind; blue), $f = 0.1$ (green), and $f = 0.01$ (red). Note the strong differences of the electron-scattering wing on the red flank of the emission line.

3 Preliminary results

Very preliminary results indicate that for all our sample stars, models with constant clumping (typically $f \sim 0.1$ above 2 R_*) throughout the entire wind are able to reproduce both the UV/optical and the mid-IR spectrum. However, models with identically clumped inner wind but with an increasingly smooth outer wind fail to generate enough free-free excess

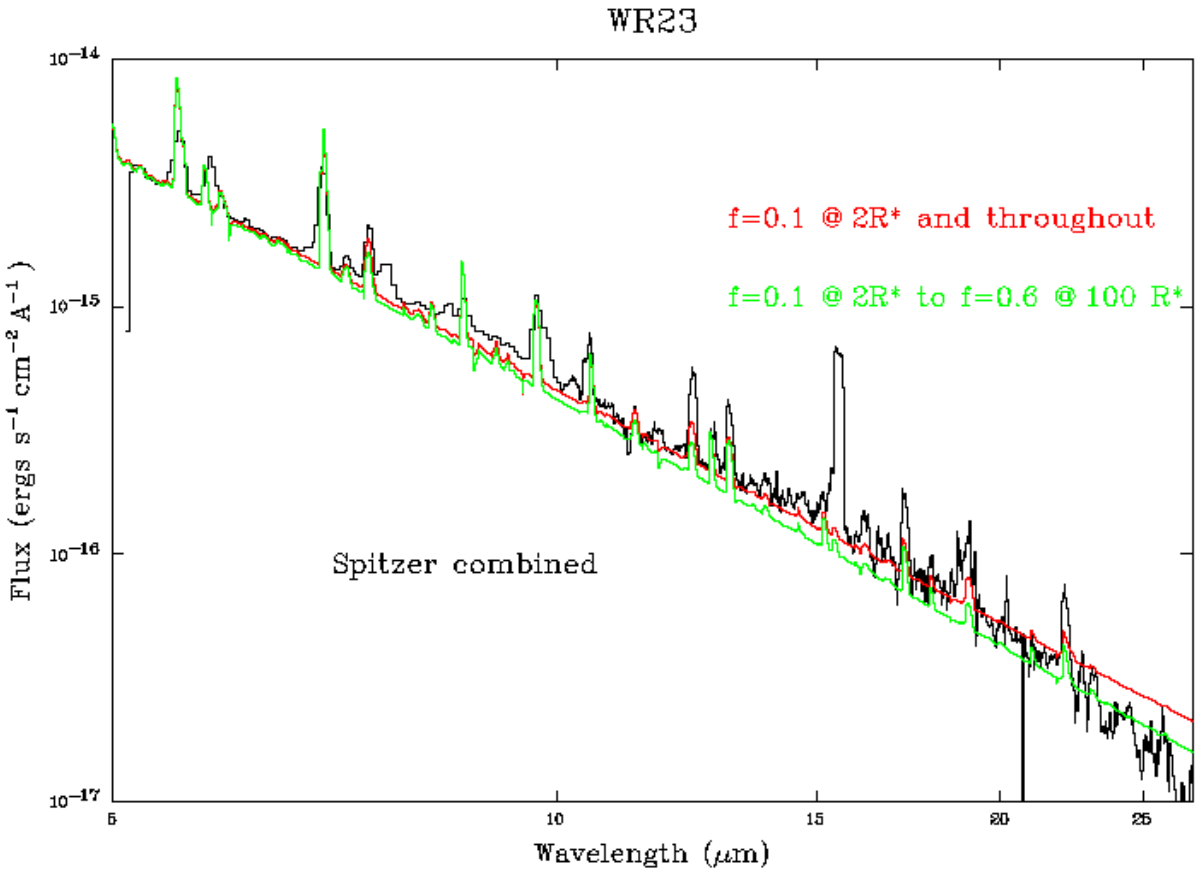

Figure 3: Spitzer data (5 to 35μm) of WR23. Overplotted are two model atmospheres, one with constant ($f = 0.1$ above 2 R_*; red) and one with a clumping that decreases outwards again (green). The constant-clumping model repreduces the observed continuum slope much better. Neon has not yet been included in the model, so that e.g. the strong [NeIII]λ15.5μm line is not reproduced.

in the mid-IR. Due to the broad spectral coverage of our mid-IR data and the rather pronounced effect clumping has on the mid-IR continuum, even slight changes in the clumping of the outer wind can be easily noticed. However, a more thorough analysis is required. Major points are the robustness of the clumping law in terms of the onset of the clumping roll-off, and its slope.

Provisionally using constant volume-filling factors throughout the wind and mass-loss rates, and Dessart et al.'s (2000) approach to derive Ne abundances, we find that the Ne fraction in our sample stars is $\sim$ 1% by mass. These results are in line with what is expected from model calculations of reaction rates and new solar abundances.

We would like to thank our co-investigators on the Spitzer IRS programme, Drs. P.W. Morris, P.M. Williams, K. van der Hucht, A.J. Willis, J.D. Smith, and D.J. Hillier.

References

Dessart, L., Crowther, P.A., Hillier, D.J., Willis, A.J., Morris, P.W., van der Hucht, K.A. 2000, MNRAS, 315, 407

Hillier, D.J. 1991, A&A, 1991, 247, 455

Hillier, D.J., Miller, D.L. 1998, ApJ, 496, 407

Maeder, A. 1983, A&A, 120, 113

Runacres, M.C., Owocki, S.P. 2002, A&A, 381, 1015

Ignace: How do errors for the absolute flux calibration affect your slope fitting?

Schnurr: Certainly, the quality of the flux calibration is an issue that will have to be discussed, but while we are aware of it, we have not yet looked into it.

Barniske: Do you see signs of dust present in the mid-IR spectra?

Schnurr: Presently, we think that non of our program stars shows a dust excess (after all, we have chosen WC4 to WC8 types for this reason), but yes, we will have to be careful.

Oskinova: Did you study the shape of forbidden [Ne] emission lines?

Schnurr: So far, we have not even included neon into our model atmosphere, but in principle, [Ne] lines give some information about the velocity structure. These lines form in the outer wind and therefore should be flat-topped. Unfortunately, the SPITZER-IRS spectral resolution does not allow for a more sophisticated analysis of the line profiles.

Najarro: Are the neon lines sensitive to the radial structure of clumping compared to the constant clumping models?

Schnurr: Yes, they are.

Clumping in Hot Star Winds
W.-R. Hamann, A. Feldmeier & L.M. Oskinova, eds.
Potsdam: Univ.-Verl., 2008
URN: http://nbn-resolving.de/urn:nbn:de:kobv:517-opus-13981

On the influence of clumping on O and Wolf-Rayet spectra

D. J. Hillier
University of Pittsburgh, USA

Overwhelming observational and theoretical evidence suggests that the winds of massive stars are highly clumped. We briefly discuss the influence of clumping on model diagnostics and the difficulties of allowing for the influence of clumping on model spectra. Because of its simplicity, and because of computational ease, most spectroscopic analyses incorporate clumping using the volume filling factor. The biases introduced by this approach are uncertain. To investigate alternative clumping models, and to help determine the validity of parameters derived using the volume filling factor method, we discuss results derived using an alternative model in which we assume that the wind is composed of optically thick shells.

1 Introduction

Evidence for clumping is widespread. It is evident in images of nebulae, it manifests itself through continuum, line and polarization variability (e.g., Lépine 1999, Eversberg et al. 1998), through the relative strength of electron scattering wings to their adjacent line (Hillier 1991), in the unusual strength of certain resonance lines (e.g., P V) and subordinate lines (e.g., O V 1371Å)(Crowther et al. 2002; Hillier 2003; Hillier et al. 2003; Bouret et al. 2003; Massa et al. 2003), and in the profiles of X-ray wind lines (e.g., Kramer et al. 2003). Theoretically, clumping is expected to occur in winds produced by radiation pressure acting on bound-bound transitions (Lucy & Solomon 1970; Owocki et al. 1988).

Clumping influences spectra formation in several ways. First, it enhances (relative to a smooth spherical wind) the strength of emission lines, such as recombination lines and collisionally excited lines, that depend on the square of the density. Consequently, clumping allows a given observed emission line spectrum to be reproduced using a lower mass-loss rate. As some features depend only linearly on the density (e.g., electron scattering wings, P V in some O stars) the relative strength of features can be changed in a way that cannot be achieved by any other reasonable mechanism. Second, clumping allows for the wind to be porous, enabling photons to escape more freely. This has been invoked to explain X-ray line profiles (e.g., Oskinova et al. 2006). Third, clumping potentially allows a wider range of ionization stages to be present in the wind (see, e.g., Hillier 2003).

The incorporation of clumping into radiative transfer calculations is extremely difficult. First, clumping requires 3D radiative transfer, which is computationally expensive. Homogenous 3D models are at least three orders of magnitude more expensive than similar 1D models, while clumping introduces even more computational requirements because of the need for finer spatial and angular grids. Second, the properties of clumps in stellar winds are poorly known (but see Dessart & Owocki 2002, 2003, 2005). In general, we need to specify the size, density, and velocity of clumps (locally and as a function of radius), their internal structure, the nature of the interclump medium, and the mechanical energy deposition rate. Third, clumping introduces additional complexities into the radiative transfer. As noted by Williams (1992), for example, individual clumps can be optically thick and hence have their own ionization structure. Further, clumps can shield other clumps from the radiation field, affecting the level populations and hence the observed spectrum. Fourth, clumped winds may be inherently non-spherical, especially if rotation and/or pulsations play an important role in producing clumping. Evidence for non-sphericity is provided by the presence of "Discrete Absorption Components" (DACs) in UV resonance profiles, and other UV variability. Finally we note that clumping introduces additional free parameters potentially exacerbating degeneracies. We note, for example, that a disk causes many of the same effects as clumping. As a consequence of the difficulties outlined above, and the extreme computational effort, approximate techniques are generally used to allow for the effects of clumping.

A computationally expedient technique for incorporating clumping is the use of the volume filling factor (f). It provides a method for treating clumping exactly under the assumption that the medium is made of small, uniform density, optically thin clumps which occupy a fractional volume "f". While in practice these conditions are unlikely to be met, it does provide an excellent fit to spectral features insensitive to clumping in both Wolf-Rayet (W-R) and

O stars while not destroying the fit to clumping sensitive features (e.g., Hα). Another advantage of the volume filling factor approach is that one only needs to specify a single parameter ($f(r)$) at each radius — in practice one allows f to vary smoothly with radius in which case a minimum of 2 parameters are needed (Hillier & Miller 1999). Other techniques for treating clumping, with different assumptions, are also being developed (e.g., Oskinova et al. 2007).

In W-R stars the volume filling factor approach provides a means to fit the electron scattering wings on emission lines, while simultaneously allowing the strength of most emission lines and continuua to be fit (e.g., Hamann & Koesterke 1998; Hillier & Miller 1999). It is still difficult to get a simultaneous fit to both high and low ionization lines, and this may be a consequence of the simplicity of the volume filling factor approach. In O stars, the volume filling factor allows models to be developed which fit most diagnostics. In particular, it provides a means of matching the strength of the P V resonance lines, the O V 1371Å subordinate lines, and strong photospheric lines simultaneously with emission lines such as Hα (Hillier et al. 2003, Bouret et al. 2003)

2 Shell model

An alternative approach to incorporate clumping is to assume that the wind is composed of dense spherical shells. While this approach has its obvious limitations it has three important strengths. First, the non-LTE problem can be solved exactly in a situation where optical depth effects in the clumps are important. Second it allows the influence of clumps on spectra to be investigated using qualitatively different assumptions. Third, it provides test results for other techniques.

We have computed shell-like models for the O star AV83 (O7 Iaf) and a W-R WN5-like star (e.g., HD 50896). In the model the shells were assumed to be equally spaced in $\log r$ and the shell size/density was adjusted to give the required volume filling factor. An illustration of a sample density structure is shown in Figure 1.

For AV83 reasonable quality fits to the spectra were obtained — a quality similar to that obtained with the volume filling factor approach. Additional calculations are being undertaken, and a more rigorous comparison will be published elsewhere.

For the WN5 star the conclusions are dramatically different. The shell model provides a very poor fit to a WN5 spectrum. In particular optically thick emission lines are much weaker than in the volume filling factor approach, while the continuum fluxes, and optically-thin line fluxes, are very similar (Fig. 2). The changes show some similarities to that seen for the optically-thick clump model of Oskinova et al (2007). The weakening of the lines can be explained by optical depth effects in the clumps. For the continuum, the clumps are effectively thin and thus their strengths remain similar. Unfortunately the correct line strengths cannot be recovered by increasing the mass-loss rate, as this would increase the continuum fluxes, destroying the agreement with observation. The distinct behavior of lines and continuua in W-R stars provides a mechanism for investigating the presence of optially-thick clumps in winds. The present modeling (albeit limited) argues that the clumps in W-R stars are better treated as optically thin. In O stars, it might be possible to use IR through radio fluxes, in combination with line measurements, to make similar inferences although in such cases it is also necessary to allow for the variation of clump properties with location in the wind.

The ionization structure of the shell model, and the equivalent volume filling factor model, are qualitatively similar. Both models show, for example, that helium is doubly ionized in the inner wind, and singly ionized in the outer wind. However, in the shell model the ionization does not vary smoothly with radius — the low density regions exhibit a higher ionization than do the denser shells. While the He II departure coefficients show a global similarity to that seen for the volume filling factor model, the variation across the shells is complicated. In the inner region, for example, the shell model tends to have large departure coefficients due to the enhanced photon trapping in optically thick lines.

The shell models reveal some interesting computational aspects. First, the Sobolev approximation is no longer valid. This occurs because photon escape is affected by the finite size of the clumps — photons can escape from the clump surface much easier than from the center of the clump. If the lateral size of the clumps is comparable to their radial size (as suggested by the studies of Dessart & Owocki (2002, 2003, 2005) fragmenting the shells might potentially have a significant effect, since it would increase the surface area from which photons could escape. Second (and as noted by Hamann during the meeting), the shell model has velocity porosity (a term introduced by Owocki, this meeting) because the shells are located at distinct radii, and hence at distinct velocities. Since the shells are complete, there is limited "volume" porosity; there is some porosity due to the finite number of shells. Third, it is necessary to treat a large number of rays in order to fully resolve the radiation field. In the non-LTE calculation we used a fine spatial grid across the shells, and a much coarser grid for the inter-shell medium. This is probably an adequate approach as the moment equations are used to solve for the mean intensity; the angular dependance of the radiation field only enters through the Eddington factors, and the denser material generally dominates spectral formation. For the calculation of the formal spectrum we initially adopted the usual approach, and chose the impact parameters according to the radius grid. This approach is inadequate, and produced "spiked profiles", an effect

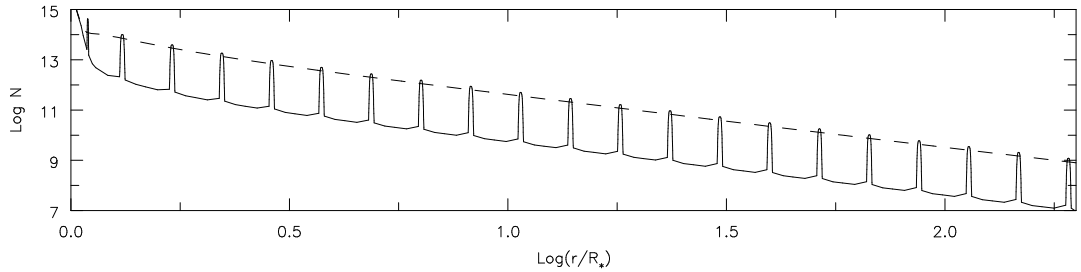

Figure 1: Illustration of the density (atoms/cm^3) structure of a WN5 shell model as a function of radius. Also shown (solid line) is the density of the model which uses the volume filling factor approach.

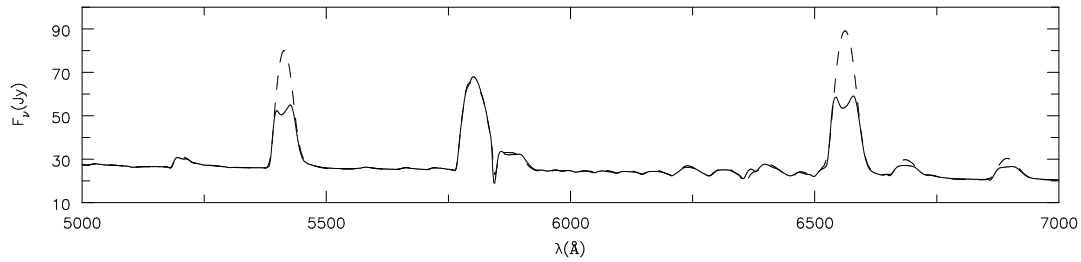

Figure 2: Spectral comparison between the WN5 shell model (solid) and volume filling factor model (dashed). The later model was scaled by a factor of 0.945 to facilitate line comparison. Notice that optically thick lines (e.g, He II 5411Å) are significantly reduced in intensity while other lines (e.g., C IV/He I complex at 5800 to 5900Å) are unchanged.

related to velocity porosity (along a given sight-line only some velocities are represented). To solve this problem additional rays, with impact parameters located in the inter-clump medium, had to be inserted.

3 Conclusion

The volume filling factor approach has proved a worthwhile tool, and has allowed simultaneous excellent fits to be obtained to multiple features, both clumping-sensitive and clumping-insensitive, in W-R and O stars. However the approach is simplistic, and its basis and adequacy needs to be tested via very detailed spectroscopic studies, through theoretical studies of clump generation, and through the use of alternative methods for treating clumping. For W-R stars, an alternative approach using optically thick shells appears to be less able to quantitatively match observed spectra.

DJH wishes to thank Stan Owocki for supplying a clumped model of Zeta Pup.

References

Bouret, J.-C., Lanz, T., Hillier, D. J., et al. 2003, ApJ, 595, 1182
Crowther, P. A., Hillier, D. J., Evans, C. J., et al. 2002, ApJ, 579, 774
Dessart, L., Owocki, S. P. 2002, A&A, 383, 1113
Dessart, L., Owocki, S. P. 2003, A&A, 406, L1
Dessart, L., Owocki, S. P. 2005, A&A, 437, 657
Eversberg, T., Lépine, S., Moffat, A. F. J. 1998, ApJ, 494, 799
Hamann, W.-R., Koesterke, L. 1998, A&A, 335, 1003
Hillier, D. J. 1991, A&A, 247, 455
Hillier, D. J., Miller, D. L. 1999, ApJ, 519, 354
Hillier, D. J., 2003, in *A Massive Star Odyssey: From Main Sequence to Supernova*, IAU Symp. 212, eds, K. van der Hucht, A. Herrero, C. Esteban, p .70
Hillier, D. J., Lanz, T., Heap, S. R., et al. 2003, ApJ, 588, 1039
Kramer, R. H., Cohen, D. H., Owocki, S. P. 2003, ApJ, 592, 532
Lépine, S., Moffat, A. F. J. 1999, ApJ, 514, 909
Lucy, L. B., Solomon, P. M. 1970, ApJ, 159, 879
Massa, D., Fullerton, A. W., Sonneborn, G., Hutchings, J. B. 2003, ApJ, 586, 996
Oskinova, L. M., Feldmeier, A., Hamann, W.-R. 2006, MNRAS, 372, 313
Oskinova, L. M., Hamann, W.-R., Feldmeier, A. 2007, A&A, 476, 1331
Owocki, S. P., Castor, J. I., & Rybicki, G. B. 1988, ApJ, 335, 914
Williams, R.E. 1992, ApJ, 392, 99

Najarro: Have you checked the parameterized shell model for ζ Pup in the UV? Would you see stronger effects in the optical in this star if the clumping would start at smaller radii?

Hillier: The current models have only been run for two cases, an AV83 like model, and a WN5 like model. Any effect on optical lines for ζ Pup will crucially depend on the exact mass loss rate, and where the clumping starts. As yet I have not had a chance to study the influence on lines in detail, and more test calculations need to be run.

Hamann: I agree that we are (almost) perfectly happy with the agreement between models and observations of WR spectra. Macroclumping can only spoil this happiness. However, for O stars we need to solve the P v discrepancy, that is why macroclumping is so interesting. Maybe WR clumps are smaller than O star clumps?

Hillier: Whether WR clumps are smaller than O star clumps remains to be seen, obviously one difference between O and WN5 stars is that the former contain H and the latter (generally) do not. As for the O stars I think it is important not to concentrate on P v and Hα only; there are other lines which also show sensitivity to lower mass loss rates and/or clumping. Furthermore, to understand the P v problem it is important to do detailed modelling in order to get the correct ionization structure. As I understand it to date, detailed modelling of O stars using the approximate volume filling factor approach has led to at most a factor of ten reduction (usually less, see Bouret's talk). Porosity may decrease this reduction by a factor of two, but it is clear that mass loss rates are lower than values derived from Hα.

Ignace: For lines from discrete spherical shells, some had a double-horned appearance. Are those the effect of escape from a thick shell dominating that line?

Hillier: The lines showing the horns are indeed optically thick. However the models are still rather preliminary, and there are some issues that I still need to resolve for computing accurate line profiles from these clumped media. It is also possible that the horns will disappear in models where the shells are broken up into detached pancakes.

Clumping in Hot Star Winds
W.-R. Hamann, A. Feldmeier & L.M. Oskinova, eds.
Potsdam: Univ.-Verl., 2008
URN: http://nbn-resolving.de/urn:nbn:de:kobv:517-opus-13981

Discussion: Spectral modeling

Moderator: Alex Fullerton

Hirschi: What is the importance of the clump size?

Townsend: We do not see individual clumps in a wind, so the clump sizes must be under some threshold, but is otherwise unconstrained. Porosity can work independently of the clump size, the key parameter is the porosity length $h \equiv L^3/l^2$, where L is the interclump distance and l is the clump size.

Moffat: But one has a distribution of sizes according to some power law, so does your lack of sensivity to unique clump size at a given radius also apply?

Fullerton: Something else we should try to keep in mind is how structure on various spatial scales merges together. Basically, what mental picture should we have of these winds? What would they look like if we could get closer to them? Evidently many or most have large-scale structures or disturbances like CIRs or whatever causes DACs. But as we zoom in, they are also comprised of physically smaller inhomogeneities, which may or may not be optically thick depending on a variety of things, including what wavelength you use as a probe. How does all this structure manage to coexist?

Cohen: I think the optically thick absorption lines in clumps (optically thick clumps) provide means of getting at clump sizes. This is because of the requirement that clumps be optically thick. If a model reproduces the absorption lines, and assumes optically thick clumps, then the line opacity and density determine a minimum clump size.

Moffat: The $\dot{M}$ correction does not depend on size but rather densities, although both are coupled.

Najarro: What is the mass loss correction the "community agrees" upon, 1, 3 or 10?

Puls: So far, we have dealt mostly with the density stratification (micro-/macroclumping), but it is similarly important to consider the velocity field. Mostly, the velocity field inside the clumps is assumed to follow the standard law, while the hydrodynamic simulations show that the velocity field inside the clump changes considerably, becoming rather flat and multiply non-monotonic. This should have a considerable effect particularly for resonance lines, since the $\bar{J}$ depends crucially on the local escape, which is controlled by $\mathrm{d}v/\mathrm{d}r$.

Townsend: As reply to Puls' comment about incorporation of velocity fields in clumped models: this is already being done in the statistical models of Stan Owocki and Wolf-Rainer Hamann and also (just last week) in my Monte Carlo code.

Najarro: Would the ionization of P V not be frozen in the interclump medium?

Cassinelli: In a paper by Brown et al. (2004, A&A, 426, 323), we addressed the role of clumps in regards to the classic wind momentum problem for Wolf-Rayet stars. It was typically found that the wind momentum rate $\dot{M}v_\infty$ exceeded the radiation momentum rate L/c by factors of order 30. This was explained away in two parts. Theorists realized that more momentum by about a factor of five to ten could be extracted from the radiation field by way of multiple scatterings (Lucy & Abbott 1993, ApJ, 405, 738; Gayley et al. 1995, ApJ, 442, 296). Observers found that mass loss rates derived from radio free-free fluxes could have been overestimated by factors of $1/(\text{filling factor})^{1/2}$ owing to clumpiness of the winds. The filling factors are very small, in the range 10^{-4} to 10^{-3}. In Brown et al., it is shown that the two effects of multiple scattering and enhanced radio flux compete rather than complement each other. This is because clumpiness of the extent needed leads to very long photon mean free paths, and this increases the escape of the radiation and eliminates the possibility of multiple scattering and thus leaves the momentum problem unsolved.

Townsend: In answer to Joe Cassinelli's point about porosity/clumping reducing radiative driving in WR stars: this will only occur if there is a significant difference in optical depth between the clumps and the interclump medium. Only if you can create channels, by which photons can easily escape the medium, you will suffer a reduction in the radiative force.

Hamann: In principle, radiation driving is hampered by macroclumping: material which hides itself in optically thick clumps experiences no radiation pressure, as you (Joe Cassinelli) have pointed out in your paper Brown et al. However, optically thick lines do not contribute much to the radiative driving anyhow. A further effect predicted by strong macroclumping is a residual intensity in the absorption minima of P Cygni lines. Here I have a question to the instrument specialists. From the good old IUE times I remember that we could never trust the background subtraction. So what we did was just to

take a long ruler and draw the zero-intensity level from *assuming* that the deepest absorption minima, e.g. of the C IV or the N V resonance lines, are completely black. Could a rest intensity of a few percent therefore have escaped from detection?

Massa: New IUE data reductions and STIS suggest that there cannot be more than $1-2\,\%$ of flux there.

Gull: In reference to STIS echelle spectra and black troughs, some caution must be applied. The STIS calibration had to address a wavelength-dependent point spread function. Ideally, totally black interstellar absorption lines were used where possible, but they are inconveniently spaced across the UV. Broad "black" wind absorptions were also used to extend those studies, which were done in the initial operational phase. While there is little or no evidence for errors in calibration, e.g. no negative fluxes beyond photon statistical level, the observer should consider a 1% level as the limit without further independent tests.

Sonneborn: Independent of the calibration and spectral extraction, the strong ISM lines (Ly α, C II, etc.) will be saturated (and black) for any star beyond ~ 100 pc from the sun. Use these lines to check on any low level residual flux in the stellar wind lines.

Prinja: I think it is very important to remember that substantial variability is seen in the UV resonance lines and Balmer lines of O stars, early B supergiants and late B stars. Their fluctuations over a smaller time scale (hours to days) are not due to the (small scale) clumping that is dominating our discussions. These characteristic changes are diagnostics of the substantial role of other (large scale) structures in the wind. Small scale clumps are not going to change the equivalent width of Hα in a B supergiant by a factor of $\sim$ seven over a day or so.

Moffat: It is time for observers to become more innovative. Some ideas come to mind: e.g. in eclipsing binaries perhaps one can constrain clump sizes during eclipses, or in massive X-ray binaries looking at X-ray flares.

Feldmeier: It is not just the clump size that matters, but also the clump shape. Since the outflow is strongly radial, spherical clumps, and therefore isotropic turbulence, may not be expected. Instead, the clumps should be rather "flat", and oriented perpendicular to the outflow direction. If the X-ray emission really originates from small, fast clumps crashing into big, slow clumps, then this clump shape (spherical vs. flat) has a large influence on the X-ray line shape.

Puls: It has to be stressed that multiple non-monotonic v-fields do create a black trough, but can modify the red emission part considerably with respect to its shape. I guess that the precise shape should depend on the distribution and shape of the clumps, and might be used as a diagnostic tool. Would it be possible to use interferometry to obtain information on the structure at least in the outer regions of not too thin winds (as was done earlier for P Cygni)?

Feldmeier: In our time-dependent hydrodynamic simulations, we have recently (2006, A&A) began to include this multiple scattering in non-monotonic velocity fields in the calculation of the radiative line force, using the source function iteration procedure of Rybicki & Hummer (1978, ApJ). At each of some 20,000 time steps of the simulation, the source function is calculated by standard lambda iteration (which converges quickly due to the small number of discrete coupling points) over the full spatial mesh.

Townsend: In answer to Alex Fullerton's question about "what is the key issue?" I would like to understand what the clumps actually look like. Are they pancakes? Spheres? The small scale structure seen in the 2D line-driven instability calculations by Stan Owocki and Luc Dessart? And to answer this question, we really need to get a handle on what causes the clumping.

Cohen: Can the line-driven instability make structures at arbitrarily small radii?

Feldmeier: It does not seem so. Even if you apply large photospheric perturbations, say Langevin turbulence with a velocity dispersion on the order of the sound speed, a pronounced wind structure develops only when the wind reaches about one third of the terminal speed. But there are also delicate issues about growth rates when applying the EISF force instead of the SSF force, so it is really difficult to know if there is pronounced structure close to the star.

Ignace: What does MOST tell us about hot stars? I am specifically thinking of producing structure in the deep wind.

Moffat: MOST has observed several WR and OB stars. The variation in OB stars (m-magnitude) comes mostly from non-radial pulsations due to p-mode and g-mode. In WR, a WN8 star is highly variable at the 10% level, which must be due to pulsations at multiple frequencies, not due to clumping, since the variation amplitude is large.

Massa: Doublets contain additional information that has not been tapped. I will be talking about that tomorrow. This will give a way to determine parameters for simple models that may help guide us to the next level.

Cassinelli: I see a problem in your assumption that the ion stage is P V inside the clumps, and which allows you to get the total column density of P V. If shock fronts at the face of the clumps are the sites for the formation of the X-rays, then the X-ray mean

intensity inside the clumps can be very high, and in this case the dominant ionization stage can be changed owing to the Auger effect. In the case of elements with fewer than ten electrons, K shell absorption by the dominant ion leads to the ejection of two electrons, and for heavier elements, like Phosphorus, an even larger number of electrons can be ejected by the Auger process (Odegard & Cassinelli 1982, ApJ, 256, 568). The net effect would be that the mass loss rates might not be reduced by anywhere near as much as you have calculated under the assumption that P V is the dominant stage everywhere in the wind.

Hamann: With present interferometry facilities, there is no chance to resolve clumps in hot-star winds. Given the relatively large distance to the OB and WR stars, one would need a resolution of about 10^{-5} arcsec, while e.g. ESO-VLTI can resolve only milli-arcseconds.

Prinja: The impressive upgrades to radio facilities such as e-MERLIN and EVLA will provide greater sensivity that permits us to conduct deeper surveys of clumping as a function of stellar parameters ($T_{\rm eff}$, $v_{\rm rot}$, $\dot{M}$). A survey that includes not only O supergiants, but also (weak wind) O main-sequence and B giants is now going to be possible.

Massa: I would just like to add that as we detect stars with weaker winds we will be sampling deeper into the wind. This will make interpreting the observations more difficult, but also provide more information.

Owocki: It is perhaps important to distinguish between multi-D radiation hydrodynamic models for small vs. large-scale structure. The latter can be done using a generalized CAK/Sobolev approach for the line force, which is purely local and thus quite tractable in even a 3D model.But small-scale structure arising from the line-driven instability can have a size near and below the mean Sobolev length, making a Sobolev treatment useless. Instead, this requires a fuller *non-local* treatment of the time-dependent transport, using various approximations based on integral escape probabilities (such as the "Smooth Source Function" (SSF) or "Escape Integral Source Function" (EISF) methods). It is now relatively routine to carry out instability simulations in simple 1D models. But 2D or 3D models are still a real challenge, and have only been done in approximations that ignore the lateral components of the radiation force, e.g. the 2D hydrodynamic and 1D radiation models computed by Luc Dessart. My basic point is that there are still great challenges if we want to model such small-scale clumping in multi-D. But at least these initial efforts give some clues that we should pay attention to as we develop more phenomenological descriptions involving the clumping factor and porosity.

Cohen: Even at the national labs the full 3D radiative transfer is not being done. And they have quasi-infinite resources.

Hydrodynamic modeling (stationary)

Chairs: R. Ignace, P. Najarro

Clumping in Hot Star Winds
W.-R. Hamann, A. Feldmeier & L.M. Oskinova, eds.
Potsdam: Univ.-Verl., 2008
URN: http://nbn-resolving.de/urn:nbn:de:kobv:517-opus-13981

Clumping in hydrodynamic atmosphere models

G. Gräfener
Universität Potsdam, Germany

We investigate the effect of wind clumping on the dynamics of Wolf-Rayet winds, by means of the Potsdam Wolf-Rayet (PoWR) hydrodynamic atmosphere models. In the limit of micro-clumping the radiative acceleration is generally enhanced. We examine the reasons for this effect and show that the resulting wind structure depends critically on the assumed radial dependence of the clumping factor $D(r)$. The observed terminal wind velocities for WR stars imply that $D(r)$ increases to very large values in the outer part of the wind, in agreement with the assumption of detached expanding shells.

1 Hydrodynamic PoWR models

The new hydrodynamic PoWR models are the first model atmospheres that solve the full wind hydrodynamics in line with a detailed NLTE radiative transfer. The models have been applied to different Wolf-Rayet (WR) subtypes, from H-free WC stars with extremely hot core temperatures (Gräfener & Hamann 2005) to late-type WN stars with much lower temperatures and considerable amounts of hydrogen at their surfaces (Gräfener & Hamann 2006, 2007). The basic result from these computations is that the enhanced WR-type mass loss is primarily triggered by the proximity to the Eddington limit.

When stars approach the Eddington limit their effective surface gravity is reduced. The large density scale height then supports the formation of optically thick stellar winds. For such winds the critical point is located at large optical depth, close to the point of zero effective gravity (see Nugis & Lamers 2002). Their mass loss thus depends on the flux-mean opacity in deep atmospheric layers, and on the Eddington factor Γ_e. Particularly because of the ρ,T–dependence of the mean opacity, these winds have qualitatively different properties than classical OB star winds (see Gräfener & Hamann 2006, 2007).

The large optical depth of their stellar winds is chiefly responsible for the observed properties of WR stars. Photons are typically absorbed and re-emitted τ^2 times, which causes the large observed wind momenta ($\dot{M} v_\infty \approx \tau \cdot L/c$). The efficient re-distribution of ionizing photons in the wind leads to recombination cascades which are responsible for the observed emission line spectra. Note that the dominance of recombination processes leads to an over-population of excited energy levels which is the basic reason for the sensitivity to wind clumping (see Sect. 2).

Large Eddington factors are a prerequisite for the formation of WR-type winds. According to our models the most massive stars can reach this state already at the end of their main-sequence lifetime, i.e., still in the pase of central H-burning. Less massive objects enter the Wolf-Rayet stage after the onset of He-burning. For two extremely luminous, H-rich WNL stars in Carina OB 1 (WR 22 and WR 25) we derive masses of at least 80–100 $M_\odot$. Such stars are presumably the direct descendants of the most massive stars in the galaxy (Gräfener & Hamann 2007).

2 The role of wind clumping

Wind clumping is routinely taken into account in spectral analyses to fit the electron scattering wings of strong WR emission lines. Its main effect is that the mean $<\rho^2>$ increases and the derived mass loss rates, relying on ρ^2-diagnostics, decrease with $\dot{M} \propto 1/\sqrt{D}$ (see Hamann & Koesterke 1998). In our previous work we have shown that clumping also affects the wind acceleration in O supergiant (Gräfener et al. 2002, Gräfener & Hamann 2003) and WR star winds (Gräfener & Hamann 2005, 2007). The specific choice of the clumping factor $D(r)$ has a major influence on the wind dynamics in our models.

The reason for this is that due to the increase of $<\rho^2>$ in a clumped wind, more excited energy levels are populated by recombination. For the weak lines connected to these levels, a clumped wind thus mimics the opacity of an un-clumped wind with a factor of $\sqrt{D}$ larger density. The radiative force from these lines in a clumped wind is thus similar to an un-clumped wind with higher density. In effect the wind acceleration is larger by a factor $\sqrt{D}$.

At this point it is necessary to emphasize that we assume small-scale clumps, or micro-clumping in our models. In this limit the separation between clumps is so small that the mean opacity can be used in the radiative transfer. In the limit of large clump separation, or macro-clumping, the optical depth of individual clumps may become large. Brown et al. (2004) have shown that in this case the radiative ac-

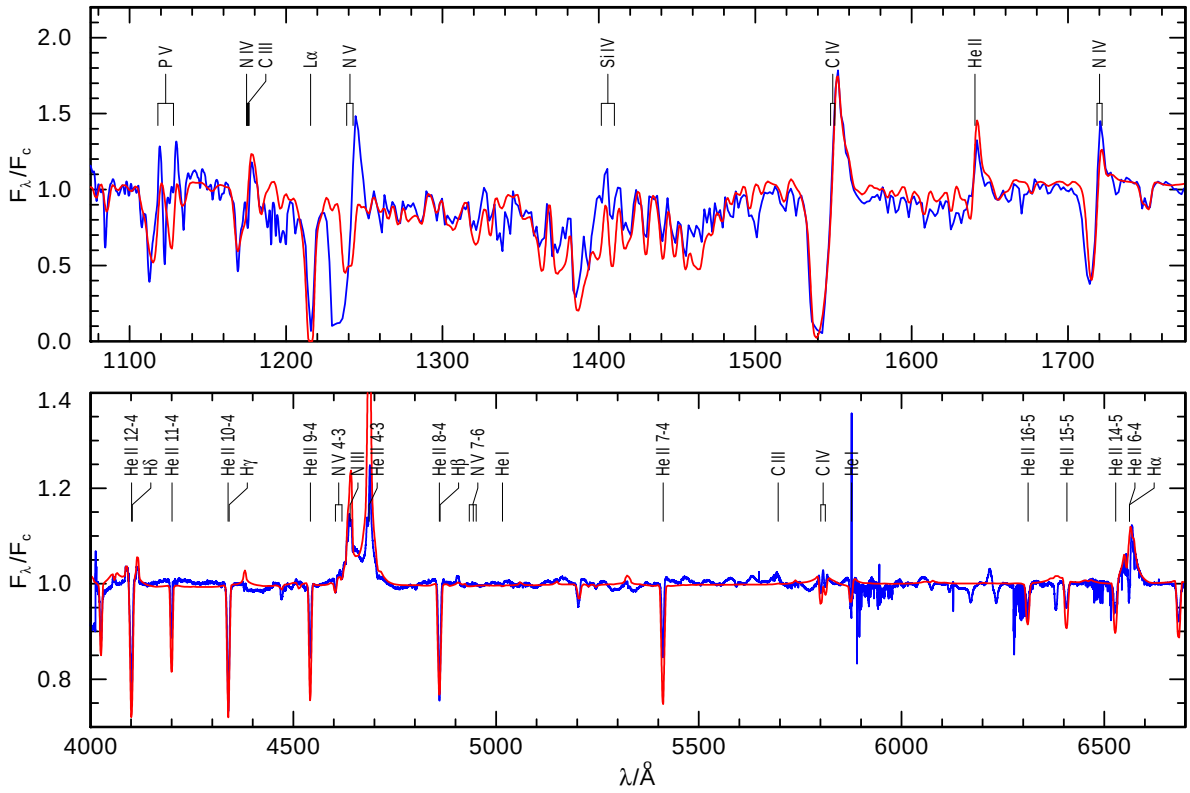

Figure 1: Self-consistent wind model for ζ Pup, with an increasing clumping factor ($D \propto v$, see text for more details). For a metallicity of $Z = 2/3\, Z_\odot$ the observed spectrum is reproduced with a very low mass loss rate ($\dot{M} = 7.4\,10^{-7} M_\odot/\mathrm{yr}$). Note that the discrepancy for the N V resonance line at 1240 Å is presumably caused by the neglect of X-ray radiation in this model.

celeration is reduced by geometrical effects. Moreover, Oskinova et al. (2007) have demonstrated that macro-clumping can considerably affect the spectral line diagnostics. We thus have two counteractive effects which may both affect our results. Micro-clumping increases the radiative acceleration with $a_{\rm rad} \propto \sqrt{D}$, and macro-clumping decreases $a_{\rm rad}$ dependent on the detailed clump-geometry. In our present models only micro-clumping is taken into account.

First results from our hydrodynamic models clearly favor large clumping factors. WR wind models with the typical observed values around $D = 10$ underestimate the terminal wind speeds of early to intermediate subtypes (WC 5 and WN 6–7). To fit the observed wind velocities, larger clumping factors of the order of $D \approx 40$ are needed (see Gräfener & Hamann 2005). Our models with $D = 10$ thus underestimate $a_{\rm rad}$ in the outer wind layers by a factor of two. Admittedly, a part of this deficiency might be due to the neglect of trace elements like Ne, Ca, and Mg in our models. On the other hand, a very plausible solution of this problem is the assumption of a radially increasing clumping factor.

For radially increasing $D(r)$ the electron scattering wings, which are formed close to the star, still indicate low clumping factors while the clumping factors can be much larger in the outer wind where the acceleration to v_∞ takes place. Note that such an increase of D is indeed expected due to the wind expansion. E.g., for a geometry with spherically expanding, detached shells of constant thickness, the clumping factor would increase with $D \propto v$. First test models for WNL stars indeed provide larger terminal wind speeds, even slightly above the observed values.

3 Low O star mass loss rates

From the strength of the unsaturated P V resonance lines in OB star spectra, clumping factors of the order of 10–100 have recently been deduced (Crowther et al. 2002, Hillier et al. 2003, Bouret et al. 2003, 2005, Fullerton et al. 2006). If micro-clumping dominates, the observed mass loss rates should thus be revised downward by factors of 3–10. For the common OB star wind models this would however introduce massive problems. While the observed mass loss rates go down, the predicted values are expected

to increase due to micro-clumping (see the previous section). For the classical wind models it is thus necessary to introduce a combination of micro and macro-clumping to retain consistency (See also de Koter & Muijres, and Krtička et al., this volume). The strong downward revision of the OB star mass loss rates could be avoided in this way.

From a spectroscopic point of view the introduction of macro-clumping is however unnecessary. Models with micro-clumping reproduce the observed spectra of OB stars in an impressive way (e.g., Bouret et al. this volume). It remains to be shown if the same fit quality can be achieved under realistic model assumptions for macro-clumping. Moreover, the analysis of X-ray line profiles by Cohen et al. (this volume) strongly favors micro-clumping. In the present work we address the question if micro-clumping alone can account for the observed spectral properties of OB stars and the wind acceleration simultaneously.

Note that the classical wind models for OB stars generally employ the Sobolev approximation for the spectral line transfer. On the other hand, stellar atmosphere models like the CMFGEN code by Hillier & Miller (1998) and the PoWR models are based on a detailed radiative transfer in the CMF. These models reproduce the observed wind momenta of WR and OB stars only, if clumping factors of the order of 10 or larger are assumed (Gräfener et al. 2000, 2002, Gräfener & Hamann 2005, Herald et al. 2001, Hillier 2003, Hillier et al. 2003). The reason for the differences with respect to the Sobolev models is not yet fully understood (but see the discussion in Hillier et al. 2003 and the recent work by Lucy 2007). Nevertheless, it seems that the introduction of macro-clumping can be avoided for the CMF models because they predict a priori lower mass loss rates.

For our present OB star models we assume an outward increasing clumping factor, in analogy to our previous WR models. However, we only prescribe the growth rate of the clumping factor close to the stellar photosphere From $D = 1$ at $\tau_{\rm Ross} = 0.35$ to $D = 3$ at $\tau_{\rm Ross} = 0.03$ (which corresponds to a radius of $1.2\,R_\star$). Above this point we assume an increase with $D \propto v$, as expected for detached spherical shells of constant thickness. For the ζ Pup model in Fig. 1 this leads to a significant amplification of the clumping factor up to $D \approx 300$, just because of the wind expansion. Above $\approx 10\,R_\star$ a point is reached where the thermal pressure within a shell would exceed the external pressure due to the wind acceleration. From this point on we let the clumps expand with sonic speed, which leads to a fast decline of D. With an extremely low mass loss rate of $7.4\,10^{-7} M_\odot$/yr the model reproduces the observed strength of Hα and slightly underestimates P V. Under the assumption of pure micro-clumping, our present models thus seem to favor very low mass loss rates for OB stars.

References

Bouret, J.-C., Lanz, T., & Hillier, D. J. 2005, A&A, 438, 301

Bouret, J.-C., Lanz, T., Hillier, D. J., et al. 2003, ApJ, 595, 1182

Brown, J. C., Cassinelli, J. P., Li, Q., Kholtygin, A. F., & Ignace, R. 2004, A&A, 426, 323

Crowther, P. A., Hillier, D. J., Evans, C. J., et al. 2002, ApJ, 579, 774

Fullerton, A. W., Massa, D. L., & Prinja, R. K. 2006, ApJ, 637, 1025

Gräfener, G. & Hamann, W.-R. 2003, in IAU Symp., Vol. 212, A Massive Star Odyssey: From Main Sequence to Supernova, ed. K. A. van der Hucht, A. Herrero, & E. César (San Francisco: ASP), 190

Gräfener, G. & Hamann, W.-R. 2005, A&A, 432, 633

Gräfener, G. & Hamann, W.-R. 2006, in ASP Conf. Ser. 353: Stellar Evolution at Low Metallicity: Mass Loss, Explosions, Cosmology, ed. H. J. G. L. M. Lamers, N. Langer, T. Nugis, & K. Annuk, 171

Gräfener, G. & Hamann, W.-R. 2007, A&A, submitted

Gräfener, G., Hamann, W.-R., & Koesterke, L. 2000, in ASP Conf. Ser., Vol. 204, Thermal and Ionization Aspects of Flows from Hot Stars, ed. H. J. G. L. M. Lamers & A. Sapar (San Francisco: ASP), 215

Gräfener, G., Koesterke, L., & Hamann, W.-R. 2002, A&A, 387, 244

Hamann, W.-R. & Koesterke, L. 1998, A&A, 335, 1003

Herald, J. E., Hillier, D. J., & Schulte-Ladbeck, R. E. 2001, ApJ, 548, 932

Hillier, D. J. 2003, in IAU Symp., Vol. 212, A Massive Star Odyssey: From Main Sequence to Supernova, ed. K. A. van der Hucht, A. Herrero, & E. César (San Francisco: ASP), 70

Hillier, D. J., Lanz, T., Heap, S. R., et al. 2003, ApJ, 588, 1039

Hillier, D. J. & Miller, D. L. 1998, ApJ, 496, 407

Lucy, L. B. 2007, A&A, 468, 649

Nugis, T. & Lamers, H. J. G. L. M. 2002, A&A, 389, 162

Oskinova, L. M., Hamann, W.-R., & Feldmeier, A. 2007, A&A, 476, 1331

Feldmeier: Abbott (1982) showed that the flux distribution as function of frequency and the opacity distribution match very well, which is the reason for the efficient wind driving of O stars. WR stars should be even more efficient in wind driving. But your plot suggests that there is an offset between the flux and opacity distribution. Is this a contradiction?

Gräfener: The flux is partly blocked in the photosphere by Fe lines. This is something which would not happen if you use Sobolev approximation or if you treat the lines as scattering lines. And it definitely lowers the radiative acceleration.

Puls: At which radius is the density contrast decreased in ζ Pup (in order to obtain a correct radio flux)?

Gräfener: The decrease due to gas pressure sets in at $10\,R_*$, well before the radio regime.

Hillier: In the inner wind for ζ Pup there are obviously issues with the effect of microturbulence on the line force. However, in the outer wind I think you are significantly underestimating the line force by not including Ar, Ne, Cl, etc. In the outer wind, CMFGEN does not have significant problems in getting the appropriate line force, in fact with a small volume filling factor we can have the opposite problem (too much line force).

Gräfener: Alright, so I should include these elements, too.

Cassinelli: It appears your clumping occurs very close to the photosphere. How could clumps occur here?

Gräfener: Yes, the clumping sets in well below the sonic point and thus affects the mass loss rate. One could explain this for instance by the ideas of Shaviv about the formation of a photospheric structure when a star approaches the Eddington limit. Nevertheless, even if the formation of the clumps is difficult to explain I find it interesting that it is possible to produce O stars with low mass loss rates in this way, which are in agreement with the observed spectral diagnostics.

Owocki: Sobolev theory can in principle include multiple scattering or even branching of lines. So when you cite that there is a difference between Sobolev and CMF I think it is important to examine whether it is these effects of failure of Sobolev localization due to, e.g. large microturbulent broadening.

Gräfener: Yes it is important to find the reason. Concerning the line blocking I see the possibility that the treatment of line opacities as pure scattering opacity might be responsible. Generally, NLTE effects can change things, e.g. in case of an outward increasing line source function.

Ignace: IR forbidden lines form at very large radii in WR winds. A useful test of spectral models would be to reproduce observed line ratios, such as [Ne II] / [Ne III].

Clumping in Hot Star Winds
W.-R. Hamann, A. Feldmeier & L.M. Oskinova, eds.
Potsdam: Univ.-Verl., 2008
URN: http://nbn-resolving.de/urn:nbn:de:kobv:517-opus-13981

Advances in mass-loss predictions

J.S. Vink[1], P. Benaglia[2], B. Davies[3], A. de Koter[4] & R.D. Oudmaijer[5]
[1]*Armagh Observatory, Northern Ireland, UK*
[2]*Instituto Argentino de Radioastronomia, Argentina*
[3]*Rochester Institute of Technology, USA*
[4]*Astronomical Institute Anton Pannekoek, University of Amsterdam, The Netherlands*
[5]*School of Physics & Astronomy, University of Leeds, UK*

We present the results of Monte Carlo mass-loss predictions for massive stars covering a wide range of stellar parameters. We critically test our predictions against a range of observed mass-loss rates – in light of the recent discussions on wind clumping. We also present a model to compute the clumping-induced polarimetric variability of hot stars and we compare this with observations of Luminous Blue Variables, for which polarimetric variability is larger than for O and Wolf-Rayet stars. Luminous Blue Variables comprise an ideal testbed for studies of wind clumping and wind geometry, as well as for wind strength calculations, and we propose they may be direct supernova progenitors.

1 Introduction

This contribution consists of two complementary aspects of hot-star winds. We first describe the results of mass-loss predictions – widely used in current massive star models in the galaxy, and beyond. In particular, we test our predictions as a function of effective temperature against recent radio data, and we discuss the potential implications for the clumping properties of supergiants of various spectral types (Sect.2). We also discuss mass-loss predictions for the winds of Luminous Blue Variables (LBVs), and we present results of the clumping-induced polarimetric variability of hot-star winds (Sect. 3), before we conclude.

2 Monte Carlo mass-loss predictions

Our method to predict the mass-loss rates of massive stars is based on Monte Carlo radiative transfer calculations (see Vink et al. 1999, de Koter et al. 1997). In short, we compute non-LTE level populations for all relevant ions from hydrogen to zinc, before we follow the fate of a large number of photon packets through the wind. We predict the efficiency of the momentum transfer from the photons to the gas, generally assuming a pre-described velocity law (but see Vink et al. 1999, Müller & Vink, *in prep.*). We derive wind efficiencies, $\eta = (\dot{M}v_\infty)/(L/c)$, for a range of stellar parameters (including metallicities).

2.1 Results: successes

To gauge the success of our models and to be able to identify discrepancies, we test our predictions against a survey of radio mass-loss rates (Benaglia et al. 2007) from the free-free emission in hot-star winds.

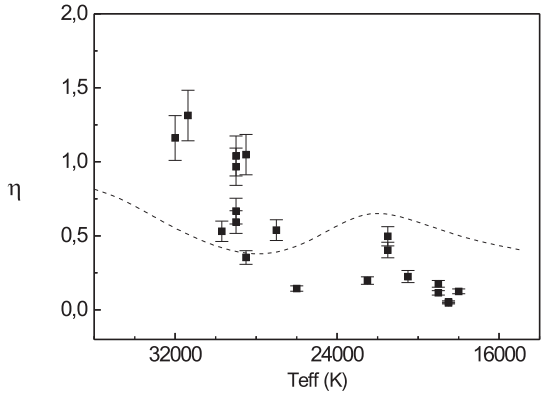

Figure 1: Radio wind efficiency vs. effective temperature (Benaglia et al. 2007). Overplotted are mass-loss predictions (Vink et al. 1999). Note the possible bi-stability jump at 21 000 K.

In Fig. 1, we plot the wind efficiency versus effective temperature in the regime of the wind bi-stability, where winds are predicted to change from

lower $\dot{M}$, fast winds, on the hot side, to higher $\dot{M}$, slow winds on the cool side – a result of a change in the Fe ionisation that drives the wind. We overplot the mass-loss predictions around the bi-stability jump (dashed line) and focus on the general trends, before we continue our discussion on quantitative aspects, and their implications, in Sect 2.2.

The overall behaviour shows that η declines when the temperature drops. At the highest temperatures, the flux and the opacity show large overlap and the momentum transfer efficiency is maximal. At lower effective temperature, the flux is gradually emitted towards lower wavelengths, and there is a growing mismatch between the flux and the ultraviolet line opacity. Figure 1 shows that our predictions of this overall behaviour are confirmed by the radio survey. Our second prediction is that there should be an increase in the mass-loss rate due to the opacity increase when Fe recombines from Fe IV to Fe III. Our radio data appear to confirm the presence of a local maximum around 21 000 K, although data around this critical temperate is, as yet, sparse.

The bi-stability limit is relevant for stellar evolution calculations when stars evolve off the main sequence towards the red part of the Hertzsprung-Russell diagram (HRD). It may also play a role for LBV winds, when LBVs such as AG Car, change their temperatures – and radii – on timescales of the S Dor variations (of the order of years to decades). This variable wind behaviour – predicted by Vink & de Koter (2002) – is anticipated to result in circumstellar media consisting of concentric shells with varying wind densities. Kotak & Vink (2006) recently suggested that the quasi-periodic modulations seen in the radio lightcurves of some supernovae may imply that LBVs could be *direct* supernova progenitors. At first this seems at odds with stellar evolution calculations, which do not predict LBVs to explode. However, there is a growing body of evidence hinting that LBVs may nonetheless explode (Pastorello et al. 2007, Smith 2007, Gal-Yam et al. 2007).

Despite the success of our models in explaining LBV mass-loss variability, the bi-stability jump, and the scaling of $\dot{M}$ with metallicity (see de Koter, this volume), we turn to discrepancies of our models against empirical mass-loss rates.

2.2 Results: discrepancies

Discrepancies have been noted between the Vink et al. (2000) predictions and empirical mass-loss rates in several areas of the HRD. One group of objects is that of low L ($\log L/L_\odot < 5.2$) O dwarfs, where the data of Martins et al. (2005) fall well below predictions, by factors of 10 or more. The reason for this discrepancy is as yet not understood. Another area of discrepancies is that of the B supergiants where empirical rates have been found to be much lower than predicted rates (Vink et al. 2000, Trundle & Lennon 2005).

The most worrisome however is the situation with garden-variety type O stars! Figure 1 shows that the Vink et al. (2000) predictions are *lower* than the observed rates. The radio rates are likely to be upper limits as the radio free-free emission is a ρ^2 process, and any form of clumping leads to a maximal $\dot{M}$. Mokiem et al. (2007) and Puls (this volume) noted that *if* this discrepancy is related to wind clumping – and theoretical rates are unaffected – the empirical ρ^2 mass-loss rates must be down-revised by a factor 2-3, suggesting a clumping factor $f \sim 5$. Recent massive star evolution models would not be effected by such modest clumping factors as these already use the theoretical Vink et al. (2000) rates.

If $f \sim 5$ were universal, one would expect the empirical $\dot{M}$ for B supergiants to be *lower* than indicated in Fig. 1 and the discrepancy would amount to an order of magnitude, or more. This implies there are some serious issues with our theoretical understanding of hot-star winds, and we need to reconsider even our most basic modelling assumptions, such as sphericity and homogeneity, which can be tested with linear polarimetry.

3 Linear polarisation variability

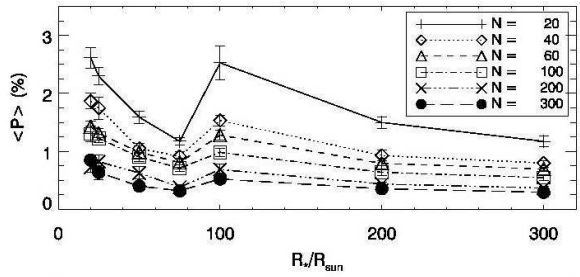

Figure 2: Polarisation variability vs. stellar radius – for different clump ejection rates. $N = \dot{N}\ t_{\rm fl}$, where $\dot{N}$ is the clump ejection rate (related to the mass-loss rate) and $t_{\rm fl} = R/v_\infty$ (see Davies et al. 2007).

Linear polarimetry is a tool to measure asymmetries. Davies et al. (2005) performed a polarimetric survey of LBVs and found asymmetries in a majority of them. When the position angle (PA) of the polarisation shows a straight line in the Stokes QU diagram this is generally attributed to a large-scale, axisymmetry, e.g. a disk. Davies et al. (2005) found time-variable PAs for objects such as AG Car and attributed these to wind clumping. Subsequently, Davies et al. (2007) constructed an analytic clumping model, releasing clumps with a certain ejection

rate per wind flow-time, N, from the wind base. The average polarisation of the clump ensemble was calculated; the results for LBVs with a range of temperatures and radii are shown in Fig. 2.

When the LBVs decrease their radii, the clumps become smaller and denser, and produce more polarisation. This behaviour reverses at the temperature of the bi-stability jump where the wind becomes faster, and the clumps spend less time at the wind base. As a result the polarisation drops. Figure 2 also shows that when the ejection rate increases, the polarisation drops as the wind approaches that of a smooth outflow leading to zero polarisation.

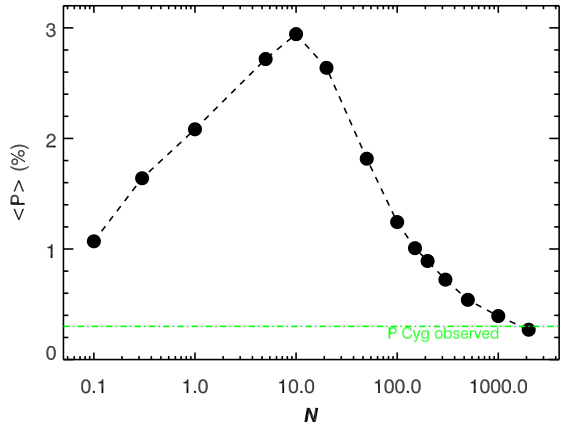

Figure 3: Polarisation variability vs. clump ejection rate. The presence of a maximum implies there are two solutions compared to the observed level of P Cyg.

We now consider the average polarisation as a function of ejection rate. The right-hand side of Fig. 3 shows the regime of many optically thin clumps. A maximum is reached at $N \sim 10$ where the clumps become optically thick and multiple scattering becomes important. The left-hand side represents the optically-thick clump regime. The observed level of polarisation of P Cyg is shown as a horizontal line that intercepts both branches. The data either point to a wind with low N, or to one with $N \sim 1000$. We distinguish between these two branches using timescale information of the polarimetric variations. Preliminary results from our recent monitoring campaign indicate that the high-N scenario is likely to be the correct one (Davies et al. *in prep*), which would suggest that LBV winds consist of thousands of optically thin clumps close to the photosphere.

4 Conclusion

Polarimetry is a tool to constrain the clumping properties of hot-star winds. This may become a powerful means by which to constrain non-LTE models and mass-loss predictions. We anticipate to witness an increased understanding of hot-star winds – an important endeavour because of the impact mass loss has on massive star evolution modelling.

References

Benaglia, P., Vink, J.S., Marti, J., Maiz Apellaniz, J., Koribalski, B., Crowther, P.A., 2007, A&A 467, 1265

Davies, B., Oudmaijer, R.D., Vink, J.S., 2005, A&A 439, 1107

Davies, B., Vink, J.S., Oudmaijer, R.D., 2007, A&A 469, 1045

de Koter, A., Heap, S.R., Hubeny, I., 1997, ApJ 477, 792

Gal-Yam, A., Leonard, D.C., Fox, D.B., et al., 2007, ApJ 656, 372

Kotak, R., Vink, J.S., 2006, A&A 460, 5

Martins, F., Schaerer, D., Hillier, D.J., et al., 2005, A&A 441, 735

Mokiem R., de Koter, A., Vink, J.S., Puls, J., et al., 2007, A&A, in press

Pastorello, A., Smartt, S.J., Mattila,S., 2007, MNRAS 377, 1531

Smith, N., 2007, AJ 133, 1034

Trundle, C., Lennon, D.J., 2005, A&A 434, 677

Vink, J.S., de Koter, A., Lamers, H.J.G.L.M., 1999, A&A 350, 181

Vink, J.S., de Koter, A., Lamers, H.J.G.L.M., 2000, A&A 362, 295

Vink, J.S., de Koter, A., 2002, A&A 393, 543

Puls: In how far do the results depend on model details (e.g. on the opening angle), and will you be able to derive clumping factors? In Lunteren, you quoted a clumping factor of two.

Vink: For optically thin clumps, the exact shape/opening angle of the clumps is not so important, as long as the clumps do not become too large. Deriving clumping factors is tricky, as we only constrain the polarization from the clumps and not from the interclump medium. Using a range of diagnostics, this may well be constrained (polarimetry will provide geometrical constraints).

Groh: When you compare your predictions with the observations for AG Car, should clumping and rotation not be taken into account in your models in order to obtain results?

Vink: We make assumptions when modelling the radiative acceleration (homogeneity and sphericity). We are working to improve these assumptions (e.g. by polarimetric modelling of LBV winds).

Cassinelli: The importance of the angular size of the clump is that it determines the fraction of the stellar light that is scattered.

Vink: Once the clump becomes very large, you need to look at the detailed shapes indeed. In our modelling, the clumps are small and the exact opening angle is less relevant to determine $\langle\rho\rangle$.

Ignace: Although the data do not appear to support the idea of optically thick clumps, in principle the polarization from thick clumps depend on their shape.

Vink: Yes, I agree. For thick clumps you need to do Monte Carlo simulations. Nonetheless, the point of our analysis is that the average polarization will drop once you go to low injection rates, the exact function how $\langle P\rangle$ falls of with low N (number of clumps) is less relevant for our arguments.

Smith: In order to see a net polarization, where you jump around randomly on the Q-U plot: does that require some large scale asymmetry in the wind, i.e. are there sporadic mass ejections in random directions?

Vink: First results from our recent polarimetric monitoring campaign seem to suggest that we are working in the "high-ejection rate" regime, resulting in a "stochastic" low level of average polarization (producing short timescale variability) rather than sporadic mass ejections.

Clumping in Hot Star Winds
W.-R. Hamann, A. Feldmeier & L.M. Oskinova, eds.
Potsdam: Univ.-Verl., 2008
URN: http://nbn-resolving.de/urn:nbn:de:kobv:517-opus-13981

The influence of clumping on predicted O star wind parameters

J. Krtička[1], J. Puls[2] & J. Kubát[3]
[1] *Masarykova universita, Brno, Czech Republic*
[2] *Universitätssternwarte München, München, Germany*
[3] *Astronomický ústav, Ondřejov, Czech Republic*

We study the influence of clumping on the predicted wind structure of O-type stars. For this purpose we artificially include clumping into our stationary wind models. When the clumps are assumed to be optically thin, the radiative line force increases compared to corresponding unclumped models, with a similar effect on either the mass-loss rate or the terminal velocity (depending on the onset of clumping). Optically thick clumps, alternatively, might be able to decrease the radiative force.

1 Introduction

Theoretical models of hot star winds led to the conclusion that mass-loss has a significant impact on the stellar evolution in the upper HRD. This conclusion was supported by a relatively good agreement between these models and observational data.

However, both theoretical predictions and observational values were derived, in a first approximation, by assuming the stellar wind to be a smooth, spherically symmetric outflow. This picture might be inadequate due to the existence of a strong instability related to radiative line driving (see Feldmeier, this volume, and references therein). The influence of corresponding spatially inhomogeneous wind structures ("clumps") on the basic wind properties (i.e., mass-loss rate and velocity field) and the emergent spectrum was believed to be insignificant.

This changed with the application of NLTE models that were able to account for the influence of clumping on hot star wind spectra. The reason that the effect of clumping is not immediately apparent in the wind spectra is that most diagnostical features depend on the *product* $\sqrt{C_\mathrm{c}}\dot{M}$, where the "clumping factor" $C_\mathrm{c} \geq 1$ relates the density inside the clump ρ^+ with the mean wind density $\langle\rho\rangle$,

$$\rho^+ = C_\mathrm{c}\langle\rho\rangle. \qquad (1)$$

Consequently, spectra from winds with a large clumping factor but small mass-loss rate can mimic those from winds with weak clumping but large mass-loss rate. If $C_\mathrm{c} > 1$, then the mass-loss rates derived from such diagnostics are overestimated by a factor of $\sqrt{C_\mathrm{c}}$. Fortunately, some spectral properties may be used to break this degeneracy, and to "observationally" estimate the value of C_c. For example, Martins et al. (2005b) derived clumping factors of 10 and 100 for studied Galactic O-stars, implying a decrease of the estimated mass-loss rate by factors of 3 and 10 (see also Bouret, this volume, and Puls et al., this volume, and references therein).

Thus, if the actual mass-loss rates of hot stars are really lower than assumed before, then there is a significant discrepancy between the observations and theory. The reason for this discrepancy is not yet known. A possibility might be that clumping may shift the ionization balance in such a way that the final radiative force is lower, resulting in lower mass-loss rates. To test this possibility we have included clumping into our wind models and studied its influence on the basic wind properties of hot stars.

2 Model stars

The wind models are calculated for O-type stellar parameters based on the recent calibrations by Martins et al. (2005a, see also Fig. 1).

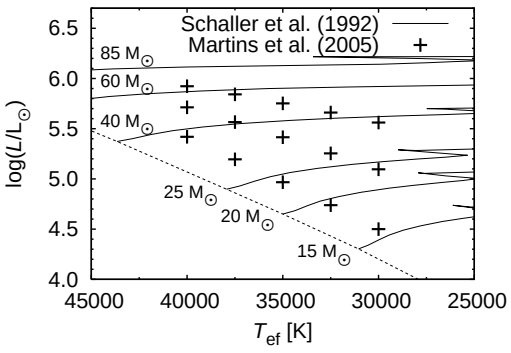

Figure 1: Parameters of studied stars in the HR diagram. Overplotted are the evolutionary tracks from Schaller et al. (1992).

3 Wind models

For our study we used the spherically symmetric, stationary wind models developed by Krtička & Kubát (2004). These models solve the equations of statistical equilibrium together with the equations of radiative transfer. The calculated occupation numbers are used to derive the radiative force (in the Sobolev approximation) and the radiative heating/cooling terms. This enables us to obtain the radial stratification of velocity, density and temperature in the wind and finally to predict the wind mass-loss rate $\dot{M}$ and terminal velocity v_∞. For the studied O-stars, $\dot{M}$ derived from our models depends on the stellar luminosity L and the effective temperature $T_{\rm eff}$ on average as

$$\left(\frac{\dot{M}}{1\,{\rm M}_\odot\,{\rm yr}^{-1}}\right) = 8.13\times10^{-7}\left(\frac{L_*}{3\times10^5\,{\rm L}_\odot}\right)^{2.05} \times\left(\frac{T_{\rm eff}}{3.5\times10^4\,{\rm K}}\right)^{3.78}. \quad (2)$$

The advantage of our models is the self-consistent solution of the momentum equation, though the radiative transfer is treated in a simplified way.

4 Optically thin clumps

The assumption of optically thin clumps is widely used for studying the influence of clumping on the wind spectra (e.g., Martins et al. 2005b, Puls et al, this volume).

To include optically thin clumps into our models we modified the equations of statistical equilibrium, by using an electron density $\rho_{\rm e}^+ = C_{\rm c}\langle\rho_{\rm e}\rangle$, opacity $\langle\chi\rangle = \chi^+/C_{\rm c}$, and emissivity $\langle\eta\rangle = \eta^+/C_{\rm c}$. The superscript + denotes values inside the (homogeneous) clumps and the quantities inside brackets corresponding volume averages.

4.1 Influence of clumping

To investigate the influence of clumping on the stellar wind we have calculated a wind model of an O-type giant at $T_{\rm eff} = 35\,000$ K, assuming the wind to be smooth ($C_{\rm c} = 1$) close to the star ($r < 2R_*$), and to be clumped ($C_{\rm c} = 10$) in the outer regions ($r > 2R_*$, see Figs. 2, 3).

The presence of clumping leads to an increase of the electron density inside the clumps. Consequently, the recombination rates become higher and the wind less ionized (see Fig. 2). Since lower ions are able to accelerate the stellar wind more efficiently than the higher ones (due to a larger number of driving lines), the radiative force increases, which, in our case, leads to an increase in wind velocity (see Fig. 3).

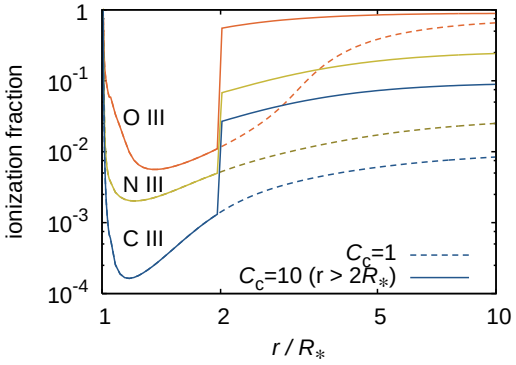

Figure 2: Influence of clumping on the ionization fractions of selected ions.

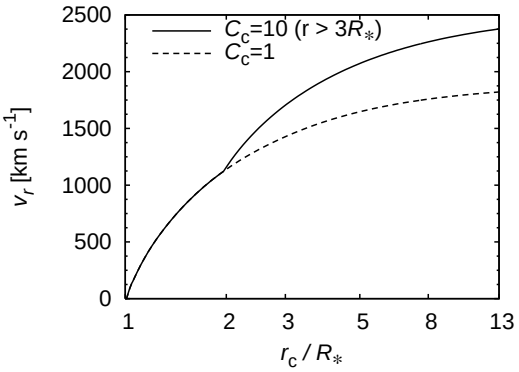

Figure 3: Influence of clumping on the wind velocity.

4.2 Radially constant clumping factor

The influence of clumping on the wind parameters depends on the radial onset of clumping. If clumping starts above the critical point (below which the mass-loss rate is determined), then the terminal velocity increases (see Fig. 3). On the other hand, if clumping starts below the critical point, then the wind mass-loss rate becomes larger.

Table 1: Average increase of $\dot{M}$ for constant $C_{\rm c}$

$C_{\rm c}$	1	3.16	10	31.6	100
$\dot{M}(C_{\rm c})/\dot{M}(C_{\rm c}=1)$	1	1.48	2.15	3.17	4.57

In case of radially constant clumping, the mass-loss rate increases significantly, and the predicted wind-momentum rate is much higher than for a smooth wind at same parameters (see Fig. 4).

5 Clumps larger than $L_{\rm Sob}$

Individual clumps may be larger than the Sobolev length $L_{\rm Sob}$. Assuming the velocity gradient inside the clumps to be the same as in the corresponding smooth wind, we account for clumps being larger than $L_{\rm Sob}$ by using the same modifications as in the case of optically thin clumps, but additionally increasing the Sobolev optical depth by $C_{\rm c}$, and decreasing the radiative force per unit of volume by a factor of $C_{\rm c}$.

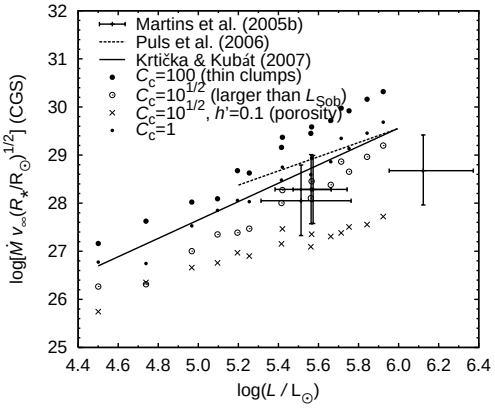

Figure 4: Influence of wind inhomogeneities on the modified wind-momentum rate.

The inclusion of clumps larger than $L_{\rm Sob}$ into our wind models leads to a decrease of the radiative force. Thus, and for radially constant $C_{\rm c}$, the mass-loss rate decreases significantly (Fig. 4).

6 Influence of porosity

Wind porosity (Owocki et al. 2004) can be introduced into the wind models by additional decreasing the continuum opacity, $\chi_{\rm eff} = \langle\chi\rangle/(1 + rh'\langle\chi\rangle)$, where $h'r$ is the porosity length. The continuum emissivity has to be modified by the same amount.

This effect leads to a significant increase of the wind ionization. Thus, porosity leads to a decrease of the radiative force, and also the mass-loss rate may decrease if the wind is porous below the critical point (see Fig. 4 for the results for radially constant $C_{\rm c}$ and h').

7 Discussion

Our results are in agreement with those derived from a similar investigation conducted by de Koter & Muijres (this volume): Indeed, *wind inhomogeneities influence the predicted wind parameters*. An approach which roughly corresponds to the results of time-dependent simulations (i.e., clumps which are optically thin at most frequencies, "starting" above the critical point) does not improve the agreement between theory and observations. Clumps assumed to be larger than the Sobolev length (and starting below the critical point) may provide a better agreement between theory and observations, both in terms of mass-loss rates (Fig. 4) and P V ionization fractions (Fig. 5). Note, however, that the approach chosen by us strongly contrasts an important aspect of time-dependent simulations, namely that the velocity gradient inside the clumps is predicted to be much shallower than that of a corresponding smooth wind. This problem will be considered in a follow-up investigation.

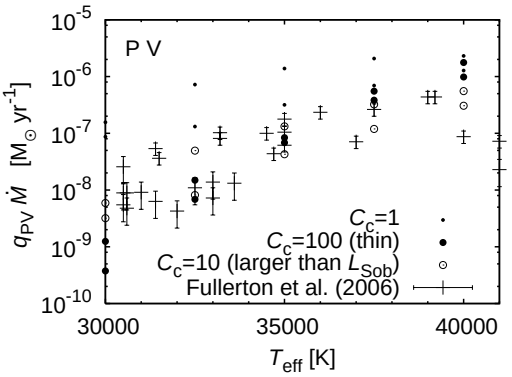

Figure 5: Influence of different types of wind inhomogeneities on the P V ionization.

This research was supported by grants GA ČR 205/07/0031 and GA AV ČR B301630501.

References

Fullerton, A. W., Massa, D. L., & Prinja, R. K., 2006, ApJ, 637, 1025

Krtička, J., & Kubát, J. 2004, A&A, 417, 1003

Martins F., Schaerer D., & Hillier D. J., 2005a, A&A, 436, 1049

Martins F., Schaerer, D., Hillier, D. J., et al. 2005b, A&A, 441, 735

Owocki, S. P., Gayley, K. G., & Shaviv, N. J., 2004, ApJ, 616, 525

Schaller, G., Schaerer, D., Meynet, G., & Maeder, A. 1992, A&AS, 96, 269

Cassinelli: With regards to P V: It decreased because of the recombination – owing to higher N^2?

Krtička: Yes. In the models with optically thin clumps the ionization fraction of P V decreases due to the increase of the electron density and consequently due to higher recombination rates. In the models with optically thick clumps the product $q(\mathrm{P\,V})\,\dot{M}$ decreases also due to the decrease of $\dot{M}$.

Puls: These calculations are a first step to account for clumping in stationary wind models. We are aware of the problem of the velocity field, and hope to include a more realistic description of $v(r)$ inside the clump soon.

Clumping in Hot Star Winds
W.-R. Hamann, A. Feldmeier & L.M. Oskinova, eds.
Potsdam: Univ.-Verl., 2008
URN: http://nbn-resolving.de/urn:nbn:de:kobv:517-opus-13981

Hydrodynamic simulations of clumps

A. Feldmeier, W.-R. Hamann, D. Rätzel & L. M. Oskinova
Universität Potsdam, Germany

Clumps in hot star winds can originate from shock compression due to the line driven instability. One-dimensional hydrodynamic simulations reveal a radial wind structure consisting of highly compressed shells separated by voids, and colliding with fast clouds. Two-dimensional simulations are still largely missing, despite first attempts. Clumpiness dramatically affects the radiative transfer and thus all wind diagnostics in the UV, optical, and in X-rays. The microturbulence approximation applied hitherto is currently superseded by a more sophisticated radiative transfer in stochastic media. Besides clumps, i.e. jumps in the density stratification, so-called kinks in the velocity law, i.e. jumps in $\mathrm{d}v/\mathrm{d}r$, play an eminent role in hot star winds. Kinks are a new type of radiative-acoustic shock, and propagate at super-Abbottic speed.

1 Line Driven Instability in 1-D

Clumps in hot star winds can be created by shock compression, where the shocks occur as result of the line driven instability, as first suggested by Lucy & Solomon (1970). First numerical simulations of this process were presented in a seminal paper by Owocki et al. (1988), and became possible through two novel "inventions": (1) The introduction of an exponential cutoff in the CAK (1975) power law distribution of line opacities. Perturbation growth through the line driven instability only terminates when highly accelerated gas is optically thin even in the strongest line transitions. Without an opacity cutoff, the instability-induced gas acceleration and rarefaction cannot be handled numerically. (2) The introduction of a photospheric Schuster-Schwarzschild reversing layer that allows for self-absorption in spectral lines via an inner boundary condition. Without this devise, the instability disrupts the flow already at the inner boundary. Owocki et al. (1988) treated only pure line absorption, but this shortcoming was overcome with the smooth source function method (SSF, Owocki 1991). This method is extensively reviewed in the literature (e.g. Owocki & Puls 1996), and is therefore not further discussed here.

The flow structure resulting from the line driven instability is shown in Fig. 1. (1) The instability steepens the velocity field of the wind on a macroscopic scale of order R_*. The basic action of the instability is to amplify positive velocity perturbations, in a cycle $\delta v \rightarrow -\delta\tau \rightarrow \delta F \rightarrow \delta g_l \rightarrow \delta v$ (with radiative flux F, and line force g_l). In words: a positive velocity perturbation Doppler-shifts a gas parcel out of the absorption shadow of gas lying closer to the star. The optical depth towards the parcel drops, the parcel experiences a stronger radiative flux from the star, and thus a larger line force, which *further* increases the velocity perturbation. (2) The highly accelerated and rarefied gas streams are decelerated in strong reverse shocks, by overdense shells. Due to the deceleration, the shells have a negative velocity gradient, and are no longer subject to the instability (Martens 1979). Ahead of the shells resides gas close to the stationary CAK density and velocity of the wind, however with negative velocity perturbations and again not subject to the instability. This gas acts as reservoir for the rarefied gas stream hitting the next outer shell. (3) From the outer rim of this reservoir, lumps of gas at CAK densities are ablated and radiatively accelerated through the almost void intershell space, until they hit the next outer shell, causing detectable X-ray emission (Feldmeier et al. 1997). X-ray emission from hot stars is covered in the contributions by Cassinelli et al., Oskinova et al., Cohen et al., and Leutenegger et al., in these proceedings. The gas reservoir is exhausted at around $7\,R_*$, and X-ray emission ceases. Figure 2 shows clumps propagating through void intershell space in snapshots from a numerical simulation.

This sequence of rarefied gas upstream of a dense shell, of the shell itself, and of a gas reservoir at CAK densities downstream of the shell can also be understood as one cycle of a radiative-acoustic Abbott wave. Initially, this is a harmonic wave, which then undergoes nonlinear deformation. This corresponds to the solution of Burgers' equation (that describes the kinematics of fast gas overtaking slow gas), where accelerating regions become ever broader in course of time, and decelerating regions become ever narrower, eventually turning into shock transitions. Since numerical simulations of the line driven instability do not adopt the Sobolev approximation, this is another hint that Abbott waves are not an artefact of the latter, as is occasionally uttered. Similarly, the line driven instability can be understood in the context of the Sobolev approximation, if second order terms including the curvature of the velocity

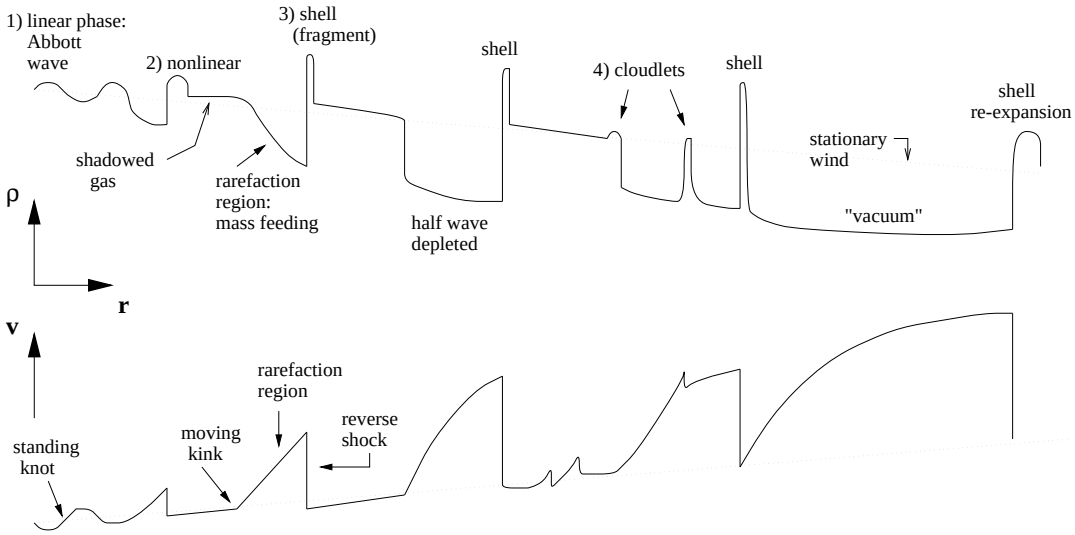

Figure 1: Radial wind structure that develops from the line driven instability.

field are included (Feldmeier 1998), and is then given by the cycle $\delta v \rightarrow \delta v'' \rightarrow -\delta\tau \rightarrow \delta F \rightarrow \delta g_l \rightarrow \delta v$ (with $v'' = \partial^2 v/\partial r^2$). In words: a positive velocity perturbation, or an elevation of the thermal band, increases the absolute curvature of the velocity field. By this, the Sobolev optical depth decreases (a second-order effect), the stellar radiative flux and the line force increase, and the velocity perturbation is further amplified.

2 Line Driven Instability in 2-D

In 1-D simulations assuming spherical symmetry, all flow structures correspond to shells. A key question is that for the real lateral scale of wind structure. Two basic scenarios are plausible: the Rayleigh-Taylor instability could fragmentize extended shell-like structures via eddies or fingers; and the line driven instability could amplify photospheric seed perturbations that have ab initio tiny lateral scale. This question is not decided yet. Another open question is whether the wind structure is essentially isotropic or not. X-ray line profiles look different for spherical (Owocki & Cohen 2006) and pancake-shaped, aligned absorbers (Feldmeier et al. 2003). However, due to the large number of model assumptions and free parameters in X-ray fitting, the data do so far not allow to make a conclusive decision.

Figure 3 shows a hypothetical sketch of the expected 2-D structure of an O star winds. At low and intermediate radii (out to a few stellar radii), three compression levels can be distinguished: (1) typical CAK densities, (2) shock compression one or two orders of magnitude above the CAK density, resulting from the line-driven instability, and (3) essentially void regions. As mentioned before, the gas (1) at CAK densities is ablated in form of small clumps from extended gas reservoirs directly above the dense shells, and the clumps are accelerated through void intershell regions (3), until they collide with the next outer shell (2), creating an observable X-ray flash. The gas reservoir (1) should be depleted by about seven stellar radii. The role of the void regions (3) in allowing X-rays to escape from the wind is discussed in Feldmeier et al. (2003, wind fragmentation) and Owocki & Cohen (2006, wind porosity).

At present, the only 2-D wind simulations of the line driven instability are by Dessart & Owocki (2003, 2005). In their first paper, a purely radial radiative force is assumed. The resulting wind structure is laterally incoherent, i.e. neighboring wind cones are completely independent. The question is whether lateral photons can cause some "lateral organization" of the flow. In their second paper, Dessart & Owocki used a tailored spatial mesh on which the single lateral photon ray considered crosses cell corners i, j and $i \pm 1, j \pm 1$, in order to minimize extrapolations. Models with high radial resolution show then indeed a high degree of lateral coherence. More specifically, the shells created by the line driven instability do *not* break up into clumps. However, the tailored mesh itself poses problems: in order that the photon ray hits cell corners as specified above, the radial mesh distance has to grow very fast with radius, which causes strong artificial dispersion of instability-generated structure.

We have recently started to program a short characteristics method for 2-D radiation hydrodynamics on a standard spatial mesh. An advantage of using short characteristics within the SSF approach

is that the latter only requires a high-precision calculation of optical depths, whereas for the intensity and source function rather simplified expressions are sufficient. Parabolic interpolation of intensity, which is often cumbersome in the short characteristics approach, can then be replaced by linear interpolation of optical depth, which has to be performed in the comoving frame however.

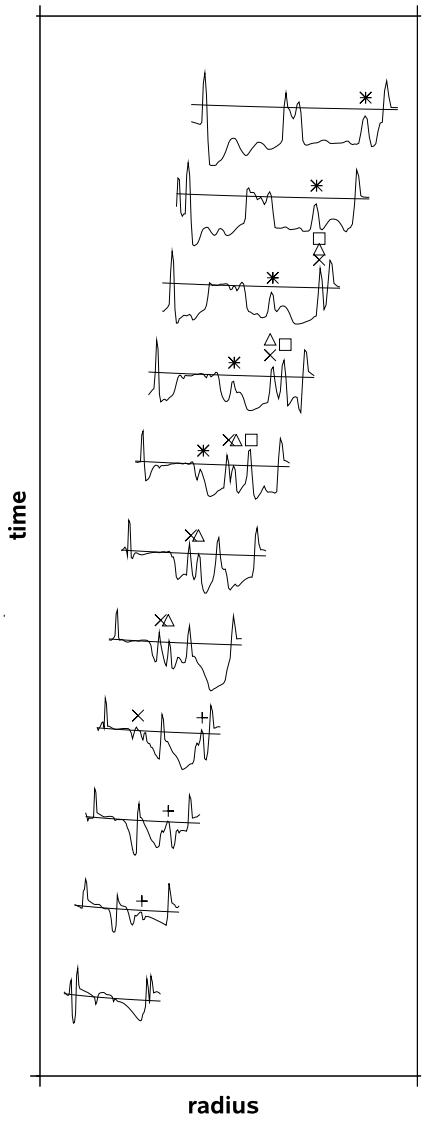

Figure 2: Clouds (marked $+$, $\times$, $\triangle$, $\square$, and $*$) are ablated from the gas reservoir ahead of a dense shell, propagate through a void region, and collide with the next outer shell.

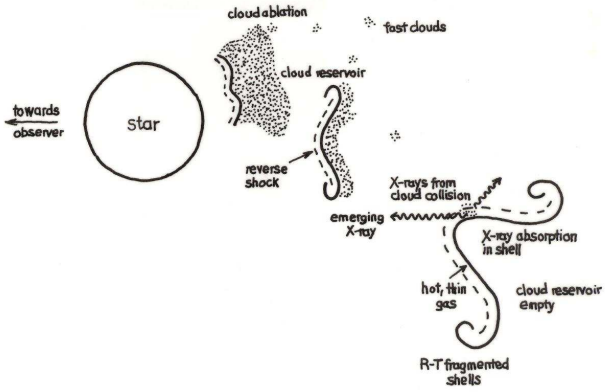

Figure 3: Sketch of wind structure expected from the line driven instability.

3 Multiple Radiative Resonances

If the velocity law of the wind is not monotonic, as is the case for clumpy winds, a photon can be absorbed in the same line transition at different loci. In the SSF approach, this is accounted for in the calculation of the total optical depth along a ray, but not in the calculation of the line source function. We have recently generalized an iteration method devised by Rybicki & Hummer (1978), to determine the line source function in presence of multiple resonances (Feldmeier & Nikutta 2006). Knowledge of the geometric shape of the resonance region is not required in this method, as the μ integral in the calculation of S is transformed to an r integral. A major problem of the method, however, which was not addressed by Rybicki & Hummer, is that "resonance caps," i.e. spherical fragments of finite angular size but tiny radial extent, can contribute significantly to the source function, while being badly resolved on a discrete radial mesh. We gave a remedy for this, and the lambda iteration proposed by Rybicki & Hummer converges then within a few iteration steps, if the number of resonance locations is small (three, in the above paper). This allows to calculate the source function at *each* time step of a hydrodynamic calculation on the *full* spatial mesh.

The method assumes validity of the Sobolev approximation in the calculation of the optical depth, whereas S is calculated via iteration as solution of the exact transfer equation. This is complementary to the SSF method, where τ is calculated (numerically) exact, whereas S is adopted from Sobolev approximation. It seems therefore natural and worthwhile to merge the two approaches in the near future.

4 Kink Propagation

Essentially all hydrodynamic simulations of hot star winds show the occurence of *kinks* in the velocity and density law of the wind. Kinks are discontinuities in the first spatial derivative of the wind speed or density, as opposed to shocks, which are discontinuities in the speed and density themselves. Kinks are found in overloaded or choked winds (Feldmeier & Shlosman 1999), in thin winds where metal ions and the H/He background plasma switch abruptly to a shallow solution branch in order to avoid decoupling (Krtiĉka & Kubát 2000), and in centrifugally-supported flows (Madura et al. 2007). Kinks are also thought to be connected to so-called discrete absorption components (DACs) observed in non-saturated P Cygni line profiles from OB stars. DACs could originate in an extended wind velocity plateau that termiantes in a kink (Cranmer & Owocki 1996): no clumping (i.e. density enhancement) is required to explain the "extra" absorption in a DAC. Still, outer wind clumps may be responsible for the formation of the extended velocity plateau and kink.

In standard hydrodynamics, kinks propagate at the sound speed. Similarly, Cranmer & Owocki suggest that the kink that terminates the velocity plateau should propagate upstream at the Abbott wave speed. The speed (in the stellar rest frame) at which the kink propagates away from the star is then (much) slower than the wind speed, and this would explain the observed slow frequency drift of DACs, which is roughly a factor of five smaller than expected from the wind acceleration.

The radiative force from line scattering in an optically thick gas parcel is proportional to the width of the frequency interval in which stellar radiative flux is intercepted, which in a strongly accelerating medium is proportional to the velocity shift $\mathrm{d}v$ across the parcel; and is inversely proportional to the mass of the parcel, which scales with its diameter $\mathrm{d}r$. Hence, the radiative force g_l scales with $\mathrm{d}v/\mathrm{d}r$ (not with v!). This leads to an interesting modification of the solution topology of line driven winds as compared to the solar wind and Laval nozzle flow. In the latter two cases, the critical or sonic point is a saddle point in the $r - v$ plane, whereas for line driven flows, the critical point is a saddle point in the $r - \mathrm{d}v/\mathrm{d}r$ plane (Bjorkman 1995). It is therefore not clear whether the concept of a *weak* discontinuity, i.e. a jump in the first spatial derivative of v and ρ that propagates at the sound speed, carries over from standard hydrodynamics to line driven flows. From analytical considerations we could recently show that radiative kinks propagate upstream at *super*-Abbottic speed (Feldmeier et al. 2008). Kinks or weak discontinuities in line driven flows behave therefore like *shocks* in standard gasdynamics, the shock being a strong discontinuity, i.e. a jump in v and ρ.

The essential argument is simple: the radiative or Abbott wave speed is given by $A = -\partial g_l/\partial v'$, and describes the response of the radiative force to perturbations of the velocity *gradient*. A careful treatment of the kink discontinuity leads to a kink speed $U = -[g_l]/[v']$ in the comoving frame, where the square bracket stands for the difference in a quantity across the kink. Since the CAK power law index is $\alpha < 1$, the function $g_l(v')$ at a given radius r is concave from below, hence the kink speed is faster than the Abbott speed. In this argument, $g_l(v')$ replaces the Hugoniot adiabate $p(\rho)$ from standard gasdynamics.

Regarding DACs in O star winds, this super-Abbottic upstream propagation of kinks causes an even slower outward propagation in the stellar rest frame then was assumed hitherto, which could further help to understand the slow evolution time of DACs.

5 Stochastic Transfer

The basic distinction between micro- and macroturbulence was introduced by Traving (1964): for microturbulence, hydrodynamic turbulence elements in a stellar atmosphere or the ISM are optically thin even at the center of a spectral line, and the turbulence is indistinguishable from thermal motion, and can be accounted for by a microturbulence velocity that is added to the thermal line broadening. For macroturbulence, on the other hand, a full line profile forms in every turbulence element, and one has to add these statistically independent, Doppler-shifted profiles to obtain the emergent line profile.

If the turbulent medium, or more generally any multi-phase medium, can be described statistically, i.e. if the density and velocity law are *random functions*, the radiative transfer has to be solved separately for each of the possible realizations of the medium, and the emergent intensity is obtained from averaging over all the realizations. This approach includes both the micro- and macroturbulence limit. In the microturbulence limit that the different phases cannot be distinguished from ordinary atoms by the photons, i.e. that the photon mean free path is much larger than the phase elements, the "averaging over realizations" can be replaced by a simpler "averaging over opacities", i.e. an effective opacity can be introduced, and the radiative transfer is solved once and for all on an "average" medium (e.g. filling factor approach).

By contrast, if the phase patches are *larger* than the photon mean free path, averaging of the emergent intensity over all realizations of the stochastic medium is unavoidable (e.g. in a Monte Carlo approach), since then $\langle e^{-\tau} \rangle \neq e^{-\langle \tau \rangle}$, where $\langle\, . \,\rangle$ indicates averaging. The latter inequality is readily understood, by writing out $\tau = \int \mathrm{d}\tau$, and expanding the exponential into a power series. The left and right hand side are then only identical if all n-point

correlation functions $\langle \mathrm{d}\tau(r_1)\mathrm{d}\tau(r_2)\ldots\mathrm{d}\tau(r_n)\rangle$ (with $r_1 < r_2 < \ldots < r_n$) are zero. But this is only true in the microturbulence or "atomic mix" limit that the clump size is smaller than the photon mean free path.

The calculation of n-point correlation functions is the biggest challenge of hydrodynamic turbulence theory, since (by definition) there are always large-scale eddies in hydrodynamic turbulence that cause large distance correlations, thus preventing n-point correlation functions from vanishing. Similarly, the radiation field that emerges from a medium with large-scale clumps obviously carries information about the stochastic properties of this medium, e.g. of the size distribution (power law vs. exponential) of the clumps.

Transfer theory in stochastic media was developed since the 1950ies (theory of Poisson processes), with applications e.g. to neutron transport in nuclear reactor walls. A modern landmark paper is Levermore et al. (1986), which demonstrates the mathematical complexity involved. The authors solve the "formal" transfer problem (pre-specified source function $S = B$) in a two-phase Markovian mix fully analytically. We quote here only a limiting case, for a medium that consists of infinitely dense absorbers in a background vacuum. For pure absorption ($S = 0$), the emergent intensity is then $I = I_0 \exp(-z/h)$, where h is the mean free path between the absorbers. This is the result for a fully *porous* wind, with porosity length h (see Hamann et al., Owocki et al., and Cohen et al., these proceedings).

A novel way to describe properties of stochastic media is via *percolation theory* (see reviews by Isichenko 1992 and Stauffer & Aharony 1992), which considers *stochastic clusters* in space, and transport upon them. Indelman & Abramovich (1994) derive an expression for the opacity of a two-phase medium via percolation theory. Their result is used to determine the degree of polution of rivers and lakes, and is used by Shaviv (1998) in a model for the inhomogeneous atmosphere of η Car. In its simplest form, percolation theory deals with two- and three dimensional, infinite grids, on which each position is either "filled" or "empty". When nearest-neighbor points are "filled", one speaks of a connection (which could mean e.g. that a current or heat flows). A celebrated result from percolation theory is that above a well-defined critical value for the space density of filled positions, the so-called percolation threshold, there exists one single-connected structure on the grid. Because of the long-range correlations near the percolation threshold, the latter is a *phase* transition. This explains the large interest in percolation theory in the settings of statistical mechanics.

The distinction between diffusion theory and percolation theory is, according to Broadbent & Hammersley (1957), that diffusion theory describes the stochastic motion (random walk) of a particle through a regular, ordered medium, whereas percolation theory describes an ordered, macroscopic motion (hydrodynamic fluid or electrical current) in a random medium. Diffusion theory was successfully applied by Ruszkowski & Begelman (2003) to describe the angular dependence of the radiation intensity in a medium with strong density contrasts, as in atmospheres of stars or accretion disks near the Eddington limit.

References

Bjorkman J.E. 1995, ApJ, 453, 369
Broadbent S.R. & Hammersley J.M. 1957, Proc. Cambridge. Philos. Soc., 53, 629
Castor J.I., Abbott D.C., & Klein R. 1975, ApJ, 195, 157 (CAK)
Cranmer S.R. & Owocki S.P. 1996, ApJ, 462, 469
Dessart L. & Owocki S.P. 2003, A&A, 406, L1
Dessart L. & Owocki S.P. 2005, A&A, 437, 657
Feldmeier A. 1998, A&A, 332, 245
Feldmeier A. & Shlosman I. 1999, ApJ, 526, 344
Feldmeier A. & Nikutta R. 2006, A&A, 446, 661
Feldmeier A., Puls J., & Pauldrach A. 1997, A&A, 322, 878
Feldmeier A., Oskinova L., & Hamann W.-R. 2003, A&A, 403, 217
Feldmeier A., Rätzel D., & Owocki S.P. 2008, ApJ, in print
Indelman P. & Abramovich B. 1994, Water Resources Research, 30, 3385
Isichenko M.B. 1992, Rev. Mod. Phys., 64, 961
Krtiĉka J. & Kubát J. 2000, A&A, 359, 983
Levermore C.D., Pomraning G.C., Sanzo D.L., & Wong J. 1986, J. Math. Phys., 27, 2526
Lucy L.B. & Solomon P.M. 1970, ApJ, 159, 879
Madura T.I., Owocki S.P., & Feldmeier A. 2007, ApJ, 660, 687
Martens P.C.H. 1979, A&A, 75, L7
Owocki S.P. 1991, in Stellar atmospheres: beyond classical models, eds. Crivellari L., Hubeny I., & Hummer D.G., Kluwer, Dordrecht, 235
Owocki S.P. & Puls J. 1996, ApJ, 462, 894
Owocki S.P. & Cohen D.H. 2006, ApJ, 648, 565
Owocki S.P., Castor J.I., & Rybicki G.B. 1988, ApJ, 335, 914
Ruszkowski M. & Begelman M.C. 2003, ApJ, 586, 384
Rybicki G.B. & Hummer D.G. 1978, ApJ, 219, 654
Shaviv N.J. 1998, ApJ, 494, L193
Stauffer D. & Aharony A. 1992, Introduction to Percolation Theory, Taylor & Francis, London
Traving G. 1964, Zeitschrift f. Astrophysik, 60, 167

Puls: a) In how far are kinks physical, since their properties depend crucially on the Sobolev theory. b) Might it be that the stochastic treatment simplifies, since we are interested in $\langle(1-\exp(-\tau))/\tau\rangle$ instead of $\langle\exp(-\tau)\rangle$.

Feldmeier: a) I have no real answer, since we are not yet able to apply our analytic method to a more realistic line force that avoids the Sobolev approximation, e.g. the SSF line force. But kinks are not just an artifact of the Sobolev approximation, since they also appear in numerical simulations applying the SSF force. b) This is a very interesting comment. As far as I remember the results from the papers by Levermore and Pomraning, you are indeed right, but I would have to look up the details.

Owocki: In response to comment/question by J. Puls: non-Sobolev SSF models of corotating interaction regions give very similar results to CAK simulations, with the kinks just somewhat rounded, but otherwise the inward propagation is very similar.

Clumping in Hot Star Winds
W.-R. Hamann, A. Feldmeier & L.M. Oskinova, eds.
Potsdam: Univ.-Verl., 2008
URN: http://nbn-resolving.de/urn:nbn:de:kobv:517-opus-13981

Dynamical simulation of the "velocity-porosity" reduction in observed strength of stellar wind lines

S. P. Owocki
University of Delaware, Newark, DE USA

I use dynamical simulations of the line-driven instability to examine the potential role of the resulting flow structure in reducing the observed strength of wind absorption lines. Instead of the porosity length formalism used to model effects on continuum absorption, I suggest reductions in line strength can be better characterized in terms of a *velocity* clumping factor that is insensitive to spatial scales. Examples of dynamic spectra computed directly from instability simulations do exhibit a net reduction in absorption, but only at a modest 10-20% level that is well short of the ca. factor 10 required by recent analyses of PV lines.

1 Spatial clumping and porosity

Historically the wind clumping that is the focus of this workshop has been primarily considered for its effect on diagnostics that scale with the square of the density, e.g. free-free emission, and emission or absorption from atomic states that are populated by collisional excitation or recombination. The strength of such diagnostics is *enhanced* in a clumped medium, leading to an overestimate of the wind mass loss rate that scales with $\sqrt{1/f}$, the inverse square-root of the clump volume filling factor f.

Over the past couple of years, there also has been considerable attention to an additional "*porosity*" effect that can *reduce* the strength of *single*-density diagnostics. In particular, Oskinova et al. (2006) have claimed a porous reduction in bound-free continuum absorption of X-rays emitted from wind shocks can help explain the unexpected relative symmetry of X-ray emission lines observed by Chandra and XMM. However, Owocki & Cohen (2006) have argued this requires an unrealistically large value for the wind *porosity length* $h \equiv \ell/f$, defined by the ratio the clump scale ℓ to their volume filling factor f.

A recent follow-on preprint by Oskinova et al. (2007) has now applied an analysis based on this porosity length to argue for a reduction in the strength of *line* absorption in structured stellar winds. If substantiated, such a reduction might help explain the unexpected weakness of PV lines observed by FUSE (Fullerton et al. 2004), which otherwise might require a substantial, factor-ten or more reduction in wind mass loss rate.

A key point of the present paper is to argue that a description based on the *spatial* porosity that is central to reducing *continuum* absorption is *not* well suited to characterizing the effects on *line* absorption, which instead depend on a kind of "*velocity porosity*" (or "vorosity"?) that is relatively insensitive to the spatial scale of wind structure. The next section suggests a simple analytic scaling based on a simplified description of the velocity structure arising in numerical hydrodynamics simulations of the line-driven instability. The follow-on section uses line-absorption profiles formed in actual dynamical instabilty models to show that the reduction in overall line absorption is typically quite modest, only about 10-20%.

2 The 'velocity clumping factor'

The left panel of figure 1 illustrates the typical result of 1D dynamical simulation of the wind instability, plotted here as a time-snapshot of velocity vs. a mass coordinate $M(r)$ instead of radius r. The intrinsic instability of line-driving leads to a substantial velocity structure, with narrow peaks corresponding to spatially extended, but tenuous regions of high-speed flow, which bracket dense, spatially narrow clumps/shells that appear here as nearly flat, extended velocity plateaus in mass.

The right panel of figure 1 illustrates a simplified, heuristic model of such wind structure for a representative wind section, with the velocity clumping now represented by a simple "staircase" structure, compressing the wind mass into discrete sections of the wind velocity law, while evacuating the regions in between. The structure is characterized by a "velocity clumping factor" f_v, set by the ratio between the internal velocity width δv to the velocity separation Δv of the clumps. The straight line through the steps represents the corresponding smooth wind flow.

The effect of the velocity structure on the line-absorption profile depends on the local Sobolev optical depth, which scales with the inverse of the mass derivative of velocity, $\tau_x \sim 1/(dv/dm)$, evaluated at

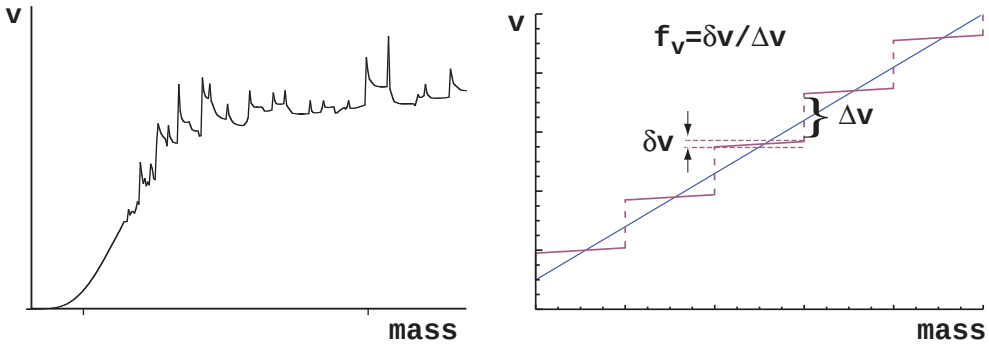

Figure 1: Left: Self-excited velocity structure arising in a 1D SSF simulation of the line-driven instability, plotted versus a mass coordinate, $M(r) = \int_R^r 4\pi\rho r'^2\, dr'$. Note the formation of velocity plateaus in the outer regions of the wind. Right: Velocity vs. mass in a wind seqment with structure described by a simplified velocity staircase model with multiple large steps Δv between plateaus of width δv. Here the associated velocity clumping factor $f_v \equiv \delta v/\Delta v = 1/10$. The straight line represents the corresponding smooth CAK/Sobolev model.

a resonance location r_s where the velocity-scaled, observer-frame wavelength $x = -v(r_s)/v_\infty$. In a smooth wind with Sobolev optical depth τ_x, the absorption profile is given simply by

$$A_x = 1 - e^{-\tau_x}\,. \tag{1}$$

In the structured model, the optical thickness of individual clumps is increased by the inverse of the clumping factor $1/f_v$, but they now only cover a fraction f_v of the velocity/wavelength interval. The net effect on the averaged line profile is to *reduce* the net aborption by a factor

$$R_A(\tau_x, f_v) = f_v\, \frac{1 - e^{-\tau_x/f_v}}{1 - e^{-\tau_x}}\,. \tag{2}$$

Note that for optically thick lines, $\tau_x \gg 1$, the reduction approaches a fixed value, given in fact by the clumping factor, $R_A \approx f_v$. If the smooth-wind line is optically thin, $\tau_x \ll 1$, then $R_A(\tau_x, f_v) \approx (1-e^{-\tau_x/f})/(\tau_x/f_v)$, which is quite analogous to the opacity reduction for *continuum* porosity (cf. Owocki & Cohen 2006, eqn. 4), if we just substitute for the clump optical depth, $\tau_c \to \tau_x/f_v$.

But a key point here is that, unlike for the continuum case, the net reduction in line absorption no longer depends on the spatial scale of the clumps. Instead one might think of this velocity clumping model as a kind of velocity form of the standard venetian blind, with f_v representing the fractional projected covering factor of the blinds relative to their separation. The $f_v = 1$ case represents closed blinds that effectively block the background light, while small f_v represent cases when the blinds are broadly open, letting through much more light.

3 Line-absorption profile from instability simulations

Because the line-driven instability occurs at scales near or below the Sobolev length, dynamical simulations of the resulting structure cannot rely on the standard CAK/Sobolev form for the line-force, but rather must use expressions that require a *non-local* spatial integration of the line-optical depth at a sample of observer-frame wavelengths $x = -v/v_\infty$. The output of such simulations thus readily provide dynamical, non-Sobolev results for the total radial optical depth from the stellar surface to an observer at the outer boundary,

$$\tau_x = \int_{R_*}^{R_{max}} dr'\, \kappa\rho(r')\, \phi(\tilde{x}(r'))\,. \tag{3}$$

Here κ is the mass-absorption coefficient of the line, ρ is the density, and $\tilde{x}(r') = (xv_\infty + v(r'))/v_{th}$ is the local co-moving-frame wavelength at radius r', in units of the thermal velocity width v_{th} of the line profile function ϕ. Use of eqn. (3) in place of the Sobolev optical depth in eqn. (1) then provides a full *non-Sobolev* computation of the line-absorption trough in this dynamical model.

Figure 2 shows results for line-absorption spectra from a typical wind instability simulation, which starts with a smooth, CAK initial condition, and is then evolved forward using the standard "Smooth Source Function" (SSF) formulation for the line-force (Owocki & Puls 1996, 1999). Although there are no explicit perturbations, the intrinsic, self-excited nature of the instabilty leads to extensive wind structure above a radius of about $r \approx 1.5R_*$. The upper panels of figure 2 show the corresponding effect on the dynamic spectra for a weak, mediuim,

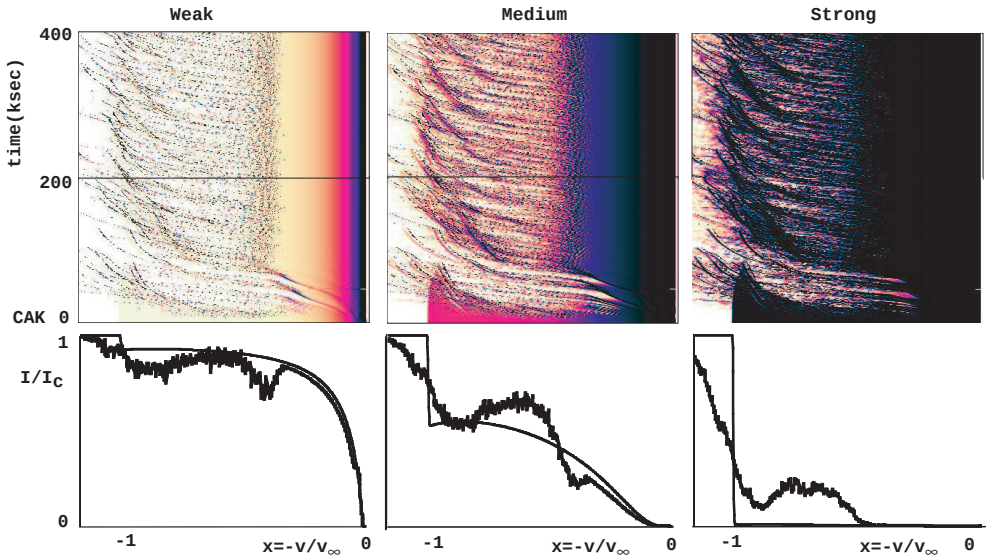

Figure 2: *Lower panels:* Absorption trough of time-averaged P-Cygni line profile plotted versus velocity-scaled observer wavelength $x = -v/v_\infty$ from line-center, for a weak, medium, and strong line. The smooth curves correspond to the smooth, CAK initial condition, while the jagged curves represent results for 1D dynamical instability simulations using the Smooth Source Function (SFF) method. *Upper panels:* Color-scale plots of the associated dynamical spectra, with time increasing vertically from the CAK initial condition. Note that, although for simplicity the re-emission from scattering is ignored, the line absorption profiles here are not the result of a Sobolev model, but instead are computed from the full spatial integral of the line absorption from the stellar surface to the outer boundary (set here to $R_{max} = 100R_*$).

and strong line. The lower panels compare the associated time-average profile with that of the smooth CAK initial condition.

Because of the restriction here to pure-absorption along a single radial ray in a 1D instability model, the synthetic profiles here have an artificially fine level of structure and variability, but they illustrate quite vividly the key effects that can alter line absorption. The high level of velocity clumping leads to many tracks of enhanced, even saturated absorption, while at the same time exposing channels between the clumps that allow for increased tranmission of the stellar surface flux. The time-averaged profiles in the lower panels thus show a general *reduction* in the absorption compared to the smooth, CAK model, most notably at middle wavelengths ($-x = v/v_{th} \approx 0.3 - 0.8$) relative to blue edge for the CAK terminal speed. On the other hand, the unstable flow faster than the CAK v_∞ extends the absorption beyond $x = -1$, leading to notable softening of the blue edge.

The net effect is still to reduce the overall absorption equivalent width of the medium and strong lines, though only by about 10-20%. Thus while the dynamical simuations of wind instabilities do confirm the basic velocity porosity effect, they indicate the net reduction in line absorption may be quite modest, and thus may only play a minor part in the factor 10 reduction thought to be necessary to explain the observed strength of PV lines.

This work was supported in part by NSF grant AST-0507581, and NASA Chandra grant TM7-8002X.

References

Fullerton, A. W., Massa, D. L., & Prinja, R. K. 2006, ApJ, 637, 1025

Oskinova, L. M., Hamann, W., & Feldmeier, A. 2007, A&A, 476, 1331

Oskinova, L. M., Feldmeier, A., & Hamann, W.-R. 2006, MNRAS, 372, 313

Owocki, S. P., & Cohen, D. H. 2006, ApJ, 648, 565

Owocki, S. P., & Puls, J. 1996, ApJ, 462, 894

Owocki, S. P., & Puls, J. 1999, ApJ, 510, 355

Townsend: Is it not likely that the velocity porosity you discuss will be augmented by spatial porosity?

Owocki: In principle it could be. But it would require relatively large spatial porosity lengths ($h > R$), which might be unrealistic. A key result of this analysis is that "velocity porosity" can occur even when the spatial porosity for continuum absorption is entirely in the microclumping limit ($h \ll R$), for which there is little or no reduction in the absorption. For example, Wolf-Rainer quoted in his talk that the Oskivova et al. analysis implies a notable reduction in line absorption even with a spatial porosity length $h = 0.25\,R_*$. Indeed, for a moderately strong line, i.e. with a smooth wind Sobolev depth $\tau > 1$, velocity clumping on *any* scale should in principle lead to an absorption reduction.

Hamann: It is very interesting how you have modeled the porosity effect for line opacity. I want to emphasize that your "vorosity" is equivalent to the model of Oskinova et al. which I have presented in my talk this morning. Some details, however, are slightly different. You are using a Sobolev opacity over a clump which has a velocity gradient, and we assume a Gaussian distribution of velocities inside the clump for our CMF optical depth.

Owocki: I agree there are some similarities, but in my eyes the scaling picture I emphasize is conceptually distinct from the "porosity length" formalism followed in Oskinova et al. I do not assume, or propose, that the clump has a positive velocity gradient. Rather the key parameter in my picture is the "velocity clumping factor", effectively the *ratio* of the clump velocity width (which might be turbulent, using your "Gaussian" picture) over the velocity separation between clumps. A key point is that this parameter is, unlike the porosity length, entirely independent of any assumed spatial length scale. Finally, I would emphasize that, however one chooses to describe the effect in terms of simple scaling parameters, the latter half of my talk uses radiation hydrodynamic models in which the optical depth is computed not from any Sobolev model, but from numerical integration of the profile-weighted line optical depth through the complex velocity and density structure. In this model we do indeed see clearly that moderately strong lines have an effective absorption reduction of a few tens of percent.

Puls: I think one can actually use this step-function (maybe with a single velocity "step" at different locations) to get a correct description of the radiation field, where the step function is constructed from averaging over the hydrodynamic simulations.

Owocki: That is an interesting idea. I am in the process of trying to develop a formalism to derive an effective "velocity porosity" for any given complex structure obtained from instability simulations.

Feldmeier: The "venetian blind" distance in your model is apparently a stochastic quantity. We discussed yesterday the statistical properties of cloud turbulence, i.e. its length distribution according to Kolmogoroff's law. What is the statistical distribution function of your velocity turbulence?

Owocki: That is a good question. I think the key here is to focus not on the *spatial* distribution and whether it follows Kolmogoroff, but really the *velocity* distribution. That is what my "velocity clumping" parameterization attempts to capture for a simple two-component medium, but I agree that a more realistic model requires some statistical description of how much material is clumped into a distribution of velocity bins. Such a description is still to be developed.

Clumping in Hot Star Winds
W.-R. Hamann, A. Feldmeier & L.M. Oskinova, eds.
Potsdam: Univ.-Verl., 2008
URN: http://nbn-resolving.de/urn:nbn:de:kobv:517-opus-13981

Large-scale wind structure due to magnetic fields

A. ud-Doula
Bartol Research Institute, Newark, USA

Magnetic fields influence the dynamics of hot-star winds and create large scale structure. Based on numerical magnetohydrodynamic (MHD) simulations, we model the wind of θ^1 Ori C, and then use the SEI method to compute synthetic line profiles for a range of viewing angles as function of rotational phase. The resulting dynamic spectrum for a moderately strong line shows a distinct modulation, but with a phase that seems at odds with available observations.

1 Introduction

Magnetic fields can influence hot star winds significantly. Their overall influence on the wind dynamics can be characterized by a single magnetic confinement parameter,

$$\eta_* \equiv \frac{B_{eq}^2 R_*^2}{\dot{M} v_\infty}\,, \qquad (1)$$

which characterizes the ratio between magnetic field energy density and kinetic energy density of the wind (ud-Doula & Owocki 2002).

Extensive magnetohydrodynamic (MHD) simulations show that, in general, for the stellar models with weak magnetic confinement ($\eta_* < 1$) field lines are stretched dynamical timescale into radial configuration by the strong outflow. However, even for magnetic confinement as weak as $\eta_* \sim 1/10$ the field can influence the wind density by diverting the wind material from higher latitudes towards the magnetic equator.

For stronger confinement ($\eta_* > 1$), the magnetic field remains closed over a limited range of latitude and height about the equatorial surface, but eventually opens into a nearly radial configuration at large radii. Within closed loops, material is channeled toward loop tops into shock collisions, leading to X-ray emission that is generally consistent with that derived in the original "magnetically confined wind shock" (MWCS) model first developed by Babel & Montmerle (1997). But in MHD simulations, once shocked material cools and becomes dense, it eventually is pulled by gravity back onto the star in quite complex and variable inflow patterns. Within open field flow, the equatorial channeling leads to oblique shocks that eventually forms a thin, dense, slowly outflowing disk at the magnetic equator (see Fig. 1).

Such large scale wind structures are inferred most directly from time variability in the blueshifted absorption troughs of UV P Cygni profiles. The study here thus uses the SEI (Sobolev with Exact Integration; Lamers et. al. 1987) to synthesize line profiles in MHD models of the O5.5 V star θ^1 Ori C, and then compares these with a sample UV line profiles observed by *FUSE*.

2 MHD model of θ^1 Ori C

θ^1 Ori C (O5.5 V) is the brightest member of the Orion Nebula. With a measured surface magnetic field of ca 1100 G (Donati et al. 2002), it is currently only one of two known magnetic O stars (the other being HD 191612, Donati et al. 2006). *Chandra* observations show that it is an unusually hard X-ray source with modulated flux on a rather long 15-day rotation period.

To model the magnetized outflow of of θ^1 Ori C, we perform 2D-MHD simulations wherein a dipole magnetic field with prescribed strength is suddenly introduce into an already relaxed spherically symmetric wind. Since the star rotates slowly, the rotation is relatively unimportant and can be ignored. The model then is allowed to evolve in time for a long period, ca. 1500 ksec or 17 days. Magnetic field quickly guides the wind material from opposite hemispheres towards the magnetic equator, where they shock and cool, emitting X-rays. The modeled emission matches remarkably well with X-rays observation (Gagné et al. 2005) with very little fine-tuning of free parameters.

This type of MCWS model also leads to a dense equatorial region wherein material within closed loops fall back onto the star as radiation is unable to drive the dense material, and the plasma in the outer region above the magnetosphere flows out relatively slowly. Such large-scale structure should leave distinct imprints on UV P Cygni profiles, and in this work we use these MHD models to compute synthetic UV line profiles with the SEI method, following closely the work of Cranmer & Owocki(1996).

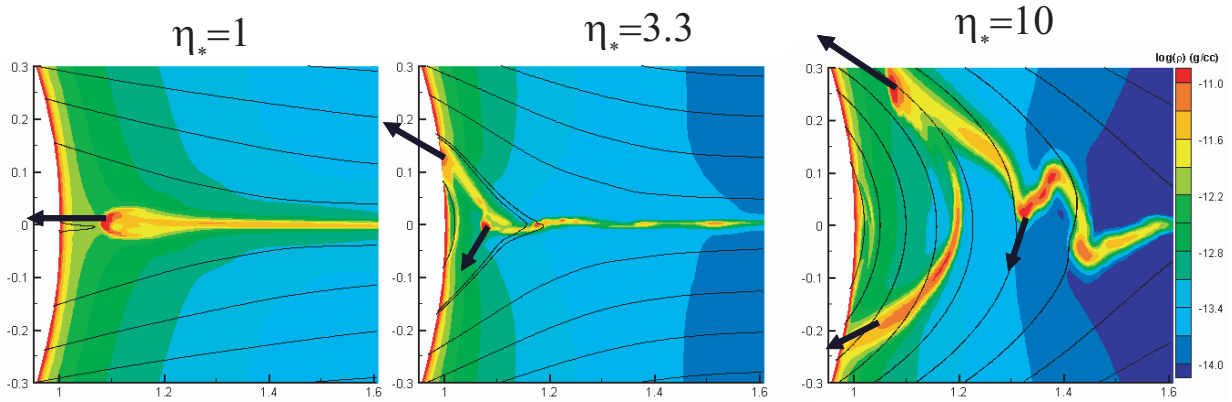

Figure 1: Logarithmic density for models with various magnetic confinement parameter η_*, as indicated, at arbitrarily chosen time to show structure created by magnetic fields.

3 Dynamical SEI line profiles

Ultraviolet P Cygni profiles are excellent diagnostics for probing wind structure in hot stars. Their time variations tell us something about the temporal evolution of the structure as well.

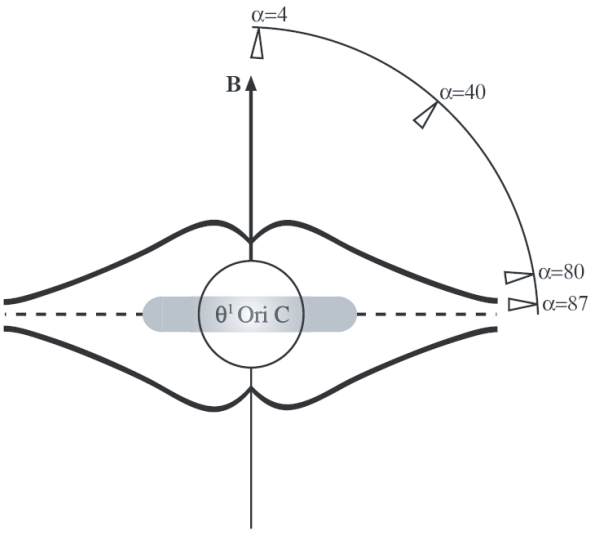

Figure 2: Schematic view of θ^1 Ori C. The vector indicates the magnetic axis and the semicircle represents the viewing angles in degrees spanning the rotational phases of 0 to 1.0. [Figure adopted from Gagné et al. (2005).]

Here we compute time variable synthetic UV line profiles from our simulations by positioning an 'observer' at different viewing angles α between the line of sight and the magnetic pole. If β is the obliquity (the angle between the rotational and magnetic axes), i the inclination angle, and ϕ is the rotational phase of the observations, then α can computed from (Gagné et al. 2005):

$$\cos\alpha = \sin\beta\cos\phi\sin i + \cos\beta\cos i\,. \qquad (2)$$

Quite fortuitously, for θ^1 Ori C $\beta \approx i \approx 45^o$. This implies that the viewing angle α covers a full hemisphere, i.e. from co-latitude $\theta = 0$ to 90 degrees for the northern part, as shown in Fig. 2, or possibly from 90 to 180 degrees for the southern part, as there is an ambiguity about which pole of the star is facing the earth. Our 2D-MHD simulations are fairly north-south symmetric, and so either choice yields similar results. To mimic time variability on a rotational time scale, we choose time $t = 0$ to be an arbitrary time snapshot from our simulation, and then allow the observer to move around the star, as depicted in Fig. 2 (see also, Gagné et al. 2005).

The left panel of Fig. 3 shows the total SEI flux quotient, the absorption plus the emission, expressed as the deviation from the time average, and computed for a relatively strong line. Over the poles (near phases 0 and 1) the strong absorption of relatively dense and fast wind broadens the line by ca. 4000 km/s. By contrast, near the magnetic equator (phase 0.5), the absorption trough is relatively narrow, due to slowly moving, very dense, equatorial disk-like outflow. There is also a weak signature of red-shifted absorption from the dense material that falls backs onto the stellar surface near the magnetic equator (phase 0). Although the equator represents only a geometrically small region in this figure, in the phase variation it occupies a relatively large interval, due to the particular geometry that keeps the equator facing the earth for longer period of time than the poles (see Eq. 2).

The right panel in the same figure shows the ob-

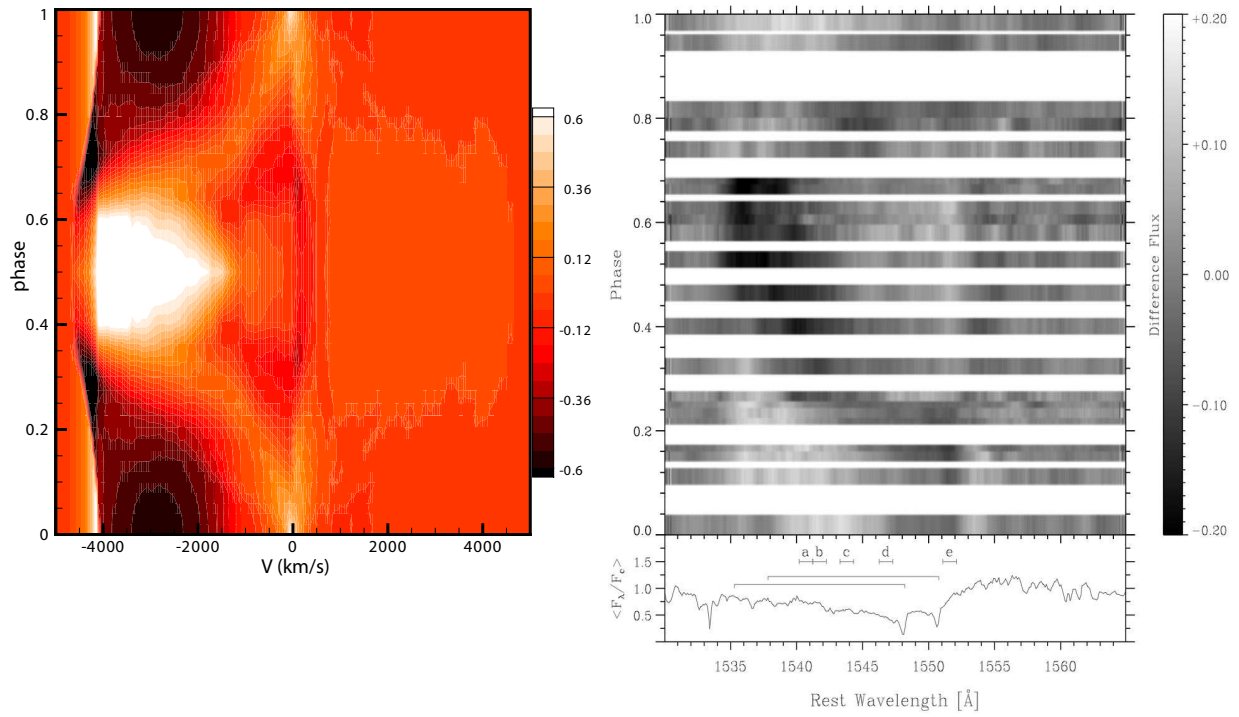

Figure 3: Left Panel: Computed SEI flux quotient (deviation from the time average) for a strong line. Right panel: Observed flux quotient (courtesy of Alex Fullerton).

served *FUSE* UV profile for the C IV doublet line (courtesy of Alex Fullerton), plotted also as a flux quotient. The model variability is a factor two or so stronger than the observations, and moreover exibits almost an opposite sense with phase. However, there is a possibility that phase of the observed data has been miscalculated by ca 0.6 or so, in which case the match will be significantly better. This issue is currently under investigation. Moreover, the observed data also lacks the clear symmetry around the phase 0.5 that our simulation model predicts. Such discrepancies are puzzling and will require further study.

4 Conclusion

In this work, we have shown that the magnetic fields can create large scale structure that is directly related to wind magnetic confinement parameter, η_*. Computed SEI synthetic UV P Cygni profiles show clear temporal and spatial variation. However, such computed profiles do not match the observed data very well. Further studies are under way to investigate this discrepancy.

References

Babel, J., & Montmerle, T. 1997, A&A, 323, 121

Cranmer, S. R., & Owocki, S. P. 1996, ApJ, 462, 469

Donati, J.-F., Howarth, I. D., Bouret, J.-C., Petit, P., Catala, C., & Landstreet, J. 2006, MNRAS, 365, L6

Donati, J.-F., Babel, J., Harries, T. J., Howarth, I. D., Petit, P., & Semel, M. 2002, MNRAS, 333, 55

Gagné, M., Oksala, M. E., Cohen, D. H., Tonnesen, S. K., ud-Doula, A., Owocki, S. P., Townsend, R. H. D., & MacFarlane, J. J. 2005, ApJ, 628, 986

Lamers, H. J. G. L. M., Cerruti-Sola, M., & Perinotto, M. 1987, ApJ, 314, 726

ud-Doula, A., & Owocki, S. P. 2002, ApJ, 576, 413

Townsend: Just a remark: I believe redshifted absorption features have already been detected in the wind of θ' Ori C. So, already there is an encouraging match between observations and your model for the star.

Feldmeier: Owocki, Cranmer & Gayley showed a few years ago how important non-radial forces are in wind-compressed disk calculations: these forces may be small, but they alter velocities that are themselves small, so may be important. How significant is the neglect of non-radial forces in your model?

ud-Doula: Non-radial forces in MHD models are not very important, because magnetic fields make the wind flow in a constrained motion towards the magnetic equator. In WCD models only a small force can disrupt the "disk", but here you need a much larger force. In my direct comparison models, non-radial forces make a difference on a scale $10 - 15\,\%$.

Cohen: Soft X-ray lines are broad in θ' Ori C (implying that instabilities are present), but hard X-ray lines are narrow (they come from magnetically confined wind shocks). So, both small and large structures co-exist. What is the lateral scale of structure in your 3D simulation?

ud-Doula: My simulation extends to $R = 10\,R_*$, and covers a cone of 45°. As such, I estimate lateral structures to be a few tenths of a stellar radius.

Owocki: Just to be explicit, these 2D and 3D MHD models are based on a CAK/Sobolev method for the line force. Such models would be far more difficult with non-local force treatments (SSF), because these require computationally expensive integrations.

Clumping in Hot Star Winds
W.-R. Hamann, A. Feldmeier & L.M. Oskinova, eds.
Potsdam: Univ.-Verl., 2008
URN: http://nbn-resolving.de/urn:nbn:de:kobv:517-opus-13981

Hydrodynamical models of clumping beyond 50 R_*

M. C. Runacres
Erasmushogeschool Brussel, Belgium

We present one-dimensional, time-dependent models of the clumps generated by the line-deshadowing instability. In order to follow the clumps out to distances of more than 1000 R_*, we use an efficient moving-box technique. We show that, within the approximations, the wind can remain clumped well into the formation region of the radio continuum.

1 Introduction

The line-driven stellar winds of hot stars are subject to a strong line-deshadowing instability (e.g. Owocki & Rybicki 1984), which causes the wind to become highly structured. This structure takes the form of strong shocks, strong density contrasts and regions of hot, but generally rarefied, gas.

The structure caused by the line-deshadowing instability is small-scale and stochastic in nature, as opposed to the large-scale, coherent structure associated with discrete absorption components and related features in ultraviolet spectral lines of hot stars (Prinja 1998) We use the word *clumping* to refer to the small-scale density structure only, with the line-deshadowing instability as its most likely cause.

The degree of clumping at a certain distance r from the star is most readily described by the clumping factor $f_{\rm cl}$, defined as

$$f_{\rm cl}(r) = \frac{\langle \rho^2 \rangle}{\langle \rho \rangle^2},$$

where $<>$ denotes the time-averaging of the quantity between brackets. If all of the mass is concentrated in the dense clumps, then the clumping factor is the inverse of the volume filling factor, and is equal to the overdensity of the clumps with respect to the mean wind:

$$f_{\rm cl} = \frac{1}{f_{\rm volume}} = \frac{\rho_{\rm clump}}{\langle \rho \rangle}.$$

The mass-loss rate derived from a density-squared dependent observational diagnostic is inversely proportional to the square root of the clumping factor.

Most theoretical studies of clumping are limited to the wind below 30 stellar radii (R_*). There is, however, ample reason to study clumping at much larger distances from the star. The radio continuum used to derive the mass-loss rates of hot stars is formed by free-free emission and hence is strongly sensitive to clumping. To know the true value of the mass-loss rate, we therefore need to know the degree of clumping. The same holds for other diagnostics of the mass-loss rate that are proportional to the density squared, such as $H\alpha$. As is shown throughout these proceedings, this is a surprisingly difficult thing to do. All mass-loss rate diagnostics are affected by uncertainties. One way to reduce such uncertainties, is to combine different observational mass-loss rate diagnostics, formed in different parts of the wind, to obtain the radial stratification of clumping. Such a study has been performed by Puls et al. (2006).

Even from such a study, it is impossible to derive absolute values of the clumping factor. If one derives a certain radial stratification of the clumping factor assuming the clumping vanishes in the radio formation region, then the observations can also be explained by this clumping factor multiplied by a constant factor, providing the mass-loss rate is lowered accordingly. The derived value of the clumping factor (and hence the value of the mass-loss rate) thus depends on the assumption one makes about the amount of clumping in the radio formation region. Therefore it is important to gain insight in how clumps evolve as they move out to large distances, and to investigate whether clumps can survive as far as the radio formation region.

2 Hydrodynamical models

2.1 Hydrodynamical models including the line-deshadowing instability

We solve the conservation equations of hydrodynamics, using the time-dependent hydrodynamics code VH-1, developed by J. M. Blondin, and modified by S. P. Owocki to include the acceleration due to line driving. Our models are one-dimensional. The radiative acceleration is included in the model using the smooth source function method (Owocki 1991). The structure is self-excited, in the sense that there are no external perturbations at the base of the wind. The structure is seeded by internal base perturbations, that arise as radiation is scattered back

to the base from the structured outer wind. (Initial structure arises as the wind solution adapts from the smooth initial condition). In the absence of detailed knowledge of the photospheric perturbations acting at the base of a real wind, self-excited structure can be seen as a conservative estimate of wind structure.

Radiative and adiabatic cooling are included in the energy equation. Photo-ionisation heating is mimicked by imposing a distance-dependent floor temperature, below which the temperature is not allowed to drop. Details are given in Runacres & Owocki (2002). From test calculations performed in that paper, we have learned that the amount of clumping depends on the value adopted for the floor temperature, as well as on the strength of the line-driving. Also, it is necessary to maintain a rather fine spacing of the radial mesh, in order to adequately resolve the structure. On the other hand, clumping does not depend on the radiative force beyond 30 R_*. This reduces the outer-wind evolution to a pure gasdynamical problem, allowing us to construct vastly more economical models, which will be presented in the next section.

2.2 Moving-box models

For a star like ζ Pup, about half of the radio continuum is formed beyond 100 R_*. So in order to make meaningful predictions about the effect of clumping on the radio mass loss rate, we need to model structure out to very large distances from the star. Even without the evaluation of the radiative force, evolving the entire stellar wind (between 1 and say 1000 R_*) at the required high spatial resolution is still very expensive. A solution is suggested by realising that the structure generated by the instability, apart from being stochastic, is also quasi-regular in the sense that similar features are repeated over time. Therefore it is not necessary to keep track of the whole stellar wind during the duration of the simulation. It is enough to select a limited but representative portion of the structure, and follow this "box" as it moves out at the terminal speed. Following a portion of the wind entails transforming the conservation equations to a moving reference frame. This is not possible directly, as the spherical equations of hydrodynamics are not invariant under a Galilean transformation. This problem can be circumvented by rewriting the equations in a pseudo-planar form. In this form, the equations resemble the planar equations of hydrodynamics, while still describing a spherical geometry. We impose periodic boundary conditions on the box, i.e. structures that flow out of the box on one side, are made to enter it on the other side. Details can be found in Runacres & Owocki (2005).

In the following section, we use a periodic box model, starting from a hydrodynamical model including the line-deshadowing instability, to predict the radial stratification of wind clumping. The adopted model parameters are the same as in Runacres & Owocki (2005).

3 Results

Fig. 1 shows the density contrast (density divided by mean density) within the box as a function of radius and time, as the box moves out from $\sim$ 100 to $\sim$ 1300 R_*. The backward running streaks are shells that are somewhat slower than the terminal speed, the forward running streaks are faster than the terminal speed. The streaks broaden as they evolve, reflecting the fact that shells expand (at a few times the sound speed) as they move out. Within the assumptions of the model, the clumpiness is maintained by collisions between shells. As shells collide, they form denser shells, counteracting their pressure expansion.

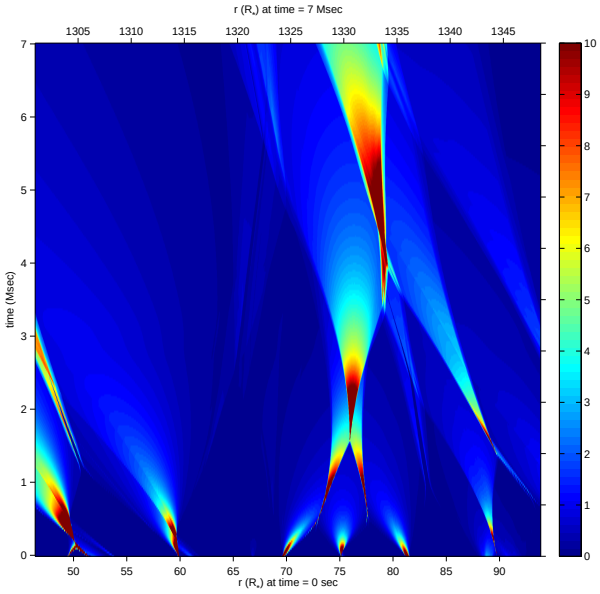

Figure 1: Image of the density contrast as a function of space and time. The intensity scale has been truncated to highlight the kinematics of the shells. The adopted model parameters are the same as in Runacres & Owocki (2005).

The clumping factor for a moving-box model extending out to $\sim$ 1300 R_* is shown in Fig. 2. Below 100 R_* the model is a line-driven instability model, above 100 R_* it is a moving-box model. It is clear that these models predict that the winds stays clumped well into the radio formation region, with clumping factors beyond 200 R_* ranging from 2.5 to

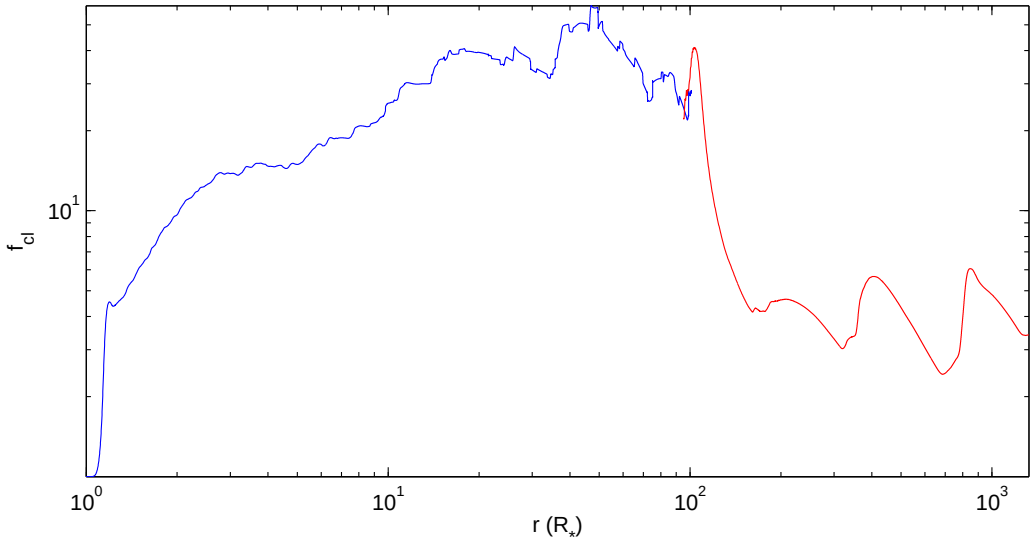

Figure 2: The clumping factor as a function of radius, predicted by our theoretical models. Below 100 R_* the model is a line-driven instability model, above 100 R_* it is a moving-box model.

6. Inferred mass-loss rates would therefore be overestimated by a factor of two.

4 Discussion and conclusions

Our models predict an increase of the clumping factor from the base of the wind to $\sim 50\ R_*$ (Fig. 2), after which the clumping factor decreases, maintaining a level of residual clumping beyond 200 R_*. This does not quite match the clumping factors derived from observations by Puls et al. (2006), which start to tail off closer to the star ($\sim 10\ R_*$). As has been mentioned before, the observations do not tell us whether or not there is residual clumping at very large distances from the star.

There are of course a number of limitations to our model. As has been mentioned above, we have used self-excited structure without external perturbations. Also, we have not attempted to model different spectral types. In particular, the important difference between dense and less dense winds found by Puls et al. (2006) has not been investigated at all in our models.

A key limitation of the present model is of course its restriction to just one dimension. The focus here is entirely on the extensive radial structure, and the instabilities that are likely to break up the azimuthal coherence of the structure are not accounted for. It remains to be seen to what extent this changes the global evolution of instability-generated wind structure. We plan to extend the present models to 2-D in the near future.

References

Owocki, S. P. 1991, in Stellar Atmospheres : Beyond Classical Models, ed. L. Crivellari, I. Hubeny & D. G. Hummer (Dordrecht: Kluwer), 235

Owocki, S. P., & Rybicki, G. B. 1984, ApJ, 284, 337

Prinja, R.K.. 1998, in Cyclical Variability in Stellar Winds, ed. L. Kaper & A. W. Fullerton (Garching: ESO)

Puls, J., Markova, N., Scuderi, S., Stanghellini, C., Taranova, O. G., Burnley, A. W., & Howarth, I. D. 2006, A&A, 454, 625

Runacres, M. C., & Owocki, S. P. 2002, ApJ, 381, 1015

Runacres, M. C., & Owocki, S. P. 2005, ApJ, 429, 323

Hamann: In your diagram with modeling results, it looks as if the clumping factor drops drastically just about a radius of $100\,R_*$, i.e. where your modeling method changed. Is that not something that makes you suspicious?

Runacres: Well, it is a logarithmic scale on the plot, so the decrease of the clumping factor happens over a distance of $100\,R_*$, which is not so small. However, when doing models one always needs to be cautious, so I will check your remark by extending a regular model out to $250\,R_*$. That is easily done.

Cassinelli: You said "once clumped it is hard to get unclumped". That is surprising. Is that not just because your model is 1D?

Runacres: The wind basically stays clumped out to such large distances because the clumps continue to collide and form denser clumps. In this regard, the 1D assumption is indeed crucial, and needs to be checked carefully. I intend to extend this study to 2D in the near future.

Feldmeier: You emphasized the importance of shell collisions at large radii. In my own simulations on X-ray emission I found only very little emission in self-excited models, because there are essentially no shell-cloud collisions. So have you done any models with turbulent photospheric perturbations?

Runacres: No, I have not, but it is on the agenda.

Puls: In your simulations for the outermost structure, is the usual approximation that $\langle\varrho^2\rangle/\langle\varrho\rangle^2_{\rm temporal} \approx \langle\varrho^2\rangle/\langle\varrho\rangle^2_{\rm spatial}$ still valid?

Runacres: Yes, that is still a valid approximation. In fact, the clumping factor in the moving box model has been calculated by replacing time-averages by spatial averages using an ergodic approximation. This was done because calculating a time average at an uncertain position in space, involves some awkward bookkeeping in a moving box model.

Owocki: It is necessary to use time-averaging because in 1D there are too few clumps within a radial range that is uniform enough (without radial evolution). But by ergodic argument, this should be a proxy for volume averages in more realistic 2D/3D models.

Puls: I agree.

Clumping in Hot Star Winds
W.-R. Hamann, A. Feldmeier & L.M. Oskinova, eds.
Potsdam: Univ.-Verl., 2008
URN: http://nbn-resolving.de/urn:nbn:de:kobv:517-opus-13981

Discussion: Hydrodynamic modeling

Moderator: Jorick Vink

Hirschi: From the stellar evolution point of view, a mass loss reduction of three is possible, but ten would imply many critically rotating stars and a low WR/O ratio, and models would not fit observations as well.

Townsend: In answer to Jorik's question (are diagnostics indicating clumping very close to the star incompatible with the result that the line-driven instability does not kick in until a little bit away from the star?) – there are of course photospheric processes that could seed the instability at the wind base. I do not know, however, whether the Lucy drag effect would quench any perturbations introduced at the base.

Hamann: I want to ask those of you who are calculating the hydrodynamic models to consider critically your inherent approximations and assumptions: which of your predictions are robust against the approximations, and which might be actually artifacts? I must say that I am still not fully convinced that Abbott waves are real, and not only an artifact of the Sobolev approximation. My opinion very much depends on the day of the week. On Monday I am skeptical, but till Friday Achim (Feldmeier) has convinced me of their existence. Over the weekend I recover, and next Monday I am doubtful again. For example, is the radiation transfer treated sufficiently correct in the time-dependent hydrodynamic simulations? When the wind encounters a shock, the velocity makes a huge jump downwards. Hence, for optically thick lines the opacity is shifted back into its own shadow, and will hardly intercept any pressure from the stellar radiation. Are such effects properly taken into account in the time-dependent wind models?

Feldmeier: Most of the material in the shock jump is highly rarefied and not optically thick. What is really relevant for these issues of non-monotonic velocity laws, of multiple resonances, and of self-shadowing is the material in the dense shells. The velocity coverage of these shells is, as Stan pointed out in his venetian-blind model for velocity porosity, at most 10%, and clearly not 100%. Furthermore, the effect of multiple resonances on the optical depth is actually included in the simulations. And we have recently started to also include the effect of multiple resonances on the source function, using the iteration method developed by Rybicki & Hummer (1978).

Townsend: To add to what Joe said: 1. Massive stars do have convection zones below the surface, as any stellar structure model made since the early 1990s will show. Around 200,000 K, where the iron opacity bump is located, the blocking effect of the opacity leads to the onset of convection. 2. Even without convection, there are processes, such as the Tayler-Spruit dynamo mechanism, that can generate magnetic fields in radiative envelopes.

Pollock: It is certain that there are magnetic fields in some WR binary systems, those that are non-thermal radio sources. It remains to be seen if the fields are in some way connected to the stellar surfaces or whether the colliding plasmas make up their own fields in order to satisfy the boundary conditions.

Moffat: In the case of magnetic fields in WR stars, we still only have few real empirical constraints from Zeeman data. Nicole (St-Louis), a PhD student and myself have only found modest upper limits to B of 20-40 G in two stars looked at so far (EZ CMa and γ Vel). We still cannot exclude much higher fields at the hydrostatic core ($\sim 10^{3-4}$ G) if they scale as a global dipole. So, we cannot a priori exclude magnetic driving of WR winds.

Feldmeier: I would like to ask Stan whether Alfvén waves could propagate outward through the wind and lead to a large magnetic pressure at large radii, so that the magnetic field would actually have a strong influence at large distances from the star, like e.g. in the afterburner effect in the solar wind.

Owocki: In principle, yes. But as transverse waves, Alfvén waves along a more or less radially oriented magnetic field line would be expected to be strongly damped by the lateral line-drag effect in a radiatively driven flow. But to be honest, there has not been any very extensive modeling or detailed analysis published on the potential role of Alfvén waves in a line-driven wind, so I guess the mechanisms you mentioned might still be relevant. But I would note that the non-radial divergence of field lines in MHD simulations, e.g. by Asif ud-Doula, do show a clear effect in increasing the wind speed in regions of open field in a line-driven wind.

Townsend: One remark – perhaps the final one – about magnetic fields. Jirí Krtička made a good point earlier today, that if you play around with a wind below the critical point, you can change the

overall mass loss rate. So, even small-scale, high-order fields that do not really extend into the wind, and have no detectable signature, can lead to a very inhomogeneous mass loss across the stellar surface. This could serve as seed for the line-driven instability to amplify into clumping.

Owocki: If the pulsations are relatively low-order in l and m, then in principle one can model their effects on a stellar wind using the multi-D CAK/Sobolev hydrodynamic approach, ignoring the small-scale instability. I think this should be one focus for future research.

Kellermann: Is there an influence of the rotation (uniformly versus differential rotation) on the pulsation of the star? There are some influences on the oscillation in neutron star models.

Townsend: In massive stars, neither p modes nor g modes probe the convective core, they are both reflected, due to the variation in the Lamb and Brunt-Väisälä frequencies. There is some evidence claimed in one β Cep star of differential rotation, revealed by p mode frequency splitting, but the evidence is rather marginal.

Owocki: Regarding critical points, these in my opinion are really a somewhat artificial consequence of assuming a steady-state solution. A time-dependent model has no such critical points, but nonetheless a time-dependent simulation will generally relax quite quickly to something quite close the steady, critical solution derived by a CAK analysis. In such CAK models, the sonic point represents the transition between the nearly hydrostatic atmosphere where gas pressure balances gravity, and the wind where the radiative force is able to overcome gravity and accelerate a net outflow. The CAK critical point is where it is the most difficult for the line-driving to sustain the mass flux. But since at the sonic point the flow inertia is effectively canceled by the gas pressure term, the line force there can drive an arbitrarily large mass flux simply through an increased velocity gradient. The CAK critical point thus occurs *above* the sonic point, when gas pressure becomes negligible and the line force must balance both the gravity and wind inertial acceleration.

Feldmeier: To emphasize Stan's answer: the critical point lies very close to the star not because it coincides with the sonic point, but because photons are predominantly lateral close to the star, and therefore cannot carry $\dot{M}$ away from the star in radial direction. The critical point has his name for good reasons: it is the point where the radiation field has the hardest time to lift the wind mass against stellar gravity. This is in complete analogy with the Laval nozzle, where the critical point coincides with the location of minimum nozzle area, i.e. with the nozzle constriction. The critical point in an O star wind has to do with the radiative force, and hence the flow becomes super-Abbottic there, not supersonic.

Moffat: One should look at the ISM, even if detailed conditions are different (e.g. no radial fall-off of driving).

Massa: The evidence for clumping starting near the stellar surface comes from O stars. Could it be that clumping does not begin close to the surface in WRs but it does in O stars?

seems to be surprisingly similar between different object classes. For WN stars, we (Liermann & Hamann, these proceedings) found that clumping in the line-forming region is about three times stronger than in the radio region – i.e. similar in tendency but less pronounced than what Puls et al. (2006) obtained for O-type supergiants. Moreover, all studies show evidence that clumping is already strong at velocities of the order of the sound speed. These properties are puzzling and not quantitatively explained by the hydrodynamic models of the line-driven instability.

Gräfener: In our optically thick wind models it happens that the dependence on ρ and T dominates over the CAK-α effect. Close to the Fe-opacity peaks, the radiative force increases due to the outward decrease of ρ and T and *not* due to the α-effect. In such a case the sonic point becomes the critical point. Other effects that strongly deviate from the CAK asssumptions are extreme line-overlaps due to a pronounced ionization structure and an "active" line transfer. In extreme cases (e.g. outwardly increasing line source functions) the latter can even cause negative fluxes in the line core. So, as far as I see, there are many effects not taken into account in the CAK approach which may significantly alter the wind physics.

Hirschi: How does metallicity affect clumping and the different mass loss diagnostics?

Fullerton: I think that Raphael (Hirschi) is correct to raise the issue of abundances. Certainly, the current controversy about the solar oxygen abundance is a reminder that determining absolute abundances is a very tricky business. In the case of phosphorus, I think we are on reasonably solid ground. As I mentioned yesterday, the abundance really does appear to be solar along eight sightlines recently studied with FUSE spectra (Lebouteiller et al. 2005, A&A). This is the material from which Galactic O stars formed "the day before yesterday", so it is hard to see how it could be lower by factors of three or ten. Furthermore, the mass loss discrepancy between P V and Hα persists in both the LMC and SMC; so it is also hard for me to see how abundance can play a key role in resolving the problem. Of course, for his work Raphael is primarily concerned with the abundances of the elements that actually drive the wind. Phosphorus is completely unimportant in this regard.

Weis: Is there a difference between the phosphorus lines comparing LMC and galactic objects?

Magnetic fields

Chair: R. Prinja

Clumping in Hot Star Winds
W.-R. Hamann, A. Feldmeier & L.M. Oskinova, eds.
Potsdam: Univ.-Verl., 2008
URN: http://nbn-resolving.de/urn:nbn:de:kobv:517-opus-13981

Circumstellar Magnetic Field Diagnostics from Line Polarization

R. Ignace[1] **& K. G. Gayley**[2]
[1]*Department of Physics, Astronomy, & Geology, East Tennessee State University, USA*
[2]*Department of Physics & Astronomy, University of Iowa, USA*

1 Introduction

Given that dynamically significant magnetic fields in at least some massive stars have now been measured, our contribution addresses the question, to what extent can fields be directly detected in circumstellar gas? The question speaks directly to the very interesting topic of line-driving physics coupled with magnetized plasmas, and how this coupling produces structure in the wind flow. The major goal of this effort is the hope of relating direct measurements of photospheric magnetic fields in massive stars, for example via the methods of Donati & Cameron (1997), with direct measurements of the circumstellar magnetic field from wind lines. Aside from non-thermal emissions, direct detection of magnetic fields derives from the Zeeman effect. Already, Donati et al. (2005) has reported the detection of circularly polarized lines in the disk of FU Ori, signifying that the time is ripe for modeling diagnostics of circumstellar magnetic fields to help guide observers in similar future searches.

We focus our attention on weak-field diagnostics. These come in two main types: the Hanle effect, which pertains to coherence effects for linear polarization from line scattering, and the weak longitudinal Zeeman effect, which pertains to circular polarization in lines.

2 The Hanle Effect for Winds

The Hanle effect refers to how a magnetic field can alter the linear polarization of a scattering line. When the splitting of magnetic sublevels by the Zeeman effect $\Delta\nu_Z$ remains comparable to the natural width of those sublevels $\Delta\nu_N$, a situation of quantum coherence exists. Normally, in the absence of a magnetic field, a coherent scattering line (such as a resonance line) produces linear polarization following a dipole emission pattern (like that of a free electron), but with an amplitude that depends on the details of the particular transition. In the presence of a relatively weak magnetic field, the magnetic sublevels start to become non-degenerate in energy, leading to an adjustment of the polarization amplitude, which becomes a function of scattering direction with respect to the local magnetic field vector (Stenflo 1994).

A description of this effect in terms of classical damped harmonic oscillators is quite helpful because of its visual nature. For simplicity, consider a level transition that has a polarization amplitude of 100% when scattering through a right angle, just like Thomson scattering. The scattering of unpolarized incident light, typical of the case for illumination by starlight, is pictured as the excitation of two orthogonal dipole oscillators. Forward and backward scattered radiation is unpolarized.

Now consider a magnetic field that is perpendicular to the direction of incident radiation. The magnetic field exerts a Lorentz force on the oscillating bound electron such as to precess the oscillation about the axis of the field direction. The competition here is between the Larmor frequency $\omega_L = g_L B/m_e c$ that sets the rate of precession and the Einstein A-value that sets the rate at which radiation is scattered. For a small ratio of ω_L/A, precession is minimal, and the scattering is essentially non-magnetic. But when ω_L/A is large, precession leads to a full rotation of the oscillator before much damping of the amplitude occurs. Consequently, the scattered light when viewed along the magnetic field becomes completely depolarized. We refer to this limit as "saturated", because information about the field strength is lost – one knows the field is relatively strong, but the low polarization is a hindrance for determining exactly how strong, yet there is still information about the magnetic field direction. In terms of synthetic polarization spectra from models, the saturated limit is valuable for interpreting the results because of its simplistic properties – complete depolarization along the field, but no precession of the dipole oscillator that is parallel to the field. At its heart the Hanle effect is about redistributing scattered light relative to the zero field case.

There have been a series of papers highlighting applications of the Hanle effect to scattering lines

from winds (Ignace et al. 1997; Ignace et al. 1999; Ignace 2001a; Ignace 2001b; Ignace et al. 2004). These have dealt exclusively with line polarizations from optically thin scattering. Ignace et al. (2004) consider the impact of line optical depth on the polarization through a single-scattering approximation, whereby optical depths below unity adopt the single-scattering results, but zero polarization contributions are assumed from regions where the optical depth exceeds unity. The series has dealt with spherical wind flows, expanding disks, and simplified considerations of oblique magnetic rotators.

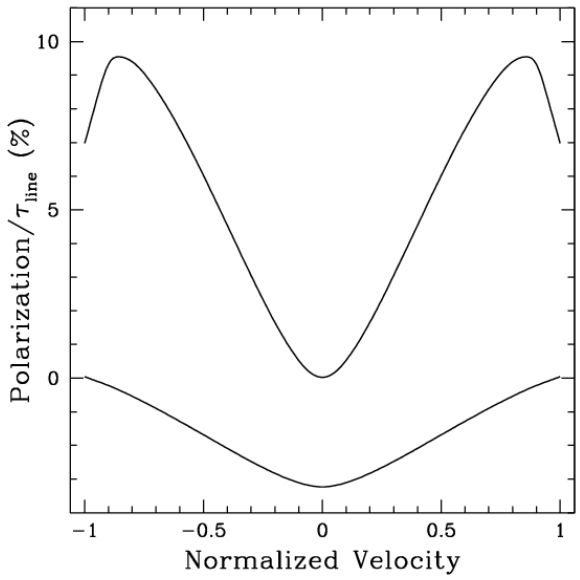

Figure 1: The Hanle effect for a thin scattering line from a Keplerian disk seen edge-on. The polarization is normalized to the line optical depth $\tau_{\rm line} < 1$. The upper curve shows the polarization without a magnetic field. Lower curve is for a toroidal field in the saturated limit. The sign change signifies a rotation of the polarization position angle by 90°.

A new model presented at this meeting was a calculation for an optically thin line from an axisymmetric Keplerian disk, with results shown in Figure 1. The upper curve shows the total flux emission profile, and the lower curve shows two curves for the polarized line profile. These are plotted against velocity shift normalized to the Keplerian speed at the stellar radius. In the lower panel, the upper curve is the polarization without a magnetic field, and the lower one is with a toroidal field, $B_\varphi \propto r^{-1}$, in the saturated limit. Note that these profiles assume an edge-on viewing perspective and normalized to line optical depth, τ. Going to higher inclinations can affect the profile shape, but the dominant effect is to lower the amplitude of the polarization. Also, this calculation does not take account of absorption of the photospheric continuum, nor contamination by photospheric lines, nor stellar occultation of the rearward disk (e.g., the approach of Ignace 2000). However, with the disk velocity field being right-left anti-symmetric, the effects will be symmetric about line-center.

Of particular interest is that the line-integrated polarization is non-zero, and so even narrow-band polarimetry could be used in order to increase signal-to-noise to detect the influence of the Hanle effect. Different lines that are sensitive to different field strengths would yield not only different levels of polarization, but even net position angle rotations.

There are plans to measure the Hanle effect for the first time in stars other than the Sun. The Far Ultraviolet Spectro-Polarimeter (FUSP, see www.sal.wisc.edu/FUSP; Nordsieck et al. 2003; Nordsieck & Ignace 2005) will have the capability at a resolving power of $R \approx 1800$ of measuring the linear polarization across wind-broadened P Cygni lines of bright stars. This is a rocket payload mission expected to have multiple flights. The stars targeted for detecting the Hanle effect are ζ Ori and ξ Per in the missions second launch, currently scheduled for late 2009.

3 Zeeman Effect for Winds

As is well known, the Zeeman effect describes how a magnetic field leads to splitting of atomic sublevels. In a standard Zeeman triplet, one generally has an unshifted line component that can be linearly polarized (referred to as a "π" component) and a pair of equally shifted components left and right of line center range (referred to as "σ" components). The σ components are circularly polarized when viewed along the magnetic field, in which case the unshifted π component will not be seen, but are linearly polarized when viewed orthogonal to the magnetic field.

In the weak-field limit – not so weak as to be in the Hanle regime, but sufficiently weak that the Zeeman splitting is small compared to other broadening processes, the Zeeman components will be strongly blended. In the Hanle regime, the σ components maintain a phase relation, leading to linear polarization effects owing to the coherent superposition of left and right circular polarizations. In the weak Zeeman regime, the σ components are distinctly split relative to their respective natural broadening, and the circular polarizations of the two components add incoherently. Consequently, blending from thermal, turbulent, rotational, or wind broadening strongly diminishes the net circular polarization of the line.

Ignace & Gayley (2003) explored the Zeeman effect in the Sobolev approximation in order to de-

termine the scaling of the circular polarization on magnetic field and wind properties. In the context of the longitudinal Zeeman effect, that relates to the net circular polarization of a line, and scales with the net projected magnetic flux along the line-of-sight, the circular polarization is derived from a Taylor expansion of the difference in intensity between the two σ components. Following that paper, we define $I_\pm$ as left (blueshifted) and right (redshifted) circularly polarized intensities as given by

$$I_\pm \approx \frac{1}{2} I_0(\Delta\lambda \mp \Delta\lambda_B \cos\gamma), \quad (1)$$

where I_0 is the intensity profile shape in the absence of a magnetic field, $\Delta\lambda$ is the wavelength shift from line center, and

$$\cos\gamma = \hat{B} \cdot \hat{z}, \quad (2)$$

for $\hat{B}$ the magnetic field unit vector and $\hat{z}$ a unit vector directed toward the observer. For the intensity of circularly polarized light, we have Stokes $V = I_+ - I_-$, yielding

$$V = -\Delta\lambda_B \cos\gamma \left(\frac{dI_0}{d\lambda}\right)_{\Delta\lambda} \quad (3)$$

In the Sobolev approximation for spherical winds, one builds up a line profile by considering isovelocity surface "cuts" through the wind flow, and integrating the intensities across these surfaces, accounting for stellar occultation and absorption of the photospheric continuum. In the weak-field regime of interest, the fluxes $F_\pm$ are identical in shape but slightly shifted from one another. The difference of these profiles gives the flux of circular polarization F_V. Focusing on only the emission for illustration, Ignace & Gayley derive the formula:

$$F_V^{\rm emis}(\Delta\lambda_z) = -\frac{2\pi}{D^2} \int_{\Delta\lambda_z} \Delta\lambda_B \cos\gamma \times \times \frac{d}{d\Delta\lambda_z} \left[S_\lambda \left(1 - e^{-\tau_S}\right)\right] p\, dp \quad (4)$$

where τ_S is the Sobolev optical depth, $\Delta\lambda_z$ identifies the wavelength shift in the profile from line center that spatially corresponds to an isovelocity zone, S_λ is the position-dependent source function, D is the source distance, and p the polar radius in observer coordinates. Implicit is that the wind is spherical, that the field is axisymmetric, and that the viewer perspective is along the field symmetry axis (otherwise there would be an integration in observer azimuth α since the intersection of the field topology with the isovelocity zones would not generally be azimuthally symmetric). Consequently, equation (4) is maximized for the net magnetic flux through isovelocity zones, and the resultant circular polarizations represent best-case scenarios.

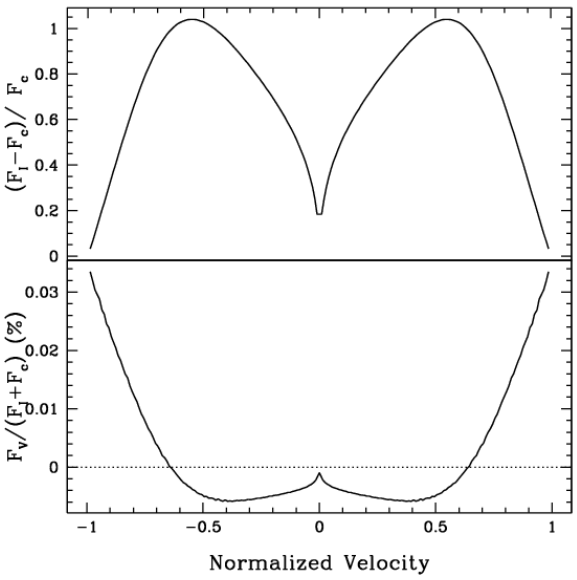

Figure 2: Upper panel shows the emission line profile from a Keplerian disk (relative to and normalized by the continuum level). Lower panel displays the percent circularly polarized profile assuming a toroidal magnetic field with $B_* = 100$ G for an optical line.

Ignace & Gayley derived polarized line profiles for simplified models of resonance and recombination lines, assuming a velocity law that was linear with radius and using simple field distributions such as a split monopole. As expected, the overall peak amplitude of the polarization scales with v_Z/v_∞, for v_Z the velocity splitting of the Zeeman components. Peak polarizations of about 0.05% were found, assuming a surface field strength of 100 G and a modest terminal wind speed of 1500 km/s. Such values are challenging, but not beyond the capability of existing and upcoming telescopes, such as the Potsdam Echelle Polarimetric and Spectroscopic Instrument ("PEPSI", see www.aip.de/pepsi; Hofmann et al. 2002; Andersen et al. 2005).

We are taking steps in developing approaches for computing line polarization for more realistic stellar winds. The two main practical considerations are: (1) what geometries are of most interest and (2) what geometries are most observationally feasible? The answers to both questions would seem to be the same, namely circumstellar disks. Disks in Keplerian (or near Keplerian) rotation are relatively common: for example protostellar disks, interacting binaries, and Be disks. The scaling of polarization amplitude with $v_Z/v_{\rm max}$, where $v_{\rm max}$ is the maximum flow speed in a system, is robust, and Keplerian disks are limited by the speed of critical rotation of their central star, which is typically a factor of 3

smaller than wind speeds. Consequently, line polarizations will be larger by a similar factor for a given surface field strength.

As an example, we consider a Keplerian disk with a purely toroidal magnetic field. As noted previously, the isovelocity zones of an axisymmetric rotating disk are left-right symmetric, in contrast to the back-front symmetry for spherically expanding winds. For disks the isovelocity zones are loops. As for the calculation with the Hanle effect, we focus on just the emission contribution and for now ignore absorption and stellar occultation. For modeling the disk emission, we follow the escape probability approach of Rybicki & Hummer (1983).

A useful notational device is to scale the Zeeman splitting to a Doppler shift in the units of an equivalent line-of-sight speed v_Z, and then the simplest preliminary result can be obtained assuming a toroidal disk field obeying $B_\varphi \propto r^{-1/2}$. Then the Zeeman shifts of the $\sigma_\pm$ components, characterized by v_Z, scale in direct proportion to the actual Keplerian speed v_ϕ. As a result, the isovelocity zones for the respective $\sigma_\pm$ components are identical to Keplerian but with v_ϕ scaled *uniformly* larger or smaller, by $(v_\phi \pm v_Z)/v_\phi$, for each circular polarization.

In this special case, the resultant Stoke-V flux for the line profile is given by the expression

$$F_V^{\rm emis} = F_+^{\rm emis} - F_-^{\rm emis} \quad (5)$$

$$= -2\left(\frac{v_B}{v_{\rm rot}}\right)\left[F_I + \Delta\lambda_{\rm z}\left(\frac{dF_I}{d\lambda}\right)\right], \quad (6)$$

where v_B is v_Z evaluated for a surface field strength at the equator of the star with $B_* = 100$ G, and $v_{\rm rot} = 500$ km/s is the Keplerian rotation speed at the radius of the star. The resultant profile shape is shown in the lower panel of Figure 2, with the upper panel displaying the Stokes F_I profile for the line emission. The profiles are plotted against observed velocity shift normalized to $v_{\rm rot}$. Note that the F_I profile shows the characteristic double-peak morphology, whereas the polarized line shows its strongest values at the extreme line wings. The circularly polarized emission from a disk is seen to be left-right *symmetric*, in contrast to a spherical wind that is *antisymmetric* about line center.

4 Observing Strategies

We have emphasized what lies ahead for the future opportunities in direct detection of circumstellar magnetic fields, in order to test models of magnetized plasma flows. It is significant that efforts in this regard are already underway. As mentioned, Donati et al. (2005) have claimed a detection of magnetic fields in the circumstellar disk of FU Ori. Hubrig et al. (2007) have also claimed a detection of circular polarization in the circumstellar line of a couple of Herbig Ae stars; however, this has been contested by Wade et al. (2006). Eversberg et al. (1999) and St-Louis et al. (2007) have searched for the Zeeman effect in lines of Wolf-Rayet stars, although they have no confirmed detections as yet. The key point is that observers are undertaking these searches, albeit with difficulty. More detections are to be expected, so diagnostic procedures are needed to connect the data with models of magnetized winds and disks.

This raises the obvious question, how are the Zeeman and Hanle effects to be most effectively employed? Bear in mind that the Hanle effect only works for scattering lines, but it is sensitive to quite weak fields, in the range 1–100 G. For hot stars this generally relegates its usefulness to UV spectropolarimetry, which of course requires space-borne instrumentation. Fortunately, FUSP should give us our first opportunity of sampling the Hanle effect in the UV lines of hot stars.

On the other hand, there are limited classes of objects where even Hα can act as a scattering line, significant for the fact that it can be observed from the ground, and sensitive to fields of around 1 G. Such sources include yellow hypergiants and some blue supergiants (e.g., Verdugo et al. 2005). Another important class are supernovae, as for example the polarization from Hα seen in SN1987A (Jeffery 1987, 1991). Studies of polarization in SNe suggests that observed variations can arise in part from line scattering effects e.g., Hoffman 2006). In those cases where the polarization arises from line scattering, comparisons of the polarizations between different lines and in relation to the continuum polarization from Thomson scattering could reveal the presence of the Hanle effect and thereby constrain magnetic fields in the ejecta of SNe.

The magneto-rotational instability (MRI – Balbus & Hawley 1991) has been found to be a robust mechanism for producing turbulent magnetic fields. In particular in a Keplerian disk, simulations indicate that for an initially vertical field threading the disk, the MRI leads to two primary field components: one that is predominantly toroidal (like that of our model profiles) and one that is turbulent or "randomized". Moreover, the toroidal field likely switches direction between the upper half disk and the lower half. So for the Zeeman effect, the oppositely directed toroidal field essentially leads to net zero magnetic flux around the disk for optically thin emission, and so would not produce observable circular polarization. This would not be the case for the Hanle effect, as the result shown in Figure 1 does not depend on the handedness (or reversals) of the toroidal field in the disk.

A distinct advantage of the Hanle effect in *turbulent* magnetic regions is that it is not canceled by line-of-sight magnetic field reversals, the way the longitudinal Zeeman effect is. Indeed, the Hanle

effect has been employed as a diagnostic of turbulent solar magnetic fields (Stenflo 1982; Stenflo et al. 1998). (Note however that for an unresolved source, a field that is tangled on a spatial scale that is small compared to the Sobolev length will likely lead to complete depolarization from that region.)

Perhaps the best strategy is to employ the Zeeman and Hanle effects in a complementary fashion. The Hanle effect will likely be best sensitive to weak fields from scattering lines in regions where the line is optically thin (Ignace et al. 2004), even if the surface field is quite strong, because the circumstellar field will typically drop rather rapidly with radius (as for multipole fields). The Zeeman effect will be sensitive to strong photospheric fields, and possibly circumstellar fields in the inner wind or disk. Both of these should be used along with additional sources of information about the source, such as the continuum polarization that may arise from electron scattering, and line profile shapes in Stokes-F_I.

We suggest that one promising target for honing these diagnostics is σ Ori E. This Bp star has a Zeeman detection (Landstreet & Borra 1978), has anomalous X-ray behavior (Groote & Schmitt 2004), and cyclic variations in its Hα emission (Townsend et al. 2005), all that been successfully interpreted in terms of a strongly magnetized circumstellar envelope (Townsend & Owocki 2005). This and similar sources where the magnetic field properties are already highly constrained would be good targets for detecting the Zeeman and Hanle effects in circumstellar lines.

The authors would like to thank Ken Nordsieck for discussions of the Hanle effect in SNe, and Jennifer Hoffman for a preview of recent line polarization data in SNe.

References

Andersen, M., et al. 2005, in High Resolution Infrared Spectroscopy in Astronomy, (eds) Käufl, Siebenmorgen, Moorwood, 57

Balbus, S., & Hawley, J. 1991, ApJ, 376, 214

Donati, J.-F., & Collier Cameron, A. 1997, MNRAS, 291, 1

Donati, J.-F., Paletou, F., Bouvier, J., Ferreira, J. 2005, Natur, 438, 466

Eversberg, T., Moffat, A., Marchenko, S. 1999, PASP, 111, 861

Groote, D., & Schmitt, J. 2004, A&A, 418, 235

Hofmann, A., Strassmeier, K., Woche, M. 2002, Astr. Nach., 323, 510

Hoffman, J. L. 2006, to appear in Circumstellar Media and Late Stages of Massive Stellar Evolution, RMxAA Conf. Ser. (astroph/0612244)

Hubrig, S., Yudin, R., Schöller, M., Pogodin, M. 2006, A&A, 446, 1089

Ignace, R. 2000, A&A, 363, 1106

Ignace, R. 2001a, in Advanced Solar Polarimetry – Theory, Observation, and Instrumentation, ASP Conf. Ser. 236, (ed) Sigwarth, 227

Ignace, R. 2001b, ApJ, 547, 393

Ignace, R., Cassinelli, J., Nordsieck, K. 1999, ApJ, 520, 335

Ignace, R., Gayley, K. 2003, MNRAS, 341, 179

Ignace, R., Nordsieck, K., Cassinelli, J. 1997, ApJ, 486, 550

Ignace, R., Nordsieck, K., Cassinelli, J. 2004, ApJ, 609, 1018

Jeffery, D. 1987, Nature, 329, 419

Jeffery, D. 1991, ApJS, 77, 405

Landstreet, J., & Borra, E. 1978, ApJ, 224, L5

Nordsieck, K., et al. 2003, in Polarimetry in Astronomy, (ed) S. Fineschi, Proceedings of the SPIE, 4843, 170

Nordsieck, K., & Ignace, R. 2005, in Astronomical Polarimetry: Current Status and Future Directions, ASP Conf. Ser. 343, (eds) Adamson, Aspin, Davis, Fujiyoshi, 284

Rybicki, G., & Hummer, D. 1983, ApJ, 274, 380

St-Louis, N., 2007, to appear in Mass Loss from Stars and the Evolution of Stellar Clusters, (eds) de Koter, Smith, Waters

Stenflo, J. O. 1982, Solar Phys., 32, 41

Stenflo, J., Solar magnetic fields: polarized radiation diagnostics, 1994, (Dordrecht: Kluwer)

Stenflo, J., Keller, C., Gandorker, A. 1998, A&A, 329, 319

Townsend, R., Owocki, S. 2005, MNRAS, 357, 251

Townsend, R., Owocki, S., Groote, D. 2005, ApJ, 630, L81

Verdugo, E., et al. 2005, in The Nature and Evolution of Disks Around Hot Stars, ASP Conf. Ser. 337, (eds) Ignace and Gayley, 324

Wade, G., et al. 2006, in Solar Polarization 4, ASP Conf. Ser. 358, (eds) Lites, 369

Nielsen: The Zeeman effect does not affect all spectral lines, but is dependent on the Lande factor. Consequently, you need to be careful and choose spectral lines wisely. How do you know what lines to use?

Ignace: I failed to mention that $\delta\lambda_B$ contained the Landé factor. Your comment is appreciated, but I would leave line selections to observers. My results (although simple) will just scale in amplitude with the Landé factor.

Puls: Not only in SNe, but also in A-type supergiants (the visually brightest blue supergiants with radiation driven winds) Hα becomes a quasi-resonance line. So also here the Hanle effect might become visible.

Ignace: You are correct, and I have spoken with Eva Verdugo about these sources. However, if one assumes that magnetic flux is conserved, the surface fields in these large stars may be too small for Hanle.

Kholtygin: Recently a large number of magnetic field measurements for B stars was made by S. Hubrig et al. They used the FORS1 spectropolarimeter at VLT and found a field for most of the studied stars.

Owocki: As I recall, Svetlana Hubrig has reported spectropolarmetric evidence of complex field in disks of a few Be stars, but with a very low upper limit to large-scale dipole.

Ignace: I was not aware of this. Observationally, it seems very challenging to draw such conclusions from circularly polarized lines in relation to a "complex field". Perhaps there is phase information that helps.

Sonneborn: The Hα polarisation in SN1987A is not associated with any magnetic field, but with a symmetric distribution of scatterers as in the SN envelope on the line of sight. What magnetic field strength would be needed for the Hanle effect to compete with the large velocities ($\pm$1000 km/s) and scattering geometries in SN ejecta?

Ignace: The Hanle effect merely modifies line scattering polarization: it either elevates or diminishes it. Hα is sensitive to fields of a few Gauss. High speed flow does present a challenge to the Hanle effect, in contrast to the Zeeman effect. The Hanle effect is coherent scattering whereas Zeeman is incoherent.

Vink: Regarding those QU loops you showed. We see a majority of Herbig Ae stars showing these kind of QU loops (Vink et al. 2002, MNRAS) and this is suggestive of a rotating medium.

Clumping in Hot Star Winds
W.-R. Hamann, A. Feldmeier & L.M. Oskinova, eds.
Potsdam: Univ.-Verl., 2008
URN: http://nbn-resolving.de/urn:nbn:de:kobv:517-opus-13981

Magnetic fields and wind variability in massive stars

R.S. Schnerr[1,2] & H.F. Henrichs[2]
[1] *SRON, Sorbonnelaan 2, 3584 CA Utrecht, the Netherlands and*
[2] *Astronomical Institute of the Univ. of Amsterdam, Kruislaan 403, 1089 SJ Amsterdam, the Netherlands*

This paper describes the thesis work of Schnerr (2007) entitled "Magnetic fields and mass loss in massive stars", which aimed at a better understanding of the impact of magnetic fields on the winds of massive stars.

1 Introduction

The goal of this PhD project was to increase our understanding the role of magnetic fields in massive stars ($M \geq 10\ M_\odot$), as magnetic fields strongly impact both their formation and evolution, and many unexplained phenomena observed in massive stars are likely related to magnetic fields. In this paper we list the known magnetic massive stars, summarise the indirect evidence for the presence of magnetic fields in these stars, such as various types of variability observed in UV wind lines, report new direct measurements of their magnetic field strengths, and discuss results of models of the impact of magnetic fields on the structure of the stellar wind.

2 Indirect evidence for magnetic fields in massive stars

The most important indirect evidence of magnetic fields in massive stars is the observed, rotationally modulated, variability in their UV wind lines (see e.g. Henrich et al. 2005). Examples of such variability are shown in Fig. 1. Magnetic fields have been suggested as a possible cause for this variability (see also Sect. 2.1).

Ud-Doula & Owocki (2002) showed that the type of variability caused by a magnetic field can be characterised by the magnetic confinement parameter η_*:

$$\eta_* = \frac{B_{*,\mathrm{eq}}^2 R_*^2}{\dot{M} v_\infty}, \qquad (1)$$

where $B_{*,\mathrm{eq}}$ is the magnetic field strength at the stellar equator, R_* the stellar radius, $\dot{M}$ the mass-loss rate and v_∞ the terminal wind velocity. All currently known magnetic massive stars (listed in Table 1) have $\eta_* \gg 1$, which means that the behaviour of their winds is dominated by the magnetic field. Such stars are called oblique rotators. For stars with $\eta_* < 1$, the wind dominates over the magnetic field, but even such a weak field could still result in observable variability in the wind. The fact that only relatively strong magnetic fields have been detected is likely due to the sensitivity of the current instrumentation. The known population of magnetic massive stars might only be the tip of the iceberg.

Other indicators for the presence of a magnetic field are non-thermal radio emission likely due to synchrotron radiation (White 1985, see also Schnerr et al. 2007c), anomalous X-ray emission (e.g. Oksala et al. 2005 and Waldron & Cassinelli 2001), chemical peculiarities related to reduced mixing due to magnetic fields, and variable (double peaked) emission lines such as Hα and He II (e.g. Moffat & Michaud 1981, Rauw et al. 2001 and Stahl et al. 1996).

2.1 Types of UV wind-line variability

A thorough investigation of OB stars observed with IUE by ten Kulve (2004, see also Howarth & Prinja 1989, Kaper et al. 1996, Fullerton 2003 and Henrichs 2005) revealed three different types of UV wind-line variability (Fig. 1). Next to the known DAC-type variability observed at high velocities (near v_∞) and the magnetic-type variability close to line centre, a third type is found with variability at intermediate velocities.

All known magnetic massive stars observed by IUE show magnetic-type variability, except ω Ori and θ^1 Ori C which show DAC-type variability. In all these stars the UV wind-line variability is stricly periodic (see Fig. 2), except perhaps ω Ori where the periodicity was only observed for a period of three days (Peters 1996). Most O stars show DAC-type variability, usually with a cyclic behaviour but not strictly periodic. Cranmer & Owocki (1996) presented a model to explain this type of variability by a disturbance at the base of the wind. As a cause for this disturbance both magnetic fields and non-radial pulsations have been suggested. However, the observed periods of the variability are of the order of the stellar rotation period, and no pulsations modes

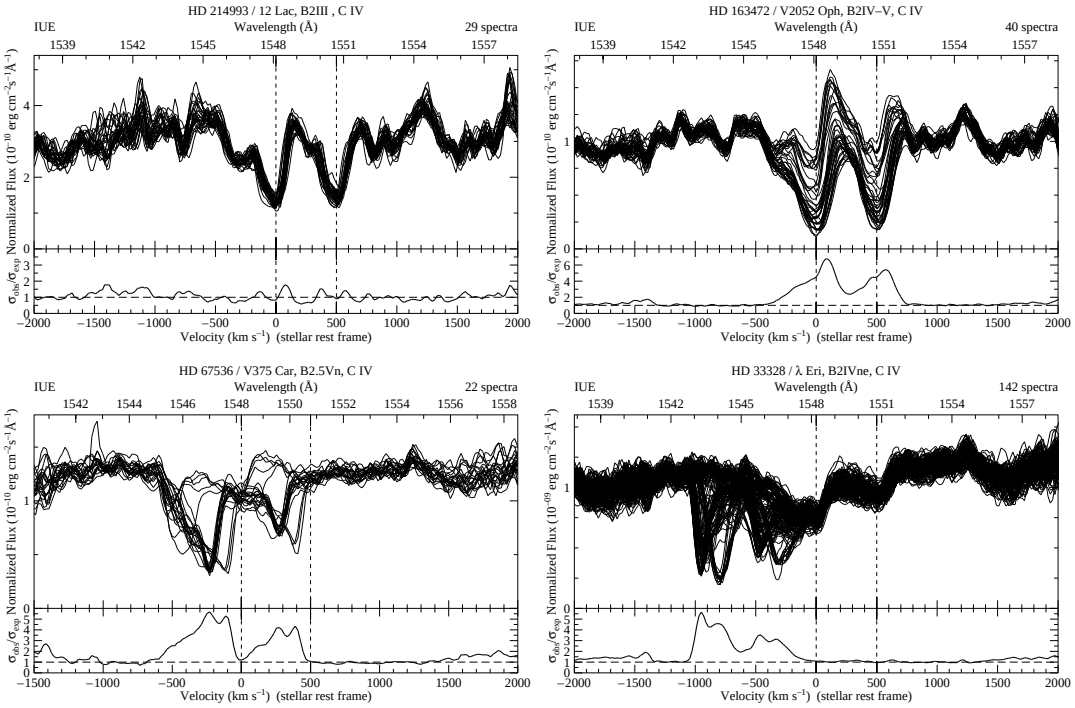

Figure 1: Examples of the different types of variability found in the UV wind lines of massive stars. Shown are: a non-variable star (12 Lac - top left), magnetic type variability (V2052 Oph - top right), intermediate type variability (V375 Car - bottom left) and DAC-type variability (λ Eri - bottom right). Figures after ten Kulve (2004).

(or beating of different modes) with the right periods have been observed (see e.g. Henrichs 1999).

3 Line profile modeling

To investigate the impact of a magnetic field on the stellar wind of a massive star, we have modeled the case of the B1IV star β Cephei using a MHD code to determine the wind geometry in the presence of a magnetic field (see ud-Doula et al. 2002) and a SEI based code to calculate corresponding line profiles. We find that for simple phenomenological models with enhanced density in the magnetic equator (presumably due to magnetic channeling of the wind) the observed variability of the wind lines is qualitatively reproduced. However, when full 2D-MHD models are used to determine the geometry of the stellar wind, significant differences are encountered that are likely due to X-ray ionisation which has not been included in the models (see Schnerr et al. 2007b).

4 New B-field measurements

Currently only a rather small sample of magnetic massive stars is known (see Table 1). To increase this number we have started a large observational program to search for new magnetic massive stars. For this program we have observed 11 O-type stars at three different epochs with FORS1 at the VLT and obtained a total of 136 magnetic field measurements of 25 OB stars with Musicos at the TBL (Schnerr et al. 2007a). Typical 1σ errors of the order of 40-100 gauss were achieved, but no new magnetic fields have been detected. From this we conclude that if magnetic fields are responsible for the observed UV wind-line variability in massive stars, they must either be weak ($\eta_* = 0.1 - 1$) or relatively small scale (perhaps similar to sunspots), or both.

5 Conclusions

The winds of many massive stars are highly variable. For the stars that are known to have strong magnetic fields (which are listed in Table 1) the (periodic) variability observed in their UV-wind lines is clearly related to the magnetic field. However, other types of variability are also observed of which the cause has not yet been established. Our working hypothesis is that magnetic fields are related to all types of UV wind-line variability, and that the type of variability is determined by the magnetic wind confinement

Table 1: The known magnetic massive stars and their properties.

Object	Spectral Type	Mass ($M_\odot$)	$B_{\rm polar}$ (G)	$P_{\rm rot}$ (days)	Reference
θ^1 Ori C	O4-6V	45	1100±100	15.4	Donati et al. (2002)
HD 191612	O6-8	∼30	∼1500±	538?	Donati et al. (2006a)
τ Sco	B0.2V	∼15	∼500±	41	Donati et al. (2006b)
β Cep	B1IV	12	360±40	12.00089	Henrichs et al. (2000)
V2052 Oph	B1V	10	250±190	3.63883	Neiner et al. (2003)
ζ Cas	B2IV	9	340±90	5.37045	Neiner et al. (2003)
ω Ori	B2IVe	8	530±200	1.29	Neiner et al. (2003)
14 pulsating stars	B1–B8	2-14	few 10^2	>1	Hubrig et al. 2006
He-peculiar (∼25)	B1–B8	$\lesssim$10	10^3–10^4	0.9–22	

parameter η_* and the magnetic field configuration.

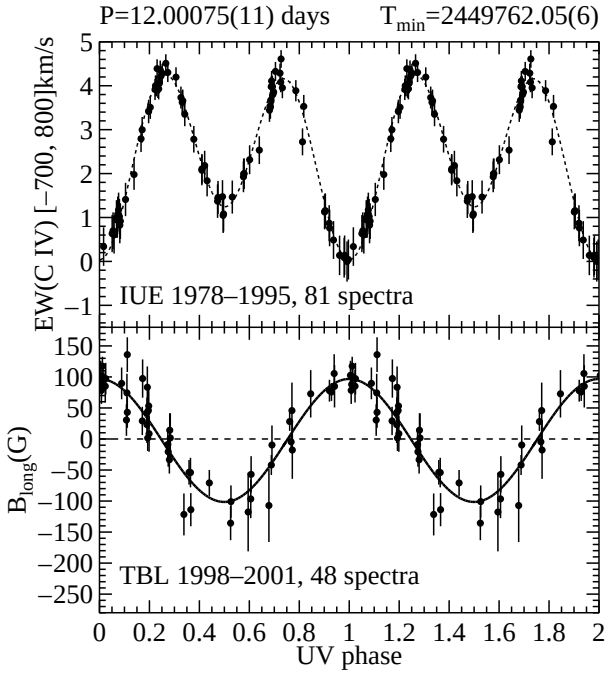

Figure 2: The variability of the equivalent width of the CIV line (top) in β Cephei shows the same period as the magnetic field (bottom), which is the rotational period of the star. Figure after Henrichs et al. (2005).

References

Cranmer, S.R., Owocki, S.P. 1996, ApJ, 462, 469

Donati, J.-F., Babel, J., Harries, T.J., et al. 2002, MNRAS, 333, 55

Donati, J.-F., Howarth, I.D., Bouret, J.-C., et al. 2006a, MNRAS, 365L, 6

Donati, J.-F., Howarth, I.D., Jardine, M.M., et al. 2006b, MNRAS, 370, 629

Fullerton, A.W. 2003, ASPC, 305, 333

Henrichs, H.F. 1999, Proc. IAU Coll. 169, Eds. Wolf et al., Lect. Notes in Phys., Vol. 523, 305

Henrichs, H.F., de Jong, J.A., Donati, J.-F., et al. 2000, Proc. IAU Colloquium 175, ASP, Vol. 214, p.324

Henrichs, H.F., Schnerr, R.S., & ten Kulve, E. 2005, ASPC, 337, 114

Howarth, I.D. & Prinja, R.K. 1989, ApJS, 69, 527

Hubrig, S., Briquet, M., Schöller, M., et al. 2006, MNRAS, 369L, 61

Kaper, L., Henrichs, H.F., Nichols, J.S., et al. 1996, A&AS, 116, 257

Kulve, E. ten, 2004, Master Thesis, Univ. of Amsterdam

Moffat, A.F.J., Michaud, G. 1981, ApJ, 251, 133

Neiner C., Geers V.C., Henrichs H.F., et al. 2003a, A&A, 406, 1019

Neiner C., Hubert A.-M., Fremat, Y., et al. 2003b, A&A, 409, 275

Neiner C, Henrichs H.F., Floquet, M., et al. 2003c, A&A, 411, 565

Oksala, M.E., Gagné, M., Cohen, D.H., et al. 2005, ASPC, 337, 289

Peters, G. 1996, Be Star Newsletter, 31, 16

Rauw, G., Morrison, N.D., Vreux, J.-M., et al. 2001, A&A, 366, 585

Schnerr, R.S. 2007, PhD thesis, University of Amsterdam

Schnerr, R.S., Henrichs, H.F., Neiner, C. et al. 2007a, A&A, submitted

Schnerr, R.S., Henrichs, H.F., Owocki, S.P., et al. 2007b, ASPC, 361, 488

Schnerr, R.S., Rygl, K.L.J., van der Horst, A.J., et al. 2007c, A&A, 470, 1105

Stahl, O., Kaufer, A., Rivinius, T., et al. 1996 A&A, 312, 539

ud-Doula, A., & Owocki, S.P. 2002, ApJ, 576, 413

Waldron, W.L., Cassinelli, J.P. 2001, ApJ, 548L, 45

White, R.L. 1995, ApJ, 289, 689

Kubat: If β Cep is not a Be star, what is the source of the Hα emission?

Schnerr: Using spectro-astrometic observations we have shown in Schnerr et al. (2006, A&A) that the Hα emission actually originates from the binary companion of β Cep, which is likely a normal Be star.

Cassinelli: Steve Shore found that for stars with strong fields the outflow was out of the magnetic polar region. But you said that for β Cep the flow cut the B field equator.

Cohen: In θ' Ori C it also was assumed that the wind is strongest over the magnetic poles, but once the field was measured it turned out that the strongest wind is in fact in the magnetic equatorial plane.

Sonneborn: Shore's work on mass loss/wind in oblique rotators is for stars with strong magnetic fields, so mass loss along the magnetic poles is not surprising.

Schnerr: I agree that the very high field strength may explain the different behavior.

Clumping in Hot Star Winds
W.-R. Hamann, A. Feldmeier & L.M. Oskinova, eds.
Potsdam: Univ.-Verl., 2008
URN: http://nbn-resolving.de/urn:nbn:de:kobv:517-opus-13981

The effects of clumping on wind line variability

D. Massa[1], R.K. Prinja[2] & A.W. Fullerton[3]
[1] *SGT, Inc., USA*
[2] *University College London, England*
[3] *Space Telescope Science Institute, USA*

We review the effects of clumping on the profiles of resonance doublets. By allowing the ratio of the doublet oscillator strenghts to be a free parameter, we demonstrate that doublet profiles contain more information than is normally utilized. In clumped (or porous) winds, this ratio can lies between unity and the ratio of the f-values, and can change as a function of velocity and time, depending on the fraction of the stellar disk that is covered by material moving at a particular velocity at a given moment. Using these insights, we present the results of SEI modeling of a sample of B supergiants, ζ Pup and a time series for a star whose terminal velocity is low enough to make the components of its Si VI$\lambda\lambda$1400 independent. These results are interpreted within the framewrok of the Oskinova et al. (2007) model, and demonstrate how the doublet profiles can be used to extract infromation about wind structure.

1 Introduction

Clumping has been apparent from time series for many years (Kaper et al. 1999, Prinja et al. 2002). In this contribution we will first show how clumping affects doublet ratios and then use a time series to demonstrate the presence of clumping in winds.

2 Clumping

It is well known in the AGN community that doublet ratios are sensitive to clumping, with the ratio related to the covering factor of the clumped medium (e.g., Ganguly et al. 1999). For an extended source, the optical depth ratio determined from a doublet lies between the ratio of the blue and red f-values ($\alpha \equiv f_{\rm B}/f_{\rm R}$) and unity, depending on the covering factor of the source. Further, it is possible to interpret the observed doublet ratio within the framework of the Oskinova et al. (2007) model. In their model, the doublet components have an *observed* optical depth ratio of

$$\frac{\tau^{\rm B}_{\rm rad}}{\tau^{\rm R}_{\rm rad}} = \frac{\kappa^{\rm B}_{\rm eff}}{\kappa^{\rm R}_{\rm eff}} = \frac{1-e^{-\tau^{\rm B}_{\rm C}}}{1-e^{-\tau^{\rm B}_{\rm C}/\alpha}} \,, \qquad (1)$$

which varies between 1 and α (see, massa:Massa, for a definition of $\tau_{\rm rad}$, and Oskinova et al. for definitions of the other symbols). Consequently, if we allow the ratio of f-values to be a free parameter,

$$\frac{\tau^{\rm B}_{\rm rad}}{\tau^{\rm R}_{\rm rad}} = \frac{f'_{\rm B}}{f'_{\rm R}} = \frac{\kappa^{\rm B}_{\rm eff}}{\kappa^{\rm R}_{\rm eff}} \,. \qquad (2)$$

Thus, $f'_{\rm B}/f'_{\rm R}$ (determined by the fit) gives $\kappa^{\rm B}_{\rm eff}/\kappa^{\rm R}_{\rm eff}$ and, hence $\tau^{\rm B}_{\rm C}$. Oskinova et al. also relate the measured and smoothed opacities (or optical depths) and the clump optical depths as follows: $\kappa_{\rm eff}/\kappa_{\rm f} = (1-e^{-\tau_{\rm C}})/\tau_{\rm C}$. Since $\dot{M}q$ (where $\dot{M}$ is the mass loss rate and q is the ionization fraction, see, e.g., Massa et al. 2003) should be derived from $\kappa_{\rm f}$, the observed $\dot{M}q$ must be corrected as follows

$$\dot{M}q = (\dot{M}q)_{\rm obs}\left(\frac{\tau_{\rm C}}{1-e^{-\tau_{\rm C}}}\right) \qquad (3)$$

Fig. 1 shows how the "observed ratio" defines a point on the y-axis which gives $\tau^{\rm B}_{\rm C}$. $\tau^{\rm B}_{\rm C}$ then gives the ratio of the effective to actual opacity, $\kappa^{\rm B}_{\rm eff}/\kappa^{\rm B}_{\rm f}$. Note: *to obtain* $\kappa^{\rm B}_{\rm eff} \ll \kappa^{\rm B}_{\rm f}$ *and* $\dot{M}$*'s near expected values*, requires $\tau^{\rm B}_{\rm C} \gtrsim 5$, which implies $\kappa^{\rm B}_{\rm eff}/\kappa^{\rm R}_{\rm eff} \lesssim 1.1$.

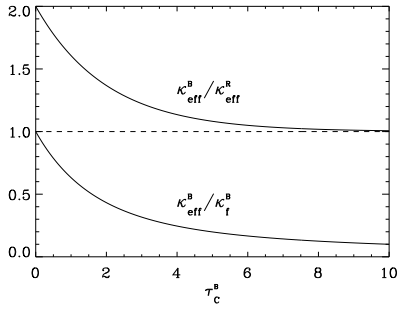

Figure 1: Ratio of effective opacities, $\kappa^{\rm B}_{\rm eff}/\kappa^{\rm R}_{\rm eff}$, (top) and effective to smooth opacities, $\kappa^{\rm B}_{\rm eff}/\kappa^{\rm B}_{\rm f}$, (bottom) versus clump optical depth, $\tau^{\rm B}_C$, for a doublet with $\alpha = 2$.

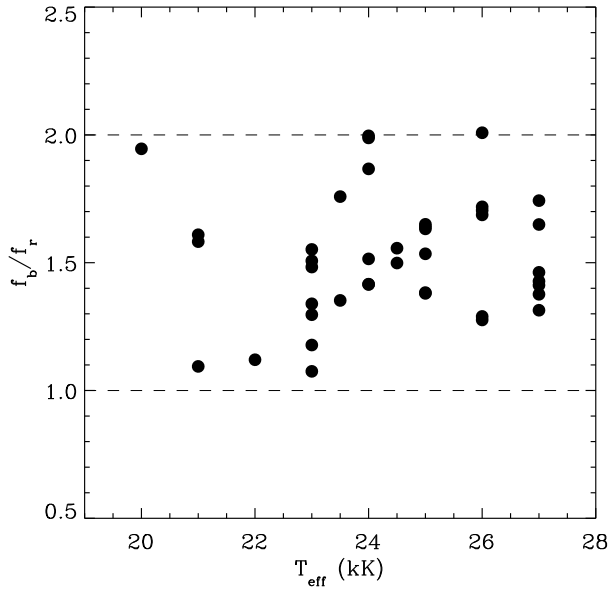

Figure 2: Derived ratios of oscillator strengths versus $T_{\rm eff}$ for Si IV $\lambda\lambda$1400 in B supergiants with wind lines $0.3 \leq \tau_{\rm rad} \leq 5$ (weaker have inadequate optical depth information and stronger are too saturated).

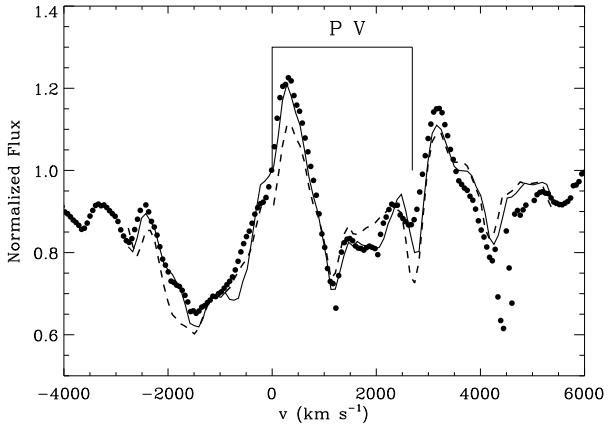

Figure 3: P V in ζ Pup. Points are data, dashed curve is SEI fit with fixed f-values, solid curve allowed the ratio of f-values to vary.

It must now be determined whether this additional information is present in the observed profiles. As a first test, we fit the Si IV$\lambda\lambda$1400 doublet in the sample of B supergiants given in Prinja et al. (2005) using a variable f-value. The results are shown in Figure 2. Notice that all of the f-value ratios lie between 1 and 2, as expected for a clumped wind.

As a second test, we fit *Copernicus* data of the P V$\lambda\lambda$1117, 1128 doublet in ζ Pup. Two least squares SEI (Lamers et al. 1987) fits are shown in Fig. 3. Both use a T_{eff} = 40kK, $\log g$ = 3.5 TLUSTY model photosphere. The dashed fit uses the actual ratio of f-values, 2.02. The solid fit varied the ratio, giving a best fit value of 1.84. This 10% change clearly improves the fit, making the blue absorption weaker relative to the red. The fit gives $\tau_{\rm C}^{\rm B} \simeq 0.5$ and $\kappa_{\rm eff}^{\rm B}/\kappa_{\rm f}^{\rm B} \simeq 0.5$. Thus, the correction to $\dot{M}q$ is only 1.3, increasing ratio of P V to radio mass loss rates given by Fullerton et al. (2006) from 0.11 to 0.14 – *still far smaller than expected*, even if q(P V) ~ 0.5. Thus the mass loss rate in this case is truly smaller than expected.

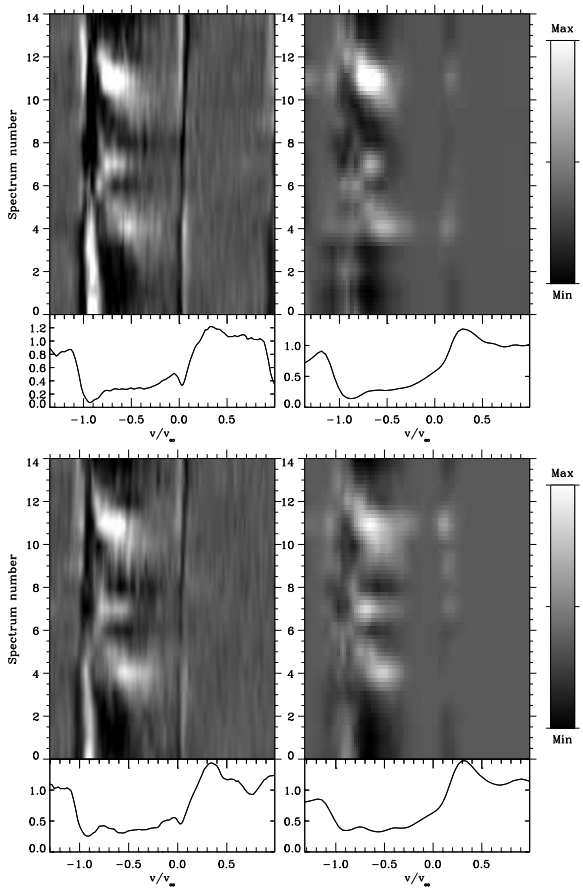

Figure 4: Dynamic spectra of the observed (left) and modeled (right) spectra of the blue (top) and red (bottom) components of Si IV$\lambda\lambda$1400 in HD 47240. The spectra are normalized by their means.

3 Clumping and time series

Time series for stars with $v_\infty \geq 2c\Delta\lambda/\lambda$, where $\Delta\lambda$ is the doublet separation, present a valuable test for the effects of clumping on wind lines. The B1 Ib,

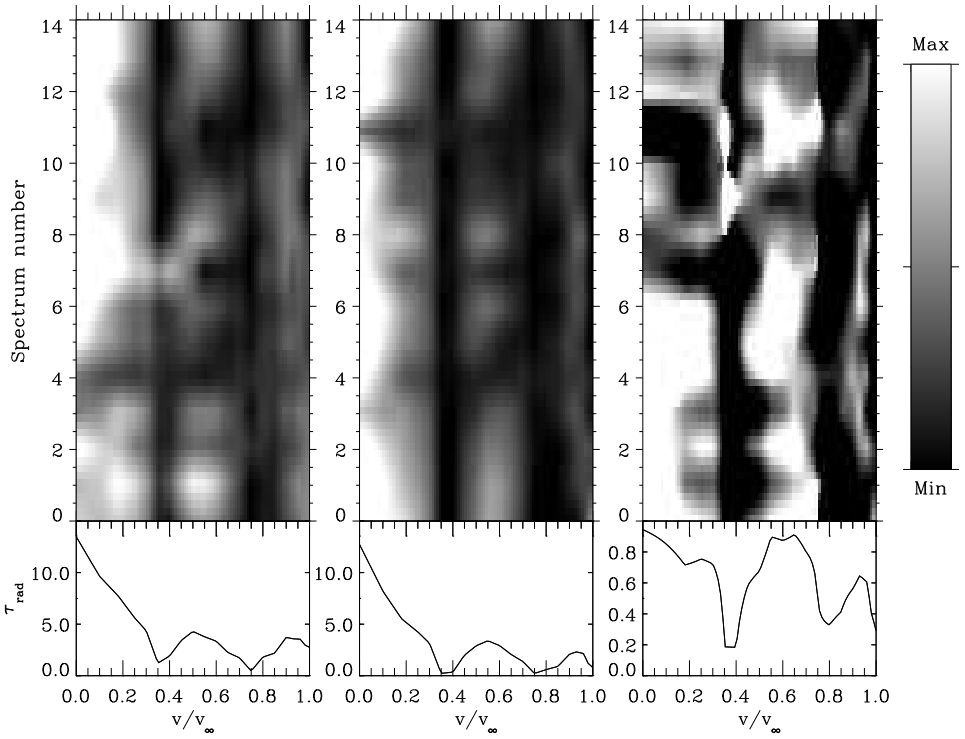

Figure 5: Dynamic spectra for $\tau^{\rm B}_{\rm rad}$ (left), $\tau^{\rm R}_{\rm rad}$ (middle) and $\tau^{\rm R}_{\rm rad}/\tau^{\rm B}_{\rm rad}$ (right) in HD 47240.

HD 47240, is such a star with $v_\infty = 980$ km s^{-1}. Consequently, each of its Si iv components are effectively independent. Thus, they were fit independently. The result is equivalent to allowing $f_{\rm B}/f_{\rm R}$ to be a function of velocity. The results are shown in Fig. 4, which shows the observed and modeled normalized dynamic spectra versus spectrum number for each component, and Fig. 5, which shows the unnormalized optical depths and their ratio. Several points are noteworthy. First, *both* components show similar, persistent velocity dependent structure. The fits of many B supergiants given by Prinja et al. (2005) had similar structure appearing in different ions in the same star. Thus, this structure may be real. Whether it results from density inhomogeneties or velocity plateaus, cannot be determined. Second, when $\tau_{\rm rad}$ is greater than a few tenths and well-defined, the ratio of optical depths varies between 1 (clumped) and 0.5 (unclumped). Third, it appears that the ratio (clumping) decreases at velocities where the density decreases. Fourth, there seems to be a general decrease in the clumping at larger velocity, similar that seen in O stars by Puls et al. (2006).

4 Discussion

It has been demonstrated that resonance doublets contain more information than is usually exploited, that this information is related to clumping, and that it can be interpreted by the Oskinova et al. (2007) model. Our ultimate goal is to apply these techniques to a large number of stars with a range of stellar and wind parameters. This will allow us to examine how these relate to the empirically determined clumping parameters and provide clues to the physical agents responsible for wind clumping.

References

Fullerton, A.W., Massa, D.L., & Prinja, R.K. 2006, ApJ, 637, 1025

Ganguly, R. et al. 1999, AJ, 117, 2594

Kaper, L., et al. 1999, A&A, 344, 231

Lamers, H.J.G.L.M., et al. 1987, ApJ, 314, 726

Massa, D., et al. 2003, ApJ, 586, 996

Oskinova, L. M., Hamann, W.-R. & Feldmeier, A. 2007, A&A, 476, 1331

Prinja, R.K., Massa, D. & Searle, S.C. 2005, A&A, 430, L41

Prinja, R.K., Massa, D., & Fullerton, A.W. 2002, A&A, 388, 587

Puls, J., et al. 2006, A&A, 454, 625

Moffat: Why do you not see the small scale clumping directly via variable sub-peaks on the emission lines in the UV, as we see in the optical? Is it a question of signal-to-noise?

Massa: In a way, yes. In OB stars, we only see the wind in resonance lines. In which case, we can only see emission on the red part of the profile. As a consequence, any excess emission is seen against the average emission of a huge constant velocity surface. This makes it hard to detect sub-peaks compared to the absorption which is seen along a column to the stellar disk. Nevertheless, we do see faint, migrating emission features in a few cases like the MEGA data for HD 64760.

Moffat: 1. For your plot of mean radial optical depth that has two minima, is the radial optical depth essentially always low near the minima? 2. How does the assumption of spherical SEI affect your interpretation of the "banana" features?

Massa: 1. Yes, the radial optical depth is always low near the minima. 2. I am sure that SEI has some effect on the results but, unfortunately, there is currently nothing better. Nevertheless, it seems to produce reasonable results, so it cannot be mucking things up too badly. Furthermore, deJong et al. showed the presence of "bananas" by comparing dynamic spectra of the Si IV 1400 doublet at high velocity and the N IV 1718 excited state line at low velocity.

Oskinova: Thank you for showing us your very interesting results. Do your results imply that porosity effects are important also for clump optical depths less than one?

Massa: Thank you. Yes, they do make a detectable difference for small optical depths.

Clumping in Hot Star Winds
W.-R. Hamann, A. Feldmeier & L.M. Oskinova, eds.
Potsdam: Univ.-Verl., 2008
URN: http://nbn-resolving.de/urn:nbn:de:kobv:517-opus-13981

Corotating Interaction Regions and clumping

R. Blomme
Royal Observatory of Belgium

We present hydrodynamical models for Corotating Interaction Regions, which were used by Lobel (2007) to model the Discrete Absorption Components in HD 64760. We also discuss our failure to model the rotational modulations seen in the same star.

1 Introduction

Discrete Absorption Components (DACs) seen in ultraviolet lines are one of the clearest indicators of large-scale structure in the winds of hot stars. Cranmer & Owocki (1996) attributed these DACs to Corotating Interaction Regions (CIRs) which are formed when slow and fast streams collide in the wind. In their model, CIRs are produced by introducing a spot on the stellar surface. The spot can literally be a spot, but can also simulate the effect of non-radial pulsations, or a magnetic field.

In the present work, we attempt a *quantitative* fit to the DACs seen in the Si IV λ 1395 line of the B0.5 Ia star HD 64760. This paper describes the hydrodynamical models used for this fit and discusses the problems in fitting the rotational modulations, which are an additional feature seen in the P Cygni profiles of this star. In a companion paper (Lobel 2007), the radiative transfer code and the fitting of the observed DACs is discussed.

2 Hydrodynamics

To construct the hydrodynamical models, we use the Zeus3D code (Stone & Norman 1992). We solve the 3-dimensional equations of hydrodynamics, limited to the equatorial plane. This approximation is justified by the high $v \sin i$ value of HD 64760, which suggests that it is seen (nearly) equator-on.

In our model, we largely follow Cranmer & Owocki (1996). We include the radiative acceleration due to the spectral lines as well as the rotation of the star and the wind (through angular momentum conservation). The energy equation is also solved (including radiative cooling and a floor temperature), but this turned out to be unimportant in the present calculations. We further introduce a circularly symmetric spot on the stellar surface, with its centre on the equator. This spot is specified by its brightness $A_{\rm sp}$ and its angular diameter $\Phi_{\rm sp}$.

Contrary to Cranmer & Owocki, we allow the spot to rotate with a velocity $v_{\rm sp}$ *that can be different from the rotational velocity* $v_{\rm rot}$. The main justification for this is that the recurrence time of the DAC is measured to be 10.3 d while the rotation period is only 4.1 d (see Lobel 2007). A similar assumption was also made by Kaufer et al. (2007) in their model for the Hα variations in HD 64760.

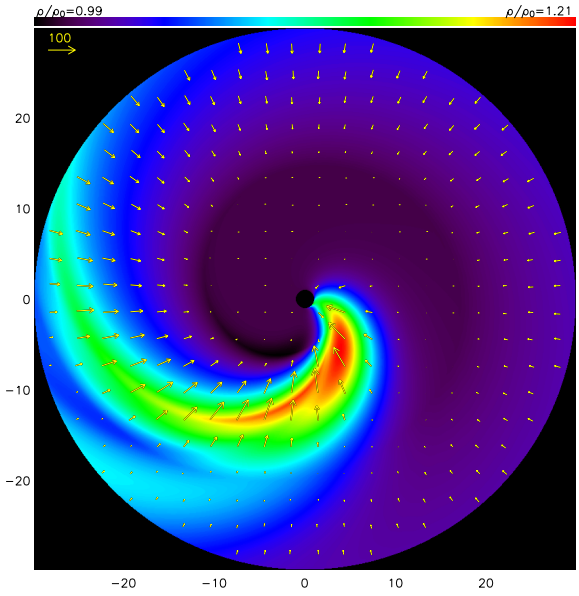

Figure 1: The colour scale presents the density contrast of the CIR with respect to the smooth wind. The velocity vectors plotted show the differences with respect a smooth wind. The model parameters are: $A_{\rm sp} = 0.1$, $\Phi_{\rm sp} = 50^o$, $v_{\rm sp} = v_{\rm rot}/2.5$.

The effect of a spot on the hydrodynamics of the wind is easiest to understand if there is no rotation. In that case, there is a sector above the spot with a different wind (i.e. a different mass-loss rate and terminal velocity) compared to the smooth wind around it. When the star rotates, these different winds collide and a spiral-shaped density enhancement is formed (see Fig. 1). Trailing this density

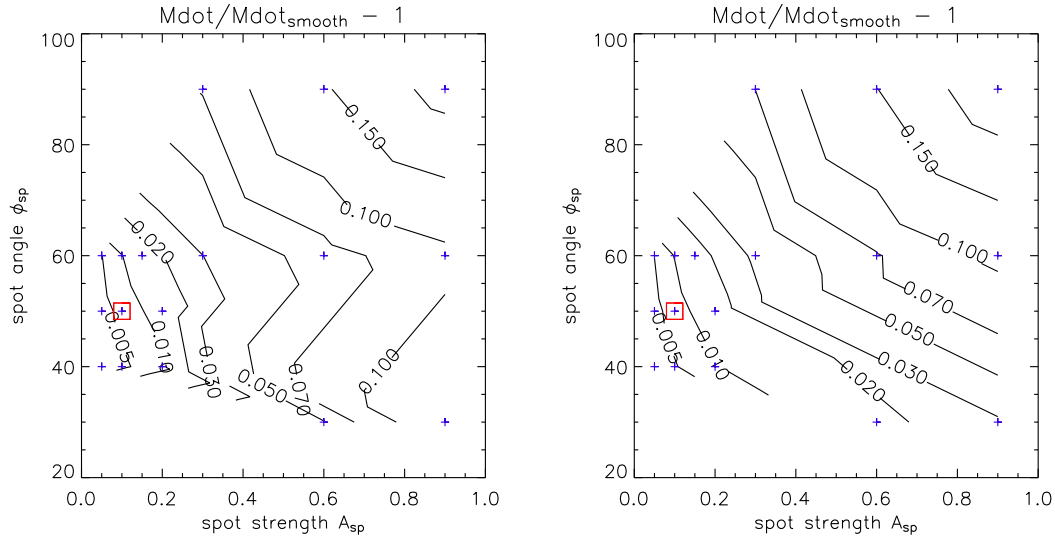

Figure 2: Contour lines of the effect of a CIR on the mass-loss rate as a function of spot brightness and angle. The plusses indicate the models we calculated. The best-fit model is shown with a red square. The left panel shows the values measured from the hydrodynamical models, the right panel the results from the approximation in Eq. 2.

wave is a region with a velocity plateau, which is mainly responsible for the formation of the DAC (Lobel 2007). One should also note that the CIR is not a stream of material particles, but is a pattern in the wind. If we follow trace particles, we see that they can cross the whole width of the CIR as they move out almost radially.

We constructed a large grid of hydrodynamical models, from which the DACs were then calculated using the WIND3D code. The best fit to the Si IV λ 1395 line of HD 64760 was then determined (see Lobel 2007). The hydrodynamical model of this best fit is shown in Fig. 1.

The total mass-loss rate of the structured wind ($\dot{M}_{\rm struct}$) is easy to calculate if we assume the star to be non-rotating:

$$\dot{M}_{\rm struct} = \frac{\Omega}{4\pi}\dot{M}_{\rm spot} + \left(1 - \frac{\Omega}{4\pi}\right)\dot{M}_{\rm smooth}, \qquad (1)$$

where Ω is the solid angle of the spot, $\dot{M}_{\rm smooth}$ is the mass-loss rate in the smooth wind and $\dot{M}_{\rm spot}$ that above the spot. Using the approximate relation that $\dot{M} \propto L^{1/\alpha}$, we can rewrite this as:

$$\frac{\dot{M}_{\rm struct}}{\dot{M}_{\rm smooth}} \approx \frac{\Omega}{4\pi}\left(1 + A_{\rm sp}\right)^{1/\alpha} + \left(1 - \frac{\Omega}{4\pi}\right). \qquad (2)$$

A rotating star will have a structure that is quite different from the non-rotating model, but close to the stellar surface the differences will be small. We can therefore use the density and velocity measured near the surface to determine the mass-loss rate. The results for a series of models are presented in Fig. 2. Our best-fit model for the HD 64760 DAC corresponds to an additional mass loss of only 0.6 %.

3 Rotational modulations

Encouraged by the good fit we obtained for the DAC, we also tried to fit the "rotational modulations" present in the dynamic spectrum. These are the banana-shaped, nearly-flat absorption components seen in Fig. 3. All our models fail however to reach the terminal velocity sufficiently quickly. Our failure is surprising in view of the good agreement presented by kinematical models such as those by Owocki et al. (1998) and Brown et al. (2004).

To investigate this further, we switched to using the kinematical models developed by Brown et al. We find that these models can indeed explain the observations, provided the $v_{\rm rot}/v_\infty$ ratio is small (~ 0.05). In such a case, the rotational modulation does reach the terminal velocity sufficiently quickly (dotted white line in Fig. 3). For HD 64760 however, we have that $v_{\rm rot}/v_\infty \approx 0.16$ and we obtain the solid white line in Fig. 3, which does not fit the observations. Because we consider the spot velocity as a free parameter, we can of course introduce a slower-moving spot (thereby getting a more favourable $v_{\rm sp}/v_\infty$ ratio). However, the recurrence time scale then becomes longer, stretching out the time-axis, and we again obtain a bad fit which is in-

distinguishable from the high $v_{\rm rot}/v_\infty$ solution (solid white line).

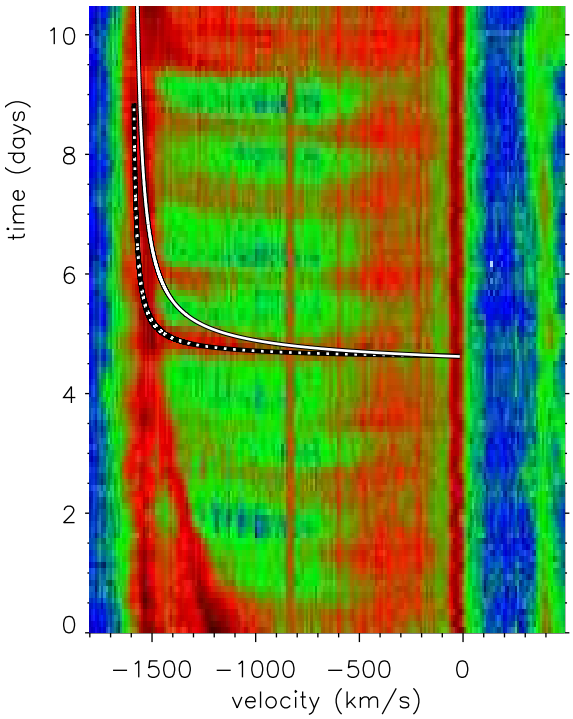

Figure 3: The dynamic spectrum of the Si IV λ 1395 line in HD 64760. One of the observed rotational modulations is fitted with a kinematical model based on Brown et al. (2004). The dashed white line has $v_{\rm rot}/v_\infty = 0.05$, the solid one has $v_{\rm rot}/v_\infty = 0.16$ and is indistinguishable from the $v_{\rm sp}/v_\infty = 0.05$ solution.

4 Conclusions

Lobel (2007) and the present paper show that the DACs of HD 64760 can be well fitted with hydrodynamical models for CIRs. The recurrence time of the HD 64760 DACs requires that the spots responsible for the CIRs rotate considerably more slowly than the stellar surface (by a factor of 2.5). The spots cannot be fixed on the surface, thereby excluding magnetic fields as a possible cause. As suggested by Kaufer et al. (2007), a beat-pattern due to non-radial pulsations seems to be the only valid explanation for the spot.

The additional mass-loss rate put into the wind is very small and no shocks are formed due to the (weak) CIR in HD 64760. The CIRs can therefore not be responsible for the clumping discussed at this workshop, nor for the X-ray emission of these stars. As Owocki (1998) showed, CIRs are sensitive to the amount of instability in the wind. Too large an amount of clumping could therefore destroy the CIRs responsible for the DACs. As the DACs are almost ubiquitous in hot-star winds, this imposes important constraints on the amount of clumping.

Finally, our failure to reproduce the rotational modulations seen in HD 64760 suggests that we still lack a key component in our understanding of these stellar winds.

We thank Asif ud-Doula for making his version of the Zeus3D code available to us.

References

Brown, J.C., Barrett, R.K., Oskinova, L.M., et al. 2004, A&A, 413, 959

Cranmer, S.R., & Owocki, S.P. 1996, ApJ, 462, 469

Kaufer, A., Stahl, O., Prinja, R.K., & Witherick, D. 2006, A&A, 447, 325

Lobel, A. 2007, these proceedings

Owocki, S.P. 1998, "Cyclical Variability in Stellar Winds", Eds. L. Kaper & A.W. Fullerton, ESO, 325

Owocki, S.P., Cranmer, S.R., & Fullerton, A.W. 1995, ApJ, 453, L37

Stone, J.M., & Norman, M.L. 1992, ApJS, 80, 753

Hamann: Can you offer a plausible physical explanation for the nature of the "spot" at the CIR footpoint, which explains why it is running like mad counterwise to the stellar rotation?

Blomme: Kaufer et al. (2006) invoke a beat-pattern of NRPs for this. Admittedly, their value for the spot velocity is not the same as ours. We took their work to mean that we could count the spot velocity as a free parameter. Its value is then of course determined by the ratio of the recurrence time of the DAC (10.3 d) against the rotational period (4.1 d). We did not model a specific beat-pattern that could give this spot velocity.

Prinja: I would just like to echo the point made by Ronny that invoking substantial amounts of clumping must not then destroy the CIR-type structures, since the spectral signatures of the latter are so widespread in OB stars.

Owocki: The 2D SSF simultations of CIRs show that velocity plateaus and (somewhat rounded) "kinks" are not an artifact of the Sobolev approximation.

Clumping in Hot Star Winds
W.-R. Hamann, A. Feldmeier & L.M. Oskinova, eds.
Potsdam: Univ.-Verl., 2008
URN: http://nbn-resolving.de/urn:nbn:de:kobv:517-opus-13981

Hα line profile variability in the B8Ia-type supergiant Rigel (β Ori)

N. D. Morrison, S. Rother, & N. Kurschat
Ritter Astrophysical Research Center, The University of Toledo, USA

Hα observations of Rigel obtained on 184 nights during the past ten years with the 1-m telescope and échelle spectrograph of Ritter Observatory are surveyed. The line profiles were classified in terms of morphology. About 1/4 of them are of P Cygni type, about 15% inverse P Cygni, about 25% double-peaked, about 1/3 pure absorption, and a few are single emission lines. Transformation of the profile from one type to another typically takes a few days. Although the line stays in absorption for extended intervals, only one high-velocity absorption event of the intensity reported by Kaufer et al. (1996a) was observed, in late 2006. Late in this event, Hα absorption occurred farther to the red than the red wing of a plausible photospheric absorption component, an indication of infalling material. In general, as the absorption events come to an end, the emission typically returns with an inverse P Cygni profile. The Hα profile class shows no obvious correlation with the radial velocity of C II λ6578, a photospheric absorption line.

1 Introduction

Rigel is a hot, luminous star that is well known to show mass loss. Studies of the Mg II resonance lines have shown its terminal wind speed to be about 230 km s^{-1} (Kaufer et al. 1996b). According to Gilheany (1991), Mg II in this star shows episodes of increased mass-loss rate and edge velocity, as well as DAC-like behavior. Hα is also well known to be highly variable, with profile morphologies ranging from P Cygni to double-peaked to inverse P Cygni (Kaufer et al. 1996b, Israelian et al. 1997).

A non-LTE, line blanketed model atmosphere analysis by Przybilla et al. (2006) derived $T_{\rm eff} \simeq 12,000$ K, $\log g \simeq 1.7$, and $L \simeq 2 \times 10^5 L_\odot$. Thus, the star is in a physical regime where the wind is partially ionized. Accordingly, the number of neutral H atoms, and hence the strength of Hα absorption, can be expected to be sensitive to density perturbations, because of not only column density effects but also ionization effects. Therefore, this physical regime is a particularly interesting one for the study of structure in stellar winds.

The purpose of this report is to make an initial survey of the results of more than ten years of spectroscopic monitoring of this star.

2 Observations and reductions

The observations were made with the 1-m telescope, fiber-fed échelle spectrograph, and Wright Instruments CCD camera of Ritter Observatory (U. Toledo, OH, USA). The CCD encompasses a 70-Å range around Hα, plus 8 other such ranges. The entrance slit width gives a resolution element about 4.3 pixels wide, which corresponds to $\lambda/\Delta\lambda = 26,000$. The spectra have signal-to-noise ratios ranging from about 30 to several hundred per pixel and have not been smoothed. Figure 1 shows a typical spectrum. Experience with this instrumentation shows that the underlying continuum is linear; the apparent curvature of the local continuum in this and similar stars is due to broad Hα emission wings that are thought to be a non-LTE effect (Hubeny & Leitherer 1989).

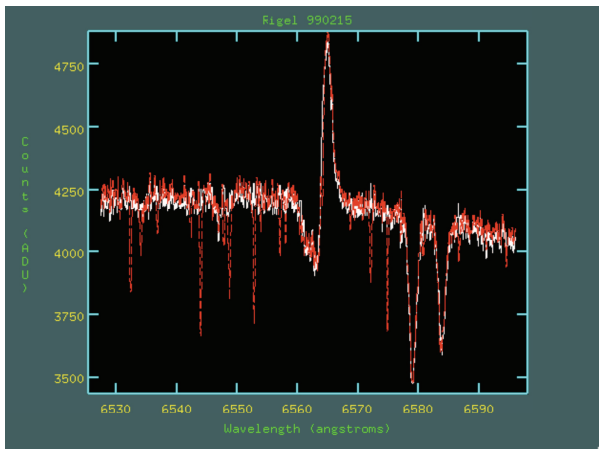

Figure 1: A typical Hα spectrum of Rigel taken on 15 Feb. 1999 (UT), before continuum normalization. The red overplot shows the spectrum before removal of telluric lines.

Data reduction was carried out by standard proce-

dures with IRAF. Telluric water lines were removed, and the spectra were normalized to a linear fit to the apparent continuum at the ends of the spectral range observed. The Hα profiles were classified visually into seven morphological classes: P Cygni, inverse P Cygni, absorption (in which weak emission wings may be present), pure emission, double emission, double absorption, and triple absorption. In the last of these, the spectrum just reaches the continuum between the absorption components.

Our data set consists of 193 observations made on 184 nights during 1996–2007. During each observing season, a typical 20-night interval includes 4 observations.

3 Results

The radial velocity of C II λ6578 was measured from the same data. It is variable with an amplitude of about 10 km s^{-1} and a mean of +21.5 km s^{-1}, which we adopted as the systemic radial velocity. There is no obvious correlation between the C II radial velocity and the Hα profile class.

Figure 2 shows examples of an inverse P Cygni, a double-peaked, and a P Cygni profile. It illustrates the behavior, previously noted by Kaufer et al. (1996b), that the blue and red peaks rise and fall while remaining approximately stationary. In keeping with this behavior, our results show a tendency for the Hα absorption velocity to be more negative than the systemic velocity, except that it is more positive than systemic when the profile morphology is inverse P Cygni.

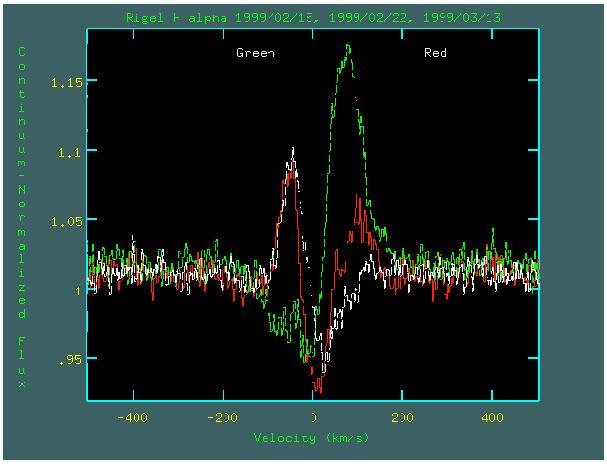

Figure 2: Typical examples of an inverse P Cygni (white), a double-peaked (red), and a P Cygni profile (green). In this and later figures, the abscissa is heliocentric radial velocity.

Hα often appears in pure absorption, sometimes symmetrical and near systemic velocity. Occasions when, on the other hand, it is asymmetric or blueshifted, we call "absorption events." Absorption events tend to be followed by inverse P Cygni profiles.

Figure 3 shows the number of occurrences of each profile class. About 2/3 of the time, the profile is in one of the three emission states. On the other hand, if all the absorption-type profiles are counted together, they become the most numerous class.

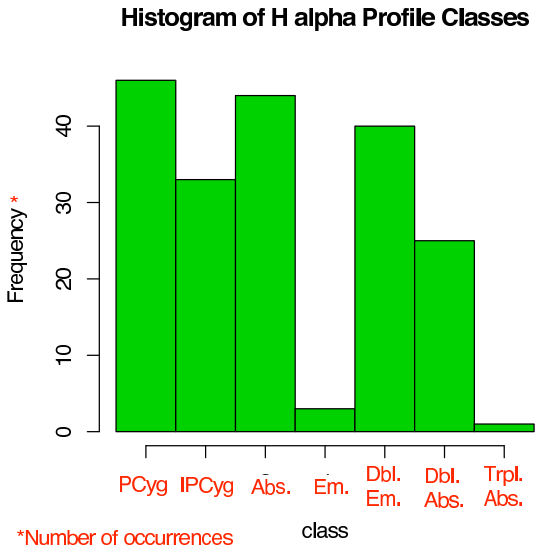

Figure 3: Frequency of each Hα profile class.

We estimated the persistence times of the various profile classes from sequences of observations that were densely sampled enough to exclude the profile changing to another type and back again during the sequence. The P Cygni and inverse P Cygni profile classes have a median persistence time of 5 days or less, compared to 10 to 13 days for the other profile classes, but the ranges of values of persistence time for all the profile classes overlap.

We also studied the time scale for Hα profile variations to occur. No significant differences were observed between spectra obtained during the course of one to two hours. Minor changes were sometimes observed during the course of 24 hours, while significant morphological changes occur in 2 to 3 days or more. These time scales are much shorter than the relevant physical time scales, which are the rotation period, $P/\sin i = 164 \pm 13$ d (based on Przybilla et al. 2006), and the dynamical time scale of the wind, 20 to 60 d (Kaufer et al. 1996a). Therefore, they indicate that the wind has structure on a scale that is small compared to the volume of the wind and/or

is rapidly changing.

In addition to several weaker absorption events exhibiting lower absorption velocities, we observed one strong, high-velocity absorption event of the intensity reported by Kaufer et al. (1996a). Our one spectrum taken during this event is shown in Figure 4. For comparison is shown a sample photospheric model profile—not fully realistic for this star, since it comes from a model that is 3,000 K hotter.

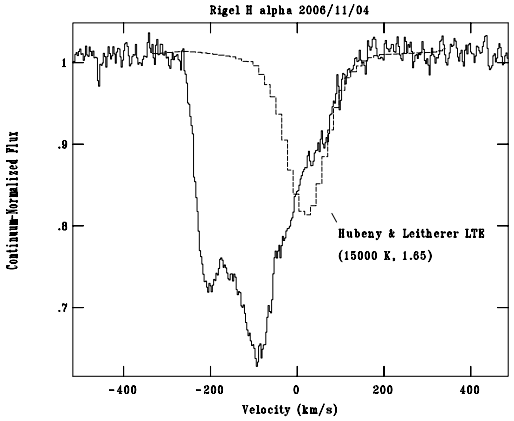

Figure 4: Full line: spectrum obtained during a high-velocity absorption event. Dashed line: fiducial photospheric profile, shifted upward to match the local continuum.

On the basis of Hα profiles similar to that shown in Figure 5, Israelian et al. (1997) claimed infalling material, which they proposed is due to control of the wind by magnetic loops. In a weak wind, however, redshifted absorption could be caused by the wind being translucent at that wavelength, so that the photospheric absorption shows through. In order to demonstrate the existence of infall, one has to show that the absorption on the red wing is deeper than any likely photospheric profile at that wavelength. This condition is fulfilled in Figure 5 unless the true photospheric profile is significantly deeper and wider than the example shown here.

4 Conclusions and future work

Although the spectrum of this star is often depicted in the literature to have P Cygni emission in Hα, most of the time the line has another emission profile type or is in absorption. It is reasonable to conclude that the wind is highly variable in structure, with significant departures from spherical symmetry. Accordingly, the star's mass-loss rate may be lower than commonly estimated.

In future work, we plan to search for (quasi)periodic behavior in the Hα profile.

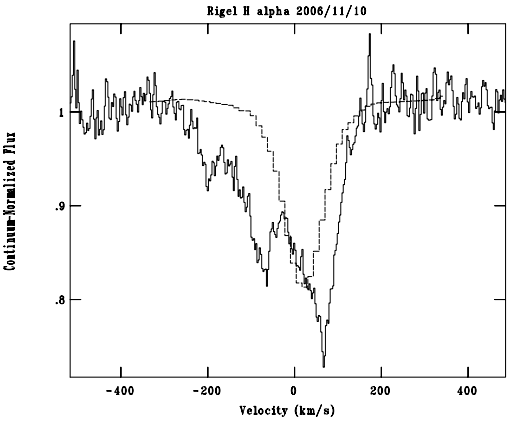

Figure 5: Spectrum that may show evidence for infalling material. The dashed line is as in Figure 4.

Research and operations at Ritter Observatory are supported by NSF-PREST grant AST-0440784 and by The University of Toledo. Technical support was provided by Observatory Technician R. J. Burmeister. Observations were obtained and pipeline data reduction carried out by C. L. Mulliss, D. C. Knauth, J. P. Wisniewski, D. R. Long, and E. N. Hesselbach. Additional observations were obtained by K. S. Bjorkman, A. Miroshnichenko, G. B. Thompson, and N. D. Richardson.

References

Gilheany, S. 1991, Vistas Astron., 34, 249

Hubeny, I. & Leitherer, C. 1989, PASP, 101, 114

Israelian, G., Chentsov, E., & Musaev, F. 1997, MNRAS, 290, 521

Kaufer, A., Stahl, O., Wolf, B., Gäng, Th., Gummersbach, C. A., Jankovics, I., Kovács, J., Mandel, H., Peitz, J., Rivinius, Th., & Szeifert, Th. 1996a, A&A, 314, 599

Kaufer, A., Stahl, O., Wolf, B., Gäng, Th., Gummersbach, C. A., Kovács, J., Mandel, H., & Szeifert, Th. 1996b, A&A, 305, 887

Przybilla, N., Butler, K., Becker, S. R., & Kudritzki, R. P. 2006, A&A, 445, 1099

Prinja: Do you see any evidence that the high-velocity absorptions in Hα are correlated in some way with disturbances (velocities, strength) in the photospheric lines such as C II λ 6578?

Morrison: In the present data, which I showed in the boxplot, the correlation is very weak, if any. If we cross-correlate with a time lag, we may find a stronger relationship.

Moffat: 1. Are there any variations that are cyclic on a rotation period? 2. Has this star been looked at using spectropolarimetry?

Schner: We did observe this star spectropolarimetrically occasionally. At least we can say that there is no strong magnetic field present.

Puls: The predicted deep-seated photospheric emission in Hα is usually reduced (though not destroyed) if you include winds into the atmospheric models (Hubeny's calculation is based on hydrostatic models.).

Morrison: Thank you. When we observe this star with our new, larger-format CCD camera, we will be better able to determine the continuum level and hence the amplitude of the scattering wings.

Clumping in Hot Star Winds
W.-R. Hamann, A. Feldmeier & L.M. Oskinova, eds.
Potsdam: Univ.-Verl., 2008
URN: http://nbn-resolving.de/urn:nbn:de:kobv:517-opus-13981

Wind variabilities and asymmetries in Luminous Blue Variables

T. Szeifert
ESO, Alonso de Cordova 3107, Santiago 19, Chile

Luminous Blue Variables show strong changes in their stellar wind on time scales of typically years to decades when they expand and contract radially at approximately constant luminosity. Micro-variability on shorter time scales and amplitudes can be observed superimposed to the larger scale radial changes. I will show long-term time series of high resolution spectra which we have collected in the past 20 years for many of the well known LBVs together with a few time series of weekly sampling (HR Car, R40, R71, R110, R127, S Dor) covering a time windows of up to a few months.

Wind variability is seen on short and intermediate time scales with the line profiles changing from P Cygni to inverse P Cygni and double peeked profiles sometimes for the same star and spectral line. On longer time scales the ionisation levels for all chemical elements change drastically due to the strong change of the temperature on the stellar surface.

While on the long term the characteristic radial changes may have impact on the over all mass loss rates, the variabilities and asymmetries on short and intermediate time scales may cause false estimates of the mass loss rates when confronting models with the observed line profiles

1 Introduction

Luminous Blue Variables (LBVs) play an important role in the evolution of the most massive stars. They at least contribute to the mass loss history of the massive stars if they are not the only link between the early phases of the evolution with very high actual mass and hydrogen rich surface chemistry and the surface hydrogen poor Wolf Rayet stars. With the reduced mass loss rates in the O-star and WR-star phases due to the implementation of clumping in the stellar wind models the importance of the LBV phase has increased and the role of the LBVs should be further investigated.

LBVs show photometric and spectroscopic variability on different time scales and magnitudes, which I will classify as micro-variability, characteristic variability and outburst:

The micro-variability of LBVs appears on time scales of 10 to several 100 days with photometric amplitudes of tenth of magnitudes. These variations appear like semi-periodic pulsation like motions with the time scale P proportional to the inverse square root of the mean density ρ^{-1}. Similar variations are observed for all of the most luminous B and A-supergiants.

The characteristic LBV variability occurs on longer time scales of a few years to a few decades. The stars undergo enormous contraction and expansion phases at approximately constant bolometric luminosity. The stars can change from spectral types WN11 or early BIa at visual minimum light to typically late A-types at visual maximum light. Many of these stars change their parameters continuously and can be rarely found in any stable phase at either minimum or maximum visual phase.

LBV outbursts like for η Car are very rare events. During an outburst an outer shell of 10 solar masses or more can be expelled from the star which will lead to a significant and spontaneous change of the stellar mass and the later stellar evolution of the remaining star.

A massive blue supergiant should be classified as LBV after observing either the characteristic LBV variability or an η Car like outburst. Stars which are spectroscopically very similar to LBVs may be called LBV candidates. Other stars which show LBV nebulae, but no variability like HD 168625 are difficult to classify in this scheme, because the old age of the nebulae and the possibility that the star may never again enter in an active LBV phase.

LBVs overlap in some respect with the parameter space of hydrogen rich Wolf Rayet stars, while for other parameters they can be well separated. The show colder temperatures then WR-stars and the wind momentum transferred to the wind is typically below the single scattering value. The surface abundances of the LBVs show nitrogen enrichment and in some cases like for R 71 in the LMC helium appears already significantly enriched (see Lennon et al. 1993).

2 Examples

The galactic LBV HR Car together with R 127 and S Dor are here selected from a larger list of stars monitored over the past 20 year with various instruments. For two more stars AG Car and HD 160529 the data was discussed in a comprehensive way by Stahl et al. 2001 and Stahl et al. 2003, respectively. All data reduction has been repeated with the latest version of the data reduction software including a global fit of the wavelength solution over many orders and optimum extraction techniques (CASPEC, HEROS, FEROS).

HR Car went through two cycles of characteristic LBV variability in the last 20 years with visual maxima of 7.2 magnitudes in 1991 and 2001 and minima of about 8.2 magnitudes before 1987, in 1992 and after year 2004. Interestingly the star shows rotational broadening of the order of 70km/s during minimum light estimated in Si III and N II line while in the other phases the metal lines have shown P Cygni or more complex profiles which prevented to search for the spin down of the outer stellar photosphere when the star is radially expanding. The later has been observed by Groh et al. 2006 for the galactic LBV AG Car. During most phases the line profiles are rather complex with multiple discrete absorption components. With the circumstellar emission in the forbidden [Fe II] line a reference, the observation appears even more complex since in all phase except of the maximum light the apparent P Cygni-profile appear at an offset red-shifted radial velocity, while at maximum light the Balmer lines appear more like classical P Cygni profiles but blue-shifted in respect to the circumstellar lines. The complexity of the profiles indicate that the velocity fields and wind geometry may deviate significantly from a spherical symmetric stellar wind beyond the observation of clumping in the wind.

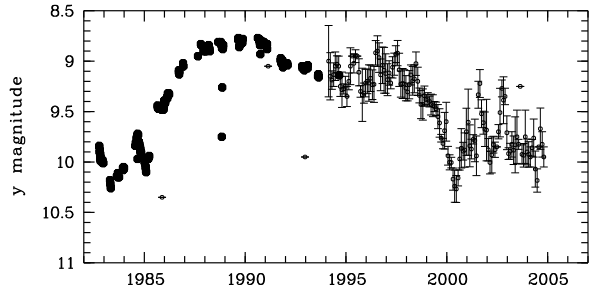

Figure 1: Light curve of the LBV R 127 in the LMC. The data has been collected from the literature (Sterken et al. 1995 and references therein) and from the visual RASNZ observations.

R 127 located in the Large Magellanic cloud was in the 1970s spectroscopically classified as OF/WN9 star of 11th magnitude. Since then is has radially expanded until 1991 when it has shown a spectrum strongly dominated by singly ionized metal lines (also see Wolf et al. 1988). The star has not undergone another minimum phase during the last two decades. It showed as indicated in Figure 1 a slow decline in visual brightness since 1991 superimposed with a steep but temporary decline in starting in 1999. During this period the emission part of the P Cygni profile has strongly increased. Like for HR Car we take the radial velocity of the circumstellar shell of R 127 as the reference for the system velocity of the star.

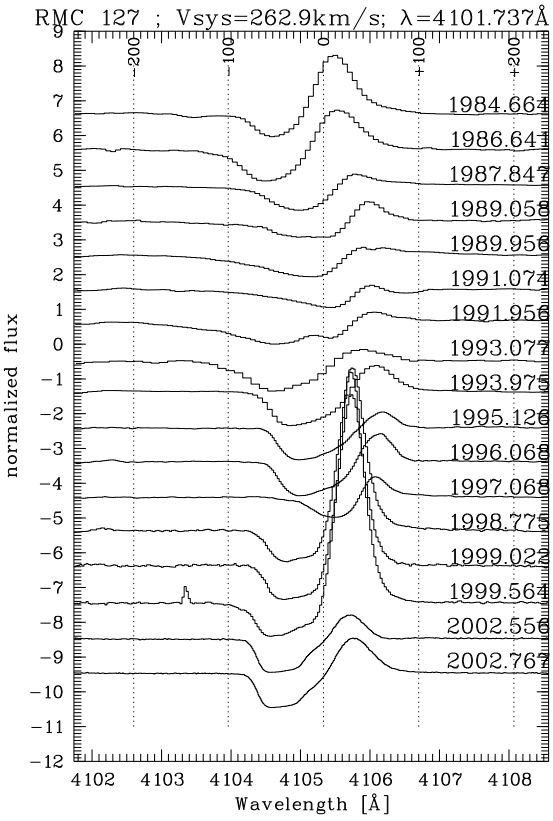

Figure 2: Long-term spectral variation of the Hδ-line of R 127. The indicated velocities are the system velocities in respect to the velocity of the circumstellar shell.

Again I have found that the P Cygni profile do not appear at the radial velocity at which it would be expected following a text book like interpretation of these profiles for an monotonous accelerated radially expanding stellar wind. The strongest red-shift of the profile was found in 1997 when there was no

apparent change in the light curve seen. After reaching the visual maximum in 1991 the star has undergone a phase when inverse P Cygni components were indicating in-falling gas, but at relatively high velocities of 60km/s seen in respect to the circumstellar shell.

In 2002 the star was monitored with higher frequency with UVES in service mode. The spectra show multiple discrete absorption components in the Fe II lines ($\lambda = 4233$Å can be taken as an example) . However unlike for cases of clumps in the wind these components appear not to be accelerated within a period of 80 days covered by the monitoring.

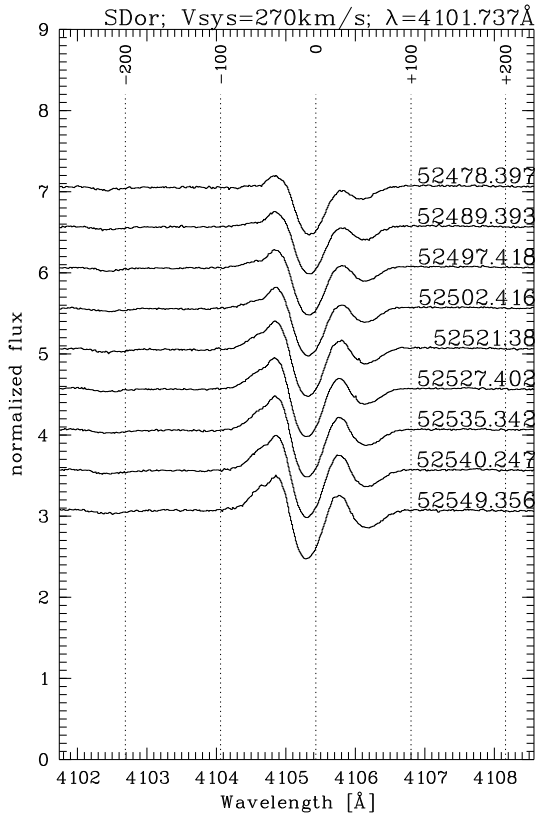

Figure 3: Short-term spectral variation of the Hδ-line of S Dor. The data was obtained in year 2002.

S Dor of the LMC has been observed close to maximum visual brightness phase for most of the time since in 1989 and since 1996. During two periods, in 1985 and 1993 it was observed in a phase when it has been 1 magnitude fainter then during the maximum light. The star has been frequently observed with inverse P Cygni profiles which appears to persist for a relatively long long time (see Wolf & Stahl 1990). A higher level of complexity was reached during 2002 when the star was monitored with higher time resolution (see Figure 3). We find for the Balmer lines (Hγ, Hδ) two emission peaks and two absorption peaks at the same time. The absorption minima are at blue- and red-shifted velocities (about -10km/s and +50km/s respectively) while the peak emission were found at -40km/s and +20km/s. The relative intensity of these components have significantly changed during the 80 days monitoring campaign with overall stronger absorption and emission components at the end.

3 Discussion

During their extreme radial expansion and contraction episodes the LBVs are very often observed with complex line profiles, which are very puzzling in the sense that even when the lines appear as text book like P Cygni profiles these profiles are shifted in respect to the circumstellar shells taken as a reference for the system velocity. The velocity fields in the stellar wind appear to be very complex even if some of these effect can be explained by unusual radially changing excitation or ionization states. Considering the variability of the profiles is appears more likely that the overall geometry is more complex then the classical radially expanding stellar wind with or without clumps. It is however extremely complicate to derive the geometry of the none stationary LBV winds from the observed time series of line profiles.

The data presented here were taken by the hot star group of the Landesternwarte Heidelberg (Berhard Wolf, Otmar Stahl, Andreas Kaufer, Thomas Rivinius, Franz-Josef Zickgraf and others) at ESO telescopes in La Silla and Paranal. I acknowledge with thanks the variable star observations from the AAVSO International Database and the RASNZ observations.

References

Groh, J. et al. 2006, ApJ, 638, L33

Lennon, D.J. et al. 1993, SSRv, 66, 207

Stahl, O. et al. 2001, A&A, 375, 54

Stahl, O. et al. 2003, A&A, 400, 279

Sterken, C. et al. 1995, A&AS, 113, 31

Wolf, B. et al. 1988, A&AS, 74, 239

Wolf, B. , Stahl, O. 1990, A&A, 235, 340

Groh: The fact that HR Car shows an absolute low value of $v_{\rm rot} \sin i$ does not necessarily mean that it is a slow rotator. You have to compare $v_{\rm rot} \sin i$ with the value of the critical rotational velocity, which requires the knowledge of M, L and R.

Szeifert: I agree! For reasonable stellar parameter estimates the rotation does not reach critical rotational velocities. The most uncertain parameter in case of HR Car is the distance.

Weis: Can you define to me what an LBV outburst is? If you need it as a definition of an LBV none of the objects you showed have been LBVs.

Szeifert: This is a misunderstanding: My definition was that LBVs are evolved massive supergiant stars with characteristic variability at approximately constant bolometric luminosities. An LBV outburst like η Car's I have added in a footnote to the class of LBVs even though this outburst will change dramatically the bolometric luminosity.

Clumping in Hot Star Winds
W.-R. Hamann, A. Feldmeier & L.M. Oskinova, eds.
Potsdam: Univ.-Verl., 2008
URN: http://nbn-resolving.de/urn:nbn:de:kobv:517-opus-13981

Rapidly accelerating clumps in the winds of the very hot WNE Stars

A.-N. Chené[1], A.F.J. Moffat[1] & P.A. Crowther[2]
[1] *Université de Montréal, Canada*
[2] *University of Sheffield, UK*

We study the time variability of emission lines in three WNE stars : WR 2 (WN2), WR 3 (WN3ha) and WR152 (WN3). While WR 2 shows no variability above the noise level, the other stars do show variation, which are like other WR stars in WR 152 but very fast in WR 3. From these motions, we deduce a value of $\beta \sim 1$ for WR 3 that is like that seen in O stars and $\beta \sim 2$–3 for WR 152, that is intermediate between other WR stars and WR 3.

1 Clumping in Wolf-Rayet Winds

Previously in these proceedings, one of us (AFJM) showed how the motion of subpeaks over the broad emission lines in the spectra of Wolf-Rayet (WR) stars can be associated with the motion of clumps in the wind. He also reminded us how Lépine & Moffat (1999) followed the trajectory of subpeaks in the spectra of 9 WR stars and determine their velocity law, with the assumption of a β-law for which a value of βR_* is calculated (R_* is the radius of the base of the wind). For all these stars, the value of βR_* found ranges between 20 and 80 $R_\odot$. Taking the values of stellar radius from the literature and assuming that the base of the wind is at this radius, they obtained values for β which are much greater than 1, indicating that the WR winds have very slow acceleration. However, all the stars studied by Lépine & Moffat (1999) are WC or WNL stars showing broad emission lines formed at radii where the wind has reached a velocity near terminal (v_∞) while none of them are hot, weak-line WNE stars.

2 The Spectrum of WR2, WR3 and WR152

In this study, we were initially interested in the spectrum of WR3, which shows weak, narrow triangular emission lines (Marchenko et al. 2004), indicating that, in contrast to the previously studied WR stars, the lines in WR3 come from regions of great acceleration, i.e. regions at radii near the base of the wind. If we can assume that the wind is spherically symetric and optically thin, it is then possible to estimate the velocity regime of the line formation using the deprojected emission function (Lépine & Moffat 1999). In Table 1 is listed in the third column the value $\langle v \rangle$, which is the velocity regime where the maximum emissivity of the line occurs, and in the fourth column the value Δv, which is the extension of the line formation region in velocity space for 4 different lines in the spectrum of WR3. Also are shown the same values for the He II λ4686 line of WR2 and WR152, two other WNE stars that we observed to compare with WR3.

Table 1: Line formation region

Star	Transition	$\langle v \rangle$ (km s^{-1})	Δv (km s^{-1})
WR3	N III λ4604	155-1500±10	60-900±5
	N V λ4620	145-1500±10	60-900±5
	He II λ4686	1520±5	900±5
	N V λ4945	145±5	60±5
WR2	He II λ4686	2340±5	750±5
WR152	He II λ4686	1240±5	610±5

The formation region of the He II λ4686 line of the three stars spans over a wide velocity range, going from moderate velocities to velocities near v_∞ (WR2: $v_\infty = 3100\,\mathrm{km\,s^{-1}}$, WR3: $v_\infty = 2500\,\mathrm{km\,s^{-1}}$ and WR152: $v_\infty = 2000\,\mathrm{km\,s^{-1}}$; Hamann et al. 1995). One can also see in Table 1 that the formation region of the N V λ4945 line in WR3 occurs at very low velocity. This allows us to probe radii near the base of the wind. Interestingly, both N III λ4604 and N V λ4620 present two components in the deprojected emission function, i.e. one at low and one at high velocity.

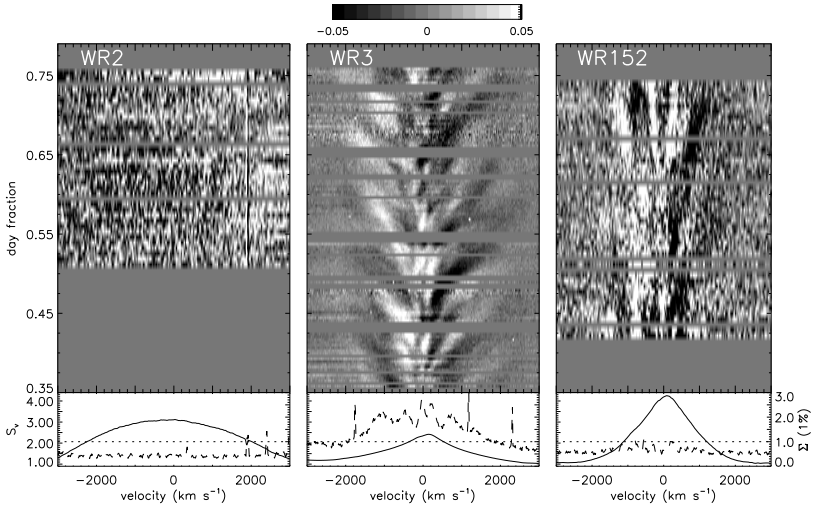

Figure 1: Spectral variability of the He II λ4686 line for WR2, WR3 and WR152. *Bottom panel*: Mean spectrum (solid line) and Σ spectrum (dashed line). Σ is proportional to the variability at each wavelength. The variability at a given wavelength is significant if Σ is higher than 1.0 (dotted line). *Upper panel*: Time-resolved plot of the residuals after subtracting the mean spectrum.

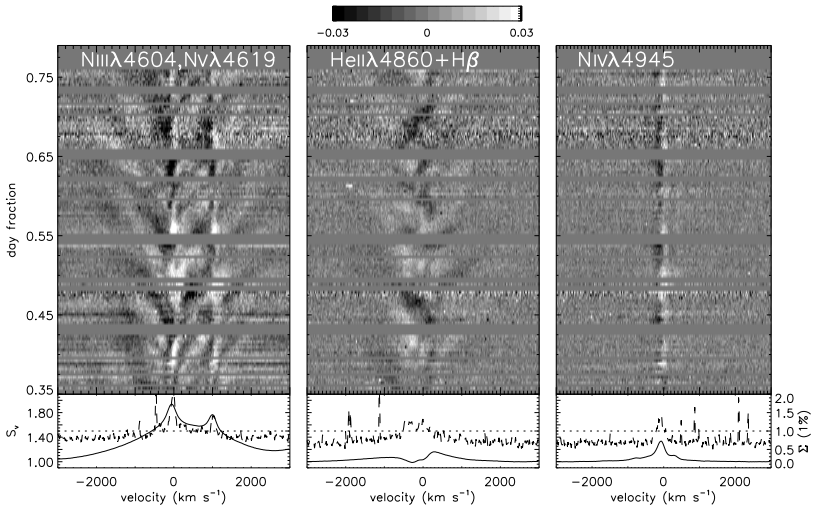

Figure 2: As in Fig. 1, but for N III λ4604 and N V λ4620 (left), He II λ4860 (middle) and N V λ4945 (right) in WR3.

3 Spectral Variability and the Velocity Law

Intense time-series of high-resolution spectra of the three WNE stars have been obtained at the Observatoire du mont Mégantic. Three nights were dedicated to WR2, eight to WR3 and six to WR152. Spectra with mean SNR $\sim$ 90 were obtained every 10 minutes. During an additional night at the William Hershel Telescope, spectra of WR3 with a mean SNR $\sim$ 120 were obtained every 5 minutes, allowing the analysis of weak-lines such as N V λ4945 line.

In Fig. 1 we present in the *upper panel* one example of the spectral variability observed during one night on the He II λ4686 line of the three stars WR2, WR3 and WR152. In the *lower panel* is plotted the Σ spectrum (Fullerton et al. 1996). If the value of Σ is higher than 1.0 at a given wavelength, this means that the spectrum is significantly variable at this wavelength at a confidence level of 99 %. For the three stars follow details.

3.1 WR2 (WN2)

Surprisingly, no variability at all was observed for WR2, even if the signal-to-noise ratio (SNR) was sufficiently high to allow a 2-3σ detection of a subpeak as small as 1% of the He II λ4686 line intensity, for a temporal resolution of 10 minutes. Moreover, the Σ spectrum never reaches a value higher than 1.0 all along the spectrum. Thus, no value of βR_* can be determined for this star.

3.2 WR3 (WN3ha)

While the spectrum of all the stars studied by Lépine & Moffat (1999) show slowly moving subpeaks that last for $\sim$ 10 hours, the spectrum of WR3, on the other hand, shows subpeaks that appear stochastically on the emission lines, move rapidly toward the edges of the line, and disappear within $\sim$3 hours. The curvature of the subpeak trajectories on the He II λ4686 line indicates that the acceleration of the wind at radii corresponding to its formation region is not constant. These subpeaks have an intensity of 1-1.5 % of the line intensity. In Fig. 2, we present the spectral variability of emission lines due to N III λ4604, N V λ4620, He II λ4686, He II λ4860 and N V λ4945. When comparing all these lines, we see they all are variable, that their subpeaks all lie between 1.0 and 1.5 % of the line intensity, and that the pattern of variability is comparable for lines sharing similar formation regions. Indeed, the trajectories of the subpeaks are similar on the He II λ4686 and He II λ4860+Hβ lines, but are not clearly associated with the the trajectories traced on the N V λ4945 line. Interestingly, the two N III λ4604 and N V λ4620 lines show a variability pattern that resembles a combination of the variability pattern of the He II λ4686 and the N V λ4945 lines.

To determine the velocity law of WR3, we first assume that the acceleration of clumps is not too far from a constant value. Then we can deduce a mean radial velocity ($v_{\rm m}$) and a mean radial acceleration ($a_{\rm m}$) of each clump with a linear regression of their trajectory. The relation $a_{\rm m}(v_{\rm m})$ is approximated by (Lépine & Moffat 1999) :

$$a_{\rm m}(v_{\rm m}) = \frac{\left[v_{\rm m} \ln(\frac{v_{\rm m}}{\mu v_\infty})\right]^2}{\mu \beta R_*}, \qquad (1)$$

where μ is the cosine of the angle of the clump trajectory with the line-of-sight, and βR_* is the parameter to be determined. In Fig. 3, each trajectory for a subpeak on the line He II λ4686 is represented by a point in the plot $a_{\rm m}(v_{\rm m})$. All these points cannot be fitted, because the change of μ from one trajectory to another implies different values of $a_{\rm m}(v_{\rm m})$, even with a single value of βR_* for all trajectories. However, βR_* can be estimated from the two curves of $a_{\rm m}$ with μ=-1 and μ=1 that englobe the bulk of the points. In Fig. 3 are plotted two different solutions of βR_* possible within the uncertainties of the measurements. As a result, βR_*=2.8-3.1 $R_\odot$ for WR3. Then, if R_*=2,5 $R_\odot$ (Hamann et al. 1995), β=1.1-1.2, a value significantly lower than what was determined for previously studied WR stars (Lépine & Moffat 1999). One can see that in Fig. 3, no point is present in the area near $a_{\rm m}$=0, defined by the curve $a_{\rm m}(v_{\rm m})$ and the dashed line. Then, at a velocity too high with an acceleration too low, no clump is present. This can be translated to a maximum radius where clumps are seen on the He II λ4686 line, leading to $R_{\rm max}$=3.5 $R_\odot$.

3.3 WR152 (WN3)

The motion of the subpeaks on the lines of WR152 is not as rapid as the motion of subpeaks on the lines of WR3 and lasts for $\sim$ 10 hours. However, from the $a_{\rm m}(v_{\rm m})$ curves, we deduce βR_*=5.0-7.0 $R_\odot$. If R$_*$=2.7 R$_\odot$ (Hamann et al. 1995), β=1.9-2.6. This is an intermediate case between WR3 and the stars of Lépine & Moffat (1999). No $R_{\rm max}$ could be deduced.

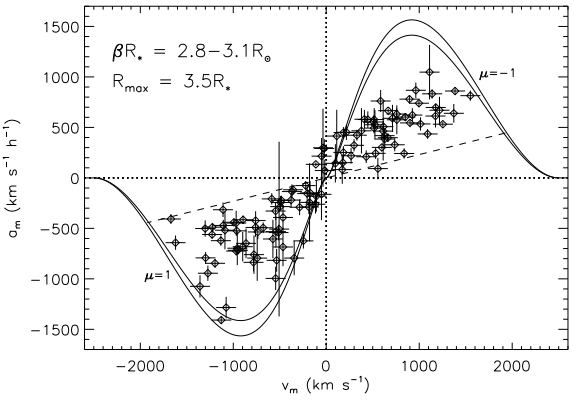

Figure 3: Comparison of $a_{\rm m}$ and $v_{\rm m}$ for all the clumps on He II λ4686 in WR3. In solid lines are plotted two solutions for βR_* = 2.8 and 3.1 $R_\odot$. The dashed line gives $R_{\rm max}$.

References

Fullerton, A.W., Gies, D.R., & Bolton, C.T. 1996, ApJS, 103, 475

Hamann, W.-R. et al. 1995, A&A, 299, 151

Lépine, S., & Moffat, A.F.J. 1999, ApJ, 514, 909

Marchenko, S.V. et al. 2004, MNRAS, 353, 153

Prinja: Since line profile variability is so widespread in WR stars and OB stars, it is very interesting when you come across a star that does *not* vary! Can you comment on what might be special in the case of WR2, where the lines are so steady and there is no evidence for moving sub-peaks on the emission lines?

Chene: Not that much. All I can say is, assuming that clumping produces line-profile variability of a level of 1 % of the line intensity, according to our signal to-noise ratio, we should have seen moving sub-peaks, if there were any. Maybe the lines observed in WR2 are formed in a highly optically thick region.

Hamann: Your results show that clumping is a universal phenomenon in WN stars of all sub-types, with the one exception you have shown, WR2, where you found no line-profile variability. I want to point out that WR2 has a very peculiar spectrum. Among all galactic WN, it is the only one which shows round-shaped emission-line profiles. (There is a similar counterpart in the LMC.) Such round-shaped profiles cannot be reproduced by the models at all. In Hamann et al. (2006,A&A 457) we have shown that a convolution with rotational broading gives a good fit to the observation, if $v_{\rm rot} \sin i = 1\,900\,{\rm km/s}$ is assumed. This demonstrates that something very strange is going on with WR2.

Ignace: In some cases, $\beta\, R_*$ is quite small. To what extent does the assumption of a β-law bias your implied values of R_*?

Chene: Maybe I did not make my point clear enough, but a small $\beta\, R_*$ does not imply a small R_*, but a small value of β. The value for R_* is taken from literature (e. g. Hamann 1995).

Hamann: I want to emphasize that the value of $\beta\, R_*$ that one obtains from the analysis of line-profile variability depends sensitively on the adopted radius of formation for the considered spectral line. This formation radius can only be inferred from adequate model atmospheres.

Clumping in Hot Star Winds
W.-R. Hamann, A. Feldmeier & L.M. Oskinova, eds.
Potsdam: Univ.-Verl., 2008
URN: http://nbn-resolving.de/urn:nbn:de:kobv:517-opus-13981

Modelling the induced clumping stochastic line profile variability

A.F. Kholtygin
Astronomical Institute of Saint-Petersburg University, Russia

We model the line profile variability (lpv) in spectra of clumped stellar atmospheres using the Stochastic Clump Model (SCM) of the winds of early-type stars. In this model the formation of dense inhomogeneities (clumps) in the line driven winds is considered as being a stochastic process. It is supposed that the emission due to clumps mainly contributes to the intensities of emission lines in the stellar spectra. It is shown that in the framework of the SCM it is possible to reproduce both the mean line profiles and a common pattern of the lpv.

1 Introduction

In the beginning of 70th the first indications of the presence of high density regions (blobs or clumps) in the atmospheres (winds) of the early-type (hot) stars were emerged. Now the strong inhomogeneity of the winds of the early-type stars appears to be evident both from theoretical works and observations.

This inhomogeneity can be described in the *clump model*. In this model a stellar wind is proposed to be composed of the numerous dense clumps and more rarefied interclump medium. Total number of the clumps exceeds 10^3. The ions of the low and moderate ionization stages are located dominantly in the clumps while the interclump medium is strongly ionized.

2 Stochastic clump model

A random character of the clump connected lpv allows us to conclude that clumps born and dissipate randomly. A random ensemble of clumps in the atmosphere may be described in the framework of the Stochastic clump model suggested by Kostenko & Kholtyhin (1999) and Kudryashova & Kholtygin (2001) and close to that propose by Lepine & Moffat (1999). In this case one can say only about the probability for clump has a determined values of the mass, size, flux in the line and other parameters. For each cloud these values are defined through the distribution of clumps on masses, sizes and other parameters.

The total flux in the line formed by a clumped atmosphere in a frequency interval $[\nu, \nu + d\nu$ can be presented as

$$F(\nu)\nu = F^{\rm icl}(\nu)\nu + F^{\rm cl}(\nu)\nu + F^{\rm cl-icl}(\nu)\nu\,. \quad (1)$$

Here the value of $F^{\rm icl}(\nu)$ is the part of the line flux formed by the homogeneous interclump medium only, $F^{\rm cl}(\nu)$ is the clumps contribution and $F^{\rm cl-icl}(\nu)$ refers to the contribution of the clump - interclump medium interactions to the line profile.

As it was shown by Kostenko & Kholtygin (1999) the contribution of the interclump medium into the total intensity of many lines in the hot star spectra (e.g. lines of ions CIII, HeI-II, etc.) is small. The interaction of clumps with the interclump medium give contribution mainly in the X-ray region and weakly impacts on the profiles of optical and UV lines considered. It means that the intensity of these lines are mainly determined by clumps.

Due to of the large velocity gradients in the winds the contributions of the separate clumps into the total line flux can be considered independently and a part of the total line flux formed by clumps

$$F^{\rm cl}(\nu) = \int_{(4\pi)}\int_{M_{min}}^{M_{max}}\int_{R_*}^{\infty} N_{cl}(M_{\rm cl}, R, \Omega) \times F_{\rm cl}(R,\nu)\, d\Omega\, dM_{\rm cl}\, dR\,. \quad (2)$$

Here $M_{\rm min}$ and $M_{\rm max}$ are the minimal and maximal masses of clumps in the whole clump ensemble; a function $N_{\rm cl}(M_{\rm cl}, R, \Omega)$ describes a distribution of clumps on masses $M_{\rm cl}$, distances from the centre of a star R (R_* is a stellar radius) and directions Ω.

Studies of lpv for O and WR stars (Kaper et al. 1999, Lépine & Moffat 1999) specify that clumps are mainly formed in a narrow area of an atmosphere near the stellar core. It means that distribution of clumps on distances from the stellar core, masses and directions can be considered independently:

$$N_{\rm cl}(M_{\rm cl}, R_{\rm cl}, \Omega) = N_m(M_{\rm cl})\, N_r(R_{\rm cl}) N_\Omega(\Omega)\,. \quad (3)$$

2.1 Modelling the clump ensemble

We present a distribution of clumps on masses in atmospheres of early-type stars as $N_m(M_{\rm cl}) \sim (M_{\rm cl})^{-\gamma}$ and adopt the values of $\gamma \approx 2.0$ (see arguments in a paper by Kudryashova & Kholtygin 2001).

For modelling the distribution $N_r(R_{\rm cl})$ we suppose that clumps are formed near the stellar core, the total clump number in the atmosphere is constant and their distribution on radius R is determined by a relation $R^2 N_r(R)(R) V_{\rm cl}(R) = const$. For clump velocity $V_{\rm cl}(R)$ we adopt standard β-law. We use mainly the spherical-symmetric distribution $N_\Omega(\Omega)$ of directions of clumps.

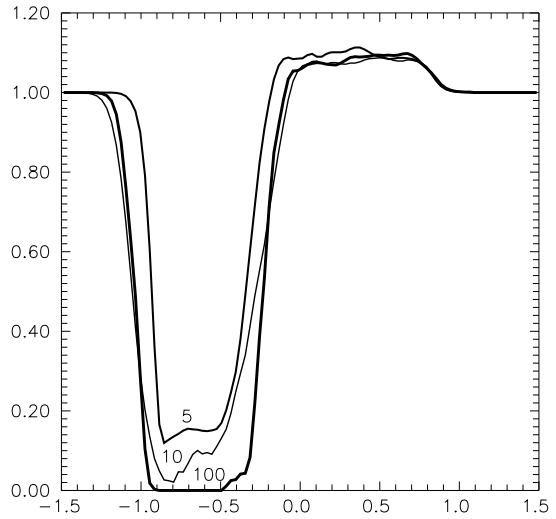

Figure 1: Mean line profile in the SCM in a dependence on a parameter $\tau_{\rm cl}^{\rm max}$.

We assume that each clump forms a detail of the line profile (subpeak) with gauss distribution of intensity. Dependencies of a total flux in the different lines formed by separate clump at the distance R to star were calculated by Kostenko & Kholtygin (1999). Follow Lépine (1994) we suppose that the full fluxes of subpeaks $F_i \propto \sigma_i^2$, where σ_i^2 is a velocity dispersion inside a clump with number i.

Follow Kudryashova & Kholtygin (2001) we suppose that mean clump *lifetime* is determined by a relation $T^{\rm cl} = T_{\rm cl}^{\rm max} (F_{\rm cl}^{\rm max}/F_{\rm cl})^\gamma$, where $T_{\rm cl}^{\rm max}$ is a *lifetime* of a clump with the maximal flux $F_{\rm cl}^{\rm max}$ and $\gamma \approx 1$ (see Lépine (1994 for details). We suppose that after its *lifetime* a clump can exists by does not emit in the considered line. It means that *lifetime* of clump depends of the line considered.

The resonance lines of the most of ions in the atmospheres of hot stars have the strong absorption components. Assume the next procedure taking into account the absorption in the violet wing of the line. Suppose that clumps which are located on a line of sight can absorb the radiation of the stellar photosphere and the total optical depth for absorption of the continuum radiation can be presented as a sum of all optical depths of the clumps on a line of sight. To calculate an optical depth $\tau_i(\nu)$ of a clump with a number i in the central frequency of the considered line we use the scaled relations $\tau_i(0) = \tau_{\rm cl}^{\rm max}(F_i/F_{\rm max})^{\mu_\tau}$, where $\tau_{\rm cl}^{\rm max}$ is an optical depth of a clump with a maximal line flux $F_{\rm max}$. From the calculations of the ionization structure of the hot stars (Kostenko & Kholtygin 1999) we can conclude that parameter $\mu_\tau \approx 2$.

2.2 Results of the line profile calculations

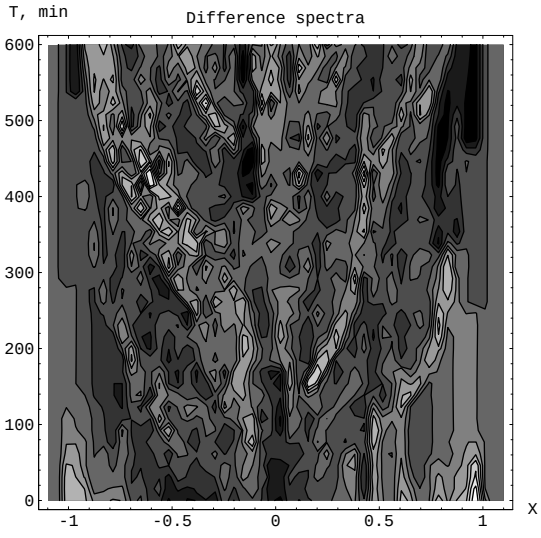

Figure 2: Dynamical spectra in the SCM for parameters $\sigma_{max} = 0.20$, $\varepsilon = 10^{-3}$ and $\tau_{cl}^{max} = 0$ and for 10^h of total time of "quasi-observations".

The relation (2) gives us the *instantaneous* line profile only, whereas the observed line profiles are the mean of all instantaneous profiles over the whole interval of the observations. For evaluating the *quasi-observed* line profile we average all *instantaneous* line profiles on the typical time of observations of one line profile – ΔT.

For obtaining the difference spectra we calculate the averaged *quasi-observed* line profiles over the whole period of observation $T_{\rm obs}$. The difference spectra are an individual quasi-observed profile minus this average profile.

For example we plot a dependence of mean line profile versus $T_{\rm cl}^{\rm max}$ in Fig. 1 for a resonance doublet CIV λ 1548,1550. For the sake of simplicity we use a dimensionless frequencies in a line $x = (\nu - \nu_{ik})/\Delta\nu_\infty$, where $\Delta\nu_\infty = \nu_{ik}(V_\infty/c)$ is a full width of a line, ν_{ik} is the central frequency of the line, and V_∞ is a wind terminal velocity.

Main parameters of the model are σ_{max}, ε and τ_{cl}^{max}, where σ_{max} is a velocity dispersion in a clump with a maximal flux, ε is a ratio of a minimal and

a maximal fluxes of line formed by an ensemble of clumps. For an illustration we plot the typical dynamical spectra for line CIII $\lambda\,5696$ for the typical parameters of a clump ensemble at a total duration $T^{\rm full} = 10^h$ of *quasi-observations*.

2.3 Using wavelets for testing clumps

For OB stars the clump contribution in the total line profile is not so significant as for WR ones. Because of this we need to use the more elaborate methods for testing a clump contribution in the line profile. The most convenient tool for solving such problem is a wavelet analysis. Kholtygin et al. (2006) described a procedure of construction the *dynamical wavelet spectra* for lines in spectra of OB stars. Those are the wavelet transform of the difference spectra for studied line in the velocity V space in a dependence of the time of observation t for the fixed scale S. For scales in an interval $S = 1 - 5\,$km/s the dynamical wavelet spectra is determined by the noise contribution mainly, whereas for large scales $S > 25\,$km/s mainly regular variations in the *dynamical wavelet spectra* can be detected (see Kholtygin et al. 2006) for details.

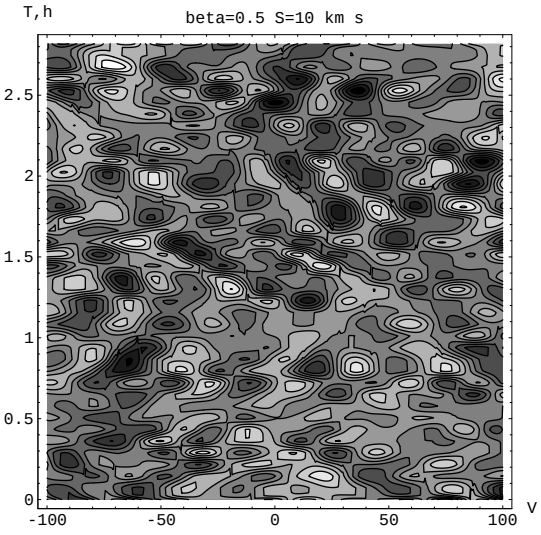

Figure 3: Dynamical wavelet spectra for the Hα line in the spectrum of δ Ori A

At the same time for intermediate scales ($S \in [5-25]\,$km/s) the contribution of the stochastic lpv, connected with the clumps contribution can be seen. Figure 3 illustrate the stochastic variations in the dynamical wavelet spectra of line H_α in a spectra of a bright triple system δ Ori A (O9.5II) for scale $S = 10\,$km/s with using the Mexican Hat as a Mother wavelet.

3 3-phase model of winds of early-type stars

Early-type stars are the powerful sources of X-Ray emission (e.g., Oskinova et al. 2006). For explanation both the UV optical an X-Ray spectra of these stars we postulate the *3-phase model* of winds. In this model we suppose that wind consist of 3 phase: homogeneous warm wind with a mean temperature $\approx 10^5\,K$, cold clumps with $T \approx 10^4\,K$ and hot clumps (hot zones with T up to $10^8\,$K. Warm wind and cold clumps emit in an optical and UV range, whereas a radiation of hot zones are mainly in a X-Ray region.

For WR stars clumps give the *main contribution* in the line emission, but for OB stars clumps give the smaller one. There exist a phase transitions between hot and cold phases. Cold clumps can be heated by shocks up to $10^8\,$K (Bychkov & Aleksandrova 2000), whereas hot zones cool very fast with cooling time is less than 1 min and convert to cold clumps. In a support of our model we can mention a connection between optical and X-Ray variability (see Oskinova et al. 2001 and reference therein).

Acknowledgements. The author is grateful for the support provided by the RFBR grant 05-02-16995.

References

Bychkov, K.V., Aleksandrova, O.A. 2000, Astronomy Reports, 44, 781

Kaper, L., Henrichs, H.F, Nichols, J.S. 1999, A&A, **344**, 231

Kholtygin, A.F., Burlakova, T.E., Fabrika, S.N., Valyavin, G.G., Yushkin, M.V. 2006, Astronomy Reports, 50, 887

Kostenko, F.V., Kholtygin, A.F. 1999, Astrophysics, 41, 277

Kudryashova, N.A., Kholtygin, A.F. 2001, Astronomy Reports, 45, 287

Lépine, S. 1994, ASpSci, 221, 371

Lépine, S., Moffat, A.F.J. 1999, ApJ, 514, 909

Oskinova, L.M., Clarke, D., Pollock, A.M.T. 2001, MNRAS, A&A, 378, L21

Oskinova, L.M., Feldmeier, A., Hamann, W.-R. 2006, MNRAS, 372, 313

Moffat: In the time-series spectra of the few O stars that have been observed so far (e. g. ζ Pup, HD93129A), the sub-peaks seem to have similar velocity compared to those seen in WR stars. Is this compatible with your statement that clumps in O star winds have spatially smaller clumps compared to these in WR stars?

Kholtygin: As far as I remember, direct evidence for clumps in the atmosphere of an O star is only found for ζ Pup. But this star is untypical for O stars and the properties of its clump ensemble can be very different from that of other O stars. We have estimated the clump sizes for α Cam and found that these clumps are really smaller than in WR stars. For other O stars this conclusion must be checked.

Clumping in Hot Star Winds
W.-R. Hamann, A. Feldmeier & L.M. Oskinova, eds.
Potsdam: Univ.-Verl., 2008
URN: http://nbn-resolving.de/urn:nbn:de:kobv:517-opus-13981

Discussion: Magnetic fields, variability

Moderator: Joe Cassinelli

Owocki: We intuitively associate increased absorption with a high spatial density, since this leads to an increased column density. But for line opacity the absorption at any frequency scales with the column density within a Sobolev length about the resonance point for that frequency, and that in turn depends on the inverse of the velocity gradient. In hydrodynamic models of wind structure, for example of corotating interaction regions (CIRs, see, e.g. Cranmer and Owocki 1996), discrete absorption features tend to come from regions of a relative velocity plateau, not from dense compressions as had been anticipated.Such plateaus form behind discontinuities in the positive velocity gradient, i.e. at "kinks" in the velocity law. They represent a new and interesting feature of line-driven outflows, wherein the driving force depends on the velocity gradient, and often arise upstream from a barrier, such as a slower moving dense compression. As such, discrete absorption components (DACs) in UV wind lines from hot stars may be providing a diagnostic of a new hydrodynamical phenomenon that we are still trying to fully understand.

Feldmeier: As for the propagation properties of these kinks: as we recently found analytically (Feldmeier, Raetzel, & Owocki, 2008, ApJ), kinks propagate upstream faster than Abbott waves. A pronounced kink like in the Cranmer & Owocki (1996, ApJ) CIR simulations propagates roughly at twice the Abbott speed. Due to this fast upstream motion of kinks, their outward evolution through the wind, and that of the associated velocity plateau causing DACs, is rather slow and may indeed match the slow, observed DAC evolution timescale.
Regarding Wolf-Rainer Hamann's criticism towards the Sobolev approximation: someone should really generalize the amazing Greens function analysis by Owocki & Rybicki (1986, ApJ) for the pure absorption case, to include line scattering, if only in some simplified fashion. This would once and for all do away with any qualms about the existence of Abbott waves.
Finally, with regard to the temperature stratification of the X-ray emitting gas: the exact run of temperature, density, and ionization in the postshock region of a radiatively cooling shock is well know, e.g. from the analytical calculations by Chevalier & Imamura (1982, ApJ). We (Feldmeier et al. 1997, A&A) applied this to obtain fits to ROSAT spectra, which were clearly better than from corresponding isothermal-shock fits.

Massa: I hear a lot about velocity plateaus. But these enhance the absorption for a fixed column density. So am I being told that the mass loss rates are even lower because the column density is less?

Puls: May it be that the maximum observed infall velocity (which could be observed on the red side of the profile) is related to the magnetic parameter η_*?

ud-Doula: The infall velocity of dense material is always smaller than the free fall velocity. Assuming no rotation, the magnetic confinement parameter decides how far away from the stellar surface the material is collected. The further out this happens, the higher is the infall velocity.

Massa: A result from our 2003 paper is that the ion fraction of O VI is correlated with terminal velocity. To me, this suggests that shocks and not magnetic fields are dominating the clumping.

Blomme: We indeed require that the spot velocity is different from the rotational velocity. The fact that the spot is not fixed on the surface makes it difficult to attribute it to magnetic fields, which are expected to be fixed on the surface.

Hamann: Can somebody make clear the relation between the periods of DACs and modulations? For ζ Pup, as far as I remember, the IUE MEGA campain data gave the DAC repetition time equal to the rotation period of $\sim$ five days, and a modulation period that is much shorter (19 h) and not an integer fraction of the former.

Blomme: These are the correct values for ζ Pup. But for HD 64760, we have a recurrence time for the DAC of 10.3 d and a rotational period of 4.1 d (or 4.8 d if you believe that the rotational modulations are stuck on the surface). The values are not compatible, so you need a spot velocity that is lower than the rotation velocity.

Lobel: The shape of the DAC is very much dependent on the spot velocity with respect to the surface rotation velocity. It is determined by the velocity plateaus behind the CIR and how they are geometrically distributed over time with respect to an observer. The DAC optical depth estimated by the Sobolev approximation is $\tau = \rho q_i / |\mathrm{d}v/\mathrm{d}r|$, so if $|\mathrm{d}v/\mathrm{d}r|$ is small there is large line optical depth in

the DAC. Close to the surface that approximation may break down, however, because there is also the projection effect in the observer's line of sight which will determine the morphology of the DAC.

Binaries, colliding winds and LBVs

Chair: A. de Koter

Clumping in Hot Star Winds
W.-R. Hamann, A. Feldmeier & L.M. Oskinova, eds.
Potsdam: Univ.-Verl., 2008
URN: http://nbn-resolving.de/urn:nbn:de:kobv:517-opus-13981

Eta Carinae viewed from different vantages

T. R. Gull
NASA/GSFC/ASD, USA

The spatially-resolved winds of the massive binary, Eta Carinae, extend an arcsecond on the sky, well beyond the 10 to 20 milliarcsecond binary orbital dimension. Stellar wind line profiles, observed at very different angular resolutions of VLTI/AMBER, HST/STIS and VLT/UVES, provide spatial information on the extended wind interaction structure as it changes with orbital phase. These same wind lines, observable in the starlight scattered off the foreground lobe of the dusty Homunculus, provide time-variant line profiles viewed from significantly different angles. Comparisons of direct and scattered wind profiles observed in the same epoch and at different orbital phases provide insight on the extended wind structure and promise the potential for three-dimensional imaging of the outer wind structures. Massive, long-lasting clumps, including the nebular Weigelt blobs, originated during the two historical ejection events. Wind interactions with these clumps are quite noticeable in spatially-resolved spectroscopy. As the 2009.0 minimum approaches, analysis of existing spectra and 3-D modeling are providing bases for key observations to gain further understanding of this complex massive binary.

1 The Eta Carinae System

Eta Carinae is a very luminous binary stellar system near the end of its hydrogen-burning phase (Davidson & Humphreys, 1997). It experienced two major events seen by astronomers: in the 1840s, a major brightening accompanied by ejection that we see as the dusty, neutral Homunculus, a bipolar shell thought to contain at least 12 $M_{\odot}$(Smith et al., 2003a); and in the 1890s a lesser event with ejecta that we see as the interior, ionized Little Homunculus which contains about 0.5 $M_{\odot}$(Ishibashi et al, 2003). The central source is a massive wind that enshrouds two massive stars with a 5.54-year spectroscopic and X-ray period (Damineli, 1996, Corcoran, 2006). Beginning with the 1998.0 minimum with particular focus on the 2003.5 minimum, several campaigns were conducted to observe the X-ray, visible and UV changes of Eta Carinae including the accompanying responses of the immediately surrounding ejecta. A large number of atlases and papers have been published derived from these observations. Analysis is continuing along with increasingly detailed models to explain the observations and to predict phased behavior of Eta Carinae leading to crucial tests to differentiate between various models of this massive binary system.

The massive ejecta are very rich in nitrogen and helium, very poor in oxygen and carbon. Indeed the N/O and N/C ratios seen by Verner et al., 2002 and Verner, Bruhweiler & Gull, 2005 are consistent with models of evolved massive stars with high angular rotation at the end of their CNO cycle (Meynet & Maeder, 2003).

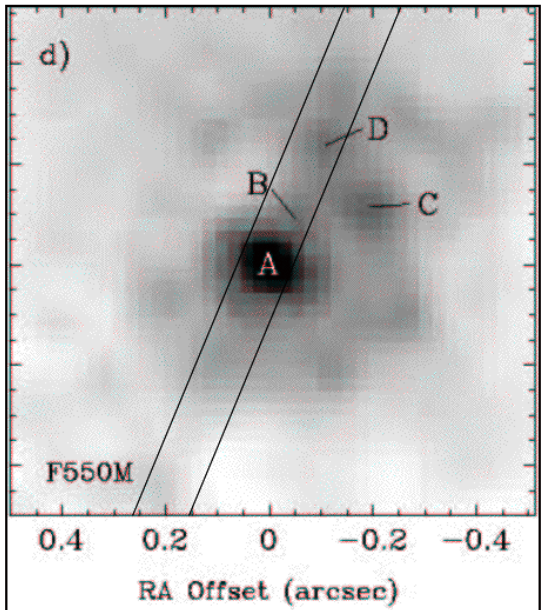

Figure 1: Eta Carinae and its wind/ejecta structure imaged by HST at 5500Å. Spatially-resolved HST/STIS spectra indicate that the interacting winds extend out to 0.4". Weigelt B, C, and D are very luminous narrow-line emission structures located in the downwind cavity carved by the hot secondary and are directly excited by the hot companion. Other clumps complete a ring around Eta Carinae (A) but are shielded by the massive primary stellar wind.

An evolved, massive star is well past the H-burning phase, moving into the He-burning phase that ultimately leads to C and O overabundances at late stages. Recently Smith & Owocki, 2006 pointed out that, with the lowered mass loss rate for an O star during its main sequence lifetime, most mass lost before the supernova event must occur through multiple major ejection events. Eta Carinae, with its N-rich ejecta appears to have just begun a series of major ejections that C- and O-rich Wolf Rayet stars have progressed beyond. Given the transient nature of the Homunculus, historically recent ejecta of Eta Carinae, and the accessibility to studying the material as it responds to the periodically variable FUV and X-ray excitation by the central source, we can learn much about this early phase of massive stellar evolution.

2 Observations

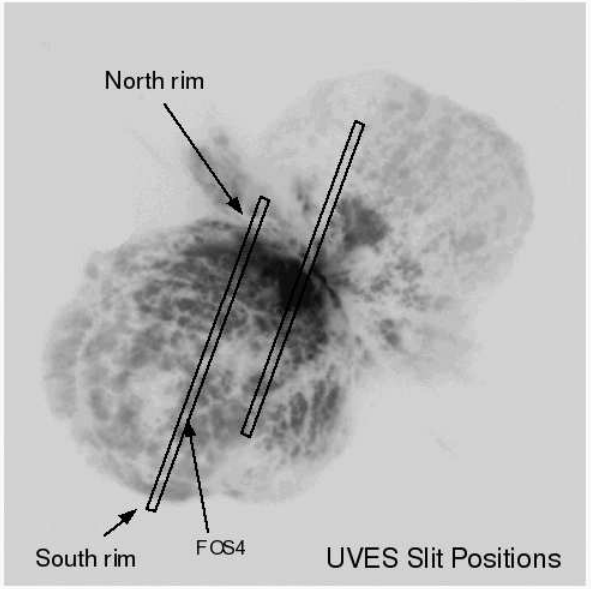

Figure 2: Eta Carinae and the Homunculus as imaged by HST. FOV is about 20". The UVES slit positions for Eta Carinae and for the nebular observations (FOS4) are overlaid. The foreground lobe scatters starlight off the cap and the background wall, resulting in a double-velocity profile. However along the rim, nebular absorption lines and the stellar wind profiles indicate scattering primarily at a single velocity. We use this (see Figure 3) to view the central source from a very different viewing angle relative to line of sight.

Direct imagery of Eta Carinae and the Homunculus (Figures 1 and 2) show extensive structure in the dusty, bipolar and disk ejecta. Figure 1, which is of the central 1" field, includes a number of condensations. The three labeled B, C and D are the Weigelt blobs (Weigelt & Ebersberger, 1986)Spatially resolved spectroscopy at varying angular and spectral resolutions tell much additional detail.

Smith et al., 2003b, using HST/STIS spatially-resolved spectra with $\delta\theta \approx 0.1$" and spectral resolving power, R = 8000, noticed that the hydrogen Bα line terminal wind velocity in the scattered starlight off the center of the foreground Homunculus lobe is greater than that measured in line of sight. We suggested a latitudinal wind dependence especially across the broad spectroscopic maximum of the 5.5-year period. Weis et al, 2005, Stahl et al., 2005 and Davidson et al., 2005, used VLT/UVES observations with seeing-limited angular resolution, $\theta \approx 1$–2" and R≈80,000, to monitor changes across the 2003.5 spectroscopic minimum. They confirmed that the wind lines seen by scattered starlight in the center of the foreground lobe, labeled FOS4 in Figure 2 showed higher terminal wind velocities. They also noted that the wind profiles seen directly in line of sight and scattered off the foreground lobe included temporal bumps and wiggles that were not easily explained by a single wind that varied uniformly by latitude.

The highest angular resolution currently possible is with the VLTI/AMBER at 2 microns at 4 mas and 1500 or 12,000 resolving power (Weigelt et al., 2007). Comparison of the hydrogen Bγ and He I 2.06μ line profiles and visibilities with continuum visibilities led to a model wind structure in the shape of a prolate spheroid with major axis aligned with the bipolar axis. The dominant source of continuum in the infrared is the extended primary, thought to be at least 200 times brighter at those wavelengths that the secondary, which, if a normal O or WN star, dominates in the FUV. Current VLT/AMBER measures place an upper limit of the secondary at 1/50th the flux of the primary.

AMBER measures a FWHM continuum diameter of 4.2 mas (10 AU at 2300 pcs). The wind line FWHM diameters are 6.5 mas for the He I 20.6 μ and 9.6 mas for the H Brγ line, consistent with the more extended optical depth of line transitions and decreasing excitation requirements. The He I line profiles originate from singlet and triplet levels requiring much higher temperatures and/or excitation/ionizing photons that does the H Brγ transition. One peculiar aspect was that the He I profile, most noticeably the absorption component was measured to be blue shifted by several hundred km/s relative to the H I profile.

The HST/STIS medium dispersion, long slit spectra (0.1" angular resolution with R=8000) recorded from 1998.0 to 2004.3 across the 2003.5 minimum provides insight to the velocity shift.

(Nielsen, et al., 2007). The model, discussed by Nielsen, 2007 suggests that while the H I wind lines, along with Fe II wind lines, originate from the overall wind, dominated by the massive, cooler primary wind, the He I wind line originates in the wall of the cavity carved out of the primary wind by the less massive, energetic secondary wind. However, the FUV radiation from the hot secondary penetrates the wall for a significant distance into the primary wind. The blue-shifted He I profile indicates that the secondary star, in the highly elliptical orbit, spends most of the orbit on the near side of the primary.

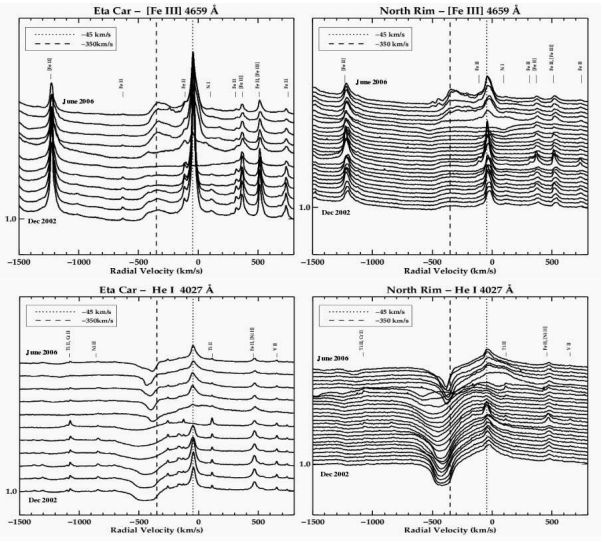

Figure 3: VLT/UVES line profiles recorded from December 2002 through June 2006 (K. Weis, PI). Top row: [Fe III] 4659Å. Bottom row: He I 4027Å. Left: Line profiles direct from of Eta Carinae. Right: Line profiles scattered off of the northern rim. Both [Fe III] and He I emission disappear during the 2003.5 minimum.

We learn much about the wind interaction by probing the scattered starlight at different positions across the Homunculus. The wall of the foreground lobe, in line of sight, registers strong absorption lines at −513 km/s (Gull et al., 2005). We have identified over two thousand metal and molecular absorption lines in the STIS UV ($\delta\theta$ ≈.06", R≈110,000) and VLT/UVES ($\delta\theta$ ≈1-2", R≈80,000) spectra. Many of these lines, while smeared out in the center of the lobe are still observed in the rim structures.

We compare windline profiles in line of sight and scattered off the northern rim (Figure 3). He I and [Fe III] lines originate from two very different regions: He I from the wind-wind interaction region as discussed above and [Fe III] from the outer, lower density regions, photo-excited by the FUV emission of the secondary star. Careful examination of the two sets of spectra indicates that 1) the narrow emission component of [Fe III] is much weaker in the view seen from the northern rim and 2) the He I absorption is significantly more robust in the northern rim view compared to direct line of sight.

3 Discussion & Conclusions

The wind line profiles are very different when viewed at different angles due to the extended, veiling wind-wind interaction. The wind line profiles change with time, primarily due to binary orbital motion and their interacting winds. However irregular features appear and disappear at shorter intervals. Some may be due to long term changes of the wind opacity, but much is likely due to clumping within the massive winds. With appropriate angular and spectral resolutions, the opportunity is available to get information leading to that a 3-D image of the near side wind structure. Data from these instruments provide very complimentary information that will lead not only to gross properties of the winds but also of the massive clumps ejected during major outbursts.

We thank our many collaborators who share in this major ongoing study. Funding was provided through the Hubble Space Telescope Project.

References

Corcoran, M. 2005, AJ, 129, 2018

Damineli, A. 1996, ApJ, 460, L49

Davidson, K, & Humphreys, R. 1997, ARAA, 35, 1

Davidson et al., 2005, AJ, 129, 900

Gull, T., et al., 2005, ApJ, 620, 442

Ishibashi, K, et al. 2003 AJ 125, 3222

Meynet, G. & Maeder, A., 2003, A&A, 404, 975

Nielsen, K. 2007, this volume

Nielsen, K., et al. 2007, ApJ, 660, 669

Smith et al. 2003a, AJ 125, 1458

Smith et al. 2003b, ApJ, 586, 432

Smith, N., & Owocki, S. 2006, ApJ, 645, L45

Stahl, O. et al., 2005, A&A, 435, 303

Verner, E., et al. 2002 ApJ, 581, 1154

Verner, E., et al. 2005, ApJ, 624, 973

Weigelt, G., & Ebersberger, J., 1986, A&A 163, L5

Weigelt, G. et al., 2007 A&A, 464, 87

Weis, K. et al., 2005, AJ, 129,1694

Weis, K. 2007, this volume

Cassinelli: You have been discussing the disk wind. Is this related to the "extended skirt" seen off to the side of Homunculus?

Weis: Across the skirt there is low energy X-ray emission.

Gull: The [Fe III], [Ar III], [S III], [Ne III] emission appears to come from the interior disk edge, but this region is photoionized by the hot secondary companion.

de Koter: You showed that you probed the iron lines on many positions in the Homunculus, also quite far out. Do you have any information on the abundances of iron? This may be very important in better understanding the dust formation (or subsequent destruction/re-formation).

Gull: Hillier's models of the primary star assume normal abundances. As to nebular abundances, Verner et al. (2001,2003) demonstrate He/H $\sim$ 1, N/O, N/C $\sim$ 100. In the line of sight, the Homunculus shows Ti/Ni, etc. to be large. The metal-ionized nebula (Sr-Filament) has Ti/Ni $\sim$ 80 solar and Cr/Ni $\sim$ 20 solar. We suspect these strange abundance ratios to be caused by low C, O abundances leading to many metals, ordinarily formed as oxides and precipitated on dust grains, to be trapped in the gaseous phase. Ti, V, Sc, Sr, Y have been identifed in emission in the Sr filament and in absorption at -513 km/s in line of sight (Homunculus).

Moffat: I really admire your and others' work! But we will not understand what is going on until we actually resolve and track (spatially or spectroscopically) both stars. One clearly needs high spatial resolution and the "right" spectral window.

Gull: Gerd Weigelt and team place an upper limit to the secondary of 1/50 of the primary. Models suggest an O star would be 1/200. Recent improvements in VLTI/AMBER with the auxiliary telescopes should reach to 1/300. In the UV, FUSE observations do detect flux that disappears during the minimum (Iping et al. 2005), but foreground absorption and wind scattering prevents wind line identification.

Clumping in Hot Star Winds
W.-R. Hamann, A. Feldmeier & L.M. Oskinova, eds.
Potsdam: Univ.-Verl., 2008
URN: http://nbn-resolving.de/urn:nbn:de:kobv:517-opus-13981

On irregular line profiles in the optical spectrum of Eta Carinae

K.E. Nielsen
Catholic University of America, Washington DC 20064, United States &
NASA Goddard Space Flight Center, Code 667, Greenbelt MD 20771, United States

The optical spectrum of Eta Carinae (η Car) is prominent in H I, He I and Fe II wind lines, all of which vary both in absorption and emission with phase. The phase dependance is a consequence of the interaction between the two objects in the η Car binary (η Car A & B). The binary system is enshrouded by ejecta from previous mass ejection events and consequently, η Car B is not directly observable. We have traced the He I lines over η Car's spectroscopic period, using *HST*/STIS data obtained with medium spectral, but high angular, resolving power, and created a radial velocity curve for the system. The He I lines are formed in the core of the system, and appear to be a composite of multiple features formed in spatially separated regions. The sources of their irregular line profiles are still not fully understood, but can be attributed to emission/absorption near the wind-wind interface and/or a direct consequence of the η Car A's, massive, clumpy wind.

This paper will discuss the spectral variability, the narrow emission structure of the He I lines and how clumpiness of the winds may impede the construction of the reliable radial velocity curve, necessary for characterizations of especially η Car B.

1 Introduction

Eta Carinae (η Car) provides a unique opportunity to investigate a massive star in a late evolutionary phase and how CNO processed material is ejected into the ISM. Investigation of the material surrounding η Car is reported to show similar characteristics as Gamma Ray Burst progenitors (Prochaska et al. 2006). Consequently, investigating η Car may provide clues about other extreme objects such as hypernovae and supernova impostors.

Most observations up through the mid-1990s could be interpreted as arising from either a single star or binary system (Davidson 1997). Current consensus favors the binary scenario. However, little is directly known about the companion star. Many indirect signatures of η Car B are observed in the form of periodic behavior.Two X-ray cycles, each characterized by a gradual increase in brightness just before a rapid decline to a low-state, were observed with the *RXTE* and fine-tuned η Car's spectroscopic period to 5.54 yr (Corcoran 2005). The Weigelt condensations follows the 5.54 yr period with emission lines from ionized spectra, such as [Ar III] and [Fe IV], disappearing during the spectroscopic low-state. While the flux of the primary star with $T_{\rm eff}\sim$15,000 K is sufficient to excite the Weigelt condensations during the spectroscopic low-state (Verner et al. 2002), the flux of an O or WN star with $T_{\rm eff}\sim$35,000 K is needed to excite the Weigelt blobs during the rest of the period (Verner et al. 2005).

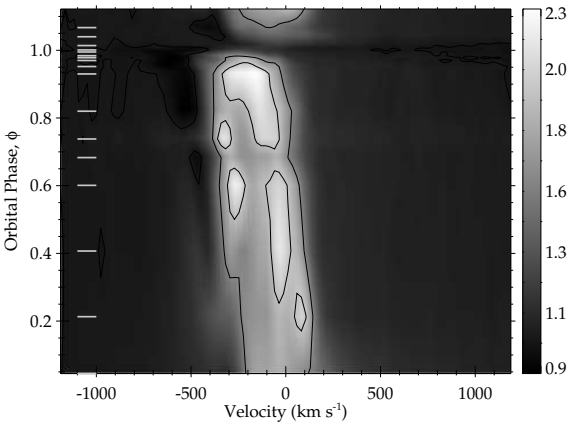

Figure 1: Surface plot for He I λ7067. The line profile's variation with phase is presented with intensity ranging from black to white with increasing line emission. All spectra used in the figure are normalized to the flux level at -1200 km s^{-1}. The observed phases are marked to the left in the figure. Note the structure of the emission at, especially, ϕ=0.6.

Unfortunately, η Car is enshrouded in multiple ab-

sorption shells (Gull et al. 2005), associated with the Homunculus and the Little Homunculus, which prevent direct observations of the radiation source in the core of the nebula including η Car A and its hot companion. A hot companion star can usually be detected at short wavelengths. However, the spectrum obtained with *FUSE* (905−1175 Å) is severely blanketed by iron-group resonance and strong interstellar molecular hydrogen absorption. Iping et al. (2005) found potential signatures in the *FUSE* spectrum of a companion star that disappeared just before the X-ray declined in 2003.5, and reappeared after the X-ray low-state. The *FUSE* spectrum does, however, not provide much information about the nature of η Car B. The medium resolution *HST* STIS E140M/E230M spectra (1140−2360 Å) are dominated by ejecta absorption, especially, in the iron-group elements and H_2 in the Homunculus (Nielsen et al. 2005). Longward of 2500 Å the line density decreases and wind lines are easier to identify and analyze. For this analysis we use velocity and intensity variation of spectral features, in the optical wavelength region, formed in the wind-wind interface region between the two massive stars as a proxy for the orbital motion. The data used in this analysis are high angular, medium spectral, resolution *HST*/STIS CCD spectra.

2 Analysis

The He I lines are dramatically blue-shifted with respect to the system velocity over the entire cycle. Their excitation, peculiar line profiles and velocity variation over the spectroscopic period (Fig. 1) suggest that the He I lines are formed in the vicinity of the wind-wind interface region. Consequently, by tracing these lines we can obtain information regarding the orbital parameters of the system including the mass ratio of the objects. The He I lines appear to be a composite of a weak broad P-Cygni wind line, likely formed in η Car A's wind, with narrow emission components superposed on top. The narrow components are likely from spatially separated regions, for example along the two arms of the bow-shock cone. The origin of the He I emission lines is easier to confine to the interface region than the absorption, and would be preferred for deriving a radial velocity curve. However, the complexity of the narrow He I emission, both regarding line profile and number of narrow components, makes the measurements of the radial velocities difficult and inaccurate. The He I absorption is fairly well behaved, easier to measure, and was therefore used to constructed the radial velocity curve (Fig. 2). The velocities were measured through line profile fitting where the absorption and emission were assumed to be decoupled, i.e. originating from different parts of the nebula.

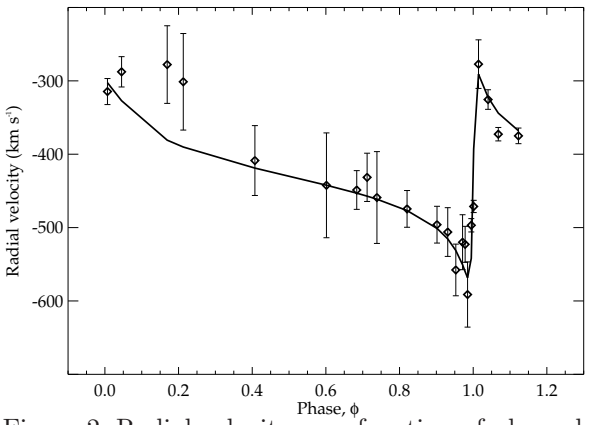

Figure 2: Radial velocity as a function of phase derived from the He I absorption. Solid curve: fit to the data using an eccentricity, e=0.90, velocity amplitude, K=140 km s^{-1} and system absorption velocity, γ=−430 km s^{-1}. The error bars represent estimated uncertainty of the individual fits.

The radial velocity curve is similar to one for a standard binary system, however, the derived parameters from this particular fit, are difficult to interpret. The width of the He I absorption components and their blue-shifts just before periastron indicate that the velocity variations are caused by the motion of η Car A. However, the large velocity amplitude over periastron imply that we are tracing the least massive star of the system. η Car A is more luminous and, therefore, assumed to be the more massive star. The radial velocities are clearly difficult to attribute to the motion of one of the objects alone. The measured velocity are likely the sum of the orbital motion of η Car A and the velocity of the part of η Car A's wind that is ionized by the hot η Car B. To understand how the radiation from η Car B alters the derived radial velocity curve, detailed modeling of the ionization structure in the central parts of the system is required, but even then it is difficult to correct the radial velocities for the ionization in line-of-sight. An accurate radial velocity curve is necessary to derive the relation between the masses, but an alternative method to derive it is necessary. The measurements and the radial velocity curve are discussed in detail in Nielsen et al. (2007).

3 The Next Step

Most of the winds lines in the optical spectrum show asymmetric line profiles with narrow peaks. These profiles are difficult to explain with a spherical symmetric wind model. Their line structure may be caused by a clumpy wind or additional emission

from the surrounding nebula in lines-of-sight. The He I lines distinguish themselves from the rest of the wind lines with a larger blue-shift and a much greater velocity amplitude at periastron, indicating that the lines are formed very close to central part of the system (<100 AU). Other observed wind lines can be used to investigate the ionization structure of η Car A's wind. These lines are also used as a comparison to the spectral characteristics in He I. The H I lines are assumed to be formed in a large portion of the primary wind. As demonstrated by Damineli et al. (2000), H I shows spectral variations over the 5.54 yr spectroscopic period but with a smaller velocity amplitude than He I. While H I and Fe II show similar characteristics as the He I lines, they are strongly dominated by the primary stellar wind extending ∼1000 AU from η Car (Hillier at al. 2006). Line profiles in Fe II transitions vary considerably due to local physical conditions and population of lower upper energy levels. The intensity variation over the spectroscopic period is likely due to the variation in Balmer continuum from the central source, causing a population shift within Fe^{+}.

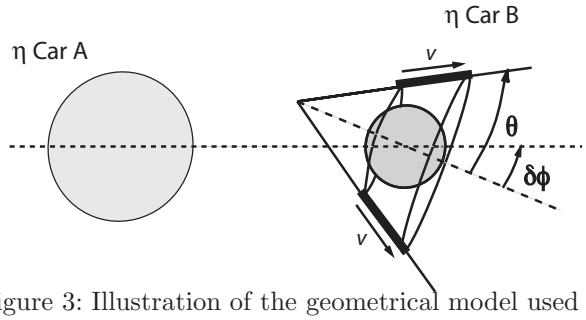

Figure 3: Illustration of the geometrical model used to derive orbital parameters for WR 42 and WR 48. v is the flow velocity along the shock-cone, θ the half-opening angle and $\delta\phi$ is the deviation due to the Coriolis force. The two measurable quantities: the full-width, fw, and the radial velocity, rv, are related to the orbital parameters as $fw = c_1 + 2v \sin\theta \sqrt{1 - \sin^2 i \cos^2(\phi - \delta\phi)}$ and $rv = c_2 + v \cos\theta \sin i \cos(\phi - \delta\phi)$, respectively, where i is the inclination, ϕ is the orbital phase and c_1, c_2 are constants.

Analysis of the Fe II and H I line profiles will provide valuable information about the excitation conditions in η Car A's wind and the influence by η Car B.

We are confident that the He I emission is formed in the vicinity of the wind-wind interface region. If the lines are formed along the bow-shock then they are dependent on temperature and density along the bow-shock and the momentum ratio of the two objects. The bow-shock can be approximated by a cone (see Fig. 3) with the emission originating at some distance from the apex of the cone. The observed spectrum would be a sum of the emission from the spatially separated arms of the interface region, which would give a double peaked emission feature. Emission features like this have previously been observed in WR star spectrum and have been modeled with simple geometrical models. The model developed by Lührs (1997) can be applied to the narrow components observed in the He I emission profiles to produce a radial velocity curve. This method has a successfully been used in other massive binaries such as WR 42 and WR 48 (Hill et al. 2002).

The next step in our analysis will be to model the He I emission components in a similar way as earlier has been done for the WR spectra. This would provide a radial velocity curve that would be easier to interpret, than the corresponding curve for absorption, and would provide the necessary tool to estimate the mass ratio of the two objects, but also constrain the orbital parameters.

We thank our many collaborators, especially John Hillier (U. Pittsburgh), Ted Gull, Mike Corcoran and Kenji Hamaguchi (NASA GSFC), who share in this major ongoing study. Funding was provided through the *Hubble Space Telescope* Project.

References

Corcoran, M. F. 2005, AJ, 129, 2018

Damineli, A., et al. 2000, ApJL, 528, L101

Davidson, K. 1997, NewA, 2, 387

Gull, T. R., et al. 2005, ApJ, 620, 442

Hill, G. M., Moffat, A. F. J., & St-Louis, N. 2002, MNRAS, 335, 1069

Hillier, D. J., et al. 2006, ApJ, 642, 1098

Iping, R. C., et al. 2005, ApJL, 633, L37

Lührs, S. 1997, PASP, 109, 504

Nielsen, K. E., Gull, T. R., & Vieira Kober, G. 2005, ApJS, 157, 138

Nielsen, K. E., et al. 2007, ApJ, 660, 669

Prochaska, J. X., Chen, H.-W., & Bloom, J. S. 2006, ApJ, 648, 95

Verner, E. M., et al. 2002, ApJ, 581, 1154

Verner, E., Bruhweiler, F., & Gull, T. 2005, ApJ, 624, 973

Moffat: In other WR+O systems with WN component (e.g. V444 Cyg, CQ Cep, CX Cep) we do see blueshifted He I components (in addition to broad components) that vary around the orbit, arising when the curved bow shock passes across the line of sight.

Nielsen: We have, so far, not found a WR system where the absorption variations are comparable with what we see in the η Car spectrum. However, it is worth the effort to investigate this further.

Ignace: Can the variations in [Fe II] and [Fe III] lines be used with your He I data to resolve some of the radial velocity issues?

Nielsen: Likely, but not in a straightforward way, since the lines presumably are formed in different parts of the wind. The [Fe II] and [Fe III] lines will help us to understand the ionization structure of the winds, and especially the influence of the hot companion star.

Sonneborn: Could you explain again the interpretation of the very large negative radial velocity curve of η Car?

Nielsen: Since we are measuring radial velocities in the absorption component, we will get a significantly larger negative velocity compared with corresponding values derived with the emission component. The measured velocity is consistent with the terminal velocity for η Car A's wind.

Owocki: As I understand it, your "light curve" is not of a fixed object/star but of an outflowing wind that is tied, in some complex way, to an orbiting star. But now that we have 3D hydrodynamic simulations of the wind interaction, I think it should be possible to correct for the various dynamic and projection effects to derive an orbital solution for the wind's source.

Nielsen: Correct, we interpret the radial velocity curve as sum of the orbital motion of the primary star (η Car A) and the velocity of the absorbing part of the primary wind in the line of sight. The contribution of the latter is very difficult to derive, and new 3D hydrodynamic simulations will be a valuable tool for understanding how the hot companion influences the ionization structure in the central parts of the system. However, one concern may be that the 3D simulations include too many "unknowns", especially since we have very little information about the geometry of the bow shock.

Hillier: Augusto Damineli has a paper in preparation which discusses ground-based optical data obtained through the last two cycles. There are differences in the time behavior of lines throughout the 5.5 year cycle, and particularly around periastron. These variations tell us much about the interaction between the companion star and η Carinae and the circumstellar material. Additional comment: the major difficulty in interpreting the radial velocity light curve is that the orbit is highly eccentric. As a consequence there are complicated changes in the bow shock structure around periastron, as nicely illustrated by the movie of Atsuo Okazaki shown by Ted Gull. Unfortunately this (i.e. periastron) is where most of the radial velocity changes occur.

Clumping in Hot Star Winds
W.-R. Hamann, A. Feldmeier & L.M. Oskinova, eds.
Potsdam: Univ.-Verl., 2008
URN: http://nbn-resolving.de/urn:nbn:de:kobv:517-opus-13981

Wind relics: clumps, inhomogeneities and outflows in LBV nebulae

K. Weis
Astronomisches Institut, Ruhr-Universität Bochum, Germany
Lise-Meitner fellow

The most massive stars are those with the shortest but most active life. One group of massive stars, the *Luminous Blue Variables (LBVs)*, of which only a few objects are known, are in particular of interest concerning the stability of stars. They have a high mass loss rate and are close to being instable. This is even more likely as rotation becomes an important factor in stellar evolution of these stars. Through massive stellar winds and sometimes giant eruptions, LBV nebulae are formed. Various aspects in the evolution in the LBV phase lead, beside the large scale morphological and kinematical differences, to a diversity of small structures like clumps, rims, and outflows in these nebulae.

1 A primer to LBVs and LBV nebulae

All massive evolved stars do have a certain potential to enter the LBV phase. Initial mass, metalicity, strength and structure of the stellar wind, and in particular stellar rotation seem to impact the star's evolution and therefore its passage through an LBV phase see, cf. Meynet & Maeder (2005) and Meynet et al. (2007). Models with rotation of 300 km/s show that stars with masses even as low as about 20 $M_\odot$ (for Z=0.02) may encounter the LBV phase (40 $M_\odot$ without rotation). In contrast, these models also show that rotating star with very high mass will totally skip the LBV phase and directly enter the Wolf-Rayet phase. LBVs—as the name indicates—are characterized being luminous (blue) stars, and posses photometric as well as spectral variabilities with various amplitudes (both in time and brightness). A variability intrinsic to LBVs, is the S Dor variability. Depending on the direction of its evolution the star gradually brightens in the V band by up to 3^{mag} in roughly 10 years, as the spectrum changes from a hot O-B to a cooler A-F star. It dims on its return to the hot phase. The Balmer lines are seen in emission (P Cygni profiles), during the hot phase He I and He II lines pop up too. LBVs do have a high mass loss rate and may undergo giant eruptions, likely due to their closeness to the Eddington/break-up limit. This predestinates the formation of LBV nebulae.

LBV nebulae formed through the continuous stellar winds (mixed with swept-up ISM) and eruption in which larger amounts of mass are carried away in a more instant event. LBV nebulae can be identified through the presence of CNO processed material, e.g. more nitrogen. The abundances are enhanced even more, if the star rotates and material from deeper layers is mixed up and peeled off. Expansion velocities and morphologies are manifold. For a more comprehensive description the reader is refereed to e.g. van Genderen (2001), Weis (2001, 2003) and references therein. Here only a short description and summary of the basic parameters of LBV nebula, e.g. their morphology and kinematics is given. Fig. 1 already visualizes the manifold of morphologies and sizes of the majority of known and resolved LBV nebulae. The images are either taken with Hα and/or [N II] filters and F656N or F658N filters for the HST images (S119, R127, S61, R143, η Car, AG Car, HD 168625). The Pistol star was observed with the NICMOS F187N filter (Brγ). All images are drawn to scale. There is a small tendency that the LMC LBVs are larger in size compared to their Galactic mates, see also Weis (2003). From pure morphological aspects 5 (38%) of the LBVs show indications for a bipolar structure. The expansion velocities for LBV nebulae, excluding η Car, generally range between 20-100 km/s, a few are as high as 150-170 km/s (P Cygni, HR Car). η Car is an exceptional case with an expansion velocity of roughly 600 km/s for the Homunculus and the outer ejecta escaping with up to 2500 km/s, giving rise to X-ray emission, see Weis et al. (2004). Kinematic analyses add R127 and WRA 751 to the list of nebulae which posses bipolar structures (the caps) to some degree. The current, obviously poor statistics yields about 50% of the nebulae having indications for bipolar structures, about 40% are roughly spherical and 10% (1 object=R143) is irregular. On smaller scales the nebulae are highly complex, and their characteristics depend even more on the history of stellar winds, the interstellar surrounding, stellar rotation and instabilities.

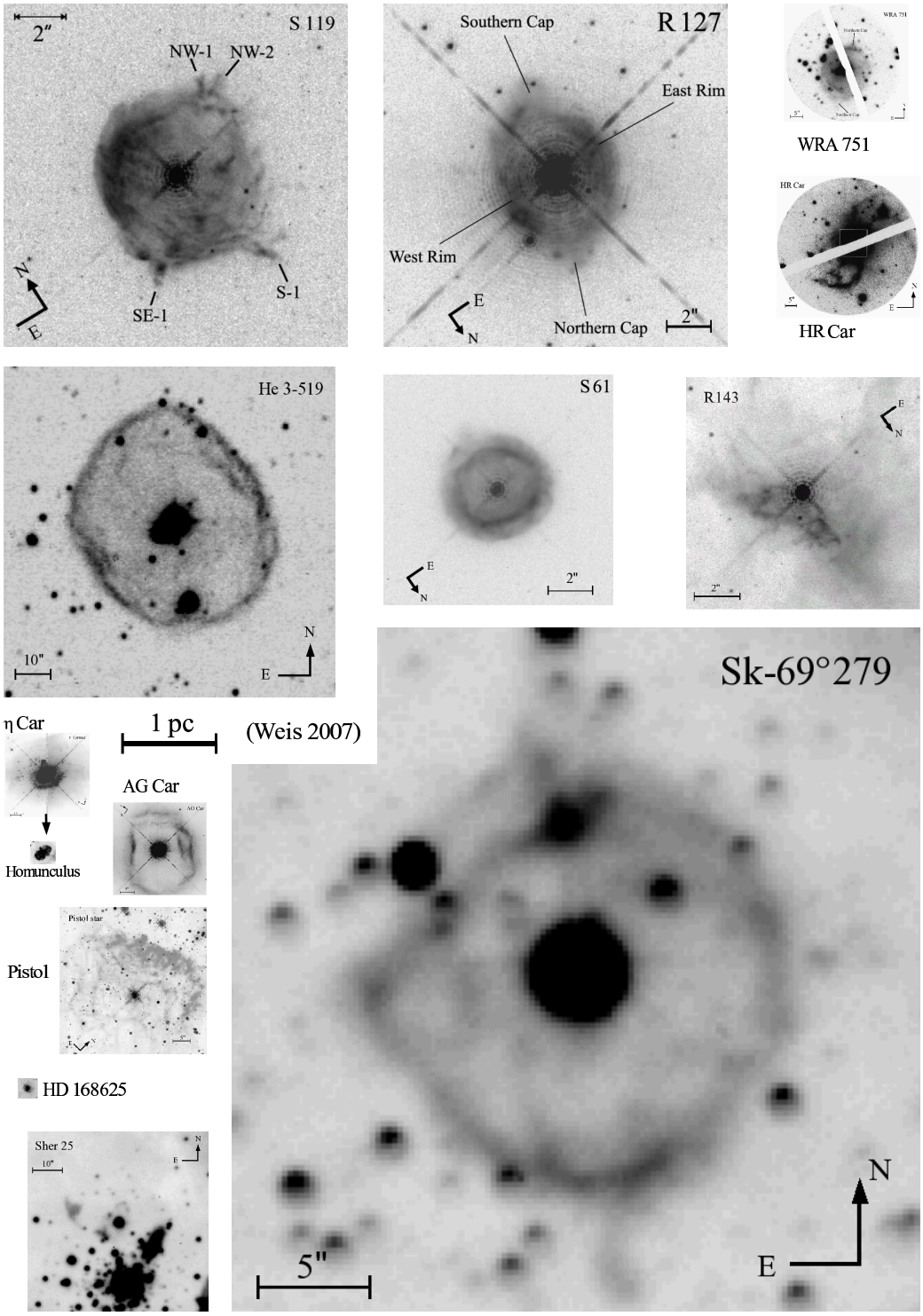

Figure 1: LBV nebulae drawn to scale. Sk-69 279: Weis et al. (1997); Pistol: Figer et al. (1999); WRA 751: Weis (2000); S119: Weis et al. (2003); S61, R127, R143: 2003; η Car, HR Car, HD 1682625, AG Car, Sher 25: Weis(2001); He 3-519: (Weis 2007, in prep)

2 Nebulae as imprints of stellar and interstellar parameters

During the LBV phase several parameters will influence the final—the currently observed—structure and properties of the nebula. The most obvious are discussed here.

WIND. Being formed by stellar winds the properties of the winds are among the most important that determine the shape and kinematics of LBV nebulae. The wind during the star's main sequence phase already pre-structures the environment and can lead to the formation of bubbles with lower density. This bubble expands and already sweeps up ISM around the star. Several such bubbles might merge and even enclose whole OB associations. In the evolved phase the characteristics of the stellar wind changes back and forth between fast and slow wind velocities, high and low mass loss rates, and last but not least higher and lower fractions of clumpiness. By compression, material from the different wind phases (and eruptions) forms the LBV nebula, uniform or already fragmented. Different wind phases could be for instance be the explanation for the shape of the nebula around S61 (see Fig.1). Diffuse less dense material possibly from an earlier faster wind phase is found outside the brighter ring.

ISM. Staring right from the formation, a massive star's stellar wind will impact the ISM. The ISM is different in e.g. density for each birth cloud. In this way the surrounding of a star evolving into an LBV is individual. The combination of the initial structure of the ISM and influence of stellar wind forms bubble of different sizes, different densities, density gradients, clumps etc. During the formation process, therefore the ISM surrounding the LBV, shapes the nebula. The image of S119 is an example of a density gradient, with denser material detected in the (north-)east, leading to a more compressed rim of the LBV nebula on this side.

ROTATION. In recent years the in-cooperation of rotation in stellar models has changed our picture of the stellar evolution, in particular concerning instabilities, mass loss and the lifetime spend in different phases. The most massive stars are therefore even more likely to reach break up, and according to the models may not enter the LBV phase at all. More importantly rotation also influences the 3D topology of the wind and consequently the nebula. It seems natural to connect the presence of bipolar LBV nebulae η Car, HR Car, or Sher 25 with the fact that rotation does play an important role for the evolution and winds of massive stars.

INSTABILITIES/OUTFLOWS. Nebulae are very likely to encounter instabilities. This will sometimes lead to the disintegration of the confining shell structure and can even give rise to outflow of material. From a hydrodynamic perspective the nebulae are subject to Rayleigh-Taylor and Vishniac instabilities. In the first case due to an external density gradient fragments of the nebula shell are left behind as the less dense interior expands out. Spike like structure form and material is torn outwards by the wind. An example for such an instability seem the filamentary structures of the Pistol nebula. In Vishniac instabilities, an expanding shell with an already intrinsic density contrast expanding into an uniform medium, enhances the density contrast (clumpiness) as ram pressure and thermal pressure are not perpendicular to each other. Sheer forces therefore lead the clumps grow even further. Small subclumps in the nebula around S119 (towards the north and south) are an example for such a process.

3 Summary: What's wind got to do with it?

Analyzing various aspects of LBV nebulae provides an additional tool to obtain information about stellar parameters. The nebulae manifest relics of the star's wind (former envelope) and are therefore sensitive to wind properties like density, abundances, velocity, clumpiness and asymmetry.

References

Figer, D.F., Morris, M., Geballe, T.R., Rich, R.M., Serabyn, E., McLean, I.S., Puetter, R.C., & Yahil, A. 1999, ApJ, 525, 759

van Genderen, A.M. 2001 A&A 366, 508

Meynet, G., & Maeder, A. 2005, A&A 429, 581

Meynet, G., Eggenberger, P., & Maeder, A. 2007, IAU Sym 241, (astro-ph/0702515v1)

Weis, K. 2000, A&A, 357, 938

Weis, K. 2001, Reviews in Modern Astronomy 14, 261, (astro-ph/0104214)

Weis K. 2003, A&A, 408, 205

Weis, K., Chu, Y.-H., Duschl, W.J., Bomans, D.J. 1997 A&A 325, 1157

Weis, K., Duschl, W.J., & Bomans, D.J. 2003, A&A, 398, 1041

Weis, K., Corcoran, M. F., Bomans, D. J., & Davidson, K. 2004, A&A, 415, 595

Cassinelli: Some of the LBV nebulae appear like shocked shells, like one would get from fast with slow wind interactions. Do you have X-ray information?

Weis: Only for a few LBVs X-ray measurements have been made. From the low expansion velocities ($20-90\,\mathrm{km/s}$) except in η Car a shock in X-rays is not expected.

Cassinelli: X-rays from wind/ISM?

Gull: The Homunculus interacts with the residual wind. Indeed weak shocks are seen in Hα, [N II], [S II], but too weak that X-rays are detected.

Owocki: I really like your comparison to LBV nebulae at fixed spatial scale, which makes η Car look small and insignificant. But of course the reason is that we are lucky to see η Car at a relatively young phase, when the nebula from outburst has not expanded much. This implies, if ever we want to find other η Car analogs, we need to think of what η Car would look like thousand years from now.

Clumping in Hot Star Winds
W.-R. Hamann, A. Feldmeier & L.M. Oskinova, eds.
Potsdam: Univ.-Verl., 2008
URN: http://nbn-resolving.de/urn:nbn:de:kobv:517-opus-13981

Clumping effects on non-thermal particle spectra in massive star systems

A. Reimer
W. W. Hansen Experimental Physics Laboratory & Kavli Institute for Particle Astrophysics & Cosmology, Stanford University, 452 Lomita Mall, Stanford, CA 94305, USA

Observational evidence exists that winds of massive stars are clumped. Many massive star systems are known as non-thermal particle production sites, as indicated by their synchrotron emission in the radio band. As a consequence they are also considered as candidate sites for non-thermal high-energy photon production up to gamma-ray energies. The present work considers the effects of wind clumpiness expected on the emitting relativistic particle spectrum in colliding wind systems, built up from the pool of thermal wind particles through diffusive particle acceleration, and taking into account inverse Compton and synchrotron losses. In comparison to a homogeneous wind, a clumpy wind causes flux variations of the emitting particle spectrum when the clump enters the wind collision region. It is found that the spectral features associated with this variability moves temporally from low to high energy bands with the time shift between any two spectral bands being dependent on clump size, filling factor, and the energy-dependence of particle energy gains and losses.

1 Introduction

Evidence for particle acceleration to relativistic energies mediated by the supersonic winds of massive, hot stars comes from the observation of non-thermal radio emission (e.g., Abbott et al. 1986). This has been interpreted by synchrotron emission on the basis of the measured spectra (much steeper than the canonical value $\alpha_r \sim +0.6$, $F_\nu \propto \nu^{\alpha_r}$) and high brightness temperatures of $\sim 10^{6-7}$K, far exceeding $\sim 10^4$K expected from free-free emission from a steady-state isothermal radially symmetric wind (Wright & Barlow 1975). Those particles has been suggested to be accelerated either in shocks caused by the instability of radiatively driven winds (White 1985), in the shocked wind collision region of multiple systems (e.g., Eichler & Usov 1993) or in the termination shock (Völk & Forman 1982).

Through a statistical study the presence of non-thermal radio emission has been linked to the binarity status of the stellar systems (Dougherty & Williams 2000), which is in support of a scenario where particles being predominantly accelerated at the forward and reverse shocks from the colliding supersonic winds from massive stars. Therefore, in this work I am considering the non-thermal particle spectra from being produced in the collision region of a typical long-period massive binary system.

By now ample evidence has accumulated that hint towards the clumpiness of WR- and O-star winds: non-converging mass loss rates from various methods (thermal radio, H_α, UV-lines, X-ray and IR diagnostics, etc.), polarization and photometric variability, stochastically variable substructures in lines (e.g., Eversberg et al. 1998), the observation of non-thermal radio emission even in some short period binaries (e.g., CygOB2#8A: Blomme 2005) where self-absorption in the optically thick winds should prevent the visibility of a non-thermal component, etc. Still open, however, remains a qualitative assessment about the filling factors, typical clump sizes, clumping startification, etc.

2 Emitting electron spectrum

This work considers, for the first time, the effect of clumpiness in the colliding winds of binary systems on the resulting non-thermal electron spectrum in the collision region at a given orbital phase, assuming that the particles to be accelerated stem from the pool of thermal wind particles. It requires a fully time-dependent treatment of particle injection, acceleration and losses.

For this purpose I describe diffusive particle acceleration and losses (radiatively, and via escape from the collision region with rate T_0^{-1}) that governs the non-thermal emitting electron spectrum, by the kinetic equation:

$$\frac{\partial}{\partial t}N(E,t)+\frac{\partial}{\partial E}\dot{E}\,N(E,t)+\frac{N(E,t)}{T_0}=Q(E,t) \quad (1)$$

where $\dot{E}=aE-\dot{E}_{\rm loss}$, the radiative energy loss rate $\dot{E}_{\rm loss}=(b_{\rm syn}+b_{\rm IC})E^2$ from synchrotron and inverse

Compton losses in the Thomson regime, the acceleration rate $a = \frac{V_{\rm OB}^2(c_r-1)}{3c_r\kappa_{\rm a}}$ (Reimer et al. 2006) with c_r the shock compression ratio, and $\kappa_{\rm a}$ the diffusion coefficient, $T_0 = \frac{r_0}{V}$ the escape time scale for a constant post-shock flow velocity V, and the size of the acceleration region, assumed cylinder-shaped for simplicity, with $r_0 = \kappa_{\rm a}/V$. In this picture the clumpiness of the wind translates into a variable injection rate $Q(E,t)$, while for a homogenuous wind $Q(E,t) \propto \delta(E-E_0)$.

In the following I consider the typical setting of a colliding wind region (see e.g., Eichler & Usov 1993) at a given orbital phase with a clumpy wind of volume filling factor $f_{\rm vol}$ defined as the total volume occupied by the clumps with respect to the total wind volume, $f_{\rm vol} = V_{\rm clump}/V_{\rm tot}$. The simplified picture of a constant particle density within the clump and no particles in the interclump medium used here is sufficient to expose the basic properties of variability in a non-thermal component from a clumpy wind. Furthermore, $f_{\rm vol}$ and $V_{\rm OB}$ shall be constant sufficiently close to the shock region.

$Q(E,t) = Q_0\delta(E-E_0)H(t-t_0)H(t_v-t)$ describes the particle injection into the shock region for a clump of size $l_{\rm clump} = V_{\rm OB}(t_v-t_0)$. The solution is analytic, and shown in Fig. 1 for $t_v \to \infty$. With the spectral index s of the emitting electron spectrum, $\propto E^{-s}$, determined by the acceleration rate and escape, the exponential built-up of the electron spectrum up to a maximum energy $E_c = a/(b_{\rm syn}+b_{\rm IC})$ (see Fig. 2, solid line) is governed by both, energy gains and losses. Steady-state is reached on hours time scale in the typical settings of the colliding wind region in long-period binary systems.

The interclump phase is described by $Q(E,t) \propto E^{-s}\delta(t-t_v)$ as the source term in Eq. 1. For $a > 0$ in this phase the solution of Eq. 1 implies a continued acceleration with the maximum electron energy increasing further exponentially (see Fig. 2, dashed line): the particle acceleration appears as a multi- (here: two)-stage process. For $a = 0$ further acceleration ceases and the emitting electron spectrum declines on typically hour times scales in the astrophysical environment considered here. Variations of the acceleration rate a may be plausible considering that possible variations of the shock conditions (e.g. compression ratio, etc.) as the clumpy winds collide re not unexpected.

Combining injection and interclump phases and taking into account past clump injections into the shock results in a temporally evolving electron spectrum in the wind collision region. An example for $l_{\rm clump} = 10^{12}$cm is shown in Fig. 3. Clearly visible are the spectral features from injection phases, and they propagate from low to high energies as time progresses. Thus the flux variations from clumpy particle injections into the acceleration process in the shock at low energies are anticipated to precede the flux variations at high energies. Ultimately, the underlying physical reason for this time shift is the unavoidable energy dependence of the radiative particle energy losses, and their gains in the acceleration process. In addition to the clump size and volume filling factor, the expected time shift is therefore dependent on the electron energy losses and gains.

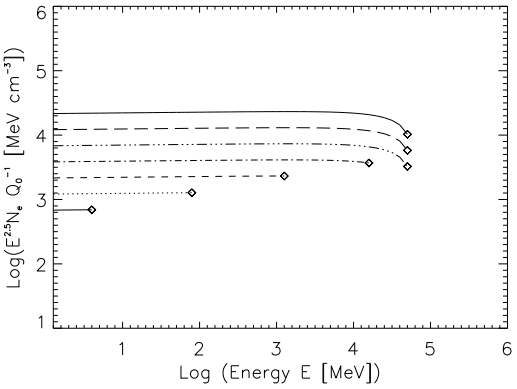

Figure 1: Injection phase: Resulting emitting electron spectrum at times 1, 3, 5, 7, 10, 15 and 20 ksec (correspondingly, lower to upper lines) after $t_0 = 0$ in response to injecting particles into the acceleration process starting at t_0. Parameters used for all figures presented in this work: bolometric luminosity $L_{\rm OB} = 10^6 L_\odot$ and effective temperature $T_{\rm eff} = 45000$K of the star closer to the stagnation point, terminal wind velocities $V_{\rm WR} = V_{\rm OB} = 2000$km/s, mass loss rates of the OB, $\dot{M}_{\rm OB} = 10^{-6}M_\odot$/yr, and WR-star, $\dot{M}_{\rm WR} = 10^{-5}M_\odot$/yr, constant magnetic field in the shock region B=1 G, a stellar separation of $D = 5\cdot 10^{14}$cm, postshock flow velocity $V = 0.6V_{\rm OB}$, diffusion coefficient $\kappa_a = 10^{19}$cm^2/s, shock compression ratio $c_r = 4$ and $E_0 = 1$MeV. Steady-state is reached on hours time scale.

3 Discussion and Outlook

In this work consideration has been given to the effects on the non-thermal electron spectra, as produced in a diffusive shock acceleration process from the pool of thermal wind particles, when the massive star winds are clumped as they collide. In this case, the electron injection into the shock varies with time, dependent on the volume filling factor and typical clump size. Consequently, flux variations are expected in non-thermal particle and photon spectra,

in addition to the thermal emission component. I have shown that those flux variations are expected to appear time shifted when comparing various spectral bands, with the low energy flux variations preceding those at high energies. This clumping signature in non-thermal spectra probes wind clumping in the very vicinity of the collision region, and may possibly show up in multifrequency observations at energy bands that are dominated by non-thermal emission, provided sufficiently dense data sampling.

A metallicity dependence of clumping in non-thermal spectra may be probed by comparing clumping signatures from non-thermal ion spectra, appearing eventually in the gamma-ray domain only through π^0-decay photon emission, with those from non-thermal electron spectra. For this purpose we plan to apply the presented prescription to clumpy ion injections as well.

The presented scenario describes a simplified clumping picture, which nonetheless proves to be sufficient to expose the basic properties of a variable particle injection into the acceleration process in colliding wind regions. This general prescription allows to also account for more complex clumping configurations (e.g. density structure within clump and/or interclump medium, irregular nested clump sizes on various scales, etc.), by modifying the injection term $Q(E,t)$ accordingly.

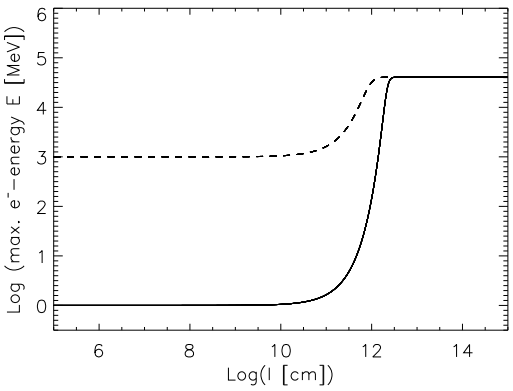

Figure 2: Exponential increase of maximum energy as a function of time with $l = V(t - t_0)$. During the clump injection phase the maximum energy reaches a level $\frac{1}{E_{\mathrm{max},1}(t)} = \frac{1}{E_c} - \left(\frac{1}{E_c} - \frac{1}{E_0}\right) \exp\left(-a\frac{l_{\mathrm{clump}}(t)}{V}\right)$ (solid line). During the interclump phase the maximum particle energy increases further if $a > 0$ as $\frac{1}{E_{\mathrm{max},2}(t)} = \frac{1}{E_c} + \left(\frac{1}{E_{\mathrm{max},1}} - \frac{1}{E_c}\right) \exp\left(-a\frac{l_{\mathrm{interclump}}(t)}{V}\right)$ (dashed line). $E_{\mathrm{max},1} = 10^3$ MeV and the rate of energy gain a =const at all phases is used here for demonstration.

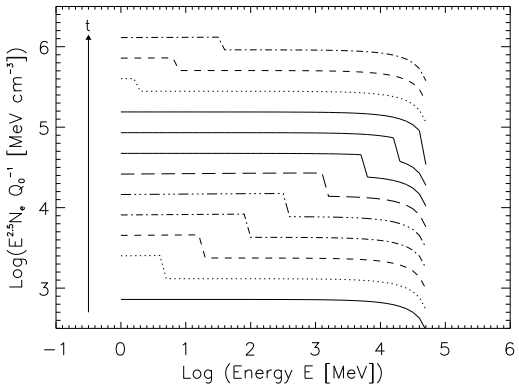

Figure 3: Temporal evolution of the total emitting electron spectrum in the wind collision region with clumpy particle injection and clump size $l_{\mathrm{clump}} = 10^{12}$cm. A temporal step size of Δt = 1ks is used. All spectra are separated artificially in normalization for optimal visibility. a =const at all phases is used here as an example.

References

Abbott, D.C., Bieging, J.H., Churchwell, E. & Torres, A.V. 1986, ApJ, 303, 239

Blomme, R. 2005, Proceedings of "Massive Stars and High-Energy Emission in OB Associations", Liége (Belgium), 2005, Eds. G. Rauw, Y. Nazé, R. Blomme, & E. Gosset, p. 45

Dougherty, S.M. & Williams, P.M. 2000, MNRAS, 319, 1005

Eichler, D. & Usov, V. 1993, ApJ, 402, 271

Eversberg, T., Lepine, S. & Moffat, A.F.J. 1998, ApJ, 494, 799

Reimer, A., Pohl, M. & Reimer, O. 2006, A&A, 644, 1118

Völk, H.J. & Forman, M. 1982, ApJ, 253, 188

White, R.L. 1985, ApJ, 289, 698

Wright, A.E. & Barlow, M.J. 1975, MNRAS, 170, 41

Moffat: Could you not use X-ray light curves of wind-wind collision systems to also probe the clump structure as it makes the X-ray flux flare up as clumps enter the bow shock?

A. Reimer: This should in principle be possible. However, please note that I considered only the non-thermal behaviour of the clumps when they enter the shock. Depending on the X-ray energy band the X-ray flux may however rather be dominated by the thermal hot gas. The resulting thermal spectra when the clumps enter the shock may show different properties than the non-thermal spectra I have been considering here in my talk.

Romero: Anita, can you specify a bit more the physical conditions you are assuming for the clumps? What is the clump density? What is the magnetic field inside the clumps?

A. Reimer: The clump density in my calculations of the non-thermal spectra from the wind-wind collision region as the clumps enter the shock is specified by the variable Q_0. Its value has been left open in the figures shown. The clump size with respect to the volume occupied by the interclump medium is defined via the volume filling factor $f = V_{\rm clump}/V_{\rm tot}$. I used $f = 0.2$ for the examples presented in the figures here. The magnetic field in my calculations is only relevant for the synchrotron losses in the shock region, and its value has been kept constant to 1G for the presented examples. I did not consider any possible interactions of a magnetic field in the clumps with the shock region when clumps enter the shock. This would require MHD calculations.

Clumping in Hot Star Winds
W.-R. Hamann, A. Feldmeier & L.M. Oskinova, eds.
Potsdam: Univ.-Verl., 2008
URN: http://nbn-resolving.de/urn:nbn:de:kobv:517-opus-13981

Using gamma-rays to probe the clumped structure of stellar winds

G.E. Romero[1,2], S.P. Owocki[3], A.T. Araudo[1,2], R. Townsend[3] & P. Benaglia[1,2]
[1]*Instituto Argentino de Radioastronomía, C.C.5, (1894) Villa Elisa, Buenos Aires, Argentina*
[2]*Facultad de Ciencias Astronómicas y Geofísicas, Universidad Nacional de La Plata, Paseo del Bosque, 1900 La Plata, Argentina*
[3]*Bartol Research Institute, University of Delaware, Newark, DE 19716, USA*

Gamma-rays can be produced by the interaction of a relativistic jet and the matter of the stellar wind in the subclass of massive X-ray binaries known as "microquasars". The relativistic jet is ejected from the surroundings of the compact object and interacts with cold protons from the stellar wind, producing pions that then quickly decay into gamma-rays. Since the resulting gamma-ray emissivity depends on the target density, the detection of rapid variability in microquasars with GLAST and the new generation of Cherenkov imaging arrays could be used to probe the clumped structure of the stellar wind. In particular, we show here that the relative fluctuation in gamma rays may scale with the square root of the ratio of porosity length to binary separation, $\sqrt{h/a}$, implying for example a ca. 10% variation in gamma ray emission for a quite moderate porosity, $h/a \sim 0.01$.

1 Introduction

High-energy gamma-rays can be produced in accreting black holes with relativistic jets, as shown by the recent detection of a high-energy flare in the classical X-ray binary Cygnus X-1 (Albert et al. 2007). In this type of system the primary object is a hot, massive star with a strong stellar wind, and the secondary is usually an accreting black hole. Since the jet propagates through the wind and the radiation field of the star, gamma-rays can be produced by inverse Compton scattering with the radiation and/or pion-decays from inelastic proton-proton collisions with the stellar wind. If the wind has a clumpy structure, then jet-clump interactions can produce rapid flares of gamma-rays which, if detected, could be used to probe the size, density, and velocity of wind inhomogeneties.

2 Gamma-ray emission from jet-clump interaction

The basic model for hadronic gamma-ray production in a microquasar with an homogeneous wind has been developed by Romero et al. (2003). The reader is referred to this paper for the basic formulae. In the case of a clumped wind, the situation is illustrated in Figure 1. The compact object is assumed to be in a circular orbit of radius a, the clump crosses the jet forming an angle Ψ with the center of the star, and the viewing angle is θ.

The spectral gamma-ray intensity (photons per unit of time per unit of energy-band) produced by the injection of relativistic protons in the clump is

$$I_\gamma(E_\gamma,\theta) = \int_V n(\vec{r'}) q_\gamma(\vec{r'}) d^3r' \,, \qquad (1)$$

where V is the interaction volume, $n(\vec{r'})$ is the clump density, and $q_\gamma(\vec{r'})$ is the gamma-ray emissivity, which depends on the proton spectrum and the interaction cross section. The spectral energy distribution is given by $L_\gamma^{\pi^0}(E_\gamma,\theta) = E_\gamma^2 I_\gamma(E_\gamma,\theta)$. Note that a change in the density of the target will be reflected in a variation of the gamma-ray luminosity. Figure 2 shows a 3D-plot of the evolution of the spectrum during the transit of a clump through the jet. For this specific calculation we have assumed the clump flow follows a typical β velocity law at an angle $\Psi = 5$ deg with the orbital plane, with a viewing angle of 45 deg. The clump density follow Gaussian profile with peak at $\sim 10^{13}$ cm^{-3} and a width of 0.01 $R_\star$. The primary star is assumed to be similar to the primary in Cygnus X-1. The fraction of the accretion power that goes to relativistic protons in the jet is 10^{-3}.

From Fig. 2 we see that a gamma-ray flare with a power-law spectrum and a luminosity of $\sim 10^{35}$ erg s^{-1} at 1 GeV is produced by the interaction. The flare duration is set by the clump crossing time, which here is a few hundred seconds. For clumps interacting at higher altitudes above the black hole, longer timescales are possible, but the luminosity de-

creases since the jet expands and hence the proton flux decreases.

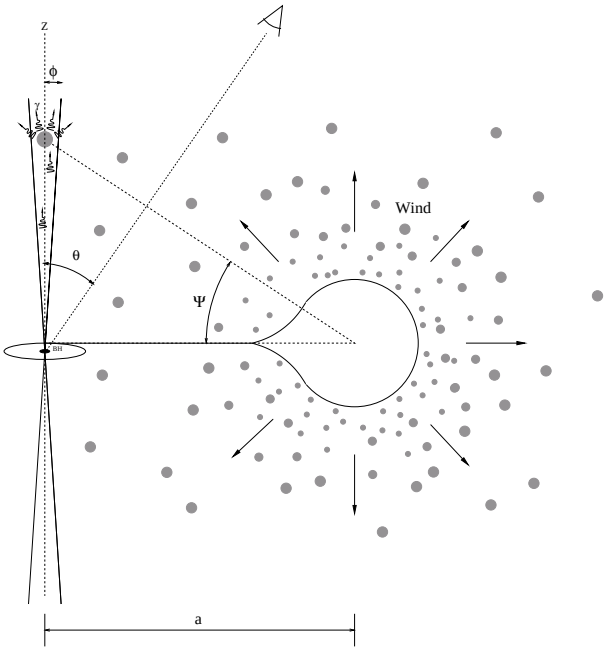

Figure 1: Sketch of a jet-clump interaction in a high-mass microquasar.

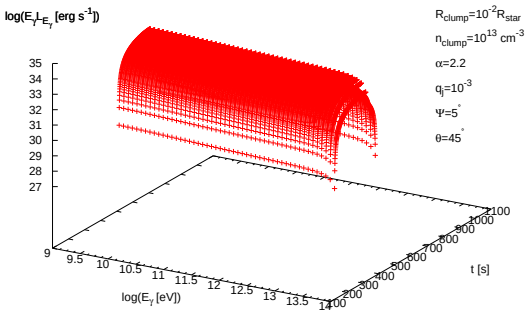

Figure 2: 3D-plot with the light curve and the spectral energy distribution resulting from a jet-clump interaction. The main parameters adopted are indicated in the figure. See text for details.

3 Porosity length scaling of gamma-ray fluctuation from multiple clumps

Individual jet-clump interactions should be observable only as rare, flaring events. But if the whole stellar wind is clumped, then integrated along the beam there will be clump interactions occurring all the time, leading to a flickering in the light curve, with the relative amplitude depending on the clump characteristics. In particular, while the mean gamma-ray emission will depend on the mean number of clumps intersected, the relative fluctuation should (following standard statistics) scale with the inverse square-root of this mean number. But, as we now demonstrate, this mean number itself scales with the same *porosity length* parameter that has been used, for example, by Owocki and Cohen (2006) to characterize the effect of wind clumps on absorption of X-ray line emission.

Let us first consider the *mean* gamma-ray emission integrated along the beam. Assuming a narrow beam with constant total energy along its length coordinate z, the mean total gamma ray emission scales as

$$\langle I_\gamma \rangle = I_b \sigma \int_0^\infty n(z)\, dz\,, \tag{2}$$

where $n(z)$ is the local mean wind density and σ represents an interaction cross-section for conversion of beam energy I_b to gamma-rays. For a steady wind with mass loss rate $\dot{M}$ and constant speed v emanating from a star at binary separation a from the z-origin at the black hole, the integral in Eq. (2) gives

$$\langle I_\gamma \rangle = \frac{I_b \sigma \dot{M}_\star}{8\mu v a}\,, \tag{3}$$

where μ is the mean wind mass per interacting particle (e.g., protons), and $\dot{M}_\star$ is the star mass loss rate.

The fluctuation in this mean emission depends on the properties of the wind clumps. A simple model assumes a wind consisting entirely of clumps of a characteristic length ℓ and volume filling factor f, for which the mean-free-path for any ray through the clumps is given by the porosity length $h \equiv \ell/f$. For a local interval along the beam Δz, the mean number of clumps intersected is thus $\Delta N_c = \Delta z/h$, whereas the mean gamma-ray production is given by

$$\Delta I_\gamma = I_b \sigma n \Delta z = I_b \sigma n \Delta N_c. \tag{4}$$

But by standard statistics for finite contributions from a discrete number N_c, the *variance* of this emission is

$$\left\langle \Delta I_\gamma^2 \right\rangle = \frac{I_b^2 \sigma^2 n^2 \Delta z^2}{\Delta N_c} = I_b^2 \sigma^2 n^2 h \Delta z\,. \tag{5}$$

The total variance is then just the integral that results from summing these individual variances as one allows $\Delta z \to dz$,

$$\delta I_\gamma^2 = I_b^2 \sigma^2 \int_0^\infty n^2 h dz \,. \quad (6)$$

Taking the square-root of this yields an expression for the relative rms fluctuation of intensity

$$\frac{\delta I_\gamma}{\langle I_\gamma \rangle} = \frac{\sqrt{\int_0^\infty n^2 h \, dz}}{\int_0^\infty n \, dz} \,. \quad (7)$$

As a simple example, for a wind with a constant velocity and constant porosity length h, the relative variation is just

$$\frac{\delta I_\gamma}{\langle I_\gamma \rangle} = \sqrt{h/a} \, \frac{\sqrt{\int_0^\infty dx/(1+x^2)^2}}{\int_0^\infty dx/(1+x^2)} = \sqrt{h/\pi a} \,. \quad (8)$$

On the other hand, for the Owocki & Cohen (2006) uniform expansion model with $v \sim r$ and $h = h'r$, we find $\rho \propto 1/r^3$ and thus,

$$\frac{\delta I_\gamma}{\langle I_\gamma \rangle} = \sqrt{h'} \, \frac{\sqrt{\int_0^\infty dx/(1+x^2)^{5/2}}}{\int_0^\infty dx/(1+x^{3/2})} = \sqrt{2h'/3} \,. \quad (9)$$

Typically then, if $h \sim 0.03a$,

$$\frac{\delta I_\gamma}{\langle I_\gamma \rangle} \approx 0.1.$$

This implies an expected flickering at the level of 10% for a wind with such porosity parameters. The variability timescale will depend on the wind speed, the size of the clumps, and the width of the jet, with a typical value of $\sim$ an hour.

4 Prospects

Fluctuations of 10% in a source with a luminosity of 10^{34-35} erg s^{-1} on timescales of $\sim 10^3$ s could be detectable with GLAST and CTA if the source is located at a few kpc. This means that gamma-ray astronomy can be used to probe the structure of stellar winds through dedicated observations of microquasars with massive donor stars. If additional information on the wind can be obtained through X-ray observations (Owocki & Cohen 2006) and the source can be detected with neutrino km^3-telescopes, we can also gain valuable insights in the relativistic proton content of the jets.

G.E.R., A.T.A. and P.B. are supported by CONICET (PIP 5375) and the Argentine agency ANPCyT through Grant PICT 03-13291 BID 1728/OCAR. S.P.O. acknowledges partial support of NSF grant 0507581 and NASA Chandra grant GO3-3024C.

References

Albert, J. et al. (MAGIC coll.) 2007, ApJ Lett, in press [arXiv:0706.1505]

Owocki, S.P., & Cohen, D.H. 2006, ApJ, 648, 565

Romero, G.E., et al. 2003, A&A, 410, L1

Puls: A couple of years ago it has been suggested that the winds themselves may be the source of γ-rays (second order Fermi acceleration between shock and final decay). May this process contaminate the scenario you have discussed?

Romero: I am a bit skeptic about γ-ray production in the stellar winds. Particles should be accelerated at shocks in the wind. In such an environment, losses should be very important for electrons (inverse Compton interactions with stellar photons) and for protons size constraints on the acceleration region should cut off the particle spectrum at low energies. In addition, the particle injection mechanism is unclear. So, I do not expect any contamination at high energies ($E > 10$ GeV).

Cassinelli: In the case of SS 433: in Hα one sees speeds of order $0.25\,c$ which is much smaller than the energy you are discussing. What are the relations? Secondly. The primary star provides the disk. Does it also produce the clumps in the region you are considering?

Romero: The velocity of the order of 0.25 c inferred for the jets of SS433 corresponds to the bulk velocity or the macroscopic outflow. In the model I am presenting, a small fraction of macroscopic kinetic energy is transformed into microscopic energy of some particles. These particles can be highly relativistic and generate the γ-rays when they interact with the clump material. Concerning the second question, yes, the clumps are produced by the same massive primary star that feeds the compact object through accretion.

O. Reimer: Are you considering heavier nuclei in the hadronic interactions than just pp for realistic modelling?

Romero: Yes. We introduce a phenomenological parameter that accounts for the presence of heavier nuclei in the jets.

Clumping in Hot Star Winds
W.-R. Hamann, A. Feldmeier & L.M. Oskinova, eds.
Potsdam: Univ.-Verl., 2008
URN: http://nbn-resolving.de/urn:nbn:de:kobv:517-opus-13981

VHE gamma-rays from Westerlund 2 and implications for the inferred energetics

O. Reimer[1], F. Aharonian[2,3], J. Hinton[4], W. Hofmann[2], S. Hoppe[2], M. Raue[5], and A. Reimer[1]
[1] *W.W. Hansen Experimental Physics Laboratory & Kavli Institute for Particle Astrophysics and Cosmology, Stanford University, USA*
[2] *Max-Planck-Institut für Kernphysik, Heidelberg, Germany*
[3] *Dublin Institute for Advanced Studies, Ireland*
[4] *School of Physics & Astronomy, University of Leeds, UK*
[5] *Institut für Experimentalphysik, Universität Hamburg, Germany*

The H.E.S.S. collaboration recently reported the discovery of VHE γ-ray emission coincident with the young stellar cluster Westerlund 2. This system is known to host a population of hot, massive stars, and, most particularly, the WR binary WR 20a. Particle acceleration to TeV energies in Westerlund 2 can be accomplished in several alternative scenarios, therefore we only discuss energetic constraints based on the total available kinetic energy in the system, the actual mass loss rates of respective cluster members, and implied gamma-ray production from processes such as inverse Compton scattering or neutral pion decay. From the inferred gamma-ray luminosity of the order of 10^{35}erg/s, implications for the efficiency of converting available kinetic energy into non-thermal radiation associated with stellar winds in the Westerlund 2 cluster are discussed under consideration of either the presence or absence of wind clumping.

1 The stellar cluster Westerlund 2 in the HII region RCW 49

The prominent giant HII region RCW 49 is characterized by still ongoing massive star formation (Whitney et al. 2004). The regions surrounding the central stellar cluster Westerlund 2 appear evacuated by stellar winds and radiation, and dust is distributed in fine filaments, knots, pillars, bubbles, and bow shocks throughout the rest of the HII complex (Churchwell et al. 2004, Conti & Crowther 2004). Radio continuum observations revealed two wind-blown shells in the core of RCW 49 (Whiteoak & Uchida 2004), surrounding the central region of Westerlund 2, and the prominent Wolf-Rayet star WR 20b. There is an ongoing controversy over the distance to Westerlund 2, and consequently about the association of WR 20a with Westerlund 2, as will be discussed later. The stellar cluster contains an extraordinary ensemble of hot and massive stars, at least a dozen early-type O-stars, and two remarkable WR stars. One of them, WR 20a was only recently established to be a binary (Rauw et al. 2004, Bonanos et al. 2004) by presenting solutions for a circular orbit with a period of 3.675, and 3.686 days, respectively. Based on the orbital period, the minimum masses were found to be $(83 \pm 5)\,M_\odot$ and $(82 \pm 5)\,M_\odot$ for the binary components (Rauw et al. (2005)). At that time, WR 20a was classified as the most massive of all confidently measured binary systems in our Galaxy. Synchrotron emission has not yet been detected from the WR 20a system, presumably because of free-free-absorption in the optically thick stellar winds along the line of sight. Although WR 20a has been detected in X-rays (Belloni & Mereghetti 1994), the non-thermal and thermal components of the X-ray emission remain currently indistinguishable. Detectable VHE gamma-radiation from the WR 20a binary system was only predicted in a pair cascade model (Bednarek 2005), although detailed modeling of the WR 20a system in other scenarios (e.g. as of Reimer et al. (2006) when produced either by optically-thin inverse Compton scattering of relativistic electrons with the dense photospheric stellar radiation fields in the wind-wind collision zone or in neutral pion decays, with the mesons produced by inelastic interactions of relativistic nucleons with the wind material) is still pending. In VHE γ-rays, photon-photon absorption would modulate (and diminish) the observable flux from a close binary system such as WR 20a.

2 H.E.S.S. observations towards Westerlund 2

The H.E.S.S. (High Energy Stereoscopic System) collaboration observed the Westerlund 2 region between March and July 2006, and obtained 14 h (12.9

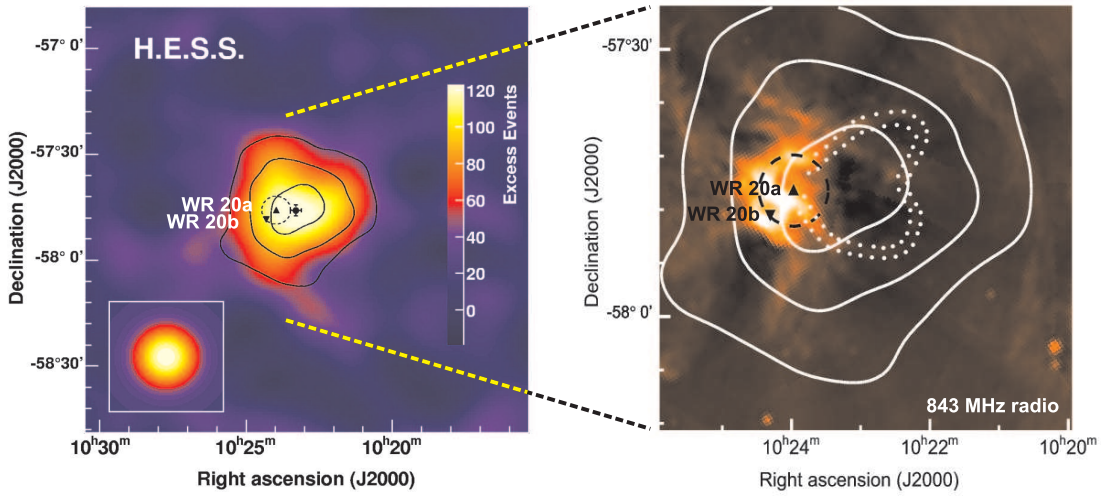

Figure 1: Left: H.E.S.S. gamma-ray sky map of the Westerlund 2 region, smoothed to reduce the effect of statistical fluctuations. The inlay in the lower left corner shows how a point-like source would have been seen by H.E.S.S. The WR stars WR 20a and WR 20b are marked as triangles, and the stellar cluster Westerlund 2 is represented by a dashed circle. Right: Significance contours of the gamma-ray source HESS J1023–575 (corresponding 5, 7 and 9σ), overlaid on a radio image from the Molonglo Observatory Synthesis Telescope. The wind-blown bubble around WR 20a, and the blister to the west of are seen as depressions in the radio continuum. The *blister* is indicated by white dots, and appears to be compatible in direction and location with HESS J1023–575.

h live time) of data, incorporating targeted observations of WR 20a and data from the ongoing H.E.S.S. Galactic plane survey. The data were obtained under zenith angles in the range between 36° and 53°, resulting in an energy threshold of 380 GeV for the analysis. A point source analysis on the nominal position of WR 20a resulted in a clear signal with a significance of 6.8σ, and further investigations revealed an *extended* excess with a peak significance exceeding 9σ. The center of the excess was derived by fitting the two-dimensional point spread function of the instrument folded with a Gaussian to the uncorrelated excess map: $\alpha_{2000} = 10^{\rm h}23^{\rm m}18^{\rm s} \pm 12^{\rm s}$, δ_{2000} = -57°45'50" ± 1'30". The systematic error in the source location is 20" in both coordinates. The source is clearly extended beyond the appearance of a point-like source for the H.E.S.S. instrument (Fig. 1), and a fit of a Gaussian folded with the PSF gives an rms extension of $0.18° \pm 0.02°$. The differential energy spectrum can be described by a power law $\mathrm{d}N/\mathrm{d}E = \Phi_0 \cdot (E/1\,\mathrm{TeV})^{-\Gamma}$ with a photon index of $\Gamma = 2.53 \pm 0.16_{\rm stat} \pm 0.1_{\rm syst}$ and a normalization at 1 TeV of $\Phi_0 = (4.50 \pm 0.56_{\rm stat} \pm 0.90_{\rm syst}) \times 10^{-12}\,\mathrm{TeV}^{-1}\,\mathrm{cm}^{-2}\,\mathrm{s}^{-1}$. The integral flux for the whole excess above the energy threshold of 380 GeV is $(1.3 \pm 0.3) \times 10^{-11}\,\mathrm{cm}^{-2}\,\mathrm{s}^{-1}$. No significant flux variability or the characteristic orbital periodicity of WR 20a could be detected in the data set. Full details regarding the discovery of HESS J1023–575 at VHE γ-rays are given in Aharonian et al. (2007).

3 Size constraints and energetics

The detection of extended VHE γ-ray emission towards Westerlund 2 is indicative of the presence of extreme high-energy particle acceleration in this young (∼2-3 Myrs; Piatti et al. 1998) star forming region. Following the HEGRA detected source TeV J2032+4130 and its suggested connection to the Cygnus OB2 cluster (Aharonian et al. 2002), HESS J1023–575 and Westerlund 2 is the second but even more prominent association between VHE γ-ray emission and an extraordinary assembly of young, hot and massive stars in our Galaxy. Given that the size of the γ-ray emission does not resemble the nominal size of the stellar cluster as known from radio, infrared to optical, and X-ray energies very well, but stretches further out in the direction of the *blister* (Whiteoak & Uchida 2004), we discuss the implied energetics based on the most simple possible, and accordingly least model-dependent considerations. A central problem for any stringent energetic assessment lies in the still unsettled dispute on the distance to Westerlund 2, when even recent determinations differ apparently by more than a factor of 3 (see Fig. 2): The distance to

Westerlund 2 is uncertain in the range of values between ∼2.2 kpc (Brand & Blitz 1993) and 7.9 kpc (Moffat et al. 1991), and intermediate values of 4.2 kpc were derived from 21 cm absorption line profile measurements (McClure-Griffiths et al. 2001), 5.75 kpc from the distance estimate towards the prominent WR star WR 20a (van der Hucht 2001), and 6.4 kpc from photometric measurements (Carraro & Munari 2004). Recently, Rauw et al. (2007) presented a compelling re-determination of the distance to Westerlund 2 by spectrophotometric measurements of 12 cluster member O-type stars of (8.3±1.6) kpc, a value in very good agreement with the (8.0±1.0) kpc as measured by Rauw et al. (2005) as determined from the light curve of the eclipsing binary WR 20a. We adopt the value of the weighted mean of (8.0±1.4) kpc (Rauw et al. 2007) throughout this manuscript, thereby associating WR 20a as a cluster member of Westerlund 2. Note, however, that Ascenso et al. (2007) and Dame (2007) put forward significantly lower values.

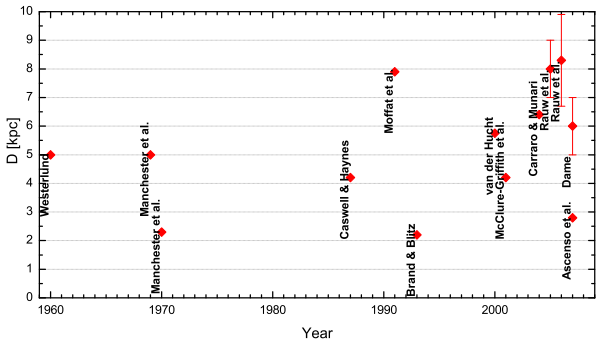

Figure 2: Distance measures for Westerlund 2 and/or WR 20a. The lasting distance ambiguity from different methodological approaches translates into the energetic constraints imposed by the detection of VHE γ-radiation.

With a projected angular size of submilliarcsecond scale, the WR 20a binary system, including its colliding wind zone, would appear as a point source for observations with the H.E.S.S. telescope array. At a distance of 8 kpc, the measured γ-ray source extension is equivalent to a diameter of 28 pc. Unless there are extreme differences in the spatial extent of the particle distributions producing radio, X-ray, and VHE γ-ray emission, scenarios based solely on particle acceleration in the colliding wind zone of WR 20a are unlikely to account for the observed source extent of 0.18° in the VHE γ-rays. Therefore the bulk of the γ-rays cannot energetized to TeV energies close to WR 20a. The apparent size of the VHE photons is however consistent with theoretical predictions of bubbles blown from massive stars into the ISM (Castor et al. 1975).

We estimated the γ-ray luminosity above 380 GeV to $\sim 1.5 \times 10^{35}$erg/s (at 8 kpc), corresponding to 0.2% (smooth wind: $\dot{M} = 2.5{\times}10^{-5} M_{\odot}$/yr) or 0.7% (clumped wind: $\dot{M} = 8.5{\times}10^{-6} M_{\odot}$/yr) of the total kinetic energy available from the colliding winds of WR 20a, and 0.2% (smooth wind: $\dot{M} = 5.3{\times}10^{-5} M_{\odot}$/yr) or 0.7% (clumped wind: $\dot{M} = 1.7{\times}10^{-5} M_{\odot}$/yr) of the kinetic energy of WR 20b, respectively. With up to 1.4% of the available E_{kin} in the WR-winds alone, a canonical value of 10% acceleration efficiency, the implied γ-ray production efficiency ($L_{\gamma,\mathrm{VHE}}/L_{\mathrm{particle}}$) is as high as 14% in case of clumped winds, or 4% for the less realistic case of smooth winds. These estimates, however, do not consider additional mass loss from other hot and massive stars present in Westerlund 2, which needs to be included when the H.E.S.S. result is interpreted in terms of collective stellar wind outflows. The energetic constraint is further relaxed when the distance to Westerlund 2 is indeed lower than the 8 kpc assumed, due to the accordingly higher integral γ-ray luminosity, and lower efficiency $L_{\gamma,\mathrm{VHE}}/L_{\mathrm{particle}}$.

In summary, the inferred γ-ray luminosity from the detection of VHE γ-ray emission from Westerlund 2 implies a rather high conversion efficiency when considering the mass loss rates for clumped winds from the two WR stars. This constraint can be relaxed if Westerlund 2 is indeed more closer than 8 kpc, as well as by considering mass loss transfer from the O- and B-stars in the stellar cluster.

References

Aharonian, F. et al. 2002, A&A 393, L37
Aharonian, F. et al. 2007, A&A 467, 1075
Ascenso, J. et al., 2007 A&A 466, 137
Bednarek, W. 2005, MNRAS 363, L46
Belloni, T. & Mereghetti, S. 1994, A&A 286, 935
Bonanos, A.Z. et al. 2004, ApJ 611, L33
Brand, J. & Blitz, L. 1993, A&A 275, 67
Carraro, G. & Munari, U. 2004, A&A 347, 625
Castor, J. et al. 1975, ApJ 200, L107
Churchwell, E. et al. 2004, ApJS 154, 322
Conti, P.S. & Crowther, P.A. 2004, MNRAS 255, 899
Dame, T.M. 2007, ApJ 665, L163
McClure-Griffiths, N.M. et al. 2001, ApJ 551, 394
Moffat, A.F.J. et al. 1991, AJ 102, 642
Piatti, A.E. et al. 1998, A&AS 127, 423
Rauw, G. et al. 2004, A&A 420, L9
Rauw, G. et al. 2005, A&A 432, 985
Rauw, G. et al. 2007, A&A 463, 981
Reimer, A. et al. 2006, ApJ 644, 1118
van der Hucht, K. 2001, New Astron. Rev 45, 135
Whiteoak, J.B.Z. & Uchida, K.I. 1997, A&A 317, 563
Whitney, B.A. et al. 2004, ApJS 154, 315

Gull: Models of superbubbles would suggest that the extended structure of Wd2/WR20a might be due to first generation stars that have contributed winds and ejecta. A good test would be a study of Constellation III in the LMC, where a core of remnant stars are surrounded by second generation stars not becoming SNe, see Brohweiler et al. and Kafatos et al.

Owocki: I am confused. You seem to imply that clumping and the implied mass loss rates would relieve the energetics problem of explaining observed TeV γ-ray luminosity, but would not the reduced wind kinetic energy make that problem worse?

O. Reimer: No, that is not what I was trying to say. I just thought that we have to invoke wind clumping in order to treat the energetics correctly. Clumped winds would imply less energy content from the particles whereas the γ-ray luminosity remains unchanged. If we back up to smooth wind, we would ease energetic constraints, but (to my understanding) at the expense of a more realistic description of the situation. Other factors come to play independently of the clumping problem: A lower distance to Wd2 will yield a lower γ-ray emissivity as the one I obtained for a distance of 8 kpc; if we consider not only WR20a – which itself may not account solely for the observed extended γ-ray emission – but also WR20b, and if the hot and massive stars in Wd2 will take their share, we can avoid a crisis concerning the γ-ray efficiency, which is thought to be comfortable only when it is below 10 %.

Romero: Is there any evidence for a high-energy cut-off in the HESS spectrum of Westerlund 2?

O. Reimer: Not on the basis of the HESS data taken so far. A single power law fit to the VHE spectrum is the preferred representation from a threshold energy of 380 GeV up to 20 TeV.

Moffat: Just for clarification: The stars in WR20a are not classical WR stars, rather they are close to solar-hydrogen, main-sequence stars well before any kind of Roche lobe overflow can occur. The strong winds are merely due to the extremely high luminosity of the stars.

Clumping in Hot Star Winds
W.-R. Hamann, A. Feldmeier & L.M. Oskinova, eds.
Potsdam: Univ.-Verl., 2008
URN: http://nbn-resolving.de/urn:nbn:de:kobv:517-opus-13981

Discussion: Binaries, colliding winds, LBVs and high energy radiation

Moderator: Nicole St-Louis

Hamann: I want to ask Andy Pollock one more question about the incredibly high mass obtained for WR 25 (344 $M_\odot$). What can be wrong with this mass estimate? And if the mass you get is not correct, will the mass loss rate still be okay?

Moffat: We now have binary-based masses of similar stars to WR 25, which have masses of order $100M_\odot$, not $> 300M_\odot$.

Gräfener: From our most recent spectral analyses we deduce a very large luminosity for WR 25. The result depends upon the adopted distance and the interstellar reddening law and lies between $10^{6.4}\,L_\odot$ and $10^{6.7}\,L_\odot$. From our hydrodynamic models we deduce masses of 110 and 210 $M_\odot$ respectively. This is not too far away from Andy's results.

Puls: In reply to Gräfener: When one believes in your hydrodynamic models, the mass should be quite constrained from the luminosity and the requirement that Γ is close to unity.

Moffat: The most massive, classical (He-burning) WR star has a mass of $\sim 20M_\odot$, while the most massive H-rich WR star is close to $120M_\odot$ (NGC 3603/AI).

Ignace: What actually constitutes a WR star?

Hillier: "Wolf-Rayet" is a spectral designation denoting the presence of certain emission lines; it is not an evolutionary designation. During the 1980ies, WR stars became associated with stars that were core He burning, and had lost much of their H envelope. However, in young massive clusters (e.g. 30 Dor, Carinae) many of the WR stars are H rich, and are probably still H-core burning. As emphasized by Stan, the reason for their emission lines are their high mass loss rates (and hence wind densities) which arise from their high luminosities.

Pollock: The abundances seem fairly well determined in the brightest WR 140 spectrum. The lines here are fairly regular in shape. After periastron, where the spectrum is much fainter, the lines are much more irregular, probably because there is now contribution from shocked O star material, which near periastron was seen through the shocked WR star material, which is probably optically thick.

Gull: Again, what is the definition of a clump? How long do clumps last? Are clumps we see in ejecta all from major events or do some originate from winds? η Carinae's Homunculus shows multiple absorption systems with velocities ranging from -128 km/s to -1500 km/s. The -513 km/s (Homunculus) and -146 km/s (little Homunculus) are clearly associated with historical events. Intermediate velocity systems are present from -385 to -508 km/s, almost periodically spaced. Excitation drops with increasing velocity and STIS nebular spectra show these absorptions to be associated with internal shells. Are these originating with each periastron event? Do they indicate decreasing activity after each major event leading up to new activity analogous to seismic activity? Does this provide insight to the periodic wind variations and a predictor of future events?

Moffat: The clumps we observe in WR stars have lifetimes of ~ 10 h in the observed lines. This does not exclude that the clumps continue to propagate without significant radiation in that line.

Pollock: The depth and shape of the eclipse depends very sensitively on the geometry. It would be essential to calibrate the method on objects for which the eccentricity and inclination are known by independent means. WR 133 is a possible example.

Weis: The classical picture of a nebula goes back to the Weaver et al. model in which a homogenous wind expands into an also homogenous medium. If the wind is already clumped, such a model is not valid anymore and the question is how large is the impact of those clumps onto the nebula formation.

X-rays

Chair: J.-C. Bouret

Clumping in Hot Star Winds
W.-R. Hamann, A. Feldmeier & L.M. Oskinova, eds.
Potsdam: Univ.-Verl., 2008
URN: http://nbn-resolving.de/urn:nbn:de:kobv:517-opus-13981

X-raying clumped stellar winds

L.M. Oskinova, W.-R. Hamann & A. Feldmeier
Universität Potsdam, Germany

X-ray spectroscopy is a sensitive probe of stellar winds. X-rays originate from optically thin shock-heated plasma deep inside the wind and propagate outwards throughout absorbing cool material. Recent analyses of the line ratios from He-like ions in the X-ray spectra of O-stars highlighted problems with this general paradigm: the measured line ratios of highest ions are consistent with the location of the hottest X-ray emitting plasma very close to the base of the wind, perhaps indicating the presence of a corona, while measurements from lower ions conform with the wind-embedded shock model. Generally, to correctly model the emerging X-ray spectra, a detailed knowledge of the cool wind opacities based on stellar atmosphere models is prerequisite. A nearly grey stellar wind opacity for the X-rays is deduced from the analyses of high-resolution X-ray spectra. This indicates that the stellar winds are strongly clumped. Furthermore, the nearly symmetric shape of X-ray emission line profiles can be explained if the wind clumps are radially compressed. In massive binaries the orbital variations of X-ray emission allow to probe the opacity of the stellar wind; results support the picture of strong wind clumping. In high-mass X-ray binaries, the stochastic X-ray variability and the extend of the stellar-wind part photoionized by X-rays provide further strong evidence that stellar winds consist of dense clumps.

1 Introduction

All OB-stars with spectral types earlier than B1.5 have X-ray luminosities $L_{\rm X}$ exceeding $10^{30.5}\,{\rm erg\,s^{-1}}$. Remarkably, their X-ray luminosity roughly correlates with stellar bolometric luminosities as $L_{\rm X}{\approx}10^{-7}L_{\rm bol}$ (Seward et al. 1979, Berghöfer et al. 1994). The high-resolution X-ray spectra of two O-stars, ζ Pup and ζ Ori, are shown in Figure 1. The spectra are dominated by strong emission lines that reflect stellar wind abundances, e.g. nitrogen lines are more prominent in the spectrum of the more evolved star ζ Pup. X-ray spectra of single non-magnetic massive stars can be explained as emitted by optically thin plasma heated to temperatures $kT_{\rm X}{\lesssim}0.6\,{\rm keV}$ (e.g. Wojdowski & Schulz 2005).

There are different hypotheses for the generation of X-rays in stellar winds. Lucy & White (1980) put forward a theory where X-rays originate from bow shocks around blobs (see also Cassinelli et al., these proceedings). Cassinelli & Swank (1983) proposed an analogy with coronal stars where X-rays originate from magnetically confined regions at the wind base. Owocki et al. (1988) performed simulations of the evolution of instabilities in radiatively driven stellar winds and predicted a development of reverse shocks with temperatures in the range $10^6 - 10^7\,{\rm K}$ (i.e. as inferred from the observed X-ray spectra). Feldmeier et al. (1997) developed a model explaining the X-rays as originating from cooling zones behind shock fronts and were able to reproduce the low-resolution ROSAT spectra of ζ Pup and ζ Ori.

In massive binaries a copious amount of X-ray emission is produced by the collision of two powerful stellar winds. X-ray spectra of colliding wind binaries reveal that the X-ray emitting plasma departs from collisional equilibrium (e.g. Pollock et al. 2005). Colliding wind systems tend to have somewhat higher X-ray luminosities and their X-ray spectra can be "harder" compared to the single stars.

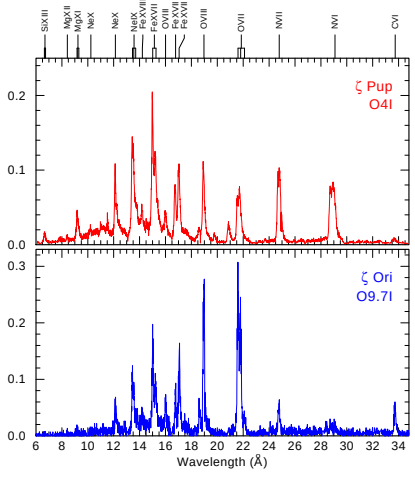

Figure 1: High-resolution X-ray spectra of ζ Pup *(top panel)* and ζ Ori *(bottom panel)* obtained with *XMM-Newton*. Prominent emission lines are identified.

Another type of X-ray emitting plasma is found in high-mass X-ray binary systems (HMXBs) that consist of an OB supergiant and a degenerate companion, usually a neutron star (NS) deeply embedded in the stellar wind of the primary. Stellar wind accretion onto a NS powers strong X-ray emission that has a characteristic power-law spectrum, while the surrounding stellar wind is photoionized by this X-ray emission.

Independent on the formation mechanism, the X-rays registered by the observer are attenuated in the stellar wind and interstellar medium. The transport of X-rays in stellar winds can often be treated as pure absorption (Baum et al. 1992, Hillier et al. 1993). This leads to a great simplification of the radiative transfer problem and allows modeling even in the case when the absorbing medium is inhomogeneous.

2 X-ray emission of single stars as a probe of clumped stellar wind

2.1 Line ratios in spectra of He-like ions

One of the key spectral diagnostics is provided by the ratio of line fluxes from He-like ions. These ions show characteristic '*fir* triplets' of a forbidden (f), an intercombination (i) and a resonance (r) line. In OB-type stars, the $\mathcal{R} \equiv f/i$ line ratio is sensitive to the local mean intensity of the UV radiative field, J_ν. The UV photons with wavelength $\lambda_{\rm f\rightarrow i}$ excite the metastable ^{3}S level to the ^{3}P level, so that $\mathcal{R} \propto (1+\phi(J_\nu))^{-1}$, where $\phi(J_\nu)$ is the photoexcitation rate (constants and collisional terms are omitted). Neglecting the limb darkening, the average intensity can be substituted by the diluted photospheric flux, $W(r)H_\nu$. *If* the photospheric flux H_ν is known, the dilution factor W can be inferred from $\mathcal{R}$. This constrains the radius $R_{\rm fir}$ where the X-ray emitting plasma is located.

For wavelengths in the observable part of the UV the flux can be, in principle, directly inferred from observations. Unfortunately, especially for giant and supergiant stars, the photospheric fluxes are often contaminated by wind lines. E.g. O VI resonance doublet coincides with the $\lambda_{\rm f\rightarrow i}$ transition at 1033 Å for the Mg XI line. The O VI doublet itself can only be reproduced by stellar atmosphere models if an X-ray field causing Auger ionization is included (e.g. Oskinova et al. 2006). This example highlights the need of a full radiative transfer treatment for the correct interpretation of the *fir* line ratios – a task that has not been accomplished yet.

Commonly, the fluxes H_ν at the wavelengths of interest are obtained from stellar atmosphere models. Leutenegger et al. (2006) analyzed the lines of He-like ions in the spectra of four O-type giants and supergiants. The parameters of the O-stars were taken from Lamers & Leitherer (1993) and used to select a stellar atmosphere model from the TLUSTY static plane-parallel model grid. Leutenegger et al. find that the minimum radius of X-ray formation is typically in the range of $1.25 < R_{\rm fir}/R_* < 1.67$.

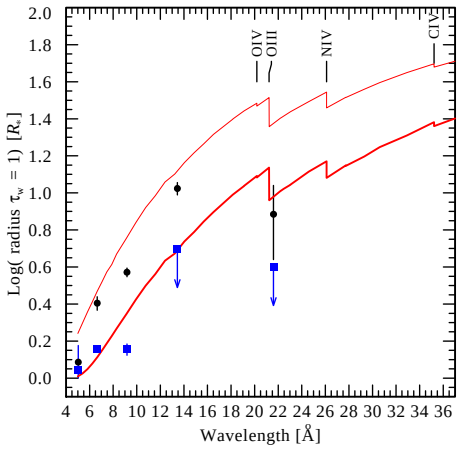

Figure 2: Logarithm of the radius were the radial optical depth of the wind becomes unity in ζ Pup according to PoWR stellar atmosphere models. Thick line: model with $\dot{M}$=2.5×10^{-6} $M_\odot$/yr; thin line: $\dot{M}$=8.7×10^{-6} $M_\odot$/yr. The radii of the X-ray emission derived from different He-like ions are indicated by dots (from WC07) and squares (Leutenegger et al. 2006).

Waldron & Cassinelli (2007, WC07) analyzed *fir* line ratios for 17 OB stars, using plane-parallel Kurucz models, and found, in agreement with their earlier results, that high-Z ions are predominantly located closer to the photosphere. They highlighted a *"near-star high-ion" problem*. This problem can be illustrated by the S XV line in ζ Puppis. WC07 constrained $R_{\rm fir}$ for this line to $< 1.22\,R_*$. This is in agreement with the results of Leutenegger et al. (2006) who estimated the minimum value of $R_{\rm fir}$ as $1.1^{+0.4}_{-0.1}\,R_*$. The emissivity of S XV has its maximum at $T \approx 16$ MK. The presence of plasma with such high temperatures at $\approx 1.1\,R_*$, i.e. close to the photosphere, is contrary to the expectations from the shocked-wind model, but supports the base-corona model.

WC07 notice a correlation between the radius where the ambient cool wind becomes transparent for the X-rays $R(\tau_{\rm wind})$=1, and the predominant location of He-like ion X-ray emission. This is illustrated in Fig. 2. We use a spherically-symmetric PoWR atmosphere model of ζ Pup to calculate $R(\tau_{\rm wind})$=1. The calculations are performed for two

different $\dot{M}$ evaluated under the assumption of unclumped wind (Repolust et al. 2004) and allowing for macroclumping (Oskinova et al. 2007). The measurements of $R_{\rm fir}$ by WC07 and Leutenegger et al. (2006) are also shown. As can be seen in Fig. 2, there is a good agreement between the measurements by WC07 of the *fir*-inferred radii and $R(\tau_{\rm wind})$=1. However, there is an apparent disagreement with the results of Leutenegger et al. (2006). This can be due to a difference in measuring $\mathcal{R}$ and/or different approaches to the analysis (see WC07).

Because we preferentially see X-rays that are generated close to the $\tau_{\rm wind} = 1$ surface (e.g. Ignace et al. 2000), the results of Leutenegger et al. imply a reduced mass-loss rate, while the WC07 results are consistent with the $\dot{M}$ estimates of Puls et al. (2006) and Oskinova et al. (2007).

2.2 X-ray emission line profiles

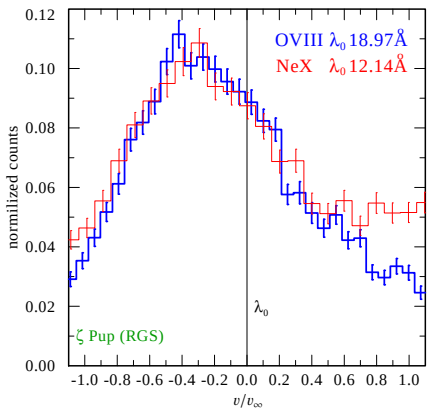

Figure 3: O VIII (thick blue) and Ne X (thin red) lines in the spectrum of ζ Pup plotted versus wavelength in velocity units. The redward shoulder in Ne X line is due an unresolved Fe emission feature.

The analysis of *fir*-lines suggests that lines from lower Z ions are formed further out in the wind. Therefore, assuming that the wind velocity monotonically increasing with the radius, lines from ions with lower Z should be broader than from ions with higher Z. Contradictory to this expectation, the observed widths of all X-ray lines are similar (e.g Kramer et al. 2003; Pollock 2007). To illustrate this, the lines of Ne X and O VIII in spectrum of ζ Pup are shown in Fig. 3 (see also lines of C VI and Ne X in ζ Ori spectrum shown in Pollock 2007). Thus, there is a discrepancy between the location of the emission region inferred from the *fir* line ratios and from the fitting of the line profiles.

Radiative transfer in homogeneous wind predicts that the redshifted emission from the back side of the wind is more suppressed by the continuum opacity along the line of sight, than the blueshifted emission from the front hemisphere. This should lead to skewed, almost triangular-shaped profiles of the emission lines (MacFarlane et al. 1991; Ignace 2001; Owocki & Cohen 2001). Because the atomic opacity κ_ν increases at longer wavelengths, the lines of ions with lower Z are expected to be more skewed compare to the higher Z ions. However, the majority of observed stellar X-ray lines are only slightly skewed and the shifts are similar for lines of all ions (WC07).

There are a number of different hypotheses to explain the puzzling properties of observed line profiles. Pollock (2007) proposes that X-rays originate in collisionless shocks. Two-component wind expansion is invoked by Mullan & Waldron (2006). Ignace & Galley (2002) show that if the X-ray emitting plasma is optically thick this would result in more symmetric line profiles (see also Leutenegger et al., these proceedings). Waldron & Cassinelli (2001) suggest that nearly symmetric line profiles can be explained by low opacity of the stellar wind.

Waldron & Cassinelli (2001) note that the wind opacity could be reduced if a large fraction of the wind were photoionized by X-rays. However, they observe that this is not compatible with the presence of low-ionisation species, e.g. C IV in the UV spectra. Our recent PoWR models of O star winds confirm this suggestion: there is no significant change in the ionisation structure of the wind when a realistic X-ray intensity is included.

Waldron & Cassinelli (2001) further suggest that if the adopted mass-loss rate is reduced this would lead to a better agreement between modeled and observed line shapes. This suggestion is supported by the modeling of line profiles emerging from a homogeneous wind by Kramer et al. (2003) and Cohen et al. (2006). They infer the wind optical depth by fitting a model with four free parameters to the lines observed in the X-ray spectra of ζ Pup and ζ Ori. The optical depth in the smooth wind with a monotonic velocity law scales with a parameter $\tau_* = \kappa_\nu \dot{M}(v_\infty R_*)^{-1}$ (Owocki & Cohen 2001). Inferring τ_* from the model fits and assuming that the wind atomic opacity κ_ν is a constant, Kramer et al. (2003) and Cohen et al. (2006) conclude that X-ray lines can be fitted only if $\dot{M}$ for ζ Pup and ζ Ori are strongly reduced (see also Cohen, these proceedings). More realistic mass-absorption coefficients κ_ν are presented in Oskinova et al. (2006). We use the best-fit values of τ_* obtained for different lines from Table 1 in Kramer et al. (2003) to estimate the mass-loss in ζ Pup, however there is large disagreement when different lines are considered.

The smooth-wind line profile formalism can be easily adapted for an inhomogeneous wind, where *all* clumps are optically thin at *any* given wavelength (so-called microclumping approximation). The empirical mass-loss rates based on ρ^2 diagnostics are

lower when microclumping is adopted, compared to models that assume a smooth wind. The mass-loss rates obtained from the fitting of X-ray lines by Kramer et al. (2003) can be reconciled with the radio and Hα measurements only if clumping filling factors are very small (see Puls et al. 2006). Overall, the use of microclumping approximation, at least in dense winds, is questionable (see Hamann, these proceedings).

Waldron & Cassinelli (2001) also note that a *clumped wind* can be effectively optically thin even in stars with large $\dot{M}$. This suggestion was exploited in Feldmeier et al. (2003) by waiving the microclumping approximation.

Assume that the flow of clumps that constitutes the wind obeys the equation of continuity. The number of clumps per unit volume is $n(r) \equiv n_0 v(r)^{-1} r^{-2}$, where n_0 is a constant. The effective opacity of clumped wind, $\kappa_{\rm eff} = n(r)\sigma_{\rm clump}\mathcal{P}$, is the product of the clump number density $n(r)$, the clump cross-section $\sigma_{\rm clump}$, and the probability of an X-ray photon being absorbed when it encounters a clump, $\mathcal{P} = 1 - \exp(-\tau_\nu^{\rm clump})$ (Feldmeier et al. 2003).

The optical depth across an average clump at the distance r is $\tau_\nu^{\rm clump} = \tau_* R_* v_\infty r^{-2} n_0^{-1}$. When $\tau_\nu^{\rm clump} \gg 1$ the effective opacity $\kappa_{\rm eff}$ does not depend on the atomic opacity κ_ν (because $\mathcal{P} \to \infty$). Therefore, the wind effective opacity becomes grey.

To calculate emission line profiles, we assume for simplicity that the emission with emissivity η originates between some specific radii r_1 and r_2 in the wind. The formal integral for the line profile reads $F_\mu \sim \int_{r_1}^{r_2} \eta(r) r^2 {\rm e}^{-\tau_{\rm w}} {\rm d}r$, where μ is the direction cosine.

Evaluating the wind optical depth as an integral over effective opacity along the line-of-sight z gives:

$$\tau_{\rm w} = n_0 \int_{z_\nu}^{\infty} \frac{\sigma}{v(r) r^2} (1 - {\rm e}^{-\tau_\nu^{\rm clump}}) {\rm d}z. \qquad (1)$$

To understand how the clump geometry alters the line profile shape, let us consider two extreme cases and compare isotropic clumps (balls) and anisotropic clumps in the form of infinitesimally thin shell-fragments (pancakes) oriented perpendicular to the radial direction, so-called a "Venetian blind" model. Assuming that the clumps keep constant solid angle as they propagate outwards, in the direction z a ball has the cross-section $\sigma \propto r^2$, while a pancake has $\sigma \propto |\mu| r^2$. Recalling that $dz = dr/\mu$ and inserting the above expressions for the cross-sections in the Eq. (1), it is immediately clear that in the case of pancakes the integral Eq. (1) transforms into an integral over r, while it stays an integral over z in case of the balls. The consequence is that pancakes yield nearly symmetric emission line profiles, similarly to the observed (Oskinova et al. 2006).

Owocki & Cohen (2006) applied a porosity length formalism (Owocki et al. 2004) with $\kappa_{\rm eff} = h(r)^{-1}(1 - \exp(-\tau_\nu^{\rm clump}))$, where $h(r)$ is a parameter. They studied a case of isotropic opacity, and concluded that large porosity lengths $h(r) \approx 1 R_*$ are required to reproduce the observed X-ray line profiles. However, Oskinova et al. (2006) computed synthetic X-ray lines for anisotropic opacity. Stellar wind parameters, i.e. κ_ν, $\dot{M}$, and $v(r)$ were adopted from most recent stellar atmosphere models and it was assumed that the average separation between clumps at distance r is $R_* v(r)/v_\infty$, as compatible with predictions of hydrodynamic simulations (e.g Feldmeier et al. 1997). Synthetic lines were computed *without allowing any free parameter* and compared with the observed lines. The remarkable similarity between synthetic and observed lines provides an evidence that the wind clumps are not optically thin, and are compressed in radial direction.

3 X-ray emission of binaries as a probe of clumped stellar wind

The collision of stellar winds in massive binary systems (CWB) results in a bow shock that concaves around the star with the weaker wind. In close binaries the shocked material cools radiatively and hence the intrinsic X-ray luminosity is $L_{\rm X} \propto \dot{M} v^2$ (Pittard & Stevens 2002). In the wide binaries with sufficiently large separation d, the shocked material cools adiabatically resulting in $L_{\rm X} \propto \dot{M}^2 d^{-1} v^{-1.5}$ (Stevens et al. 1992).

Hydrodynamic studies of colliding *clumped* winds were conducted by Walder & Folini (2002) and Pittard (2007). Walder & Folini considered WR 140 at periastron. They showed that the collision of clumped winds in a radiatively cooling system leads to the fragmentation of the colliding wind region (CWR). Carbon enriched dense WR-wind clumps with dimensions exceeding 10^{11} cm can effectively cool and serve as the seeds for the formation of the dust. Pittard (2007) considered WR 140 at apastron when the CWR is likely to cool adiabatically. It was shown that in this case the CWR becomes highly turbulent. This leads to a rapid destruction of the clumps in the CWR. Therefore in adiabatic CWB, wind clumping does not affect the intrinsic X-ray luminosity. Therefore such systems may provide a diagnostic of mass-loss that is independent on clumping.

The X-rays generated in the bow shock propagate along the line of sight through the stellar wind of the foremost star, resulting in X-ray eclipses due to the orbital motion. The duration and the depth of the eclipses depends on the orbital parameters, the wind geometry, and its opacity. When the intrinsic X-ray luminosity from the bow shock is known, the stellar mass-loss rate can be probed by inferring the absorbing column from the X-ray spectrum.

Schild et al. (2004) derived the mass-loss rate of the WC8 component of γ Vel in this way. The ob-

tained $\dot{M}$ is a factor of four smaller than what is derived from spectral analysis with homogeneous wind models. This was interpreted in terms of WR wind clumping, with a volume filling factor of $f_{\rm V} \approx 0.06$. For η Car, Pittard & Corcoran (2002) derived a mass-loss rate from an analysis of the X-ray spectrum that is lower by a factor of few compared to the conventionally adopted value, thus indicating wind clumping. Similarly, Pollock et al. (2005) derived smaller than expected wind absorption from their analysis of the X-ray spectrum of WR140.

Supergiant HMXBs consist of a supergiant OB star and (usually) a neutron star (NS), that orbits deep inside the stellar wind. An X-ray emission with a power-law spectrum results from the accretion of the stellar wind onto the NS. These X-rays photoionize the surrounding stellar wind. The wind X-ray spectrum shows a large variety of emission features, including a number of fluorescent lines. Sako et al. (2003) reviewed the spectroscopic results obtained with X-ray observatories for several wind-fed HMXBs. They concluded that the observed spectra can be explained only as originating in a wind where cool dense clumps are embedded in rarefied photoionized gas. Sako et al. (1999) constrained the volume filling factor of clumps in the wind of Vela X-1 as $f_{\rm V} \approx 0.04$. Similar conclusions were reached by Van der Meer et al. (2005). They studied the X-ray light curve of 4U 1700-37 and found that the feeding of the NS by stellar wind clumps explains the observed stochastic variability. The clump separation at the distance $2R_*$ was constrained to $0.4R_*$. Recently, the advances in the γ-ray and X-ray observations lead to the discovery of new HMXBs that are highly absorbed and display fast stochastic variability. This spectral and temporal variability is consistent with strong wind clumping. The inferred clumping parameters are similar to those obtained from the analysis of X-ray emission in single stars and in CWBs (see Romero et al. and Walter et al., these proceedings).

4 Conclusions

The spectral and temporal properties of the X-ray emission from single stars, colliding wind binaries and high-mass X-ray binaries provide consistent evidence of wind clumping. The multitude of data requires strongly clumped winds where clumps are separated by a few tenths of the stellar radius in the wind acceleration zone. The approximation that clumps are optically thin at *all* wavelengths in the X-ray band is not justified and cannot be applied universally. Clumped stellar winds have a reduced opacity for X-rays, compared to a homogeneous wind, due to a reduction of empirically determined mass-loss rates and to the effect of wind porosity.

References

Baum, E., Hamann, W.-R., Koesterke, L., & Wessolowski, U., 1992, A&A, 266, 402

Berghöfer, T.W., Schmitt, J.H.M.M., Danner, R., & Cassinelli, J.P., 1997, A&A, 322, 167

Cassinelli, J.P. & Swank, J.H., 1983, ApJ, 271, 681

Cohen, D.H., et al., 2006, MNRAS, 368, 1905

Feldmeier, A., Puls, J., & Pauldrach, A.W.A., 1997, A&A, 322, 878

Feldmeier, A., Oskinova, L., & Hamann, W.-R., 2003, A&A, 403, 217

Hillier, D.J., Kudritzki, R.P., Pauldrach, A.W., et al., 1993, A&A, 276, 117

Ignace, R., 2001, ApJ, 549, 119

Ignace, R. & Gayley, K.G., 2002, ApJ, 568, 954

Ignace, R., Oskinova, L.M., & Foullon, C., 2000, MNRAS, 318, 214

Kramer, R.H., Cohen, D., & Owocki, S.P., 2003, ApJ, 592, 532

Lamers, H.J.G.L.M. & Leitherer, C., 1993, ApJ, 412, 771

Leutenegger, M.A., et al., 2006, ApJ, 650, 1096

Lucy, L.B. & White, R.L. 1980, ApJ, 241, 300

MacFarlane, J.J., et al., 1991, ApJ, 380, 564

Mullan, D.J. & Waldron, W.L. 2006, ApJ, 637, 506

Oskinova, L.M., Feldmeier, A., & Hamann, W.-R., 2004, A&A, 422, 675

Oskinova, L.M., Feldmeier, A., & Hamann, W.-R., 2006, MNRAS, 372, 313

Oskinova, L.M., Hamann, W.-R., & Feldmeier, A., 2007, A&A, 476, 1331

Owocki, S.P., Castor, J.I.,& Rybicki, G.B. 1988, ApJ, 335, 914

Owocki, S.P & Cohen, D.H., 2001, ApJ, 559, 1108

Owocki, S.P., Gayley, K.G., & Shaviv, N.J., 2004, ApJ, 616, 525

Owocki, S.P & Cohen, D.H., 2006, ApJ, 648, 565

Pittard, J.M. & Stevens, I.R., 2002, A&A, 388, 20

Pittard, J.M., & Corcoran, M.F., 2002, A&A, 383, 636

Pittard, J.M., 2007, ApJ, 660, 141

Pollock, A.M.T., et al., 2005, ApJ, 629, 482

Pollock, A.M.T., 2007, A&A, 463, 1111

Puls, J., et al., 2006,A&A, 454, 625

Repolust, T., Puls, J., & Herrero, A., 2004, A&A, 415, 349

Sako, M., et al., 1999, ApJ, 525, 921

Sako, M., et al., 2003, astro-ph/0309503

Schild, H., et al., 2004, A&A, 422, 177

Seward F.D., et al., 1979, ApJ, 234, 55

Stevens, I.R., Blondin, J.M., & Pollock, A.M.T., 1992, ApJ, 386, 265

van der Meer, A., et al., 2005, A&A, 432, 999

Walder, R. & Folini, D., 2002, ASPC, 260, 595

Waldron, W.L & Cassinelli, J.P. , 2001, ApJ, 548, 45

Waldron, W.L & Cassinelli, J.P. , 2007, ApJ, 668, 456 (WC07)

Wojdowski, P.S. & Schulz, N.S., 2005, ApJ, 627, 953

Feldmeier: Lida, there are two central effects that affect the X-ray emission line profile, first the wind porosity and second the geometric shape of the clouds or clumps, namely whether they are spheres or pancakes. Although both effects are included in the paper, I suggest that we all work together to do this more systematically and statistically.

Oskinova: I totally agree with you. It is important to compare the results obtained by different groups and to join the efforts in order to explain the X-ray line-profiles. I would very much welcome any possible collaboration.

Ignace: 1. What do you find for the inner radius of the X-ray emitting gas? 2. So as a limiting case, if $\tau(E) \gg 1$ for all energies, a flat continuum spectrum would remain flat?

Oskinova: 1. Our results roughly constrain the line emission region between $1.5\,R_*$ and $5\,R_*$. 2. Yes, in case when wind clumps are optically thick for all energies, a flat continuum spectrum would remain flat.

Pollock: When looking through a porous wind, what would be the chances of the small neutron star appearing in a line of sight with NO absorption?

Oskinova: I believe the neutron star significantly disturbs the wind in its immediate vicinity. Existing hydrodynamic simulations predict at least two dense structures close to the neutron star, an accretion column and a photoionization wake. I am not sure whether it is known how predictions of these models will be modified for a porous wind. So I would be careful in answering your question till the models of wind dynamics in HMXBs can account for wind clumping.

Clumping in Hot Star Winds
W.-R. Hamann, A. Feldmeier & L.M. Oskinova, eds.
Potsdam: Univ.-Verl., 2008
URN: http://nbn-resolving.de/urn:nbn:de:kobv:517-opus-13981

Quantitative analysis of resolved X-ray emission line profiles of O stars

D.H. Cohen[1], M.A. Leutenegger[2], & R.H.D. Townsend[3]
[1]*Department of Physics and Astronomy, Swarthmore College, Swarthmore, Pennsylvania, United States*
[2]*Columbia Astrophysics Laboratory, Columbia University, New York, New York, United States*
[3]*Bartol Research Institute, University of Delaware, Newark, Delaware, United States*

By quantitatively fitting simple emission line profile models that include both atomic opacity and porosity to the *Chandra* X-ray spectrum of ζ Pup, we are able to explore the trade-offs between reduced mass-loss rates and wind porosity. We find that reducing the mass-loss rate of ζ Pup by roughly a factor of four, to 1.5×10^{-6} $M_\odot$ yr^{-1}, enables simple non-porous wind models to provide good fits to the data. If, on the other hand, we take the literature mass-loss rate of 6×10^{-6} $M_\odot$ yr^{-1}, then to produce X-ray line profiles that fit the data, extreme porosity lengths – of $h_\infty \approx 3$ R_* – are required. Moreover, these porous models do *not* provide better fits to the data than the non-porous, low optical depth models. Additionally, such huge porosity lengths do not seem realistic in light of 2-D numerical simulations of the wind instability.

1 Introduction

The X-ray emission lines from O stars are wind-broadened but are surprisingly symmetric. Asymmetry should arise due to the preferential absorption of red-shifted photons, which are produced on the far side of the wind and seen through a larger column density of cold, absorbing material. The very modest asymmetry in the observations implies that mass-loss rates are lower than has been presumed, which is, of course, in line with other recent observations. Alternatively, it has been suggested that the mass-loss rates are actually high, but the effective opacity of the wind is reduced due to porosity, or macroclumping (Oskinova et al. 2006).

In this very brief paper, in which we focus on one strong representative line in the *Chandra* grating spectrum of ζ Pup, we explore whether the measured profile shapes can discriminate between mass-loss reduction and porosity. Even if they cannot, by fitting models to data we can quantitatively explore the trade-off between the key parameters: fiducial optical depth, $\tau_* \equiv \kappa \dot{M}/4\pi v_\infty R_*$, and the terminal porosity length, h_∞. Here we do this by fitting the Owocki & Cohen (2001) profile model to one strong line in the *Chandra* HETGS/MEG spectrum of ζ Pup. We then fit a modified profile model, where the opacity is adjusted for porosity according to Owocki & Cohen (2006).

2 Fitting Models to the Data

There are 560 counts in the Fe XVII line shown in Fig. 1, accumulated during an exposure time of 68 ks. The line is well resolved and clearly asymmetric, with the characteristic blue shifted and skewed line shape that is expected from a spherically symmetric, beta-velocity wind with embedded X-ray emission and continuum absorption from the cool, dominant component of the wind. The first model we fit to the data is the simplest – a non-porous Owocki & Cohen (2001) model where the optical depth depends on the atomic opacity. We note that this model does not preclude microclumping of the sort that affects density-squared emission diagnostics, but does not affect column-density based diagnostics like X-ray emission line profiles. However, this standard profile model does *not* include large scale porosity, or macroclumping, with $h \equiv \ell/f > r$, where h is the porosity length, defined as the clump size scale to the volume filling factor (Owocki & Cohen 2006). We do fit porous models later in this paper.

We fit the model, along with a fixed power-law continuum, within XSPEC, to the line over the wavelength range shown in Fig. 1. The fitting routine in XSPEC adjusts the free parameters of the model: R_0, the radius below which there is no X-ray emission, τ_*, the fiducial wind optical depth, and the normalization, until the global minimum of the fit statistic – here the C statistic (Cash 1979), which is the maximum likelihood statistic for Poisson-distributed data – is found. The best-fit model, with $R_0 = 1.5 \pm .2$ R_* and $\tau_* = 2.0 \pm .5$, is plotted over the data in Fig. 1.

The uncertainties on the parameters can be estimated by evaluating ΔC, the difference between the C statistic value for a given choice of parameters and that of the best-fit model. The distribution of ΔC is the same as that of $\Delta\chi^2$ and a specific value cor-

responds to a formal confidence limit. By drawing contours of constant ΔC in the parameter space of interest, we can see the extent of a given parameter's possible range and the correlation between parameters, as we show in Fig. 2.

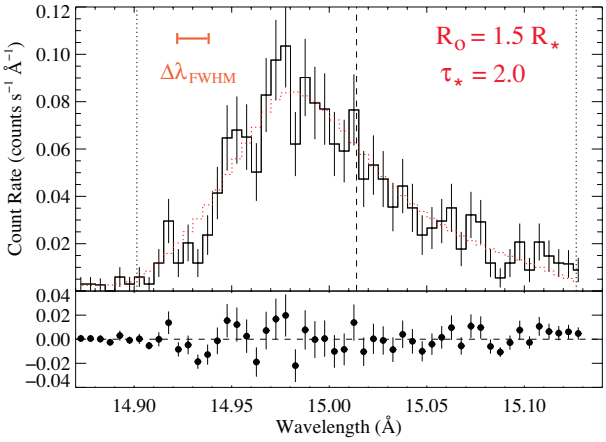

Figure 1: An Fe XVII emission line, formed in a thermal plasma at a few 10^6 K, with Poisson error bars. The approximate spectral resolution is indicated by the orange bar. The best-fit non-porous model is shown.

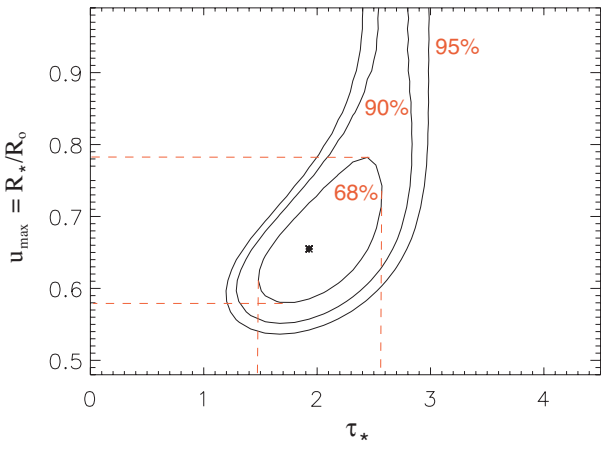

Figure 2: These confidence contours in the R_0 - τ_* parameter space of the fit of the non-porous model to the Fe XVII line, shown in Fig. 1, enclose 68%, 90%, and 95% of the model parameter space where the true model parameters lie, given the data and the assumed model.

The value of τ_* we derive from the model fitting, $\tau_* = 2.0 \pm .5$, implies a mass-loss rate of $\dot{M} = 1.5 \pm .4 \times 10^{-6}$ M$_\odot$ yr^{-1}, given an X-ray opacity at 15 Å of 70 cm^2 g^{-1} (Waldron et al. 1998). If, on the other hand, we take the mass-loss rate of ζ Pup to be $\dot{M} = 6 \times 10^{-6}$ M$_\odot$ yr^{-1} and use $R_* = 19$ R$_\odot$ and $v_\infty = 2250$ km s^{-1} (Puls et al. 1996), then we expect the wind to have a fiducial optical depth of $\tau_* = 8$. The best-fit model is favored over a $\tau_* = 8$ model with $> 99.99\%$ confidence ($\Delta C = 79$). In Fig. 3 we show the optimal model with a fixed $\tau_* = 8$ (R_0 and normalization are free parameters) along with the global best-fit model.

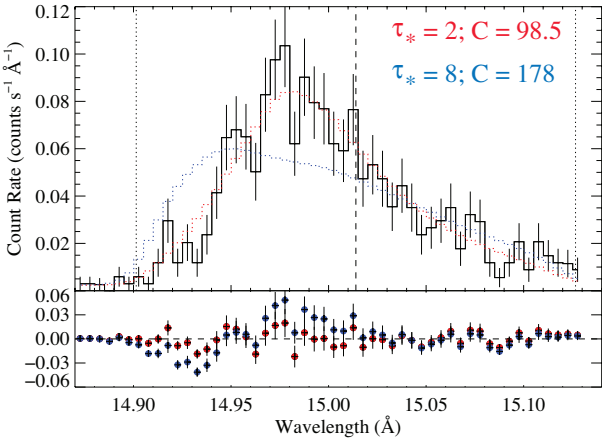

Figure 3: The global best-fit non-porous wind model is shown in red and the best-fit model with the wind opacity expected based on the standard mass-loss rate is shown in blue.

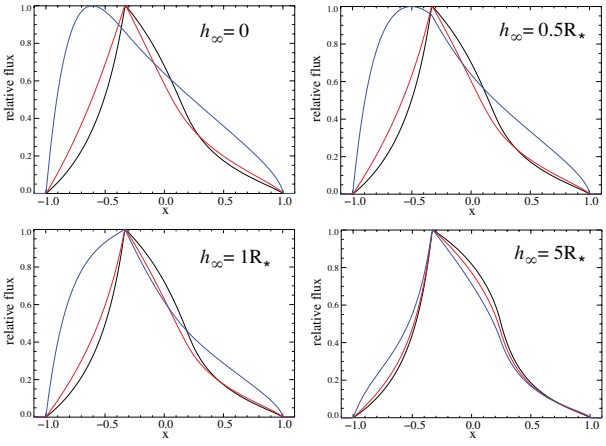

Figure 4: Suite of porous line profile models, shown at infinite resolution. Within each panel, three optical depth values are represented, $\tau_* = 1, 2, 8$: black, red, blue.

We next fit models that allow for porosity, but are

otherwise identical to the Owocki & Cohen (2001) models fit in the previous subsection. In these porous models, the opacity is not atomic, but rather geometric, and due to optically thick clumps of size ℓ and filling factor f. The optical depth is thus modified according to $\kappa_{\rm eff} = \kappa(1 - e^{-\tau_c})/\tau_c$, where κ is the microscopic opacity and τ_c is the clump optical depth, $\tau_c = \kappa\ell\langle\rho\rangle/f$, where $\langle\rho\rangle$ is the local mean wind density (Owocki & Cohen 2006). We parameterize the porosity length as $h(r) = h_\infty(1 - R_*/r)^\beta$ and fix $\beta = 1$, leaving the terminal porosity length, h_∞ as the single additional parameter of the model. As can be seen in Fig. 4, porosity has only a weak effect, even at $h_\infty = 1$ R$_*$. Values above unity are required before the profiles are strongly affected.

Now, by fitting this porous line profile model to the data, we can examine the joint constraints on the key parameters: τ_* and h_∞, while allowing R_0 and the normalization to also be free parameters of the model fit. When we do this, we find a best-fit terminal porosity length of $h_\infty = 0.0$. In other words, the non-porous model is preferred over the porous one. In Fig. 5 we show the joint confidence limits on h_∞ and τ_*.

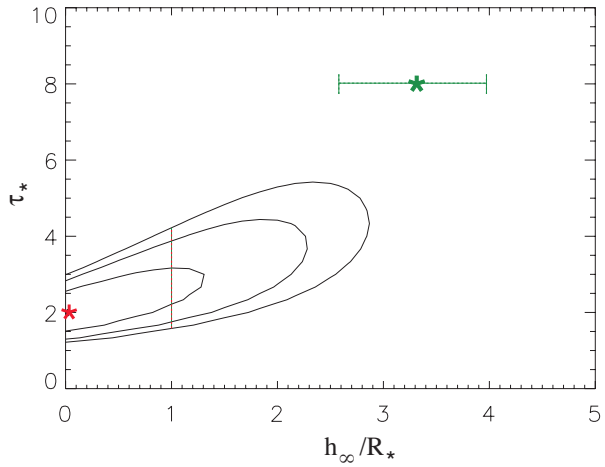

Figure 5: The 68%, 90%, and 95% confidence contours in τ_* - h_∞ parameter space, with the best-fit global model shown as the red star. The green star is the location of the optimized model with $\tau_* = 8$ fixed at the value implied by the literature mass-loss rate. The green line denotes the 68% confidence range on the terminal porosity length, h_∞ when $\tau_* = 8$. The vertical red line emphasizes that even with $h_\infty = 1$, the wind optical depth is only a little higher than the non-porous value of $\tau_* = 2.0$.

From this figure, we can see that the model with low optical depth and no porosity is preferred with a high degree of formal significance over the model with high optical depth and a large porosity length. We can also see, from the shape of the confidence contours, that the porosity length does not appreciably change the optical depth derived from the data until $h_\infty >$ R$_*$. This is in accord with the expectations from the sensitivity of the model profiles to the value of this parameter (as shown in Fig. 4).

We stress that the porous model with the higher mass-loss rate provides an adequate fit to the data, just not as good a fit as the non-porous model. It is possible that a porous model with a different description of porosity could fit the data as well as the non-porous model fit we show. However, we can definitively say two things from the model fitting we have reported on here: (1) Porosity cannot explain the only modestly asymmetric line profiles in ζ Pup any better than a non-porous model with a reduced mass-loss rate can; if anything, it provides a worse fit. And, (2) in order to fit the data with a high mass-loss rate, high porosity model, terminal porosity lengths of several R$_*$ are required.

Regarding this last point, two-dimensional simulations of the line-driven instability show numerous very small structures, as the compressed shells created by the instability break up laterally. Constraints on moving emission bumps seen in WR winds using these 2-D simulations shows that the clumps subtend about 3 degrees, or 1/20 steradian, implying linear clump scales of 1/20 the local stellar radius, and thus quite small porosity lengths (Dessart & Owocki 2003, 2005).

References

Cash, W. 1979, ApJ, 228, 939

Dessart, L., & Owocki, S.P. 2003, A&A, 406, L1

Dessart, L., & Owocki, S.P. 2005, A&A, 437, 657

Oskinova, L.M., Feldmeier, A., & Hamann, W.-R. 2006, MNRAS, 372, 313

Owocki, S.P., & Cohen, D.H. 2001, ApJ, 559, 1108

Owocki, S.P., & Cohen, D.H. 2006, ApJ, 648, 565

Puls J., et al. 1996, A&A, 305, 171

Waldron, W.L., Corcoran, M.F., Drake, S.A., & Smale, A.P. 1998, ApJS, 118, 217

Feldmeier: You suggest a reduction of the wind mass loss rate by a factor of a few, and at the same time you suggest that the wind is not clumped. So what then has gone wrong with $\dot{M}$-estimates from radio and IR so far?

Cohen: It is the destinction between "clumping" and "porosity". What I called a "smooth wind" model I should more properly call a "non-porous" model. The clumps are too small to lead to porosity, in my opinion.

Hamann: 1. There are two ways to reduce the opacity that attenuates the X-rays: by reducing the mass loss rate, or by introducing porosity. Therefore I am not surprised by the similarity of your results to Lida Oskinova's. 2. The predicted X-ray emission depends on the radius where the emitting plasma is located. This is constrained by the fir analyses, but not very well known. 3. The occurence of porosity effects is not up to our free choice. As we have to assume a specific clump filling factor/density contrast, and a plausible separation between the clumps of the order of R_*, the effect just follows automatically, whether we like it or not.

Cohen: 1. Right, porosity leads to a reduction in effective opacity, but this effect is only significant when the porosity length $h \gtrsim r$. There are differences between the detailed line profile shapes, but they are subtle. 2. Please see Leutenegger et al. (2006) for the only analysis that assumed a spatially distributed source of X-rays in the fir analysis. The locations inferred from the line ratios are completely consistent with the profiles of these lines without having to assume large scale ($h \gtrsim r$) porosity. 3. I completely agree: the physics decides. But I am skeptical that the physics is telling us that $h > r$.

Clumping in Hot Star Winds
W.-R. Hamann, A. Feldmeier & L.M. Oskinova, eds.
Potsdam: Univ.-Verl., 2008
URN: http://nbn-resolving.de/urn:nbn:de:kobv:517-opus-13981

Resonance scattering in the X-ray emission lines profiles of ζ Puppis

M.A. Leutenegger[1], D.H. Cohen[2], S.M. Kahn[3], S.P. Owocki[4], & F.B.S. Paerels[1]
[1] *Columbia Astrophysics Laboratory, USA*
[2] *Swarthmore College, USA*
[3] *Stanford University and Stanford Linear Accelerator Center, USA*
[4] *Bartol Research Institute, USA*

We present XMM-*Newton* Reflection Grating Spectrometer observations of pairs of X-ray emission line profiles from the O star ζ Pup that originate from the same He-like ion. The two profiles in each pair have different shapes and cannot both be consistently fit by models assuming the same wind parameters. We show that the differences in profile shape can be accounted for in a model including the effects of resonance scattering, which affects the resonance line in the pair but not the intercombination line. This implies that resonance scattering is also important in single resonance lines, where its effect is difficult to distinguish from a low effective continuum optical depth in the wind. Thus, resonance scattering may help reconcile X-ray line profile shapes with literature mass-loss rates.

1 Introduction

Recent studies of X-ray emission line Doppler profiles from O stars have found that the profiles are too symmetric to be explained in the context of a smooth-wind model, assuming the published mass-loss rates of O stars are correct (e.g. Kramer et al. 2003, Cohen et al. 2006).

There is mounting evidence from studies of UV absorption profiles as well as other lines of inquiry that the true mass-loss rates of O stars are at least a factor of a few smaller than those derived from density-squared diagnostics (e.g. Bouret et al. 2005, Fullerton et al. 2006). However, some of the observed X-ray profiles appear to require mass-loss rate reductions of an order of magnitude (e.g. Kramer et al. 2003, Cohen et al. 2006).

Two alternative explanations for X-ray profile shapes may mitigate the requirement for large mass-loss rate reductions. *Porosity*, the formation of very large, optically thick clumps, could reduce the effective opacity of the wind to X-rays (e.g. Oskinova et al. 2006, Owocki & Cohen 2006). *Resonance Scattering* could change the local angular distribution of emitted X-rays, symmetrizing line profiles and mimicking the symmetric profiles of a wind with little absorption (Ignace & Gayley 2002).

2 He-like emisison line profile discrepancy

In Leutenegger et al. (2007) we present over 400 ks of net XMM-*Newton* Reflection Grating Spectrometer (RGS) data from observations of ζ Pup. This is by far the highest signal-to-noise high-resolution X-ray spectrum available for any O star. In figures 1 and 2 we show this data with the line profile models for the N VI and O VII He-like triplets of ζ Pup, respectively. The profile model is described in Owocki & Cohen (2001) and Leutenegger et al. (2006). Because of photoexcitation of the metastable 1s2s $^3S_1$ state, there are effectively only two lines in each triplet, resonance (r) and intercombination (i). Note however that the models *do* correctly account for the radial dependence of the forbidden-to-intercombination line ratio, as described in Leutenegger et al. (2006). This can be seen in the weak, broad forbidden lines (f).

The models shown have been chosen to fit the red wing of the intercombination line in order to show that the model resonance line is obviously too blueshifted for both complexes. The best-fit models, presented in Leutenegger et al. (2007), have strong residuals in both lines. In both cases, the model clearly does not fit the data, and the r and i lines clearly have different shapes. The observed difference in the profile shapes is an empirical fact, and it is independent of modelling assumptions.

This is remarkable, because we expect these lines to have almost the same profile (modulo the small difference caused by the changing forbidden-to-intercombination line ratio at large radii). This is because both of these lines originate from transitions in the *same ion*.

Resonance scattering can symmetrize lines with high optical depths. The difference in observed profile shapes suggests that this effect is responsible for

the shape of the resonance line, which has a high oscillator strength, while it does not affect the intercombination line, which has a low oscillator strength.

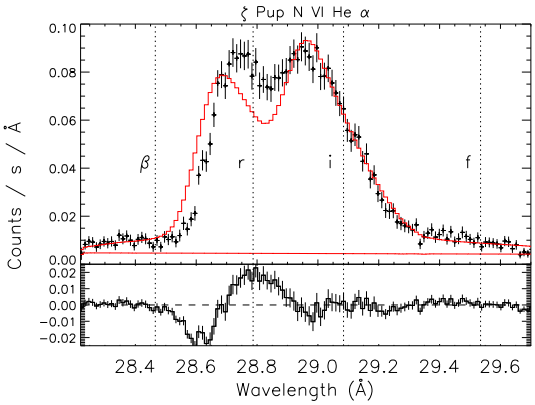

Figure 1: N VI He-like triplet from ζ Pup observed with RGS. The model (red line) does not include resonance scattering and is chosen to fit the red wing of the intercombination line. The dashed lines labelled r, i, f, and β indicate the rest wavelengths of the resonance, intercombination, and forbidden lines, and the C VI Lyβ line, respectively. The lower red line gives the continuum strength.

3 Profiles including resonance scattering

The theory of resonance scattering in O star X-ray line profiles is discussed in Ignace & Gayley (2002) and Leutenegger et al. (2007). In both these analyses, radiative transfer is considered in the Sobolev approximation.

One of the main results of Sobolev theory is that the optical depth of a strong line at a given point depends on the local line-of-sight velocity gradient. In a spherically symmetric radial outflow, the velocity gradient in the radial direction is just the velocity gradient of the flow, dv/dr. In the lateral direction, the line-of-sight velocity gradient is a consequence of the spherical divergence of the wind, v/r.

For a wind with a $\beta = 1$ velocity law, $v/r > dv/dr$ beyond two stellar radii. Far out in the wind, the radial velocity gradient is negligible. Photons emitted primarily from far out in the wind thus see a much higher optical depth in the radial direction than in the lateral direction, and they escape preferentially in the lateral direction. Since the projected velocity is the product of the outflow velocity times the direction cosine, profiles formed by photons emitted preferentially in the lateral direction will be more symmetric than profiles resulting from isotropic emission. This will be the case in typical X-ray line profiles, as long as the continuum optical depth is high enough to obscure photons coming from the inner part of the wind.

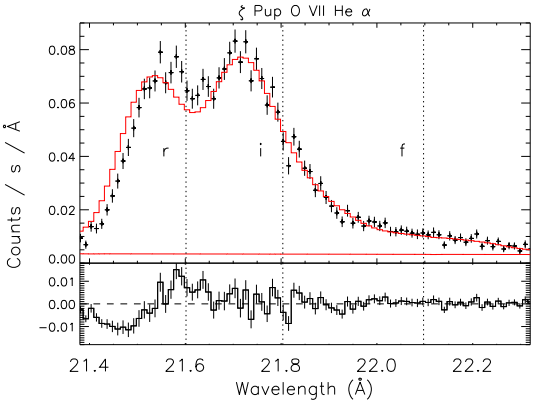

Figure 2: Same as Fig. 1, but for O VII.

In Leutenegger et al. (2007), we introduce a new free parameter, $\tau_{0,*}$, which gives the characteristic Sobolev optical depth for a given line. In Figure 3 we plot model profiles with different values of $\tau_{0,*}$. The models all have the same parameters, other than the variation of the characteristic line optical depth. The effect of resonance scattering is to significantly symmetrize a line profile, with higher optical depths causing stronger symmetrization. For a more in depth discussion of the derivation of this model and its parameters, see Leutenegger et al. (2007).

4 Application of resonance scattering models to data

In figures 4 and 5 we show the best fit models for N VI and O VII including the effects of resonance scattering. These models obviously fit the data much better than the models without resonance scattering. The fact that we observe the same effect in two different ions suggests that this is not a spectroscopic artifact or anomaly. The O VII complex requires a moderate line optical depth, while the N VI complex requires a high line optical depth.

5 Conclusions

By comparing the shapes of line profiles from resonance and intercombination lines originating from the same He-like ion in the X-ray spectrum of ζ Pup,

we find that resonance scattering is important in the formation of the resonance lines and causes them to be significantly more symmetric than the intercombination lines.

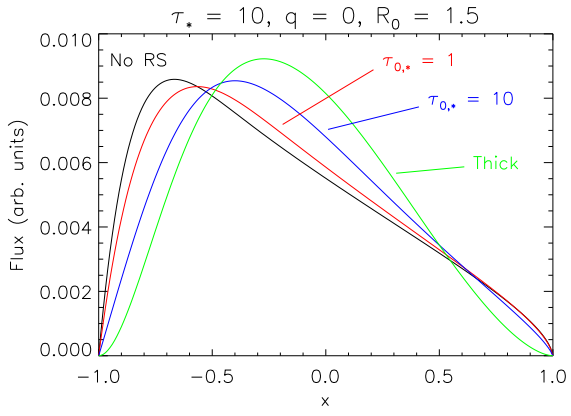

Figure 3: Comparison of different values of the characteristic line optical depth $\tau_{0,*}$.

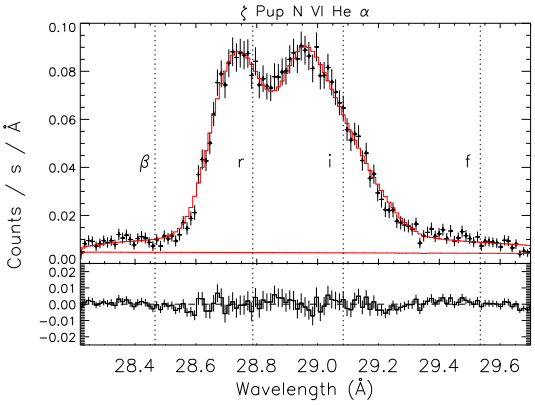

Figure 4: As Fig. 1, but showing the best fit model including resonance scattering for N VI.

This effect could be important for many lines in O stars with high mass-loss rates, and any future analyses of line profiles should take it into account. However, we expect that this effect will be more marginal for K-shell lines of Ne and higher Z elements and L-shell lines of Fe due to their lower elemental abundances.

Accounting for this effect in modelling will allow a partial reconciliation with published mass-loss rates based on density-squared diagnostics, but will likely still require reductions in O star mass-loss rates of a factor of a few. We estimate that our measured values of the continuum optical depth τ_* are consistent with a mass-loss rate of $\sim 1.5 \times 10^{-6}\,M_\odot\,yr^{-1}$, which is a factor of a few greater than the mass-loss rate suggested by modeling profiles without including the effect of resonance scattering. Furthermore, we also estimate that our values of τ_* are consistent with those inferred from the fits to the 15.014 Å line of Fe XVII and the Lyα line of Ne X in the *Chandra* HETG spectrum of ζ Pup presented by Cohen et al. in these proceedings.

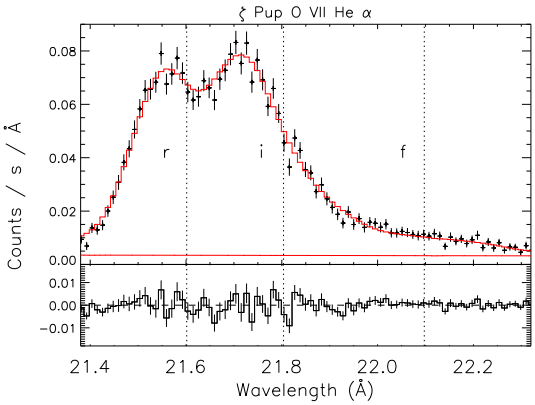

Figure 5: As Fig. 4, but for O VII.

References

Bouret, J.-C., Lanz, T., & Hillier, D.J. A&A 2005, 438, 301

Cohen, D.H., Leutenegger, M.A., Grizzard, K.T., Reed, C.L., Kramer, R.H., & Owocki S.P. 2006 MNRAS, 368, 1905

Fullerton, A.W., Massa, D.L., & Prinja, R.K. 2006 ApJ, 637, 1025

Ignace, R. & Gayley K.G. 2002 ApJ, 568, 954

Kramer, R.H., Cohen, D.H., & Owocki S.P. 2003 ApJ, 592, 532

Leutenegger, M.A., Paerels, F.B.S., Kahn, S.M., Cohen, D.H. 2006 ApJ, 650, 1096

Leutenegger, M.A., Owocki, S.P., Kahn, S.M., & Paerels, F.P. 2007, ApJ, 659, 642

Oskinova, L.M., Feldmeier, A., & Hamann, W.-R. 2006 A&A, 372. 313

Owocki, S.P., & Cohen, D.H. 2001 ApJ, 559, 1108

Owocki, S.P., & Cohen D.H. 2006 ApJ, 648, 565

Puls: In our investigation, we provide only upper limits for $\dot{M}$, which would be true if the outer wind is unclumped. If "your" $\dot{M}$ is a factor of two lower, this would mean that the clumping factor outside is four, which still seems to be reasonable.

Pollock: 1. What difference does C VI Lyβ make to the N VI resonance line? 2. Can you do a similar job for Fe XVII with LGS?

Leutenegger: 1. C VI Lyβ is included in the model; it is weak but it does blend with the blue wing of the N VI resonance line. The fit is fine. 2. I have fit Fe XVII 16.78, which is not a resonance line. It has a τ_* that is consistent with N VI and O VII. Fitting Fe XVII 15.01, a strong resonance line, is on my to-do list.

Clumping in Hot Star Winds
W.-R. Hamann, A. Feldmeier & L.M. Oskinova, eds.
Potsdam: Univ.-Verl., 2008
URN: http://nbn-resolving.de/urn:nbn:de:kobv:517-opus-13981

X-ray line emission produced in clump bow shocks

J.P. Cassinelli[1], R. Ignace[2], W. Waldron[3], J. Cho[1,4], N. Murphy[1], & A. Lazarian[1]
[1] *University of Wisconsin-Madison, USA* [2] *Eastern Tennessee State University. USA*
[3] *Eureka Scientific Inc. USA* [4] *Chungnam National University, Korea*

We summarize CHANDRA observations of the emission line profiles from 17 OB stars. The lines tend to be broad and unshifted. The forbidden/intercombination line ratios arising from Helium-like ions provide radial distance information for the X-ray emission sources, while the H-like to He-like line ratios provide X-ray temperatures, and thus also source temperature versus radius distributions. OB stars usually show power law differential emission measure distributions versus temperature. In models of bow shocks, we find a power law differential emission measure, a wide range of ion stages, and the bow shock flow around the clumps provides transverse velocities comparable to HWHM values. We find that the bow shock results for the line profile properties, consistent with the observations of X-ray line emission for a broad range of OB star properties.

1 Chandra observations of OB line emission

CHANDRA Observations provided many surprises relative to pre-launch expectations, of MacFarlane et al. (1991). We expected X-rays to be forming in driven-wave shocks, where the incident speed relative to the shock front provides the temperature of the shocked gas. The high density at the contact surface is determined by the the square of the incident flow Mach number $\times$ the density of the incident material, $\rho_{\rm wind}$. This picture led to predictions that line profiles should be very broad, and depending on the overlying cool wind column density, either nearly flat topped, or skewed significantly, such that the "blue (shortward) side", arising from the near side of the star, is at a significantly higher flux than the "red side" arising from the far side of the star. Thus, the lines were predicted to be broad, skewed, and with a peak flux shifted toward the blue side.

Observations of lines from 17 OB stars have been presented by Waldron and Cassinelli (2007). The properties of three luminosity classes are considered (Supergiants, Giants, and MS stars). As expected, almost all lines are found to be broad with a typical $HWHM = 0.4 \times v_\infty$. However, the lines are symmetric, showing negligible shift of line centroid, and are well represented by Gaussian line profiles. Figure 1 shows the derived radial dependence of the normalized HWHM and peak line shift, V_P. The radial dependence, expressed in terms of the ambient velocity, is determined from the fir-inferred radii (R_{fir}) obtained from the He-like f/i line ratios, as discussed by Waldron and Cassinelli (2007).

CHANDRA high energy resolution data provides a means to derive information about the radial distances to the X-ray sources (here, clump shocks) by using the forbidden, intercombination, resonance (fir) lines from Helium-like ions. In order of increasing ionization stage along with their associated r-line wavelength, the strongest He-like fir ions that have been observed by CHANDRA are: O VII (21.60 Å), Ne IX (13.45 Å), Mg XI (9.17 Å), Si XIII (6.65 Å), and S XV (5.04 Å).

A surprising result found even in the earliest CHANDRA observations of Waldron and Cassinelli (2001) is that the lower energy He-like ion stages (longer wavelengths) originate farther out in the wind as compared to the higher energy He-like ion stages. We explained this by the fact that "cool" wind continuum opacity to X-rays increases roughly as λ^3, and that the R_{fir} corresponds rather well to the radii of X-ray optical depth unity in the wind. This nice correlation still holds in our survey, especially for the supergiants, *but* only if one assumes the standard mass loss rates for these stars instead of the reduced mass loss rates that we have been discussing here (e.g., Fullerton et al. 2006). Although the giants and MS stars with lower mass loss rates (smaller optical depths) show more dispersal in the relationship, there is no evidence of any X-ray emission arising from below the associated optical depth unit radii. Furthermore, regardless of luminosity class, *none of the stars show high energy ion stages forming far from the star.* Thus, another major problem revealed by X-ray lines is that the high ion stages such as S XV form *too near* the star, i.e., where $U_{\rm shock\,jump} > v_{\rm wind}$.

In Figure 2, temperatures from the line ratios of H-like to He-like ions are plotted versus, R_{fir}. For the supergiants, one does not see ions arising from below a depth that corresponds well continuum op-

tical depth unity.

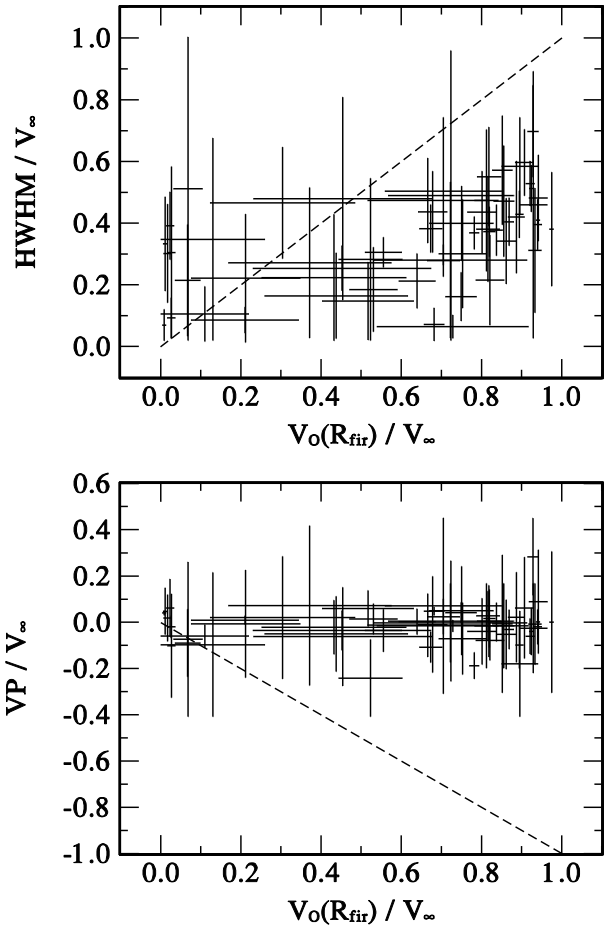

Figure 1: The upper panel shows CHANDRA X-ray line widths, (HWHM) vs. wind speed at line formation radius (R_{fir}), for lines in 17 OB stars. The widths show a distribution for 0. to 0.6 V_∞, with no clear indication of a radial dependence. In the Lower panel are the centroid line shifts vs. wind speed; note that the lines are always nearly unshifted and do not have the expected blueshift

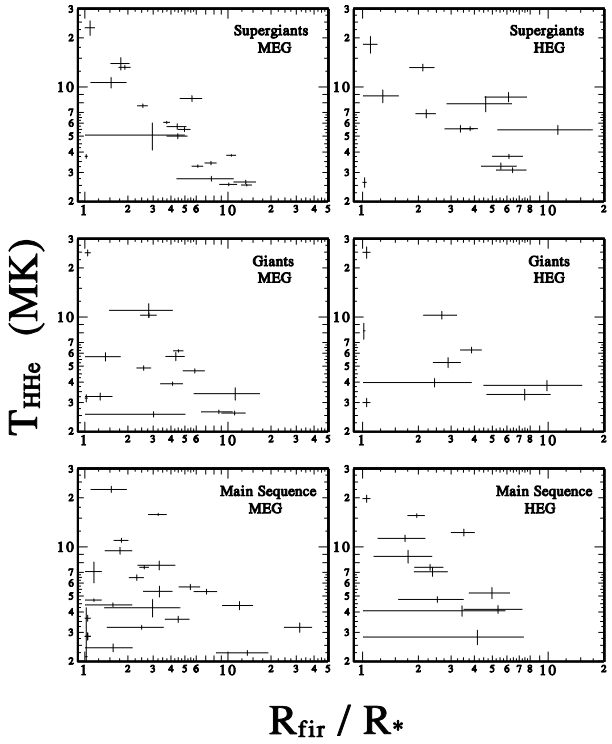

Figure 2: The X-ray source temperature versus radius distributions for three OB luminosity classes, using both the CHANDRA Medium Energy Grating and High Energy Grating. The temperatures from the H-like to He-like line ratios are plotted versus the R_{fir} line formation radii.

For the lower luminosity classes in Figure 2, one sees ions originating at a broader range of radii, but even for these stars, high ions are found not to arise at large radial distances.

Another important property of OB-star X-rays has been found by Wojdowski and Schultz (2005), who derive the stellar Differential Emission Measure (DEM) ($= dEM/d\log T$ vs. log T). For most OB stars, the DEM is a simple downward sloping power-law, from $T = 10^6$ up to a $T_{\max} > 10^7$ K. (Highly magnetic stars can have DEM increasing with T.)

2 Bow shock modeling

We have used the hydrodynamical code (ENO) of Cho and Lazarian (2001) to derive the temperature, velocity, density structure of post shock region for a wind colliding with an impenetrable sphere. We find a power law differential emission measure, in Figure 3, which is similar to that found observationally by Wojdowski and Schulz (2005). Thus, there is a wide range of ionization at each clump, with the maximum temperature set by $T_{\max} = 14$ MK $(v_{1000})^2$. The emission measure for the lower temperatures (and hence the lower ion stages), arises from the fact that a bow shock has an increased area toward the wings where the shock is increasingly oblique. Across an oblique shock there is a reduced change in flow speed and hence a reduced temperature increase is expected. The hydrodynamical models also show a significant flow of X-ray emitting gas around the clump face with a sideways speed of about 45% the incident wind speed.

We find, in contrast with Planar shocks (e.g., Feldmeier 1995), that the density behind the shock does

not rise above 4× the wind density and so the X-ray emission is from near the shock front. Hence, we say that we can use the "On the Shock" or $OTSh$ approximation for a simple analyses of bow shocks.

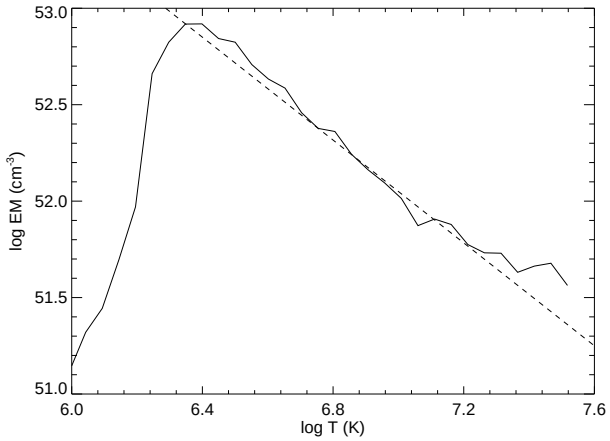

Figure 3: The Emission Measure versus Temperature power law distribution, with the maximum T set by the speed of the incident wind relative to the shock, $U_\circ$.

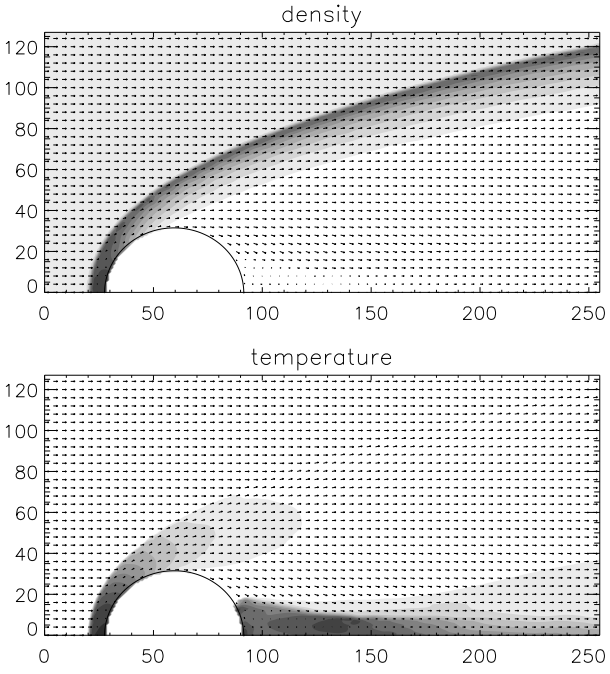

Figure 4: Bow shock structure. The X-ray production mostly occurs very near the shock at uniform density near $4\rho_{\rm wind}$.

As for the observed near-zero velocity shift and broad HWHM of the lines, these can best be explained if we have the X-ray line emission arising from the sides of the star as seen by the observer (i.e., perpendicular to the line-of-sight). This region contains a spread in speeds around the, $v_z = 0$, isovelocity surface. A concentration of emission from that sector of the wind would occur if the cool clump absorbs the line emission from the bow shock at its star-ward face. Thus we see an enhanced contribution from the regions at, and symmetric about, $v_z = 0$. This counters the expected tendency to see the blueward-shifted and -skewed line emission.

There is also the problem regarding the very high temperatures and correspondingly high high ions that are inferred to be present at small radii, the "near-star high-ion problem", as we call it. This could perhaps be explained by the infalling clump idea proposed by Howk et al. (2000). They point out that this could work for stars with lower wind momentum fluxes that produce a smaller drag force. As for the other stars, there are other possibilities for producing high relative speeds between the wind and the clumps.

In summary, accounting for bow shocks around clumps in winds can potentially explain: a) the zero centroid shift problem, ($V_p \approx 0.0$), (if the radiation is primarily from clumps to the side of the star). b) the broad line widths, because the bow shock sideways velocity plus a range in v_z is comparable to the HWHM) c)the DEM power laws, which follows directly from the wind -oblique shock interaction. d) the large range in ions and ion temperatures, also arising from the oblique shocks, and perhaps e) the concentration of the highest ions and highest temperatures relatively near the star, if clumps can have large speeds relative to the wind near the star.

We acknowledge support from NASA grant TM4-5001X, and the NSF Center for Magnetic Self Organization in Lab. and Astrophysical Plasmas.

References

Cho, J., Lazarian, A. 2005. Theo. Comp. Fluid Dyn. 19, 127

Feldmeier, A. 1995, A&A, 299, 523

Howk, J.C., Cassinelli, J.P., Bjorkman, J.E., & Lamers, H.J.G.L.M. 2000, ApJ, 534, 348

MacFarlane, J.J., Cassinelli J.P., Welch. B.Y., Vedder, P.W., Vallerga, J.V., & Waldron, W.L. 1991, ApJ, 380, 564

Waldron, W.L. & Cassinelli, J.P. 2001, ApJ, 548, L45

Waldron, W.L. & Cassinelli, J.P. 2007, ApJ, in press

Wojdowski, P., & Schulz, J.P. 2005, ApJ, 627, 953

Najarro: What if clumping disappears towards the outer regions of the winds. Would that not be consistent with a need for a reduction of the mass loss rate in regards to the UV lines of P V and with X-rays from the outside?

Cassinelli: Certainly one of the possible solutions to the P V problem, that seems to require a large reduction in mass loss rate, is to have Phosphorus Auger-ionized to even higher stages of ionization by the X-rays passing through the winds. An advantange of clumps is that the X-rays would be produced in close proximity to the clumps. In the $\dot{M}$ reduction papers, it is assumed that P V is the dominant stage of ionization even in the dense clumps, and so the P V line absorption is independent of clumping. However with a strong source of nearby X-ray emission the dominant stage of ionization could be P VII or P VIII. As for the location of the clumps and their associated X-rays: it certainly seems plausible that the clumpiness could decrease with radius, or that the velocity of the clumps relative to the ambient wind could decrease with radius, which would result in the production of softer X-rays. If the mass loss rate is actually the high, traditional value, one needs to find a way to change the ionization stage of P V. If the mass loss rate is actually very low, as has been proposed, one would not need to have the X-rays do anything to the ionization of P V. However, my feeling is that if we know that there is clumping it is inevitable that X-rays are produced. If the X-rays were to be absent in the outer regions then one would get less of a P change at high Doppler shift, and I do not think that is what is observed. The radio flux tends to form in the outer regions, and clumpiness seems to be needed to enhance that flux. The UV line profiles are broad and these indicate that the line is formed over a wide range in velocity and hence in radius. The fraction of the wind that is hot enough to produce X-rays is really quite small, like 10^{-3}, typically, and the R_{fir} diagnostic shows that the X-rays are formed over a range in radii from near the star out to say $10\,R_*$. So I do not see that eliminating the clumping in the outer regions helps much.

Cohen: Why do you assume that the jump velocity at a shock is half the wind speed?

Cassinelli: It is based on the shock models of Glenn Cooper that he did in his thesis at U. Delaware and work in Madison. Also the shock models of Achim Feldmeier et al. (1997) typically showed jumps of about half the speed of the incident gas. Subsequent infall of a clump would allow for a shock jump to be larger than the local wind speed, producing the high temperatures that seem to be needed.

Puls: Which temperature and which emission radius are you proposing from your X-ray studies.

Cassinelli: The highest ion stages in the Waldron and Cassinelli (2007) study are of S XV and S XVI and of Si XIII and Si XIV and these two pairs of ions form in temperatures in the range 13 to 25 million K and 10 to 16 million K, respectively. The fir radii are in the range 1.1 to 2.5 R_*. So we see the "near star high ion problem" as an important new property of hot-star winds.

Feldmeier: You suggest that clumps fall back to the star. Stan and I recently did some simulations where we increased and decreased the base density by up to a factor of 300. The effect of the density decrease was the creation of a velocity plateau, as I showed in my talk yesterday. But there is essentially no effect of a density increase. So I am a bit uncertain about how one can actually create a backfalling clump.

Cassinelli: In the Howk et al. paper (2000, ApJ, 534, 348), we assumed that the density in the clump is increased relative to the ambient wind by a factor (Mach number)^2. This is an even larger factor than you assumed. The high density (and a specific mass range, near 10^{19} gram) means that the cross sectional area is rather small and this area determines the continuum radiation driving, i.e. there is no velocity gradient in the clump. The dominant outward acceleration on the clump is the wind drag force acting on the area πR^2 of the clump, and since the clump is assumed to form where its velocity is less than the escape speed, it could fall back, and hence lead to the large shock speed needed for the hard X-ray emission (of τ Sco). The enhancement of ρ in your velocity plateau is smaller than what we are envisioning.

Clumping in Hot Star Winds
W.-R. Hamann, A. Feldmeier & L.M. Oskinova, eds.
Potsdam: Univ.-Verl., 2008
URN: http://nbn-resolving.de/urn:nbn:de:kobv:517-opus-13981

Probing clumpy stellar winds with a neutron star

R. Walter[1,2], J. Zurita-Heras[3] & J.-C. Leyder[4]
[1] *Observatoire de Genève, Université de Genève, Chemin des Maillettes 51, CH-1290 Sauverny*
[2] *INTEGRAL Science Data Centre, Chemin d'Ecogia 16, CH-1290 Versoix*
[3] *Laboratoire AIM, CEA/DSM-CNRS-Université Paris Diderot, DAPNIA/SAP, F-91191 Gif-sur-Yvette*
[4] *Institut d'Astrophysique et de Géophysique, Université de Liège, Allée du 6-Août 17, B-4000 Liège*

INTEGRAL tripled the number of super-giant high-mass X-ray binaries (sgHMXB) known in the Galaxy by revealing absorbed and fast transient (SFXT) systems. Quantitative constraints on the wind clumping of massive stars can be obtained from the study of the hard X-ray variability of SFXT. A large fraction of the hard X-ray emission is emitted in the form of flares with a typical duration of 3 ksec, frequency of 7 days and luminosity of 10^{36} erg/s. Such flares are most probably emitted by the interaction of a compact object orbiting at $\sim 10\ R_*$ with wind clumps ($10^{22\cdots23}$ g) representing a large fraction of the stellar mass-loss rate. The density ratio between the clumps and the inter-clump medium is $10^{2\cdots4}$. The parameters of the clumps and of the inter-clump medium, derived from the SFXT flaring behavior, are in good agreement with macro-clumping scenario and line-driven instability simulations. SFXT are likely to have larger orbital radius than classical sgHMXB.

1 Introduction

Indirect measures of the structure of massive-star winds are possible in X-ray binaries through the analysis of the interaction between the compact companion and the stellar wind. In this report we summarize the constraints obtained on wind clumping in HMXB using the hard X-ray variability observed by the IBIS/ISGRI instrument on board INTEGRAL (Winkler et al., 2003). Further details can be found in Walter and Zurita (2007) and Leyder et al. (2007).

Classical wind-fed, Roche-lobe underflow, super-giant HMXB (sgHMXB) are made of a compact object orbiting within a few (1.5 to 2.5) stellar radii from a super-giant companion. Recently INTEGRAL almost tripled the number of sgHMXB systems known in the Galaxy and revealed a much more complex picture with two additional families of sources: (1) the highly-absorbed systems which have orbital and spin periods similar to those of classical sgHMXB but much higher absorbing column densities on average (Walter et al., 2006) and (2) the fast transient systems which are characterized by fast outbursts and by a very low quiescent luminosity (Sguera et al., 2006, Negueruela et al., 2007).

2 Sources and data analysis

Several sources have now been proposed as candidate super-giant fast X-ray transient based on their hard X-ray variability characteristics, and, for a subset of them, optical counterpart spectral type. Contrasting statements have however been made on specific sources for what concerns their persistent or transient nature. In the frame of the current study we have considered all SFXT candidates together with several persistent and absorbed super-giant HMXB for comparison. Among them, we specifically excluded known Be systems, sources detected only once by INTEGRAL, blended INTEGRAL sources, long period systems and the sgB[e] system IGR J16318−4848.

We analyzed the available INTEGRAL data for 12 candidate SFXT (table 1) that have large variability factors and compared them with the classical and absorbed sgHMXB systems that have a typical variability factor $\lesssim 20$. The sources of the sample are located along the galactic plane that has been heavily observed by INTEGRAL. All public data available until March 2007 are considered in this study. Individual ISGRI sky images have been produced for each INTEGRAL pointing in the energy band 22–50 keV. The detection of the sources of the sample is forced in each image and the source count rate extracted.

Source flares have been detected by requiring a minimum of 25 ksec of inactivity between them. Flare duration of the order of a single INTEGRAL pointing (2 ksec) have been observed in all sources (excepting IGR J16465−4507). Their typical duration is 3 ksec. Fewer longer (> 15 ksec) flares have also been detected but in most cases could be interpreted as a serie of shorter flares or a long activity period. They will not be discussed further here.

Table 1: List of SFXT candidates with quiescent flux $F_{\rm q}$, source observing elapsed time $T_{\rm obs}$ and flaring characteristics: maximum count rate $F_{\rm fl}$, number of flares $N_{\rm fl}$ and the average flare duration $t_{\rm fl}$.

Source	$F_{\rm q}$ ct/s	$F_{\rm fl}$ ct/s	$N_{\rm fl}$	$t_{\rm fl}$ ks	$T_{\rm obs}$ days
SFXT systems					
IGR J08408−4503	< 0.1	3.9	2	3.6	52.0
IGR J17544−2619	0.06	24	8	2.5	127.0
XTE J1739−302	0.08	28	12	4.2	126.4
SAX J1818.6−1703	0.18	45	11	2.9	76.9
IGR J16479−4514	0.2	19	38	3.6	67.0
AX J1841.0−0536	< 0.1	15	4	5.8	51.9
AX J1820.5−1434	< 0.1	5.3	4	3.9	59.4
Intermediate systems					
AX J1845.0−0433	0.2	6.2	6	4.0	55.2
IGR J16195−4945	0.2	4.8	6	2.2	71.8
IGR J16465−4507	0.1	6.9	3		66.7
IGR J16207−5129	0.4	9.2	11	4.3	73.7
XTE J1743−363	0.5	9.2	19	2.5	122.9

Table 1 lists the sources together with their quiescent count rate ($F_{\rm q}$), average flare count rate ($F_{\rm fl}$), number of flares ($N_{\rm fl}$), range of flare durations ($t_{\rm fl}$) and total source observing elapsed time ($T_{\rm obs}$). As the probability to detect a flare decreases when the source gets outside of the fully-coded field of view, the effective observing time for flare detection can be estimated as $0.6\ T_{\rm obs}$.

The sources have been separated in two categories. The SFXT include systems featuring hard X-ray variability by a factor $\gtrsim 100$. "Intermediate" systems are candidate SFXT with smaller variability factors that could be compared with those of classical systems. From the variability point of view, sources closer to the bottom of the table are more similar to classical sgHMXB.

3 Discussion

The distances to the SFXT systems has been evaluated (2–7 kpc) in a few cases. We will assume, for the rest of the discussion, a distance of 3 kpc. The average count rate observed during flares lies between 3 and 60 ct/s which translates to hard X-ray luminosities of $(0.2-4)\times10^{36}$ erg/s. Such luminosities are not exceptional for sgHMXB but very significantly larger than the typical X-ray luminosity of single massive stars of 10^{30-33} erg/s at soft X-rays (Cassinelli et al., 1981).

As the sources are flaring at most once per day, their average hard X-ray luminosity is very low, reaching $(0.2-4)\times10^{34}$ erg/s. It is therefore very unlikely that those systems have average orbital radius lower than 10^{13} cm i.e. $\sim 10\ R_*$. One expects orbital periods larger than 15 days and underflow Roche lobe systems (note that no orbital period has yet been derived in any of these systems).

Wind clumps

The interaction of a compact objet with a dense clump formed in the wind of a massive companion leads to increased accretion rate and hard X-ray emission.

The free-fall time from the accretion radius $R_a = 2\times10^{10}$ cm towards the compact object is of the order of $(2...3)\times10^2$ sec. As the intrinsic angular momentum of the accreted gas is small (Illarionov and Beloborodov, 2001) the infall is mostly radial (down to the Compton radius) and proceeds at the Bondi-Hoyle accretion rate.

With a duration of $t_{\rm fl} = 2...10$ ksec, the observed short hard X-ray flares are significantly longer than the free-fall time. The flare duration is therefore very probably linked with the thickness of the clumps which, for a clump radial velocity $V_{\rm cl} = 10^8$ cm/s, is $h_{\rm cl} = V_{\rm cl}\times t_{\rm fl} \sim (2...10)\times10^{11}$ cm.

The average hard X-ray luminosity resulting from an interaction between the compact object and the clump can be evaluated as $L_{\rm X} = \epsilon\ M_{\rm acc}c^2/t_{\rm fl}$ (where $\epsilon \sim 0.1$) and the mass of a clump can then be estimated as $M_{\rm cl} = (R_{\rm cl}/R_{\rm a})^2\ M_{\rm acc} = (R_{\rm cl}/R_{\rm a})^2\ L_{\rm X}\ t_{\rm fl}/(\epsilon\ c^2)$ where $R_{\rm cl}$ is the radius of the clump perpendicular to the radial distance. In the case of a spherical clump, $M_{\rm cl} = \left(\frac{L_{\rm X}}{10^{36}\ {\rm erg/s}}\right)\left(\frac{t_{\rm fl}}{3\ {\rm ks}}\right)^3\ 7.5\times10^{21}$ g.

If $\dot{N}$ is the rate of clumps emitted by the star, the observed hard X-ray flare rate is given by $T^{-1} = \dot{N}(R_{\rm cl}^2/4R_{\rm orb}^2)$. The rate of mass-loss in the form of wind clumps can then be estimated as $\dot{M}_{\rm cl} = \left(\frac{10{\rm d}}{T}\frac{L_{\rm X}}{10^{36}{\rm erg/s}}\frac{t_{\rm fl}}{3{\rm ks}}\right)\left(\frac{R_{\rm orb}}{10^{13}{\rm cm}}\right)^2\ 3\times10^{-6}\ {\rm M}_\odot/{\rm yr}$.

For a $\beta = 1$ velocity law and spherical clumps, the number of clumps located between $1.05R_*$ and $R_{\rm orb}$ can be evaluated as $N = \left(\frac{10\ {\rm d}}{T}\right)\left(\frac{3\ {\rm ks}}{t_{\rm fl}}\right)^2\left(\frac{R_{\rm orb}}{10^{13}\ {\rm cm}}\right)^3\ 3.8\times10^3$.

Assuming spherical clumps, the clump density at the orbital radius is $\rho_{\rm cl} = \left(\frac{L_{\rm X}}{10^{36}\ {\rm erg/s}}\right)\ 7\times10^{-14}$ g cm^{-3} and the corresponding homogeneous wind density is $\rho_h = \dot{M}_{\rm cl}/(4\pi R_{\rm orb}^2 V_{\rm cl}) = \left(\frac{10\ {\rm d}}{T}\frac{L_{\rm X}}{10^{36}\ {\rm erg/s}}\frac{t_{\rm fl}}{3\ {\rm ks}}\right)\ 1.5\times10^{-15}$ g cm^{-3}. The clump volume filling factor at the orbital radius is $f_{\rm V} = \frac{\rho_h}{\rho_{\rm cl}} = \left(\frac{10\ {\rm d}}{T}\frac{t_{\rm fl}}{3\ {\rm ks}}\right)\ 0.02$ and the corresponding porosity length is $h = \frac{R_{\rm cl}}{f_{\rm V}} = \left(\frac{T}{10\ {\rm d}}\right)\ 15\times10^{12}$ cm.

If the density of a clump decreases with radius as $r^{-2\beta}$ and its mass remains constant, the averaged homogeneous wind density within $R_{\rm obs}$ is

$\overline{\rho_h} = NM_{\rm cl}/(\frac{4}{3}\pi R_{\rm orb}^3) = \left(\frac{10\ {\rm d}}{T}\frac{L_{\rm X}}{10^{36}\ {\rm erg/s}}\frac{t_{\rm fl}}{3\ {\rm ks}}\right)\ 7\times 10^{-15}$ g cm^{-3} and the average clump volume filling factor and porosity length could be estimated as 0.1 and 3×10^{12} cm, respectively.

The variety of $t_{\rm fl}$, T and $F_{\rm fl}$ that are observed probably reflects a range of clump parameters and orbital radii. Several of the average clump parameters estimated above, in particular the clump density, filling factor and porosity length do not depend on the orbital radius, which is unknown, and only slowly depend on the observed quantities.

These average parameters match the macro-clumping scenario of Oskinova et al. (2007) to reconcile clumping and mass-loss rates. The number of clumps derived above is also comparable to evaluations by Lepine and Moffat (1999), Oskinova et al. (2006). The volume filling factor, porosity length and the clump mass-loss rate are also similar to those derived by Bouret et al. (2005) from the study of ultraviolet and optical line profiles in two super-giant stars.

The column density through a clump can also be estimated as $N_H = \frac{M_{\rm cl}}{R_{\rm cl}^2 m_p} = \left(\frac{L_{\rm X}}{10^{36}{\rm erg/s}}\frac{t_{\rm fl}}{3{\rm ks}}\right)\ 5\times 10^{22}{\rm cm}^{-2}$. The clumps remain optically thin in the X-rays.

Inter-clump medium

The variation of the observed X-ray flux between flares and quiescence provides in principle a direct measure of the density constrast between the wind clumps and the inter-clump medium.

Density contrasts of $> 10^{2-4}$ and 15–50 have been observed in SFXT and "Intermediate" sources, respectively. The density contrast is larger in SFXT than in "Intermediate" and, of course, classical systems. Density contrasts are probably stronger when clumping is very effective.

Numerical simulations of the line driven instability (Runacres and Owocki, 2005) predict density contrasts as large as 10^{3-5} in the wind up to large radii. At a distance of 10 R_*, the simulated density can vary between 10^{-18} and 10^{-13} g cm^{-3} and the separation between the density peaks are of the order of R_*. These characteristics are comparable to the values we have derived.

What about classical sgHMXB ?

Classical sgHMXB are characterized by small orbital radii $R_{\rm orb} = (1.5-2.5)\ R_*$, and by flux variability of a factor $\lesssim 10$. Such variabilities were modelled in terms of wind inhomogeneities largely triggered by the hydrodynamic and photo-ionisation effects of the accreting object on the companion and inner stellar wind (Blondin et al., 1991, Blondin, 1994). At small orbital radii, the companion is close to fill its Roche lobe, which triggers tidal streams. In addition the X-ray source ionizes the wind acceleration zone, prevents wind acceleration and generates slower velocities, denser winds, larger accretion radius and finally larger X-ray luminosities. Whether or not the stellar wind is intrinsically clumpy at low radius, the effect of the compact object on the wind is expected to be important.

The main difference between SFXT and classical sgHMXB could therefore be their orbital radius (Leyder et al. (2007)). At very low orbital radius ($< 1.5\ R_*$) tidal accretion will take place through an accretion disk and the system will soon evolve to a common envelope stage. At low orbital radius ($\sim 2\ R_*$) the wind will be perturbed in any case and efficient wind accretion will lead to copious and persistent X-ray emission (10^{36-37} erg/s). At larger orbital radius ($\sim 10\ R_*$) and if the wind is clumpy, the SFXT behavior is expected as described above. If the wind clumps do not form for any reason, the average accretion rate will remain too low and the sources will remain mostly undetected by the current hard X-ray survey instruments.

References

Blondin, J., Stevens, I., Kallman, T., 1991, ApJ, 371, 684

Blondin, J., 1984, ApJ, 435, 756

Bouret, J.-C., Lanz, T., Hillier, D., 2005, ApJ, 438, 301

Cassinelli, J.-P-, Waldron, W., Sanders, W. et al., 1981, ApJ, 250, 677

Illarionov, A., Beloborodov, A., 2001, MNRAS, 323, 159

Lepine, S., Moffat, A., 1999, ApJ, 514, 909

Leyder, J.-C., Walter, R., Lazos, M., et al., 2007, A&A, 465, L35

Negueruela, I, Smith, D., Torrejon, J. et al., 2007, arXiv:0704.3224v2

Oskinova, L. M., Feldmeier, A., Hamann, W.-R., 2006, MNRAS, 372, 313

Oskinova, L. M., Hamann, W.-R., Feldmeier, A., 2007, A&A, 476, 1331

Runacres, M., Owocki, S., 2005, A&A, 429, 323

Sguera, V., Bazzano, A., Bird, A. et al., 2006, ApJ, 646, 452

Walter, R., Zurita-Heras, J., Bassani, L., et al., 2006, A&A, 453, 133

Walter, R., Zurita-Heras, J., 2007, A&A, submitted

Winkler, C., Courvoisier, T., Di Cocco, G. et al., 2003, A&A, 411, L1

O. Reimer: What are the considered time scales if you invoke the TeV-emission connection of the integral absorbed binaries, when having clumps involved?

Walter: The protons are accelerated extremely rapidly in the magnetosphere gaps and are released as soon as the gyration radius exceeds the Alfvén radius. Those protons that will interact with the dense clump will generate TeV emission immediately. I therefore expect the TeV to be correlated with the X-ray light curve.

Cassinelli: So you have a clump of density 10^4 times the density of the wind that directly collides with the neutron star? Also the factor of 10^4 is not far from the $\mathrm{Ma}^2\,\rho_{\mathrm{wind}}$ from the driven wave model I have discussed here.

Walter: The density ratio seems to vary from source to source. However in some sources indeed the ratio reaches 10^4.

Moffat: Are you saying there is essentially only one clump size? Or do you see a distribution in clump masses, and if so, what kind of a distribution?

Walter: We are observing clumps with sizes between 10^{11} to 10^{12} cm, assuming spherical geometry. I cannot exclude smaller clouds that would not be massive enough to be considered within our current analysis.

Clumping in Hot Star Winds
W.-R. Hamann, A. Feldmeier & L.M. Oskinova, eds.
Potsdam: Univ.-Verl., 2008
URN: http://nbn-resolving.de/urn:nbn:de:kobv:517-opus-13981

Discussion: X-rays

Moderator: Joachim Puls

Feldmeier: David, why is always exactly the porosity length $h = 0$ in your confidence plots? This is statistically significant. One would instead expect a distribution around $h = 0$.

Cohen: The mean value is not significant, but only the error interval.

Feldmeier: The wind fragmentation model was invented to help understand the data. Now you say it is of no use. How can this be understood physically?

Cohen: Because fragments are wrong. It should be Rayleigh-Taylor fingers like in Dessart & Owocki (2003, A&A).

Feldmeier: But that latter model is problematic because the radiative transfer is only 1D there, not accounting for the lateral line force.

Cohen: Rayleigh-Taylor breakup of radially compressed shells seems physically plausible to me. Fragmentation while the fragments of the shells retain their radial compression and lateral coherence seems less likely to me, but certainly not out of the question.

Oskinova: I am worried whether it is methodologically correct to use fitting software in order to discriminate between models. Fitting software is a wonderful tool to infer parameters for a given underlying model. However, it is unclear to me how to treat the situation when a physically unsound model would provide a statistically good fit to observations, e.g. due to a large number of free parameters. I would say that good fitting statistics *per se* may be necessary, but it is certainly not sufficient to physically validate the input model.

Pollock: The HMXBs show me at least that there is no chance that you can see in X-rays to the other side of an O star. These accreting neutron star X-rays sources are always very heavily absorbed. As they emerge from eclipse the X-ray reach the observer first through the upper layers of the companion star and then through the lower layers of the wind. The column density falls from $10^{24}\,\mathrm{cm}^{-2}$ or more but never gets lower than $10^{22}\,\mathrm{cm}^{-2}$.

Oskinova: The column density is largest when we are directly looking at the neutron star because of the absorption column. In order to emit, a neutron star should accrete. Therefore, talking about direct component in the spectra of HMXBs, I would say we always would see the neutron star absorbed, otherwise it would not be X-ray active.

Prinja: It is interesting to note that in terms of large-scale structure (e.g. DACs), the UV time series show that the coherence of the structures evident is greater as you go from early O stars (like ζ Pup), to mid-O (like ξ Per) and finally early B stars (such as HD 64760). Perhaps this behavior should also be examined in connection to any pattern in the shapes and shifts in the X-ray profiles (e.g. in the survey of Waldron & Cassinelli, 2007).

Hillier: I agree wholeheartedly with Joachim Puls that taking another look at the soft X-ray band for ζ Pup would be extremely beneficial. There are some interesting issues that could be looked at. Does He III recombine? Is porosity important for seeing the soft X-rays? Do the soft X-rays originate at larger radii? I also have a question regarding the X-ray properties of O stars. ζ Pup seems to be the prototypical example of what we expect the X-ray spectrum of an O star to look like. Can someone address the other O stars, and their X-ray properties?

Hamann: The radius where the X-ray emitting plasma is located is determined by the f/i line ratios of He-like ions. This diagnostic yields the dilution factor of the UV radiation field that depopulates the metastable levels. Thus the results and their uncertainty depend on having a good model for the stellar UV radiation field. Which model did you use, and it this a major source of uncertainty?

Cassinelli: We considered both the Kurucz and Hubeny atmospheric models. There was some difference in the f/i radii, but not a large amount. If the wavelength of the f-i transition were to fall at the wavelength of a broad FUV or EUV line, that would make the R_{fir} value smaller, and if the wavelength were at an emission line, R_{fir} would be larger. But the conclusion that the high ions form near the star, and that low ions can form at all radii is a good one.

Leutenegger: X-ray emitting regions formed far out in the wind cannot cool efficiently, so X-ray emission can persist to large radii. Also, since most O stars observed in X-ray have lower mass loss rates than ζ Pup by a factor of a few, and since the highest values of τ_* I measure in ζ Pup are of order four, the highest values of τ_* measured in other stars should be of order unity. This produces nearly symmetric

profiles. Thus, it is not surprising that we see relatively narrow, almost symmetric profiles from most O stars.

Hamann: Stan Owocki doubts whether porosity plays a role in the continuum absorption of X-rays, but he agrees that its effect can reduce the P V resonance line. I want to point out that a similar clump separation (of the order of one stellar radius) has been aplied in our X-ray modelling as well as in our recent modelling of the UV and optical lines. The only difference is that shell fragments ("pancakes") have been adopted for the X-ray attenuation, while the recent line-formation study is still restricted to isotropic clumps.

Oskinova: In our models of X-ray line profiles we assumed that a clump is "launched" once per flow time in each radial direction. Thus, the clump separation at v_∞ is one stellar radius. But in the wind acceleration region, the clump separation is much smaller. This is a plausible choice of parameters and is supported by observations. In denser winds, because our models conserve mass, these clumps are not necessarily optically thin, therefore smooth wind models are not adequate to model X-ray lines. The assumption of anisotropic opacity within clumps, e.g. that clumps are shell-fragments, leads to more symmetric line profiles compared to the isotropic case. Therefore, X-ray emission line profiles provide a wonderful tool to gain insight into the clump geometry.

Runacres: Paco, I think it is important to realize that you do not know whether the clumping factor *disappears* in the radio formation region. You may know that the clumping factor is *lower* in the radio formation region than in the region close to the star (by comparing the radio continuum with other diagnostics), but you do not know whether it is zero. This means, as was mentioned before by Joachim (Puls), that the $\dot{M}$ we derive actually the largest possible value. The actual numbers depend on the residual amount of clumping in the radio formation region.

Leutenegger: The He-like profiles from my paper support Joe's idea of seeing down to the radius of optical depth unity, but for a lower mass loss rate than Cassinelli & Waldron claim. This is just because they assume a single radius of formation, while we fit the entire profile with a model that accounts for f/i as a function of radius.

Feldmeier: Refering to Mark: it should be easy to replace the current approximation of a constant clumping factor with radius, or of some simple power law, with a more realistic law obtained from numerical simulations. The line-driven instability operates mostly in the accelerating part of the velocity law where de-shadowing occurs, and it does not form significant new wind structure at large distances from the star where the wind speed is almost constant. There are, therefore, only two competing processes that determine the clumping factor at large radii: clump-clump collisions in the stochastic clump ensemble; and pressure expansion of clumps.

Future observations and conference summary

Chair: J.-C. Bouret

Clumping in Hot Star Winds
W.-R. Hamann, A. Feldmeier & L.M. Oskinova, eds.
Potsdam: Univ.-Verl., 2008
URN: http://nbn-resolving.de/urn:nbn:de:kobv:517-opus-13981

Imaging and spectroscopy with the James Webb Space Telescope

G. Sonneborn
NASA's Goddard Space Flight Center, USA

The James Webb Space Telescope (JWST) is a large, infrared-optimized space telescope scheduled for launch in 2013. JWST will find the first stars and galaxies that formed in the early universe, connecting the Big Bang to our own Milky Way galaxy. JWST will peer through dusty clouds to see stars forming planetary systems, connecting the Milky Way to our own Solar System. JWST's instruments are designed to work primarily in the infrared range of 1 - 28 μm, with some capability in the visible range. JWST will have a large mirror, 6.5 m in diameter, and will be diffraction-limited at 2 μm (0.1 arcsec resolution). JWST will be placed in an L2 orbit about 1.5 million km from the Earth. The instruments will provide imaging, coronography, and multi-object and integral-field spectroscopy across the 1 - 28 μm wavelength range. The breakthrough capabilities of JWST will enable new studies of massive star winds from the Milky Way to the early universe.

1 Mission Overview

The James Webb Space Telescope (JWST) is a large (6.5 m), cold ($T < 50$ K), infrared-optimized space observatory being built for launch in 2013 on an Arianespace Ariane 5 ECA rocket into orbit around the Sun-Earth Lagrange point L2. The observatory will have four instruments: a camera, a multi-object spectrograph, and a tunable filter imager will cover the near-infrared spectrum ($0.6 < \lambda < 5.0\mu$m). A mid-infrared instrument will provide imaging and spectroscopy from $5.0 < \lambda < 28$ μm. Coronography will also be possible across the entire JWST bandpass. JWST is a cooperative project between NASA and the European and Canadian Space Agencies (ESA and CSA).

The JWST science goals, observatory design, operational concept, and expected performance are described in detail by Gardner et al. (2006, see the link on the JWST web site www.jwst.nasa.gov/science.html) to download the reprint of this large paper). The present contribution is a highly abbreviated version of the information contained in Gardner et al.

The JWST science goals are divided into four themes. The End of the Dark Ages: First Light and Reionization theme is to identify the first luminous sources to form and to determine the ionization history of the early universe. The Assembly of Galaxies theme is to determine how galaxies and the dark matter, gas, stars, metals, morphological structures, and active nuclei within them evolved from the epoch of reionization to the present day. The Birth of Stars and Protoplanetary Systems theme is to unravel the birth and early evolution of stars, from infall on to dust-enshrouded protostars to the genesis of planetary systems. The Planetary Systems and the Origins of Life theme is to determine the physical and chemical properties of planetary systems including our own, and investigate the potential for the origins of life in those systems.

To enable these observations, JWST consists of a telescope, an instrument package, a spacecraft and a sunshield. The instrument package contains the four science instruments (SIs) and a fine guidance sensor. The spacecraft provides pointing, orbit maintenance and communications. The sunshield provides passive thermal control. The JWST operations plan is based on that used for previous space observatories, and the majority of JWST observing time will be allocated to the international astronomical community through annual peer-reviewed proposal opportunities. JWST will be operated by Space Telescope Science Institute.

The telescope is a deployable optical system consisting of 18 hexagonal beryllium segments that provide diffraction-limited performance at 2 μm using active wavefront sensing and control. The wavelength range of JWST and the SIs spans 0.6 to 29 μm, limited at the short end by the gold coatings on the primary mirror and at the long end by the detector technology. The sunshield passively cools the telescope and SIs.

JWST is designed to provide instantaneous sky coverage over the solar elongation range of 85° to 135° (95° to 45° from the anti-solar direction). A continuous viewing zone within 5° of both the north and south ecliptic poles is available throughout the year. Thirty percent of the sky can be viewed continuously for at least 197 continuous days. All regions

of the sky have at least 51 days of continuous visibility per year. The JWST architecture provides an instantaneous visibility of ∼40% of the sky.

The sunshield reduces the ∼ 200 kW incident solar radiation that impinges on it to milliwatts incident on the telescope and SIs. This solar attenuation is a result of the five-layer configuration of the sunshield. Its physical size and shape determine the instantaneous sky coverage for the observatory. By reducing the solar radiation to the milliwatt level, the observatory has an intrinsically stable point spread function at all solar orientations.

Many JWST observations will be background limited. The background is a combination of in-field zodiacal light, scattered thermal emission from the sunshield and telescope, scattered starlight, and scattered zodiacal light. Over most of the sky, the zodiacal light dominates at wavelengths $\lambda < 10\mu m$. The flux senstivities of the JWST instruments are given in Table 1.

2 JWST Science Instruments

JWST has four science instruments: NIRCam, NIRSpec, TFI, and MIRI (described in Section 6.5). A cryo-cooler will be used for cooling MIRI and its Si:As detectors. The near-infrared detector arrays in the other instruments are passively cooled HgCdTe. In addition, the instrument module has the Fine Guidance Sensor (FGS, provided by CSA) and a computer that directs the daily science observations based on plans received from the ground. The science instruments and FGS have non-overlapping FOVs. Simultaneous operation of all science instruments is possible. This capability will be used for parallel calibration, including darks and possibly sky flats. FGS is used for guide star acquisition and fine pointing. Its FOV and sensitivity are sufficient to provide a greater than 95% probability of acquiring a guide star for any valid pointing direction and roll angle.

2.1 Near-Infrared Camera (NIRCam)

NIRCam provides filter imaging and coronagraphy in the 0.6 to 5.0 μm range with wavelength multiplexing. It includes the ability to sense the wavefront errors of the observatory. NIRCam uses a dichroic to simultaneously observe the short (0.6 to 2.3 μm) and long (2.4 to 5.0 μm.) wavelength light paths.

The instrument contains a total of ten 2k×2k detector chips, including those in the identical redundant optical trains. The short wavelength arm in each optical train contains a 2×2 array of these detectors, optimized for the 0.6 - 2.3 μm wavelength range, with a small gap (∼3 mm = ∼5 arcsec) between adjacent detectors. The detectors arrays are HgCdTe of HAWAII II heritage. The detectors will all have thinned substrates to avoid cosmic ray scintillation issues, as well as to extend their sensitivity below 0.85 μm. Each optical train contains a dual filter and pupil wheel, containing a range of wide-, medium- and narrow-band filters and the WFS&C optics.

To enable the coronagraphic imaging, each of the two identical optical trains in the instrument also contains a traditional focal plane coronagraphic mask plate held at a fixed distance from the detectors, so that the coronagraph spots are always in focus at the detector plane. Each coronagraphic plate is transmissive, and contains a series of spots of different sizes, including linear and radia-sinc occulters, to block the light from a bright object.

2.2 Near-Infrared Spectrograph (NIRSpec)

NIRSpec is a near infrared multi-object dispersive spectrograph provided by ESA that is capable of simultaneously observing up to ∼100 sources over a field-of-view (FOV) larger than 3 × 3 arcmin. In addition to the multi-object capability, it includes fixed slits and an integral field unit (IFU) for imaging spectroscopy. Six gratings will yield resolving powers of R ∼ 1000 and ∼ 3000 in three spectral bands, spanning the range 1.0 to 5.0 μm. A single prism will yield R ∼ 100 over 0.6 to 5.0 μm.

Targets in the FOV are normally selected by opening groups of shutters in a micro-shutter assembly to form multiple apertures. The micro-shutter assembly itself consists of a mosaic of 4 subunits producing a final array of approximately 750 (spectral) by 350 (spatial) individually addressable shutters with 200 × 450 milliarcsec (mas) openings and 250 × 500 mas pitch. The minimum aperture size is 1 shutter (spectral) by 1 shutter (spatial) at all wavelengths. Multiple pointings may be required to avoid placing targets near the edge of a shutter and to observe targets with spectra that would overlap if observed simultaneously at the requested roll angle. The nominal slit length is 3 shutters in all wavebands. In the open configuration, a shutter passes light from the fore-optics to the collimator. A slitless mode can be configured by opening all of the micro shutters. As the shutters are individually addressable, long slits, diagonal slits, Hadamard transform masks, and other patterns can also be configured with them.

In addition to the slits defined by the micro-shutter assembly, NIRSpec also includes five fixed slits that can be used for high-contrast spectroscopy. They are placed in a central strip of the aperture focal plane between sub-units of the micro-shutter assembly. Three fixed slits are 3.5 arcsec long and 200 mas wide. One fixed slit is 4 arcsec long and 400 mas wide for increased throughput at the expense of spectral resolution. One fixed slit is 2 arcsec long and 100 mas wide for brighter targets.

Table 1: JWST Instrument Sensitivities

Instrument/Mode	λ (μm)	Bandwidth	Sensitivity
NIRCam	1.1	R=4	12.1 nJy, AB=28.7
NIRCam	2.0	R=4	10.4 nJy, AB=28.9
TFI	3.5	R=100	126 nJy, AB=26.1
NIRSpec/Low Res	3.0	R=100	120 nJy, AB=26.2
NIRspec/Med Res	2.0	R=1000	1.64×10^{-18} erg s^{-1} cm^{-2}
MIRI/Broad-Band	10.0	R=5	700 nJy, AB=24.3
MIRI/Broad-Band	21.0	R=4.2	7.3 μJy, AB=21.7
MIRI/Spect.	9.2	R=2400	1.0×10^{-17} erg s^{-1} cm^{-2}
MIRI/Spect.	22.5	R=1200	5.6×10^{-17} erg s^{-1} cm^{-2}

NOTE – Sensitivity is evaluated for a point source detected at 10 σ in 10000 s

2.3 Tunable Filter Imager (TFI)

The TFI, built by CSA, provides narrow-band near-infrared imaging over a field of view of 2.2 × 2.2 arcmin^2 with a spectral resolution R ∼ 100. The etalon design allows observations at wavelengths of 1.6 μm to 2.6 μm and 3.1 μm to 4.9 μm, although this design is still prelminary. The gap in wavelength coverage allows the single channel to reach more than one octave in wavelength.

The TFI incorporates four coronagraphic occulting spots permanently to one side of the field of view, and occupying a region 20 by 80 arcsec. A set of selectable apodization masks is located at the internal pupil images of each channel by the filter wheels. The coronagraph is designed to deliver a contrast ratio of $\sim 10^4$ (10σ) at 1 arcsec separation. The sensitivity is limited by speckle noise. Contrast ratios of 10^5 may be achievable at sub-arcsec scales using roll or spectral deconvolution techniques.

2.4 Mid-Infrared Instrument (MIRI)

MIRI, provided by a consortium of European and U.S. institutions, is designed to obtain imaging, coronography, and spectroscopic measurements over the wavelength range 5 to 28 μm. A cryo-cooler will keep the MIRI Si:As detectors $T \sim 6$ K. The optical bench contains two actively cooled subcomponents, an imager and IFU spectrograph, plus an on-board calibration unit. The imager module provides broad-band imaging, coronagraphy, and low-resolution (R∼100, 5-10 μm) slit spectroscopy using a single 1024×1024 pixel Raytheon Si:As detector with 25 μm pixels. The coronagraphic masks include three phase masks for a quadrant-phase coronagraph and one opaque spot for a Lyot coronagraph. The coronagraphic masks each have a square field of view of 26 × 26 arcsec and are optimized for particular wavelengths.

The IFU obtains simultaneous spectral and spatial data on a small region of sky. The spectrograph field of view is next to that of the imager so that accurate positioning of targets will be possible by locating the image with the imager channel and offsetting to the spectrograph. The light is divided into four spectral ranges by dichroics, and two of these ranges are imaged onto each of two detector arrays. A full spectrum is obtained by taking exposures at each of three settings of the grating wheel. The spectrograph uses four image slicers to produce dispersed images of the sky on two 1024 × 1024 detectors, providing R ∼ 3000 integral field spectroscopy over the 5 to 29 μm wavelength range, although the sensitivity of the detectors drops longward of 28 μm.

References

Gardner, J. P., et al. 2006, Sp. Sci. Rev., 123, 485-606

Cassinelli: You mentioned that NIRSPEC has 62000 microshutters! That sounds dangerous, i.e. depending on so many moving parts to work.

Sonneborn: The microshutter array (171 × 365) has been tested at 40 K for over 100 000 operations. A significant duty cycle is part of the design, and has been tested at cryogenic temperatures in the lab. Each shutter is independent, so even if one shutter fails, there are many more to do the job.

Massa: Why do the simulations for the Fabry-Perot show a speckle pattern?

Fullerton: In the context of coronography, "speckles" are artifacts caused by imperfections in the primary mirror. For JWST, they will be dominated by mid-frequency errors irregularities on intermediate spatial scales. These errors are termed chromatic, because they scale with λ / D, where D is the diameter of the mirror. So a particularly cool feature of the Tunable Imager is its capability of scanning in wavelength. This permits weak astrophysical sources (brown dwarfs, planets) to be distinguished from the background of "speckle noise".

Clumping in Hot Star Winds
W.-R. Hamann, A. Feldmeier & L.M. Oskinova, eds.
Potsdam: Univ.-Verl., 2008
URN: http://nbn-resolving.de/urn:nbn:de:kobv:517-opus-13981

General Discussion

Moderator team: A.F.M. Moffat, J. Hillier, W.-R. Hamann, S. Owocki

Cassinelli: Could you explain why clumping affects the red wing of the line? Does it have something to do with iso-velocity surfaces, i.e. more scattering of photons from the back side of the star?

Hillier: In WR stars and P Cygni stars the electron scattering wings (proportional to density) are always too strong in homogeneous winds when we fit the emission line strengths (generally proportional to density squared) with our models. The only way to reduce the strength is to introduce clumping. In P Cygni stars, with low outflow velocities, the wings are fairly symmetric about the emission line whereas in WR stars the wings are mainly seen on the red, as originally predicted by Auer and van Blerkom. While it easy to deduce that $f < 1$ (say 0.1) it is quite difficult to determine an accurate value. In O stars the electron scattering wings created in the wind are usually too weak to provide meaningful constraints.

As to your question the simplest explanation can be provided by assuming that we have an outflow, electron thermal motions are negligible, the photon is initially emitted near the core at zero velocity, and scatters off an electron moving with velocity v. To a good approximation the electron scattering process is coherent in the electron restframe, and hence the incident photon will be redshifted in the electron's frame. Since in the observer's frame the electron can be either moving towards or away from the observer, the photon will pick up an additional red- or blueshift. For a photon scattered in the same direction as the incident photon, the net shift will be zero, but for a photon scattered through 180 degrees the redshift will correspond to $2v$. In Wolf-Rayet stars the outflow velocities dominate over electron thermal motions, but in P Cygni the reverse is true.
The same effect can be seen when we look at emission lines, arising in the central source, that are scattered off out-flowing dust in the Homunculus associated with Eta Carinae. The reflected emission lines are always redshifted.

Hamann: Regarding the question whether *all* hot-star winds are clumped, I want to nominate possible exceptions. The Galactic WN star WR 2 is the only one for which Cheneé and Moffat (this meeting) could not find any line-pofile variability. The spectrum of WR 2 looks different from all other Galactic WN spectra because of the round shape of the emission-line profiles that cannot be reproduced by any of our models. But, strikingly, the spectrum can be nicely matched by a model after convolution with rotational broadening of $v \sin i = 1900$ km/s (see Hamann et al. 2006). I know that just a convolution is not an adequate model for a rotating stellar wind, but still this may indicate that WR 2 is a very rapidly rotating star close to its breakup limit. Maybe that this rapid rotation leads to a different wind dynamics where the line-driven instability cannot develop? Recently we realized that there is a counterpart in the LMC, Brey 6, which shows a very similar spectrum with the same round-shaped profiles, which are again reproduced with a rotationally broadened model spectrum.

Schnurr: Regarding the rotationally broadened lines of WR2 and Brey 6: can you reproduce the spectrum by taking a normal line spectrum and diluting it?

Puls: Round-shaped profiles can be explained by optically thick shells, as already shown by John Castor in 1970 (MNRAS).

Pollock: Just out of interest: WR2 is one of the apparently single WN stars that does have X-ray emission.

Moffat: If WR 2 is a fast rotating WR, could this be a candidate for a GRB since it is believed that approximately one in 10^3 WR stars can become a GRB. There we have one star among ~ 300 WR stars known in the Galaxy.

Owocki: Well, it may be interesting that observations can be fit with such a huge rotation, but of course it makes little physical sense to have an outflowing wind simply be forced to have such a huge rigid-body rotation. If it were from a magnetic field, then there should be complex structure from regions of wind confinement, and surely it would become more oblate than spherical. So I am at a loss to know how to develop a dynamical model for this.

Cassinelli: Regarding the DAC effect: plateaus in velocity do not lead to the density increase that I am interested in. Is the DAC effect analogous to the weak shock in the wings of a bow shock?

Hillier: How universal are DACs?

Prinja: It now seems that in all cases of line-driven winds the spectral signature of migrating

DACs are seen in the UV resonance lines: this includes O stars, B supergiants, PN central stars and WR stars (WR24). The only time-series data of variable UV wind-formed lines that do not show DACs, are the disk winds from cataclysmic variables.

Owocki: As I noted above, it may be that DACs are the consequence of relative velocity plateaus that seem to occur naturally after kinks that form ahead of some slower moving compression. In this view, they would be a characterisitc feature of structure in a line-driven flow. I did not know that disk winds from cataclysmic variables did not show DACs, and I will have to think why. Perhaps it means they are not primarily line-driven?

Townsend: When considering the role played by pulsation in producing clumped winds, it is important to remember that pulsational instabilities are rather universal in massive stars. The instability strips associated with the κ mechanism (either iron bump or deep iron bump), and with strange modes, cover most of the hot, high-mass HRD. Of course, we do not see a coherent pulsation signature in massive stars. But that could very well be, because the instability excites a few thousand pulsation modes, each a small amplitude, rather than a couple of individual modes to a detectable amplitude. The effectively incoherent velocity perturbations caused by these thousands of modes could be what we observe as macroturbulence and could seed the line-driven instability at the wind base, leading to clumping.

Puls: I just want to mention that Lefever, Puls and Aerts (2007) performed an investigation of periodically variable B supergiants in order to investigate the possibility of the κ mechanism. Interestingly, we choose 12 comparison stars which were not known to be periodically variable. After our investigation, it turned out that 9 of these 12 are very similar to the confirmed variables. This shows that at least among B supergiants pulsations are more the rule than the exception.

Feldmeier: I have a question to Rich Townsend: You spoke about the 2000 or so excited pulsation modes in a massive star. For acoustic modes there are the famous results by Poincare and others that when you feed an atmosphere with a spectrum of sound waves, there is a large amount of energy that accumulates at the acoustic cutoff period. And such a strong oscillation signal is indeed seen on sun. Would something similar happen for pulsations, i.e. that they pump energy into one single frequency? This could be interesting to understand the recurrence time of DACs.

Townsend: There are two cutoffs when we consider non-radial pulsation: one at high frequencies and one at low frequencies. For the sorts of modes that are unstable in massive stars, the frequencies fall well inside these cutoffs, and so in principle we expect complete reflection of the modes at the stellar surface. However, this analysis (and all others to date) neglects the effect of wind outflow. The only exception is the PhD thesis of Steve Cranmer. Steve did a very insightful local analysis of wave propagation in an expanding isothermal atmosphere and showed that complete wave reflection is impossible. Some fraction of the wave energy will always leak out into the wind, possibly seeding the line-driven instability.

Massa: I have no explanation for the recurrence time of the DACs in ζ Pup. They are what they are. In HD 64760, the "bananas" have roughly the same ionization structure. Perhaps Alex Fullerton can add something. He is the one who did the time series analysis.

Fullerton: Concerning the "spiral" modulations in HD 64760: Fourier analysis of the periodic modulations shows that lower ions lag the higher ions very slightly. This is consistent with higher ions being preferentially (but not exclusively) located along the leading edge of the spiral feature. So, in addition to the "every second spiral" ionization effect which Derck Massa mentioned, there seems to be a small ionization shift across a spiral feature.

Hamann: Concerning the DACs, we have shown in a widely ignored paper (Hamann et al. 2001) that the corotating interaction region (CIR) model cannot explain their remarkably slow frequency drift. A simple kinematical model reveals that the apparent acceleration of a CIR feature is even higher than the clump acceleration without rotation. However, the observations can be understood if the DACs are formed by structures which are travelling upstream in the wind with something like the Abbott speed.

Feldmeier: Twice the Abbott speed!

Hamann: Okay, twice the Abbott speed according to your newest result about the motion of kinks.

Schnurr: So far, continuum-driven winds have not been mentioned in this meeting. So, I wonder whether continuum-driven LBV outbursts produce clumps, as are seen in LBV nebulae?

Townsend: Stan Owocki has done quite a bit of work on this issue. For a star above the Eddington limit (from which we expect continuum-driven mass loss) the whole envelope is above the Eddington limit, not just the surface layers. The star will therefore try to drive the whole envelope off in a massive wind outflow. This will invariantly fail, due to effects such as photon tiring, and the outflow will fragment and partly fall back to the star. But now that we have a clumpy wind, it is possible for porosity to allow a steady (albeit non-homogenous) outflow. Owocki, Gayley and Shaviv (2004) demonstrated how porosity can modulate the continuum

radiative force, and allow the atmosphere of a super-Eddington star to transition from hydrostatically bound to accelerating outward.

Cassinelli: Regarding continuum-driven winds: Rico Ignace and I studied the IR line profiles from ISO to derive a velocity law of WR stars. The WR should be small, $\sim 1R_\odot$ from evolution models, but $\sim 10R_\odot$ from line profile wind analyses. It seems there must be a slowly accelerating outflow deep down and a transition to a rapid accelerating wind at larger radii.

Ignace: In describing the inner, slowly accelerating WR wind, the necessary conditions appear to be very delicate. Surely, WR stars have non-zero rotation. Do you have an idea of how rotation will affect this delicate force balance? I mean, in light of the fact that most WR stars are not intrinsically polarized.

Massa: Can I get a consensus of what a wind might look like? When Vink produced a grid of mass loss rates versus stellar parameters that was great since it gave observers a paradigm to test. It seems to me that when I talk to different theorists that I get a general picture of bow shocks and that these may be clumped in some way to make coherent features such as DACs and "bananas". Is that correct? What does the panel think?

Lobel: The CIRs in our hydrodynamical models are large-scale density and velocity structures that produce slowly drifting features in the P Cygni profiles called DACs. For the DACs we modelled in HD 64760 there is no shock surface. There is only a kind of "smooth" density wave. If the radiative driving mechanism is unstable in these CIRs, they may fall apart in "clumps", but this idea for the origin of clumps is not going to resolve the $\dot{M}$ discrepancies because such density waves do not require large changes of $\dot{M}$. The hydrodynamic simulations show that changes of $\dot{M}$ of less than 1% suffice to produce the CIRs. We need the CIRs to make the DACs observed in many O and B type stars, so the CIR should be a stable feature in the wind that is not easily disrupted. If it can be broken up, it should build up again very fast. The coherent CIR structure results from a steady mass injection at the base of the wind which I think is very different from the source of the clumps we are talking about.

Blomme: CIRs can survive a limited amount of breakup due to the instability mechanism. But they would not survive a large amount of instability. The DACs would disappear.

Hillier: I wonder whether DACs could be produced not by an outflow, but by some type of coherent phenomena (density wave). By analogy with a traffic jam, the pile up of cars at the traffic jam is determined mainly by local conditions, and not by where the cars are from.

Feldmeier: Referring to Joe Cassinelli's bow shock model that was mentioned by Derck: I think this model runs into the problem first raised by John Hillier in his ROSAT paper 1993: once you have created clumps, the interclump density is much lower than the CAK density: the material is sitting in the clump and is lost between the clumps, where now the density is very low. This is indeed seen in the hydrodynamic wind simulations. Now when you have this thin material crashing into the clump at high speeds, it may create sufficiently high temperatures for X-ray emission, but it does not produce sufficiently large X-ray flux.

Cassinelli: I envision the high density of these clumps as arising at the contact surface of a driven wave, giving $\rho = \mathrm{Ma}^2\,\rho_{\mathrm{wind}}$. This high density shell breaks up owing to, say, Rayleigh-Taylor instability and forms clumps onto which the wind collides producing the bow shock. The clump probably would have the same velocity from front edge to rear edge so there is no line driving force on it but rather only the continuum radiation force on πR^2_{clump} (and the drag force of the wind passing by).

Hamann: In your (Joe Cassinelli's) sketch you have placed the bow shocks of clumps around their bottom side. This seems to be the common understanding, and is supported by the hydrodynamic modelling by e.g. Achim Feldmeier, where smaller cloudlets are strongly accelerated and ram from below into bigger, denser shells. However, the original idea by Lucy & White (1980) to explain the X-ray emission had been that the clumps are ploughing through a slower ambient wind, the bow shocks thus preceeding the clumps. I would like to reconsider this scenario, for two reasons. First, in the Monte-Carlo X-ray modelling by Lida (Oskinova et al.) we found no reasonable fit of the observed emission if the emitters are always attached to the bottom side of clumps. Second, there is no reason to assume that the radiative acceleration of blobs is smaller than for lower-density material. Rather on the contrary, hydrodynamic plus non-LTE modelling by Götz Gräfener has shown that in denser material the excited atomic energy levels are more populated, while at low densities all ions tend to be in their ground state. Moreover, ionization degrees are lower in the denser blobs, again providing more line opacities. These density effects are not taken into account in the present time-dependent models by Stan Owocki and Achim Feldmeier. I can imagine that the densest clouds are actually accelerated more rapidly than the ambient gas of lower density, forming their bow shock on the upper side.

Cassinelli: Regarding the depth of formation of X-rays: In the bow shock picture, an important contribution to the width (HWHM) is from the sideways (lateral flow) past the curved front of the bow. Also the high ions form deep and that is okay in your

picture because the continuum optical depth is $\lesssim 1$. The O VII lines form at the larger radius, as you show.

Ignace: In terms of anticipating the structured flow expected from fully 3D time dependent simulations, Puls and I discussed the possibility that one might have something like the patch method ("1D sectors") but with partially overlapping sectors (more or less). In this case there would still be clump collisions, but this would lead to "shredding" and a cascade of structure with lateral spatial scale. However, perhaps such effects will be governed by Rayleigh-Taylor instability if this is faster.

Puls: I just want to remind you that the observed "macroturbulence" in hot supergiants ($3\,v_{\rm sound}$) has not been explained so far. We do not know where it comes from and what its relevance with respect to clumping is.

Hamann: David Cohen has argued that porosity effects may be negligible for the attenuation of X-rays from O stars like ζ Pup. But look at our diagram showing the radius where the radial optical depth becomes unity. At wavelengths of the observed X-ray emission line, this radius lies at several stellar radii, even if taking the clumping-reduced mass loss rate of $\log \dot{M} = -5.56$. However, from the width of the X-ray lines, as well as from the expectation that the strongest shocks are located in the acceleration zone, one should expect that the X-rays are produced below a radius of about $2\,R_*$. Only porosity can explain how these X-rays manage to emerge from the star.

Leutenegger: The opacity plot Wolf-Rainer Hamann showed for ζ Pup is oversimplified. Using realistic opacities and line profile models shows that there is no inconsistency between profile widths (velocities) and the continuum optical depth of the wind.

Pollock: I have a way of reducing the line widths which none of you seem to like and that is to get a shock to randomize v_∞. Velocity randomization is what shocks do. Then you share the velocity from one dimension into three and the component along the line of sight is naturally narrower than X-ray material moving with the bulk velocity of the wind. In ζ Ori, the maximum velocity seen on both, the red and blue sides of the line, is about 80 or 90% of the maximum expected values (Pollock 2007).

Hillier: It is clear that when making inferences from X-ray analyses, and discussing the appropriateness of different results, that a detailed comparison of the adopted wind opacity must be done. This means verifying the cross-sections, adopted ionization structure, and abundances. This is particularly important because of the recent suggestion by Asplund that CNO abundances in the sun should be revised downwards.

Hamann: Is there still a P V problem and how can it be solved?

Fullerton: To the issue of whether there is still a P V problem: My hope is that we have all agreed that there is a problem; that the discrepancy is real. Beyond that, there are a large number of issues that remain to be resolved. These concern, e.g., the exact ion fraction of P V, the effect of X-rays and the extent to which "macroclumps" are present and optically thick to resonance-line radiation. Beyond an ill-defined feeling that an order of magnitude reduction in $\dot{M}$ is probably too large, I have not sensed any concensus on the resolution of these issues. So my answer is that the problem remains; and in fact we do not know what the mass loss rates of O stars are to the desired accuracy.

Puls: I also think that there is a P V problem: As we have heard, P V can be made consistent with $\dot{M}$ from other diagnostics, but the degree of the reduction in $\dot{M}$ depends crucially on our assumptions. If we have microclumping, this reduction is of the order of ten, and if we include macroclumping, we might be able to have a reduction of "only" a factor of three. Due to the difficulties in the statistical modelling (porosity, vorosity etc.), we have to carefully test these models, agree on them and apply them to a wide range of parameters and diagnostics. Only then we will be able to say which $\dot{M}$ reduction P V actually implies.

Prinja: We should note that it is not just a "P V problem" but also extends to sulphur and silicon, the latter is the case in B supergiants. All their diagnostics point to a need for low $\dot{M}$, compared to the smooth wind case.

Gräfener: As far as I see it there is no observational evidence against the low P V mass loss rates plus microclumping. We saw that the O star spectra are convincingly reproduced (Bouret, this volume) and also that the X-ray line profiles favor microclumping plus low mass loss (Cohen, this volume, and Leutenegger, this volume). Moreover, my own wind models with large microclumping factors nicely reproduce the low mass loss rates.

Owocki: Does Achim Feldmeier want to comment on the intercloud lengthscale?

Feldmeier: From your and my simulations, the biggest shells or shell fragments have a radial distance of order $1\,R_*$ for reasonable base perturbation periods. But you suggest that for isotropic clumps one would need seperations of even a few R_*, and I cannot see how to achieve this. But for the pancake-shaped clumps a distance of $1R_*$ between clumps may be sufficient to explain the observed X-ray emission line profiles.

Owocki: Well, the pancake shape does help to increase the effective porosity, but only marginally.

And I would argue that dynamically they would be likely to break up into clumps with comparable lateral and radial size. Based on the simulations done so far, it seems that stochastic structure arising from the line-driven instability is likely to have too small a porosity length to explain the X-ray profile symmetry. Perhaps larger scale structure seeded by, e.g. pulsations, would work better, but that seems a less universal mechanism.

Townsend: I would like to emphasize that we can still get a porous wind with clumps that are close together. So long as the clumps are optially thick (i.e."macroclumping"), all that determines the radiative transfer properties of the wind is the porosity length $h = L^3/l^2$, where L is the clump separation and l is the clump size. So, with small L we can still obtain large h, as long as l is small, too. Of course, with very small clumps, it can be problematic to ensure that the clumps remain optically thick. The density in the clumps (relative to the interclump medium) must be very large, which may be unphysical.

Hamann: I want to emphasize that the criterium whether porosity effects will make the medium effectively more transparent, does not only depend on the average clump separation L. The effect occurs when the optical depth across a clump becomes larger than unity, and this optical depth scales also with the density contrast: $\tau_C = \kappa_D\ D^{2/3}\ L$.

Owocki: Yes, assuming that the κ_D is the wind opacity for the *mean* density (with units of inverse length), then the quantity $D^{2/3}L$ is just what I call the "porosity length". If l is the clump size then $D = (L/l)^3$ is the inverse of what I have called the volume filling factor, $f = 1/D$, giving the porosity length $h = l/f$, and so clump optical thickness $\tau_C = \kappa_D h$. For a given mean opacity κ_D, the key to having a significant porosity effect is thus to have a porosity length h that is large enough to make the individual clumps optically thick.A key point, though, is that the (continuum) photon mean free path between optically thick clumps is also set by this porosity length h, and not, for example, by the clump separation scale L.

Feldmeier: I have a similar question to Stan Owocki as George Sonneborn, but even without rotation: What would you expect for the shape of the clumps? In your paper with Luc Dessart you find shell fragments, maybe similar to Joe Cassinelli's suggestion of clumps with bow shocks. I remember that a few years ago you made an interesting suggestion that the wind structure may look like a 1D spray or stream coming out of a tube of toothpaste, which is very curly and goes to all different lateral directions. Do you think such a spaghetti stream could stay coherent, or would it break up laterally into separate clumps?

Owocki: If I understand you correctly, this is essentially what Luc Dessart has done. But the key approximation has been to ignore the lateral radiation forces, which in principal may regulate the lateral scale at which Rayleigh-Taylor instabilities can operate.

Runacres: The moving box models described in my talk can certainly be extended to 2D: a first toy model would be to examine whether clump collisions in 2D still produce density enhancements predicted by the 1D models, or whether instabilities may inhibit such density enhancement. A further idea would be to build on the Dessart & Owocki (2003, 2005) models and extend them to large distances ($\sim 250\,R_*$).

Owocki: Yes, this would be interesting. For the radial direction, the computational box could have the quasi-periodic boundary conditions developed by the pseudo-planar model, but also use real periodic conditions in the lateral direction. In this way, clumps would have another degree of freedom and not be forced to repeatedly collide as in 1D mdoels, and this would certainly be more realistic.

Hamann: Stan Owocki has argued that clumps move strictly radially, because high lateral velocities would have been observed. I want to contradict here, as I think that lateral velocity components cannot be distinguished observationally from the component of the radial motion projected on the line of sight.

Blomme: The material essentially moves out radially. Only close to the surface of the star do you see some effect of rotation (through angular momentum conservation).

Ignace: Comparing bow shocks for radiative vs. adiabatic cooling: for hypersonic flow, our simulations (Cassinelli et al.) give bow shocks that are roughly parabolic. Raga has an analytic solution for a similar scenario but with strong radiative cooling and the bow shock (downwind) is much more "confined", implying less lateral flow.

Owocki: Backfalling clumps can arise in MHD models when material is trapped in closed loops. Infall can also occur if the wind becomes overloaded, for example from rapid rotation or temporal modulation in base driving. But in ordinary hydrodynamic models of CAK winds with or without instability, we see no evidence of infalling clumps.
As for lateral velocity, the analyses of WR emission bumps by Carmelle Robert and by Sebastian Lepine seem to show that the bumps have smaller width at line center than at line wings, which is consistent with a much smaller velocity dispersion in the lateral than radial direction. Indeed, this feature is reproduced quite well in Luc Dessart's "patch" models with *no* lateral velocity. Physically, it seems reasonable that the lateral velocity should be much smaller since the radiative driving is primarily radial.

Until one accounts for lateral radiation transport, the main lateral force is from gas pressure, which can only give a lateral velocity dispersion up to the sound speed. So from both theory and observations, it seems the radial velocity dispersion is greater than that in the lateral direction.

Cassinelli: At the very high temperatures of 10 to 15 million K at the peak of the bow shock, radiation losses are far below the cooling runaway. So the adiabatic shock structure should be appropriate.

Hamann: Before I spoil any relations, I want to emphasize that all of you who are doing the wind hydrodynamic modelling: Stan Owocki, Achim Feldmeier, Joachim Puls and others, are doing the best calculations that are feasible today, and even more than that (*laughter*). Nevertheless, we should always remain critical and compare the model predictions with the observational evidence. I feel that there are still a couple of severe discrepancies which should keep us alert that the models might not be fully adequate yet:
1. Mass loss rates from CAK-type stationary wind models are said to be in very good agreement with observed mass loss rates from OB stars. However, when $\dot{M}$ is revised downwards by more and more clumping, I wonder why there is not too much wind driving now predicted by the models.

Puls: The predicted mass loss rates became also lower because of the revision of stellar parameters from line blanketing!

Hamann: Okay, but at least if mass loss is revised downward further, by more than a factor of three compared to the unclumped Hα diagnostics, you will get into troubles. But I have three more points:
2. The velocity law predicted by the models approaches the terminal speed sooner than is observed. The best fits are obtained with a gradual further acceleration extending to larger distances from the star.
3. In the time-dependent hydrodynamic models, the shocks and clumps develop in the acceleration zone and slowly die out at large distances. The observations seem to indicate (for O stars at least) that the clumps already exist close to the sonic point, and survive into the radio region.
4. Clumping properties have been shown in this workshop to be amazingly universal, from WR stars to OB stars, even to the low-mass central stars of Planetary Nebulae. If clumping is caused by the line-driven instability: would you not expect a significant dependence on the parameters, i.e. on mass loss rate and luminosity, which vary over orders of magnitude?

Puls: Actually, the observed O supergiant mass loss rates from Hα are a factor of two to three larger than the stationary hydrodynamic predictions. This factor has already been mentioned by Puls et al., Markova et al. and Repolust et al. (2003, IAUS 212; A&A 2004) and clumping was invoked to explain the difference. If the presently observed $\dot{M}$ are decreased by a factor of three, there is no contradiction to models. If they are decreased by a factor of ten, then there will be a big discrepancy.

Vink: With respect to empirical mass loss rates from Hα versus theoretical line acceleration calculations: I think one should be aware that in parallel to the realization that clumping may affect the Hα mass loss rate in O stars (with $f_{\rm cl} \sim 4-5$, i.e. $\dot{M}$ Hα reductions of $\sim 2-3$), it has also been shown that line blanketing reduces O star temeratures (Crowther, Martins etc.), which affects the empirical luminosities and counteracts the clumping effect. As a result, at this point in time there is no systematic difference between moderately reduced $\dot{M}$ (by a factor 2-3) Hα rates and theoretical O star predictions by Vink et al. (2000), Pauldrach et al. (2003), and Krtička & Kubát (2004). If the *real* clumping factor turns out to be $\gtrsim 5$, then we produce too much driving with our current line force models.

Fullerton: This is a question for the atmosphere modellers: how robust is the result that the clumping must start very near the photosphere? I understand that it appears to be required to get the best fits. But we here also heard that clumping is implemented in the simplest possible way. Could this result be an artifact of the implementation of clumping? It is a crucial issue.

Najarro: Implementation is important. In our current prescription we are using two or three parameters and this means that we cannot easily derive a precise radial value for where clumping starts. To do so, a step function should be implemented. Concering the region where clumping sets on, we are obtaining two sorts of regions, either very close to the photosphere (close to the sonic point) or at much higher velocities ($\sim v_\infty/3$).

de Koter: Someone mentioned "free parameter heaven". Indeed, in principle, the radial stratification structure of clumping offers many free parameters; one $f_{\rm cl}$ at every radius. So it is essential that in constraining $f_{\rm cl}$ the diagnostics should significantly overlap. Note, for instance, that the UV line formation region would only overlap with, say, 10% of the mm-flux zone. Overlap needs to be stronger. Is this the case?

Hillier: I have several comments.
1. Observations by Moffat of ζ Pup show that the variability starts at low velocities in that star (and that the velocity law is consistent with $\beta = 1$).
2. The X-ray modelling finds that the X-ray emission starts at 1.5 R_*, and hence that the shock structure is well developed at this radius. This clearly implies that the clumping and wind structure must start at

lower radii.
3. With smooth winds ($f = 1$) many difficulties in modelling O stars were encountered. The adoption of the volume filling factor approach allowed many of these difficulties (i.e. P V resonance line, O V 1371) to be simultaneously alleviated. While there are discrepancies, these are at a much smaller level than previously.

Schnurr: Referring to what Paco said about the possibility to constrain the properties of wind clumping. The same is true for WR winds, i.e. we are probing different regions of the wind, and can tell what the clumping has to be in different parts of the wind from lines, electron scattering wings, and the spectral energy distribution (Spitzer/Herschel).

Puls: I guess all modellers agree that we need a stratifaction of clumping. The important point, however, as raised by Wolf-Rainer is whether clumping starts close to the wind base. In WR stars, this question cannot be "directly" answered, because one cannot see so far down. If, indeed, clumping sets in very deep, the standard description of a void interclump medium might influence the result (as long as photospheres are not completely clumped as well).

Massa: In regards to lateral coherence, I have never seen a feature simply vanish at intermediate velocity so, at least for DACs, there is no evidence for small lateral structures in UV wind line variability.

Vink: To assess the role of clumping on stellar evolution I do not think we should look too much at GRB, as they are really quite exceptional (high rotation, low Z, binarity?, etc.). A factor of two reduction in absolute $\dot{M}$ will already have an effect on canonical stellar evolution models (e.g. Meynet et al. 1994).

de Koter: Concerning Jorick's remark how a factor of three reduction would affect massive star evolution: I do think that a factor of three decrease would prevent Galactic stars to spin down significantly on the main sequence. If so, partial cumulative projected radial velocities for SMC, LMC and Galactic stars should be similar for young clusters, if the initial $v_{\rm rot}$ distribution does not depend on the environment.

Ignace: We observe GRBs, and some are associated with supernovae, and so connected with massive stars. To what extent is the frequency of GRBs dependent on mass loss issues discussed here for single stars, or can all GRBs be explained with effects from binary star evolution?

de Koter: I am no expert in binary evolution. However, it is discussed that the binary fraction may be less at lower Z. If so, the possibility of having GRBs as the result of single star evolution becomes more important, perhaps even essential.

Vink: Regarding stellar evolution. It is crucial to determine the precise offset between UV, X-ray diagnostics and the ρ^2 diagnostic from Hα. If it is only a factor of two to three, the agreement with theory is good and stellar evolution models that use the Vink et al. (2000) $\dot{M}$ rates would not be affected. If the *real* empirical mass loss rates are a factor of five to seven lower compared to Hα, and a factor of two to three lower than theory, then stellar evolution will be affected quite dramatically.

Gräfener: In our recent WN analyses (Hamann et al. 2006) we found that the luminosities of the Galactic H-free WN stars are all below the Humphreys-Davidson-limit, while H-rich WNL stars (WNLha) tend to lie above it. This could mean that the H-free WN stars are all post RSG/YSG stars, and there would be no need for large O star mass loss to explain their existence. According to our hydrodynamic models the WNLha stars have large masses and are thus still in the H-burning phase.

Hillier: Analyses of wind-blown bubbles have had problems with the energetic for years, and one possible solution is that mass loss rates have been overestimated. With the lower O star mass loss rates it would be worthwhile exploring this issue in further detail.

Weis: I think it also depends highly on how large the bubble is. We distinguish between single-star and total OB association bubbles. For single stars the wind might not be the driving mechanism of the bubble, but only the adiabatic expansion.

de Koter: I showed before that for SMC, LMC and Galactic stars our results on clumping in O stars do apparently not depend on metallicity. My question is, does one expect clumping to depend on Z?

Owocki: In the line driven instability, the growth rate scales with the mean acceleration divided by the ion thermal speed. As such, its formal "direct" dependence on metallicity Z should be the same as the line force itself, i.e. as $Z^{(1-\alpha)}$, where α is the CAK power index. But that is just the growth rate, and in practise the effect on wind structure is more subtle, depending on the nonlinear evolution, as well as, for example, the overall density and its role is setting the cooling length. Generally, as one lowers Z, the smaller number of optically thick lines will make the instability less effective, and the reduced density for radiative cooling will tend to make structure stay hot rather than cool into dense clumps.

Vink: Regarding the Z-dependence of the clumping, for O stars, Mokiem et al. (2001) give some hints that the clumping factor may be the same for the SMC, LMC and Galaxy. For WR stars, Marchenko et al. (2007) show a Z-independent behavior of moving sub-peaks.

Sonneborn: What is the limit of "no metallicity dependence"? 0.1 solar? 0.01 solar?

Hillier: While clumping is prevalent in all stars, it is not clear that its characteristics are the same. Evidence in LBVs and P Cygni stars seems to indicate that while present, it is less important. Metallicity might provide a Z-dependence since it affects v_∞. Furthermore metallicity affects the cooling of shocked X-ray gas, and hence the shock structure. For example, cooling of shocked X-ray gas will be much more efficient in galactic stars as compared with SMC stars.

Hamann: With the hydrodynamic modelling of WR winds, we have found (Gräfener & Hamann 2007) that low-metallicity stars can still drive a strong wind, if they are close enough to the Eddington limit. Even at one thousands of the solar metallicity, high mass loss rates (but only low wind velocities) can be achieved. The helium and CNO lines are obviously capable to provide enough opacity.

Puls: Nobody has discussed the consequences of clumping for the emission from wind-wind collisions. Any comments?

Pollock: Reducing the mass loss rate in WR 140 will correspondingly increase the plasma cooling lengths which are already of the order or greater than the dimensions of the shocked region.

Ignace: In some WR and OB star winds, the OB wind is dominated by the WR wind. So in those cases, reductions in $\dot{M}$ for the OB winds might not impact the wind collision interaction *except* perhaps how clumping in the WR wind might alter radiative braking effects (e. g. in V444 Cyg).

Hillier: The problem with using LBVs, and A stars, is that H can recombine in the radio region, and this can provide another mechanism for providing structure. Such effects are seen in P Cygni.

Cohen: I would urge Joachim, John Hillier and Wolf-Rainer to include detailed X-ray cross sections in their wind models. We need κ_λ to better than a factor of two.

Leutenegger: The He ionization balance strongly influences the soft X-ray opacity of O star winds.

Pollock: I think there is another clumping independent mass loss rate diagnostic which is the residual X-ray flux in eclipse. This presumably simply counts the number of electrons in the wind.

Sonneborn: The physics of O/WR mass loss may be relevant to other astrophysical problems where mass loss or outflow is important: the early universe (Pop III stars, reionization of H and EUV escape fraction), AGN/QSO outflows, galactic winds, young stars, and planetary system formation. We should look how what we have learned this week applies or can be extended.

de Koter: George Sonneborn very nicely summarizes a number of high profile fields in astronomy that may be expected to show great interest in our knowledge of the mass loss properties of stars. For instance, he refers to T Tauri stars. One should certainly add the Herbig Ae/Be stars, i. e. young intermediate mass stars with protoplanetary disks. Eventually the stellar radiation field clears these disks from gas remnants, transforming them into debris disks. Mass loss may play a role in these processes, though one should not expect to obtain constraints on $\dot{M}$ from, say, protoplanetary disk versus debris disk statistics.

Posters

Clumping in Hot Star Winds
W.-R. Hamann, A. Feldmeier & L.M. Oskinova, eds.
Potsdam: Univ.-Verl., 2008
URN: http://nbn-resolving.de/urn:nbn:de:kobv:517-opus-13981

Modelling the polarimetric variability of hot stars

B. Davies[1,2], J.S. Vink[3,4,5] & R.D. Oudmaijer[2]
[1]*Rochester Institute of Technology, USA*, [2]*University of Leeds, UK*
[3]*Imperial College London, UK*, [4]*Keele University, UK*, [5]*Armagh Observatory, UK*

Many hot stars exhibit stochastic polarimetric variability, thought to arise from clumping low in the wind. Here we investigate the wind properties required to reproduce this variability using analytic models, with particular emphasis on Luminous Blue Variables. We find that the winds must be highly structured, consisting of a large number of optically-thin clumps; while we find that the overall level of polarization should scale with mass-loss rate – consistent with observations of LBVs. The models also predict variability on very short timescales, which is supported by the results of a recent polarimetric monitoring campaign.

Introduction & description of the model

Hot stars have long been known to exhibit polarimetric variability. In a recent study, we showed that in the case of Luminous Blue Variables the magnitude of the intrinsic polarization can reach up to 1% (Davies et al. 2005). The stochastic nature of this variability seems to rule-out the presence of a disk / interacting-wind binary as the cause, and instead seems to be caused by wind-clumping. To investigate the conditions required to reproduce this variability, we have constructed an analytic model.

In our model clumps are given a constant angular size, thickness, initial electron density, and ejection rate per wind-flow-time. The clumps are ejected from random positions on the star's surface and move radially outward through the wind according to a β-type velocity law. The total polarization at each time-step is then found from the vector sum of each clump's polarization. We first allow the model to reach steady-state (when the first clumps reach 10 $R_\star$), and then run for 50 flow-times, after which the time-averaged polarization, $\langle P \rangle$, is determined. Here, we summarize the results and predictions, which are published in Davies et al. (2007).

Results & implications

Briefly, we find that the observed level of $\langle P \rangle$ is reproduced in two regimes: optically-thick clumps, with ejection-rates of a few per year; and optically-thin clumps, with hundreds of clumps produced per day (see also Vink et al., these proceedings). The previously-observed shorter timescale variability precludes the dense clumps / few ejections-per-year regime, *therefore we conclude that the polarimetric variability is caused by thousands of optically-thin clumps in a slightly-fragmented wind.*

In this regime, the model predicts that the residual level of polarization should scale with mass-loss rate – consistent with the findings of Davies et al. (2005) that P is generally higher for stars with strong Hα emission. In addition, we expect variability on very short timescales (<1 day) due to the high ejection-rate. This is supported by recent polarimetric monitoring observations (Fig. 1), where we found the magnitude and timescale of AG Car's variablity to be similar to that predicted by a simulation using AG Car-like parameters and an ejection-rate of 200/day (Davies et al., *in prep*). We also find the polarization to be wavelength independent – consistent with electron scattering.

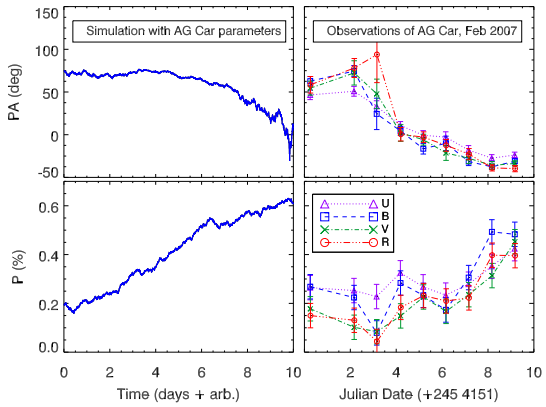

Figure 1: *Left*: snapshot of a simulation using stellar parameters appropriate for AG Car. *Right*: the observed intrinsic polarimetric variability of AG Car. The two have similar variability timescales and magnitudes.

References

Davies, B., Oudmaijer, R.D., & Vink, J.S. 2005, A&A, 439, 1107
Davies B., Vink J.S., Oudmaijer R.D., 2007, A&A, 469, 1045

Clumping in Hot Star Winds
W.-R. Hamann, A. Feldmeier & L.M. Oskinova, eds.
Potsdam: Univ.-Verl., 2008
URN: http://nbn-resolving.de/urn:nbn:de:kobv:517-opus-13981

Far-ultraviolet spectroscopy of O+O binaries in the Magellanic Clouds

R.C. Iping[1], G. Sonneborn[1], D.L. Massa[1], D. Gies[2] & S. Williams[2]
[1] *NASA/GSFC Greenbelt, USA*
[2] *Georgia State University Atlanta, USA*

We report FUSE observations in 2005–2006 of three O-type, double-lined spectroscopic binaries in the Magellanic Clouds. The systems have very short periods (1.4–2.25 d), represent rare, young evolutionary stages of massive stars and binaries, and provide a unique glimpse at some of the most massive systems that form in dense clusters of massive stars. Improved orbit parameters, including revised masses, for LH54-425 are derived from new CTIO spectroscopy. The systems are: LH54-425 in the LMC (O3V + O5V, P=2.25 d, 62+37 $M_\odot$), J053441-693139 in the LMC (O2-3If + O6V, P=1.4 d, 41+27 $M_\odot$), and Hodge 53-47 in the SMC (O6V + O4-5IIIf, P=2.2 d, 24+14 $M_\odot$, where the O4 star appears to be less massive than the O6 star). Their short periods indicates that wind interaction and mass transfer are likely important factors in their evolution. The spectra provide quantitative and systematic studies of phase-dependent stellar wind properties, wind collision effects in O+O binaries at lower metallicities, improved radial velocity curves, and FUV spectro-photometric changes as a function of orbital phase.

LH54-425 (LMC). This binary, with P=2.2475 d, is one of the most massive known. Its binary nature was discovered by Ostrov (2002, MNRAS 336, 309), who derived masses of 100 $M_\odot$ for the primary and 50 $M_\odot$ for the companion. New optical spectroscopy obtained by one of us (SW) at the CTIO 1.5m provide a new radial velocity curve, slightly updated period, and significantly improved values of the orbital parameters. The revised stellar masses are 62 and 37 $M_\odot$ and spectral types are O3V and O5V. Ostrov found the primary to be O3 III (f*), but the new optical spectra (Hα profile) indicate $\log g$=4.0 and a main-sequence luminosity class. However, comparison of FUV spectra of LH54-425 with other early O stars in the LMC show the P-Cygni emission of S VI and O VI may be more consistent with O3 III. The v_∞ of the stellar wind of LH54-425 is 2800 km/sec. LH54-425 is the earliest type star, and one of the most luminous, in the LH54 OB association.

Hodge 53-47 (SMC). Classified as O6V+O4-5III(f) by Morrell et al. (2003, MNRAS 341, 583) who performed the first orbit analysis and found masses of 24 ± 3 $M_\odot$ for the O6 star and 14 ± 3 $M_\odot$ for the O4 star. The periodicity of 2.206 days was discovered in the OGLE survey. It is remarkable that the O4 star is the secondary (less massive) star, indicating that the mass ratio of the system has reversed due to mass transfer and/or loss. H53-47 has undergone significant mass transfer to arrive at the current situation of mass inversion. This may be a short-lived transition phase to a Wolf-Rayet stage. Since H53-47 has undergone significant mass transfer, the current secondary, formerly the more massive star, may show enhanced CNO abundances in its atmosphere. The O6 primary might also have increased CNO abundances as the result of mass accretion from its companion. FUSE observed H53-47 in Oct 2005 and in Nov 2006. Another star (H53-46) 3 arcsec from H53-47 required the use of a narrow slit, and this resulted in incomplete wavelength coverage of the FUV spectrum of H53-47.

J053441-693139 (LMC). Discovered by the MACHO project and catalogued as MACHO 81.8763.8. It is one of the brightest of 611 new eclipsing binaries discovered in their survey of the LMC (Alcock et al. 1997, AJ 114, 326). The system does not appear to have been previously cataloged as a binary or even as an O star. The spectral classification of O3If*+O6V was determined by Ostrov (2001, MNRAS 321, 250), who also performed the first orbit analysis and found stellar masses of 41 ± 1 $M_\odot$ and 27 ± 1 $M_\odot$. The spectral classification was revised by Walborn et al. (2002, AJ 123, 2754) to O2-3 If* + O6:V, making the primary one of the few stars in the new O2 spectral type. With P=1.4047 d, this is one of the shortest periods of any O+O binary, and the most massive of any O binary with $P < 2$ days. The orbital solution of Ostrov (2001) shows that the stars are in over-contact, as might be expected from the derived masses and very short period. This stage of evolution must be quite short, making this object unique. A single FUSE observation was obtained on Sep. 22, 2006 for 28 ksec spanning about half of a binary orbit. The P V 1118, 1128 and Si IV 1122 lines vary significantly with orbital phase for all three O-type, double-lined spectroscopic binaries.

Clumping in Hot Star Winds
W.-R. Hamann, A. Feldmeier & L.M. Oskinova, eds.
Potsdam: Univ.-Verl., 2008
URN: http://nbn-resolving.de/urn:nbn:de:kobv:517-opus-13981

Moving absorption bumps in the spectra of Be stars

J. Kubát[1], **& S. M. Saad**[2]
[1]*Astronomický ústav AV ČR, 251 65 Ondřejov, Czech Republic*
[2]*National Research Institute for Astronomy and Geophysics, 11421 Helwan, Egypt*

Several Be binaries exhibit an absorption bump moving across the blue wing of hydrogen emission lines towards the line center. This bump is demonstrated for the case of two bright Be stars, κ Dra and 4 Her. It is not clear what is the reason for this travelling bump.

4 Her (HR 5938, HD 142926) is a bright (V=5.75) rapidly rotating Be star and a single-line spectroscopic binary (Harmanec et al. 1973). Koubský et al. (1997) found an absorption bump moving across the blue wing of the Hα profile. This bump follows the orbital period and appears twice during the orbital period (see Fig. 2). Very interesting is the fact that the radial velocity of this absorption bump is *always* negative.

κ Dra (HR 4787, HD 109387) is a variable (V=3.75–3.95) Be star, which was proved to be a binary by Juza et al. (1991). Similarly to the case of 4 Her, Saad et al. (2005) found an absorption bump moving in the blue part of the Hα and Hβ line profiles (Figure 1). The bumps are indicated by an arrow. Comparing available profiles of Hα and Hβ lines observed at the same time we can see that the bump velocity in the Hβ lines is always slightly smaller. The radial velocities of these bumps are plotted in the Figure 2.

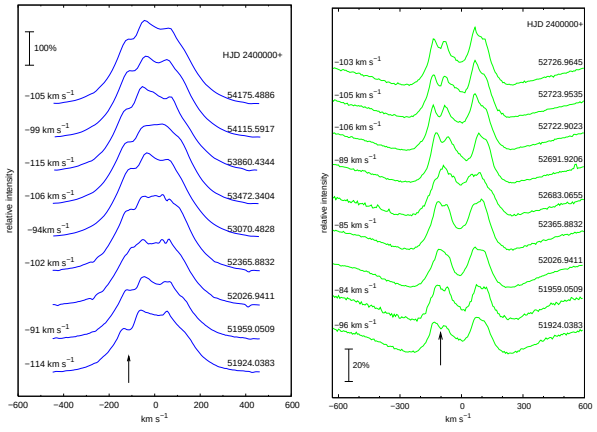

Figure 1: The Hα (left panel) and Hβ (right panel) line profiles of κ Dra with the moving absorption bump (denoted by an arrow) in the blue wing of the profile.

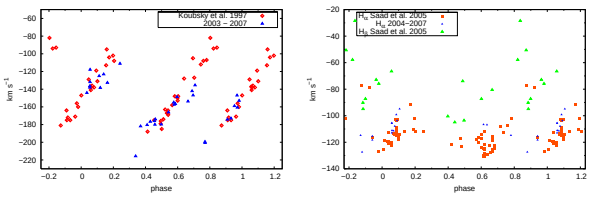

Figure 2: Radial velocities of the moving absorption bump in the Hα line of 4 Her (left panel) and in the Hα and Hβ lines of κ Dra (right panel), both folded with orbital periods.

Discussion: Both binary systems display a lot of similarities. They are both systems with a rapidly rotating late Be star primary and a low-mass secondary. Their orbital period is of the order of tens of days. Both stars display also V/R variations locked with the orbital period. All these similarities suggest that also the reason for the appearance of the moving absorption bumps could be similar. However, the explanation of the absorption feature is not clear. Possible polar jets connected with the Be star are not able to explain orbital variations of the bumps. On the other hand, corotating structure does not explain the exclusively negative radial velocities of these bumps.

There are indications that similar features may be present in other systems with Be stars as well, like in V743 Mon (Pogodin 1997).

We used data from the Ondřejov 2m-telescope data archive. This work has been supported by a grant 205/07/0031 (GA ČR).

References

Harmanec, P., et al. 1973, A&A 22, 337
Juza, K., et al. 1991, BAICz 42, 39
Koubský, P., et al. 1997, A&A 328, 551
Pogodin, M. A. 1997, A&A 317, 185
Saad, S. M., et al. 2004, A&A 419, 607
Saad, S. M., et al. 2005, Astr. Space Sci. 296, 173

Clumping in Hot Star Winds
W.-R. Hamann, A. Feldmeier & L.M. Oskinova, eds.
Potsdam: Univ.-Verl., 2008
URN: http://nbn-resolving.de/urn:nbn:de:kobv:517-opus-13981

Radiative transfer in CV disk winds

D.-J. Kusterer[1], T. Nagel[1], K. Werner[1] & A. Feldmeier[2]
[1] *Universität Tübingen, Germany*
[2] *Universität Potsdam, Germany*

Mass accretion onto compact objects through accretion disks is a common phenomenon in the universe. It is seen in all energy domains from active galactic nuclei through cataclysmic variables (CVs) to young stellar objects. Because CVs are fairly easy to observe, they provide an ideal opportunity to study accretion disks in great detail and thus help us to understand accretion also in other energy ranges. Mass accretion in these objects is often accompanied by mass outflow from the disks. This accretion disk wind, at least in CVs, is thought to be radiatively driven, similar to O star winds. WOMPAT, a 3-D Monte Carlo radiative transfer code for accretion disk winds of CVs is presented.

The first detection of outflows in CVs dates back to the late 1970ies and early 1980ies when blueshifted absorption troughs and P Cygni profiles in ultraviolet (UV) resonance lines were discovered (Heap et al. 1978). Such signatures of outflows are mainly seen during outbursts and high states of CVs, as the disk is hotter and creates more radiation pressure for driving a wind. The observational evidence is such that detailed models of CVs, at least in outburst, have to include outflows.

Within the Tübingen group a code for modeling NLTE accretion disk atmospheres was developed and successfully used to model spectra of CVs and ultracompact X-ray binaries (Nagel et al. 2004, Werner et al. 2006). Our goal is to develop a whole package with which we are able to model a complete CV including the accretion disk, the white dwarf and the outflow.

At the moment we implemented a kinematical biconical wind model by Shlosman & Vitello (1993) for the outflow structure. To contrast the kinematical model a hydrodynamical approach is taken by implementing a wind structure based on CAK theory following Feldmeier & Shlosman (1999). Monte Carlo techniques are used to do the radiative transfer in this three-dimensional wind structure. Photon packets, which represent a monochromatic family of photons, are created on the disk or the WD and are then followed through the wind. All parts of a photon packet's life, the creation, interaction points and -processes, new directions of flight, etc. are determined via probabilities. Optical depths are acquired by numerical integration of local opacities along the photon's line of flight. Thus no Sobolev approximation is needed. Furthermore line opacities can be calculated with either Doppler or Stark broadening. The spectra are determined by detecting escaping parts of photon packets in a virtual detector located at infinity.

Typical P Cygni wind lines, such as the CIV 1550 Å resonance line, (Fig. 1) are reproduced by our model. One interesting point to note is, using the same parameters the assumption of Doppler broadening yields much stronger lines compared to the use of Stark broadening. In order to get the P Cygni profile for Stark broadening one could assume a higher abundance of C in the wind as compared to the standard solar value. Other possible solutions currently probed for this problem are different temperatures and higher accretion rates. Even clumping like in O-star winds might prove useful.

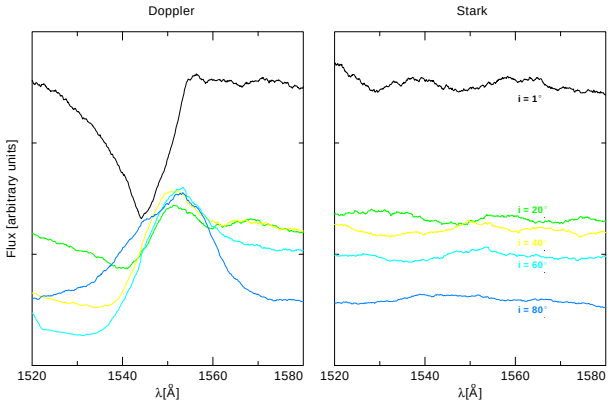

Figure 1: Calculated CIV 1550 Å resonance line for different inclination angles.

References

Feldmeier, A., & Shlosman, I., 1999, ApJ, 526, 344
Heap, S. R., et al., 1978, Nature, 275, 385
Nagel, T., et al., 2004, A&A, 428, 109
Shlosman, I., & Vitello, P., 1993, ApJ, 409, 372
Werner, K., et al., 2006, A&A, 450, 725

Clumping in Hot Star Winds
W.-R. Hamann, A. Feldmeier & L.M. Oskinova, eds.
Potsdam: Univ.-Verl., 2008
URN: http://nbn-resolving.de/urn:nbn:de:kobv:517-opus-13981

Clumping in Galactic WN stars: a comparison of mass loss rates from UV/optical & radio diagnostics

A. Liermann & W.-R. Hamann
Universität Potsdam, Germany

The mass loss rates and other parameters for a large sample of Galactic WN stars have been revised by Hamann et al. (2006), using the most up-to date Potsdam Wolf-Rayet (PoWR) model atmospheres. For a sub-sample of these stars exist measurements of their radio free-free emission. After harmonizing the adopted distance and terminal wind velocities, we compare the mass loss rates obtained from the two diagnostics. The differences are discussed as a possible consequence of different clumping contrast in the line-forming and radio-emitting regions.

The Potsdam Wolf–Rayet model atmospheres were applied by Hamann et al. (2006) (HGL06) to analyze the UV/optical spectra of Galactic WN stars. Radio continuum emission measurements are available for 12 of these stars (Wendker 1995; Leitherer et al. 1997; Cappa et al. 2004), leaving out known binary systems. For 10 more stars only upper limits of their radio emission could be estimated. We derive mass loss rates with the relation from Wright & Barlow (1975) for free-free emission. Multiple radio measurements were averaged for WR 87, WR 89 and WR 105. The free-free Gaunt factor $g_{\rm ff}$ is calculated following Leitherer & Robert (1991) with a constant electron temperature $T_{\rm e} = 10000$ K. The mean molecular weight μ is taken from our analysis (HGL06) and the mean number of electrons per ion is $\gamma = 1$ – exept for WR 2 and WR 3 where our models indicate that He remains fully ionized. Terminal velocities v_∞ and distances d are taken from HGL06 for consistency.

While UV/optical lines are formed in regions between $1 \ldots 10\ R_*$, the radio emission emerges from $\approx 1000\ R_*$. The empirical mass loss rates from both diagnostics scale with the adopted clumping contrast ($\dot{M} \propto D^{-1/2}$) at their corresponding formation radius. The UV/optical mass loss rates from HGL06 were derived under the assumption of clumping ($D_{\rm opt} = 4$), whereas the radio mass loss rates are derived for an unclumped plasma ($D_{\rm radio} = 1$).

We find that the mass loss rates from the two diagnostics agree remarkably well (see Fig. 1), the average difference in $\log \dot{M}$ being only $\Delta \log \dot{M}(\text{opt-radio}) = -0.05 \pm 0.10$. This average difference would vanish completely when choosing $D_{\rm opt} = 3.2 \times D_{\rm radio}$. For OB stars, Puls et al. (2006, and this volume) found a higher degree of clumping in the line-forming region, relative to the radio regime.

There are evidences (from electron-scattering line wings) that the clumping contrast in the line-forming region of WR stars is $D_{\rm opt} = 4...10$, typically. This implies, together with our present result, that density imhomogeneities are not entirely smoothed out in the radio-emitting region.

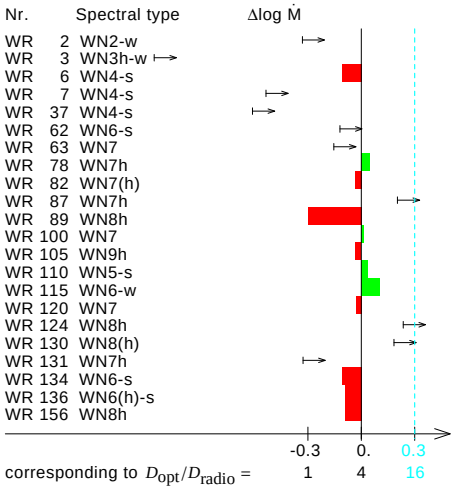

Figure 1: Analysed sample of WN stars

References

Cappa, C., Goss, W. M., & van der Hucht, K. A. 2004, AJ, 127, 2885

Hamann, W.-R., Gräfener, G., & Liermann, A. 2006, A&A, 457, 1015 (HGL06)

Leitherer, C., Chapman, J.M., & Koribalski, B. 1997, ApJ, 481, 898

Leitherer, C., & Robert, C. 1991, ApJ, 377, 629

Puls, J., Markova, N., Scuderi, S., Stanghellini, C., Taranova, O. G., Burnley, A. W., & Howarth, I. D. 2006, A&A, 454, 625

Wendker, H.J. 1995, A&AS, 109, 177

Wright, A. E., & Barlow, M. J. 1975, MNRAS, 170, 41

Clumping in Hot Star Winds
W.-R. Hamann, A. Feldmeier & L.M. Oskinova, eds.
Potsdam: Univ.-Verl., 2008
URN: http://nbn-resolving.de/urn:nbn:de:kobv:517-opus-13981

Wavelets for looking for clumping in the wind of OB stars

A.F. Kholtygin
Astronomical Institute of Saint-Petersburg University, Russia

The wind of hot stars are strongly structured and carry the numerous clumps of very different sizes and masses. Contrary to the Wolf-Rayet stars, the individual clumps in the winds of OB stars are rather small and not very long-lived objects. This makes the detecting clumps in OB star wind a hard problem. We use the wavelet analysis as a powerful tool for searching the details of the line profiles, connected with clumps. We use the dynamical wavelet spectra of line profile variations (lpv) for studying a regular and a stochastic lpv.

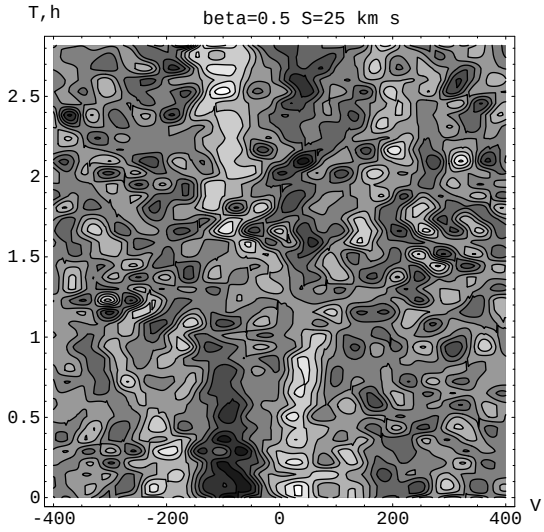

Figure 1: Dynamical wavelet spectra for line HeII $\lambda\,4686$ in a spectra of the star δ Ori A for the scale=25 km/s.

The clump contribution in the total line profile for OB stars is smaller than for WR ones and can be restored using the wavelet analysis via the *dynamical wavelet spectra* (Kholtygin et al. 2006). Those are the wavelet transform of the line difference spectra in the velocity V space for the fixed scale S. For scales in an interval $S = 1 - 5$ km/s the dynamical wavelet spectra is determined by the noise contribution, whereas for large scales $S > 25$ km/s mainly regular variations in the *dynamical wavelet spectra* can be detected.

For intermediate scales the contribution of the stochastic lpv for line HeII $\lambda\,4686$ in a spectra of a triple system δ Ori A (O9.5II) connected with the clumps can be seen in Fig. 1. The *dynamical wavelet spectra* for the same line for scale $S = 50$ km/s show mainly the regular components of lpv (Fig. 2), connected with the non-radial pulsations of the main component δ Ori Aa[1] (Kholtygin et al. 2006).

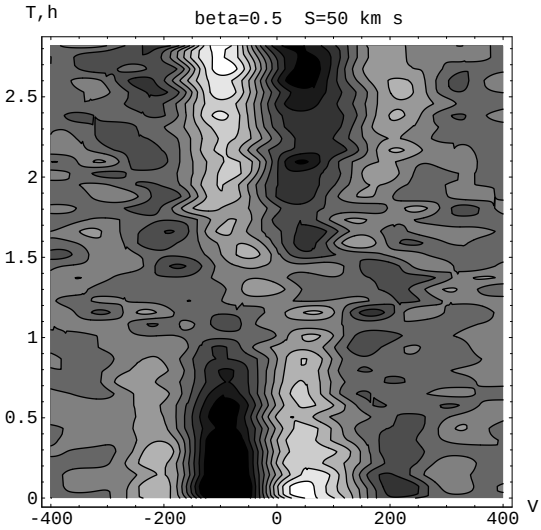

Figure 2: The same as in a Fig. 1 but for the scale=50 km/s.

The author is grateful for the support provided by a RFBR grant 05-02-16995.

References

Kholtygin, A.F., Burlakova, T.E., Fabrika, S.N., Valyavin, G.G., Yushkin, M.V., Astronomy Reports, 2006, 50, 887

Clumping in Hot Star Winds
W.-R. Hamann, A. Feldmeier & L.M. Oskinova, eds.
Potsdam: Univ.-Verl., 2008
URN: http://nbn-resolving.de/urn:nbn:de:kobv:517-opus-13981

XMM-Newton observations of Zeta Orionis (O9.7 Ib): A Collisional Ionization Equilibrium model

A.J.J. Raassen[1,2], K.A. van der Hucht[1], N.A. Miller[3] & J.P. Cassinelli[4]
[1]*Netherlands Institute for Space Research (SRON), Utrecht, The Netherlands*
[2]*Astronomical Institute "Anton Pannekoek", Amsterdam, The Netherlands*
[3]*Dept. of Physics & Astronomy, Universiy of Wisconsin-Eau Claire, Eau Claire, USA*
[4]*Dept. of Physics & Astronomy, Universiy of Wisconsin at Madison, Madison, USA*

We present the analysis of XMM-Newton observations of ζ Orionis. The analysis is based on fitting to the total spectrum as well as diagnostics of individual line.

1 CIE model

We have fitted the RGS, EPIC-MOS and EPIC-pn spectra applying a three temperature collisional ionization equilibrium (CIE) model for optically thin plasma, from SPEX in combination with MEKAL. The ionization equilibrium is based on calculations by Arnaud & Rothenflug (1985). The obtained temperatures, Emission measures (EM) and abundances are given in Table 1. The temperatures range from $\approx$ 0.1 ... 0.6 keV. The EM values are in units of 10^{54}cm^{-3}. The abundances are close to solar photospheric values, except for Ne, Mg, and Si which are somewhat higher. The values are relative to solar photospheric values (Anders & Grevesse 1989) except for Fe (Grevesse & Sauval 1999).

Table 1: Multi-temperature fit

Parameter	Value	Abun	
kT_1	0.073 (.006)	C	1.04 (0.19)
EM_1	8.2 (2.7)	N	1.10 (0.12)
kT_2	0.201 (.004)	O	0.92 (0.08)
EM_2	3.76 (0.31)	Ne	1.34 (0.18)
kT_3	0.551 (.013)	Mg	1.94 (0.24)
EM_3	1.57 (0.18)	Si	1.41 (0.21)
		Fe	1.13 (0.10)

2 He-like line ratio diagnostic

Based on forbidden line versus intercombination line diagnostics in He-like ions we conclude that the ions in the hot plasma are formed at an average distance from the stellar surface of 3.9 (1.7) R_* for Mg XI, 4.8 (1.8) R_* for Ne IX, 12.5 (1.5) R_* for O VII, and 34 (10) R_* for N VI.

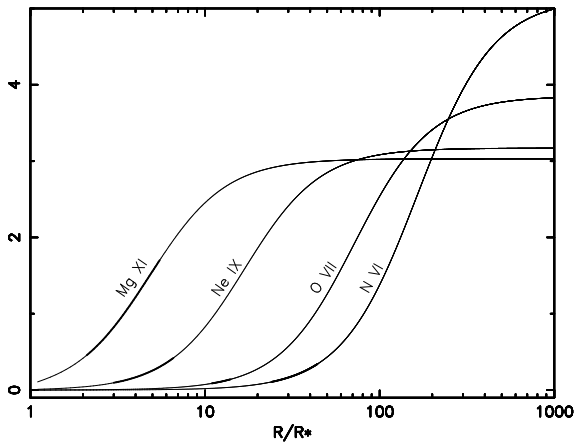

Figure 1: The curves show the theoretical f/i ratios (thin lines) and the measured values (thickened portions).

References

Anders, E., & Grevesse N. 1989, Geochimica et Cosmochimica Acta, 53, 197

Arnaud, M., & Rothenflug, J. 1992, A&AS, 60, 425

Grevesse, N., & Sauval, A.J. 1999, A&A, 347, 348

Clumping in Hot Star Winds
W.-R. Hamann, A. Feldmeier & L.M. Oskinova, eds.
Potsdam: Univ.-Verl., 2008
URN: http://nbn-resolving.de/urn:nbn:de:kobv:517-opus-13981

3D numerical model for an asymmetrical superbubble

J. Reyes-Iturbide[1], P. Velázquez[2] & M. Rosado[1]
[1] *Instituto de Astronomía, UNAM. México*
[2] *Instituto de Ciencias Nucleares, UNAM. México*

Massive stars usually form groups such as OB associations. Their fast stellar winds sweep up collectively the surrounding insterstellar medium (ISM) to generate superbubbles. Observations suggest that superbubble evolution on the surrounding ISM can be very irregular. Numerical simulations considering these conditions could help to understand the evolution of these superbubbles and to clarify the dynamics of these objects as well as the difference between observed X-ray luminosities and the predicted ones by the standard model (Weaver et al. 1977).

1 Numerical simulation

We only considered the interaction between OB stellar winds and the surrounding ISM. To do the 3D numerical simulation, we considered that the plane of the sky is in the xy plane of our simulation. From the same xy star configuration, three possible z coordinates distribution were generated by randomly choosing the z value. The different stellar configurations define different models in our simulations as we will see below. The cluster is limited by two molecular clouds at the North and South-West. These clouds are modelled as two bars which have high densities compared with the surrounding ISM.

Considering this scenario, we have carried out 3D numerical simulations with the Yguazú-a code (Raga et al. 2000, 2002). Its main characteristic is that it is an adaptive grid code. In our case five grid levels were employed with a maximum resolution of 7.26×10^{16}cm. A computational domain of $512 \times 512 \times 128$ pixels was considered in the x, y and z axis, respectively.

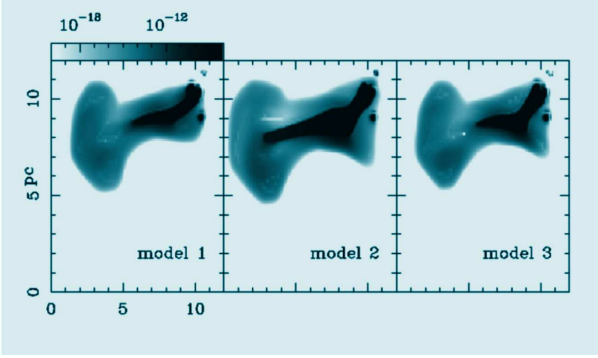

Figure 1: Simulated X-ray emission maps obtained from the models. The logarithmic scale is given in erg s^{-1} cm^{-2} sr^{-1}

2 Results

Figure 1 shows the X ray emission map for the three models, corresponding to an integration time of 2.1×10^5 years. The elongated shape observed in all models is produced by the presence of the two bars. Individual stellar winds begin to collide each other producing a stellar cluster wind. This stellar cluster wind interacts with both bars, which allow the cluster wind gas freely flow to the left, forming an asymmetric superbubble wind. The mechanism of stellar cluster wind formation is more efficient in the case of model 2 because its z-distribution of the stars reveals that they are located closer to each other. The total X-ray luminosities for the three models are quite similar to each other (see Table 1).

Table 1: Total X-ray luminosities

Model	L_X(erg s^{-1})
1	7.0×10^{33}
2	8.6×10^{33}
3	6.3×10^{33}

References

Raga A. C., Navarro-González R., Villagrán-Muniz M., 2000, Rev. Mex. Astron. Astrofis., 36, 67

Raga A. C., de Gouveia Dal Pino E. M., Noriega-Crespo A., Mininni P. D., Velázquez P. F., 2002, A&A, 392, 267

Weaver R., McCray R., Castor J., Shapiro P., Moore R., 1977, ApJ, 218, 377

Clumping in Hot Star Winds
W.-R. Hamann, A. Feldmeier & L.M. Oskinova, eds.
Potsdam: Univ.-Verl., 2008
URN: http://nbn-resolving.de/urn:nbn:de:kobv:517-opus-13981

Clumping in [WC]-type Central Stars from electron-scattering line wings

H. Todt, W.-R. Hamann & G. Gräfener
Universität Potsdam, Germany

While there is strong evidence for clumping in the winds of massive hot stars, very little is known about clumping in the winds from Central Stars. We have checked [WC]-type CSPN winds for clumping by inspecting the electron-scattering line wings. At least for three stars we found indications for wind inhomogeneities.

Clumping in Central Star winds

Hillier (1991) showed for WR atmospheres that clumpiness can be estimated from the strength of electron-scattering line wings. Clumps are defined by an enhanced density, so that $\varrho_{\mathsf{clump}} = D \cdot \overline{\varrho}$ with the clumping factor D. The empirical mass-loss rates scale with the adopted $D^{-1/2}$. Hamann & Koesterke (1998) found $D \approx 4$ for WN stars and even higher values of D for WC stars.

Although the spectra of [WC] Central Stars resemble those of massive WC stars, the clumping of their winds is not well investigated. Koesterke & Hamann (2003) derived $D \gtrsim 4$ for Sand 3, which is assumed to be a former Central Star with a dissolved nebula. For O-type, hydrogen-rich CSPN Kudritzki et al. (2006) found $D = 1 \ldots 50$ from the relative strength of Hα and He II 4686Å lines. Furthermore, Grosdidier et al. (2002) observed large-scale inhomogeneities, so-called blobs, via the line profile variability at a time scale of hours, which is comparable with the flight time of the clumps.

[WC] Central Star spectra

Electron-scattering (e.s.) wings in [WC] spectra are difficult to measure. The stellar spectra are contaminated with nebular lines which often outshine the e.s. wings. The uncertainty of the stellar continuum is often comparable with the strength of e.s. wings. Moreover the e.s. wings in [WR] CSPN spectra are weaker than for massive stars of same spectral type due to the different scaling properties of the line emission and the e.s. wings (providing a potential way to discriminate between [WR] CSPN and massive WR stars).

Results

In spite of the problems mentioned before, we found evidence for wind clumping in the three early-type [WC] stars NGC 6751, NGC 5189, and NGC 1501. For these stars, homogenous wind models yield e.s. wings that are definitely stronger than observed. The clumping contrast D seems to be higher than 4, but its precise value cannot be determined.

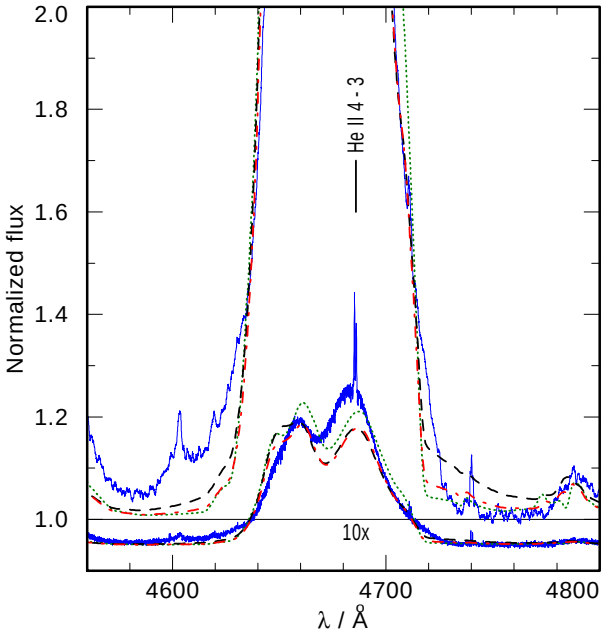

Figure 1: NGC 5189: observation (blue solid) and PoWR models: no clumping (black dashed), $D = 10$ (red dashed-dotted) and $D = 16$ (green dotted)

References

Grosdidier Y., Acker A., Moffat A.F.J., 2002, RevMexAA 12, 90
Hamann W.-R., Koesterke L., 1998, A&A 335, 1003
Hillier, 1991, A&A 247, 455
Koesterke L., Hamann W.-R., 2003, ASPCS 260, 259
Kudritzki R.P., Urbaneja M.A., Puls J., 2006, IAU Symp. 234, 119

Clumping in Hot Star Winds
W.-R. Hamann, A. Feldmeier & L.M. Oskinova, eds.
Potsdam: Univ.-Verl., 2008
URN: http://nbn-resolving.de/urn:nbn:de:kobv:517-opus-13981

Multicomponent stellar wind of hot stars

V. Votruba[1,3], A. Feldmeier[2], J. Kubát[1] & D. Rätzel[1]
[1] *Astronomický ústav, AV ČR v.v.i., Czech Republic*
[2] *Universitat Potsdam, Germany* [3] *Masarykova univerzita, Czech Republic*

We developed a time-dependent multicomponent hydrodynamical code for simulation of the stellar wind from hot stars and applied it to stars with high and low density winds.

One of the major aproximations of the CAK theory is the one component fluid aproximation. This approximation is acceptable for most cases of stellar winds from O stars and some B stars. But in fact, the radiation is acting on absorbing ions and electrons only, and these particles share momentum through Coulomb collisions with the remaining passive part of the plasma (namely protons).

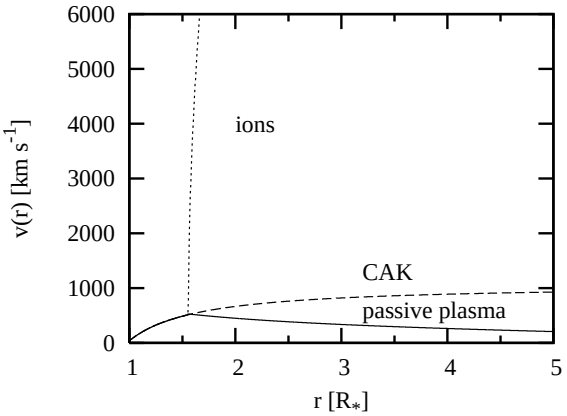

Figure 1: Final wind velocity laws for the model B5 after 55 flow time units R_*/v_∞. Absorbing ions are marked by $(\cdots)$, passive plasma by (—), and the result of the one-component code by (- - -).

Decoupling

The dynamical effect of the Coulomb collisions on plasma is well described by dynamical friction, which was first used by Chandrasekhar (1943) for the case of the gravity force, and later it was used for the electromagnetic force by Spitzer (1956). As was first shown by Springmann & Pauldrach (1992), this more detailed multicomponent description of a stellar wind predicts a runaway mechanism. This means that under certain conditions, namely low density of the wind, Coulomb interactions are so small that they stop the momentum transfer between the passive bulk of plasma and absorbing ions and, as a result, the wind decouples at a certain point. From this point, called the decoupling radius, absorbing ions are highly accelerated by radiation, while passive plasma is decelerated by gravity. We simulated the effect of decoupling for a model star B5, with stellar parameters from Krtička & Kubát (2000).

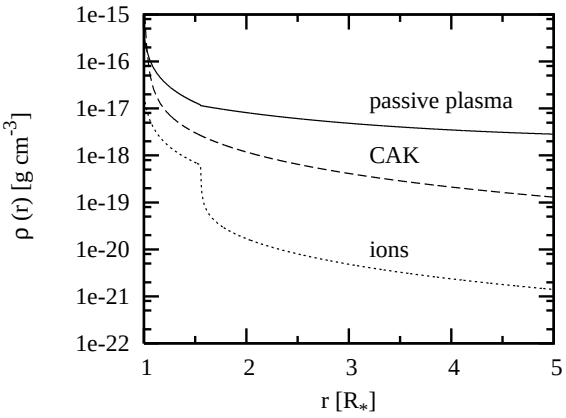

Figure 2: Wind density for the same model B5 star.

This work was supported by a GA AV CR grant B301630501.

References

Chandrasekhar, S. 1943, Principles of Stellar Dynamics, University of Chicago Press

Krtička, J., Kubát J. 2000, A&A 359, 983

Pauldrach, A., Puls, J., Kudritzki, R. P. 1986, A&A 164, 86

Spitzer, L. 1956, Physics of fully ionized gases, New York Interscience

Springmann, U.W.E., Pauldrach, A.W.A. 1992, A&A 262, 515

Author Index

Author Index